BULLETIN OF THE EARTHQUAKE RESEARCH INSTITUTE,
TOKYO UNIVERSITY. Vol. XXVIII, Parts 1-2. Jan.~June, 1950.

東京大學
地震研究所彙報

第28號　第1~2冊

昭和25年1~6月

目　次

論文及報告

			頁
1.	坐標變換にともなふ波動方程式の解の變換 I（英文）	佐藤泰夫	1
2.	水平等方彈性体表面を傳はるレーリー波（英文）	佐藤泰夫	23
3.	地表層の固体粘性が地震動の振幅に及ぼす影響（英文）	金井清	31
4.	粒狀物体を傳はる彈性波の理論 II（英文）	高橋健人 佐藤泰夫	37
5.	地球内の電磁感應およびその地球内部の電氣的性質との關係 第1報 (1)（英文）	力武常次	45
6.	捕獲岩に見出される尖晶石の產狀とその成因（英文）	森本良平	101
7.	日本における1933年から1943年までの間に起つた著しい地震の統計的研究（英文）	岸上冬彥 小高美江子	109
8.	土地の脈動の傳播性の研究（第2報）（英文）	池上良平 岸上冬彥	115
9.	昭和24年12月26日今市地震に於ける墓石顚倒より推定した地震動の加速度（英文）	池上良平 岸上冬彥	121
10.	今市地震に依る地下水位の變化（英文）	下鶴大輔	129
11.	有珠山の活動と精密水準測量（英文）	表俊一郎	133
12.	最近の有珠山の活動（其の5）噴火中 (1944-1945) に現はれた地形變動（英文）	水上武	143
13.	最近の有珠山の活動（其の6）有珠山周邊の精密水準測量（英文）	水上武 佐久間修三 岡田惇	153
14.	n 層建實在建物の各階の水平剛度を調べる一つの方法（英文）	金井清	161
15.	金井式小引（英文）	高橋龍太郎	165
16.	日本における建物に震害を受けた度數の分布（邦文）	金井清 吉澤靜代	167

所　報

(The titles in occidental languages are given on the back cover.)

本彙報ハ年4回（但シ第1號ヨリ第6號マデハ不定期ニ，第7號ハ3冊トシテ發行セリ），彙報別冊ハ不定期ニ發行ス．

本彙報掲載ノ論文及ビ報告ノ內容ニ關シテハ著者ノミニ其責任アルモノトス．

本彙報ニ關スル照會通信ハ東京大學地震研究所長ヘ宛テラレタシ．

The Bulletin is published quarterly. (Vols. I–VI were published at irregular intervals and Vol. VII consisted of three parts.)

Supplementary Volume is published at irregular interval.

The authors of the papers alone are responsible for the statements and opinions contained in their respective papers.

All communications relating to this Bulletin should be addressed to the Director of the Earthquake Research Institute, Tokyo University.

1. *Transformations of Wave-functions Related to the Transformations of Coordinates Systems. I.*

By Yasuo Satô,

Earthquake Research Institute.

(Read July 16, 1946.—Received Sept. 11, 1947.)

1. Introduction.

To find a solution satisfying given conditions on a prescribed boundary surface is one of the most difficult problems in mathematical physics. Utmost endeavours have been made to solve this problem, resulting in devices of a number of elaborate methods worked out by prominent authors. Briefly stated, the current procedure is to find solutions of fundamental equation in specified system of coordinates such that one of the coordinates is constant on the boundary surface. Even if we limit our view for the present to the problem of elastic waves, we first recall the celebrated paper of H. Lamb[1] entitled "On the Propagation of Tremors over the Surface of an Elastic Solid", in which he obtained ingeniously a formula

$$H_0^{(2)}(kr)=\frac{i}{\pi}\int_0^\infty(\xi^2-k^2)^{-\frac{1}{2}}\exp\{i\xi x-(\xi^2-k^2)^{\frac{1}{2}}y\}d\xi \;\ldots\ldots\ldots\ldots (1.1)^{2)}$$

by means of the Green's theorem. The same result was later oblained by H. Nakano[3] by making use of the elliptic coordinates. Corresponding formulae in three dimensional problems were worked out by several authors through different methods. To cite some examples, H. Lamb[4] solved a simple case by means of the same theorem as mentioned above, and T. Sakai[5] and S. Syôno[6] made use of the Weyl's transformation, while Erdélyi[7] used skillfully a method analogous to Maxwell's axial theorem.

Although the methods mentioned above are very sagacious and elegant in themselves, we cannot deny the inevitable lack of definite logical sequence of thinking to make them applicable to all the problems. The writer noticed that the equation (1.1) is nothing but a Fourier transform of Hankel's Bessel function $H_0^{(2)}(kr)$, so that we can reach the result (1.1) by introducing the Fourier's conjugate function of $H_0^{(2)}(kr)$ into the double integral theorem. This procedure may be easily extended to more general cases by means of not only Fourier's theorem but also Fourier-Bessel or Bessel-Dini's double integral theorem.

---

[1] *Phill. Trans.*, **203** (1904), 1.

[2] Notations are somewhat different with the original paper to harmonize with what are used here.

[3] *Jap. Journ. Astro. Geophys.*, **2** (1905), 1.

[4] *loc. cit.* (1)

[5] *Geophys. Mag.*, **14** (1936) 582, *Proc. Phys. Math. Soc. Japan*, **2** (1938), 100.

[6] *Geophys. Mag.*, **12** (1934) 67.

[7] *Physica*, **4** (1937) 107, *Tikyûbuturigaku-Bunken Syô*, (1937), 155.

In this paper the writer treated on this line a general problem of transformation of the coordinates systems of some wave-functions, or in other words, transformation of solutions in a system of coordinates into other system of coordinates which is convenient for boundary value problems. The boundary surfaces considered in this paper are planes, circular cylindrical sufaces and spherical surfaces.

The new results obtained in this paper are the transformations of wave-functions in polar coordinates into those referred to Cartesian coordinates in two dimensional as well as in three dimensional problems [formulae (2.21), (2.24) and (2.27)]; and transformations of wave-functions in three dimensional polar coordinates into those referred to the Cartesian [(5.27)], cylindrical [(6.8)and (6.11)], and polar [(7.9)] coordinates systems.

Part I. Two-dimentional Problem.

2. Transformation from Polar to Cartesian Coordinates.

Solution of wave equation in two dimensions is, omitting the time factor $\exp(ipt)$, written down by polar coordinates as follows:

$$\Theta(x;y)=H_m^{(2)}(kr)e^{im\theta} \qquad (2.1)$$

If we can express this function as the summation of plane waves, it will be very convenient for the treatment of boundary value problems in which boundary surfaces are illustrated as in Fig. 1. This is indeed the problem, of which the most simple case was formerly studied by H. Lamb[8] and H. Nakano[9]. Our purpose at present is—regarding $\Theta(x;y)$ as a function of x, with a parameter y—to obtain the Fourier's conjugate function of this expression.

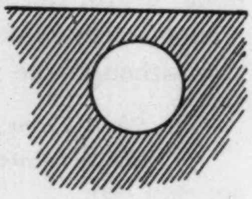
Fig. 1.

First we will consider how to express $H_m^{(2)}(kr)$ and $\exp(im\theta)$ as the function of x and y.

---

[8] *loc. cit.*

[9] *loc. cit.*

When r is real and positive, there is a well known formula[10]

$$H_m^{(2)}(\zeta)=-\frac{1}{i\pi}e^{t\pi m/2}\int_{-\infty+i\pi/2}^{\infty-i\pi/2}\exp\{-i\zeta\cosh t-mt\}dt \quad \ldots\ldots (2.2)$$

Putting here

$$e^t=\frac{2}{r}\tau$$

we have

$$H_m^{(2)}(\zeta)=\frac{1}{\pi}i^{m+1}\left(\frac{\zeta}{2}\right)^m\int_L\exp\left\{-i\left(\tau+\frac{1}{4\tau}\zeta^2\right)\right\}\tau^{-m-1}d\tau \quad \ldots\ldots\ldots (2.3)$$

where integration path is to be taken along L shown in Fig. 2.

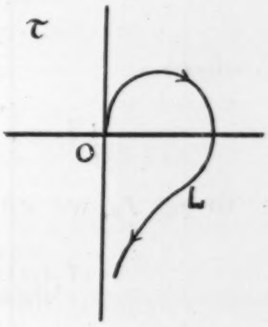

Fig. 2.

On the other hand

$$e^{im\theta}=\exp\{i\,m\tan^{-1}y/x\}=r^{-m}(x+i\,y)^m \quad \ldots\ldots\ldots (2.4)$$

Using (2.3) and (2.4)

$$\begin{aligned}\Theta(x;\,y)&=H_m^{(2)}\{k(x^2+y^2)^{\frac{1}{2}}\}\cdot\exp\{i\,m\tan^{-1}y/x\}\\&=\frac{1}{\pi}i^{m+1}2^{-m}k^m r^m\int_L\exp\{-i(\tau+k(x^2+y^2)/4\tau)\}\\&\qquad\cdot\tau^{-m-1}d\tau\cdot r^{-m}(x+iy)^m\\&=\frac{1}{\pi}i^{m+1}2^{-m}k^m(x+iy)^m\int_L\exp\{\quad ,, \quad\}d\tau \quad \ldots\ldots\ldots\ldots\ldots\ldots (2.5)\end{aligned}$$

By Fourier's double integral theorem,

$$\begin{cases}\Theta(x;\,y)=\displaystyle\int_{-\infty}^{\infty}\Theta^*(\xi;\,y)e^{i\xi x}d\xi\\ \Theta^*(\xi;\,y)=\displaystyle\frac{1}{\pi}\int_{-\infty}^{\infty}\Theta(x;\,y)e^{-i\xi x}dx\end{cases} \quad \ldots\ldots\ldots\ldots\ldots\ldots\ldots\ldots\ldots\ldots (2.6)$$

we have

$$\begin{aligned}\Theta^*(\xi;\,y)&=\frac{1}{\pi}i^{m+1}2^{-m}k^m\int_{-\infty}^{\infty}(x+i\,y)^m\Big[\int_L\exp\{-i(\tau+k(x^2+y^2)/4\tau)\}\\&\qquad\cdot\tau^{-m-1}d\tau\Big]e^{-i\xi x}dx\\&\overset{11)}{\equiv}\frac{1}{\pi}i^{m+1}2^{-m}k^m\int_L\exp\{-i(\tau+k^2y^2/4\tau)\}\tau^{-m-1}T_m(\tau)d\tau\end{aligned}$$

---

[10] WATSON, *Theory of Bessel Functions*, p. 180 (9)

[11] From the uniform convergency of integral, we may legitimately change the order of integration.

where[12]

$$T_m(\tau)=\int_{-\infty}^{\infty}(x+iy)^m\exp\{-i(k^2x^2/4\tau+x\xi)\}dx \quad\ldots\ldots\ldots\ldots\ldots\ (2.7)$$

Putting $a^2=k^2/4\tau$, $2b=\xi$, we have

$$T_m(\tau)=\exp\{i\,b^2/a^2\}\int_{-\infty}^{\infty}(x+iy)^m\exp\{-i(ax+b/a)^2\}dx\,,\ [ax+b/a=\sigma]$$

$$=\exp\{ib^2/a^2\}\cdot a^{-m-1}\int_{-\infty}^{\infty}\left\{\sigma+\left(-\frac{b}{a}+iay\right)\right\}^m\exp\{-i\sigma^2\}d\sigma$$

$$=\exp\{ib^2/a^2\}\cdot a^{-m-1}\sum_{p=0}^{m}\binom{m}{p}\left(-\frac{b}{a}+iay\right)^{m-p}\cdot I_p$$

where

$$I_p\equiv\int_{-\infty}^{\infty}\sigma^p\exp\{-i\sigma^2\}d\sigma\,.\quad\ldots\ldots\ldots\ldots\ldots\ldots\ldots\ldots\ (2.8)$$

To get I_p, we will consider the following integral

$$I_p(\alpha)=\int_{-\infty}^{\infty}\sigma^p\exp\{-i\alpha\sigma^2\}d\sigma\,.\quad\ldots\ldots\ldots\ldots\ldots\ldots\ldots\ (2.9)$$

This can be easily evaluated, for

$$I_{2q+1}(\alpha)=0$$

$$I_{2q}(\alpha)=\int_{-\infty}^{\infty}\sigma^{2q}\exp\{-i\alpha\sigma^2\}d\sigma$$

$$I_0(\alpha)=\int_{-\infty}^{\infty}\exp\{-i\alpha\sigma^2\}d\sigma=(\pi/\alpha)^{\frac{1}{2}}e^{-i\pi/4}$$

$I_{2q}(\alpha)$ is uniformly convergent near $\alpha=1$, therefore we may differentiate the above expression by α.

$$\left(\frac{d}{d\alpha}\right)^q I_0(\alpha)=(-i)^q\int_{-\infty}^{\infty}\sigma^{2q}\exp\{-i\alpha\sigma^2\}d\sigma=i^{-q}I_{2q}(\alpha)$$

$$=\sqrt{\pi}\cdot\left(\frac{d}{d\alpha}\right)^q\alpha^{-\frac{1}{2}}e^{-i\pi/4}$$

---

12) Though FOURIER's integral theorem is generally used under the condition of "limited total fluctuation" (cf. WHITTAKER and WATSON: *Modern Analysis*, p. 188) $\Theta(x;y)$ does not satisfy this condition. But as is clear from a perusal of the proof of FOURIER's theorem, any function, which diminishes in the order of $O(\zeta^{-\vartheta})$ $(0<\vartheta<1)$ can be represented by FOURIER's integral if it does not contain the above condition. (Since the proof is easy we need not write it here.) $\Theta(x;y)$ diminishes as $O(\zeta^{-\frac{1}{2}})$, and we may apply the above proposition.

$$=\sqrt{\pi}\cdot i^{2q-\frac{1}{2}}\{1\cdot 3\cdots\cdots(2q-1)/2q\}\alpha^{-q-\frac{1}{2}}$$

$$\therefore\quad I_{2q}(\alpha)=\sqrt{\pi}\cdot i^{3q-\frac{1}{2}}\,A_q\alpha^{-q-\frac{1}{2}}$$

where $A_q\equiv\{1\cdot 3\cdots\cdots(2q-1)\}$[13]

therefore

$$\begin{cases} I_{2q}\equiv I_{2q}(1)=\sqrt{\pi}\cdot i^{-q-\frac{1}{2}}A_q \\ I_{2q+1}\qquad =0 \end{cases} \qquad\cdots\cdots\cdots\cdots\cdots\cdots\cdots\cdots\cdots\cdots \text{(2.10)}$$

Substituting (2.10) into (2.8)

$$T_m(\tau)=\exp\{ib^2/a^2\}a^{-m-1}\sum_{q=0}^{\langle m\rangle}\binom{m}{2q}\left(-\frac{b}{a}+iay\right)^{m-2q}$$

$$=\sqrt{\pi}\cdot\sum_q A_q\sum_{r=0}^{m-2q} i^{m+q+r-\frac{1}{2}}\binom{m}{2q}\binom{m-2q}{r}y^{m-2q-r}$$

$$\times\exp\{i\tau\xi^2/k^2\}2^{2q+r-1}\,k^{-2q-2r-1}\,\xi^r\,\tau^{q+r+\frac{1}{2}}\qquad\cdots\cdots\cdots\cdots \text{(2.11)}$$

in which $\langle m\rangle$ means

$$\begin{cases}\langle m\rangle=m/2 & \text{when } m \text{ is even,}\\ \qquad=(m-1)/2 & \quad\text{,,}\qquad \text{odd.}\end{cases}$$

$$\therefore\quad \Theta^*(\xi;y)=\frac{1}{\sqrt{\pi}}\sum_q\sum_r A_q\,i^{2m+q+r+\frac{1}{2}}\binom{m}{2q}\binom{m-2q}{r}$$

$$\times\,2^{-m+2q+r+1}\,k^{m-2q-2r-1}\,y^{m-2q-r}\,\xi^r\,Y(\xi)$$

where

$$Y(\xi)=\int_L\exp\{-i(\tau(1-\xi^2/k^2)+k^2y^2/4\tau)\}\tau^{-m+q+r-\frac{1}{2}}d\tau\ \cdots\cdots\cdots\text{(2.12)}$$

If we change the integration variable from τ to $\rho=\tau(1-\xi^2/k^2)$, then we have, when $|\xi|<|k|$

$$Y(\xi)=\int_L\exp\left\{-i\left(\rho+\frac{1}{4\rho}\,(1-\xi^2/k^2)\,k^2y^2\right)\right\}(1-\xi^2/k^2)^{m-q-r-\frac{1}{2}}\,\rho^{-m+q+r-\frac{1}{2}}d\rho$$

$$=\pi\,i^{-m+q+r-\frac{1}{2}}\,(1-\xi^2/k^2)^{(m-q-r-\frac{1}{2})/2}(2/ky)^{m-q-r-\frac{1}{2}}$$

$$\times\,H^{(2)}_{m-q-r-\frac{1}{2}}\{(k^2-\xi^2)^{\frac{1}{2}}y\}\ \cdots\cdots\cdots\cdots\cdots\cdots\cdots\cdots\cdots\cdots\cdots\cdots \text{(2.13)}$$

$$\therefore\quad \Theta^*(\xi;y)=\sqrt{\pi}\cdot\sum_{q=0}^{(m)}\sum_{r=0}^{m-2q}A_q\,i^{m+2q+2r}\binom{m}{2q}\binom{m-2q}{r}\,2^{q+\frac{1}{2}}$$

$$\cdot\,k^{-q-r-\frac{1}{2}}(k^2-\xi^2)^{(m-q-r-\frac{1}{2})/2}\,y^{-q+\frac{1}{2}}\,\xi^r\,H^{(2)}_{m-q-r-\frac{1}{2}}\{(k^2-\xi^2)^{\frac{1}{2}}y\}$$

---

13) This notation appears in Modern Analysis p. 331.

$$=\sqrt{2\pi}\ \sum_q\sum_r{}^*\{1.3\ldots(2q-1)\}\, i^{m+2q+r}\binom{m}{2q}\binom{m-2q}{r}$$

$$\times\, k^{-m}(k^2-\xi^2)^{(m-q-r-\frac{1}{2})/2}y^{-q+\frac{1}{2}}\xi^r\, H^{(2)}_{m-q-r-\frac{1}{2}}\{(k^2-\xi^2)^{\frac{1}{2}}y\}$$

$$+\sqrt{2\pi}\ i^{3m}k^{-m}(k^2-\xi^2)^{-\frac{1}{4}}\,y^{\frac{1}{2}}\,\xi^m H^{(2)}_{-\frac{1}{2}}\{(k^2-\xi^2)^{\frac{1}{2}}y\} \quad\ldots\ldots\ldots(2.14)$$

where $\sum\limits_q\sum\limits_r{}^*$ means the summation except the case where $q=0$, $r=m$.

Now we have formulae[14)]

$$\begin{cases} H^{(2)}_{\nu+\frac{1}{2}}\{k^2-\xi^2)^{\frac{1}{2}}\,y\}=\{2/\pi(k^2-\xi^2)^{\frac{1}{2}}y\}^{\frac{1}{2}}\ \exp\{-i(k^2-\xi^2)^{\frac{1}{2}}y\} \\ \qquad\qquad\cdot\sum\limits_{s=0}^{\nu} i^{\nu-s-1}\dfrac{(\nu+s)!}{s!\,(\nu-s)!\,\{2(k^2-\xi^2)^{\frac{1}{2}}y\}^s} \\ H^{(2)}_{-\frac{1}{2}}\{(k^2-\xi^2)^{\frac{1}{2}}y\}=\{2/\pi(k^2-\xi^2)^{\frac{1}{2}}y\}^{\frac{1}{2}}\ \exp\{-i(k^2-\xi^2)^{\frac{1}{2}}y\} \end{cases}\quad\ldots\ldots\ldots\ (2.15)$$

Substituting (2.15) into (2.14), we have

$$\Theta^*(\xi;\,y)=2k^{-m}\Big[\sum_q\sum_r{}^*\{1.3\ldots(2q-1)\}\binom{m}{2q}\binom{m-2q}{r}(k^2-\xi^2)^{(m-q-r-1/2}\,y^{-q}\xi^r$$

$$\cdot\sum_s i^{2m+q+r-s}\frac{(m-q-r-1+s)!}{s!\,(m-q-r-1-s)!\,\{2(k^2-\xi^2)^{\frac{1}{2}}y\}^s}$$

$$+\,i^{3m}(k^2-\xi^2)^{-\frac{1}{2}}\xi^m\Big]\ \exp\{-i(k^2-\xi^2)^{\frac{1}{2}}y\}\ \ldots\ldots\ldots(2.16)$$

This expression may be written in the following form, if we regard this as a function of y and rearrange the part in parenthesis as a polynomial of y^{-1}.

$$\Theta^*(\xi;\,y)=\sum_N C_N\,y^{-N}\cdot\exp\{-i(k^2-\xi^2)^{\frac{1}{2}}y\}\ \ldots\ldots\ldots\ldots\ldots\ldots\ldots(2.17)$$

Now, we get back to the first and introducing (2.17) in (2.6), we have

$$\Theta(x;\,y)=H^{(2)}_m(kr)e^{im\theta}=\sum C_N\int_{-\infty}^{\infty}y^{-N}\exp\{-i(k^2-\xi^2)^{\frac{1}{2}}y+i\xi x\}d\xi\quad(2.18)$$

As $\Theta(x;y)$ is a solution of fundamental equation, the right hand side of (2.18) must also satisfy the wave equation. However, if N is not zero, functions of the type of $y^{-N}exp\{-i(k^2-\xi^2)^{\frac{1}{2}}y+i\xi x\}$ or their linear combination cannot satisfy the equation. Therefore, the above coefficents C_N must be all zero except C_0.

$$\therefore\quad \Theta^*(\xi;\,y)=C_0\ \exp\{-i(k^2-\xi^2)y\}\ \ldots\ldots\ldots\ldots\ldots\ldots\ldots(2.19)$$

---

14) WATSON; *Theory of Bessel Functions*, pp. 53, 55.

where C_0 is a function of k and ξ, in which m is involved as a parameter. Besides, $N=q+s$ and q, s are both non-negative, q and s must therefore be both zero; so that $\Theta^*(\xi\,;y)$ is obtained by putting $q=0$, $s=0$ in (2.16)

$$\Theta^*(\xi;\,y)=2k^{-m}\Big[\sum_r{}^*\binom{m}{r}(k^2-\xi^2)^{(m-r-1)/2}\,\xi^r\,i^{2m+r}$$

$$+i^{3m}(k^2-\xi^2)^{-\frac{1}{2}}\xi^m\Big]\exp\{-i(k^2-\xi^2)^{\frac{1}{2}}y\}$$

$$=2k^{-m}(-)^m\{(k^2-\xi^2)^{-\frac{1}{2}}+i\xi\}^m(k-\xi^2)^{-\frac{1}{2}}\exp\{-i(k^2-\xi^2)^{\frac{1}{2}}y\}\;\ldots\ldots(2.20)$$

Though this is obtained under the condition $|k|>|\xi|$, we may prove that the same relation holds when $|k|<|\xi|$ by analytic continuation. Therefore we have generally,

$$H_m^{(2)}(kr)e^{im\theta}=(-)^m\frac{1}{\pi}\int_{-\infty}^{\infty}k^{-m}\{(k^2-\xi^2)^{\frac{1}{2}}+i\xi\}^m(k^2-\xi^2)^{-\frac{1}{2}}$$

$$\cdot\exp\{-i(k^2-\xi^2)^{\frac{1}{2}}y+i\xi x\}d\xi\;\ldots\ldots\ldots\ldots\ldots(2.21)$$

If we put here $m=0$, we have

$$H_0^{(2)}(kr)=\frac{i}{\pi}\int_{-\infty}^{\infty}(\xi^2-k^2)^{-\frac{1}{2}}\exp\{-(\xi^2-k^2)^{\frac{1}{2}}+i\xi x\}d\xi\;\ldots\ldots\ldots(2.22)$$

and this is the result which H. Lamb and H. Nakano obtained.

We may transform (2.21) little, and have

$$H_m^{(2)}(kr)e^{im\theta}=i^m\frac{1}{\pi}\int_{-\infty}^{\infty}k^{-m}\{-\xi+i(k^2-\xi^2)^{\frac{1}{2}}\}^m(k^2-\xi^2)^{-\frac{1}{2}}$$

$$\cdot\exp\{-i(k^2-\xi^2)^{\frac{1}{2}}y+i\xi x\}d\xi\;\ldots\ldots\ldots\ldots(2.23)$$

Here, we put

$$-\xi=k\cos\varphi\,,\quad(k^2-\xi^2)^{\frac{1}{2}}=k\sin\varphi\,,\quad d\xi=k\sin\varphi\;d\varphi\,,$$

then

$$H_m^{(2)}(kr)e^{im\theta}=i^m\frac{1}{\pi}\int_C\exp\{im\varphi-ik(x\cos\varphi+y\sin\varphi)\}d\varphi\quad\ldots(2.24)$$

where the integration path C is illustrated in Fig. 3. (This path may also be deformed to the one denoted by a dotted line.)

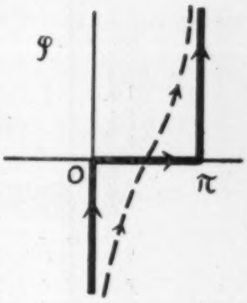

Fig. 3.

By a slight modification

$$H_m^{(2)}(kr)e^{-im\theta}=i^m\frac{1}{\pi}\int_{-\infty}^{\infty}k^{-m}\{-\xi-i\,(k^2-\xi^2)^{\frac{1}{2}}\}^m$$

$$\cdot(k^2-\xi^2)^{-\frac{1}{2}}\exp\{-i\,(k^2-\xi^2)^{\frac{1}{2}}y+i\xi x\}d\xi\ldots\ldots(2.25)$$

and

$$H_m^{(2)}(kr)e^{-im\theta}=i^m\frac{1}{\pi}\int_C \exp\{-im\varphi-ik\,(x\cos\varphi+y\sin\varphi)\}d\varphi\ldots\ (2.26)$$

(2.23) and (2.25) are Fourier transform of the wave-functions $H_m^{(2)}(kr)\exp(\pm im\theta)$ and (2.24) and (2.26) are the expressions corresponding to that of Weyl in three dimensional problems. This circumstance will become clearer in Part II, where we shall treat problems in three dimensional space.

From (2.24) and (2.26) we get generally

$$H_m^{(2)}(kr)e^{\pm im\theta}=i^m\frac{1}{\pi}\int_C \exp\{\pm im\varphi-ik\,(x\cos\varphi+y\sin\varphi)\}d\varphi\ldots\ (2.27)$$

in this expression m is assumed to be positive, but if we put $m'=-m<0$

$$\begin{aligned}H_{m'}^{(2)}(kr)e^{\pm im'\theta}&=H_{-m}^{(2)}(kr)e^{\mp im\theta}\\ &{}^{15)}=i^{-m}\frac{1}{\pi}\int_C \exp\{\mp im\varphi-ik\,(x\cos\varphi+y\sin\varphi)\}d\varphi\\ &=i^{m'}\frac{1}{\pi}\int_C \exp\{\pm im'\varphi-ik\,(x\cos\varphi+y\sin\varphi)\}d\varphi\ldots\ (2.28)\end{aligned}$$

therefore the relation (2.27) holds in cases when m is not only positive but also for all values of integer m.

3. Translation of Origin of Polar Coordinates.

When we are engaged in solving the problem in which the medium is within the bounds of two excentric circular cylinder (see Fig. 4), we must translate the origin of polar coordinates. In this article we will treat such a case, which is, in short, the problem of expressing the wave-function $H_m^{(2)}(kr)\exp(\pm im\theta)$ by new polar coordinates whose origin $0'$ is at a distance from the former one as shown in Fig. 5.

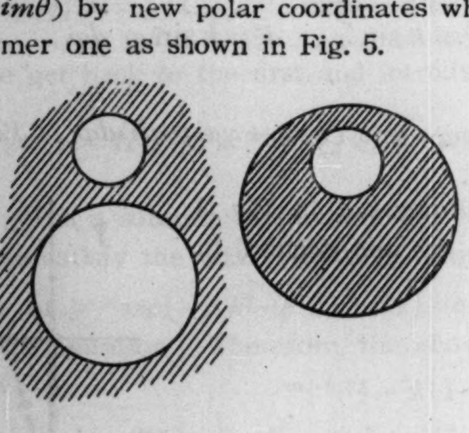

Fig. 4.

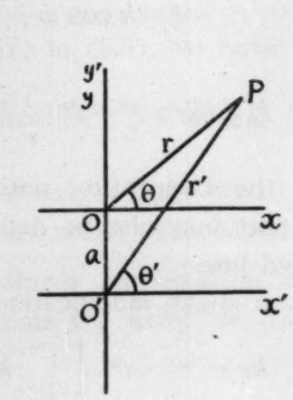

Fig. 5.

---

15) WATSON, p. 74 (7)

Using the formula (2.28) which we have obtained in § 2,

$$H_m^{(2)}(kr')e^{\pm im\theta'}=\pi^{-1}i^m\int_C \exp\{\pm im\varphi-ik(x'\cos\varphi+y'\sin\varphi)\}d\varphi \quad\ldots\ldots\ (3.1)$$

Here, introducing the relation

$$\begin{cases} x=r\cos\theta\,, & y=r\sin\theta \\ x'=r'\cos\theta'=x\,, & y'=r'\sin\theta'=y+a \end{cases} \quad\ldots\ldots\ldots\ldots(3.2)$$

we have

$$H_m^{(2)}(kr')e^{\pm im\theta'}=\pi^{-1}i^m\int_C \exp\{\pm im\varphi-ik\,(x\cos\varphi+y\sin\varphi)\}$$

$$\cdot\exp\{-ika\sin\varphi\}d\varphi \quad\ldots\ldots\ldots\ldots\ (3.3)$$

Now, in this expression

$$\exp\{-ika\sin\varphi\}=\sum_{p=0}^{\infty}\frac{1}{p!}\,\{-ika(e^{i\varphi}-e^{-i\varphi})/(2i)\}^p$$

$$=\sum_{p}\sum_{q=0}^{p}(-)^{p+q}\left(\frac{ka}{2}\right)^p\frac{1}{q!\,(p-q)!}\,e^{i(p-2q)\varphi}$$

therefore

$$H_m^{(2)}(kr')e^{\pm im\theta'}=\frac{1}{\pi}\,i^m\sum_{p}\sum_{q}(-)^{p+q}\left(\frac{ka}{2}\right)^p\frac{1}{q!\,(p-q)!}$$

$$\cdot\int_C \exp\{i(\pm m+p-2q)\varphi-ik\,(x\cos\varphi+y\sin\varphi)\}d\varphi$$

$$=(\pm)^m\sum_{p=0}^{\infty}\sum_{q=0}^{p}i^p\left(\frac{ka}{2}\right)^p\frac{1}{q!\,(p-q)!}\,H_{\pm m+p-2q}^{(2)}(kr)e^{i(\pm m-p-2q)\theta}$$

putting $p-2q=r$, and changing the summations with respect to p and q to the summation by q and r

$$=(\pm)^m\sum_{q=0}^{\infty}\sum_{r=-q}^{\infty}(-)^q i^r\left(\frac{ka}{2}\right)^{r+2q}\frac{1}{q!\,(q+r)!}\,H_{\pm m+r}^{(2)}(kr)\,e^{i(\pm m+r)\theta}$$

if we use the notation $q!$ when q is negative integer, and assume $1/q!$ as zero, $\sum\limits_{q=0}^{\infty}\sum\limits_{r=-q}^{\infty}$ may be written as $\sum\limits_{r=-\infty}^{\infty}\sum\limits_{q=0}^{\infty}$, and so the above expression becomes

$$=(\pm)^m\sum_{r=-\infty}^{\infty}i^r\,H_{\pm m+r}^{(2)}\,(kr)\,e^{i(\pm m+r)\theta}\sum_{q=0}^{\infty}(-)^q\left(\frac{ka}{2}\right)^{r+2q}\frac{1}{q!\,(q+r)!}$$

Here we notice that the summation involving q is just the infinite series representation of Bessel function $J_r\,(ka)$, hence

$$H_m^{(2)}(kr')e^{\pm im\theta'}=(\pm)^m\sum_{\nu=-\infty}^{\infty}i^\nu\,H_{\pm m+\nu}^{(2)}\,(kr)\,e^{i(\pm m+\nu)\theta}\,J_\nu\,(ka)\quad\ldots\ldots\ldots\ldots(3.4)$$

This may be transformed to a more convenient form, for writing $\nu=-\nu'$

$$H_m^{(2)}(kr')\,e^{-im\theta'}=(-)^m\sum_{\nu'=-\infty}^{\infty} i^{-\nu'}H_{-m-\nu'}^{(2)}(kr)\,e^{-i(m+\nu')\theta}\,J_{-\nu'}(ka)$$

$$=\sum_{\nu'} i^{\nu'}\,H_{m+\nu'}^{(2)}(kr)\,e^{-i(m+\nu')\theta}\,J_{\nu'}(ka)$$

Therefore we have finally,

$$H_m^{(2)}(kr')\,e^{\pm im\theta'}=\sum_{\nu=-\infty}^{\infty} i^{\nu}\,J_\nu(ka)\,H_{m+\nu}^{(2)}(kr)\,e^{\pm i(m+\nu)\theta} \quad\text{.....................}(3.5)$$

(3.5) is the relation which holds when m is any integer, but this result is not new, which was obtained half a century ago through other methods.[16)]

4. Rotation of Polar Coordinates.

The subject of this article is very simple. Using the relation between two systems $r'=r$, $\theta'=\theta-\psi$, (which is quite clear from Fig. 6), we have

$$H_m^{(2)}(kr')\,e^{\pm im\theta'}=e^{\mp im\psi}\,H_m^{(2)}(kr)\,e^{\pm im\theta} \quad\text{............................}(4.1)$$

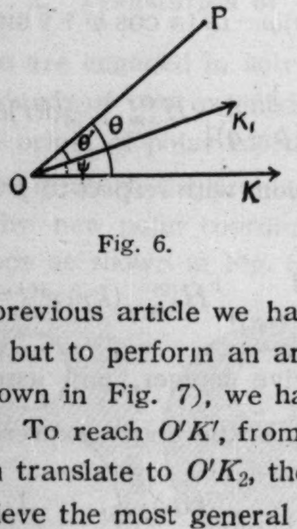

Fig. 6.

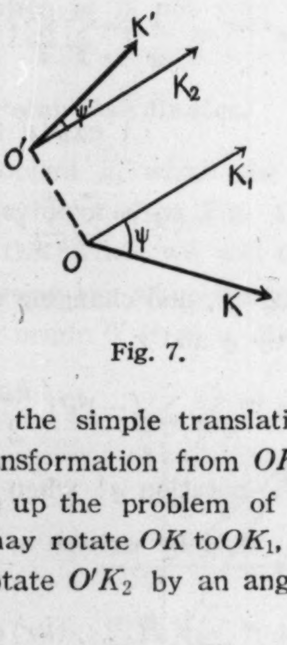

Fig. 7.

In the previous article we have treated the simple translation of polar coordinates, but to perform an arbitrary transformation from OK system to $O'K'$ (as shown in Fig. 7), we have to take up the problem of rotation of coordinates. To reach $O'K'$, from OK, we may rotate OK toOK_1, by an angle ψ, and then translate to $O'K_2$, then again rotate $O'K_2$ by an angle ψ'; thus we can achieve the most general case.

By the above study we finish the two dimentional problem.

---

16) SOMMERFELD, *Math. Ann.*, 14 (1894), 276; *ibid* 47 (1896), 356.
SCHARZSCHILD, *Math. Ann.*, 55 (1902), 177.
And see also WATSON, p. 361.

Part II Three-dimensional Problem—(1)

5. Transformation from Polar to Cartesian Coordinates.

This subject is already treated by S. Syôno[17] by an elegant method using the Weyl's integral theorem[18] in his voluminous paper "On the Propagation of Tremors over the Plane Surface of a Semi-infinite Perfect Elastic Solid," and a particular case, when the wave-function has no orientative characteristics, had been obtained by T. Sakai.[19] This is the transformation, as is easily known, necessary to get the solution satisfying conditions given on both spherical and plane surfaces.

Wave-function referred to polar coordinates is, ommitting the time factor exp(*ipt*)

$$\left\{\begin{aligned} F(x,\ y;\ z)&=(kR)^{-\frac{1}{2}}\,H^{(2)}_{n+\frac{1}{2}}(kR)\,\bar{P}^m_n(\cos\theta)\,e^{\pm im\varphi}\ ^{20)}\\ x&=R\sin\theta\cos\varphi\\ y&=R\sin\theta\sin\varphi\\ z&=R\cos\theta \end{aligned}\right. \qquad\qquad \text{(5.1)}$$

Just as Fourier's integral theorem was used in § 2, in this article we may use Fourier's double integral theorem.

As we know, any function of two variables x and y can be represented under certain conditions in the following integral, where z is a parameter.

$$\left\{\begin{aligned} F\ (x,\ y;\ z)&=\frac{1}{2\pi}\int_{-\infty}^{\infty}\int_{-\infty}^{\infty}F^*(f,\ g;\ z)\,e^{ifx+igy}\,df\,dg\\ F^*(f,\ g;\ z)&=\frac{1}{2\pi}\int_{-\infty}^{\infty}\int_{-\infty}^{\infty}F(\xi,\ \eta;\ z)\,e^{-i\xi f-i\eta g}\,d\xi\,d\eta \end{aligned}\right. \qquad\qquad \text{(5.2)}$$

Now we assume as a function F, the above-stated wave-function (5.1), and change the variables from R, θ, φ, to Cartesian coordinates ξ, η; z. Then

$$\begin{aligned} F(\xi,\ \eta;\ z)=k^{-\frac{1}{2}}(\xi^2+\eta^2+z^2)^{-\frac{1}{4}}\,H^{(2)}_{n+\frac{1}{2}}\{k(\xi^2+\eta^2+z^2)^{\frac{1}{2}}\}\\ \cdot\,\bar{P}^m_n\{z(\xi^2+\eta^2+z^2)^{-\frac{1}{2}}\}\,\exp\{\pm im\tan^{-1}\eta/\xi\} \end{aligned} \qquad\qquad \text{(5.3)}$$

Using (2.3) and (2.4), and further the formula of associated Legendre function[21]

---

17) *lcc. cit.* (6)

18) *Ann. Phys.*, 60 (1919) 481.

19) *loc. cit.* (5)

20) Here $\bar{P}^m_n(\cos\theta)$ means the associated Legendre function, defined by FERRERS, and when we adopt HOBSON's definition we denote $P^m_n(\cos\theta)$. This is the notation used by S. Syôno.

21) HOBSON, *Spherical and Ellipsoidal Harmonics*, p. 91 (5)

$$\overline{P}_n^m(\mu)=(1-\mu^2)^{m/2}\sum_{p=0}^{\langle n-m\rangle}(-)^p\,\frac{(2n-2p)!}{(n-m-2p)!}\,\mu^{n-m-2p}\quad\dots\dots\dots\dots\dots\ (5.4)$$

$$F(\xi,\eta;\,z)=\frac{1}{\pi}\,i^{n+3/2}\,k^{-\frac{1}{2}}\left(\frac{k}{2}\right)^{n+\frac{1}{2}}\frac{1}{2^n n!}\,(\xi+i\eta)^m$$

$$\cdot\sum_{p=0}^{\langle n-m\rangle}(-)^p\cdot\frac{(2n-2p)!}{(n-m-2p)!}\,z^{n-m-2p}(\xi^2+\eta^2+z^2)^p$$

$$\cdot\int_L \exp\{-i(\tau+k^2(\xi^2+\eta^2+z^2)/4\tau)\}\tau^{-n-\frac{3}{2}}\,d\tau\quad\dots\dots\dots\dots\dots(5.5)$$

$$\therefore\quad F^*(f,g;\,z)=\pi^{-2}2^{2n-\frac{3}{2}}\,k^n\,\frac{1}{n!}\cdot\sum_p i^{n+2p+\frac{3}{2}}\binom{n}{p}\frac{(2n-2p)!}{(n-m-2p)!}$$

$$\cdot\,z^{n-m-2p}\int_{-\infty}^{\infty}\int_{-\infty}^{\infty}(\xi+i\eta)^m(\xi^2+\eta^2+z^2)^p$$

$$\cdot\int_L \exp\{--i(\tau+k^2(\xi^2+\eta^2+z^2)/4\tau)\}\tau^{-n-\frac{1}{2}}\,d\tau\,e^{-i\xi f-i\eta g}\,d\xi\,d\eta$$

Here we change the integration variables from ξ, η to ζ, φ, such that

$$\xi=\zeta\cos\varphi\,,\qquad \eta=\zeta\sin\varphi\,.$$

Thus

$$F^*(f,g;\,z)=\left\{\pi^{-2}\,2^{-2n-\frac{3}{2}}\,k^n\,\frac{1}{n!}\sum_p i^{n+2p+\frac{3}{2}}\binom{n}{p}\frac{(2n-2p)!}{(n-m-2p)!}\,z^{n-m-2p}\right\}$$

$$\cdot\int_L \exp\{-i(\tau+k^2z^2/4\tau)\}\tau^{-n-\frac{3}{2}}\,d\tau$$

$$\cdot\int_0^{\infty}\zeta^{m+1}(\zeta^2+z^2)^p\exp\{-ik^2\zeta^2/4\tau\}\,d\zeta$$

$$\cdot\int_0^{2\pi}\exp\{i(\pm m\varphi-\zeta[f\cos\varphi+g\sin\varphi])\}\,d\varphi\quad\dots\dots\dots\dots\dots\ (5.6)$$

5.1 Reduction of Integration.

The above expression contains a triple integral with respect to τ, ζ, φ; and so, we will consider these ingetrations successively. First we will take up the last one which involves φ.

Putting

$$f=j\sin\delta\,,\quad g=j\cos\delta\,,\ \text{and}\ \ \varphi=\varphi'-\delta$$

$$\int_0^{2\pi}\exp\{i(\pm m\varphi-\zeta[f\cos\varphi+g\sin\phi])\}\,d\varphi$$

$$=\int_{\delta}^{\delta+2\pi}\exp\{i(\pm m(\varphi'-\delta)-j\zeta\sin\varphi')\}d\varphi'$$

[22] $$=2\pi\exp\{\mp im\delta\}J_{\pm m}(j\zeta)\qquad\ldots\ldots(5.7)$$

Introducing this result into (5.6)

$$\begin{cases} F^{*}(f,g;z)=\{\text{same with (5.6)}\} \\ \qquad\cdot\displaystyle\int_{L}\exp\{-i(\tau+k^{2}z^{2}/4\tau)\}\tau^{-n-\frac{3}{2}}\,d\tau\cdot\exp\{\mp im\delta\}\cdot 2\pi(\pm)^{m}Z \\ \text{where}\quad Z=\displaystyle\int_{0}^{\infty}\zeta^{m+1}(\zeta^{2}+z^{2})^{p}\exp\{-ik^{2}\zeta^{2}/4\tau\}J_{m}(j\zeta)\,d\zeta \end{cases}\qquad\ldots\ldots(5.8)$$

Next we will consider the integral Z which involves ζ as the integration variable. Expanding $(\zeta^2+z^2)^p$ by the binomial theorem,

$$Z=\sum_{q=0}^{p}\binom{p}{q}z^{2q}\int_{0}^{\infty}\zeta^{m+1+2p-2q}\exp\{-ik^{2}\zeta^{2}/4\tau\}J_{m}(j\zeta)\,d\zeta\qquad\ldots\ldots(5.9)$$

According to Watson,[23] when *arg* $p<\pi/4$ ……(5.10)
the following formula holds

$$\begin{cases} \displaystyle\int_{0}^{\infty}J_{\nu}(at)\exp(-p^{2}t^{2})\,t^{\mu-1}dt=\frac{\Gamma(\frac{1}{2}\nu+\frac{1}{2}\mu)\,(a/2b)^{\nu}}{2p^{\mu}\,\Gamma(\nu+1)}\exp\left(-\frac{a^{2}}{4p^{2}}\right) \\ \qquad\qquad\cdot{}_{1}F_{1}(\frac{1}{2}\nu-\frac{1}{2}\mu+1;\ \nu+1;\ a^{2}/4p^{2}) \\ {}_{1}F_{1}(\alpha;\rho;z)=\displaystyle\sum_{n=0}^{\infty}\{(\alpha)_{n}/n!\,(\rho)_{n}\}z^{n} \\ (\alpha)_{n}=\alpha(\alpha+1)\ldots\ldots(\alpha+n-1),\ \alpha_{0}=1 \end{cases}\qquad\ldots\ldots(5.11)$$

In order to apply the formula (5.11) to (5.9), we must examine the condition (5.10) carefully. For in the expression (5.9)

$$|\arg(-ik^{2}\zeta^{2}/4\tau)|=\pi/2\qquad\ldots\ldots(5.12)$$

and does not satisfy the condition (5.10).

However, as is often used in such a case, if we put small frictional term in the fundamental wave equation, *arg* (k^2) becomes positive, and so, it becomes

$$|\arg(-ik^{2}\zeta^{2}/4\tau)|<\pi/2$$

and thus the former condition holds. Therefore we may write in this case

$$\int_{0}^{\infty}\zeta^{m+1+2p-2q}\exp\{-ik^{2}\zeta^{2}/4\tau\}\,J_{m}(j\zeta)\,d\zeta$$

$$=\sum_{r=0}^{p-q}2^{m+2p-2q+1}\,i^{-m-p+q-r-1}\,k^{2m-2p+2q-2r-2}\,j^{m+r}$$

$$\cdot\frac{\Gamma(m+p-q+1)}{\Gamma(m+r+1)}(-p+q)_{r}\,\tau^{m+p-q+r+1}\exp\{i\tau j^{2}/k^{2}\}\qquad\ldots\ldots(5.13)$$

---

[22] WATSON, p. 20.

[23] WATSON, p. 394 (3).

We introduce this into the expression (5.8)

$$\left\{\begin{aligned} F^*(f,g;z)=&\pi^{-1}\sum_p\sum_q\sum_r 2^{-2n+m+2p-2q+\frac12}\, i^{n-m+p+q-r+\frac12}\\ &\cdot k^{n-2m-2p+2p-2r-2}\, j^{m+2r}\cdot\exp\{\mp im\delta\}z^{n-m-2p+2q}\\ &\cdot\frac{(2n-2p)!\,(m+p-q)!}{(n-p)!\,(n-m-2p)!\,q!\,(p-q)!\,r!\,(m+r)!}\\ &\cdot(-p+q)_r\cdot(\pm)^m T \qquad\qquad \text{......(5.14)}\\ \text{where}&\\ T=&\int_L\exp\{-i(\tau(1-j^2/k^2)+k^2z^2/4\tau)\}\tau^{-n+m+p-q+r-\frac12}d\tau \end{aligned}\right.$$

Lastly, we take up the integral T, whose integration variable is τ and is written in the last line of (5.14).

Changing the variable from τ to $\rho=\tau(1-j^2/k^2)$

$$T=(1-j^2/k^2)^{-\nu-\frac12}\int_L\exp\{-i(\rho+(1-j^2/k^2)k^2z^2/4\rho)\}\rho^{-\nu-\frac12}d\rho \quad\text{......(5.15)}$$

where $\nu=n-m-p+q-r$

Using the formula (2.3) inversely, we can express the integral in T as a Hankel's Bessel function, so we have

$$T=\pi 2^{\nu-\frac12} i^{-\nu-\frac12} k^{-\nu+\frac12}(1-j^2/k^2)^{\frac12\nu-\frac14} z^{-\nu+\frac12} H^{(2)}_{\nu-\frac12}\{(k^2-j^2)^{\frac12}z\}\text{..............(5.16)}$$

Finally, substituting (5.15) and (5.16) into (5.14), we have

$$\begin{aligned} F^*(f,g;z)=(\pm)^m&\sum_{p=0}^{\langle n-m\rangle}\sum_{q=0}^{r}\sum_{r=0}^{p-q} 2^{p-q-r}\,k^{\nu-n-\frac32}\,j^{m+2r}\exp\{\mp im\delta\}\\ &\cdot(1-j^2/k^2)^{\frac12\nu-\frac14}z^{-p+q+r+\frac12}\\ &\cdot P(n,m;p)\binom{r}{q}\frac{(m+p-q)!}{r!\,(m+r)!}(-p+q)_r H^{(2)}_{\nu-\frac12}\{(k^2-j)^{\frac12}z\} \quad (5.17) \end{aligned}$$

$$\left\{\begin{aligned} &\text{where } P(n,m;p) \text{ is the coefficient of } z^{n-m-2p} \text{ in the expansion of}\\ &P_n^{(m)}(z)\ {}^{24)},\ \text{that is } P(n,m;p)=(-)^p 2^{-n}\frac{1}{p!\,(n-p)!}\cdot\frac{(2n-2p)!}{(n-m-2p)!},\\ &\qquad\qquad {}^{24)}P_n^{(m)}(z)=\sum_p P(n,m;p)z^{n-m-2p}\\ &\qquad \text{and}\qquad \nu=n-m-p+q-r \text{ ....(5.18)} \end{aligned}\right.$$

To reduce F^* shown in (5.17) to a more simple form, we will employ that technique which we have used in §2 for simplification of $\Theta^*(\xi;y)$. For the

---

[24] Here, we define $P_n^{(m)}(z)\equiv\left(\frac{d}{dz}\right)^m P_n(z)$, and this notation will be used hereafter.

sake of convenience, we shall make consideration separately, when $n-m$ is an odd integer and when $n-m$ even.

5.11 When $n-m$ is odd.

In this case $\nu-\frac{1}{2}=n-m-p+q-r-\frac{1}{2}$ is always positive, so that using the upper formula of (2.15)

$$F^*(f, g; z)=(\pm)^m\pi^{-\frac{1}{2}}\sum_p\sum_q\sum_r\sum_{s=0}^{r-1}2^{-\nu-m-2r-s+\frac{1}{2}}\,i^{\nu+2p-s}\,k^{\nu-n-s-2}\,j^{m+2r}$$
$$\cdot\exp\{-im\delta\}\cdot(1-j^2/k^2)^{\frac{1}{2}(\nu-s-1)}\,z^{-p+q+r-s}\,P(n, m; p)\binom{p}{q}$$
$$\cdot\frac{(n+p-q)!}{r!\,(m+r)!}(-p+q)_r\cdot\frac{(\nu-1+s)!}{s!\,(\nu-1-s)!}\exp\{-i(k^2-j^2)^{\frac{1}{2}}z\}$$
$$\nu=n-m-p+q-r \qquad \ldots\ldots\ldots\ldots\ldots\ldots\ldots\ldots\ldots\ldots(5.19)$$

As before, this expression can be written as

$$F^*(f, g; z)=\sum_N C_N z^{-N}\ \exp\{-i(k^2-j^2)^{\frac{1}{2}}z\}\ \ldots\ldots\ldots\ldots\ldots\ldots\ (5.20)$$

Since

$$F(x, y; z)=\frac{1}{2\pi}\int_{-\infty}^{\infty}\int_{-\infty}^{\infty}F^*(f, g; z)\exp\{ifx+igy\}df\,dg$$

must satisfy the fundamental wave eqnation,

$$\sum C_N y^{-N}\iint\exp\{ifx+igy-i(k^2-j^2)^{\frac{1}{2}}z\}df\,dg$$

must also satisfy the same wave equation. However, this is impossible so long as C_N $(N\neq 0)$ does not vanish; so that we may legitimately conclude that all C_N except C_0 vanish after a exact summation indicated in (5.19). On the other hand $N=p-q-r+s=0$ holds only when

$$r=p-q\,,\qquad s=0\ \ldots\ldots\ldots\ldots\ldots\ldots\ldots\ldots\ldots\ldots\ldots\ldots\ (5.21)$$

because $\quad -p+q+r-s=-\{((p-q)-r)+s\}$

and $\quad (p-q)\geq r\,,\qquad s\geq 0$

Hence, putting (5.21) into (5.19), we have

$$F^*(f, g; z)=(\pm)^m\pi^{-\frac{1}{2}}\sum_{p=0}^{\langle n-m\rangle}\sum_{q=0}^{p}2^{\frac{1}{2}}\,i^{n-m}\,k^{-n-1}\,j^{m+2p-2q}\exp\{\mp im\delta\}$$
$$\cdot(k^2-j^2)^{(n-m-2p+2q-1)/2}\,P(n, m; p)\binom{p}{q}\cdot\exp\{-i(k^2-j^2)^{\frac{1}{2}}z\}\quad\ldots\ldots(5.22)$$

while

$$(\pm)^m \exp\{\mp im\delta\}=i^{-m\pm m}\{\cos\delta\mp i\sin\delta\}^m,\quad (f=j\sin\delta\,,\ g=j\cos\delta)$$

$$=i^{-m}j^{-m}\{f\pm ig\}^m$$

therefore

$$F^*(f,g;z)=(2/\pi)^{\frac{1}{2}}\sum_{p} i^{n-2m}k^{-n-1}\{f\pm ig\}^m(k^2-j^2)^{(n-m-2p-1)/2}P(n,m;p)$$

$$\cdot\sum_{q=0}^{p}\binom{p}{q}j^{2p-2q}\ (k^2-j^2)^q\exp\{-i(k^2-j^2)^{\frac{1}{2}}z\}$$

$$=(2/\pi)^{\frac{1}{2}}i^{n-m}\sum_{p=0}^{\langle n-m\rangle}k^{-n-1+2p}\{f\pm ig\}^m(k^2-j^2)^{(n-m-2p-1)/2}$$

$$\cdot P(n,m;p)\exp\{-i(k^2-j^2)^{\frac{1}{2}}z\}\ \ldots\ldots\ldots\ldots\ldots\ldots\ldots\ldots\ldots(5.23)$$

Using the formnla (5.18) inversely

$$F^*(f,g;z)=\left(\frac{2}{\pi}\right)^{\frac{1}{2}}i^{n-2m}\left\{\frac{f\pm ig}{k}\right\}^m\frac{1}{k^2}\frac{k}{(k^2-j^2)^{\frac{1}{2}}}P_n^{(m)}\{(k^2-j^2)^{\frac{1}{2}}/k\}\ldots(5.24)$$

This is the final result which we have aimed to reach.

5.12 When $n-m$ is even.

Of course, almost the same logic as above holds good with this case. The only difference is that $\nu-\frac{1}{2}=n-m-p+q-r-\frac{1}{2}$ is not always positive, but it becomes negative in a special combination of p, q, r. For, when $p=r=(n-m)/2$, $q=0$; $\nu-\frac{1}{2}$ becomes $-\frac{1}{2}$, therefore (5.17) is written as

$$F^*(f,g;z)=(\pm)^m\pi^{-\frac{1}{2}}\sum_{p}\sum_{q}\sum_{r}{}^{*}\sum_{s}[\text{same with (5.19)}]+(2/\pi)^{\frac{1}{2}}i^{n-2m}k^{n-\frac{1}{2}}j^n$$

$$\times\ \{(f\pm ig)/j\}^m(k^2-j^2)^{-\frac{1}{2}}P(n,m;(n-m)/2)\exp\{-i(k^2-j^2)^{\frac{1}{2}}z\}\ldots\ldots(5.25)$$

where $\sum\limits_{p}\sum\limits_{q}\sum\limits_{r}{}^{*}$ implies that the summation excludes the combination of p, q, r such that $p=r=(n-m)/2$, and $q=0$.

By the same reasoning with that of § 5.11, we may conclude that all terms of the form $C_N z^{-N}\exp\{-i(k^2-j^2)^{\frac{1}{2}}z\}$ vanish except the term for $N=0$, which corresponds to the case when $-p+q+r-s=0$, or $p-q=r$, $s=0$. In consequence

$$F^*(f,g;z)=\pi^{-\frac{1}{2}}\sum_{p}\sum_{q}{}^{*}\,2^{\frac{1}{2}}\cdot i^{n-m}k^{-n-1}j^{2p-2q}\{f\pm ig\}^m(k^2-j^2)^{(n-m-2p+2q-1)/2}$$

$$\cdot P(n,m;p)\binom{p}{q}\exp\{-i)k^2-j^2)^{\frac{1}{2}}z\}$$

$$+[\text{same with the last term of (5.25)}]\ldots\ldots\ldots\ldots\ldots\ldots(5.26)$$

Here $\sum_{p}\sum_{q}^{*}$ means the summation excluding the case when $p=(n-m)/2$ and $q=0$. The term correspoding to this combination of values is already represented in the last line of (5.25) or (5.26). Hence we have

$$F^{*}(f,g;z)=(2/\pi)^{\frac{1}{2}}\sum_{p=0}^{\langle n-m\rangle}\sum_{q=0}^{p} i^{n-m}k^{-n-1}j^{2p-2q}\{f\pm ig\}^{m}(k^{2}-j^{2})^{(n-m-2p+2q-1)/2}$$

$$\cdot P(n,m;p)\binom{p}{q}\exp\{-i(k^{2}-j^{2})^{\frac{1}{2}}z\}$$

This is strictly identical with (5.23), so that the formula (5.24) holds also when $n-m$ takes an even value. Therefore, for any integral value of n and m, we have

$$\left\{\begin{aligned}F(x,y;z)&=\pi^{-\frac{3}{2}}2^{-\frac{1}{2}}i^{n-2m}k^{-2}\int_{-\infty}^{\infty}\int_{-\infty}^{\infty}\left\{\frac{f\pm ig}{k}\right\}^{m}\frac{k}{(k^{2}-j^{2})^{\frac{1}{2}}}P_{n}^{(m)}\{(k^{2}-j^{2})^{\frac{1}{2}}/k\}\\&\qquad\cdot\exp\{ifx+igy-i(k^{2}-j^{2})^{\frac{1}{2}}z\}df\,dg\end{aligned}\right.$$

$$\text{where}\quad j^{2}=f^{2}+g^{2}\;\ldots\ldots\ldots\ldots\quad(5.27)$$

If we change integration variables from f, g to u, v by the formulae

$$\left\{\begin{aligned}f&=-k\sin u\cos v\\g&=-k\sin u\sin v\end{aligned}\right.\;\ldots\ldots\ldots\ldots(5.28)$$

we have

$$F(x,y;z)=\pi^{-\frac{3}{2}}2^{-\frac{1}{2}}i^{n-m}\int_{0}^{2\pi}dv\int_{W}P_{n}^{m}(\cos u)$$

$$\cdot\exp\{\pm imv-ik(x\sin u\cos v+y\sin u\sin v$$

$$+z\cos u)\}\sin u\,du\ldots\ldots(5.29)$$

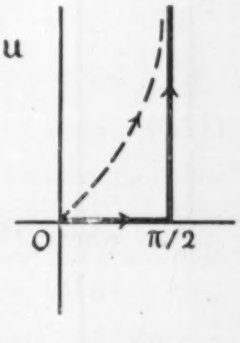

Fig. 8.

where integration path W is shown in Fig. 8 (Of course this path may be deformed to the dotted line.) This last formula is identical with what S. Syôno[25] has deduced by means of his special skillful method using Weyl's transformation. Indeed, Weyl's transformation is obtainable when we apply the change of varirbles shown in (5.28) to Fourier's transformation (5.2).

5.2 Transformation from Polar to Cylindrical Coordinates.

In the previous article we have treated the problem how to express spherical waves as summations of plane waves. Now, in this article we will consider how to express a spherical wave by means of cylindrical waves. For this purpose Hankel's double integral theorem was found to be of great use. Under several conditions,[25] we have

---

[25] *loc. cit.* (6)

$$\begin{cases} \Phi(r) = \int_0^\infty J_\nu(rs)\Phi^*(s)s\,ds \\ \Phi^*(s) = \int_0^\infty J_\nu(\rho s)\Phi(\rho)\rho\,d\rho \end{cases} \qquad \ldots\ldots\ldots\ldots\ldots\ldots\ldots\ldots\ldots\ldots (6.1)$$

As a function $\Phi(r)$, we shall take the wave-function written in spherical coordinates; that is

$$(kR)^{-\frac{1}{2}} H^{(2)}_{n+\frac{1}{2}}(kR)\,\overline{P}{}^m_n(\cos\theta)\exp(\pm im\varphi)$$

But, here, azimuthal angle φ is common in both coordinates systems, so that we may take as Φ

$$\begin{cases} G(r;\,z) = (kR)^{-\frac{1}{2}} H^{(2)}_{n+\frac{1}{2}}(kR)\,\overline{P}{}^m_n(\cos\theta) \\ \text{where } r = R\sin\theta \text{ and } z \text{ is a parameter.} \end{cases} \qquad \ldots\ldots\ldots\ldots\ldots\ldots (6.3)$$

Transforming $H^{(2)}_{n+\frac{1}{2}}$ by means of (2.3), and expressing R and θ by r and z (see Fig. 9),

$$R^2 = r^2 + z^2\,, \quad \cos\theta = z/(r^2+z^2)^{\frac{1}{2}}$$

we have

$$\begin{cases} G(r;\,z) = \pi^{-1}\, i^{n+\frac{3}{2}}\, 2^{-n-\frac{1}{2}}\, k^n \sum\limits_{p=0}^{\langle n-m\rangle} P(n,m;p) z^{n-m-2p} \\ \qquad \cdot (r^2+z^2)^p\, r^m \int_L \exp\{-i(\tau + k^2(r^2+z^2)/4\tau)\} \\ \qquad\qquad \cdot \tau^{-n-\frac{3}{2}} d\tau \\ \text{where } P(n,m;p) \text{ is the same with that in} \\ \text{(5.18)} \ \ldots\ldots\ldots\ldots\ldots\ldots\ldots\ldots\ldots\ldots (6.5) \end{cases}$$

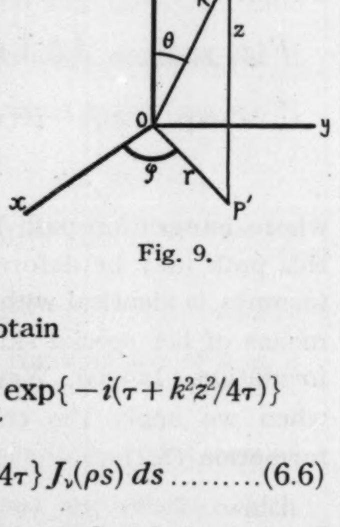

Fig. 9.

Substitusting this $G(r;z)$ for $\Phi(r)$ in (6.1), we obtain

$$G^*(s;z) = \pi^{-1}\, i^{n+\frac{3}{2}}\, 2^{-n-\frac{1}{2}}\, k^n \sum_p P(n,\,m;\,p) z^{n-m-2p} \int_L \exp\{-i(\tau + k^2 z^2/4\tau)\}$$

$$\cdot\, \tau^{-n-\frac{3}{2}} \cdot \sum_{q=0}^{p} \binom{p}{q} z^{2q} \int_0^\infty \rho^{m+1+2p-2q} \exp\{-ik^2\rho^2/4\tau\} J_\nu(\rho s)\,ds \ldots\ldots (6.6)$$

Since the last line of the above expression is perfectly identical with the integral (5.9), use is made of the result (5.11)[27] for $\nu = m$, and we have

---

26) WATSON, p. 453 (2)

27) As we may know by this process, HANKEL's double integral theorem is looked upon as a deformed scheme of FOURIER's double integral theorem, in which integration is partly performed (with respect to azimuthal angle). This circumstance is clearly noted in "COURANT und HILBERT; *Methoden der mathematische Physik*, Bd. I. p. 424".

$$G^*(s;\,z)=\pi^{-\frac{1}{2}}\sum_p\sum_q 2^{\frac{1}{2}}\,i^{n-m}\,k^{-n-1}\,s^{m+2p-2q}\,(k^2-s^2)^{(m-n-2p+2q-1)/2}$$

$$\cdot\, P(n,\,m;\,p)\binom{p}{q}\exp\{-i(k^2-s^2)^{\frac{1}{2}}z\}$$

$$=\pi^{-\frac{1}{2}}\,2^{\frac{1}{2}}\,i^{n-2m}\,k^{-2}\,P_n^m\{(k^2-s^2)^{\frac{1}{2}}/k\}\exp\{-i(k^2-s^2)^{\frac{1}{2}}\,z\}$$

$$\cdot\,\{k/(k^2-s^2)^{\frac{1}{2}}\} \quad \ldots\ldots\ldots\ldots\ldots\ldots(6.7)$$

Substituting this result into (6.1), we have at once,

$$G(r;\,z)=\pi^{-\frac{1}{2}}\,2^{\frac{1}{2}}\,i^{n-2m}\,k^{-2}\cdot\int_0^\infty J_m(rs)\,P_n^m\{(k^2-s^2)^{\frac{1}{2}}/k\}$$

$$\cdot\,\exp\{-i(k^2-s^2)^{\frac{1}{2}}z\}\cdot\{k/(k^2-s^2)^{\frac{1}{2}}\}sds\ \ldots\ldots\ldots\ldots\ldots(6.8)$$

The most simple case, where $n=m=0$, is immediately obtained from this result; that is

$$\frac{1}{kR}\exp\{-ikR\}=\left(\frac{2}{\pi}\right)^{\frac{1}{2}}\int_0^\infty J_0(rs)\exp\{-i(k^2-s^2)^{\frac{1}{2}}z\}\frac{sds}{k(k^2-s^2)^{\frac{1}{2}}}\ \ldots\ldots(6.9)$$

This is identical with what H. Lamb obtained.[28]
If we apply, in this formula, a change of integration variable

$$s=k\sin u\ \ldots\ldots\ldots\ldots\ldots\ldots\ldots\ldots\ldots\ldots\ldots\ldots\ldots\ldots\ldots\ldots\ldots\ldots\ldots(6.10)$$

$$G(r;\,z)=\pi^{-\frac{1}{2}}\,2^{\frac{1}{2}}\,i^{n-m}\int_W J_m(kr\sin u)\,P_n^m(\cos u)\exp\{-ikz\cos u\}\sin u\,du$$

$$\ldots\ldots\ldots(6.11)$$

Where W means the integration path shown in Fig. 8; here one would notice some similarity between this formula and that which is given in the previous article as (5.29). Indeed this is similar, for if we at first perform the integration with respect to v in (5.29), by the aid of formula (5.7), we can also arrive at the same result; and thus we are able to understand the relation between transformations due to Fourier, Weyl, Hankel and so on.

7. Translation of Origin of Polar Coordinates.

We have treated in § 5 and § 6 the problems how to express wave-functions in another kind of coordinates system. In this article however, we will confine our attention to the translation of origin of polar coordinates. If we are to solve problems of propagation of waves from a point within a spherical body, or scattering of spherical waves by a spherical body, we must rely upon this transformation.

---

[28] *loc. cit.*

Using the result of previous article (6.11) we put

$$G_n(r;z)\equiv(kR)^{-\frac{1}{2}}\,H^{(2)}_{n+\frac{1}{2}}(kR)\,\overline{P}{}^m_n(\cos\theta)$$

$$=(2/\pi)^{\frac{1}{2}}\,i^{n-2m}\int_W J_m(kr\sin u)\,P^m_n(\cos\theta)\,\exp\{-ikz\cos u\}\sin u\,du \qquad \ldots\ldots\ldots(7.1)$$

If we take two systems of coordinates (r,φ,z) and (r',φ',z')—as shown in Fig. 10, such that

$$\begin{cases} r'=r \\ \varphi'=\varphi \\ z'=z+a, \end{cases} \qquad \ldots\ldots\ldots\ldots\ldots\ldots\ldots\ldots\ldots(7.2)$$

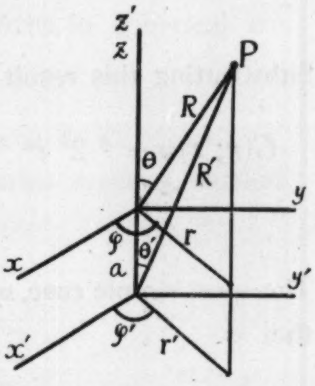

Fig. 10.

then we have

$$G_n(r',z')=G_n(r,z+a)$$

$$=(2/\pi)^{\frac{1}{2}}\,i^{n-2m}\int_W J_m(kr\sin u)\,P^m_n(\cos u)$$

$$\cdot\exp\{-ikz\cos u\}\exp\{-ika\cos u\}\sin u\,du\ldots\ldots\ldots\ldots\ldots\ldots(7.3)$$

which differs but slightly from (7.1) by an additional factor $\exp\{-ika\cos u\}$, for which we may substitute its power series $\sum_\lambda \frac{1}{\lambda!}(ika)^\lambda\cos^\lambda u$ with the result

$$G_n(r',z')=(2/\pi)^{\frac{1}{2}}\,i^{n-2m}\sum_\lambda\frac{1}{\lambda\,!}(-ika)^\lambda\int_W J_m(kr\sin u)\cos^\lambda u\,P^m_n(\cos u)$$

$$\cdot\exp\{-ikz\cos u\}\sin u\,du\ \ldots\ldots\ldots\ldots\ldots\ldots\ldots\ldots(7.5)$$

The integrand in the right hand side of this equation again differs from (7.1) only by a factor $\cos^\lambda u$. But as may be easily inferred, and proved in the following, the factor $\cos^\lambda u\ P^m_n(\cos u)$ in the integrand can be replaced by the sum

$$\cos^\lambda u\,P^m_n(\cos u)=\sum_{s=0}^{\langle\lambda+n-m\rangle}B_{2s}(n,m;\lambda)\,P^m_{\lambda+n-2s}(\cos u)\,,\quad\ldots\ldots\ldots(7.6)$$

so that the required result is obtained by the integrals which are exactly of the same forms as (7.1).

The validity of (7.6) follows from the fact that the differential equation,

$$(1-x^2)v''-2\{\lambda(1-x^2)/x+x\}v'$$

$$+[\lambda(\lambda+1)(1-x^2)/x^2+2\lambda+\{n(n+1)-m^2/(1-x^2)\}]v=0$$

for $v=x^\lambda P^m_n(x)$, is also satisfied by the series $v=\sum c_r P^m_r(x)$, provided c_r satisfies the following recurrence formula;

$$C_{r-2}\{(2\lambda-r+2)(r-1)-\lambda'+n'\}\,\frac{(r-m-1)(r-m)}{(2r-3)(2r-1)}$$

$$+C_r\Big[2\{\lambda-r(r+1)-\lambda'+n'\}\,\frac{(r-1)(r+1)}{(2r-1)(2r+3)}$$

$$+\{(2\lambda-r)(r+1)-\lambda'+n'\}\,\frac{1}{2r+3}+\lambda\Big]$$

$$+C_{r+2}\{-2\lambda(r+2)-(r+2)(r+3)-\lambda'+n'\}\,\frac{(r+m+1)(r+m+2)}{(2r+3)(2r+5)}=0$$

with $\lambda'=\lambda(\lambda+1)$, and $n'=n(n+1)$, for r between $(\lambda+n)$ and $(\lambda+n-m)$, besides

$$C_{n+\lambda}=\frac{(2n-1)!!}{(2n+2\lambda-1)!!}\,\frac{(n+\lambda-m)!}{(n-m)!},$$

$$C_{n+\lambda-2}=-\frac{1}{2}\,\frac{(2n-1)!!}{(2n+2\lambda-5)!!}\,\frac{(n+\lambda-m-2)!}{(n-m-2)!}$$

$$\cdot\left\{\frac{1}{2n-1}-\frac{(n+\lambda-m)(n+\lambda-m-1)}{(n-m)(n-m-1)}\,\frac{1}{(2n+2\lambda-1)}\right\},$$

where $(2n-1)!!=1\cdot3\cdot5\ldots\ldots(2n-1)$, and $C_{\lambda+n-2s}$ stands for $B_{2s}(n,m;\lambda)$.

Introducing, now, the above relation (7.6) into (7.5) and using the relation (7.1) conversely, we have

$$G_n(r',z')=\sum_{\lambda}(-ika)^{\lambda}\,\frac{1}{\lambda!}\,\pi^{\frac{1}{2}}\,2^{\frac{1}{2}}\,i^{n-2m}\sum_{s}B_{2s}(n,m;\lambda)$$

$$\cdot\int_W J_m(kr\sin u)\exp\{-ikz\cos u\}P^m_{\lambda+n-2s}(\cos u)\sin u\,du$$

$$=\sum_{\lambda=0}^{\infty}\{(-ika)^{\lambda}/\lambda!\}i^{-\lambda+2s}\sum_{s=0}^{\langle\lambda+n-m\rangle}B_{2s}(n,m;\lambda)\,G_{\lambda+n-2s}(r,z)\ldots\ldots(7.7)$$

in which we may take

$$B_{2s-1}(n,m;\lambda)=0\,,\qquad B_{-s}(n,m;\lambda)=0\,,\qquad(s=1,2,\;\ldots\ldots)\ldots\ldots\ldots(7.8)$$

so that

$$G_n(r',z')=\sum_{\lambda=0}^{\infty}(-1)^{\lambda+s}\,(ka)^{\lambda}/\lambda!\,\sum_{s=0}^{\lambda+n-m}B_s(n,m;\lambda)\,G_{\lambda+n-s}(r,z)\;\ldots\ldots\ldots(7.9)$$

Changing suffixes and the order of summation adequately, we have

$$G_n(r',z')=\sum_{p=-n+m}^{\infty}(-)^{p}\,K_p(n,m)\,G_{n+p}(r,z)\;\ldots\ldots\ldots\ldots\ldots\ldots\ldots\ldots(7.10)$$

where $$\mathrm{K}_p(n,m)=\sum_{\lambda=p}^{\infty}(k^{\lambda}a^{\lambda}/\lambda!)\,E_{\lambda+p}(n,m;\lambda)$$

with $B_s(n, m; \lambda)$ as shown in (7.6),

which is the required result, and may be interpreted physically as follows:

A general spherical wave

$$G_n^m(R, \theta, \varphi) \equiv (kR)^{-\frac{1}{2}} H^{(2)}_{n+\frac{1}{2}}(kR) P_n^m(\cos\theta) \exp\{\pm im\varphi\}$$

as referred to the spherical coordinates, with the origin at 0, can be expressed in terms of a different origin 0′, by the sum of the same kind of wave functions, $\sum_N G_N^m(r', \theta', \varphi)$, whose orders N are not smaller than m, while the degree m is invariably the same with that of the given wave function.

In concluding this paper we wish to express our hearty thanks to Prof. H. Kawasumi who gave us kind encouragement throughout this work.

---

1. 坐標變換にともなふ波動方程式の解の變換 I

地震研究所 佐藤泰夫

境界値問題一例へば彈性波の發生一を取扱ふさいにしばしば起つてくる困難は，いかにして境界面での條件をみたす解をうるか，といふ點にあつた．これを解決するために今世紀のはじめ以來，ラム，中野，坂井，正野等の諸大家が努力されて美事な結果を出して居られるが，ここではフーリエ，ワイル，ハンケル等の積分による變換を用いて統一的に問題をあつかふことによつて，現在迄の結果を整理するとともに，境界面が，平面，圓筒面，球面からなる場合に都合のよい公式をみちびいた．

第一部では二次元の，第二部では三次元の場合をしらべたが，三次元の球坐標の回轉についてはこれを別に扱ひたいと思ふ．

---

2. *Rayleigh Waves Propagated along the Plane Surface of Horizontally Isotropic and Vertically Aeolotropic Elastic Body.*

By Yasuo SATÔ,

Earthquake Research Institute.

(Read Nov. 15, 1949.——Received May 29, 1950.)

1. Introduction.

Since the publication of the celebrated paper on surface waves by Lord Rayleigh in 1885, considerable development has been made by a number of investigations in the field of the surface waves. But among these studies we find only a few papers concerning the theory of Rayleigh waves in aeolotropic media, none of which gives definite clue as to the conditions of existence and nature of these waves, although Dr. Nagaoka's[1] famous experiment on the elastic constants of rocks proved, in as early as 1900, strong anisotropy in most of the rocks he examined, and recent observations show that the materials in the earth's crust is not always isotropic. Therefore the present discussion is projected. Among various kinds of aeolotropy, we will consider only, in this paper, the case of horizontally isotropic medium, in view of the fact that this is the most important case in actual seismology.[2] This case has already been treated by some writers among whom Messrs. H. Homma[3] and R. Stoneley[4] are the most remarkable. The present paper being the continuation of the study of the former author, most of the equations in the first half of this paper have been obtained by Mr. Homma, to whom the writer expresses his hearty thanks for the kind permission given him to reproduce them.

---

1) H. NAGAOKA, "Elastic Constants of Rocks and the Velocity of Seismic Waves," *Publ. Earthq. Invest. Commit.*, 4 (1900), 47.

2) N. NASU and S. OMOTE, *Zisin.* 13 (1941), 91.

3) S. HOMMA, "On Rayleigh Waves in Horizontally Isotropic Elastic Body" (In Japanese), *Kensinzihô*, 12 (1942), 97.

4) R. STONELEY, "The Seismological Implications of Aeolotropy in Continental Structure," *M. N. R. A. S. Geo. Sup.*, 5 (1943), 343.

2. Equation of motion and boundary conditions.

If we confine ourselves to the problem of Rayleigh waves which are propagated along x-axis and do not vary in the direction of y-axis, then the equations of motion become as follows.* (z-axis is taken vertically downwards and free surface coincides with $z=0$.)

$$\begin{cases} \rho \dfrac{\partial^2 u}{\partial t^2} = M_1 \dfrac{\partial^2 u}{\partial x^2} + N \dfrac{\partial^2 u}{\partial z^2} + (M_3 - N) \dfrac{\partial^2 w}{\partial x\, \partial z} \\ \rho \dfrac{\partial^2 w}{\partial t^2} = (M_3 - N) \dfrac{\partial^2 u}{\partial x\, \partial z} + N \dfrac{\partial^2 w}{\partial x^2} + M_3 \dfrac{\partial^2 w}{\partial z^2} \end{cases} \quad \text{..................(2.1)}$$

where ρ is the density, u and w are the components of displacement in x and z direction respectively, and

$$\begin{cases} X_x = M_1 (x_x + y_y) - 2N_2 y_y + (M_3 - 2N_1) z_z\,, \quad Y_z = N_1 y_z \\ Y_y = M_1 (x_x + y_y) - 2N_2 x_x + (M_3 - 2N_1) z_z\,, \quad Z_x = N_1 x_z \\ Z_z = (M_3 - 2N_1)\ (x_x + y_y) + \quad M_2\ z_z\,, \\ \qquad N = N_1 \end{cases} \quad \text{............(2.2)}$$

If we assume as

$$\begin{cases} u = A_k \exp(-\sigma m Z + imx - imVt) \\ w = iB_k \exp(\quad ,, \quad) \end{cases} \quad \text{..(2.3)}$$

then we have

$$\begin{cases} (M_1 - V^2\rho - \sigma^2 N)\ A_k = \sigma\ (M_3 - N)\ B_k \\ \quad \sigma\ (M_3 - N)\ A_k = (\sigma_2 M_2 + V^2\rho - N)\ B_k \end{cases} \quad \text{..........................(2.4)}$$

Eliminating A and B, we at once have the ordinary velocity equation,

$$M_2 N \sigma^4 + \{M_3^2 - 2M_3 N - M_1 M_2 + (M_2 + N) V^2 \rho\} \sigma^2 + (M_1 - V^2\rho)(N - V^2\rho) = 0\,. \quad \text{............(2.5)}$$

Solving the above equation with respect to σ^2, and denoting the two roots by σ_1^2 and σ_2^2, we have

$$\begin{cases} u = A_1 \exp(-m\sigma_1 z) + A_2 \exp(-m\sigma_2 z) \\ w = i B_1 \exp(\quad ,, \quad) + iB_2 \exp(\quad ,, \quad) \end{cases} \quad \text{...............................(2.6)}$$

in which the common factor $\exp(imx - imvt)$ is omitted for brevity.

In this expression both (A_1, B_1) and (A_2, B_2) must be so chosen as to satisfy the equation (2. 4).

---

* We use the expressions derived by Mr. S. Homma.

Next we must consider the boundary conditions. Since at $z=0$, normal tractions must vanish, we substitute (2.6) into the expressions of Z_z and Z_x in (2.2), and equating the results to zero, we have,

$$\begin{cases} (M_3-2N)(A_1+A_2)-M_2(\sigma_1 B_1+\sigma_2 B_2)=0 \\ \sigma_1 A_1+\sigma_2 A_2+B_1+B_2=0 \end{cases} \quad \ldots\ldots(2.7)$$

We may eliminate A_1, A_2, B_1, B_2, from (2.4) and (2.8). The result

$$\begin{vmatrix} \sigma_1 & \sigma_2 & 1 & 1 \\ M_3-2N & M_3-2N & -\sigma_1 M_2 & -\sigma_2 M_2 \\ M_1-r^2\rho-\sigma_1^2 N & 0 & -\sigma_1(M_3-N) & 0 \\ 0 & M_1-V^2\rho-\sigma_2^2 N & 0 & -\sigma_2(M_3-N) \end{vmatrix}=0 \quad \ldots\ldots(2.8)$$

is the usual characteristic equation.

3. Examination of the characteristic equation.

For the sake of convenience we use the following notations

$$\begin{cases} M_1\equiv\alpha N, \quad M_2\equiv\beta N, \quad M_3\equiv\gamma N \\ \tau\equiv V^2\rho/N\equiv(V/V_s)^2, \quad \text{(where } V_s \text{ is the velocity of S wave)} \end{cases} \quad \ldots(3.1)$$

Then from (2.5)

$$\begin{cases} \sigma_1^2+\sigma_2^2=[-\gamma^2+2\gamma+\alpha\beta-(\beta+1)\tau]/\beta \\ \sigma_1^2\sigma_2^2=(\alpha-\tau)(1-\tau)/\beta \end{cases} \quad \ldots\ldots(3.2)$$

Now we will develop the determinant (2.8) and simplify it by means of the above relation. Since $\sigma_1=\sigma_2$ cannot satisfy both of the equation of motion and boundary conditions, we divide the expression above obtained by $(\sigma_1-\sigma_2)$; then we get an important equation

$$\tau(\tau-\alpha)=[\beta\tau-K]\sigma_1\sigma_2 \quad \ldots\ldots(3.3)$$

where

$$K\equiv\alpha\beta-(\gamma-2)^2 \quad \ldots\ldots(3.4)$$

From (3.3) and the second equation of (3.2) we can eliminate $\sigma_1\sigma_2$ and obtain finally the characteristic equation which determines the velocity of Rayleigh-type waves. That is

$$f(\tau)\equiv\beta(\beta-1)\tau^3-\beta(2K+\beta-\alpha)\tau^2+K(K+2\beta)\tau-K^2=0 \quad \ldots\ldots(3.5)$$

On getting this equation, however, we took the square of both members of (3.3), therefore, there is some possibility that some extraneous roots might be involved in this equation. At first we assumed σ_1 and σ_2 to be both positive. While $\tau=V^2/V_s^2$ must, of course, be positive. Thus, among the roots of $f(\tau)=0$ we must adopt only those which satisfy the following conditions.

1) τ must be positive (since $\tau=V^2/V_s^2$),
2) τ-α and $\beta\tau$-K must have same sign (since both sides of (3.3) must have same sign).

4. Possible range of values of elastic constants.*

Following Love, we write elastic constants as c_{ij} ($i, j=1, 2, 3, 4, 5, 6$), then the strain energy function W of horizontally isotropic body is written as follows:

$$2W=c_{11}(x_x+y_y)^2+c_{33}z_z^2-4c_{66}x_xy_y+2c_{13}(x_x+y_y)z_z$$
$$+c_{44}(y_z+z_x)^2+c_{66}x_y^2 \quad \ldots\ldots\ldots\ldots\ldots\ldots\ldots\ldots\ldots\ldots\ldots\ldots\ldots(4.1)$$

Since W must be positive definite form, we see at once $c_{11}>0$ by putting every strain component except x_x to zero.

Similarly we obtain the following relations,

$$c_{11}>0,\ c_{33}>0,\ c_{44}>0,\ c_{66}>0 \ldots\ldots\ldots\ldots\ldots\ldots\ldots\ldots\ldots\ldots\ldots\ldots\ldots(4.2)$$

Next, if we take $y_z=z_x=x_y=0$, W becomes

$$2W=c_{11}(x_x+y_y)^2+c_{33}z_z^2-4c_{66}x_xy_y+2c_{13}(x_x+y_y)z_z$$

So that, using the notations $\xi=x_x/z_z$, $\eta=y_y/z_z$, we get

$$F\equiv 2W/z_z^2=c_{11}(\xi+\eta)^2+c_{33}-4c_{66}\xi\eta+2c_{13}(\xi+\eta).$$

Here, F must also be positive. The condition is equivalent to

$$[F_{\xi\xi}F_{\eta\eta}-F_{\xi\eta}^2]_{\xi=\xi_0,\eta=\eta_0}>0 \text{ and } [F_{\xi\xi}]_{\xi=\xi_0,\eta=\eta_0}>0$$
$$\text{or} \quad (c_{11}-c_{66})\,c_{66}>0 \quad \text{and} \quad c_{11}>0 \quad \ldots\ldots\ldots\ldots\ldots\ldots\ldots(4.3)$$

where ξ_0, η_0 satisfies

$$\begin{cases} F_\xi=c_{11}\xi+(c_{11}-2c_{66})\eta+c_{13}=0 \\ F_\eta=c_{11}\eta+(c_{11}-2c_{66})\xi+c_{13}=0 \end{cases} \quad \ldots\ldots\ldots\ldots\ldots\ldots\ldots\ldots\ldots(4.4)$$

From this we have $\xi_0=\eta_0=-c_{13}/2(c_{11}-c_{66})$ $\ldots\ldots\ldots\ldots\ldots\ldots\ldots\ldots(4.5)$

Substituting these values into $F>0$ and simplifying, we have

$$(c_{11}-c_{66})c_{33}>c_{13}^2 \quad \ldots\ldots\ldots\ldots\ldots\ldots\ldots\ldots\ldots\ldots\ldots\ldots\ldots\ldots(4.6)$$

Now, we will collect here the conditions obtained above.

---

* This article is due to Mr. Homma's instruction.

$$\begin{cases} c_{11}>0, \quad c_{33}>0, \quad c_{44}>0, \quad c_{66}>0 \\ (c_{11}-c_{66})c_{33}>c_{13}^2 \end{cases} \qquad \text{(4.7)}$$

Our previous notations M_1, M_2, etc. bear the following relations with the notations in this article.

$$c_{11}=M_1\equiv \alpha N\ , \quad c_{33}=M_2\equiv \beta N\ , \quad c_{44}=N\ ,$$
$$c_{13}=M_3-2N\equiv(\gamma-2)N \qquad \text{(4.8)}$$

Substitution of which, and a new notation $\delta\equiv C_{66}/N$ into (4.7), gives the following relations.

$$\alpha>0\ , \quad \beta>0\ , \quad \alpha>\delta>0\ , \quad (\alpha-\delta)\ \beta>(\gamma-2)^2 \qquad \text{(4.9)}$$

In two-dimensional problems in which c_{66} is not involved, we may put $c_{66}=0$, therefore the relations (4.9) is reduced to

$$\alpha>0\ , \quad \beta>0\ , \quad K\equiv\alpha\beta-(\gamma-2)^2>0 \qquad \text{(4.10)}$$

5. Existence of Rayleigh waves.

Now we will examine the existence of solution of (3.5) under the condition (4. 10). We denote the roots of $f(\tau)=0$ lying between 0 and 1 by τ_1, τ_2 and τ_3 (where $\tau_1<\tau_2<\tau_3$; or at times τ_2 and τ_3 may not exist). The following results are obtained without difficulty:—

i) $f(\tau) \quad =(\beta\tau-K)^2(\tau-1)-\beta\tau^2(\tau-\alpha)$

So that

$$\begin{cases} f(0) & =-K^2<0 \\ f'(0) & =K(K+2\beta)>0 \\ f(K/\beta) & =(K^2/\beta^2)(\gamma-2)^2>0 \\ f(1) & =\beta(\alpha-1) \\ f(\alpha) & =(\gamma-2)^2(\alpha-1) \end{cases} \qquad \text{(5.1)}$$

ii) $\tau_n<\alpha \qquad \text{(5.2)}$

Proof; By virtue of the second equation of (3.2), it is evident that $\tau_n>\max(\alpha,1)$ or $\tau_n<\min(\alpha,1)$, but the former case is impossible. For, if it holds, from the first equation of (3.2) we know

$$\sigma_1^2+\sigma_2^2=-[(\gamma-1)^2+(\tau-1)+\beta(\tau-\alpha)]/\beta<0$$

which is contradictory to the fact that σ_1 and σ_2 must be real. Therefore

$$\tau_n<\min(\alpha,1).$$

Consequently $\quad \tau_n<\alpha. \qquad$ Q. E. D.

iii) Necessary and sufficient condition that τ_n should be a true root is $\beta\tau_n < k$.

Proof; Substitute (5.2) into (3.3), then we immediately find the result.

With the above preparation we can conclude easily; that, when $\alpha < 1$, there exists one and only one root that satisfies the required condition (i. e. one and only one sort of Rayleigh-wave exists).

Proof; $K/\beta = \alpha - (\gamma-2)^2/\beta < \alpha$.

$$\therefore \quad 0 < K/\beta < \alpha < 1.$$

From (ii) and Fig. 1 we can find

$$\beta\tau_1 < K \quad \text{but} \quad \beta\tau_2 > K,$$

therefore τ_1 is the only root that satisfies the required conditions.

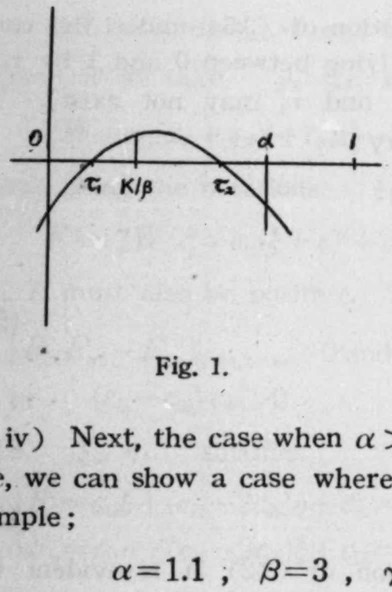

Fig. 1.

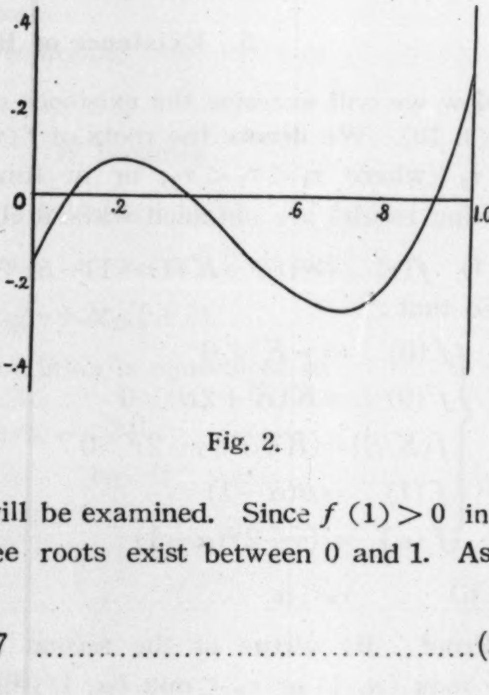

Fig. 2.

iv) Next, the case when $\alpha > 1$ will be examined. Since $f(1) > 0$ in this case, we can show a case where three roots exist between 0 and 1. As for example;

$$\alpha = 1.1 \ , \quad \beta = 3 \ , \quad \gamma = 3.7 \quad \text{..} (5.3)$$

for which

$$K = 0.41 \ , \quad K/\beta = 0.1367$$

$$\tau_1 = 0.0850 \ , \quad \tau_2 = 0.3605 \quad \tau_3 = 0.9146 \text{.............................} (5.4)$$

so that, as will be seen from Fig. 2, three roots exist. However, neither τ_2 nor τ_3 satisfies $\beta\tau_n < K$, (for $\beta\tau_2 = 1.0814 > 0.41 = K$, $\beta\tau_3 = 2.7437 > 0.41$). Therefore from the criterion iii) τ_1 is the only root.

The above case is a single example, but starting from this example, we can derive a general theorem about the existence of Rayleigh waves.

Roots of $f(\tau)=0$ are the continuous function of parameter α, β and γ. Therefore

$$\beta\tau_2-K=(\text{function of } \alpha,\ \beta,\ \gamma)\equiv\phi(\alpha,\beta,\gamma) \quad\ldots\ldots(5.5)$$

is also a continuous function of α, β and γ.

and from (5.4)

$$\phi(1.1,\ 3,\ 3.7)=0.6714>0 \quad\ldots\ldots(5.6)$$

In order to arrive at a case where τ_2 is a true root, we must start from the above example, and varying α, β and γ continuously find a combination of three parameters such that*

$$\phi(\alpha,\ \beta,\ \gamma)<0, \quad\ldots\ldots(5.7)$$

but on the way from (5.6) to (5.7) we must pass a point where

$$\phi(\alpha,\ \beta,\ \gamma)=0. \quad\ldots\ldots(5.8)$$

However, this is impossible. For, from the first equation of (5.1)

$$\begin{aligned} f(\tau_2)=0&=\phi(\alpha,\ \beta,\ \gamma)-\beta\tau_2^2(\tau_2-\alpha)\\ &=\qquad\qquad -\beta\tau_2^2(\tau_2-\alpha) \quad\ldots\ldots(5.9)\end{aligned}$$

this is self-contradictory.

Therefore we can conclude finally that ;

"One and only one sort of Rayleigh waves exists, in horizontally isotropic but vertically aeolotropic semi-infinite elastic medium."

The writer wishes to express his heartiest thanks to Mr. S. Homma. Without his instruction and encouragement, this paper could have never been completed.

2. 水平等方彈性体表面を傳はるレーリー波

地震研究所 佐藤泰夫

半無限の水平等方彈性体表面をつたはるレーリー波は常に唯一種類存在する.

---

* If there exists another domain isolated from the one involving the point $\alpha=1.1$, $\beta=3$, $\gamma=3.7$, then the proof is not complete, but the author carried out a comprehensive numerical calculation only to find no such domain.

The above result is a single example, but starting from this example, we can derive a general theorem about the existence of Rayleigh waves.

Roots of (5.4)—(5.6) are the continuous function of parameter α, β and γ. Therefore

$$\eta_1 = \eta\ (\text{function of } \alpha, \beta, \gamma) \equiv \Phi(\alpha, \beta, \gamma) \qquad (5.5)$$

is also a continuous function of α, β and γ.

and from (5.4)

$$\Phi(1, \tfrac{1}{3}, \tfrac{1}{3}) = \tfrac{1}{2}(3-\sqrt{3}) \qquad (5.6)$$

In order to arrive at a case where η_1 is a true root, we must start from the above example, and varying α, β and γ continuously, find a combination of these parameters such that*

$$\Phi(\alpha, \beta, \gamma) = 0 \qquad (5.7)$$

But on the way from (5.6) to (5.7) we must pass a point where

$$\Phi(\alpha, \beta, \gamma) = 0 \qquad (5.8)$$

However, this is impossible. For, from the first equation of (3.1)

$$F(1) = [\text{illegible}]$$

$$= [\text{illegible}] \qquad (5.9)$$

This is [illegible].

Therefore, we can conclude, finally that:

"One and only one set of Rayleigh waves exists in horizontally isotropic but vertically aeolotropic semi-infinite elastic medium."

The writer wishes to express his heartiest thanks to Mr. S. Homma. Without his instruction and encouragement, this paper could have never been completed.

13. [illegible]レーリー波

地震研究所 [illegible]

[illegible]

---

* If there exists another domain isolated from the one involving the point (1, 1) [illegible] that the point is not [illegible] and the author carried out a comprehensive numerical calculation [illegible] to find no such domain.

3. *The Effect of Solid Viscosity of Surface Layer on the Earthquake Movements.*

By Kiyoshi KANAI,

Earthquake Research Institute.

(Read July 15, 1947.—Recieved May 31, 1950.)

1. The problem of earthquake movements of the superficial layer was studied observingly by Ishimoto,[1] Saita,[2] Minakami[3] and others. The same problem was treated mathematically by Sezawa[4], Takahasi[5] and others. Owing to its increasing importance in connection with earthquake-proof constructions in our country in recent years, I again attacked this problem, particularly extending the solution to case of visco-elastic solid bodies.

In the present paper I attempt to examine the simplest case in which a distortional wave of a purely plane type propagated vertically upwards in an elastic semi-infinite medium is partly transmitted through bottom boundary of the superficial visco-elastic layer and partly reflected at this bottom as well as at the surface boundary of the same layer.

2. In the present investigation, the problem of forced vibrations will be discussed.

Let the axis of x be drawn vertically upwards from the lower boundary of the layer of thickness H and let u_1, ρ_1 μ_1, μ_1'; u_2, ρ_2, μ_2, μ_2' be the displacements, densities, elastic constants and coefficients of solid viscosity of the subjacent medium and the stratum respectively. In the case of distortional waves, the equations of motion of the two media are expressed by

$$\rho_1 \frac{\partial^2 u_1}{\partial t^2} = \left(\mu_1 + \mu_1' \frac{\partial}{\partial t}\right) \frac{\partial^2 u_1}{\partial x^2}, \qquad \rho_2 \frac{\partial^2 u_2}{\partial t^2} = \left(\mu_2 + \mu_2' \frac{\partial}{\partial t}\right) \frac{\partial^2 u_2}{\partial x^2} \quad \ldots(1),\ (2)$$

---

1) M. ISHIMOTO, *Bull. Earthq. Res. Inst.*, **10** (1932), 171; **12** (1934), 234; **13** (1935), 592; **14** (1936), 240; **15** (1937), 536.

2) T. SAITA, and S. SUZUKI, *Bull. Earthq. Res. Inst.*, **12** (1934), 517.

3) T. MINAKAMI, and S. SAKUMA, *Bull. Earthq. Res. Inst.*, **26** (1948), 61; *Bull. Inv. Comm.* Hukui Earthq., (1949).

4) K. SEZAWA, *Bull. Earthq. Res. Inst.*, **8** (1930), 1; K. SEZAWA and K. KANAI, *Bull. Earthq. Res. Inst.*, **13** (1935), 251.

5) R. TAKAHASI and K. HIRANO, *Bull. Earthq. Res. Inst.*, **19** (1941), 534.

In the case of dilatational waves, it is necessary to replace μ_1, μ_1', μ_2, μ_2' by $\lambda_1+2\mu_1$, $\lambda_1'+2\mu_1'$, $\lambda_2+2\mu_2$, $\lambda_2'+2\mu_2'$.

If the incident waves in the lower medium be of the type

$$u_0=\mathfrak{A}e^{i(pt-f_1x)} \quad \text{.......................................}(3)$$

the resulting displacement of the subjacent medium and the stratum are expressed by

$$u_1=u_0+u_0'=\mathfrak{A}e^{i(pt-f_1x)}+Ae^{i(pt+f_1x)}\,, \quad \text{..............................}(4)$$

$$u_2=Be^{i(pt-f_2x)}+Ce^{i(pt+f_2x)}\,, \quad \text{.......................................}(5)$$

where

$$p=2\pi/T\,, \qquad T=\text{the period of transmission,} \quad \text{..............}(6)$$

$$f_1^2=\rho_1p^2/(\mu_1+i\mu_1'p)\,, \quad f_2^2=\rho_2p^2/(\mu_2+i\mu_2'p)\,, \quad \text{..................}(7)$$

and A, B, C are the arbitrary constants determined by the boundary conditions.

The boundary conditions at $x=0$ are

$$u_1=u_2\,, \qquad \left(\mu_1+\mu_1'\frac{\partial}{\partial t}\right)\frac{\partial u_1}{\partial x}=\left(\mu_2+\mu_2'\frac{\partial}{\partial t}\right)\frac{\partial u_2}{\partial x}\,, \quad \text{.........}(8),\ (9)$$

while at the free surface, $x=H$ is

$$\left(\mu_2+\mu_2'\frac{\partial}{\partial t}\right)\frac{\partial u_2}{\partial x}=0\,. \quad \text{.........................}(10)$$

Assuming, for simplicity, $\mu_1'\to 0$, and substituting (3)~(5) in (8)~(10), we get

$$\left.\begin{aligned} \frac{A\Phi}{\mathfrak{A}}&=\cos f_2H-iM\sin f_2H\,, \quad \frac{B\Phi}{\mathfrak{A}}=\cos f_2H+i\sin f_2H\,, \\ \frac{C\Phi}{\mathfrak{A}}&=\cos f_2H-i\sin f_2H\,, \end{aligned}\right\} \text{......}(11)$$

where

$$\Phi=\cos f_2H+iM\sin f_2H\,, \quad M=\frac{f_2(\mu_2+ip\mu_2')}{f_1\mu_1}\,. \quad \text{..............}(12)$$

In order to avoid complexity in numerical calculations, we treated a particular case in which μ_2' is very small, then, if small quantities higher than the second order in $\mu_2'p/\mu_2$ are omitted, a characteristic equation of superficial layer becomes

$$\frac{|u_{2x-H}|}{|u_0|}\doteq\frac{2}{\sqrt{\Phi_1^2+\Phi_2^2}}\,, \quad \text{...........................}(13)$$

where $\Phi_1=\cos P\cosh Q+\sqrt{\frac{\mu_2\rho_2}{\mu_1\rho_1}}\,(R\cos P\sinh Q-S\sin P\cosh Q)$,

$$\Phi_2=\sin P\sinh Q+\sqrt{\frac{\mu_2\rho_2}{\mu_1\rho_1}}\,(R\sin P\cosh Q+S\cos P\sinh Q)\,,$$

$$P=\frac{pH\sqrt{\frac{\rho_2}{\mu_2}}}{\left\{1+\left(\frac{\mu_2'p}{\mu_2}\right)^2\right\}^{\frac{1}{4}}}\cos\left(\frac{1}{2}\tan^{-1}\frac{\mu_2'p}{\mu_2}\right),$$

$$Q=\frac{pH\sqrt{\frac{\rho_2}{\mu_2}}}{\left\{1+\left(\frac{\mu_2'p}{\mu_2}\right)^2\right\}^{\frac{1}{4}}}\sin\left(\frac{1}{2}\tan^{-1}\frac{\mu_2'p}{\mu_2}\right),$$

$$R=\frac{\cos\left(\frac{1}{2}\tan^{-1}\frac{\mu_2'p}{\mu_2}+\right)\frac{\mu_2'p}{\mu_2}\sin\left(\frac{1}{2}\tan^{-1}\frac{\mu_2'p}{\mu_2}\right)}{\left\{1+\left(\frac{\mu_2'p}{\mu_2}\right)^2\right\}^{\frac{1}{4}}}\,,$$

$$S=\frac{\frac{\mu_2'p}{\mu_2}\cos\left(\frac{1}{2}\tan^{-1}\frac{\mu_2'p}{\mu_2}\right)-\sin\left(\frac{1}{2}\tan^{-1}\frac{\mu_2'p}{\mu_2}\right)}{\left\{1+\left(\frac{\mu_2'p}{\mu_2}\right)^2\right\}^{\frac{1}{4}}}\,. \qquad \text{...........(14)}$$

Using (13), (14), some special cases are plotted in the following drawings. In Figs. 2 and 3 the cases of $\mu_2'=10^6$ and $\mu_2'=10^7$ C. G. S. besides the conditions $v_1=633$m/s, $v_2=200$m/s, $\mu_1=9\times10^9$, $\mu_2=6\times10^8$ C. G. S., $\rho_1=2.25$, $\rho_2=1.5$. Figs. 4 and 5 gives us the cases of $\mu_2'=10^6$ and $\mu_2'=10^7$ C. G. S. provided the conditions $v_1=200$ m/s, $v_2=100$ m/s, $\mu_1=6\times10^8$, $\mu_2=1.5\times10^8$ C. G. S., $\rho_1=\rho_2=1.5$. In the results of the experimental investigations,[6] the assumed values of coefficient of solid viscosity proved not to be improbable values in the superficial layer of the earth.

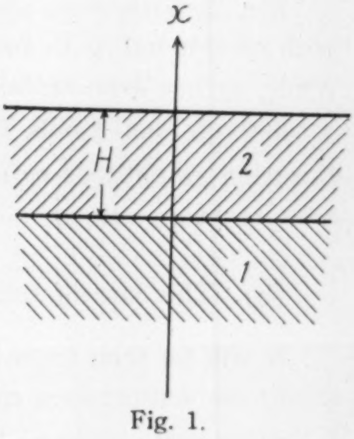

Fig. 1.

The principal results obtained in this investigation are enumerated as follows:

---

[6] K. KANAI, Meeting, Earthq. Res. Inst., Jan. 17, 1950.

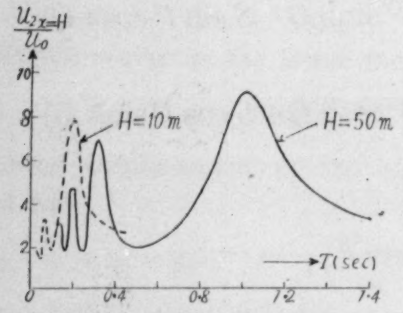

Fig. 2. $\mu_2'=10^6$ C. G. S., $v_1=633$ m/s, $v_2=200$ m/s, $\mu_1=9\times10^9$, $\mu_2=6\times10^8$ C. G. S., $\rho_1=2.25$, $\rho_2=1.5$.

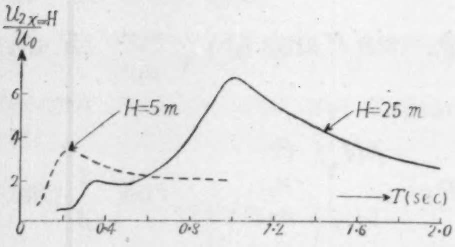

Fig. 3. $\mu_2'=10^7$ C. G. S., other constants are the same of the case of Fig. 2.

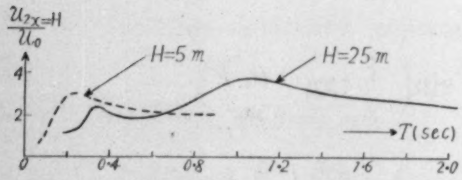

Fig. 4. $\mu_2'=10^6$ C. G. S., $v_1=200$ m/s, $v_2=100$ m/s, $\mu_1=6\times10^8$, $\mu_2=1.5\times10^8$ C. G. S., $\rho_1=\rho_2=1.5$.

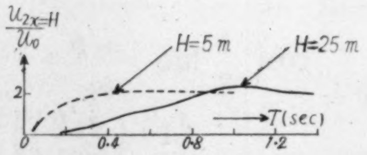

Fig. 5. $\mu_2'=10^7$ C. G. S., other constants are the same of the case of Fig. 4.

(i) The case of large solid viscosity in superficial layer.

Fig. 3 shows that, when the elasticity ratio of two media μ_2/μ_1 is small, a peak corresponding to fundamental synchronous period appears more clearly. While, as has been shown in Fig. 5, in case the elasticity ratio of two media is relatively not small, the frequency-amplitude curve is flat and then the vibration amplitudes corresponding to ordinary synchronous periods do not grow to large value.

(ii) The case of small solid viscosity in superficial layer.

It will be seen from Fig. 2 that, when the elasticity ratio of two media is small, the synchronous conditions of higher order occur successively. However, if the elasticity ratio of the two media is relatively not small, such phenomenon is not so clearly noticed as shown in Fig. 4.

At all events, the diagrammatical features of the results of the present investigations closely resemble the features[7] of the spectrogramic diagramms

---

[7] M. ISHIMOTO, *loc. cit.* 1).

of earthquake movements of the ground which were obtained by the accelerometer at several places in Tokyo and Yokohama.

---

3. 地表層の固体粘性が地震動の振幅に及ぼす影響

地震研究所 金井 清

地表層に固体粘性がある場合の地震動の振幅の性質をしらべたところ，次のようなことがわかつた．

(1) 地表層の固体粘性が大きい場合

表面層の彈性が下層のそれに比べて相當に小さい場合には，基本固有周期のところの振幅が明かに卓越するが（第3圖參照），この比が余り小さくない場合には，固有周期のところの振幅の特性をほとんど現はさない（第5圖參照）．

(2) 地表層の固体粘性が余り大きくない場合

兩層の彈性比（μ_2/μ_1）が相當に小さい場合には基本固有周期にあたる附近の振幅が無論卓越するが，高次の固有周期附近でも振幅の增大がおこる．しかし，この彈性比が余り小さくない場合には，これらの性質はそれ程はつきりしない．

以上の事柄は，一般の性質としては波動問題として容易に想像されるところではあるが，實際の場合に近い常數を入れて數値計算を行つた結果，種々の地盤に特有な地震動の性質が，この種の研究で相當程度説明できそうなことがわかつた譯である．

4. *On the Theory of Elastic Waves in Granular Substance. II.*

By Takehito TAKAHASHI,
Seijô-Gakuen High School,
and
Yasuo SATÔ,
Earthquake Research Institute.

(Read Oct. 19, 1948.—Received May 31, 1950.)

In the preceding paper, we had no space to go into details. We wish here to treat some of them.

1. *On the secular equation and its solutions of three dimensional model.* In the Paper I[1] we first considered lattice structure, then by taking the average in all directions we obtained an isotropic model. But it is not meaningless to deal directly with lattice structure, for our granular substance might have locally this lattice structure and show aeolotropic nature and we might observe some of its velocities.

In I-§ 2 we gained the equation of motion for the three dimensional granular lattice

$$(v/v_0)^2\mathfrak{A}-\sum_{j=1}^{n/2}(\mathfrak{A}\,\mathfrak{t}_j)(s\,\mathfrak{t}_j)^2\,\mathfrak{t}_j=0, \quad \dots\dots(1)$$

or

$$\left\{\begin{array}{lll} \{\lambda_{11}-(v/v_0)^2\}A_1 & +\lambda_{12}A_2 & +\lambda_{13}A_3=0, \\ \lambda_{12}A_1+\{\lambda_{22}-(v/v_0)^2\}A_2 & & +\lambda_{23}A_3=0, \\ \lambda_{13}A_1 & +\lambda_{23}A_2+\{\lambda_{33}-(v/v_0)^2\}A_3=0, & \end{array}\right. \quad \dots\dots(2)$$

where $\mathfrak{A}=(A_1,\ A_2,\ A_3)$, $\mathfrak{t}_j=(t_{j1},\ t_{j2},\ t_{j3})$

$$\lambda_{11}=\sum_{j=1}^{n/2}t_{j1}^2(s\,\mathfrak{t}_j)^2\ ,\quad \lambda_{12}=\sum_{j=1}^{n/2}t_{j1}\,t_{j2}(s\,\mathfrak{t}_j)^2, \quad \dots\dots(3)$$

Then the secular equation can be immediately written as follows

$$\begin{vmatrix} \lambda_{11}-(v/v_0)^2 & \lambda_{12} & \lambda_{13} \\ \lambda_{12} & \lambda_{22}-(v/v_0)^2 & \lambda_{23} \\ \lambda_{13} & \lambda_{23} & \lambda_{33}-(v/v_0)^2 \end{vmatrix}=0 \quad \dots\dots(4)$$

---

1) *Bull. Earthq. Res. Inst.*, 27 (1949), 11. Cited as I hereafter.

If the three roots are v_1, v_2 and v_3 $(v_1>v_2>v_3)$, from (4) we get

$$\sum_{i=1}^{3}(v_i/v_0)^2=\lambda_{11}+\lambda_{12}+\lambda_{33}=\sum_{j=1}^{n/2}(s\,\mathfrak{t}_j)^2 \quad \ldots\ldots\ldots\ldots(5)$$

1.1 *Simple cubic type. (n=6)*

	$\mathfrak{t}_1$	$\mathfrak{t}_2$	$\mathfrak{t}_3$
t_{j1}	1	0	0
t_{j2}	0	1	0
t_{j3}	0	0	1

$$(s\mathfrak{t}_j)=s_j,$$

$$\lambda_{jj}=s_j^2\ ,\quad \lambda_{ij}=0\quad (i\neq j).$$

From $$(v_i/v_0)^2=s_j^2\quad (i,\ j=1,\ 2,\ 3),\ \ldots\ldots(6)$$

$$(v_p/v_0)^2=0.6\quad \ldots\ldots\ldots\ldots(7)$$

When $s=\mathfrak{t}_i$, v_1 has its maximum value v_0. In this case only the longitudinal wave exists. (From (2) $Ai=0$ for $i\neq j$.)

1.2. *Body-centred cubic type. (n=8)*

	$\mathfrak{t}_1$	$\mathfrak{t}_2$	$\mathfrak{t}_3$	$\mathfrak{t}_4$
$\sqrt{3}\ t_{j1}$	1	−1	1	1
$\sqrt{3}\ t_{j2}$	1	1	−1	1
$\sqrt{3}\ t_{j3}$	1	1	1	−1

$$\lambda_{jj}=4/9\ ,\quad \lambda_{ij}=(8/9)\ s_is_j\ (i\neq j).$$

$$\sum_{i=1}^{3}(v_i/v_0)^2=4/3\quad \ldots\ldots\ldots\ldots(8)$$

The secular equation becomes

$$\{1-(9/4)\,(v/v_0)\}^3-4\,(s_1^2\,s_2^3+s_2^2\,s_3^2+s_3^2\,s_1^2)\,\{1-(9/4)\,(v/v_0)^2\}$$
$$+16\,s_1^2\,s_2^2\,s_3^2=0\quad \ldots\ldots\ldots\ldots(9)$$

and $$(v_p/v_0)^2=0.8\quad \ldots\ldots\ldots\ldots(10)$$

When $s=\mathfrak{t}_i$, v_1 has its maximum value.[2]

---

[2] If we put $\xi=\{(9/4)(v/v_0)^2-1\}/2$, $p=s_1^2s_2^2+s_2^2s_3^2+s_3^2s_1^2$, $q=2s_1^2s_2^2s_3^2$,
(9) becomes $\xi^3-p\xi-q=0$
By definition $p/3\geqq(q/2)^{2/3}\geqq 0$.

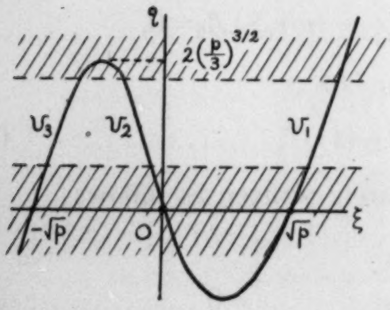

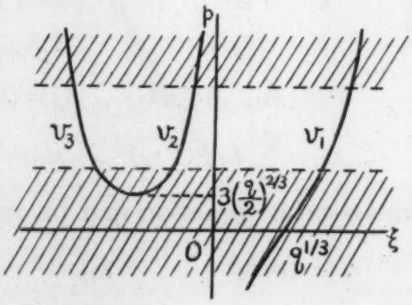

Both p and q have their greatest value when $s_1^2=s_2^2=s_3^2=1/3$. Fig. 1 shows $(q-\xi)$ and $(p-\xi)$ curves, where shadowed domains are forbidden. From these curves we see that the greatest value of ξ corresponds to the greatest values of p and q.

In this case, we have

$$p=1/3\ ,\quad q=2/27.$$

putting it in (14)

$$(\xi+1/3)^2(\xi-2/3)=0$$

or $$(v_1/v_0)^2=28/27\ ,\quad (v_2/v_0)^2=(v_3/v_0)^2=4/27 \quad\text{.....................}(11)$$

If $s=t$, from (2) we have

for v_1 , $A_1=A_2=A_3$, or $\mathfrak{A}\parallel s$. (longitudinal wave)

for v_2 and v_3 , $A_1+A_2+A_3=0$, or $(\mathfrak{A}\ s)=0$. (transversal wave)

1.3. *Face centered cubic type. (n=12)*

	t_1	t_2	t_3	t_4	t_5	t_6
$\sqrt{2}\ t_{i1}$	0	0	1	1	1	−1
$\sqrt{2}\ t_{i2}$	1	−1	0	0	1	1
$\sqrt{3}\ t_{i3}$	1	1	1	−1	0	0

$$\lambda_{jj}=(1+s_j^2)/2\ ,\quad \lambda_{ij}=s_is_j\ ,$$

$$(v_p/v_0)^2=1.2,\ \text{..........................}(12)$$

$$\sum_{i=1}^{3}(v_i/v_0)^2=2\ .\quad\text{........................}(13)$$

The secular equation becomes

$$\begin{vmatrix} (1+s_1^2)/2-(v/v_0)^2 & s_1s_2 & s_1s_3 \\ s_2s_1 & (1+s_2^2)/2-(v/v_0)^2 & s_2s_3 \\ s_3s_1 & s_3s_2 & (1+s_3^2)/2-(v/v_0)^2 \end{vmatrix}=0\text{......}(14)$$

When $s=t_i$, v_1 has its maximum value.

If we put $s=t_1$, from the secular equation we have

$$(v_1/v_0)^2=312\ ,\quad (v_2/v_0)^2=(v_3/v_0)^2=1/2\ \text{.......................................}(15)$$

From (2) we know that v_1 and v_2 (or v_3) correspond to longitudinal and transversal waves respectively.

2. *Decomposition of a symmetric tensor.*

Next we must complete the calculation involved in § 3 of the first report. That is, to accomplish the following integration,

$$C^0=\frac{1}{\Omega}\int V^*(r)\,C\,V(r)\,d\Omega\ \text{...}(1)$$

where $V(r)$ is the representation of the rotation group by means of a symmetric tensor of rank 2, or a 6–6 matrix of the coefficients of the following linear transformation[3]

---

[3] In the paper I we used the symbol x for the strain tensor, which suffers same transformation as the one used here, i. e. $V(r)$ is same in both cases.

$$\begin{pmatrix} x'^2 \\ y'^2 \\ z'^2 \\ 2y'z' \\ 2x'z' \\ 2x'y' \end{pmatrix} = V(r) \begin{pmatrix} x^2 \\ y^2 \\ z^2 \\ 2yz \\ 2xz \\ 2xy \end{pmatrix}, \quad \text{with } x'^2+y'^2+z'^2=x^2+y^2+z^2. \quad \ldots\ldots\ldots\ldots(2),\ (3)$$

(2) may be written briefly $x'=V(r)x,$ ....(2)′

x and x' being the above 1-6 matrices or vectors in a 6-dimensional space. We have transformed $V(r)$ to a orthogonal matrix $U(r)$

$$U(r)=T^{-1}V(r)T, \quad U^*(r)U(r)=1. \quad \ldots\ldots\ldots\ldots(4)$$

And (1) was written

$$C^{0T}=\frac{1}{\Omega}\int U^*(r)\, C^T U(r)\, d\Omega\ , \quad \ldots\ldots\ldots\ldots(5)$$

where

$$C^{0T}=T^*\, C^0 T\ , \quad C^T=T^* C T \quad \ldots\ldots\ldots\ldots(6),\ (7)$$

(3) means that in the considered 6-dimensional vector space $x^2+y^2+z^2$ forms an invariant one dimensional subspace. As we have no other restrictions to the six functions x^2, ..., $2yz$, ...we may expect $U(r)$ to be the sum of two irreducible parts of 1st and 5th order. (This is also a consequence of general theory of representations)

Then $U(r)$ has the following form

$$U(r)=\begin{pmatrix} 1 & 0\cdots 0 \\ 0 & \\ \vdots & U_1(r) \\ 0 & \end{pmatrix} \quad \ldots\ldots\ldots\ldots(8)$$

where $U_1(r)$ is a 5-5 matrix, irreducible and orthogonal. If C_1^T and C_1^{0T} are cofactors of c_{11}^T and c_{11}^{0T} (1-1 elements of C_0^T and C_0^{0T}) the integrand of (5) becomes

$$U^*(r)C^TU(r)=\begin{pmatrix} c_{11}^T & 0\cdots\cdots 0 \\ 0 & \\ \vdots & U_1{}^*(r)C_1^TU_1(r) \\ 0 & \end{pmatrix}$$

Then from (5) we get

$$c_{11}^{0T}=c_{11}^T\ , \quad c_{1j}^{0T}=c_{j1}^{0T}=0 \quad (j=2,\ 3,\ldots\ldots,\ 6) \quad \ldots\ldots\ldots\ldots(9)$$

$$C_1^{0T}=\frac{1}{\Omega}\int U_1{}^*(r)\, C_1^T U_1(r) d\Omega \quad \ldots\ldots\ldots\ldots(10)$$

Now C_1^{0T} commutes with all $U_1(s)$. (s means an arbitrary element of rotation group.) For

$$U_1(s)^{-1}\,C_1^{0T}\,U_1(s)=\frac{1}{\Omega}\int U_1(s)^*U_1{}^*(r)C_{11}^{T}U_1(r)U_1(s)d\Omega,\,(t=rs)$$

$$=\frac{1}{\Omega}\int U_1^*(t)C_1^TU_1(t)d\Omega=C_1^{0T}\ ,$$

Then C_1^{0T} must be a multiple of unit matrix as $U_1(r)$ is irreducible. (Schur's lemma[4])

$$C_1^{0T}=\begin{pmatrix} c_{22}^{0T} & & 0\\ & \ddots & \\ 0 & & c_{66}^{0T}\end{pmatrix},\quad c_{22}^{0T}=\cdots\cdots=c_{66}^{0T}\ \ldots\ldots\ldots\ldots\ldots\ldots\ldots\ldots(11)$$

The trace (sum of all diagonal elements) is invariant under orthogonal transformation. Comparing both sides of (10) we have

$$c_{jj}^{0T}=\frac{1}{5}\sum_{k=2}^{6}c_{kk}^{T}\ ,\quad (j\geqq 2)\ \ldots\ldots\ldots\ldots\ldots\ldots\ldots\ldots(12)$$

Before determining T, it is necessary to remark that T cannot be orthogonal. For the square sum of $x^2,\ldots\ldots,2yz,\ldots\ldots$ is not invariant under three dimensional rotations, but the sum of $x^2,\ldots\ldots,\sqrt{2}\ yz,\ldots\ldots$ is invariant. We express by χ the vector with these components: $x^*=(x^2,\ldots\ldots,\sqrt{2}\ yz,\ldots\ldots)$

Then

$$x=S\chi\ \ldots\ldots\ldots\ldots\ldots\ldots\ldots\ldots\ldots\ldots\ldots\ldots(13)$$

where

$$S=\begin{pmatrix} 1 & & & & & 0\\ & 1 & & & & \\ & & 1 & & & \\ & & & \sqrt{2} & & \\ & & & & \sqrt{2} & \\ 0 & & & & & \sqrt{2}\end{pmatrix}\ \ldots\ldots\ldots\ldots\ldots\ldots\ldots\ldots(14)$$

(4) means that the vector x is transformed by T to another vector ξ.

$$x=T\xi\ ,\quad \xi'=U(r)\xi\ \ldots\ldots\ldots\ldots\ldots\ldots\ldots\ldots(15)$$

From (13) and (15)

$$\chi=R\xi\ ,\quad T=SR\ \ldots\ldots\ldots\ldots\ldots\ldots\ldots\ldots(16)$$

As the transformation of χ is orthogonal

$$\chi'=W(r)\chi\ ,\quad W(r)W^*(r)=1\ ,\ \ldots\ldots\ldots\ldots\ldots\ldots(17)$$

from (15) and (16) $\qquad W(r)=R^{-1}\,U(r)R$

---

[4] For the proof of Schur's lemma, literature on group representations should be consulted; e. g., *H. Weyl, Classical Groups,* Chap. III. (1939).

From (4) and (17) $I = WW^* = R^{-1}\, U(r)(RR^*)U(r)^*(R^*)^{-1}$

Thus RR^* commutes with all $U(r)$, therefore it must be a multiple of unit matrix. To make calculation easier, we choose RR^* for unit matrix.

$$RR^* = 1 \quad \ldots\ldots\ldots\ldots\ldots\ldots\ldots\ldots\ldots\ldots\ldots\ldots\ldots\ldots\ldots\ldots (18)$$

As said before, one component of ξ must be $\alpha\ (x^2+y^2+z^2)$. Then (16) is written as

$$\begin{pmatrix} x^2 \\ \vdots \\ \sqrt{2}\ yz \\ \vdots \end{pmatrix} = R \begin{pmatrix} \alpha\,(x^2+y^2+z^2) \\ \vdots \\ \vdots \end{pmatrix}$$

or

$$R^{-1} = \begin{pmatrix} \alpha & \alpha & \alpha & 0 & 0 & 0 \\ & & \cdots\cdots\cdots & & & \\ & & \cdots\cdots\cdots & & & \end{pmatrix}$$

From (19) $\alpha^2 = 1/3$

and

$$R^* = \begin{pmatrix} 1/\sqrt{3} & 1/\sqrt{3} & 1/\sqrt{3} & 0 & 0 & 0 \\ & & \cdots\cdots\cdots\cdots\cdots\cdots & & & \\ & & \cdots\cdots\cdots\cdots\cdots\cdots & & & \end{pmatrix} \quad \ldots\ldots\ldots\ldots\ldots\ldots\ldots\ldots (20)$$

Putting (16) in (7)

$$C^T = R^*\, S^*\, CSR = R^* C^s R\,, \quad \ldots\ldots\ldots\ldots\ldots\ldots\ldots\ldots\ldots\ldots\ldots (21)$$

where

$$C^s = S^*\, C\, S = \begin{pmatrix} c_{11} & c_{12} & c_{13} & 2c_{14} & 2c_{15} & 2c_{16} \\ & & \cdots\cdots\cdots\cdots\cdots & & & \\ & & \cdots\cdots\cdots\cdots\cdots & & & \\ c_{61} & c_{62} & c_{63} & 2c_{64} & 2c_{65} & 2c_{66} \end{pmatrix} \quad \ldots\ldots\ldots\ldots\ldots\ldots\ldots (22)$$

From (21) $c^T_{11} = \sum\limits_{i,\,j=1}^{6} r_{i1} r_{j1} c^s_{ij} = \dfrac{1}{3}(c_{11}+c_{22}+c_{33}) + \dfrac{2}{3}(c_{12}+c_{13}+c_{23}) \ \ldots\ldots (23)$

and $t_r.C^T = t_r.C^s = c_{11}+c_{22}+c_{33}+2\,(c_{44}+c_{55}+c_{66}) \ldots\ldots\ldots\ldots\ldots\ldots (24)$

Then from (9) and (11) we get

$$c^{0T}_{11} = (1/3)\,(c_{11}+c_{22}+c_{33}) + (2/3)\,(c_{12}+c_{23}+c_{31}) \ \ldots\ldots\ldots (24)$$

$$c^{0T}_{jj} = (1/5)\,(t_r.C^T - C^T_{11}) = (2/15)\,(c_{11}+c_{22}+c_{33}) - (2/15)\,(c_{12}+c_{13}+c_{31}) \\ + (2/5)\,(c_{44}+c_{55}+c_{66})$$

(21) may be also applied to C^0.

$$C^{0S} = RC^{0T}\, R^*$$

Considering that C^{0T} is diagonal, we calculate the elements as follows,

$$c_{ij}^{0s}=\sum_k r_{ik}\,r_{jk}\,c_{kk}^{0T}=(c_{11}^{0T}-c_{22}^{0T})\,r_{i1}\,r_{j1}+c_{22}^{0T}\sum_k r_{ik}\,r_{jk}$$

$$=(c_{11}^{0T}-c_{22}^{0T})\,r_{i1}r_{i1}+c_{22}^{0T}\,\delta_{ij}\ ,$$

$$\left\{\begin{array}{l} c_{11}^{0}=c_{22}^{0}=c_{33}^{0}=(1/3)\,c_{11}^{0T}+(2/3)\,c_{22}^{0T} \\ c_{12}^{0}=c_{13}^{0}=c_{23}^{0}=(1/3)\,(c_{11}^{0T}-c_{22}^{0T}) \\ c_{44}^{0}=c_{55}^{0}=c_{66}^{0}=(1/2)\,c_{22}^{0T}=(1/2)\,(c_{11}^{0}-c_{12}^{0}) \end{array}\right. \qquad \cdots\cdots\cdots(25)$$

Putting (24) in (25) we get final results. (I. §3 (12))

Complete form of T was not necessary in our calculation, but it is of some interest to determine it.

As already said in the previous paper, five components of ξ are solid harmonics. And $\xi^*\xi$ must be invariant, therefore

$$\xi=\begin{pmatrix} (1/\sqrt{3}\,(x^2+y^2+z^2) \\ \pm\beta(-x^2-y^2+2z^2) \\ \pm\sqrt{3}\beta\,(x^2-y^2) \\ \pm2\sqrt{3}\,\beta\,yz \\ \pm2\sqrt{3}\,\beta\,xz \\ \pm2\sqrt{3}\,\beta\,xy \end{pmatrix}$$

From (16) and (19) we can determine β and R (up to signs).

$$R=\begin{pmatrix} 1/\sqrt{3} & -1/\sqrt{6} & 1/\sqrt{2} & 0 & 0 & 0 \\ 1/\sqrt{3} & -1/\sqrt{6} & -1/\sqrt{2} & 0 & 0 & 0 \\ 1/\sqrt{3} & 2/\sqrt{6} & 0 & 0 & 0 & 0 \\ 0 & 0 & 0 & 1 & 0 & 0 \\ 0 & 0 & 0 & 0 & 1 & 0 \\ 0 & 0 & 0 & 0 & 0 & 1 \end{pmatrix},\ \xi=\begin{pmatrix} (1/\sqrt{3}\,(x^2+y^2+z^2) \\ (-1/\sqrt{6})(x^2+y^2)+(2/\sqrt{6})z^2 \\ (1/\sqrt{2})\,(x^2-y^2) \\ \sqrt{2}\,yz \\ \sqrt{2}\,xz \\ \sqrt{2}\,xy \end{pmatrix}$$

T can be immediately gained by multiplying S to R.

4. 粒狀物体を傳はる彈性波の理論II

成城學園高等學校 高橋健人
地震研究所 佐藤泰夫

第一報に於ては紙面の關係でのせる事のできなかつた計算を示す. 即ち
三次元の模型で速度を決定する永年方程式を導き, その解を求めること.
彈性テンソルを既約部分に分けること.

5. *Electromagnetic Induction within the Earth and Its Relation to the Electrical State of the Earth's Interior. Part I (1)*

By Tsuneji RIKITAKE,

Earthquake Research Institute.

(Read Oct. 15, Nov. 19, 1946, and July 15, 1947.—Received Sept. 18, 1947.)

CONTENTS

Introduction.

Chapter I. Assumption on the magnetic permeability in the earth.

Chapter II. Electromagnetic induction by daily variations (so-called S_q-field)

1. The influence of the oceans.
2. Spherical harmonic analyses of S_q which have been done up to this time and their relations to the uniform core model of the earth.
3. Electromagnetic induction within the earth's model consisting of core, mantle and superficial non-conducting layer.
4. The distribution of the induced currents in the earth.

Chapter III. Electromagnetic induction by solar daily disturbance variation (so-called S_D-field).

Chapter IV. Electromagnetic induction by storm-time variation (so-called D_{st}-field).

Chapter V. Electromagnetic induction by bay-type disturbance.

1. Morphology of bay-type disturbance.
2. The analysis of bay-type disturbances.
3. The relation to the electrical state of the earth's interior.
4. The distribution of the electric currents in the earth.

Chapter VI. Electromagnetic induction by magnetic variation connected with solar eruption.

1. Radio fade-outs and magnetic variations connected with solar chromospheric eruptions.
2. The analysis of the magnetic variation accompanied by solar eruption.
3. Theory of plane-earth induction and its relation to the electrical state of the earth's interior.
4. The distribution of the induced currents in the earth.

Chapter VII. Electromagnetic induction by sudden commencement of magnetic storm.

1. The world-wide distribution of sudden commencement.
2. The analysis of sudden commencements.
3. The relation to the electrical state of the earth's interior.

4. The distribution of the induced currents in the earth.
5. The influence of the oceans.
Summary and conclusion.
Appendix.

Introduction.

As shown by Gauss[1], it is possible to separate the earth's magnetic field into parts of external and internal origins. Applying this method to the field of the daily variation, Schuster[2] was the first who found that the major part originates above the earth, but there is also a part of internal origin. According to his investigation, the latter may be the secondary field due to the electric currents induced in the earth by the variation of the external one. This hypothesis seems to be able to explain the relation between the two parts when the electrical conductivity (σ) and the magnetic permeability (μ) are distributed suitably in the earth. After Schuster's investigation, we made a good number of studies concerning this problem. Their brief outlines will be mentioned as follows.

In the above mentioned paper, Schuster, in co-operation with Lamb, showed that the conducting sphere must be smaller than the earth, that is, the outer layer of the earth must be non-conductive.

Using the observed data of 21 stations distributed widely over the earth, Chapman[3] made a more complete analysis of the daily variation field. If the thickness of the non-conducting shell is about 250 *km* and the electrical conductivity of the inner core amounts to 3.6×10^{-13} *emu*, the relation between the amplitude and phase of main harmonics becomes reasonable, while the magnetic permeability is assumed to be unity.

Chapman and Whitehead[4] studied electromagnetic induction by periodic magnetic variation in a conducting sphere whose permeability has any value. They showed that we can determine the ratio σ/μ from the observed data,

---

1) K. F. GAUSS, "*Allgemeine Theorie der Erdmagnetismus*", p. 13.
2) A. SCHUSTER, *Phil. Trans. Roy. Soc. London* A, **180** (1889), 467.
3) S. CHAPMAN, *Phil. Trans. Roy. Soc. London* A, **218** (1919), 1.
4) S. CHAPMAN and T. T. WHITEHEAD, *Trans. Cambr. Phil. Soc.*, **22** (1922), 463.

but not σ and μ separately. They also investigated the possible influence of the induced field produced by the electric current which is flowing in sea. As the electrical conductivity of sea-water amounts to the order of $10^{-10} \sim 10^{-11}$ in electromagnetic unit, it is of importance to estimate to what extent the varying magnetic field may be affected by the presence of sea. According to their estimate, the field must be considerably affected by the presence of a comparatively shallow sea which spreads all over the earth with uniform depth. In practice, as the distribution of land and sea is very irregular, the induced electric current in an ocean must presumably be far less intense, on the average, than it would be in the world-wide sea on account of the complicated ocean boundaries.

As pointed out by Chapman[5)], the average field of magnetic storms is mainly of external origin but also has a part produced within the earth. As well as in the case of the daily variation, the latter is naturally interpreted as the induced by the variation of external origin. Chapman and Whitehead[1)] made an attempt to determine the electrical conductivity from storm-time induction. Constructing the mathematical theory of electromagnetic induction by aperiodic field, they got $\sigma = 1 \sim 4 \times 10^{-13}$ *emu* in the conducting core. Their calculation was, however, somewhat rough. According to the later work, the conductivity must be higher.

The mathematics of electromagnetic induction in a sphere was fully investigated by Price[6), 7)]. In co-operation with him, Chapman[8)] studied the electrical state of the earth's interior consistent with the storm-time variation. According to their study, it was required $\sigma = 1.4 \times 10^{-13}$ *emu* for a core of almost exactly the same size in daily variation. It is remarkable that the electrical conductivity which is in accord with the daily variation and the storm-time variation differ from each other. The slower the change, the deeper do the induced electric currents penetrate into the earth. As the storm-time variation is slower than the daily one, the conductivity, which is consistent with the former is interpreted to correspond to the deeper part of the earth's interior than the one obtained from the latter. Then the earth's interior can not be uniformly conducting.

K. Terada[9)] discussed electromagnetic induction in a sphere consisting of many concentric shells whose electrical conductivity differ each other. Applying his theory to the induction by 12-hourly component of daily variation on

---

5) S. CHAPMAN, *Proc. Roy. Soc.* A, **95** (1918), 61.

6) A. T. PRICE, *Proc. Lond. Math. Soc.* ser. 2, **31** (1930), 217.

7) A. T. PRICE, *Proc. Lond. Math. Soc.* ser. 2, **33** (1931), 233.

8) S. CHAPMAN and A. T. PRICE, *Phil. Trans. Roy. Soc. London*, A, **229** (1930), 427.

9) K. TERADA, *Geophys. Mag*, **13** (1939), 63 and **16** (1948), 5.

the basis of Chapman's analysis, he got the same conclusion with Lahiri and and Price's investigation as mentioned below.

As mentioned above, the deeper part of the earth may be more conductive than the part near the surface. In order to get more precise knowledge about the conductivity-distribution, Lahiri and Price[10] studied electromagnetic induction in a conducting sphere whose conductivity varies proportionally to r^{-m} where r and m denote respectively the radial distance and at the same time a constant. According to their study, it was informed that the conductivity becomes enormously higher at the depth of 700 *km* beneath the surface.

Summing up the results of these studies, it is likely that the electrical conductivity of the earth's interior increases with the depth. Although, these investigations gave us very interesting conclusion, only the daily and storm-time variation were considered up to now. We have, however, magnetic variations of another type such as abrupt beginning of magnetic storm, solar daily disturbance variation, bay-type disturbance, pulsation and disturbance accompanying solar eruption. If we can collect a good many data from observations, these variations may also be available for our purpose. While a few of them vary with periods comparable to that of daily variation, abrupt beginning and pulsation vary very rapidly. To use these variations whose periods differ very much will be desirable for getting more complete knowledge about the conductivity-distribution in the earth. In this paper, electromagnetic induction due to variations of various types will be discussed as far as the writer can get data.

As is known in researches of seismic waves, there is a distinct discontinuity at the depth of 2900 *km* in the earth. In the core, inside this boundary, it seems very likely that the rigidity is so small that we can scarcely observe the transversal waves which come through this region, while the velocity of the longitudinal waves decreases from about 13 to 8 *km/sec* at the boundary. This is an evidence that the physical state of the material differs distinguishably at this level and consequently it may be natural to consider that the electrical conductivity also changes in- and outside this boundary. From this point of view, the writer attempts to determine the electrical conductivity in the earth's core and mantle separately.

As to the influence of sea, about which only an idealized case was investigated by Chapman, Whitehead, Lahiri and Price,[4], [10] a complete estimate for the real earth is very difficult, because the distribution of land and sea is very complicated. In this paper, the writer, intending to investigate the possible

---

10) B. N. LAHIRI and A. T. PRICE, *Phil. Trans. Roy. Soc. London*, A, 237 (1939), 509.

influence of ocean, such as the Pacific and Atlantic Oceans, calculate approximately to what extent the daily variation and the sudden commencement of magnetic storm may be affected by the presence of a sea bounded by two meridians $\pi/2$ apart in longitude.

In short, this paper is an extension of studies on electromagnetic induction in the earth which was hitherto developed by many magneticians. It is hoped that the knowledge about the electrical state of the earth's interior obtained in this study may contribute to get the more comprehensive knowledge of the internal constitution of the earth and physical properties of material in such high temperature and pressure as is in the earth.

CHAPTER I. ASSUMPTION ON THE MAGNETIC PERMEABILITY IN THE EARTH.

If μ would be larger compared to unity in the earth, the magnetically induced field must be taken into consideration for our problem together with electromagnetically induced field. Though we have not hitherto any reliable method to infer the distribution of μ in the earth, a few attempts have been tried with respect to this problem.

As pointed out by Chapman and Whitehead4), the magnetically induced part cannot be separated from the electromagnetically induced part in the case of periodic variation. On the other hand, Chapman and Price8) showed that it may be possible to make such a separation in the case of storm-time variation. According to them, it is found that the magnetically induced field will oppose the horizontal components and reinforce the vertical components of the external inducing field at the end of magnetic storms because the electromagnetically induced currents may have fairly well died away at that time. Then, if μ differs considerably from unity, the ratio of the external field to the whole field may become appreciably larger in the vertical component than in the horizontal component. They tried to find whether such effect really exists or not, examining data for several days after magnetic storms. On account of the ambiguities due to difficulties to determine the undisturbed state of the geomagnetic field and also the smallness of the later part of storm-time variation, they found no reliable indication that μ differs from unity.

Adams and Green11) investigated experimentally the influence of hydrostatic pressure on the critical temperature of magnetization for ferromagnetic materials. Five ferromagnetic metals were used in their experiment. Deter-

---

11) L. H. ADAMS and J. W. GREEN, *Terr. Mag.*, 36 (1931), 161.

minations were made at pressures up to 2000 *atmospheres* for iron and magnetite, 2200 *atmospheres* for nickel, 2600 *atmospheres* for nickel-steel, and in the case of meteorite, 3600 *atmospheres*. The results indicate that pressure has practically no-effect. However, the Curie point seems likely to decrease slightly with increasing pressure in the case of nickel-steel and meteoric iron.

An estimate of the increase of the Curie point of nickel and nickel-iron alloys was made by Slater[12) from a theoretical stand-point in which he applied Clapeyron's equation. According to him, the rate of increase for nickel with pressure must be of the order of 5×10^{-5} *degree per atmosphere*, while, in the case of nickel-iron alloys, it would become less as more iron is added. It becomes zero with 70% nickel and negative for alloys with more iron. Assuming that the temperature and the pressure amount respectively to the order of 5000 *degrees* and 10^6 *atmospheres* near the centre of the earth, it is required that the increasing rate of the Curie point must reach to the order of 5×10^{-3} *degree per atmosphere* for the ferromagnetism in that region. This magnitude is as much as one hundred times larger than the magnitude expected from the theory even for pure nickel. For this reason, it is implausible that ferromagnetic state is kept inside the earth.

Although the physical and geophysical studies mentioned above are not always applicable to real earth, it is noticeable that they are all disadvantageous to the assumption that the earth's interior could be ferromagnetic. Then, at the present stage of investigation, we naturally consider that μ does not materially differ from unity in the earth together with the impossibility of any ferromagnetic explanation of the earth's permanent magnetization.

From this point of view, the writer assumes $\mu=1$ throughout the investigations which will be developed in this paper.

CHAPTER II. ELECTROMAGNETIC INDUCTION BY DAILY VARIATION (so-called S_q-field).

1. The influence of the ocean.

In promoting the study of the electromagnetic induction in the earth, we meet a dfficulty. This is the possibility that the electric currents induced in the oceans may have an appreciable effect on the magnetic variations as often discussed by researchers of the present problem. In sea-water, whose electrical conductivity is about one hundred times larger than that of rock and soil, the induced electric currents in the ocean will become appreciably intense, especially

---

12) J. C. SLATER, *Phys. Rev.*, **58** (1940), 54.

in a deep sea. In order to investigate the influence of the oceans, Chapman and Whitehead[1] assumed that the earth is surrounded by a sea of uniform depth. According to them, the internal part of the transient magnetic field must be considerably affected by the presence of a comparatively shallow sea. As they assumed that the sea is spread all over the earth, their conclusion shows the limit to which the transient magnetic field is likely to be affected by the existing irregular distribution of land and sea. On account of the complicated ocean boundaries, the actual currents in the ocean, however, will be much less intense than it would be in such an idealized sea mentioned above. Then it is desirable to examine the extent to which the large oceans shield the inner part of the earth from the outer field. From this point of view, the writer will estimate below to what extent S_q may be affected by the presence of a sea bounded by two meridians $\pi/2$ apart in longitude.

The intensity of electric field $\overrightarrow{E}$ and the magnetic induction $\overrightarrow{B}$ in a conductor satisfy the equation

$$\mathrm{rot}\,\overrightarrow{E}=-\frac{\partial\overrightarrow{B}}{\partial t}, \tag{1.1}$$

when the phenomena are assumed to be quasistationary. Now we regard our sea as a thin conductor whose thickness and specific conductivity are respectively D and σ. When the thickness is so thin that the problem can be treated as a two-dimensional one, it is obviously sufficient for us to take into consideration only the component of rot $\overrightarrow{E}$ and $\overrightarrow{B}$ which are normal to the surface. Then, considering Ohm's law, we get

$$(\mathrm{rot}\,\overrightarrow{i}\,)_r=-D\sigma\frac{\partial B_r}{\partial t} \tag{1.2}$$

where $\overrightarrow{i}$ is electric current density and suffix r denotes the normal to the surface.

As $\mathrm{div}\,\overrightarrow{i}=0$, we can define a current-function J which gives in polar coordinate

$$i_\theta=\frac{\partial J}{a\sin\theta\partial\phi},\quad i_\phi=-\frac{\partial J}{a\partial\theta} \tag{1.3}$$

where a denotes the radius of this spherical shell.

Substituting (1.3) in (1.2), we get

$$\frac{1}{\sin\theta}\left\{\frac{\partial}{\partial\theta}\left(\sin\theta\frac{\partial}{\partial\theta}\right)+\frac{1}{\sin\theta}\frac{\partial^2}{\partial\phi^2}\right\}J=a^2D\sigma\frac{\partial B_r}{\partial t} \tag{1.4}$$

When J can be expressed by a series of the type

$$J=\sum_n\sum_m K_n^m S_n^m \qquad \text{.......................................}(1.5)$$

where S_n^m denotes spherical surface harmonic and K_n^m is a function of time, (1.4) becomes by use of well known recurrence formulae

$$-\sum_n\sum_m K_n^m(t)n(n+1)S_n^m=a^2D\sigma\,\frac{\partial B_r}{\partial t}\,. \qquad \text{..............................}(1.6)$$

Further, we assume that K_n^m can be expanded into a Fourier series of the form

$$K_n^m(t)=\sum_s K_{n,m}^{\,s}e^{ispt}\,, \qquad \text{..}(1.7)$$

whence we get from (1.6)

$$-\sum_s\sum_n\sum_m n(n+1)K_{n,m}^{\,s}S_n^m e^{ispt}=a^2D\sigma\,\frac{\partial B_r}{\partial t} \qquad \text{..........................}(1.8)$$

If we can expand the righthand-side of this equation into a series of $S_n^m e^{ispt}$, we can determine $K_{n,m}^s$ by comparing the coefficients of the corresponding harmonics.

We only deal, in this Section, with main harmonics of S_q in which magnetic flux varies so slowly that we can neglect the influence of self-induction. Then, $\frac{\partial B_r}{\partial t}$ in (1.8) can be approximately regarded as the flux-change through unit area which orignates outside of the conductor.

As already shown by Chapman[3] the equinoctial mean of S_q can be approximately expressible as

$$B_r=\sum_s P_{s+1}^s(a_{s+1}^s\cos sp\tau+b_{s+1}^s\sin sp\tau) \qquad \text{....................}(1.9)$$

where τ denotes local time. Taking (1.9) as the inducing field, we shall estimate the magnitude and direction of electric currents induced in a thin conducting shell bounded by two meridians, $\phi=0$ and $\phi=\pi/2$ on a sphere.

The normal component of the electric currents must vanish at the boundaries, namely $i_\phi=0$ at $\phi=0$ and $\phi=\pi/2$. This condition is satisfied by preferring $P_n^{2\nu}\sin 2\nu\phi$ instead of S_n^m. Then (1.8) becomes

$$-\sum_{s=1}^{\infty}\sum_{n=1}^{\infty}\sum_{\nu=0}^{\leq n/2} n(n+1)K_{n,\nu}^{\,s}\,e^{ispt}\,P_n^{2\nu}\sin 2\nu\phi=a^2D\sigma\,\frac{\partial B_r}{\partial t}\,. \qquad \text{...........}(1.10)$$

Under certain conditions, a function $f(\theta,\phi)$, defined between $\phi=0$ and

$\phi=\pi/2$, can be expanded in the next form

$$f(\theta,\phi)=\sum_{n=1}^{\infty}\sum_{\nu=0}^{\leq n/2}\gamma_{n,\nu}P_n^{2\nu}\sin 2\nu\phi \quad\text{......}(1.11)$$

where

$$\gamma_{n,\nu}=\frac{2n+1}{\pi}\int_{\theta=0}^{\pi}\int_{\phi=0}^{\pi/2}f(\theta,\phi)\,P_n^{2\nu}\sin 2\nu\phi\sin\theta\,d\theta\,d\phi \quad\text{......}(1.12)$$

From (1.9) we get

$$\frac{\partial B_r}{\partial t}=\frac{\partial}{\partial t}\sum_s P_{s+1}^s\{a_{s+1}^s\cos s(pt+\phi)+b_{s+1}^s\sin s(pt+\phi)\}$$

or in complex expression

$$=ip\sum_s se^{ispt}P_{s+1}^s\{(a_{s+1}^s\cos s\phi+b_{s+1}^s\sin s\phi)$$

$$+i(a_{s+1}^s\sin s\phi-b_{s+1}^s\cos s\phi) \quad\text{......}(1.13)$$

where t denotes $\phi=0$ meridian time.

Using (1.11) and (1.12), (1.13) becomes

$$\frac{\partial B_r}{\partial t}=ip\sum_s\sum_n\sum_\nu(a_{s+1}^s-ib_{s+1}^s)\zeta_{n,\nu}^s e^{ispt}P_n^{2\nu}\sin 2\nu\phi \quad\text{......}(1.14)$$

where

$$\zeta_{n,\nu}^s=\frac{2n+1}{\pi}\int_0^{\pi}P_{s+1}^sP_n^{2\nu}\sin\theta d\theta\int_0^{\pi/2}e^{is\phi}\sin 2\nu\phi d\phi\,. \quad\text{......}(1.15)$$

Substituting (1.15) in (1.10) and then comparing the corresponding coefficients of both sides, we get

$$K_{n,\nu}^s=\frac{a^2D\sigma ps}{in(n+1)}(a_{s+1}^s-ib_{s+1}^s)\zeta_{n,\nu}^s\,. \quad\text{......}(1.16)$$

The current-function becomes

$$J=\frac{a^2D\sigma p}{i}\sum_{s=1}^{\infty}\sum_{n=1}^{\infty}\sum_{\nu=0}^{\leq n/2}\frac{s}{n(n+1)}(a_{s+1}^s-ib_{s+1}^s)\zeta_{n,\nu}^s e^{ispt}P_n^{2\nu}\sin 2\nu\phi \quad (1.17)$$

after all. Then we get current-intensity from (1.3) and (1.17).

$\zeta_{n,\nu}^s$'s can be easily obtained from (1.15). Their numerical values for $s=1, 2, 3$, $n=2, 3, \ldots, 7$ and $\nu=1, 2, 3$ are given in Table I.

Table I $\zeta_{n,\nu}^{s}$

	ν \ n	2	3	4	5	6	7
$s=1$	1	0	$0.0817(1+i)$	0	$0.0088(1+i)$	0	$0.0019(1+i)$
	2	—	—	0	$0.0147(1-i)$	0	$0.0041(1-i)$
	3	—	—	—	—	0	$0.0052(1+i)$
$s=2$	1	0	$0.167i$	0	0	0	0
	2	—	—	0	0.0432	0	0.0110
	3	—	—	—	—	0	0
$s=3$	1	0	$-0.0278(1-i)$	0	$0.0022(1-i)$		
	2	—	—	0	$0.0051(1-i)$		

Then the first three harmonics of the real part of J become

$$J=a^2D\sigma p(C_1\cos pt+S_1\sin pt+C_2\cos 2pt$$
$$+S_2\sin 2pt+C_3\cos 3pt+S_3\sin 3pt) \quad \ldots\ldots\ldots(1.18)$$

where

$$\left.\begin{aligned}
C_1=&(a_2^1-b_2^1)\,(0.0817\,P_3^2+0.0088\,P_5^2+0.0019\,P_7^2+\ldots)\sin 2\phi\\
&-(a_2^1+b_2^1)\,(0.0147\,P_5^4+0.0042\,P_7^4+\ldots)\sin 4\phi+(a_2^1-b_2^1)\\
&(0.0052\,P_7^6+\ldots)\sin 6\phi \quad \ldots\ldots\ldots\ldots\ldots\ldots\ldots\ldots\ldots\ldots ,\\
S_1=&(a_2^1+b_2^1)\,(0.0817\,P_3^2+0.0088\,P_5^2+0.0019\,P_7^2+\ldots)\sin 2\phi\\
&+(a_2^1-b_2^1)\,(0.0147\,P_5^4+0.0042\,P_7^4+\ldots)\sin 4\phi+(a_2^1+b_2^1)\\
&(0.0052\,P_7^6+\ldots)\sin 6\phi+ \quad \ldots\ldots\ldots\ldots\ldots\ldots\ldots\ldots\ldots\ldots ,\\
C_2=&0.167\,a_3^2\,P_3^2\sin 2\phi-b_3^2\,(0.0432\,P_5^4+0.0110\,P_7^4+\ldots)\\
&\sin 4\phi+ \quad \ldots\ldots\ldots\ldots\ldots\ldots\ldots\ldots\ldots\ldots\ldots\ldots\ldots\ldots ,\\
S_2=&0.167\,b_3^2\,P_3^2\sin 2\phi+a_3^2\,(0.0432\,P_5^4+0.0110\,P_7^4+\ldots)\\
&\sin 4\phi+ \quad \ldots\ldots\ldots\ldots\ldots\ldots\ldots\ldots\ldots\ldots\ldots\ldots\ldots\ldots ,\\
C_3=&(a_4^3+b_4^3)\,\{(0.0278\,P_3^2-0.0022\,P_5^2+\ldots)\sin 2\phi\\
&-(0.0051\,P_5^4+\ldots)\sin 4\phi+\ldots\} \quad \ldots\ldots\ldots\ldots\ldots\ldots\ldots ,\\
S_3=&-(a_4^3-b_4^3)\,\{(0.0278\,P_3^2-0.0022\,P_5^2+\ldots)\sin 2\phi\\
&-(0.0051\,P_5^4+\ldots)\sin 4\phi+\ldots\} \quad \ldots\ldots\ldots\ldots\ldots\ldots\ldots .
\end{aligned}\right\} \quad \ldots\ldots \quad (1.19)$$

The lines on which C_1, S_1,...... are constant give the current-line that corresponds to the current-flows varying with t as $\cos pt$, $\sin pt$,...... respectively. For illustration, current-systems which correspond to C_1, S_1, C_2 and S_2 are shown in Figs. 1, 2, 3 and 4 respectively. The numerical values of a_{s+1}^{s}'s and b_{s+1}^{s}'s are taken from Chapman's analysis[3] of S_q, 1905 (sun-spot maximum). According to his analysis, the equinoctial mean of the harmonic coefficients

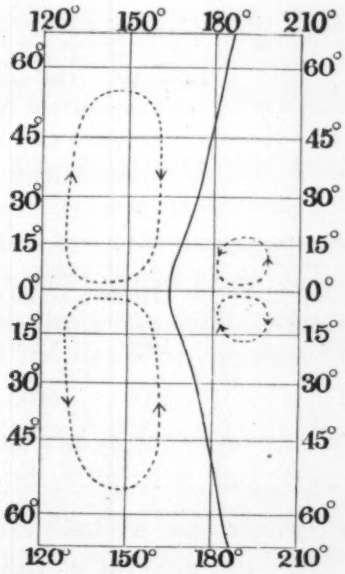
120°
150°
180°
210°
60°
45°
30°
15°
0°
15°
30°
45°
60°
60°
45°
30°
15°
0°
15°
30°
45°
60°
120°
150°
180°
210°

Fig. 1. The current-systems for cos *pt*.

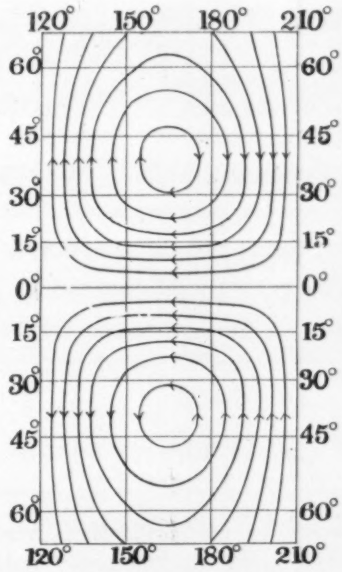
120°
150°
180°
210°
60°
45°
30°
15°
0°
15°
30°
45°
60°
60°
45°
30°
15°
0°
15°
30°
45°
60°
120°
150°
180°
210°

Fig. 2. The current-systems for sin *pt*.

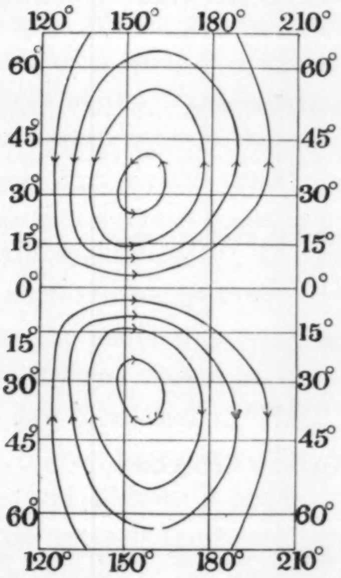
120°
150°
180°
210°
60°
45°
30°
15°
0°
15°
30°
45°
60°
60°
45°
30°
15°
0°
15°
30°
45°
60°
120°
150°
180°
210°

Fig. 3. The current-systems for cos 2 *pt*.

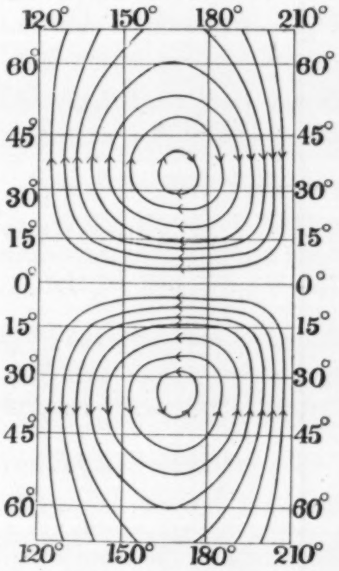
120°
150°
180°
210°
60°
45°
30°
15°
0°
15°
30°
45°
60°
60°
45°
30°
15°
0°
15°
30°
45°
60°
120°
150°
180°
210°

Fig. 4. The current-systems for sin 2 *pt*.

are given in Table II[13]. The time-origin of his analysis was taken at Greenwich midnight. When the west boundary of our ocean is assumed to be 120° E meridian which agrees roughly with that of Pacific Ocean, the harmonic coefficients referred to the 120° E meridian time or $\phi=0$ meridian time can be easily deduced from those values in Table II. These are given in Table III.

Table II. Equinoctial mean of the coef. for 1905. (after S. Chapman).

s	a^s_{s+1}	b^s_{s+1}
1	7.1 γ	−2.4 γ
2	−6.6	0.1
3	4.4	−1.5
4	1.7	0.9

Table III. Reduced coef.

s	a^s_{s+1}	b^s_{s+1}
1	−5.6 γ	−5.0 γ
2	3.2	−5.8
3	4.4	−1.5
4	−0.8	−1.9

Table IV. The amount of eletcric current flowing between two adjacent lines.

D	ΔI
100 *m*	120 *amp.*
1000	1200
5000	6000

In order to estimate the intensity of the current-flow, we take $a=6400$ *km*, $\sigma=4\times10^{-11}$ *emu*[14] and $p=2\pi/(60\times60\times24)$. Then the amount of the current-flow between two adjacent current-lines is given in Table IV in accordance with the depth of sea.

These electric currents produce magnetic fields whose potential at $P(r_0, \theta_0, \phi_0)$ is given by

$$W=a^2\int_{\theta=0}^{\pi}\int_{\phi=0}^{\pi/2} J(\theta,\phi)\,\frac{r_0\cos\gamma-a}{R^3}\sin\theta d\theta\, d\phi\,, \qquad \text{.....................(1.20)}$$

where γ is defined by

$$\cos\gamma=\cos\theta\cos\theta_0+\sin\theta\sin\theta_0\cos(\phi-\phi_0)\,.$$

Meanwhile, we get out of the earth $(r_0>a)$

$$1/R=(1/r_0)\sum_k (a/r_0)^k P_k(\cos\gamma)\,.$$

Then differentiating with respect to a, we obtain

$$(r_0\cos\gamma-a)/R^3=(1/a^2)\sum_k k(a/r_0)^{k+1}P_k(\cos\gamma)\,.$$

---

[13] According to the more recent analysis which will be referred to in § 2, these values differ slightly from those given in Table II. It is sufficient, however, to take Chapman's values to discuss the order of the influence of the oceans.

[14] CHAPMAN and BARTELS, *Geomagnetism* p. 424.

Further, considering the relation

$$P_k(\cos\gamma) = \sum_{l=0}^{k} P_k^l(\cos\theta)\, P_k^l(\cos\theta_0) \cos l(\phi-\phi_0)\,,$$

the potential is given by the next expression

$$W = \sum_k \sum_l k(a/r_0)^{k+1} P_k^l(\cos\theta_0) \int_{\theta=0}^{\pi} \int_{\phi=0}^{\pi/2} J(\theta,\phi)\, P_k^l(\cos\theta)$$
$$\sin\theta \cos l(\phi-\phi_0)\, d\theta\, d\phi\,. \quad \text{.......................}(1.21)$$

Then we can express the magnetic field on the earth's surface with sum of spherical surface harmonics. This procedure, however, is so troublesome that we can not practically get the whole distribution of the magnetic force over the earth. Besides, as our ocean, which is bounded by two meridians, is merely an idealized model, it is more practical to make an estimate approximately of the order of the field-intensity than try hard to get mathematical exactness.

Taking Fig. 2, for example, we see that the electric current-flow is fairly parallel and uniform at the point on the equator of the centre of our ocean. Then, to a fair degree of approximation, the magnetic force will be the same as that due to an infinite horizontal plane uniform current-sheet with the same direction and intensity of current-flow. Let this current-intensity be j in electromagnetic unit, the horizontal magnetic force at this point will be $2\pi j$, northwards. Giving 120, 1200 and 6000 *amperes* per 5 *degrees* of latitude to j as was shown in Table IV, we get respectively 0.1, 1.4 and 7.0 *gammas*.

By means of a similar method, we can also estimate the order of the magnetic field at the boundaries. Near the middle latitude, the magnetic field will be approximately the same with that due to a half-infinite horizontal plane uniform current-sheet with intensity j. The horizontal magnetic field produced by this current-sheet is given by πj. Then, giving the same values to j, we get respectively 0.0, 1.0 and 5.0 *gammas*, eastwards at the west boundary in the northern hemisphere.

Thus, in the same way, we can estimate the horizontal magnetic force due to current-flows shown in Figs. 1, 3 and 4. The results in the northern hemisphere are tabulated in Table V in which we do not show 8-hourly component and higher harmonics, for their magnitudes are small compared with those of 24- and 12-hourly ones.

As to the vertical force, we can easily see that it will be affected in the main at the centres of eddies and will not be influenced on the equator at all. As to the quantitative estimate, it being rather complicated in this case, we cease to discuss in detail.

Tabel V. Magnetic force produced by the induced currents in the ocean.

	Depth	C_1	S_2	C_2	S_1
North component at the middle point on the equator	100 *m*	0.0 γ	0.1 γ	−0.1 γ	0.1 γ
	1000	0.0	1.4	−1.2	1.4
	5000	0.0	7.0	−5.8	7.0
West component at the middle latitude on the west boundary of the ocean	100	0.0	0.0	0.0	0.0
	1000	0.2	1.0	−0.8	1.0
	5000	1.0	5.0	−4.2	5.0

As was mentioned above, the horizontal magnetic force produced by these oceanic currents amounts to about 10 *gammas* at the middle point of the ocean whose electrical conductivity and depth are assumed to be 4×10^{-11} *emu* and 5000 *m* respectively. At the boundaries of the ocean, it amounts, in the middle latitude, to several *gammas* adopting the same value to the depth. Near the continent, however, the magnetic force may be smaller than this value because the sea becomes shallower.

After all, we presume that the influence of the ocean will become appreciable near the centre of the ocean, while, at the boundaries between land and sea, the effect of the ocean amounts to only a few *gammas* or less. This will be apt to be hidden by local irregularities of the external part of S_q.

As the distribution of land and sea on the real earth is very complicated, we can only discuss the possibility of the ocean-effect in regard to such an idealized and simple model as has been treated in this Section. But it is obvious that S_q may not be affected so much by the ocean that the field due to induced currents in the ocean occupies its main part. Probably, the magnetic field produced by the oceanic currents may amount to the order of one tenth or less of S_q except near the centre of the ocean. Besides, it depends upon universal time, while the external part of S_q seems to depend upon local time mainly. Then, on the average, the internal part of S_q obtained from spherical harmonic analysis in which it is assumed that S_q depends on local time can be considered, to a fair degree of approximation, as that is produced by the induced currents flowing in the deeper part of the earth.

Although, it is smaller compared with the whole amplitude of S_q, the possible ocean-effects, amounting to a few *gammas*, are not so small that we can not detect them at all if we could eliminate the fields which depend solely on local time and other irregularities. It will be worth while, then, to make an effort to study whether such influences are really existing or not. However, the exact elimination of the superposing fields may be almost impossible unfortunately because the actual distribution of land and sea is very much complicated. Thus we can, in the following paragraph, only make an attempt to abstract very roughly the influence of the ocean.

As shown in several figures in this Section, the induced currents in the ocean will produce magnetic fields which are almost the same in intensity and opposite in direction at the middle point of the both boundaries of the ocean. Besides, it is notable that the fields depend on universal time and not on local time at all. If two magnetic observatories, whose latitudes are the same are situated on both sides of the ocean, the daily variation of the magnetic declination will be affected equally in their magnitudes and oppositely in their directions. Then, assuming the other part of the variation depends on only local time and neglecting local irregularities, the daily variation of the declination may be expressed as follows;

$$\left.\begin{array}{l} D_W=F(t)+f(\tau) \\ D_E=F(t)-f(\tau) \end{array}\right\} \qquad \text{(1.22)}$$

where suffices W and E denote respectively the quantities belonging to the west and east-side observatories. t and τ are respectively local and universal time.

If we take the local time at the west-side observatory as the universal time, (1.22) becomes

$$D_W=F(t)+f(t)\,, \qquad \text{(1.23 a)}$$

$$D_E=F(t)-f(t-\alpha)\,, \qquad \text{(1.23 b)}$$

where α is the difference of the local time between the two station. Subtracting (1.23 b) from (1.23 a), we get

$$D_W-D_E=f(t)+f(t-\alpha)\,. \qquad \text{(1.24)}$$

When we assume that D_W-D_E and $f(t)$ can be expanded into Fourier series of the types

$$D_W-D_E=\sum_n (A_n \cos nt+B_n \sin nt)\,, \qquad \text{(1.25)}$$

$$f(t)=\sum_n (a_n \cos nt+b_n \sin nt)\,, \qquad \text{(1.26)}$$

the righthand-side of (1.24) becomes

$$\sum_n \{a_n(1+\cos n\alpha)-b_n \sin n\alpha\}\cos nt+\sum_n \{a_n \sin n\alpha + b_n(1+\cos n\alpha)\}\sin nt \qquad \text{(1.27)}$$

Then equating the corresponding coefficients, we get

$$\left.\begin{aligned} a_n(1+\cos n\alpha)-b_n\sin n\alpha&=A_n\,,\\ a_n\sin n\alpha-b_n(1+\cos n\alpha)&=B_n\,.\end{aligned}\right\}\quad\cdots\cdots\cdots\cdots\cdots(1.28)$$

Solving (1.28), it becomes

$$\left.\begin{aligned} a_n&=\frac{A_n(1+\cos n\alpha)+B_n\sin n\alpha}{(1+\cos n\alpha)^2+\sin^2 n\alpha}\,,\\ b_n&=\frac{-A_n\sin n\alpha+B_n(1+\cos n\alpha)}{(1+\cos n\alpha)^2+\sin^2 n\alpha}\,.\end{aligned}\right\}\quad\cdots\cdots\cdots\cdots\cdots(1.29)$$

As α is known, we can get a_n and b_n from A_n and B_n. Then we are able to get $f(t)$, that is the part varies with universal time.

When we discuss the effect of Pacific Ocean, Kakioka (36.2° in latitude and 140.2° in longitude) and Tucson (32.2° in latitude and 249.2° in longitude) may approximately suffice the condition above mentioned. The harmonic coefficients of magnetic declination (+ denotes the west declination) averaged through the all international quiet days in 1924 are given in Table VI.

Table VI. Fourier coef. of declination for 1924.

	c_0	c_1	s_1	c_2	s_2
Kakioka	0.01′	−0.56′	−0.79′	−0.80′	0.70′
Tucson	0.00′	−0.25′	−1.13′	−0.35′	1.30′

Then making the difference, we get

$$A_1=0.31', \qquad B_1=0.34', \qquad A_2=-0.45', \qquad B_2=-0.60'.$$

Taking into consideration that α is nearly 16 hours, we obtain from (1.29)

$$a_1=-0.45', \qquad b_1=0.44', \qquad a_2=-0.75', \qquad b_2=0.09'.$$

In order to compare these coefficients to the estimate which has been done at the first part of this Section, we rewrite these coefficients referred to 120° *E* meridian time. Then it becomes

$$a_1=-0.33', \qquad b_1=0.54', \qquad a_2=-0.60', \qquad b_2=0.46'.$$

If we assume that the horizontal intensity of the permanent magnetic field of the earth at both stations amounts to 0.28 *Gauss*, the 24- and 12-hourly components of f can be written respectively in the next form.

$$5.2\sin(t-2.0) \text{ and } 6.2\sin(2t-3.5)\,, \quad (\text{Unit in } \gamma) \quad\cdots\cdots\cdots\cdots(1.30)$$

Meanwhile, from the estimate with respect to an idealized ocean bounded by two meridians $\pi/2$ apart in longitude, it is informed that they may become respectively

$$4.4\sin(t+0.7) \text{ and } 5.2\sin(2t-2.7), \quad (\text{Unit in } \gamma) \quad \ldots\ldots\ldots\ldots\ldots(1.31)$$

taking 4000 *m* as the depth of the ocean. This estimate was made for the year 1905. As the magnetic activities in 1905 and 1924[15] are of the same order, we may compare (1.30) to (1.31). The agreement between the theoretical estimate and that obtained from the observation seems good, especially the amplitude ratio of 24-hourly component to 12-hourly one. We must not, however, forget that we dare to make several assumptions fearlessly both in theory and in the treatment of the actual data. Accordingly, it is dangerous to conclude that the actual effect of Pacific Ocean is just of the type as expressed in (1 30) or (1.31). They are only rough approximations.

In short, according to the writer's opinion, there must be the influences of the presence of the ocean, such as Pacific Ocean, upon S_q. But they may not be so considerable that they will be almost eliminated in spherical harmonic analysis on the average assuming that S_q depends solely on local time. On the other hand, under suitable assumptions we can detect the ocean-effect though it is rather small and less reliable.

The ocean-effect on the other variations in the earth's magnetic field will be discussed later.

2. Spherical harmonic analyses of S_q which were done up to this time and their relations to the uniform core model of the earth.

As was briefly referred to in the Introduction of this paper, Chapman[3] was the first one who analyzed S_q, using data obtained from well-distributed observatories. The results of his analysis has been hitherto used by himself, Price and Lahiri, and Terada to investigate the cause of S_q and also to infer the electrical state of the earth's interior. In order to explain the relation between the external and the internal parts of S_q, both in amplitude and phase of main harmonics, Chapman took a model of the earth in which a conducting core whose electrical conductivity amounts to 3.6×10^{-13} *emu* is surrounded by non-conducting layer whose thickness is about 250 *km*. So far as we assume that the distribution of conductivity is uniform, this simple model is the best one. We shall call this "uniform core model" hereafter. We shall also call the uniform core model having the values determined by Chapman the "Chapman's model".

---

[15] The annual means of the u-measure of magnetic activity are 0.85 and 0.74 for 1905 and 1924 respectively.

After Chapman's analysis in which he used the magnetic data for 1902 and 1905 obtained from 21 stations, however, the number of magnetic observatories increased remarkably during th's 1/4 century. Using the data of the Second Polar Year, 1932~1933, Hasegawa[16] made an analysis of S_q. On the other hand, the same analysis was executed by Benkova[17] with respect to the summer of 1933. As these analyses were based upon the observed data from observatories amounting to several tens in number and distributed widely all over the world, these two analyses may be more complete and reliable than Chapman's old one.

The amplitude ratio and phase difference between the external and the internal parts of main harmonics of their analyses are shown in Table VII together with that of Chapman's study.[18] According to Nagata, the numerical values of the conductivity and q (ratio of radius of the conducting core to that of the earth) in uniform core model which are consistent with both of amplitude ratio and phase difference are given in Table VIII. As also pointed out by Nagata, the discrepancies of σ and q between those which are expected from Chapman's analysis and those obtained from recent two analyses are considerable. Especially, it is remarkable that the values of σ and q obtained from each harmonic agree fairly well in Hasegawa's and Benkova's analyses, while, in Chapman's one, they agree not so well with each other as in these two

Table VII. The results of the spherical harmonic analyses.

n	m	Chapman		Hasegawa		Benkova	
		e/i	$\epsilon-\iota$	e/i	$\epsilon-\iota$	e/i	$\epsilon-\iota$
2	1	2.8	−13°	2.30	−9°	2.34	−5°
3	2	2.2	−18°	2.43	−10°	2.30	−5°
4	3	2.5	−21°	2.25	−14°	——	——
5	4	2.7	−23°	——	——	——	——
1	1	2.5	−7°	1.98	−2°	2.15	3°

---

[16] M. HASEGAWA, Read at the Annual Meeting (1943) of the Physico-Mathematical Society of Japan.

[17] N. P. BENKOVA, *Terr. Mag.*, 45 (1940), 425.

[18] This comparison was made by Dr. T. Nagata in connexion with comment on Chapman's analysis. Read at the Dec. (1946) Meeting of the Geophysical Institute, Tokyo Imperial University.

Table VIII. σ and q of uniform core model for each analysis.

n	m	Chapman		Hasegawa		Benkova	
		$\sigma(emu)$	q	$\sigma(emu)$	q	$\sigma(emu)$	q
2	1	8.8×10^{-13}	0.920	1.7×10^{-12}	0.943	5.1×10^{-12}	0.933
3	2	4.1×10^{-13}	0.968	1.3×10^{-12}	0.940	5.2×10^{-12}	0.936
4	3	3.4×10^{-13}	0.961	0.71×10^{-12}	0.961	——	——

analyses. With the superiority of data in mind, it will be natural to prefer the results of Benkova's analysis in discussing electromagnetic induction by S_q in so far as a new analysis will be done in the future. Hence, we get $\sigma=5\times10^{-12}$ *emu* and the thickness of the non-conducting layer is about 400 *km* namely, the core must be about ten times conductive and its radius must become slightly smaller than was estimated at the first time by Chapman.

3. Electromagnetic induction in the earth's model consisting of core, mantle and superficial non-conducting layer.

Electromagnetic induction by periodic field in a uniformly conducting sphere was fully discussed by Chapman, Whitehead, and Price[19]. Its application to the earth was outlined in Section 2 of this Chapter.

As mentioned in the Introduction of this paper, we have seismological evidences[20] that there must be a distinguishable discontinuity at the depth of 2900 *km* in the earth. As this discontinuity is so notable that we must presume that physical conditions of substances may differ in- and outside this boundary, it will be worth while to attempt to find how far the electrical property differs in both regions. We do not take into consideration the other discontinuities reported from researches on seismic waves such as at the depth of 1200 *km* and 60 *km* because they are comparatively small compared with that of the boundary just mentioned. In short, the purpose of this section is to construct an electrical model of the earth which is in accord with the earth's structure inferred from seismic waves.

Mathematical theory of electromagnetic induction in a sphere which has an inner core covered by outside layer of different conductivity is easily constructed in the same way as in a uniformly conducting sphere.

In conducting region, we have vector potential $\vec{A}$, which satisfies the relation

---

[19] Mathematics of the electromagnetic induction in a uniformly conducting sphere is summarized in Chapman and Bartels' well known book "*Geomagnetism*" Vol. II, p. 732.

[20] *e.g.* B. GUTENBERG, *ZS. f. Geophysik*, 3 (1927), 371.

$$\nabla^2\overrightarrow{A}=4\pi\sigma\frac{\partial\overrightarrow{A}}{\partial t}\;\ldots\ldots\ldots\ldots\ldots\ldots\ldots\ldots\ldots\ldots\ldots\ldots\ldots\ldots(3.1)$$

for the phenomenon is assumed to be quasistationary. Here, magnetic permeability μ is assumed to be unity for the reason mentioned in Chapter I. The typical term of the solution of (3.1) can be written in polar coordinate

$$\overrightarrow{A_n^m}=af_n(t,\rho)\,[\,\overrightarrow{r}\,\mathrm{grad}\,S_n^m],\quad(\rho=r/a)\ldots\ldots\ldots\ldots\ldots\ldots\ldots\ldots\ldots\ldots(3.2)$$

where a and S_n^m denote respectively radius of the sphere in question and spherical surface harmonic. f_n is a solution of the differential equation of the next type

$$\frac{\partial}{\partial\rho}\left(\rho^2\frac{\partial f_n}{\partial\rho}\right)=\left\{n(n+1)+4\pi a^2\sigma\rho^2\frac{\partial}{\partial t}\right\}f_n\,.\;\ldots\ldots\ldots\ldots\ldots\ldots\ldots\ldots(3.3)$$

As the r, θ and ϕ components of $\overrightarrow{A_n^m}$ in (3.2) become respectively

$$0,\quad -af_n\frac{\partial S_n^m}{\sin\theta\partial\phi},\quad af_n\frac{\partial S_n^m}{\partial\theta},\;\ldots\ldots\ldots\ldots\ldots\ldots\ldots\ldots\ldots\ldots(3.4)$$

we get the components of the magnetic field as follows;

$$\left.\begin{aligned}H_r&=-\frac{1}{\rho}\,n(n+1)f_nS_n^m\,,\\H_\theta&=-\frac{1}{\rho}\frac{\partial}{\partial\rho}(\rho f_n)\frac{\partial S_n^m}{\partial\theta}\,,\\H_\phi&=-\frac{1}{\rho}\frac{\partial}{\partial\rho}(\rho f_n)\frac{\partial S_n^m}{\sin\theta\partial\phi}\end{aligned}\right\}^{21)}\;\ldots\ldots\ldots\ldots\ldots\ldots\ldots(3.5)$$

On the other hand, there is, in non-conducting medium, magnetic potential whose typical term can be written in the type

$$W_n^m=a\{e_n(t)\rho^n+i_n(t)\rho^{-n-1}\}S_n^m\,,\ldots\ldots\ldots\ldots\ldots\ldots\ldots\ldots\ldots(3.6)$$

by which we get the components of the magnetic field as follows$^{22)}$;

---

21) In the case of $\mu=1$

$$\overrightarrow{H}=\mathrm{rot}\;\overrightarrow{A}$$

or writing the components, we easily get

$$\begin{aligned}H_r&=\frac{\partial\,(A_\phi\sin\theta)}{r\sin\theta\,\partial\,\theta}-\frac{\partial\,A_\theta}{r\sin\theta\,\partial\,\phi}\,,\\H_\theta&=\frac{\partial\,A\,r}{r\sin\theta\,\partial\,\phi}-\frac{\partial\,(r\,A_\phi)}{r\,\partial\,r}\,,\\H_\phi&=\frac{\partial\,(r\,A_\theta)}{r\,\partial\,r}-\frac{\partial\,A\,r}{r\,\partial\,\theta}\,.\end{aligned}$$

22) $\overrightarrow{H}=-\mathrm{grad}\;W$

$$\left.\begin{aligned} H_r &= -\{n\boldsymbol{e}_n\rho^{n-1}-(n+1)\boldsymbol{i}_n\rho^{-n-2}\}S_n^m\,, \\ H_\theta &= -(\boldsymbol{e}_n\rho^{n-1}+\boldsymbol{i}_n\rho^{-n-2})\,\frac{\partial S_n^m}{\partial\theta}\,, \\ H_\phi &= -(\boldsymbol{e}_n\rho^{n-1}+\boldsymbol{i}_n\rho^{-n-2})\,\frac{\partial S_n^m}{\sin\theta\partial\phi}\,. \end{aligned}\right\}\quad\text{........................(3.7)}$$

In our present model of the earth, as shown in Fig. 5, the continuity of the magnetic field must be satisfied at every boundary. We get, then, from (3.5) and (3.7)

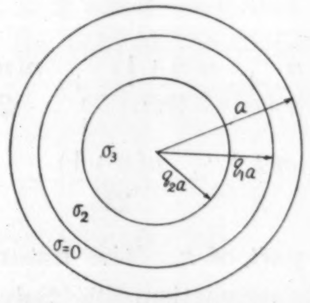

Fig. 5. Schematic view of the earth's model.

$$\left.\begin{aligned} &n(n+1)f_{2,n}(t,q_1)=n\boldsymbol{e}_nq_1^n-(n+1)\boldsymbol{i}_nq_1^{-n-1}\,, \\ &q_1^{-1}f_{2,n}(t,q_2)+\left[\frac{\partial}{\partial\rho}f_{2,n}(t,\rho)\right]_{\rho=q_1}=\boldsymbol{e}_nq_1^n+\boldsymbol{i}_nq_1^{-n-1}\,, \\ &\quad f_{2,n}(t,q_2)=f_{3,n}(t,q_2)\,, \\ &q_2^{-1}f_{2,n}(t,q_2)+\left[\frac{\partial}{\partial\rho}f_{2,n}(t,\rho)\right]_{\rho=q_2}=q_2^{-1}f_{3,n}(t,q_2)+\left[\frac{\partial}{\partial\rho}f_{3,n}(t,\rho)\right]_{\rho=q_2}, \end{aligned}\right\}\quad\text{...(3.8)}$$

where

$$f_{2,n}(t,\rho)=C_2\rho^nF_{2,n}(t,\rho)+D_2\rho^{-n-1}G_{2,n}(t,\rho)\;\text{..................................(3.9)}$$

and

$$f_{3,n}(t,\rho)=C_3\rho^nF_{3,n}(t,\rho)\,.\;^{23)}\quad\text{..................................(3.10)}$$

In these expressions, C_2, D_2 and C_3 denote functions of t, while $F_{\nu,n}(t,\rho)$ and $G_{\nu,n}(t,\rho)$ are the solutions of the equations

$$\left\{\frac{\partial^2}{\partial\rho^2}+\frac{2(n+1)}{\rho}\frac{\partial}{\partial\rho}-4\pi a^2\sigma_\nu\frac{\partial}{\partial t}\right\}f_{\nu,n}=0\,,\quad(\nu=2,3)\;\text{.........(3.11a)}$$

or writing in operational form

$$\left\{\frac{d^2}{d\rho^2}+\frac{2(n+1)}{\rho}\frac{d}{d\rho}-k_\nu^2a^2\right\}f_{\nu,n}(p,\rho)=0\;,\text{.........................(3.11b)}$$

---

23) The coefficient of $G_{3,n}(t,\rho)$ is taken to be zero because the field must remain finite at the centre.

where, putting $\partial/\partial t=p$

$$k_\nu^2=4\pi\sigma_\nu p\,. \quad \text{......................................} (3.12)$$

Solving (3.12), we obtain putting $x=k_\nu\rho$

$$F_n(x)=1+\frac{x^2}{2(2n+3)}+\frac{x^4}{2\cdot4\cdot(2n+3)\,(2n+5)}+\dots\,, \quad \text{..................} (3.13)$$

$$G_n(x)=e^{-x}\left\{1+x+\frac{2(n-1)}{2!\,(2n-1)}x^2+\frac{2^2(n-2)\,(n-1)}{3!(2n-2)\,(2n-1)}x^3+\dots\right\}, \text{...} (3.14)$$

for $x<1$ and further

$$\frac{F_{n-1}(x)}{F_n(x)}=\frac{x}{2n+1}\left\{1+\frac{n}{x}+\frac{n(n+1)}{2x^2}+\frac{n(n+1)}{2x^3}\dots\right\}, \quad \text{............} (3.15)$$

$$\frac{G_{n+1}(x)}{G_n(x)}=\frac{x}{2n+1}\left\{1+\frac{n+1}{x}+\frac{n(n+1)}{2x^2}-\frac{n(n+1)}{2x^3}\dots\right\}, \text{.........} (3.16)$$

for large values of the real part of x. The nature of F_n and G_n were fully investigated in the book "Geomagnetism"[24]. Solving the simultaneous equations (3.8) we get the relations between $e_n(t)$, $i_n(t)$, $C_2(t)$, $D_2(t)$ and $C_3(t)$ by means of operators in the forms

$$i_n(t)=I(p)e_n(t)\,, \quad \text{................................} (3.17)$$

$$C_2(t)=\overline{C}_2(p)e_n(t)\,, \quad \text{................................} (3.18)$$

$$D_2(t)=\overline{D}_2(p)e_n(t)\,, \quad \text{................................} (3.19)$$

$$C_3(t)=\overline{C}_3(p)e_n(t)\,, \quad \text{................................} (3.20)$$

in which

$$I(p)=-q_1^{2n+1}\frac{n}{n+1}\frac{\left\{1-\frac{F_{n-1}(2,1)}{F_n(2,1)}\right\}\left\{1-\frac{F_{n-1}(3,2)}{F_n(3,2)}-\frac{G_{n+1}(2,2)}{G_n(2,2)}\right\}+\tau^{2n+1}\left\{\frac{F_{n-1}(3,2)}{F_n(3,2)}-\frac{F_{n-1}(2,2)}{F_n(2,2)}\right\}\frac{F_n(2,2)}{F_n(2,1)}\frac{G_n(2,1)}{G_n(2,2)}}{\frac{F_{n-1}(2,1)}{F_n(2,1)}\left\{1-\frac{F_{n-1}(3,2)}{F_n(3,2)}-\frac{G_{n+1}(2,2)}{G_n(2,2)}\right\}+\tau^{2n+1}\left\{1-\frac{G_{n+1}(2,1)}{G_n(2,1)}\right\}\left\{\frac{F_{n-1}(3,2)}{F_n(3,2)}-\frac{F_{n-1}(2,2)}{F_n(2,2)}\right\}\frac{F_n(2,2)}{F_n(2,1)}\frac{G_n(2,1)}{G_n(2,2)}}, \tag{3.21}$$

$$\overline{C}_2(p)=\frac{1}{n+1}\frac{1}{F_n(2,1)}\frac{1-\frac{F_{n-1}(3,2)}{F_n(3,2)}-\frac{G_{n+1}(2,2)}{G_n(2,2)}}{\frac{F_{n-1}(2,1)}{F_n(2,1)}\left\{1-\frac{F_{n-1}(3,2)}{F_n(3,2)}-\frac{G_{n+1}(2,2)}{G_n(2,2)}\right\}+\tau^{2n+1}\left\{1-\frac{G_{n+1}(2,1)}{G_n(2,1)}\right\}\left\{\frac{F_{n-1}(3,2)}{F_n(3,2)}-\frac{F_{n-1}(2,2)}{F_n(2,2)}\right\}\frac{F_n(2,2)}{F_n(2,1)}\frac{G_n(2,1)}{G_n(2,2)}}, \tag{3.22}$$

$$\overline{D}_2(p)=q_2^{2n+1}\frac{1}{n+1}\frac{1}{G_n(2,2)}\frac{F_n(2,2)}{F_n(2,1)}\frac{\frac{F_{n-1}(3,2)}{F_n(3,2)}-\frac{F_{n-1}(2,2)}{F_n(2,2)}}{\frac{F_{n-1}(2,1)}{F_n(2,1)}\left\{1-\frac{F_{n-1}(3,2)}{F_n(3,2)}-\frac{G_{n+1}(2,2)}{G_n(2,2)}\right\}+\tau^{2n+1}\left\{1-\frac{G_{n+1}(2,1)}{G_n(2,1)}\right\}\left\{\frac{F_{n-1}(3,2)}{F_n(3,2)}-\frac{F_{n-1}(2,2)}{F_n(2,2)}\right\}\frac{F_n(2,2)}{F_n(2,1)}\frac{G_n(2,1)}{G_n(2,2)}}, \tag{3.23}$$

---

24) CHAPMAN and BARTELS, *loc. cit.* Vol. II, p. 738.

$$\bar{C}_3(p)=\frac{1}{n+1}\frac{1}{F_n(3,2)}\frac{F_n(2,2)}{F_n(2,1)}\frac{1-\dfrac{F_{n-1}(2,2)}{F_n(2,2)}-\dfrac{G_{n+1}(2,2)}{G_n(2,2)}}{\dfrac{F_{n-1}(2,1)}{F_n(2,1)}\left\{1-\dfrac{F_{n-1}(3,2)}{F_n(3,2)}-\dfrac{G_{n+1}(2,2)}{G_n(2,2)}\right\}+\tau^{2n+1}\left\{1-\dfrac{G_{n+1}(2,1)}{G_n(2,1)}\right\}\left\{\dfrac{F_{n-1}(3,2)}{F_n(3,2)}-\dfrac{F_{n-1}(2,2)}{F_n(2,2)}\right\}\dfrac{F_n(2,2)}{F_n(2,1)}\dfrac{G_n(2,1)}{G_n(2,2)}}. \tag{3.24}$$

For the sake of simplicity, $F(k_\nu q_\mu a)$ and $G(k_\nu q_\mu a)$ are written respectively as $F(\nu,\mu)$ and $G(\nu,\mu)$ in the above expression. We also write τ in place of q_2/q_1.

When the inducing field is periodic, the induced field becomes also periodic. In the case of period $2\pi/\alpha$, it is easily seen that the amplitude ratio i/e and the phase difference $\iota-\epsilon$ of the field at the surface ($r=a$) are given by

$$i/e=\mathrm{mod}\, I(i\alpha)\,, \qquad \iota-\epsilon=\arg I(i\alpha) \qquad\text{..........................} \tag{3.25}$$

with $i\alpha$ in place of p.
In the case of S_q, in so far as it depends solely on local time, we get

$$\alpha=2\pi m/(60\times 60\times 24) \qquad\text{..............................} \tag{3.26}$$

measuring t in seconds. m is the order of S_n^m.
We write

$$k_\nu^2 q_\mu^2 a^2=2i\beta_{\nu,\mu}^2\,, \qquad \beta_{\nu,\mu}^2=\frac{4\pi^2\sigma_\nu m q_\mu^2 a^2}{24\times 60\times 60}\,, \qquad\text{..........................} \tag{3.27}$$

so that $\beta_{\nu,\mu}^2$ is real and positive. Then it becomes

$$k_\nu q_\mu a=\beta_{\nu,\mu}(1+i)\,, \qquad 1/k_\nu q_\mu a=(1-i)/2\beta_{\nu,\mu}\,. \qquad\text{.....................} \tag{3.28}$$

As the lowest value of $\beta_{\nu,\mu}$ is about 7 in the case of daily variation, we are able to calculate approximately F_{n-1}/F_n and G_{n+1}/G_n by use of (3.15) and (3.16).
Writing

$$\frac{F_{n-1}(\nu,\mu)}{F_n(\nu,\mu)}=A_{\nu\mu}+iB_{\nu\mu}\,, \qquad \frac{G_{n+1}(\nu,\mu)}{G_n(\nu,\mu)}=C_{\nu\mu}+iD_{\nu\mu}\,, \qquad\text{.........} \tag{3.29}$$

where $A_{\nu\mu}$, $B_{\nu\mu}$, $C_{\nu\mu}$ and $D_{\nu\mu}$ are given by

$$\left.\begin{aligned}
A_{\nu\mu}&=\frac{\beta_{\nu\mu}}{2n+1}\left\{1+\frac{n}{\beta_{\nu\mu}}+\frac{n(n+1)}{4\beta_{\nu\mu}^2}\cdots\cdots\cdots\right\},\\
B_{\nu\mu}&=\frac{\beta_{\nu\mu}}{2n+1}\left\{1-\frac{n(n+1)}{4\beta_{\nu\mu}^2}-\frac{n(n+1)}{4\beta_{\nu\mu}^3}\cdots\right\},\\
C_{\nu\mu}&=\frac{\beta_{\nu\mu}}{2n+1}\left\{1+\frac{n+1}{\beta_{\nu\mu}}+\frac{n(n+1)}{4\beta_{\nu\mu}^2}\cdots\cdots\right\},\\
D_{\nu\mu}&=\frac{\beta_{\nu\mu}}{2n+1}\left\{1-\frac{n(n+1)}{4\beta_{\nu\mu}^2}+\frac{n(n+1)}{4\beta_{\nu\mu}^3}\cdots\right\},
\end{aligned}\right\} \qquad\text{..................} \tag{3.30}$$

On the other hand, it is known that F_n and G_n become approximately

$$F_n(x) = \frac{(2n+1)!}{2^n n!} \frac{e^x}{x^n} \rho_n(x) , \quad \text{[25]}$$

$$G_n(x) = -\frac{2^n(n-1)!}{(2n-1)!} x^{n+1} e^{-x} \rho_n(x) ,$$

where

$$\rho_n(x) = \frac{1}{2x} - \frac{n(n+1)}{(2x)^2} + \frac{(n-1)n(n+1)(n+2)}{2!\,(2x)^3} - \ldots\ldots .$$

Then we obtain approximately

$$\frac{F_n(x)}{G_n(x)} = \frac{(2n+1)!\,(2n-1)!}{2^{2n} n!\,(n-1)!} \frac{e^{2x}}{x^{2n+1}}$$

for large values of the real part of x.
Then it becomes

$$\frac{F_n(2,2)}{G_n(2,2)} \frac{G_n(2,1)}{F_n(2,1)} = E + iF \quad \ldots\ldots\ldots\ldots\ldots\ldots\ldots\ldots\ldots (3.31)$$

where

$$\left.\begin{aligned} E &= (\beta_{21}/\beta_{22})^{2n+1} e^{2(\beta_{22}-\beta_{21})} \cos 2(\beta_{22}-\beta_{21}) , \\ F &= (\beta_{21}/\beta_{22})^{2n+1} e^{2(\beta_{22}-\beta_{21})} \sin 2(\beta_{22}-\beta_{21}) . \end{aligned}\right\} \quad \ldots\ldots\ldots\ldots\ldots\ldots (3.32)$$

Finally, we obtain

$$I(i\alpha) = \frac{n}{n+1} q_1^{2n+1} \frac{\xi_2 + i\eta_2}{\xi_1 + i\eta_1} \ldots\ldots\ldots\ldots\ldots\ldots\ldots\ldots\ldots\ldots (3.33)$$

where

$$\left.\begin{aligned} \xi_1 = {} & A_{21}(1-A_{32}-C_{22}) + B_{21}(B_{32}+D_{22}) \\ & + \tau^{2n+1}[E\{(1-C_{21})(A_{32}-A_{22}) + D_{21}(B_{32}-B_{22})\} \\ & - F\{(1-C_{21})(B_{32}-B_{22}) - D_{21}(A_{32}-A_{22})\}] , \\ \eta_1 = {} & B_{21}(1-A_{32}-C_{22}) - A_{21}(B_{32}+D_{22}) \\ & + \tau^{2n+1}[E\{(1-C_{21})(B_{32}-B_{22}) - D_{21}(A_{32}-A_{22})\} \\ & + F\{(1-C_{21})(A_{32}-A_{22}) + D_{21}(B_{32}-B_{22})\}] , \\ \xi_2 = {} & -(1-A_{21})(1-A_{32}-C_{22}) + B_{21}(B_{32}+D_{22}) \\ & - \tau^{2n+1}\{E(A_{32}-A_{22}) - F(B_{32}-B_{22})\} , \\ \eta_2 = {} & B_{21}(1-A_{32}-C_{22}) + (1-A_{21})(B_{32}+D_{22}) \\ & - \tau^{2n+1}\{E(B_{32}-B_{22}) + F(A_{32}-A_{22})\} . \end{aligned}\right\} \ldots\ldots\ldots\ldots\ldots (3.34)$$

---

[25] CHAPMAN and BARTELS, *loc. cit* p. 739.

Now using ξ_1, η_1, ξ_2 and η_2 given in (3.33), we obtain from (3.25)

$$e/i=q_1^{-2n-1}\frac{n+1}{n}\sqrt{\frac{\xi_1^2+\eta_1^2}{\xi_2^2+\eta_2^2}}, \qquad \epsilon-\iota=\tan^{-1}\frac{\eta_1}{\xi_1}-\tan^{-1}\frac{\eta_2}{\xi_2} \quad \text{.........(3.35)}$$

Thus we can estimate the amplitude ratio and the phase difference which correspond to the given electrical conductivity in the mantle and the core of our model of the earth.

The writer applies the above mentioned theory to the actual geomagnetic problem in two cases. The first is based on Chapman's analysis by which the electrical state of the earth's interior was hitherto discussed. The second is on the basis of Benkova's analysis which seems more reliable than the former. According to Chapman's analysis which is given in Table VII, it is believed that P_3^2 is the most reliable because its coefficients remain almost constant in every analysis for different years and seasons as shown in his original paper. Then, we shall attempt to determine σ_2 and σ_3 consistent with the amplitude ratio and the phase difference for $n=3$ and $m=2$ in the first place.

As q_1 does not differ very much from unity[26], the combination of σ_2 and σ_3 by which we get approximately $\iota_3^2-\epsilon_3^2=18°$ is calculated from (3.35). As appears in Fig. 6, σ_2 is more effective than σ_3. In this calculation, q_2 is taken to be 0.540 for the inner

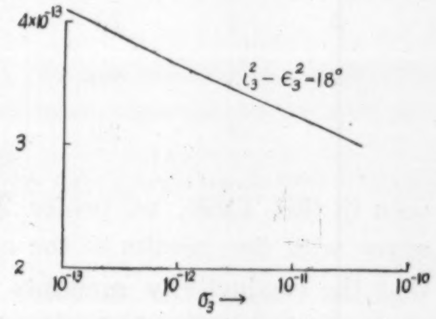

Fig. 6. Combination of σ_2 and σ_3 by which we obtain $\iota_3^2-\epsilon_3^2=18°$.

Table IX.

n \ m	σ_2 / σ_3	3.8×10^{-13} 3×10^{-13}	3.4×10^{-13} 3×10^{-12}	3.0×10^{-13} 3×10^{-11}	2.6×10^{-13} 3×10^{-10}	Chapman's Analysis
2	1	——	——	18°	——	13°
3	2	18°	18°	18°	18°	18°
4	3	18°	19°	21°	22°	21°
5	4	19°	20°	22°	24°	23°

---

[26] In such a case, the phase difference will not practically affected by the small difference of the numerical value of q_1.

boundary of the mantle is of the depth of 2900 *km*. Phase differences of main harmonics are given in Table IX for the combinations of σ_2 and σ_3, where q_1 is assumed to be nearly unity. Comparing these values to Chapman's analysis, we find that the combination $\sigma_2=3.0\times10^{-13}$ *emu*, $\sigma_3=3\times10^{-11}$ *emu* is the best. Then, taking this combination, amplitude ratio of main harmonics are calculated for several values of q_1 as appeared in Table X. As is easily seen in this Table, we prefer $q_1=0.97$ to let the calculation approximately agree with the results of the actual analysis. Ultimately, it is determined that the conductivity amounts to 3×10^{-11} *emu* in the core, 3.0×10^{-13} *emu* in the mantle and the thickness of the non-conducting layer is 200 *km* as the most probable conductivity-distribution in the earth.

Table X.

n	m \ q_1	0.985	0.980	0.975	0.970	Chapman's Analysis
2	1	2.3	2.3	2.4	2.4	2.8
3	2	2.1	2.1	2.2	2.3	2.2
4	3	2.0	2.1	2.2	2.3	2.5
5	4	2.0	2.1	2.3	2.4	2.7

As already mentioned in Section 2 in this Chapter, the newly made analyses showed us that Chapman's analysis might be somewhat rough. Then, to make the same determination of conductivity-distribution on the basis of Benkova's analysis will be worth while. Although only the coefficients of P_2^1 and P_3^2 are obtained by Benkova, we can get the most probable conductivity-distribution in the same way just mentioned. Thus, the electrical conductivity is determined to be 5.0×10^{-11} *emu* in the core and also 5×10^{-12} *emu* in the mantle, while q_1 comes to be 0.94, that is, the thickness of the outermost non-conducting layer must be about 400 *km*. The comparison of the calculation to the actual analysis is shown in Table XI.

Table XI.

n	m	e_n^m/i_n^m		$\epsilon_n^m-\iota_n^m$	
		Cal.	Obs.	Cal.	Obs.
2	1	2.29	2.34	−5.0°	−5°
3	2	2.26	2.30	−4.9°	−5°

4. The distribution of the induced currents in the earth.

Now, let us investigate how deep the electric currents induced dy S_q penetrate into the earth.

As the relation between the current-density $\overrightarrow{c}$ and the vector potential $\overrightarrow{A}$ is given by

$$\overrightarrow{c}=-\sigma\frac{\partial\overrightarrow{A}}{\partial t},\ldots\ldots\ldots\ldots\ldots\ldots\ldots\ldots\ldots\ldots(4.1)$$

we get from (3.2)

$$\overrightarrow{c}_n^m=-\sigma a\frac{\partial f_n}{\partial t}[\overrightarrow{r}\,\mathrm{grad}\,S_n^m]\ldots\ldots\ldots\ldots\ldots\ldots\ldots\ldots(4.2)$$

corresponding to the harmonic whose degree and order are respectively n and m.

Considering (3.9), (3.10), (3.18) and (3.20), we can write the expressions of current-density for the mantle and the core in operational forms such as

$$\overrightarrow{c}_{n,2}^m=-\sigma_2ap\{\overline{C}_2(p)\rho^nF_n(k_2\rho a)+\overline{D}_2(p)\rho^{-n-1}G_n(k_2\rho a)\}e_n(t)[\overrightarrow{r}\,\mathrm{grad}\,S_n^m],\ldots(4.3)$$

$$\overrightarrow{c}_{n,3}^m=-\sigma_3ap\overline{C}_3(p)\rho^nF_n(k_3\rho a)e_n(t)[\overrightarrow{r}\,\mathrm{grad}\,S_n^m],\ldots\ldots\ldots\ldots\ldots\ldots\ldots\ldots\ldots\ldots(4.4)$$

where $\overline{C}_2(p)$, $\overline{D}_2(p)$ and $\overline{C}_3(p)$ are given by (3.22), (3.23) and (3.24). Putting $p=i\alpha$, we obtain current intensity for any value of ρ by taking the moduli of $\overrightarrow{c}_{n,2}^m$ and $\overrightarrow{c}_{n,3}^m$ which correspond respectively to the mantle and the core. As the calculation can be easily performed in the same way with that of mod $I(i\alpha)$ in Section 3, we shall only describe the results, neglecting the detail of the numerical calculation.

As determined in the foregoing Section of this Chapter, we take respectively 5.0×10^{-12} and 5×10^{-11} *emu* for the electrical conductivity in the mantle and the core on the basis of Benkova's analysis. The distribution of the current-intensity in such an earth's model is shown in Fig. 7 in arbitrary scale. The rate of decrease of the current intensity seems so rapid that it becomes practically zero at $\rho=0.7$, that is, at the depth of 2000 *km*. For this reason, the currents induced in the core are very small compared with those induced in the mantle. Accordingly, the contribution of the currents flowing

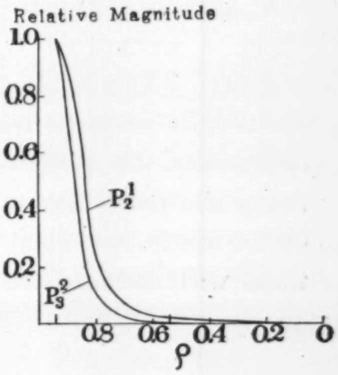

Fig. 7. The distribution of the induced currents in the earth.

in the core to the magnetic field at the earth's surface is very small. Thus, we must not forget that the determined conductivity of the core is rather ambiguous. The more accurate determination may only be effected by investigating much slower variation than S_q.

Indeed, considering that the contribution of the currents flowing in a thin shell whose radius is ρa to the magnetic field at the surface is proportional to $\rho^{n+2}|\overrightarrow{c}|$ for the harmonic whose degree is n, we obtain the contribution of the currents of any depth as shown in Fig. 8 for 24-hourly and 12-hourly components of S_q, where it is easily seen that 90% of the field are due to the currents flowing in the upper part of the mantle, from the surface of the mantle to the depth of 1400 *km* for 24-hourly component and 960 *km* for 12-hourly component. These estimates, however, are not quite accurate because the phase of the currents differ for different depths. But, as already pointed out by Chapman and Price[8)], the phase difference is slight, especially in high conducting sphere. Then, to a fair degree of approximation, we conclude that the magnetic field at the surface must be mainly due to the currents in the upper part of the mantle.

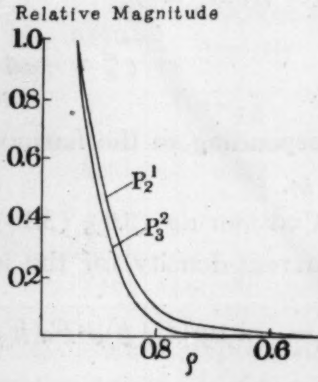

Fig. 8. The contribution of the currents to the magnetic field at the earth's surface.

Summarizing the results obtained in the present Chapter, we may say that the earth is composed of the outermost non-conducting layer, about 400 *km* in thickness, the mantle whose electrical conductivity amounts to 5.0×10^{-12} *emu*, and, as is well known from seismology, the core in which the conductivity seems likely to amount as much as ten times or more compared with that of the mantle. Though the determination of the conductivity in the core is rough, the results seem to be in accord with that of Lahiri and Price[10)] in which the increase of the conductivity with increasing depth was decisively reported. As to the more accurate determination of the conductivity in the deeper part of the earth, we must treat electromagnetic induction by much slower variations with induced currents which penetrate very deeply.

CHAPTER III. ELECTROMAGNETIC INDUCTION BY SOLAR DAILY DISTURBANCE VARIATION

(so-called S_D -field).

In a series of papers, Chapman[5, 27, 28] studied the average characteristics of magnetic disturbances or storms, deriving possible atmospheric current-systems for them. According to him, magnetic disturbances can be separated into storm-time (so-called D_{st}) and solar daily disturbance variation (so-called S_D). As already mentioned in Introduction, D_{st} was hitherto subjected to spherical harmonic analysis[4] with applications to the investigation on the earth's electrical state[8, 10]. On the other hand, S_D was not yet used for the problem in question.

On the basis of magnetic data collected by himself, Chapman proposed the atmospheric electric current-systems for S_D as shown in Fig. 9. Though the current-systems were derived for an ideal earth having its geomagnetic and geographic axes coincident, it is remarkable that the electric currents concentrate so intensely above the auroral zones that the currents above the polar caps and the low and middle latitude seem to be mere leak from the auroral zones. The characteristics of S_D current-systems was also theoretically confirmed by the writer[29] on the stand-point of "dynamo" -theory as well as the theory of bay-type disturbance.

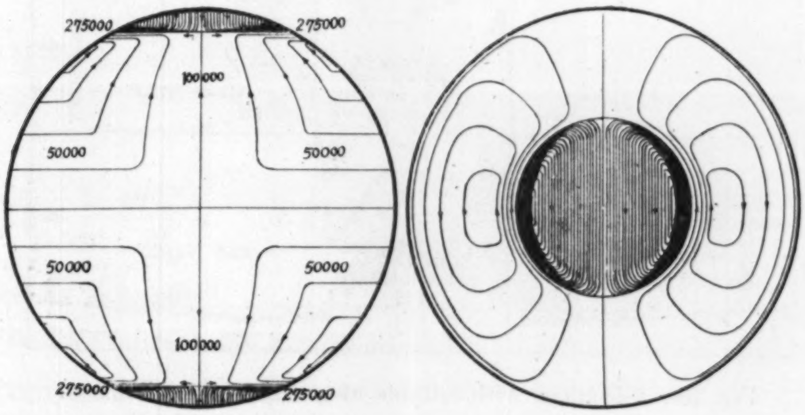

Fig. 9. Idealized current-systems in amperes for S_D, assuming magnetic and geographic axes coincident. Left: View from equator at noon meridian, Right: View from North Pole (After S. Chapman)

---

27) S. CHAPMAN, *Proc. Roy. Soc.* A, **115** (1927) 242.

28) S. CHAPMAN, *Terr. Mag.*, **40** (1935) 349.

29) T. RIKITAKE, *Rep. Ionos. Res. Japan*, **2** (1948), 57.

Since the feature of the current-systems for S_D differ very much from that for S on quiet days or S_q, it will be of interest and useful to check our foregoing studies by discussing the electromagnetic induction by S_D. However, we are obliged to treat our problem rather unsatisfactorily on account of the shortage of available data. So far as the writer could get, the most utilizable data were given by Vestine[30] who showed, as illustrated in Fig. 10, the variations with latitudes found in the maximum magnitudes of the components of S_D for dawn, noon, evening and midnight periods on the basis of data for the Second International Polar Year and auxiliary for various epochs from 1911 to 1933. With the aid of the smoothed curves drawn among the points given by observation, we can analyze in like manner with S_q. The separation of the magnetic potential into the external and the internal parts will be done only in the case of 24-hourly component because the variations of shorter period seem very small. Discussions on the phase difference between two parts will be neglected because the data are not satisfactory for this purpose.

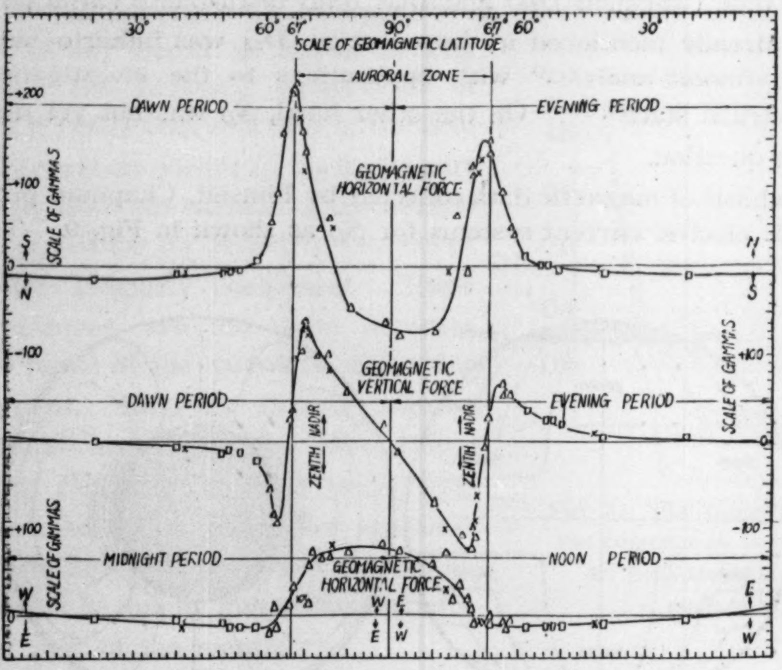

Fig. 10. Variations with latitude of maxima and minima of geomagnetic components of S_D for international disturbed minus quiet days.
(After E. H. Vestine)

When we assume that the variation depends solely on local time, the magnetic potential is generally expressed by

---

[30] E. H. VESTINE, *Terr. Mag.*, 43 (1938), 261.

$$W=\sum_{n=1}^{\infty}\sum_{m=0}^{n}\left\{\left(e_{n,a}^{m}\frac{r^n}{R^{n-1}}+i_{n,a}^{m}\frac{R^{n+2}}{r^{n+1}}\right)\cos mt\right.$$
$$\left.+\left(e_{n,b}^{m}\frac{r^n}{R^{n-1}}+i_{n,b}^{m}\frac{R^{n+2}}{r^{n+1}}\right)\sin mt\right\}P_n^m(\cos\theta) \quad\ldots\ldots\ldots\ldots\ldots(1)$$

in polar coordinate, where R denotes the earth's radius. As is well known, e_n^m's and i_n^m's are respectively the coefficients of the harmonics whose origin exist outside and within the earth. Then the components of the magnetic field at the earth's surface can be expressed as follows;

$$\left.\begin{array}{lll}
\text{North-component}: & X=\sum\limits_{n}\sum\limits_{m} n\{(e_{n,a}^{m}+i_{n,a}^{m})\cos mt & \\
 & \qquad +(e_{n,b}^{m}+i_{n,b}^{m})\sin mt\}\,X_n^m\,, & \\
\text{East-}\quad ,, & Y=\sum\limits_{n}\sum\limits_{m} n\{-(e_{n,a}^{m}+i_{n,a}^{m})\sin mt & \\
 & \qquad +(e_{n,b}^{m}+i_{n,b}^{m})\cos mt\}\,Y_n^m\,, & \\
\text{Downward-}\quad ,, & Z=\sum\limits_{n}\sum\limits_{m}\{(ne_{n,a}^{m}-\overline{n+1}\,i_{n,a}^{m})\cos mt & \\
 & \qquad +(ne_{n,b}^{m}-\overline{n+1}\,i_{n,b}^{m})\sin mt\}\,P_n^m\,. &
\end{array}\right\}\quad\ldots\ldots\ldots\ldots\ldots\ldots(2)$$

where

$$X_n^m=\frac{1}{n}\frac{dP_n^m}{d\theta}\,,\qquad Y_n^m=\frac{m}{n\sin\theta}P_n^m\,,\ldots\ldots\ldots\ldots\ldots\ldots\ldots\ldots\ldots(3)$$

as defined by Schmidt[31].

On the other hand, we get by means of spherical harmonic analysis

$$\left.\begin{array}{lll}
\text{North-component}: & X=\sum\limits_{n}\sum\limits_{m}(a_n^m\cos mt+b_n^m\sin mt)\,X_n^m\,, \\
\text{East-}\quad ,, & Y=\sum\limits_{n}\sum\limits_{m}(a_n^{m\prime}\,\mathrm{ccs}\,mt+b_n^{m\prime}\sin mt)\,Y_n^m\,, \\
\text{Downward-}\quad ,, & Z=\sum\limits_{n}\sum\limits_{m}(\tilde{a}_n^m\cos mt+\tilde{b}_n^m\sin mt)\,P_n^m\,.
\end{array}\right\}\quad\ldots\ldots\ldots(4)$$

Equating, then, the corresponding term of X and Z in (3) and (4), we have

$$n(e_{n,a}^{m}+i_{n,a}^{m})=a_n^m\,,\qquad n(e_{n,b}^{m}+i_{n,b}^{m})=b_n^m\,,$$

$$ne_{n,a}^{m}-\overline{n+1}\,i_{n,a}^{m}=\tilde{a}_n^m\,,\qquad ne_{n,b}^{m}-\overline{n+1}\,i_{n,a}^{m}=\tilde{b}_n^m\,.$$

Solving this we obtain

$$e_{n,a}^{m}=\frac{(n+1)\,a_n^m+n\tilde{a}_n^m}{n(2n+1)}\,,\qquad i_{n,a}^{m}=\frac{a_n^m-\tilde{a}_n^m}{2n+1}\,,\ \text{etc.}\ldots\ldots\ldots\ldots\ldots(5)$$

The same determination can be also done from Y and Z in (3) and (4).

---

31) AD. SCHMIDT, *Tafeln der Normierten Kugelfunktionen*, (1935).

Thus we can separate the external and internal parts of the magnetic potential from the combination of X, Z or Y, Z. In practice, the combination X and Z is taken in this Chapter.

In the case of S_D, b_n^m and $\tilde{b}_n^m$ are taken to be zero with suitable preference of the time origin, that is, it becomes, on the average, near 18 h of local time according to Vestine. Besides, as the 24-hourly component is the most predominant, we assume $m=1$. In that case we get from (4)

$$X=\sum_{n=1}^{\infty} a_n^1 X_n^1 \cos t\,, \quad \text{......................}(6)$$

$$Z=\sum_{n=1}^{\infty} \tilde{a}_n^1 P_n^1 \cos t\,. \quad \text{......................}(7)$$

On account of the orthogonality of $P_n{}^1$, the coefficients of (7) are given by

$$\tilde{a}_n^1=\frac{2n+1}{4\pi}\int_0^{\pi} Z(\theta)\, P_n^1 \sin\theta\, d\theta^{32)}. \quad \text{......................}(8)$$

To get $a_n{}^1$ from (6), we consider the expansion

$$X \sin\theta = \sum_{n=1}^{\infty} c_n^1 P_n^1 \cos t\,.$$

Meanwhile, it becomes by the well known recurrence formula

$$\begin{aligned} X \sin\theta &= \sum_{n=1}^{\infty} \frac{a_n^1}{n} \sin\theta \frac{dP_n^1}{d\theta} \cos t \\ &= \sum_{n=1}^{\infty} a_n^1 \frac{n+1}{2n+1} \left\{ \frac{\sqrt{(n+1)^2-1}}{n+1} P_{n+1}^1 - \frac{\sqrt{n^2-1}}{n} P_{n-1}^1 \right\} \cos t\,. \end{aligned}$$

Then, as is in the case of Z, multiplying both side of this equation by $P_s{}^1 \sin\theta$ and integrating from $\theta=0$ to $\theta=\pi$, we get

$$-a_2^1 \frac{3}{5} \frac{\sqrt{3}}{2} = c_1^1\,, \quad a_2^1 \frac{3}{5} \frac{\sqrt{8}}{3} - a_4^1 \frac{5}{9} \frac{\sqrt{15}}{4} = c_3^1\,,$$

$$a_4^1 \frac{5}{9} \frac{\sqrt{24}}{5} - a_6^1 \frac{7}{13} \frac{\sqrt{35}}{6} = c_5^1\,, \quad \text{........ ....}(9a)$$

or conversely

$$\begin{aligned} a_2^1 &= -1.92 c_1^1\,, \quad a_4^1 = -1.86\,(1.09 c_1^1 + c_3^1)\,, \\ a_6^1 &= -1.88\,(1.10 c_1^1 + 1.01 c_3^1 + c_5^1) \quad \text{...... ......}(9b) \end{aligned}$$

---

32) $$\begin{aligned} \int_0^{\pi} P_j{}^l P_k{}^l \sin\theta\, d\theta &= \frac{4}{2k+1} \quad \text{for } j=k \\ &= 0 \quad \text{for } j \neq k\,. \end{aligned}$$

where, as is easily gotten,

$$c_n^1 = \frac{2n+1}{4\pi} \int_0^\pi X(\theta)\, P_n^1 \sin^2\theta d\theta \;\ldots\ldots\ldots\ldots\ldots\ldots\ldots(10)$$

Here, the terms $n=2\nu$ $(\nu=1, 2, ..)$ are only taken into consideration because the current-systems concerned here are approximately symmetric with respect to the equator.

Applying the above mentioned theory to the mean values, X and Z obtained from Vestine's smoothed curves, we have

$$\left.\begin{array}{lll} a_2^1=13\,, & a_4^1=-12\,, & a_6^1=-46 \\ \tilde{a}_2^1=6.2\,; & \tilde{a}_4^1=-38\,, & \tilde{a}_6^1=-27 \end{array} \quad \text{(unit in } \pi\gamma)\right\} \ldots\ldots(11)$$

for the first three harmonics.

Then, calculating $e_n{}^1$ and $i_n{}^1$ by (5) and (11), we obtain the amplitude ratio $e_n{}^1/i_n{}^1$, which is given in Table XII together with that expected in Chapman's and Benkova's models[33] of the earth described in the preceding Chapter.

Table XII. The ratio of the external parts to the internal parts for three harmonics obtained from Vestine's data and expected from the theory of induction within Chapman's and Benkova's models.

n	m	Vestine	Chapman	Benkova
2	1	3.7	2.5	2.2
4	1	2.3	3.2	2.5
6	1	4.4	4.8	3.2

---

[33] In the case of the uniform core model, the amplitude ratio is given by

$$e_m^m/i_m^m = \frac{n+1}{n}\, q^{-2n-1}\sqrt{\frac{A^2+B^2}{(A-1)^2+B^2}}\,,$$

where

$$A = \frac{\beta}{2n+1}\left\{1+\frac{n}{\beta}+\frac{n(n+1)}{4\beta^2}\ldots\ldots\ldots\ldots\ldots\right\},$$

$$B = \frac{\beta}{2n+1}\left\{1-\frac{n(n+1)}{4\beta^2}-\frac{n(n+1)}{4\beta^3}\ldots\ldots\right\}.$$

In these expressions, β is calculated from

$$\beta^2 = \frac{4\pi^2\sigma m q^2 a^2}{24\times 60\times 60}$$

where σ, q, a denote respectively the specific electrical conductivity, the ratio of the radius of the core to that of the earth and radius of the earth.

Although the agreement between the values obtained from the actual data and the calculated ones based on the uniform core model is not quite well, it can be said approximately that the uniform core model is also roughly consistent with the electromagnetic induction by S_D, provided its conductivity amounts to the order of $10^{-12} \sim 10^{-13}$ *emu* and is covered by non-conducting layer of a few hundred *kilometers* in thickness besides.

It is desirable, however, that a more accurate discussion will be made in the future with the aid of more complete data of S_D.

CHAPTER IV. ELECTROMAGNETIC INDUCTION BY STORM-TIME VARIATION (so-called D_{st}-field).

The theory of induction by aperiodic fields in a uniformly conducting sphere was developed by Price[6), 7)], being applied to the induction by storm-time variation or D_{st}-field by Chapman and Price[8)]. Lahiri and Price[10)] also studied the induction in a non-uniform sphere with applications to the conductivity-distribution in the earth which is compatible with both S_q and D_{st}.

According to these studies, the conductivity in the core obtained from the investigations on D_{st} became larger than that of S_q as a whole, that is, it amounts to the order of 4×10^{-12} *emu*. Taking into consideration that the induced currents penetrate deeper in the case of D_{st} than of S_q, the conductivity must increase considerably with increasing depth as shown in the study of non-uniform core.

However, their discussions on the discrepancies between the results of S_q and D_{st} are all based upon the well known Chapman's analysis[3)] of S_q, which has better be criticized on the stand-point of recent investigations. As already mentioned in Section 2, Chapter II, we have, at the present stage of investigation, reasons to believe that the analyses carried out by Hasegawa and Benkova are more reliable than Chapman's one. Then, it will be worthwhile to treat the problem on the basis of newly made analyses.

Since the conductivity in the uniformly conducting core must amount to about 5×10^{-12} *emu* using Benkova's results, as Nagata[34)] pointed out, the discrepancies between the results obtained from observations and those of calculation on the basis of Chapman's model ($\sigma = 3.6 \times 10^{-13}$ *emu*, $q = 0.97$) is almost overcome leaving a small difference between the actual analysis and the calculation. For this reason, it is roughly satisfactory for us, as a first approximation, to take a uniformly conducting sphere in which the conductivity amounts to 5×10^{-12} *emu* being covered by non-conducting layer of 400 *km* in

---

34) T. NAGATA, Read at the Dec. Meeting of the Geophysical Institute, Tokyo Imperial University, 1946.

its thickness as the possible model of the earth compatible not only with S_q but also with D_{st}.

Next, taking into consideration that the conductivity in the core seems likely to be about ten times larger than in the mantle in the case of S_q, we shall discuss the electromagnetic induction by D_{st} in the earth's model described in Chapter II.

According to Chapman and Whitehead[4], the magnetic potential of magnetic storms in the low and middle latitude is expressible on the average by

$$W=a\sum_{n=1,3,5}\{e_n(t)\,(r/a)^n+i_n(t)\,(a/r)^{n+1}\}\,P_n(\cos\theta)\ \dots\dots\dots\dots\dots\dots(1)$$

where a denotes the radius of the earth. Among these harmonics, the term $n=1$ is the most important. Then the discussion will be limitted to the case $n=1$. The variations of e_1 and i_1 with time were given by Chapman and Price[8] as reproduced in Fig. 11.

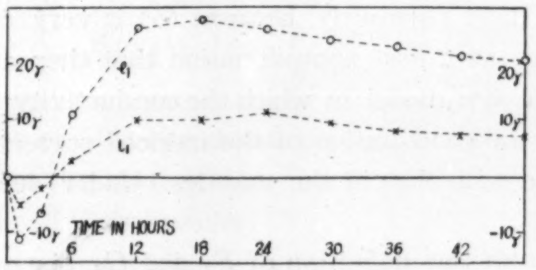

Fig. 11. (After S. Chapman and A. T. Price).

As has been done by Lahiri and Price[10], e_1 is expressed by

$$e_1(t)=Ae^{-\omega t}H(t)\ \text{or}\begin{cases}=Ae^{-\omega t} & (t>0)\\ =\ 0 & (t<0)\end{cases}\dots\dots\dots\dots\dots\dots\dots\dots(2)$$

after 18 hours passed from the beginning neglecting the initial phase, where

$$A=28\,\gamma\ ,\quad \omega=3.2\times10^{-6}\,sec^{-1}\,.$$

$H(t)$ denotes the Heaviside unit function. Writing in operational form, we get

$$e_1(t)=\frac{Ap}{p+\omega}H(t)\,.\dots\dots\dots\dots\dots\dots\dots\dots\dots\dots(3)$$

Then it becomes by (3.17) of Chapter II

$$i_1(t)=\frac{Ap\,I(p)}{p+\omega}\,H(t)\ \dots\dots\dots\dots\dots\dots\dots\dots\dots\dots(4)$$

where, as easily gotten from (3.21) of Chapter II, $I(p)$ is given by

$$I(p)=-\frac{q_1^3}{2}\,\frac{\left\{1-\frac{F_0(2,1)}{F_1(2,1)}\right\}\left\{1-\frac{F_0(3,2)}{F_1(3,2)}-\frac{G_2(2,2)}{G_1(2,2)}\right\}+\tau^3\left\{\frac{F_0(3,2)}{F_1(3,2)}-\frac{F_0(2,2)}{F_1(2,2)}\right\}\frac{F_1(2,2)}{F_1(2,1)}\,\frac{G_1(2,1)}{G_1(2,2)}}{\frac{F_0(2,1)}{F_1(2,1)}\left\{1-\frac{F_0(3,2)}{F_1(3,2)}-\frac{G_2(2,2)}{G_1(2,2)}\right\}+\tau^3\left\{1-\frac{G_2(2,1)}{G_1(2,1)}\right\}\left\{\frac{F_0(3,2)}{F_1(3,2)}-\frac{F_0(2,2)}{F_1(2,2)}\right\}\frac{F_1(2,2)}{F_1(2,1)}\,\frac{G_1(2,1)}{G_1(2,2)}} \tag{5}$$

Considering that the mantle shields the core and consequently the induced currents in the mantle contribute to the magnetic field at the surface in the main, the second terms of the numerator and the denominator of the righthand-side of (5) must be small compared with the first terms[35].

Solving the operational equation (4), we get

$$i_1(t)=\frac{A}{2\pi i}\int_L e^{pt}\frac{I(p)}{p+\omega}\,dp\ , \qquad\ldots\ldots\ldots\ldots\ldots\ldots\ldots\ldots\ldots\ldots\ldots(6)$$

where the path of integration L is taken to be Bromwich's one having all singularities on its lefthand-side in the complex plane. As to the singularities, it is difficult to get them rigorously because (5) is very complicated. However, we may assume as a first approximation that they are the same with those of the uniform core model in which the conductivity is equal to that of the mantle because the contribution of the induced current in the core seems very small compared with that in the mantle. Under such assumption, we shall calculate $i_1(t)$.

As is obvious from the definition of F_n and G_n, since it becomes in the case of $n=1$ that

$$\left.\begin{aligned}
F_0(k_\nu q_\mu a)&=\frac{\sinh(k_\nu q_\mu a)}{k_\nu q_\mu a}\ ,\\
F_1(k_\nu q_\mu a)&=\frac{3}{(k_\nu q_\mu a)^2}\left\{\cosh(k_\nu q_\mu a)-\frac{\sinh(k_\nu q_\mu a)}{k_\nu q_\mu a}\right\},\\
G_1(k_\nu q_\mu a)&=e^{-k_\nu q_\mu a}(1+k_\nu q_\mu a)\ ,\\
G_2(k_\nu q_\mu a)&=e^{-k_\nu q_\mu a}\left\{1+k_\nu q_\mu a+\frac{(k_\nu q_\mu a)^2}{3}\right\},
\end{aligned}\right\}\qquad\ldots\ldots\ldots\ldots\ldots\ldots(7)$$

the poles are approximately given by the roots of

$$\sinh(k_2q_1a)=0 \qquad (k_2^2=4\pi\sigma_2 p)\ldots\ldots\ldots\ldots\ldots\ldots\ldots(8)$$

as well as $-\omega$. Then, denoting the successive pole by $-\alpha_s$, we get

$$\alpha_s=\left(\frac{\pi s}{\kappa_{21}}\right)^2,\ s=1,2,3,\ldots\ldots\ldots\ldots \qquad \ldots\ldots\ldots\ldots\ldots\ldots(9)$$

---

[35] Really, we get the expression for uniformly conducting sphere neglecting the second terms.

where

$$\kappa_{21}^2=4\pi\sigma_2 q_1^2 a^2 \,. \qquad\qquad (10)$$

Then taking into consideration that the integral along the circumference of the semi-circle vanishes at infinity, the contour-integration shown in Fig. 12 gives when the radius of the semi-circle becomes infinitely large

$$\boldsymbol{i}_1(t)=A\left[e^{-\omega t}I(-\omega)+\frac{3q_1^3}{\kappa_{21}^2}\sum_{s=1}^{\infty}\frac{e^{-\alpha_s t}}{\alpha_s-\omega}\{1+\tau^3\phi(-\alpha_s)\}\right] \qquad (11)$$

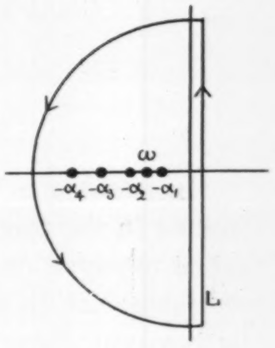

Fig. 12.

where

$$\phi(p)=\frac{F_1(2,2)\left\{\dfrac{F_0(3,2)}{F_1(3,2)}-\dfrac{F_0(2,2)}{F_1(2,2)}\right\}\dfrac{G_1(2,1)}{G_1(2,2)}}{\{F_1(2,1)-F_0(2,1)\}\left\{1-\dfrac{F_0(3,2)}{F_1(3,2)}-\dfrac{G_2(2,1)}{G_1(2,2)}\right\}} \qquad (12)$$

The calculated values of $\boldsymbol{i}_1(t)$ are shown in Fig. 13 together with those based on Benkova's model of the earth. The results of the analysis are also illustrated there. The small discrepancies between the observation and the calculation based on the uniform core model improved by introducing the core in which the conductivity is about ten times larger than the mantle.

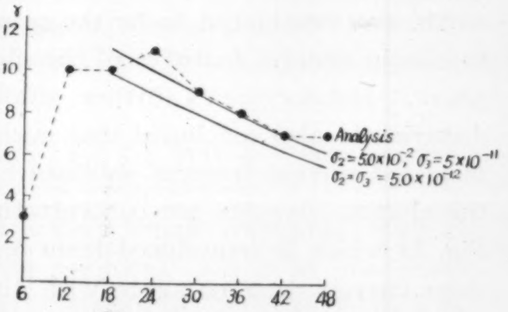

Fig. 13. Comparison of the theoretical values to the analysis.

Although the calculation carried out in this Chapter is rather rough, we may say that the electrical model of the earth obtained from the study on S_q is also compatible with the electromagnetic induction by storm-time variation.

According to Chapman and Price[10)], the core in which $\sigma=4.4\times10^{-12}$ *emu* $q=0.94$ appears to be about right for the explanation of D_{st}, while the size and conductivity in the present model fairly agree with these values. Taking into consideration that the inner core is shielded by the outer layer, then, the distribution of the electric currents in the mantle will be almost the same with that obtained by Chapman and Price. Hence we cease to study the penetration of the induced currents.

CHAPTER V. ELECTROMAGNETIC INDUCTION BY BAY-TYPE DISTURBANCE.

1. Morphology of bay-type disturbance.

In addition to the variations in the earth's magnetic field which were studied in the foregoing Chapters, we have a kind of magnetic disturbance called bay-type disturbance. Because the form of the magnetographic record resembles bay in a sea-coast. In this Chapter, the electromagnetic induction by bay-type disturbance will be investigated in the same way with the treatments of the former Chapters.

According to the studies which were carried out up to this time, it was established that the bay-type disturbance occurs nearly at the same time all over the world durating 1~5 *hours*. Its maximum amplitude often reaches to about 100 *gammas* in the middle latitudes. Among these investigations[36),37),38),39),40)] on the bay-type disturbance, Hatakeyama's[41)] investigation is one of the most excellent. In the first place, examining a large number of magnetograms obtained at Toyohara Magnetic Observatory in Sagalien, he determined both directions and magnitudes of disturbing magnetic forces and consequently those of electric currents, which, being distributed in the upper atmosphere of the earth, are considered to be the primary origin of the disturbance, and tried to obtain general features of the electric current-systems in the upper atmosphere. Hatakeyama's further studies on the world-wide character of this disturbance also concluded that such electric current-systems must exist. The idealized current-systems obtained by him seems to be fixed to the sun while the electric currents are concentrating above the auroral zones as shown in Fig. 14 which is reproduced from his original paper. We can easily see that these current-systems agree with those of S_D as already shown in Fig. 9 which was obtained by Chapman. Meanwhile, the present writer[29)] mathematically studied the mechanism of occurrence of the bay-type disturbance and S_D on the basis of " dynamo "-action in the ionosphere where the air is electric-

---

36) L. STEINER, *Terr. Mag.*, 26 (1921), 1.

37) LUBIGER, *Diss. Göttingen* (1924).

38) E. WIECHERT, *Mitt. Geophys. Warte Gr. Raum, Königsberg*, Nr. 22 (1934).

39) K. BIRKELAND, *The Norwegian Aurora Polaris Expedition*, 1902-1903, I and II (1908).

40) A. G. MCNISH, *Trans. Edinburgh Meeting Internat. Union Geod. Geophys. Ass. Terr. Mag. Electr. Bull.*, 10 (1937).

41) H. HATAKEYAMA, *Geophys. Mag.*, 11 (1937), 1 and 12 (1938), 15.

ally conducting. In that study, it was assumed that the conductivity above the auroral zones is very high compared with that of the middle and low latitudes

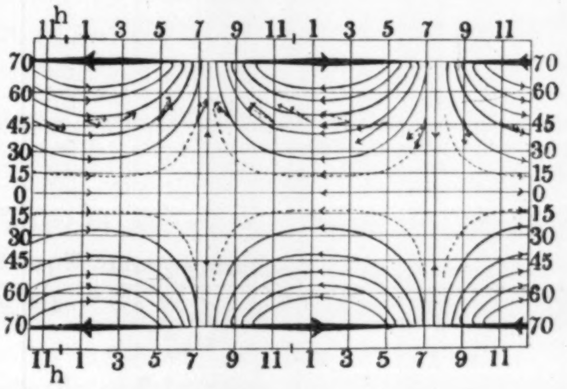

Fig. 14. Current-arrows at Toyohara and current-systems for bay-type disturbance. Broken arrows represent the disturbing forces at t_2 and thick arrows represent those at t_3. t_2 and t_3 are defined in the next Section. (After H. Hatakeyama)

with Störmer-Birkelands' theory in mind. According to the results of the writer's theoretical investigation, the current-function R_D which corresponds to the current-systems in question is given by

$$R_D = KCk_1^1C_5 \cot\theta \sin(t+\alpha_1^1)$$

in the middle and low latitudes, where K, C, $k_1{}^1$, C_5 and $\alpha_1{}^1$ are constants. θ and t denote the colatitude and the local time respectively.

As the height of the electric currents is very small compared with the radius of the earth, the components of the magnetic forces at the earth's surface which are produced by these electric current-systems, vary, to a fair degree of approximation, with θ as $\frac{d}{d\theta}\cot\theta$, $\frac{\cot\theta}{\sin\theta}$ and $\cot\theta$ in X, Y and Z respectively. Thus the magnetic field increases remarkably with increase of latitude. Then, if we take the usual spherical harmonics which are defined in the region including $\theta=0$ and $\theta=\pi$, we must take a large number of higher harmonics to express the distribution of these magnetic fields. This procedure seems to be too troublesome and less reliable to analyze the actual data except the case in which the distribution is given everywhere all over the earth. Actually the mean disturbing forces of the bay-type disturbance of Feb. 24, 1933,[42] are such as shown in Figs. 15 and 16, where, assuming that the components of the disturbing forces vary as the sine and cosine of longitude on the same latitude, Y and Z are respectively reduced on $\phi=0°$ and $\phi=90°$ meridian with respect to the geomagnetic coordinate.

---

[42] The data used in this Chapter are all taken from Hatakeyama's paper.

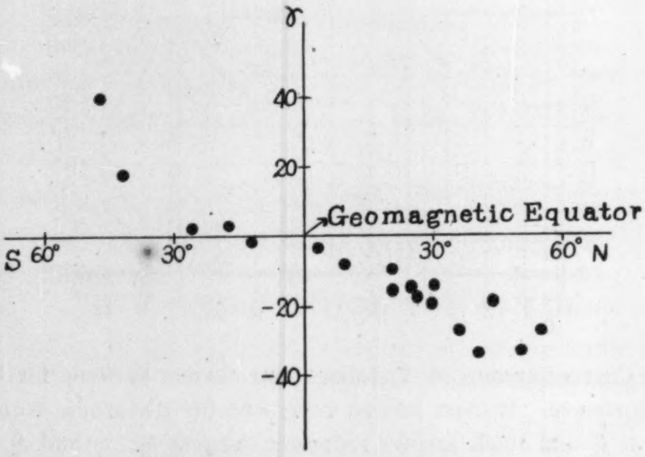

Fig. 15. The east component of the mean disturbing force of bay-type disturbance, Feb. 24, 1933. (Reduced on $\phi=0°$ meridian)

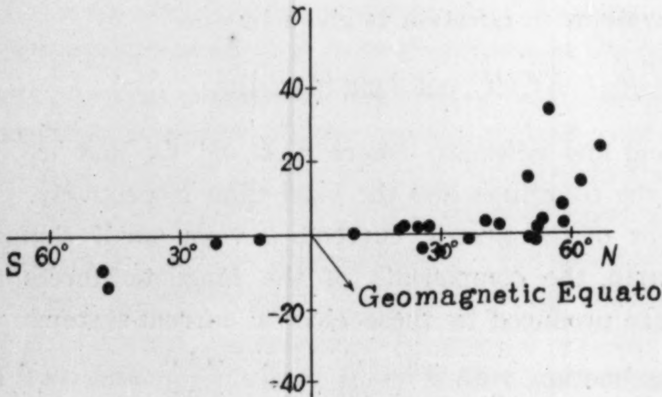

Fig. 16. The vertical component of the mean disturbing force of the bay-type disturbance, Feb. 24, 1933. (Reduced on $\phi=90°$ meridian)

2. The analysis of bay-type disturbances.

In order to analyze Hatakeyama's data, we shall introduce a system of functions which satisfy

$$\frac{d^2U}{d\theta^2}+\cot\theta\,\frac{dU}{d\theta}+\left\{n\,(n+1)-\frac{m^2}{\sin^2\theta}\right\}U=0 \quad \text{.................}(2.1\text{a})$$

in the region excluding both the north and south poles.

As is well known[43], (2.1 a) or

$$(1-\mu^2)\,\frac{d^2U}{d\mu^2}-2\mu\,\frac{dU}{d\mu}+\left\{n\,(n+1)-\frac{m^2}{1-\mu^2}\right\}U=0 \quad (\mu=\cos\theta) \quad \text{...}(2.1\text{b})$$

are satisfied by $P_n^m(\mu)$ or $Q_n^m(\mu)$ provided $\mu^2<1$, where

$$P_n^m=(1-\mu^2)^{m/2}\,\frac{d^mP_n}{d\mu^m}\,,\quad Q_n^m=(1-\mu^2)^{m/2}\,\frac{d^mQ_n}{d\mu^m}\,.$$

In like manner with the usual spherical harmonic analysis, we can generally express the magnetic potential of the disturbance as follows;

$$\begin{aligned} W=\sum_n\sum_m\Bigg\{&\left(e_{n,a}^m\,\frac{r^n}{R^{n-1}}+i_{n,a}^m\,\frac{R^{n+2}}{r^{n+1}}\right)\cos m\,\phi \\ &+\left(e_{n,b}^m\,\frac{r^n}{R^{n-1}}+i_{n,b}^m\,\frac{R^{n+2}}{r^{n+1}}\right)\sin m\phi\Bigg\}P_n^m(\cos\theta) \\ +\sum_n\sum_m\Bigg\{&\left(\tilde{e}_{n,a}^m\,\frac{r^n}{R^{n-1}}+\tilde{i}_{n,a}^m\,\frac{R^{n+2}}{r^{n+1}}\right)\cos m\,\phi \\ &+\left(\tilde{e}_{n,b}^m\,\frac{r^n}{R^{n-1}}+\tilde{i}_{n,b}^m\,\frac{R^{n+2}}{r^{n+1}}\right)\sin m\,\phi\Bigg\}Q_n^m(\cos\theta) \quad \text{......}(2.2) \end{aligned}$$

where R denotes the radius of the earth and the coordinates are taken to be geomagnetic. In the case of the bay-type disturbance, however, as the magnetic potential of the disturbing forces are nearly symmetric with respect to the geomagnetic equator as shown in Fig. 14, it is approximately sufficient for the present analysis to take into consideration only the terms which are odd functions of μ. Then, we only deal with P_n^m's where $n+m$ is odd and Q_n^m's where $n+m$ is even. Besides, as the disturbing forces seem to vary as the sine or cosine of longitude on the same latitude, the greatest part of the magnetic potential must be expressible with the sum of $P_n{}^1 \genfrac{}{}{0pt}{}{\cos\phi}{\sin\phi}$ and $Q_n{}^1 \genfrac{}{}{0pt}{}{\cos\phi}{\sin\phi}$. Meanwhile, we see in Figs. 15 and 16 that the east and vertical components both reduced on the meridian on which they become maximum increase monotonously with latitude changing the sign approximately at the equator. This fact suggests that the term including Q_1^1 [44] occupies the main part of the potential function of the disturbing forces. Thus, so far as we discuss the magnetic disturbance in the low and middle latitudes such as from 0° to 45°, we may assume without serious danger that the magnetic potential can be expressed by

---

[43] e. g. E. W. HOBSON, "*The Theory of Spherical and Ellipsoidal Harmonics,*" (1931).

$$W=\left\{\left(e_a r+i_a\frac{R^3}{r^2}\right)\cos\phi+\left(e_b r+i_b\frac{R^3}{r^2}\right)\sin\phi\right\}Q_1^1 . \;\ldots\ldots\ldots\ldots(2.3)$$

Q_1^1 and $Q_1^1/\sin\theta$ are shown graphically in Fig. 10. From (2.3), we get the magnetic forces at the surface $(r=R)$ as follows;

$$\left.\begin{aligned} X&=\{(e_a+i_a)\cos\phi+(e_b+i_b)\sin\phi\}\frac{dQ_1^1}{d\theta},\\ Y&=\{-(e_a+i_a)\sin\phi+(e_b+i_b)\cos\phi\}\frac{Q_1^1}{\sin\theta},\\ Z&=\{(e_a-2i_a)\cos\phi+(e_b-2i_b)\sin\phi\}\,Q_1^1 . \end{aligned}\right\}\ldots(2.4)$$

Then we can determine e_a+i_a and e_b+i_b from the observed data of X or Y and also e_a-2i_a and e_b-2i_b from that of Z by means of the method of least squares. Combining these coefficients we can calculate e_a, i_a, e_b and i_b. Thus the separation of the disturbing forces into the external and internal parts is over.

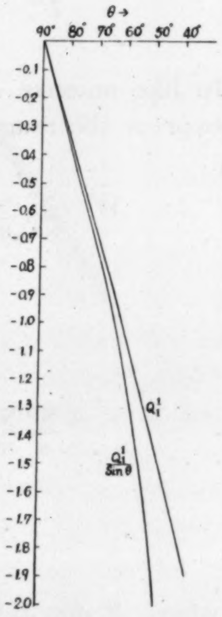

Fig. 17.

As to the application of the method described above to the actual problem, the writer used the data published by Hatakeyama who divided the course of a bay-type disturbance into six parts of equal time-interval, say t_0t_1, t_1t_2, ... , t_5t_6 determining the deviation of each component from the normal curve at t_1, t_2, ... , t_5. He collected copies of magnetograms sent from many observatories (about 30 in number) distributed widely over the earth. The determination of the disturbing forces was made in the case of the bay-type disturbances of Aug. 28, Sept. 23, 1932, Feb. 24 and Apr. 10, 1933 as reproduced in Tables XIII, XIV, XV and XVI.

Selecting the data of 16 stations whose geomagnetic latitudes are all less than 45°, the writer determined e_a, i_a, e_b and i_b from the combination of Y and Z. For example, they are tabulated in Table XVII in the case of the

---

44) $Q_1^1=-2(1-\mu^2)^{1/2}\mu\left(1+\frac{2}{3}\mu^2+\frac{3}{5}\mu^4+\ldots\ldots\right)$.

Table XIII. Disturbing forces during the bay-type disturbance of Aug. 28, 1932. (After H. Hatakeyama)

Station	Geomag-netic latitude	Geomag-netic longitude	2 *h* 10 *m*			2 *h* 43.5 *m*			3 *h* 17 *m*		
			α	ΔH	ΔZ	α	ΔH	ΔZ	α	ΔH	ΔZ
Toyohara	36.°4	206.°5	S 4°W	109γ	-2γ	S23°W	101γ	-2γ	S38°W	43γ	$+1\gamma$
Kakioka	26. 0	206. 0	S26 W	53	−34	S26 W	53	−22	S38 W	33	− 3
Tsingtau	24. 7	188. 3	S12 W	63	− 6	S23 W	50	− 6	S54 W	31	− 4
Lu-Kia-Pang	20. 0	189. 1	S13 W	67	—	S20 W	54	—	S50 W	33	—
Antipolo	3. 3	189. 8	S 7 E	35	−11	S 7 E	23	− 8	S29 W	21	− 5
Kuyper	−17. 4	175. 7	S	34	−14	S34 E	14	− 3	S45 E	6	+ 3
Watheroo	−41. 8	185. 6	S32 E	80	+ 5	S56 E	74	+19	S60 E	24	+ 5
Toolangi	−46. 7	220. 8	S15 E	119	−28	S27 E	96	−31	S23 E	52	−19
Christchurch	−48. 0	252. 6	S 2 E	89	−11	S 7 E	46	−15	S 5 E	37	− 6
Apia	−16. 0	260. 2	S 7 E	62	—	S 9 E	59	—	S19 E	31	—
Honolulu	21. 0	266. 5	S11 E	60	+ 2	S 8 E	61	+ 1	S 7 E	35	+ 3
Sitka	60. 0	275. 4	N27 E	174	+189	N63 E	68	+121	S81 E	20	+73
Agincourt	55. 0	347. 0	N28 E	126	−59	S75 E	99	−33	S62 E	60	− 7
Cheltenham	50. 1	350. 5	N38 E	134	−55	S35 E	76	−28	S50 E	68	−25
Tucson	40. 4	312. 2	S82 E	146	+14	S51 E	45	+ 5	S 3 E	50	+ 2
Teoloyucan	29. 6	326. 8	N87 E	77	+ 7	S31 E	31	− 1	S22 E	48	−11
San Juan	29. 9	3. 4	N 3 E	52	−11	N79 E	5	− 6	S43 E	22	− 8
Huancayo	−0. 6	353. 8	N 4 W	51	− 6	S35 W	40	−14	S 9 W	44	− 6
Dehra Dun	20. 5	149. 9	S11 W	26	− 2	N14 W	8	+10	N41 W	9	+ 4
Alibag	9. 5	143. 6	S17 E	17	+ 3	N51 E	13	+10	N30 E	8	+ 7
Helwan	27. 2	106. 4	N45 E	50	−10	N 1 W	54	−14	N11 W	32	− 4
Ebro	43. 9	79. 7	N 8 E	49	−20	N29 E	63	−16	N34 E	37	+ 1
Coimbra	45. 0	70. 2	—	—	—	—	—	—	—	—	—
Val-Joyeux	51. 3	84. 5	N38 W	46	−22	N20 E	59	−22	N41 E	38	−16
De Bilt	53. 8	89. 4	N21 W	45	−49	N41 E	69	−63	N55 E	47	−39
Seddin	52. 4	97. 0	N54 W	56	−44	N14 E	64	−52	N24 E	45	−34
Swider	50. 6	104. 6	N60 W	66	+27	N 6 W	61	+25	N 1 W	39	+20
Lovö	58. 1	105. 8	S63 W	112	−190	N55 W	28	−149	N 5 E	33	−61
Eskdalemuir	58. 5	82. 9	S17 W	27	−140	N56 E	37	−122	N50 E	34	−71
Lerwick	62. 6	88. 6	S 7 W	398	−270	S10 W	174	−250	S 6 E	62	−135
Tromsö	67. 1	116. 7	S37 W	248	+711	S26 W	743	+77	S25 W	248	−291
Vassouras	−11. 9	23. 9	N 8 W	57	—	N63 W	25	—	S55 W	21	—
Mauritius	−26. 6	122. 4	N64 E	30	+ 5	N54 E	44	+ 8	N58 E	32	+ 9

(Each element for 1 *h* 03 *m* and 4 *h* 24 *m* was assumed to be undisturbed.)

Table XIV. Disturbing forces during the bay-type disturbance of Sept. 23, 1932. (After H. Hatakeyama)

Station	19 *h* 48 *m*			20 *h* 18 *m*			20 *h* 48 *m*			21 *h* 18 *m*		
	α	ΔH	ΔZ	α	ΔH	ΔZ	α	ΔH	ΔZ	α	ΔH	ΔZ
Toyohara	S28°W	15γ	+1γ	S34°W	18γ	+2γ	S54°W	32γ	+2γ	S63°W	33γ	+3γ
Kakioka	S56 W	7	− 2	S52 W	11	− 3	S73 W	24	− 2	S79 W	20	+ 3
Tsingtau	S76 W	8	− 1	S37 W	10	− 2	S75 W	27	− 2	N85 W	25	0
Lu-Kia-Pang	S81 W	6	0	S45 W	11	− 1	S73 W	24	− 3	N70 W	23	− 3
Antipolo	—	0	+ 2	S	9	0	S63 W	11	+ 2	N73 W	10	0
Kuyper	N60 E	14	+ 2	N83 E	8	+ 3	S59 E	6	0	N43 E	18	+10
Watheroo	S83 E	42	+25	S86 E	31	+20	S80 E	35	+17	N89 E	50	+34
Toolangi	S18 E	25	− 5	S46 E	30	−13	S31 E	26	−10	S48 E	36	−14
Christchurch	S67 W	15	+ 4	S48 W	24	+ 2	S49 W	20	+ 2	S24 W	32	+ 1
Apia	S	6	—	S20 W	12	—	S 6 W	19	—	S21 W	17	—
Honolulu	S81 W	12	− 6	S40 W	8	− 7	S49 W	23	−15	S39 W	19	−10
Sitka	N27 W	30	+15	N63 E	27	+ 6	N31 W	12	+13	N76 E	4	+ 7
Agincourt	S41 W	28	+ 6	N18 W	26	+ 4	S32 W	21	+16	S63 E	20	+15
Cheltenham	S28 W	26	+ 2	N 3 E	17	+ 6	S 8 W	27	+ 6	S57 E	30	+14
Tucson	S77 W	9	+ 1	S59 W	6	+ 3	S13 W	13	+ 2	S19 W	18	+ 2
Teoloyucan	S	8	+ 2	S16 W	7	+ 1	S18 W	22	+ 4	S12 W	24	+ 3
San Juan	S 5 W	11	+ 1	S18 E	6	− 1	S11 E	20	+ 2	S45 E	18	− 2
Huancayo	S15 W	30	+ 1	S 9 E	12	+ 2	S 3 W	39	+ 1	S 8 W	21	0
Dehra Dun	N28 W	28	+ 5	N60 W	8	+ 1	N29 W	37	+ 9	N22 W	43	+ 5
Alibag	N	25	− 4	N 4 W	13	0	N11 W	26	− 7	N 6 W	41	+ 2
Helwan	N12 E	30	−13	N34 W	19	− 2	N 9 E	52	−19	N 6 E	51	−11
Ebro	S89 E	53	−19	N16 E	18	−10	N60 E	82	−32	N34 E	50	−11
Val-Joyeux	S79 E	65	+ 1	N 2 E	24	0	N67 E	71	− 9	N43 E	50	− 5
De Bilt	N80 E	101	−15	S83 E	23	+ 2	N59 E	91	−30	N68 E	51	−14
Seddin	N80 E	83	− 5	N80 W	18	0	N42 E	96	−25	N33 E	60	−14
Swider	N64 E	72	− 8	N12 W	14	+ 6	N28 E	74	− 3	N37 E	59	+ 5
Lovö	—	—	—	W	1	−15	N42 E	57	−61	N74 E	59	−41
Eskdalemuir	W	26	+ 9	N18 W	13	− 9	N53 E	100	−27	S84 E	30	−27
Lerwick	S64 E	100	−22	S14 W	54	−49	S73 E	75	−131	S39 E	59	−106
Tromsö	N20 E	90	0	S68 W	57	+97	S42 E	39	+189	S 1 E	177	+144
Vassouras	S12 E	14	—	S	7	—	S 4 E	16	—	W	6	—
Mauritius	N12 E	24	− 2	N22 W	11	+ 1	N 9 E	37	0	N12 E	40	+ 3

(Each element for 19 *h* 18 *m* and 22 *h* 18 *m* was assumed to be undisturbed.)

Table XV. Disturbing forces during the bay-type disturbance of Feb. 24, 1933. (After H. Hatakeyama)

Station	11 *h* 36 *m*			11 *h* 51 *m*			12 *h* 06 *m*			12 *h* 21 *m*		
	α	ΔH	ΔZ	α	ΔH	ΔZ	α	ΔH	ΔZ	α	ΔH	ΔZ
Toyohara	N80°E	36γ	0γ	N75°E	38γ	+1γ	N40°E	35γ	+1γ	N67°E	15γ	+1γ
Kakioka	N69 E	25	− 1	N44 E	37	+ 8	N43 E	25	+ 3	N63 E	11	− 3
Tsingtau	S75 E	24	+ 2	N58 E	32	0	N58 E	22	− 2	N67 E	8	− 1
Zô-se	S70 E	20	− 1	N67 E	30	− 4	N66 E	22	− 2	N80 E	11	− 1
Antipolo	S51 E	6	+ 2	N36 E	14	+ 6	N49 E	11	+ 2	N67 E	8	− 2
Kuyper	S	15	− 6	N63 W	5	− 8	N18 E	6	− 4	N45 E	6	− 2
Watheroo	S48 E	30	−30	N73 W	30	−18	N61 W	13	− 7	N	2	+ 1
Toolangi	S86 W	66	+ 1	N48 W	45	+15	N37 W	21	+13	N	2	+ 7
Christchurch	N44 W	81	+22	N25 W	47	+ 7	N33 W	20	+ 2	N68 W	5	+ 2
Apia	N51 W	28	—	N12 W	25	—	N12 W	14	—	N45 W	6	—
Honolulu	N 7 W	33	+ 3	N20 W	33	− 5	N30 W	20	− 6	N16 W	7	− 1
Sitka	S69 W	126	−78	S46 W	144	−121	S18 W	93	−118	S11 W	43	−76
Agincourt	S39 W	77	− 8	S48 W	88	− 8	S40 W	42	− 9	S45 W	14	− 6
Cheltenham	S58 W	45	− 3	S57 W	68	− 7	S69 W	39	+ 7	S75 W	20	− 7
Tucson	N59 W	51	− 1	N67 W	48	− 3	N70 W	23	− 4	N79 W	10	− 3
Teoloyucan	N60 W	28	+ 4	N69 W	30	+ 3	N67 W	21	+ 2	N74 W	7	+ 1
San Juan	W	18	+ 3	S82 W	22	+ 3	W	18	+ 1	N81 W	12	0
Huancayo	S18 W	13	+ 3	S34 W	19	+ 5	S42 W	16	+ 5	S39 W	19	+ 4
Dehra Dun	S11 E	32	− 2	S39 E	28	0	S61 E	21	+ 2	S45 E	6	+ 4
Alibag	S14 E	21	+ 3	S26 E	30	+ 3	S43 E	21	0	S41 E	9	− 6
Helwan	S 7 W	24	+ 9	S 2 E	28	+ 8	S13 E	13	0	E	2	− 3
Ebro	S18 W	22	+ 5	S13 W	37	+ 9	S 9 W	22	0	S15 E	11	− 4
Coimbra	S 7 W	26	—	S 7 W	43	—	S 8 W	27	—	S 9 E	13	—
Val-Joyeux	S 9 W	26	+ 1	S 9 W	37	0	S16 W	22	− 3	S10 W	11	− 3
De Bilt	S 4 W	43	+ 8	S 8 W	44	+ 4	S21 W	19	0	S84 E	9	+ 5
Seddin	S18 W	32	+ 6	S11 W	48	+ 4	S12 W	25	0	S14 W	8	− 1
Swider	S17 W	30	+ 5	S11 W	38	0	S11 W	20	− 6	S	5	− 3
Lovö	S19 W	37	− 2	S16 W	41	+ 8	S18 W	23	+15	S49 W	11	+12
Eskdalemuir	—	—	+ 1	—	—	+ 2	S27 W	18	+ 7	S 9 E	6	+ 2
Lerwick	S14 W	33	+ 7	S18 W	44	+20	S19 W	24	+17	S33 W	17	+13
Tromsö	N43 E	26	+22	N55 E	111	+28	N28 E	59	+23	S16 W	29	+14
Vassouras	S15 W	11	− 2	S20 W	15	− 2	S40 W	8	+ 1	S58 W	9	+ 2
Mauritius	S 2 E	24	+ 1	S 3 E	20	− 2	S 5 E	11	− 2	S	3	− 3

(Each element for 11 *h* 21 *m* and 12 *h* 51 *m* was assumed to be undisturbed.)

Table XVI. Disturbing forces during the bay-type disturbance of Apr. 10, 1933. (After H. Hatakeyama)

Station	15 *h* 00 *m*			15 *h* 18 *m*			15 *h* 36 *m*		
	α	ΔH	ΔZ	α	ΔH	ΔZ	α	ΔH	ΔZ
Toyohara	N31°W	35γ	−7γ	N36°W	17γ	−4γ	N16°W	7γ	−2γ
Kakioka	N12 W	25	+14	N22 W	18	+ 9	N	11	+ 3
Tsingtau	N	32	− 1	N15 W	23	0	N20 E	12	0
Zô-Se	N 2 E	28	− 5	N 5 W	22	− 2	N	11	0
Antipolo	N 3 W	23	+ 7	N10 W	23	− 2	N14 E	12	− 3
Kuyper	N 9 W	33	+17	N 7 W	24	+27	N	13	+16
Watheroo	N19 W	40	+10	N14 W	26	+12	N17 W	14	+ 6
Toolangi	N33 E	45	+ 8	N43 E	34	+ 7	N28 E	17	+ 5
Christchurch	N77 E	28	− 5	N82 E	22	− 1	N70 E	12	+ 2
Honolulu	N76 W	8	− 2	N59 W	6	+ 1	N56 W	4	0
Sitka	S43 W	48	+10	S55 W	40	+ 6	S48 W	13	− 2
Agincourt	S24 W	17	0	S13 E	21	0	S38 E	11	+ 1
Cheltenham	S24 W	17	− 3	S16 E	19	− 4	S24 E	12	− 2
Tucson	S 4 E	15	+ 4	S27 E	16	+ 3	S45 E	8	+ 2
Teoloyucan	S16 W	7	− 2	S22 E	5	− 2	S45 E	3	− 1
San Juan	S 8 W	7	− 1	S11 W	5	− 2	S45 E	1	− 2
Huancayo	S 6 E	9	+ 1	N25 E	19	+ 2	N21 E	22	+ 1
Dehra Dun	N37 E	26	+10	N18 E	26	+ 7	N 5 E	11	− 3
Alibag	N63 E	7	+ 2	N16 E	19	0	N17 E	14	+ 1
Helwan	S73 E	17	+ 2	N70 E	20	− 4	N49 E	11	− 2
Ebro	S25 E	17	+ 3	S72 E	13	− 6	N39 E	6	− 8
Coimbra	S11 E	20	—	E	7	—	N34 E	4	—
Val-Joyeux	S32 E	26	+ 1	S73 E	17	+ 1	N45 E	10	+ 2
De Bilt	S44 E	35	+ 1	N63 E	30	− 5	N34 E	19	+ 1
Seddin	S33 E	30	+ 2	N80 E	34	− 1	N37 E	20	+ 2
Swider	S46 E	30	− 2	N72 E	36	−11	N34 E	18	− 5
Lovö	S29 E	35	+ 4	N81 E	46	+20	N27 E	28	+12
Eskdalemuir	S24 E	32	+ 4	N47 E	21	+ 5	N27 E	22	+ 5
Lerwick	S12 E	29	+ 8	N75 E	23	+ 9	N41 E	33	+ 5
Tromsö	N59 E	108	0	N83 E	70	−18	N19 W	21	−41
Vassouras	S51 E	14	+ 1	S60 E	14	+ 2	N75 E	11	+ 3
Mauritius	S84 W	10	− 3	N61 W	10	− 3	N45 W	6	− 1

(Each element for 14 *h* 24 *m* and 16 *h* 12 *m* was assumed to be undisturbed)

Table XVII. The coef. of the magnetic potential of the disturbing force in the case of the bay-type disturbance of Feb. 24, 1933. (Unit : γ)

G. M. T.		e_a	i_a	e_b	i_b
11 *h*	21 *m*	0	0	0	0
11	36	-2.3 ± 2.2	-0.2 ± 1.3	12.9 ± 1.9	6.9 ± 1.2
11	51	-1.8 ± 2.4	-0.7 ± 1.4	15.9 ± 3.1	8.0 ± 1.3
12	06	-2.0 ± 1.6	-0.6 ± 0.9	11.9 ± 1.4	5.8 ± 0.9
12	21	-2.4 ± 1.2	-0.5 ± 0.7	6.8 ± 1.1	2.7 ± 0.7
12	51	0	0	0	0

bay-type disturbance of Feb. 24, 1933. As shown in this Table, the probable errors of the determined coefficients amount to 1~3 *gammas*. However, a part of these apparent errors may be attributed to the method of the analysis in which we did not take into consideration higher harmonics of the magnetic potential. Thus owing to the smallness of these apparent errors, we may say that the greatest part of the magnetic potential is given by the term including $Q_1^1 \cos\phi$ and $Q_1^1 \sin\phi$.

These coefficients are shown graphically in Fig. 18.

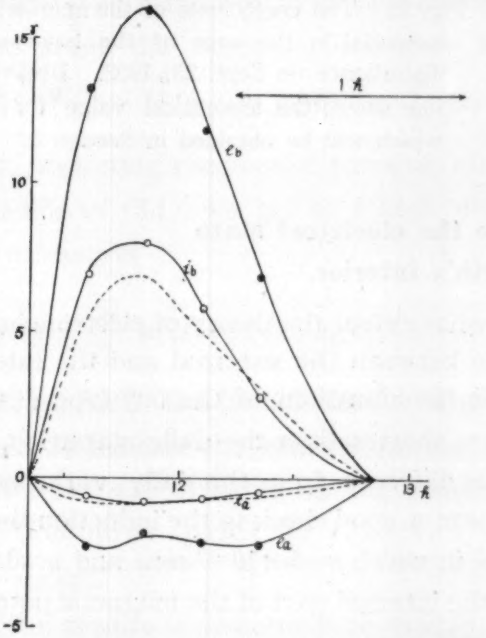

Fig. 18. The coefficients of the magnetic potential in the case of the bay-type disturbance on Feb. 24, 1933. Broken line shows the theoretical value for i which will be obtained in Section 3.

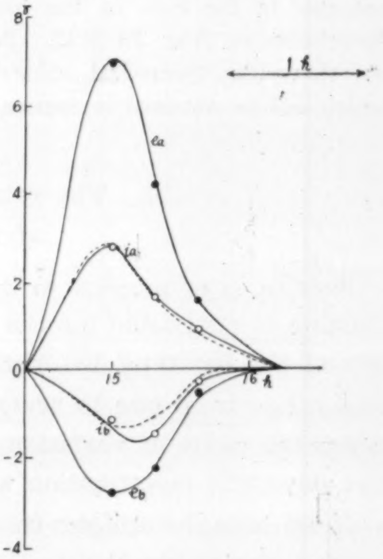

Fig. 19. The coefficients of the magnetic potential in the case of the bay-type disturbance on Apr. 10, 1933. Broken line shows the theoretical value for i which will be obtained in Section 3.

The same determination was made in each bay-type disturbance mentioned above being illustrated in Figs. 19, 20, and 21.

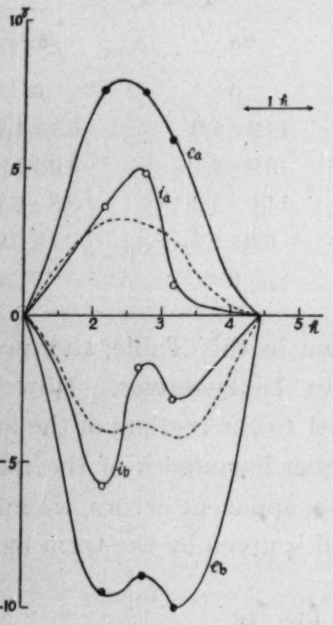

Fig. 20. The coefficients of the magnetic potential in the case of the bay-type disturbance on Aug. 28, 1932. Broken line shows the theoretical value for i which will be obtained in Section 3.

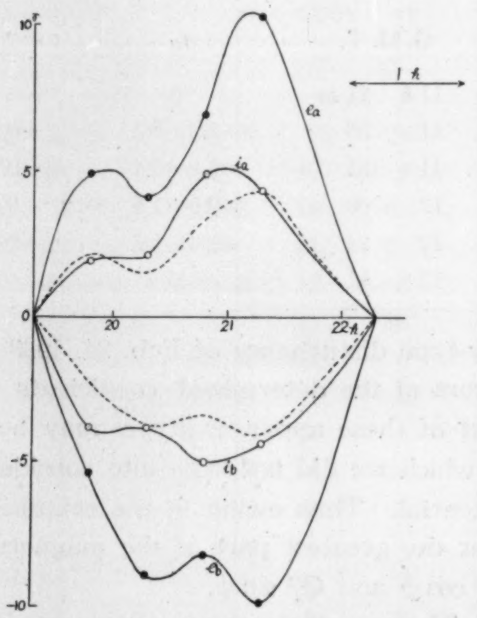

Fig. 21. The coefficients of the magnetic potential in the case of the bay-type disturbance on Sept. 23, 1932. Broken line shows the theoretical value for i which will be obtained in Section 3.

3. The relation to the electrical state of the earth's interior.

Now, it is of interest to study to what extent the theory of electromagnetic induction is applicable for the relation between the external and the internal parts of the bay-type disturbance. As the durations of the bay-type disturbances range from one to several hours, shorter than the daily variation, and besides the mode of variation is quite different from the daily variation on quiet days, the investigation will become a good check to the induction-theory.

If we take the uniform core model in which $\sigma=5\times10^{-12}$ *emu* and $q=0.94$ as already informed by the study on S_q, the internal part of the magnetic potential must be related to the external one by[6)]

$$i_n(t)=\frac{d}{dt}\int_0^t e_n(t-u)\,h(u)\,du=e_n(t)\,h(0)+\int_0^t e_n(t-u)\,h'(u)\,du \quad \ldots(3.1)$$

where $h(t)$ corresponds to $i_n(t)$ when $e_n(t)=0\ (t<0)$ and $=1\ (t<0)$.

When $n=1$, it becomes

$$h(t)=\frac{1}{2\pi i}\int_L e^{pt} I(p)\frac{dp}{p}\,, \qquad \text{......(3.2)}$$

where L is Bromwich's path of integration and

$$I(p)=\frac{q^3}{2}\left\{1-\frac{F_1(\sqrt{4\pi\sigma pqa})}{F_0(\sqrt{4\pi\sigma pqa})}\right\} \qquad \text{......(3.3)}$$

F_n was already defined in Chapter II. We get from (3.2)

$$h(t)=\frac{3q^3}{\pi^2}\sum_{s=1}^{\infty}\frac{1}{s^2}\exp\left(-\frac{\pi s^2}{4\sigma q^2a^2}\,t\right) \qquad \text{......(3.4)}$$

in like manner with the study on the induction by D_{st}. When t is small, $h(t)$ can be written as

$$h(t)=\frac{q^3}{2}\left(1-\frac{3}{\pi qa}\sqrt{\frac{t}{\sigma}}+\frac{3t}{4\pi\sigma q^2a^2}\right), \qquad \text{......(3.5)}$$

as studied by Price⑹.

In the case of Benkova's uniform core model, $h(t)$ decreses very slowly as shown in Fig. 22. The mean rate of decrese during a few *hours* from the beginning amounts to only $0.015\times\frac{q^3}{2}$ *per hour* or $4.1\times10^{-6}\times\frac{q^3}{2}$ *per second.* Then neglecting the second term of the right-hand-side of (3.1), we get to a high degree of approximation

$$i_1(t)=\frac{q^3}{2}\,e_1(t)=0.415\,e_1(t)\,. \qquad \text{......(3.6)}$$

Applying (3.6), the broken lines in Figs. 18, 19, 20 and 21 indicate the changes in the internal parts which are expected on the stand-point of induction-theory based on Benkova's uniform core model.

The results of the analyses roughly agree with those of the theory when we take into consideration the accuracy of the determination of the coefficients. Thus, we may conclude Benkova's model is approximately compatible with the induction by bay-type disturbance.

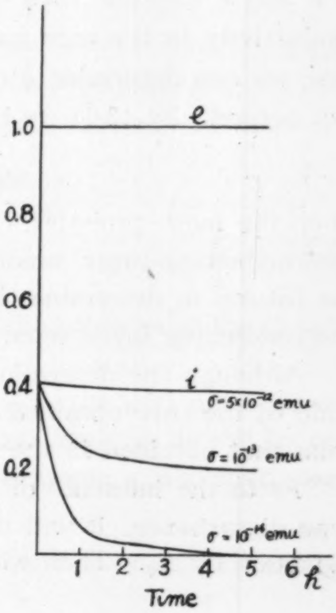

Fig. 22. The change in the induced field with the lapse of time. ($e=0$ for $t<0$, $e=1$ for $t>0$)

As shown in the figures mentioned above, however, it seems that the theoretical curves are used to be lower than those of the analysis. If this were true, it might become better to give larger values to q or to consider that the outer layer is somewhat conducting. Next, we shall determine the radius of the core on the basis of the present analysis of this Chapter.

Table XVIII.
The ratios at maximum variation.

Date	e/i
Feb. 24, 1933	2.0
Apr. 10, „	2.5
Aug. 28, 1932	1.7
Sept. 23, „	2.1

The ratio of i to e[45] when e becomes maximum are given in Table XVIII with respect to the examples of the bay-type disturbance concerned in this Chapter. As shown in this Table, its most probable value becomes 2.2±0.3. The probable error seems rather large because we have only four examples. If the conductivity in the core is smaller than the order of 10^{-12} *emu*, $h(t)$ decays rapidly as also shown in Fig. 22. Then $i(t)$ also decays rapidly. Thus the conductivity must not be materially smaller than the order of 10^{-12} *emu* in order to explain the facts, as shown in Figs. 18, 19, 20 and 21, that e/i is approximately equal to 2 and the mode of time-change of e and i resemble each other. For these reasons, we may say that the conductivity in the core amounts to the order of 10^{-12} *emu* or more. In that case, we can determine q or the radius of the core with the aid of e/i obtained just before. By (3.6) we have

$$q=\sqrt[3]{2e/i}\ .$$

Then the most probable value of q becomes 0.96, say, the thickness of the non-conducting layer amounts to about 260 *km*. However, it is desirable, in the future, to determine the conductivity in the core and the thickness of the non-conducting layer separately with the aid of more accurate analysis.

Although the determination is somewhat rough, it is interesting that the scale of the core obtained from bay-type disturbances is likely to differ slightly from that obtained in the case of S_q.

As to the influence of the ocean on the electromagnetic induction by bay-type disturbance, it will not be large by the same reason in the case of induction by S_q. Then we may neglect it.

4. The distribution of the electric currents in the earth.

We concluded in Section 3 of this Chapter that the electrical state of the earth's interior, inferred from the study on the electromagnetic induction by bay-type disturbances, nearly agrees with the uniform core model based on Benkova's analysis of S_q. Now in the present Section, we are going to study how deep the induced currents penetrate into the earth. As already investigated in the case of S_q, the estimate of the induced currents can be made as follows.

---

[45] In order to avoid errors due to the smallness of the coefficient, we have better to use $e=\sqrt{e_a^2+e_b^2}$ and $i=\sqrt{i_a^2+i_b^2}$ in place of e_a, i_a, e_b and i_b themselves.

According to the study on the electromagnetic induction within the uniformly conducting sphere, the current-density $\overrightarrow{c}{}_n^m$ which corresponds to the spherical harmonics S_n^m is given by

$$\overrightarrow{c_n^m}=-\sigma a\,\rho\,C(p)\,p\,F_n(k\rho a)\,e_n(t)\,[\overrightarrow{r}\,\mathrm{grad}\,S_n^m]^{46)}\,, \qquad\ldots\ldots(4.1)$$

whereas the notations in this expression are the same with those in Section 4, Chapter II, except $C(p)$. Since the case including Q_1^1 is the most important in the case of the bay-type disturbance, it is sufficient to take into consideration only

$$\overrightarrow{c_1^1}=-\sigma a\,\rho\,C(p)\,p\,F_1(k\rho a)\,e(t)\,[\overrightarrow{r}\,\mathrm{grad}Q_1^1\,{\cos \atop \sin}\,\phi]\,, \qquad\ldots\ldots(4.2)$$

where

$$C(p)=\frac{1}{2}\,\frac{1}{F_0(kqa)}{}^{47)}\,. \qquad\ldots\ldots(4.3)$$

In order to study the radial distribution of the electric currents in the core, we deal with the coefficient of $[\overrightarrow{r}\ \mathrm{grad}\ Q_1^1\,{\cos \atop \sin}\,\phi]$, that is

$$c(t)=-\frac{\sigma a\rho}{2}\,p\,\frac{F_1(k\rho a)}{F_0(kqa)}\,e(t)^{48)}\,. \qquad\ldots\ldots(4.4)$$

Solving the operational equation (4.4), then, we get the behavior of the change in $c(t)$ with the lapse of time together with the radial distance or ρ (its ratio to the radius of the earth). Owing to the complexity of $e(t)$ obtained, as shown in several figures in Section 2, from the actual analyses, it will be not only troublesome but unpractical to study each example. We shall here discuss an idealized case. Assuming that

$$e(t)=0\ \ (0>t)\,,\quad e(t)=Ate^{-\omega t}\,(0<t) \qquad\ldots\ldots(4.5)$$

where

$$\omega=0.278\times10^{-3}\,sec^{-1}\,,$$

we may express the general tendency of the change in the external field as shown in Fig. 23. Rewriting (4.5) in operational form we have

---

46) $k^2=4\pi\sigma p$.

47) CHAPMAN and BARTELS, *loc. cit.* Vol. II, p. 741.

48) $F_1(x)=\frac{3}{x^2}\left(\cosh x-\frac{\sinh x}{x}\right),\ F_0(x)=\frac{\sinh x}{x}$.

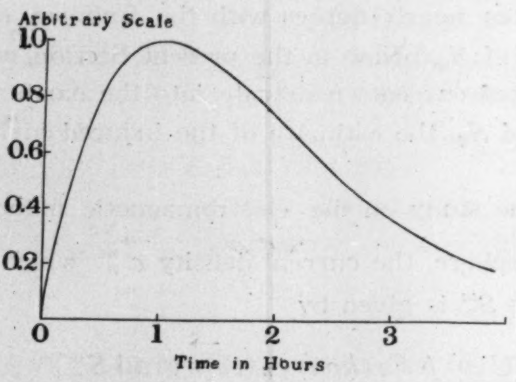

Fig. 23. Idealized change in inducing field of bay-type disturbance.

$$e(t)=\frac{Ap}{(p+\omega)^2}H(t)\ , \qquad\qquad \text{(4.6)}$$

where $H(t)$ denotes Heaviside's unit function. Substituting (4.6) into (4.4), we get

$$c(t)=-A\frac{\sigma a\rho}{2}\ \frac{F_1(k\rho a)}{F_0(kqa)}\ \frac{p}{(p+\omega)^2}H(t)\ . \qquad\qquad \text{(4.7)}$$

According to the operational calculus, the solution of (4.7) becomes

$$c(t)=-A\frac{\sigma a\rho}{4\pi i}\int_L \frac{F_1(k\rho a)}{F_0(kqa)}\ \frac{p}{(p+\omega)^2}e^{pt}dp\ , \qquad\qquad \text{(4.8)}$$

where L is Bromwich's path of integration. Taking into consideration that the poles are given by $-\omega$ (double pole) and the roots of

$$\sinh\sqrt{4\pi\sigma p}\ qa=0$$

except zero, namely, $-\alpha_s=-\dfrac{\pi s^2}{4\sigma q^2 a^2}$ $(s=1, 2, 3, \ldots\ldots)$, we can integrate (4.8) getting

$$c(t)=-A\frac{\sigma a\rho}{2}\Bigg[\Bigg\{(1+pt)\frac{F_1(k\rho a)}{F_0(kqa)} + p\frac{d}{dp}\frac{F_1(k\rho a)}{F_0(kqa)}\Bigg\}_{p=-\omega}e^{-\omega t}-\sum_{s=1}^{\infty}\Bigg\{\frac{F_1(k\rho a)}{F_0(kqa)}\Bigg\}_{p=-\alpha_s}\frac{\alpha_s}{\omega-\alpha_s}e^{-\alpha_s t}\Bigg]\ . \qquad \text{(4.9)}$$

The series in (4.9), however, converges rather slowly for small value of t. Then we shall obtain a suitable expression for small value of t as follows. Using Bessel function, F_n is expressed by

$$F_n(x)=\left(\frac{1}{2}\ ix\right)^{-n-\frac{1}{2}}\Gamma\left(n+\frac{3}{2}\right)J_{n+\frac{1}{2}}(ix)^{49)}$$

---

49) CHAPMAN and BARTELS, *loc. cit.* p. 738.

or

$$F_n(x)=\left(\frac{2}{x}\right)^{n+\frac{1}{2}}\Gamma\left(n+\frac{3}{2}\right)I_{n+\frac{1}{2}}(x)\,. \quad\ldots\ldots\ldots\ldots\ldots\ldots\ldots(4.10)$$

Meanwhile with the aid of well known asymptotic expansion

$$I_\nu(x)\simeq\sqrt{\frac{1}{2\pi x}}\,e^x\left\{1-\frac{4\nu^2-1^2}{1\,!\,8x}+\frac{(4\nu^2-1^2)(4\nu^2-3^2)}{2\,!\,8x^2}-\cdots\right\},$$

we get for large value of x

$$F_0(x)\simeq e^x/2x\ ,\quad F_1(x)\simeq 3e^x/2x^2\ ^{50)}\quad\ldots\ldots\ldots\ldots\ldots\ldots\ldots(4.11)$$

Thus substituting (4.11) into (4.7), we get

$$c\,(t)\simeq -A\,\frac{3\sqrt{\sigma}\,q}{4\sqrt{\pi}\,\rho}\,(1/\sqrt{p}\,)\,e^{-(q-\rho)\sqrt{4\pi\sigma p}\,a}\,H\,(t)\quad\ldots\ldots\ldots(4.12)$$

for large value of p. As well known in the operational calculus, the solution of an operational equation when $p\to\infty$ corresponds to the one when $t\to 0$. Then we get an expression of current-density for small value of t solving (4.12) as follows;

$$c\,(t)=-A\,\frac{3\sqrt{\sigma}\,q}{4\sqrt{\pi}\,\rho}\left[2\sqrt{\frac{t}{\pi}}\,e^{-\frac{(q-\rho)^2\pi\sigma a^2}{t}}\right.$$
$$\left.-(q-\rho)\sqrt{4\pi\sigma}\,a\left\{1-\mathrm{erf.}\sqrt{\frac{(q-\rho)^2\pi\sigma a^2}{t}}\right\}\right]^{51)}\quad\ldots\ldots\ldots(4.13)$$

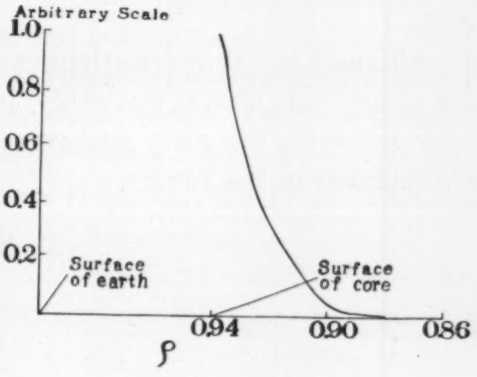

Fig. 24. The distribution of the induced current in the earth.

As to the change in the current density with increase of the depth, we can calculate from (4.9) or (4.13). For instance, the change in the current-density is shown in Fig. 24 in arbitrary scale for $t=3.6\times10^3$ *sec*, that is, after one *hour* past from the beginning and at that time e becoming maximum in our idealized bay-type disturbance. The current-density decreases very rapidly with increase of the depth. Indeed, it becomes less than one *percent* of its

---

50) $\Gamma(3/2)=\sqrt{\pi}/2$, $\Gamma(5/2)=3\sqrt{\pi}/2^2$.

51) H. JEFFREYS, *Operational Method in Mathematical Physics.*, p. 112.
$$\frac{1}{a\sqrt{p}}\,e^{-ax\sqrt{p}}=\frac{2}{a}\left(\frac{t}{\pi}\right)^{1/2}e^{-a^2x^2/4t}-x\left(1-erf.\frac{ax}{2\sqrt{t}}\right).$$

amount at the surface of the core at the depth of a few hundred *kilometers* beneath the surface of the core. As already mentioned in the study on the current-distribution in the case of S_q, the effective values of the magnetic fields observed at the surface caused by the currents flowing in a thin shell whose radius is ρa are proportional to $\rho^{n+2}|\overrightarrow{c}|$ for the harmonic whose degree is n, the contribution of the currents flowing at any depth is shown by almost the same curve in Fig. 24 because ρ does not differ materially in the effective range of the depth. Then we know from this curve that 90% of the magnetic field are caused by the induced currents flowing in the regions from $\rho=0.94$ to $\rho=0.88$, namely from the surface of the core to the depth of 1200 *km* beneath the surface of the earth.

Then the conductivity determined in this Chapter seems to correspond to that of the upper part of the core because the contribution of the currents more than 1200 *km* below is almost negligible.

Summing up the investigations in this Chapter, we may say that the electrical state of the earth's interior which is inferred from the electromagnetic induction by S_q is confirmed also by the induction by bay-type disturbances in which the distribution of the disturbing forces over the earth differ very much from that of S_q. Since bay-type disturbances generally end within several *hours*, the induced currents penetrate into the earth more shallowly than in the case of S_q. Accordingly, the electrical state which is determined by studying bay-type disturbances seems to correspond to the shallower region compared with that obtained from the study of 24- or 12-hourly component of S_q.

Although bay-type disturbances are only analyzed with respect to the low and middle latitudes in this study, it is hoped, however, that an analysis will be made including the polar regions with the aid of abundant data which will be accumulated in the future.

(*To be continued*)

5. 地球內の電磁感應およびその地球內部の電氣的性質との關係 第1報 (1)

地震研究所 力武常次

A. Schuster が地球磁場の日變化を分析し，その大半は地球外部に原因を有するが，一部は地球の內部に原因を有することを發見して以來，地球內部に原因を有する部分は，地球外部に原因を有する部分の變化に伴つて地球內部に誘導される電流に因る磁場として說明出來ることが多くの學者によつて示され，從つて地球內部の電磁氣的性質を或程度推測出來るようになつた．しかしながら，地表に於ける觀測のみでは地球內部の性質を一義的に決定することは困難であり，過去に於ては主として次の立場がとられている．即ち地球の一番外側は絕緣層であつてその內側に一樣な電氣傳導度を有する核があるとして，外部および內部磁場の關係を說明し得るように外層の厚さおよび核の電氣的性質を決定するものである．

Chapman によつて爲された日變化の研究によれば，この導電核の電氣傳導度 σ は 3.6×10^{-13} *cmu* であり，絕緣層は 250 *km* の厚さとなる．また Chapman, Whitehead および Price 等の磁氣嵐の主相（D_{st}）の研究では，上とほとんど同じ大きさの核に對して $\sigma=4.4\times10^{-12}$ *cmu* となり，S_q と D_{st} の喰違いを說明するために，S_q に比して緩漫な D_{st} によつて誘起されは電流は S_q のそれにくらべて核の內部迄浸徹し，見掛け上求められた σ はより深い部分の電氣傳導度を表わすものと考えられていた．このように σ の分布は必ずしも一樣ではないのであるから，Lahiri と Price は σ が r^{-m}（r は地球中心よりの距離）に比例して變化するようなモデルについて考察し，S_q と D_{st} の双方に對して成立つ σ の分布を求めた．また σ の違う數層よりなるモデルについては寺田一彥氏によつて研究された．

しかしながら，Lahiri と Price の研究に於ては m が相當變化しても，地表に於ける內外磁揚の關係はあまり變化せず，地球內部の電氣的性質をさらに詳細に吟味する爲にはもつとはやい變化からおそい變化迄を取扱つて種々の深さについて研究することが望ましい．

筆者は本報文に於て出來るだけ多くの種類の地磁氣の變化を取扱うべく，使用し得る資料を集めたが現在のところ，靜穩日日變化（S_q），擾亂日日變化（S_D），磁氣嵐の主相（D_{st}），灣型變化，太陽面爆發に伴う變化および磁氣嵐の急始について不充分ではあるが研究を行うことが出來た．このほかに地磁氣の脈動のような短週期の變化も存在するのであるが，地球上の廣い地域に分布している觀測資料を得ることが出來ないので他の機會にゆずることにする．

本報文に於て取扱つた地磁氣の變化は，2～3分程度の短い變化から2～3日程度の稍々長い時間にわたる變化を含んでおり，從來諸家に依つて爲された研究とならべて考察すると，地球內部の電氣的性質が或程度判明するように思われる．なお諸種の地磁氣變化が海特に大洋の存在のためにうける影響をも考察した．

第1章に於て地球內部の透磁率に關して從來行われた地球物理學的および物理學的考察を綜合すると，現在の學問では地球內部で透磁率が1より甚だしく大きいとは考えられないことを述べてある．これは地磁氣の永久磁場の說明として永久帶磁說が多くの難點をもつていることに對應する．したがつて，本報文を通じて透磁率は1に等しいとして取扱つた．

第2章は靜穩日日變化（S_q）による電磁感應であつて，はじめの部分に於て太平洋のような大洋中に誘導される電流がどのような大きさの磁場をつくるかを調べるために，90° はなれた二つ

の子午線によつてかこまれた等深の海を考えて，S_q がどの程度の影響をうけるか計算した（海の影響については従來地球全体を覆う一樣な深さの海についてのみ研究が行われている）．計算の結果は大洋の中心部を除いて振幅は S_q の $^1/_{10}$ 以下となり，變化は世界時のみにより地方時には無關係であるので，變化が地方時のみに關係するとして行つた球函數分析に於ては海洋の影響は平均として小さくなる．したがつてこの場合求められた内部磁場は大体地球内部を流れる電流によるものと考えてよい．なお適當な假定のもとに，太平洋の影響を出してみると理論値とオーダーに於て一致する値が得られた．

次に比較的最近行われた S_q に關する長谷川萬吉博士および Benkova の球函數分析の結果を使用して地球内部の電氣的性質を求めた．絕緣層および電氣傳導度一定の電導核よりなる地球については既に永田武博士によつて決定されているが，その結果は Chapman の結果と異り，核の σ が 5×10^{-12} *emu* 程度外層の厚さは 400 *km* 程度でなければならない．筆者は地震波の研究で確立されているように，地下 2900 *km* に於て急激な不連續があることから，電氣的性質にも不連續があるものとして，内核，中間層および絕緣外層よりなるモデルに就てしらべたが，結果は永田博士の與えた結果にほゞ一致する．内核に於ては一應 $\sigma=5\times10^{-11}$ *emu* という値を得たが，誘導電流はほとんど中間層内で減衰するので此の値はあまり信用することが出來ない．

第3章に於ては S_D の電磁感應をしらべたが，資料の不足から S_q の研究によつて得られた地球の電氣的モデルが S_D の内外磁場の相互關係を大略說明出來るという結果を得たにとどまる．

第4章は D_{st} の電磁感應の研究である．長谷川博士や Benkova の資料をもととして永田博士の決定した地球の電氣的モデルは Chapman の D_{st} に關する分析結果をほゞ說明出來，Chapman を中心とする一群の學者によつて取上げられたような S_q と D_{st} との喰違いは大して重要でなくなる．筆者は第2章の後半で示したように地球内核をより導電的であるとすれば，觀測と理論とのよりよい一致を期待出來ることを D_{st} について近似的に示した．しかし，S_q の場合と同じく内核に透浸徹する電流は極めて僅かであるから，あまり嚴密な議論をすることは全く無意味である．

第5章に於ては，畠山久尙博士の集めた資料にもとずいて，地磁氣灣型變化の電磁感應を研究した．畠山博士が經驗的に求めまた筆者によつてダイナモ說にもとずいて理論的に得られた灣型變化の電流系を念頭において，磁場のポテンシャルの球函數展開のうち最も重要な $Q_{1\sin}^{1\cos}\phi$ の係數を決定し，さらに外および内側に原因を有するポテンシャルの係數を求めた．決定は一つの灣型變化を通じて3または4度なされた．この係數の大きさの關係から，絕緣層におゝわれた導電核中では σ が少くとも 10^{-12} *emu* 程度で絕緣層の厚さは 300 *km* 程度でなければならないことになる．誘導電流の分布を求めてみると導電核の表面からはかつて 2〜300 *km* の深さの所ではほとんど零になることがわかる．　　　（末完）

6. Petrogenic Meaning of the Occurrence of Spinel in Xenoliths.[*]

By Ryōhei MORIMOTO,

Earthquake Research Institute.

(Read Feb. 15, 1949.—Received May 31, 1950.)

I. Introduction.

Petrological study on xenoliths sometimes informs us of the events that might have taken place during the metamorphism of xenoliths due to magmatic action. Researches on the xenoliths in effusive or hypabyssal rocks are effective in ascertaining the facts that might have taken place at an intermediate stage of metamorphism brought about in xenoliths of which we cannot be informed otherwise. Modes of occurrence of the spinel in xenoliths, now in question, is one of the most characteristic phenomena that might have taken place at an intermediate stage of metamorphism of xenoliths with argillaceous composition.

Behaviour of foreign inclusions in igneous rocks ought to be influenced not only by the original composition of foreign rocks, but by the kind of an attacking magma, and also in general by the prevailing condition to which both host and guest are exposed. It may be conceived, however, that during the metamorphism of argillaceous xenolith, events of the same kind might have been brought about almost exclusively at an intermediate stage regardless of the kind of an attacking magma. It is needless to say that each xenolith, a record of the effects of magmatic action on pre-existing rock, represents respectively each step of metamorphism brought about by a magmatic action in xenoliths or in the pre-existing rock, from which each xenolith has been derived. But in nature, xenoliths showing every step of their metamorphism are not found in equal frequency. Xenoliths recording the evidence showing an earlier and an intermediate state of metamorphism are in general scanty, when compared with those informing us of the state of metamorphism at a later stage, for we are informed of these processes from the evidences recorded in rocks that are end products of the mutual action between foreign matter and magma.

---

[*] Dedicated to the memory of late Prof. Takeo KATO.

Final goal of the metamorphism of xenolith is represented by an aggregate of the minerals that are crystallized out from the hybrid magma highly contaminated by foreign material. And the mineral assemblage of such xenoliths that reacted with magma to highly advanced state should be determined by the properties of an attacking magma. It is pointed out here that before reaching these various goals given by the characters of contaminated magma, most of argillaceous xenoliths, however, must have passed through the same course, and that the formation of spinel in xenoliths indicates one of the characteristic evidences showing such same course.

Occurrence of the xenoliths containing spinel seems to be almost restricted to those found in volcanic or hypabyssal rocks, while they seem to be scarcely found in plutonic rocks. Metamorphism of xenoliths might have easily been checked by eruption or rapid cooling of host rock. On the other hand, xenoliths in plutonic rocks were favoured in promoting the interaction with their surrounding magma sufficiently. Thus, it is difficult for us to find spinel in the xenoliths included in plutonic rocks. Even if it had been formed in the xenoliths in plutonic rocks, it must have disappeared, as the mutual reaction between xenoliths and magma have proceeded to more advanced degree. In short, occurrence of spinel in xenoliths owes much to the geologic condition that checked the metamorphism of xenoliths due to magmatic action at a moderate stage. And such a geologic condition must have prevailed in the case of the xenoliths included in volcanic or hypabyssal rocks.

Chemical composition of the original rocks is, of course, one of the essential factors that facilitate the formation of spinel in the xenoliths derived from them. We must take into our consideration the fact that the xenoliths treated by the present writer were mainly derived from the metamorphic rocks such as biotite-schist which might had already been partially rich in alumina and poor in silica on account of its metamorphic differentiation before they were influenced by the magmas related to volcanic action. And such heterogeneity in original rocks may have been favourable to appearance of the spinel in their derivative xenoliths. The andalusite or sillimanite porphyroblasts fringed with spinel grains described in the succeeding chapters may also be considered as one of the remarkable petrographic features to be ascribed to such a polymetamorphism or repeated metamorphism as shown by the pyrometamorphosed xenoliths derived from mica-schist enclosed in volcanic rocks1). There is no need to mention here that in the spinel-bearing xenoliths the writer intends to describe in this paper, xenoliths not influenced by the surrounding rock *viz.* xenoliths which were caught up mechanically and do not indicate any

---

1) A. HARKER, *Metamorphism.*, (1932), 322-326.

evidences which may be ascribed to the effects of host rock are excluded.

II. Mode of occurrence of the green spinel in the xenoliths in the garnet-biotite-andesite from Nijō volcano near Osaka.

During his petrological study on the inclusions in the garnet-biotite-andesite from Nijō volcano near Osaka, the writer pointed out the occurrence of green spinel as a common accessory constituent found in some argillaceous xenoliths. The original rock from which these spinel-bearing xenoliths are thought to have been derived is represented by such inclusions in the andesite that show no effect of magmatic action, or by those that have been only moderately metamorphosed, still with remnants of its original characters. Petrographically, these inclusions belong to so-called normal regional metamorphic rocks of the almandine-zone, staurolite-zone, and perhaps to sillimanite-zone, or to the diaphthorite derived from the former. The spinel in question is not found in these xenoliths. The first step of the metamorphism due to the attacking magma is indicated by the development of hornfelsic texture, characterized by mosaic aggregate of dark brown biotite and andesine-labradorite, among the original schistose or phyllitic texture (Fig. 1–4). Corresponding to this textural change, porphyroblasts of some aluminous minerals such as andalusite, sillimanite, and cordierite are formed. Corundum appears within the porphyroblasts of andalusite; fibrous sillimanite around the blastoporphyritic staurolite; and green spinel and calcic plagioclase around or along the cleavages of the porphyroblasts of sillimanite or of andalusite at this stage (Fig. 5–8). The appearance of corundum and spinel indicates the culmination of metasomatic action between the xenoliths or the pre-existing rock and the magma. At a further advanced stage of metamorphism which is characterized by glass invasion and by development of glomeroporphyritic aggregates of biotite and plagioclase sporadically formed in the general mass of the hornfels texture, the above-mentioned porphyroblasts of the preceding stage disappear, and are gradually replaced by andesine or sodic labradorite. Spinel is not found in such xenoliths. Metamorphism of the xenoliths is checked by effusion of the hybrid mash as a lava, and final stage of the metamorphism is represented by glomeroporphyritic aggregates of biotite and plagioclase. In other words, the xenoliths metamorphosed by the magma into an advanced degree have a mineral assemblage as if it were results from the crystallization of the contaminated magma under an intratelluric condition.

III. Examples of occurrence of spinel in xenoliths.

Andalusite or sillimanite porphyroblasts fringed by spinel—an intergrowth of the two aluminosilicates is not rare, and as far as the writer has observed, the former always tends to be replaced by the latter—are common in the xenoliths included in volcanic or hypabyssal rocks, the xenoliths caught up into host rocks only mechanically or the xenoliths sufficiently reacted on with an enclosing magma, of course, being excluded. And their occurrence have been reported by many European petrographers since the last decade of 19th century[2]. H. H. Thomas[3] described the spinel-bearing rock as a hybrid derived from an argillaceous xenolith (sillimanite-buchite) in the tholeiite sill from Mull (Fig. 9). R. Brauns[4] mentioned in his memoir on the ejecta from Laacher Seegebiet, that spinel was newly formed from staurolite, sillimanite, and andalusite during the pyrometamorphism of mica-schist due to a volcanic magma. And the spinel-bearing xenoliths were reported by G. A. Bartrum[5] in the andesite from Auckland, New Zealand.

In Japan, K Sugi[6] found the biotite-andesine-rock containing corundum and spinel as an inclusion in the quartz-porphyry from Nikkō, Pref. Tochigi, and noticed that the corundum was fringed by spinel and the former was often replaced by the latter. As compared with the above-mentioned andalusite (or sillimanite) -spinel-assemblage, this corundum-spinel-assemblage may be considered as a more extreme case showing a characteristic trend of metamorphism of argillaceous xenoliths that a xenolith becomes poor in silica, at an intermediate stage of its metamorphism, and in consequence relatively rich in alumina. Corundum is found in the xenoliths from Nijō volcano, as was mentioned in the foregoing chapter. And T. Watanabe[7] also described a xenolith containing spinel and corundum in the porphyritic granite from Suan district, Korea.

---

[2] A. LACROIX, *Les enclaves des roches volcaniques,* (1893).
F. CORNU, *Beitr. zur Paläont. und Geol. Osterreich-ungarns und des Orients,* 19 (1906), 34-47.
A. BERGEAT, *Neues. Jahrb. Mineral.,* 33 (1910), 575 629.
S. RICHARZ, *Jour. Geol.,* 32 (1924), 685-689.
G. KALB, *Min. Petr. Mitt.,* 47 (1935), 185-210.

[3] H. H. THOMAS, *Quart. Jour. Geol. Soc*, 78 (1922), 229 260.

[4] R. BRAUNS, *Die kristallinen Schiefer des Laacher Seegebietes und ihre Umbildung zu Sanidinit.,* Stuttgart (1911). usw.

[5] G. A. BARTRUM, *Trans. Roy. Soc. New Zealand,* 67 (1937), 251-280.

[6] K. SUGI, "Contact metamorphic rocks." *Iwanami Kōza Geol. & Mineralogy* (1931), 39, (in Japanese).

[7] T. WATANABE, *Jour. Fac. Sci. Hokkaido Univ.,* (ii), 6 (1943), 239.

Andalusite or sillimanite in xenoliths has often grown up to large porphyroblasts, several centimetres in their length, whose typical example was shown by a specimen collected by J. Masutomi[8] from the nevadite quarried at Shingū, Pref. Wakayama (Fig. 10). Remarkable large xenocrysts of andalusite scattered in the granite-porphyry were also described by T. Iwafune[9] from Owase, Pref. Mie.

Staurolite associated with spinel has been reported not only by Brauns in his above-mentioned memoir, but by T. Takeuchi[10] in the xenolith in the garnet-bearing andesite from Mt. Amataki, Pref. Kagawa (Fig. 11), and also by the present writer in the xenolith from Nijō volcano (Fig. 12).

IV. *Desilication* as a remarkable phenomenon characteristic of the metamorphism of argillaceous xenoliths.

Relating to this metamorphism of argillaceous xenoliths, the present writer contemplates recapitulating here that at the intermediate stage of metamorphism, a decrease in SiO_2, and an increase in Al_2O_3 take place in the chemical composition of the xenoliths. This is shown by the results of his systematic observation on the argillaceous xenoliths that are same in their origin and only different in degree of their metamorphism, as was mentioned in the foregoing description (Chapter II). And this is also consistent with geological fact that the occurrence of spinel is common from the xenoliths found in volcanic or hypabyssal rocks, while it is rare from the ones contained in plutonic rocks. The trend of this chemical change of these xenoliths is observed as the temporary appearance of spinel, usually with calcic plagioclase, sometimes with corundum, around or within the porphyroblasts of sillimanite or of andalusite in the xenoliths representing an intermediate stage of metamorphism. At the present state of his study, it may be inconceivable for the writer to make clear how the decrease in silica takes place, for the mechanism of *desilication* has never yet been analyzed. In other words, it is only considered as a result of some uncertain metasomatic processes commonly found in xenoliths or at the contact portion between wall rock and igneous mass where geological condition favourable to such processes must have been prevailing. In spite of its obscurity, however, we cannot help recognizing an important rôle played by the *desilication* in petrogenesis. If we postulate this to be one of the most primal inclination of the metasomatism brought about in xenoliths or in wall rocks due to magmatic action, many evidences observed in such rocks may be reasonably interpreted.

---

[8] J. MASUTOMI, *Our Mineral*, 9 (1940), 62-63, (in Japanese).

[9] T. IWAFUNE, "Geology and Petrology of Kinomoto and Owase District (MS)," Geol. Inst., Tokyo Univ., (1939).

[10] T. TAKEUCHI, *Jour. Jap. Assoc. Petrologists, Mineralogists, and Economic Geologists*, 26 (1941), 33-60, (in Japanese).

Thomas[11] pointed out that the plagioclase formed in the xenolith had a composition similar to anorthite and was more calcic than the plagioclase (bytownite) in the cognate inclusion. And it is often observable that the plagioclase formed in xenoliths is more calcic than those in the surrounding rocks. Concerning the garnet-biotite-andesite from Nijō volcano, R. Ōhashi[12] and T. Sugimoto[13] wrote as follows: Plagioclase enclosed in the garnet phenocryst is anorthite, while compositions of the isolated crystals of plagioclase in the andesite are An 65–40%, and the plagioclase having the composition of An 90–65 is lacking in this lava. Therefore, these garnet crystals in the andesite must have crystallized out from the magma during the cyrstallization of the plagioclase having the composition of An 90–65%. As to these garnet crystals including calcic plagioclase, it may be considered that these calcic plagioclase had been included by the garnet crystals during the formation of garnet porphyroblasts in the xenoliths or in the wall rock under the influence of the attacking magma, and were scattered into the andesite at the time of disintegration of the xenoliths into the magma.[14] The fact noted by Ōhashi and Sugimoto, whose interpretation is different from the writer's, coincides with the trend of metamorphism of xenoliths emphasized in this paper. And some of the anorthite, often found in andesite or in tholeiitic basalt as conspicuous large porphyritic minerals, may be considered as a kind of the xenoliths derived from some argillaceous rocks concealed under the volcanoes.[15] Some of them may be the extreme examples showing this trend of metamorphism. Formation of the calcic plagioclase as well as of the spinel and the corundum in xenoliths may be ascribed to the mutual reaction between xenoliths and an enclosing magma. And other metasomatic processes which might have led to the introduction of CaO, MgO, FeO, etc., into xenoliths from the attacking magma must be taken into our consideration. It may be influenced also by the least change of femic contents in xenoliths, whether the spinel appears in them or not. Nevertheless,

---

11) H. H. THOMAS, *op. cit.* 245.

12) R. ŌHASHI, *Our Mineral*, 5 (1936), 20-22, (in Japanese).

13) T. SUGIMOTO, *Our Mineral*, 5 (1936), 10-20, (in Japanese).

14) R. MORIMOTO, *Jour. Jap. Assoc. Petrologists, Geologists, and Economic Geologists*, 32 (1944), 218-225, (in Japanese).

15) K. YAGI, *Jour, Jap. Assoc. Petrologists, Mineralogists, and Economic Geologists*, 33 (1949), 13, (in Japanese).
T. ISHIKAWA, *Jour. Geol. Soc. Japan*, 53 (1947), 64, (in Japanese).
S. KÔZU, *Sci. Rep. Tohoku Univ.*, (ii), 2 (1914), 7.
J. HARADA, *Bull. Vol. Soc. Japan*, 2 (1936), 330, (in Japanese).

the writer supposes, however, that the *desilication* must have played an important rôle in making a favourable condition to form these minerals in xenoliths. Recently, H. Yamada, who described the basic xenoliths in the quartz-diorite from Senmaya, Pref. Iwate, talked about this process and explained the genesis of those inclusions.16) And it is of interest, relating to this problem, that silica mineral such as tridymite, rarely with cordierite,17) are found conspicuously in some lava containing xenoliths.18)

In conclusion, the present writer wishes to be given an opportunity to offer his cordial thanks to Prof. Seitarô Tsuboi of this Institute for his kind encouragement during this study, and his special thanks are due to Dr. Hisao Yamada of the Tokyo Institute of Technology for his kind instruction, also to Prof. Tsunehiko Takéuchi of the Tohoku University and to Mr. Junosuke Masutomi for gifts of specimens.

Some of the expense necessitated for this research was defrayed from the funds for Scientific Research of the Department of Education.

---

6. 捕獲岩に見出される尖晶石の產狀とその成因

地震研究所　森本良平

二上火山（大阪府南河內郡山田村，奈良縣北葛城郡二上村）產柘榴石黑雲母安山岩中の礬土質捕獲岩の變成過程に見られる尖晶石の消長と，各地火山岩，半深成岩中の捕獲岩中における尖晶石の產狀について記載し，礬土質捕獲岩の變成過程の特徵を述べ，特に脱珪酸作用の重要性を論じた．

---

16) H. YAMADA, *Jour. Geol. Soc. Japan*, 55 (1949), 154.

17) R. MORIMOTO, *Bull. Earthq. Res. Inst.*, 25 (1947), 33-35.
R. MORIMOTO and H. MINATO, *Bull. Earthq. Res. Inst.*, 26 (1948), 41-44.

18) Washinoyama, (Yamanouchi-mura, Ayauta-gun, Pref. Kagawa), Ishigamiyama, (Kumamoto City, Pref. Kumamoto), etc.

Explanation of Plates.

Fig. 1. Staurolite-bearing phyllite, a xenolith slightly metamorphosed by the magma. Microfolded phyllitic structure and the irregular grains of plagioclase are still reserved, though the recrystallized mosaic aggregate of plagioclase and biotite and invasion of glass are observed. Photomicrograph, polarizer only. ×ca. 20. (40IIIRM-61_{29}).

Fig. 2. Clomeroporphyritic aggregates of biotite and plagioclase (g) are formed among the matrix of the xenolith. The general mass of the rock consists of fine-grained mosaic aggregates of biotite and plagioclase, and the original schistose structure (sch) is still reserved. Photomicrograph, polarizer only. ×ca. 18. (40IIIRM-61s').

Fig. 3. Pockets of glomeroporphyritic biotite and plagioclase (g) developing in the matrix of hornfelsic texture (h). Photomicrograph of the andalusite-cordierite-biotite-plagioclase-xenolith, analyzer being inserted. ×ca. 12. (RM41123003).

Fig. 4. Hornfelsic texture reserved in the glomeroporphyritic aggregate of biotite and plagioclase. Photomicrograph of the garnet-bearing biotite-plagioclase-xenolith, analyzer being inserted. ×ca. 23 (RM41123048).

Fig. 5-6. Green spinel within and around the porphyroblast of andalusite which is partially replaced by sillimanite (s). Periphery of the porphyroblasts is embayed by the minute grains of spinel and calcic plagioclase intimately associated with each other (b), where spinel grains are arranged along the lines perpendicular to the crystal face of the andalusite. Euhedral octahedron of spinel (a) associated with clear homogeneous plagioclase is formed within the porphyroblast. Fig. 6 was photo., an analyzer being inserted. Spinel-sillimanite-andalusite-biotite-plagioclase-xenolith in the garnet-biotite-andesite from Nijō volcano. ×ca. 76. (40IIIRM-$17s_5$).

Fig. 7. Twinned sillimanite porphyroblasts fringed by green spinel (z), crystal x and crystal y penetrate each other perpendicularily. Spinel-sillimanite-biotite-plagioclase-xenolith, Nijō volcano. Polarizer only. ×ca. 35. (42 (II)-322_{15}).

Fig. 8. Relic of sillimanite porphyroblast (s) fringed by spinel (brown dirty glass) in the biotite-plagioclase-xenolith with glomeroporphyritic texture invaded by glass. Analyzer being inserted. ×ca. 19. (40IIIRM-17s).

Fig. 9. Spinel (S) forming a pseudomorph after sillimanite surrounded by anorthite (An), G being glass. A diagramatic sketch of a photomicrograph of the xenolith described by H. H. Thomas from Mull.

Fig. 10. Xenolith in the nevadite from Chihogamine, Shingū, Pref. Wakayama. Collected by J. Masutomi. Remarkable porphyroblasts are the parallel intergrowth of andalusite and sillimanite fringed by green spinel. (real size).

Fig. 11. Spinel (S)-magnetite (M)-staurolite (T)-garnet-sillimanite (S)-biotite-plagioclase (L)-rock, a xenolith coll. by T. Takéuchi from the hornblende-hypersthene-andesite, Mt. Amataki, Tsuda-machi, Pref. Kagawa. Photomicrograph, polarizer only. ×ca. 70. (RM41111403).

Fig. 12. Staurolite (T) fringed by spinel (P), associated with fibrous sillimanite (S) in the spinel-staurolite-sillimanite-cordierite-biotite-plagioclase-rock, a xenolith in the garnet-andesite from Nijō volcano near Osaka. Photomicrograph, polarizer only. ×ca. 70. (RM41123034).

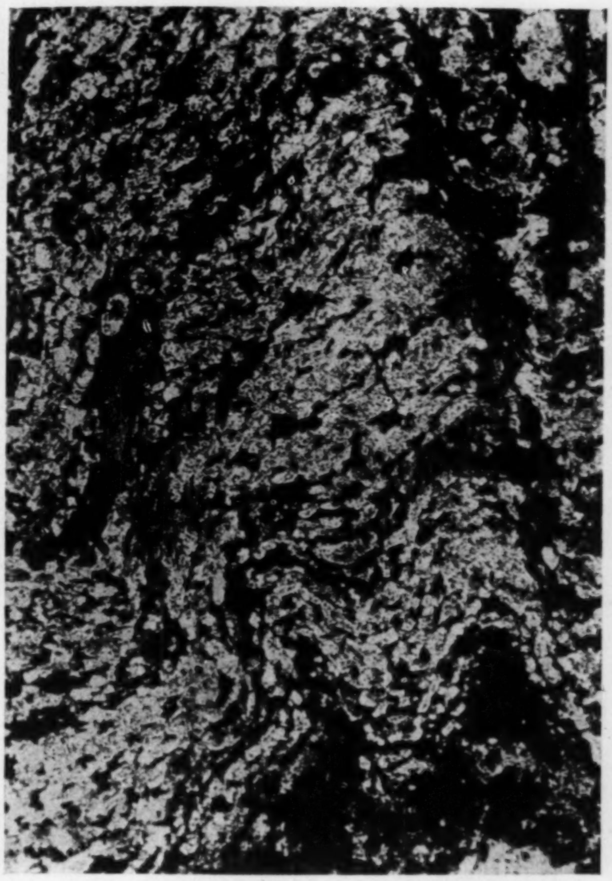

Fig. 1.

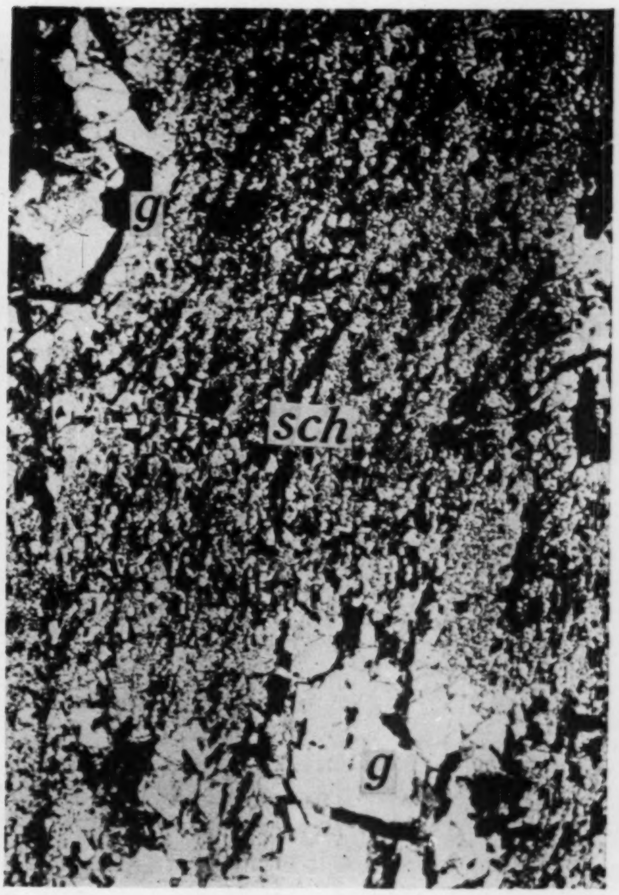

Fig. 2.

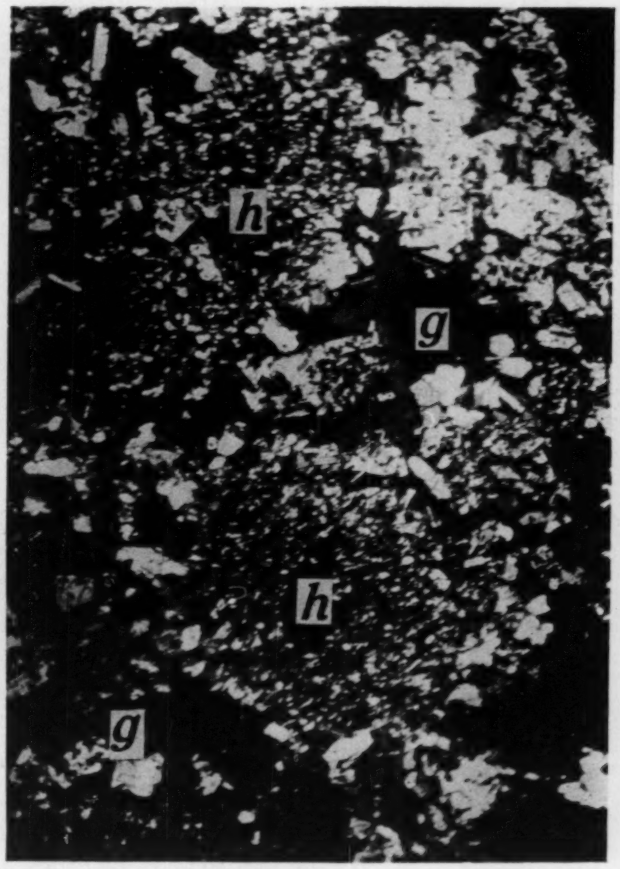

Fig. 3.

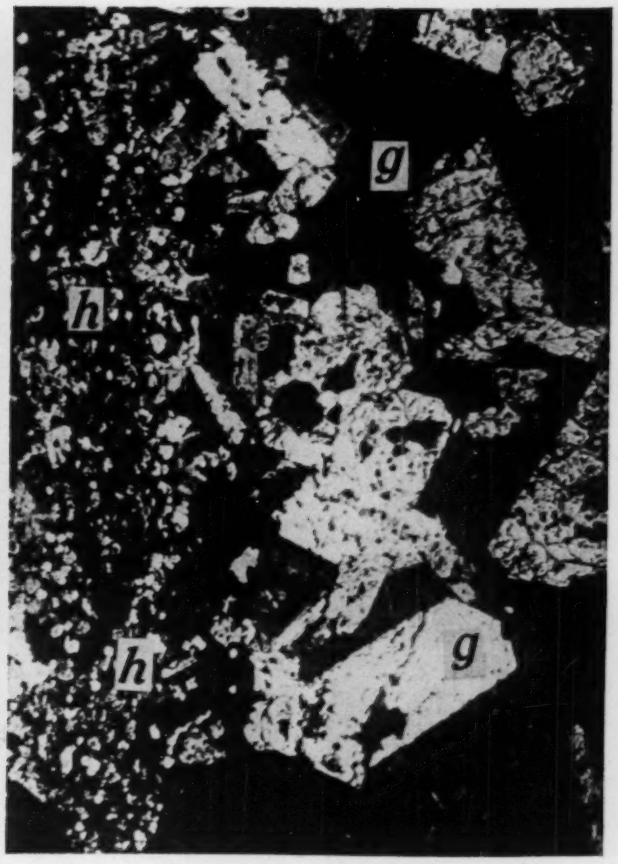

Fig. 4.

（震研彙報 第二十八號 圖版 森本）

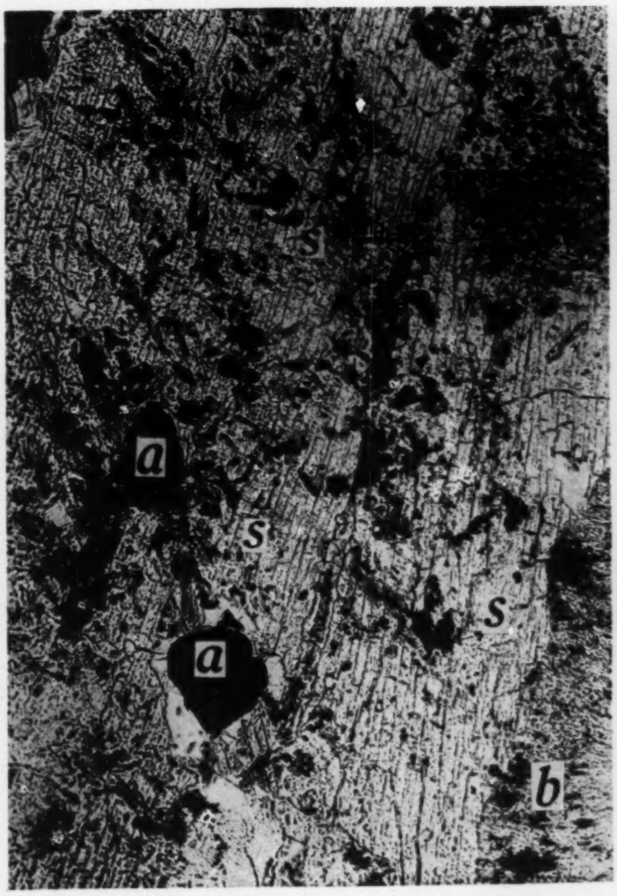

Fig. 5.

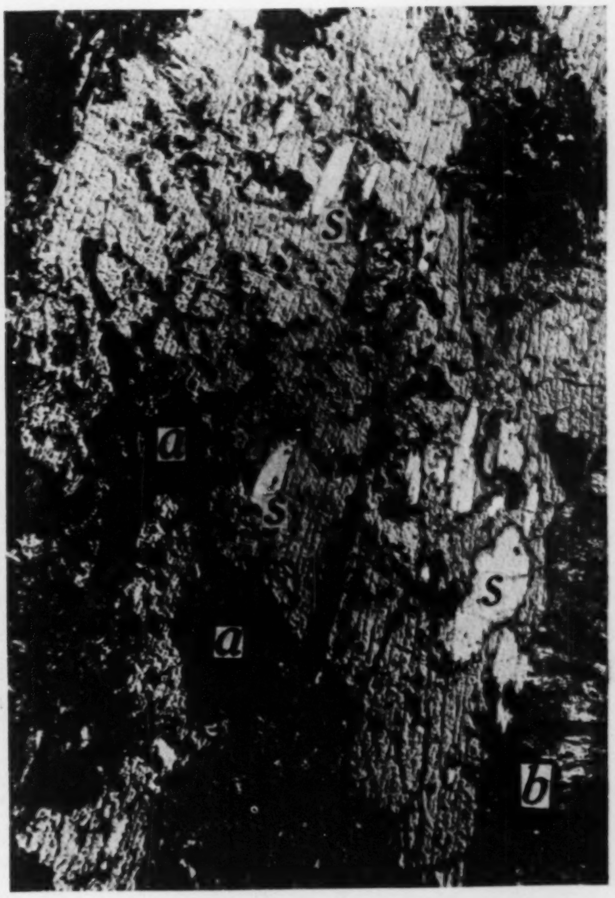

Fig. 6.

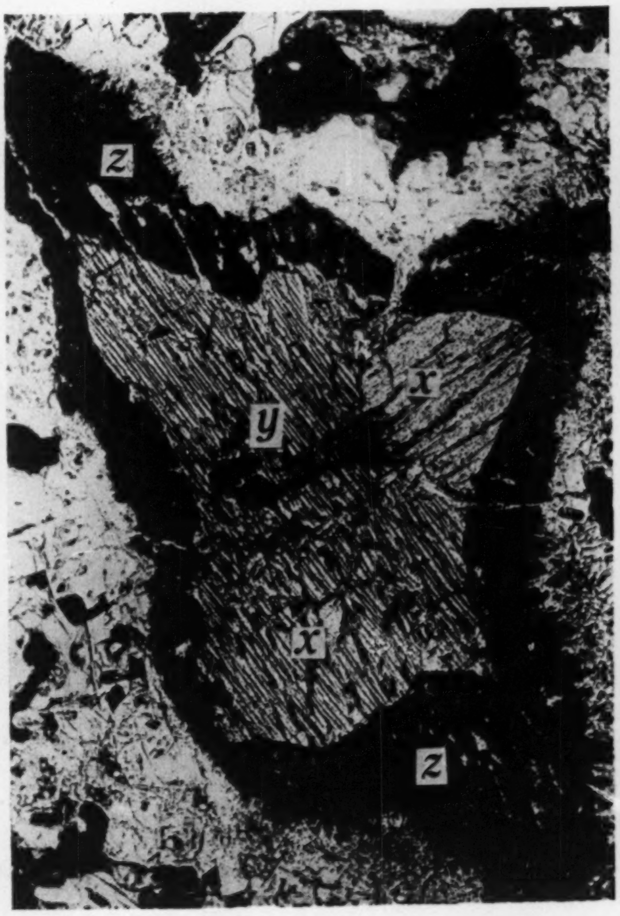

Fig. 7.

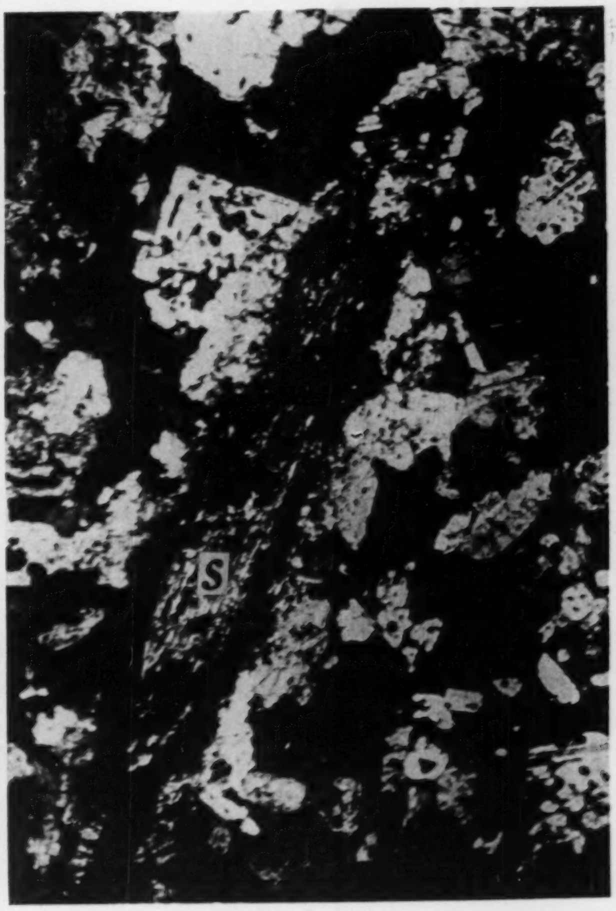

Fig. 8.

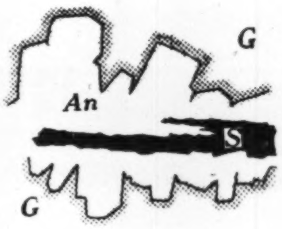

Fig. 9.

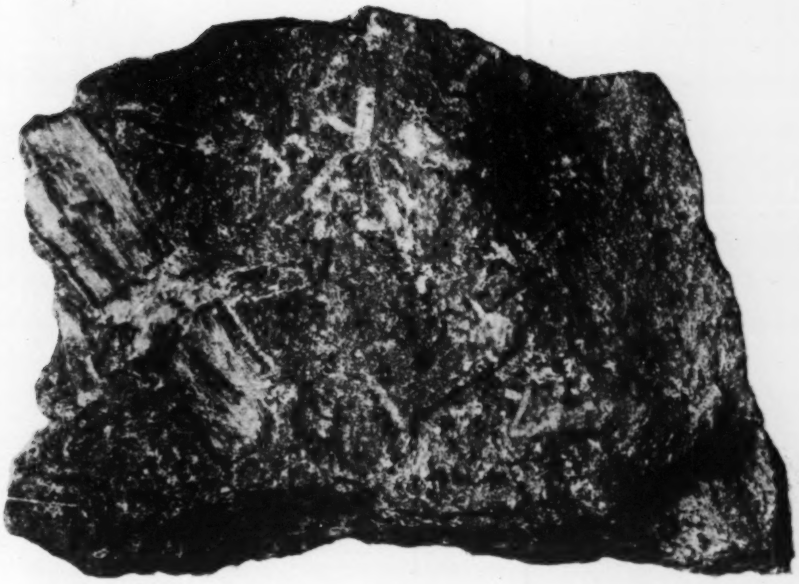

Fig. 10.

（震研彙報 第二十八號 圖版 森本）

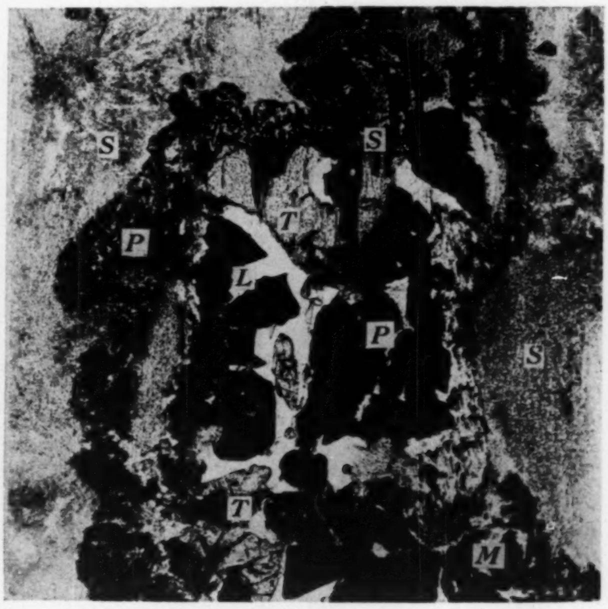

Fig. 11.

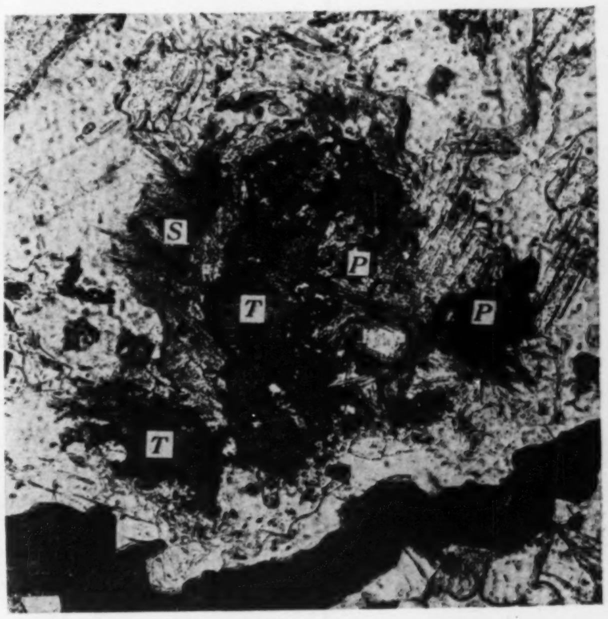

Fig. 12.

7. *A Statistical Investigation of Conspicuous Earthquakes in Japan during the Period 1933-1943.*

By Fuyuhiko KISHINOUYE and Mieko KOTAKA,

Earthquake Research Institute.

(Read Sept. 20, 1949.—Received May 31, 1950.)

1. One of the writers had made investigations on earthquakes felt at Tokyo, and the result was published in the former number of this publication.[1] We extended the investigation to conspicuous earthquakes in Japan. The seismic activity in Japan had generally been discussed so far only from data of disastrous earthquakes. But we studied it from data obtained with seismographs.

Earthquakes are classified by magnitude by the Central Meteorological Observatory of Japan in three according to the radius r of the felt area: *Remarkable earthquake* $r>300$ km.; *Moderate earthquake* $300>r>200$ km.; *Earthquake of small felt area,* $200>r>100$ km.

Neglecting the focal depth, the coordinates, time of occurrence, and class of the magnitude of the earthquakes were tabulated. Next, the difference of the time of occurrence and the distance between earthquakes which occurred in succession were entered on the table. The above-mentioned data were made use of in the following investigations.

2. Bearing and distance of the epicentres of successive earthquakes were plotted in turn as shown in Fig. 1. It may be only too natural that the bearing conformed to that of the length of the Japan Islands.

3. The frequency-distribution of the monthly numbers of earthquakes was examined with χ^2 -test to make clear which formula of distribution, Gauss's or Poisson's, fits better to the obeserved frequencies. The observed and the two calculated frequency-distributions are shown in Fig. 2. The values of χ^2 for Gaussian and Poisson's distributions were computed at 15.7 and 22.2 respectively. Therefore it may be concluded that the monthly numbers of earthquakes are distributed normally, or distributed uniformly and at random. This result applies to the case of earthquakes felt at Tokyo studied by one of the writers.

---

[1] F. KISHINOUYE, *Bull. Earthq. Res. Inst.*, 26 (1949), 73.

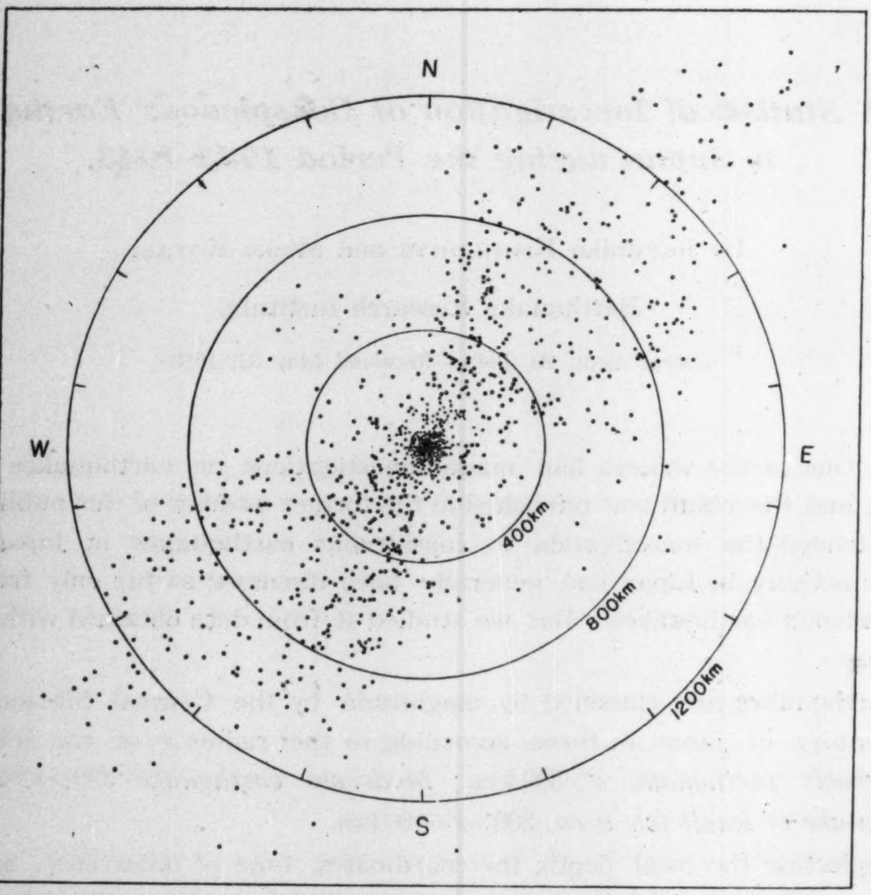
N
W
E
S
400km
800km
1200km

Fig. 1: Position of successive earthquakes.

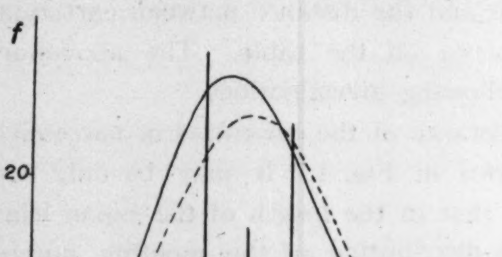

Fig. 2. Frequency-distribution of monthly number of earthquakes. (Full line: Gaussian distribution, dotted line: Poisson's distribution.)

4. The following table shows the relation of yearly numbers and the class of magnitudes of conspicuous earthquakes in Japan during 1933-1943. The χ^2 -test was applied to the table, and the value of χ^2 was computed at 33.3. The yearly number and magnitude proved to be not non-correlative, but from the data which are omitted here it became obvious that the monthly numbers were not correlative to the occurrence of remarkable earthquakes.

Table I.

Year / Magnitude	1933	'34	'35	'36	'37	'38	'39	'40	'41	'42	'43	Total
Remarkable	50	10	17	13	15	31	12	9	10	12	23	202
Moderate	40	12	23	11	21	36	17	15	22	18	22	239
Small Area	91	57	75	48	50	95	60	43	42	41	105	707
Total	181	79	115	72	86	162	89	67	74	71	150	1146

5. Relation between the distance and time interval of each succeeding earthquake is shown in Table II.

Table II.

Number of earthq. / Distance	0-1	2-3	4-5	6-7	8-9	10-20	Total
0-200 km	260	58	29	20	14	28	409
200-400	46	28	29	14	14	26	157
400-600	22	46	19	11	11	26	135
600-800	38	37	13	10	8	12	118
800-1000	30	21	20	12	5	19	107
Total	396	190	110	67	52	111	926

The contingency table was tested by the χ^2-test. Assuming non-correlation between the distance and the time interval, the value of χ^2 was computed at 160, so the distance to the next earthquake would have some relation to the time lag of occurrence.

6. The apparent velocity of propagation of seismic activity, or the ratio of distance to number of days to the next earthquake, was calculated. The mean apparent velocity was obtained as 165 km/day.

7. The difference of times of occurrence of earthquakes was reckoned successively. The relation between the two succeeding time differences in day are shown in Table III.

Table III.

n_2 / n_1	0-1	2-3	4-5	6-7	8-9	10-50	Total
0-1	222	78	40	16	14	54	424
2-3	69	53	28	25	15	27	217
4-5	45	28	18	14	7	17	129
6-7	23	18	10	8	6	9	74
8-9	21	8	12	2	5	13	61
10-50	41	31	18	11	13	25	139
Total	421	216	126	76	60	145	1044

Regarding the table as a contingency table, the χ^2-test was applied also in this case. The value χ^2 was obtained as 68.1, so the succeeding time intervals of earthquakes were considered to be not mutually independent.

8. The relation between distance and time interval of earthquakes before and those after the *remarkable* earthquakes were studied by the χ^2-test as before. The data are shown in Tables IV and V.

Table IV.

Number of earthq. / Distance	0-2	3-5	6-8	9-40	Total
0-200 km	44	4	6	6	60
200-400	14	14	9	7	44
400-600	4	8	2	6	20
600-800	7	7	4	5	23
800-1000	7	7	2	6	22
1000-2000	9	8	7	6	30
Total	85	48	30	36	199

The values of χ^2 were obtained as 40.4 and 51.6 respectively. Then there would be some relations between distance and the time differences of earthquakes which occurred before or after the *remarkable* earthquakes.

The frequency of numbers of earthquakes in the above tables (Table II and Fig. 1, Tables IV and V) will be affected by ring-shaped area limited by two distances (in the first column of the tables) which confine the interval. Multiplying the reciprocal numbers proportional to the area to the earthquake

Table V.

Distance \ Number of earthq.	0-2	3-5	6-8	9-29	Total
0-200 km	64	7	6	4	81
200-400	14	5	6	9	34
400-600	8	8	4	5	25
600-800	12	6	3	2	23
800-1000	6	5	4	6	21
1000-2000	4	9	5	6	24
Total	108	40	28	32	208

numbers, we checked the above results. But it was not necessary to change our conclusions.

9. Relation between earthquake numbers of a half-month and those of the next half-month is shown in the following table.

Table VI.

n_1 \ n_2	0-1	2-3	4-5	6-7	8-47	Total
0-1	33	37	13	5	2	90
2-3	37	44	27	11	4	123
4-5	13	27	19	5	7	71
6-7	5	9	7	4	3	28
8-47	2	7	4	3	5	21
Total	90	124	70	28	21	333

The value of χ^2 was obtained as 31.5, so it was concluded that half-monthly numbers of earthquakes are in some correlation to those of the next half-month.

10. Résumé.

Geographical and time distributions of conspicuous earthquakes which occurred in Japan during the period 1933–1943 were statistically investigated, applying χ^2-test. Monthly numbers of earthquakes were considered to be in normal distribution, so the numbers will be treated by the theory of probability, or the monthly numbers may be predicted statistically. It was also concluded that the monthly numbers were not independent of the magnitude of the earthquake.

The cost of this investigation was defrayed from the Scientific Expenditure of the Department of Education.

7. 日本における1933年から1943年までの間に起つた著しい地震の統計的研究

地震研究所 岸上冬彦
小高美江子

日本の地震活動については災害をおこした大地震によつて論じたものが多いが，こゝでは地震計によつて觀測された地震について調べた．材料は氣象要覽により，顯著・稍顯著及び小區域地震を採つた．

毎月の頻度は正規分布をなすので確率論で取扱ひ得ることを知り，地震の規模と年頻度とは無關係でないとの結果を得たことは，前に筆者の一人が東京の有感地震を調べた時と同様の結果である．その他，次の地震までの距離，次の地震の起る迄の日數等について相關表をつくり，χ^2 檢定法を應用して調べた．

---

8. *A Study on the Propagation of Microseismic Waves. Part II.*

By Ryôhei IKEGAMI and Fuyuhiko KISHINOUYE,

Earthquake Research Institute.

(Read Dec. 20, 1949.—Received May 30, 1950.)

1. We intend to solve the nature of microseisms under the assumption that microseisms are progressive waves, for their nature has not yet been ascertained in Japan and the other countries. We have already conducted the observations of microseismic waves since November, 1948 in Tôkyô, and some of the results were published.[1] From the last investigation we obtained the results of the microseisms which have the predominant period of 4 seconds in the winter season, but the microseismic storms which may be caused by the typhoons from summer to autumn have not yet been investigated by us.

For the purpose of studying the microseisms of the latter sort, we planned to observe microseisms at another place, where we have the tripartite stations situated more distantly than in the last case.

We will report in this paper a few of the results obtained, but these results did not enable us to solve the questions. Therefore we regret to say that we can not report the conclusive results in this paper.

2. We were able to use the yard of Tôkyô Astronomical Observatory through the good offices of Dr. Y. Hagihara, Mr. K. Tuzi and Mr. S. Nakano, and set up temporary stations at three places A, B and C as in Fig. 1. These three stations formed an equilateral triangle, the side of it being 285 metres.

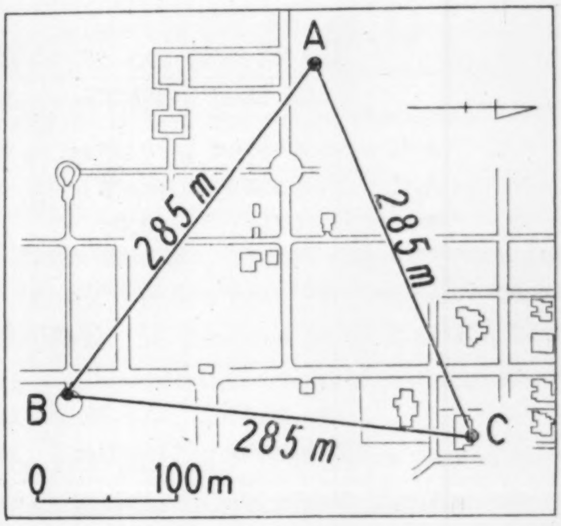

Fig. 1. Positions of temporary stations (At Tôkyô Astronomical Observatory.)

---

[1] R. IKEGAMI and F. KISHINOUYE, *Bull. Earthq. Res. Inst.*, 27 (1949), 75.

A tromometer was set up in NS-component at every station, and adjusted in the same conditions as in the last case. Every station was connected with wires, and electrical time-marks were sent out every one second from the main station (A).

3. In this paper we will report the results obtained from the observations of microseisms on October 26, 27, 28 and 29 in 1949. During these days, a typhoon (named Patricia) was sweeping from the eastern sea of Formosa to the eastern sea of Hokkaidô along Japan Islands. The track of this typhoon is shown in Fig. 2 by a bold line.

In Tôkyô the amplitudes of microseismic waves began to increase in the afternoon of Oct. 27, and became the largest in the afternoon of Oct. 28, when the center of this typhoon was passing off the eastern coast of Tôhoku district, Japan, and this condition continued until the typhoon died down.

The microseismic data obtained in this period were analysed by the same procedures as the last ones, and the mean time differences, that is to say, the mean of the differences in times of arrival between the station A and B, B and C, and A and C, were computed. These results are shown in Table I, and the bearings of wave propagation determined by these mean time differences are shown in Table II and in Fig. 2 by the arrows.

Table I.

	Oct. 26, 1949, 15*h* 26*m*.	Oct. 26, 15*h* 37*m*.	Oct. 27, 12*h* 25*m*.	Oct. 28, 17*h* 08*m*.	Oct. 29, 16*h* 43*m*.
A-B	0.054 sec.	0.159 sec.	0.042 sec.	−0.663 sec.	0.117 sec.
A-C	−0.364	−0.418	0.291	−0.807	−0.706
B-C	−0.418	−0.577	0.275	−0.145	−0.825

Table II.

	Oct. 26, 1949, 15*h* 26*m*.	Oct. 26, 15*h* 37*m*.	Oct. 27, 12*h* 25*m*.	Oct. 28, 17*h* 08*m*.	Oct. 29, 16*h* 43*m*.
Bearings	N 35° E	N 21° E	S 47° W	N 85° E	N 30° E
Velocities	626 m/sec.	478 m/sec.	877 m/sec.	329 m/sec.	318 m/sec.
Periods	3.9 sec.	3.5 sec.	2.9 sec.	6.6 sec.	5.9 sec.

These results, except the bearings on Oct. 26, show that microseismic waves came apparently from the center of this typhoon. They suggest that the dominant microseismic waves caused by deep depression such as that of a

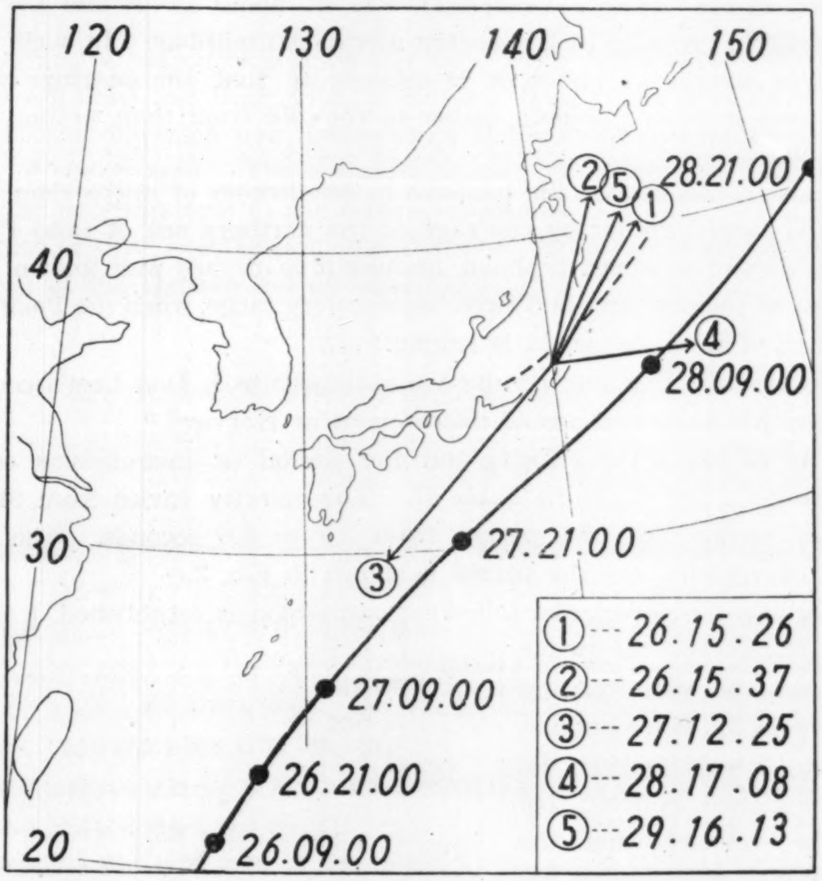

Fig. 2. Track of a typhoon (named Patricia) and bearings of microseisms on Oct. 26, 27, 28 and 29 in 1949. Dotted line shows position of a cold front on Oct. 26, at 15 *h* 30 *m*, 1949.

typhoon may be transmitted from their source. On Oct. 26, however, the bearings did not point to the center of this typhoon but to the opposite direction, namely, the bearings were N 35° E at 15*h* 26*m* and N 21° E at 15*h* 37*m*. We consider that this result suggests a substantially important problem about the cause and source of microseisms.

Judging from the weather map on Oct. 26, a few cold fronts passed over Tôhoku district from Japan Sea for the Pacific, and at about 15*h* 30*m* one of those passed over the eastern sea of Tôhoku district. On the other hand, the results of observations of sea waves and swells at a point on the Pacific (145° E, 39° N), where an observation-ship belonging to the Central Meteorological Observatory, Japan, makes oceanic observations unceasingly, reported that sea waves and swells became rough from 10 A. M. on Oct. 26 and these conditions continued till 4 P. M.

On Oct. 26 the typhoon (Patricia) was at about 24° N and 128° E, and the atmospheric pressure of her center was c. 960 millibar. In such weather conditions as mentioned above, it is noteworthy that the bearings of microseismic waves in Tôkyô pointed rather to the cold front than to the centre of that typhoon.

We must consider that the increase in amplitudes of microseismic waves in Tôkyô is caused rather by the rage of the northern sea of Bôsô Peninsula than by a distant southern typhoon, because it is already well known that the amplitudes of microseisms in Tôkyô become very large, when the Pacific Ocean of the north of Bôsô Peninsula is raging.

It is noticeable that our results are analogous to L. Don Leet's conclusions obtained by his investigations of microseisms at Harvard.[2]

4. The values of the velocity and the period of microseisms computed from these data are shown in Table II. The velocity varies from 318 to 877 metres per second, and the period from 2.9 to 6.6 seconds. The relation between the velocity and the period is shown in Fig. 3.

Concerning the waves, the following expression is established, i. e., $L=vT$, where L stands for the wave length, v for the velocity, and T for the period. If we put $L=$ 2.2 km. into this expression, the above mentioned relation between the velocity and the period applies well to this expression as shown by the curve in Fig. 3. One of the writers[3] found a similar relation in the dispersion curves of the surface waves on the occasion of his experiment on the ice of Lake Haruna, and K. SASSA[4] presented a similar relation in his paper on the seismic prospectings at Nagoya and Tottori. These relations found out by them were those of group velocity, and in these cases this relation can be explained theoretically. But we must consider that the relation found out by us was that of phase velocity, and in this case this relation can not yet be

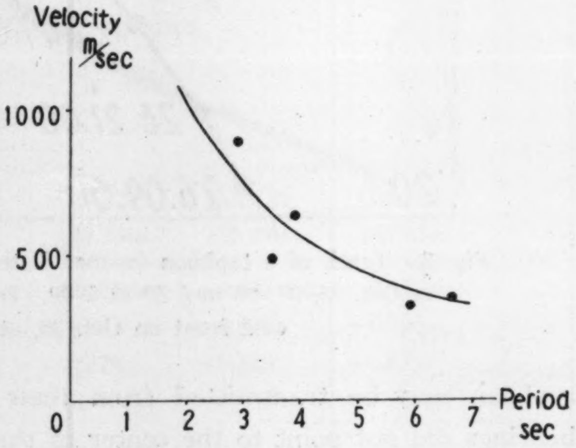

Fig. 3. Relation between measured mean velocity and period.

---

[2] L. DON LEET, *Bull. Seism. Soc. Amr.*, 38 (1948), 173.

[3] F. KISHINOUYE, *Bull. Earthq. Res. Inst.*, 21 (1943), 304.

[4] K. SASSA and others, *Disaster Prevention Res. Inst., Kyôto Univ.*, 2 (1949), 3.

explained theoretically. In consequence, our results will present a question to theorists.

The values of velocity obtained this time were remarkably smaller than the values obtained last time, viz., 2.4 km/sec. The cause of this difference passes our comprehension now, but perhaps this may be due to the geological difference of the ground. These results attract our attentions, and we will continue our investigations to solve these questions.

The cost of this investigation was defrayed from the Scientific Research Expenditure of the Department of Education.

---

8. 土地の脈動の傳播性の研究 (第2報)

地震研究所 {池上良平
岸上冬彦

脈動の傳播性その他の性質に關しての研究は多いが未だ尙多くの疑點を殘している．これらの疑點のいくらかでも解決したいと考えて三點觀測網を構成して研究して來た．前報1)では冬季一般に大きくなる脈動について研究したので今回は夏から秋にかけて平常は脈動の小さい時季に，颱風等の强い低氣壓に原因があると考えられている大振幅の脈動についてその傳播性や傳播方向を調べる目的で，東京天文臺の構內を借用し，ここで三邊夫々285米の所謂 Tripartite Stations, A, B, C を構成して同時觀測を實施した．(第1圖)．

今回の實驗は前回とは異つた場所でより大きい三角形を作り得た事，及び脈動發生の季節が異つている事等が前回の場合と異つている．

今回の觀測では1949年10月26, 27, 28, 29日の4日間にわたつて颱風 (Patricia) が臺灣東方海上から本州太平洋岸沖を北上し北海道北東方に去るまでの間に於てその進行につれて發生する脈動について研究し得た．その結果は次の通りである．

i) 颱風が臺灣東方にあつた26日には本邦三陸沖は寒冷前線の通過のため荒れていた．この日の脈動の傳播方向は一樣に，颱風の方向を示さず，むしろ荒れている三陸沖の方向を示した．(第2圖)．今迄に房總半島以北の海の荒れている時東京での脈動が常に大きくなる事はよく知られている事實であるが颱風が發生している場合でも，房總，三陸方面の海が荒れている場合には，脈動の發生は後者により多く影響されるらしいと云う事は注目すべき結果であつて，今後の研究によつて一層明らかになると思う．

ii) 颱風が九州南東方から北上して北海道北東方にぬけた27, 28, 29日には脈動は夫々その颱風の方向より傳播して來るような結果を得た．

iii) 第II表に示す如く週期は約3秒から7秒に，速度は約300米/秒から900米/秒に變化し，それら兩者の關係を圖に示すと第3圖の如くなる．この關係は $L=vT$ なる式に於て L (波長)=2.2粁としたときの v (速度) と T (週期) の關係に略一致しているようである．この結果は求めた速度が位相速度であると考える以上理論的な說明がつかぬ問題であつて，今後尙よく調べて見たいと考えている．尙速度は前回では約2.4粁/秒であつたのに今回の値がこれに比して著しく小である原因は觀測した地點が異なるためか或は他に原因があるのかも今後の問題に殘されている．

regarded theoretically. In conclusion, our results will present a question to theories.

The values of velocity obtained this time were remarkably smaller than the values obtained last time, viz. 2 km/sec. The cause of this difference passes our comprehension now, but perhaps this may be due to the geological difference of the grounds. These results attract our attention, and we will continue our investigations to solve these questions.

The cost of this investigation was defrayed from the Scientific Research Encouragement of the Department of Education.

[illegible]

[illegible]

[illegible]

[illegible]

[illegible]

[illegible]

[illegible]

[illegible]

9. *The Acceleration of Earthquake Motion Deduced from Overturning of the Gravestones in Case of the Imaichi Earthquake on Dec. 26, 1949.*

By Ryôhei IKEGAMI and Fuyuhiko KISHINOUYE,

Earthquake Research Institute.

(Read Feb. 21, 1950.—Received May 30, 1950).

1. Introduction.

The deductions of acceleration of earthquake motions drawn from the rocking or overturning of gravestones and the destruction of other constructions have played an important rôle in determining the intensity of the great earthquakes in the past. The acceleration was hitherto deduced mostly only from the ratio between height and width of the overturned gravestone, that is to say, ***the deduced acceleration of the ground motion=gravitational acceleration×width/height.*** But we believe that the deduction of the acceleration drawn only from the ratio between height and width is insufficient, for rocking or overturning of a rectangular column like a gravestone is not only related with this ratio, but also with the dimensions of height and width as shown clearly in our previous paper.[1]

In our field investigations, we often met with cases where gravestones had not overturned because of their large dimensions in spite of the small value of the ratio between height and width. In order to solve this apparently irrational phenomenon in case of the Nankai Earthquake on Dec. 21, 1946, we presented a tentative method.[2] The points of our method are as follows:

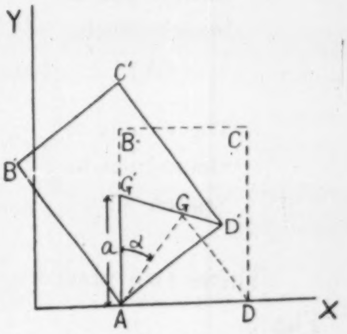

Fig. 1.

The works done by a column, while its center of gravity moves from G to G', (Fig. 1),

$$W_G=Mga\,(1-\cos\alpha)\,.\ \dots\dots\dots\dots(1).$$

On the other hand, the works done by ground motion, $\varepsilon\sin p(t+\delta)$, to the column are given in the following equation;

---

1) R. IKEGAMI and F. KISHINOUYE, *Bull. Earthq. Res. Inst.*, 25 (1947), 49.

2) *ditto.*

$$W_D=\frac{a^2M}{6}\left[\frac{m^2p^2}{(n^2+p^2)^2}\left(10+\cosh\frac{n\pi}{p}\right)-\alpha^2n^2\left(2-\cosh\frac{n\pi}{p}\right)\right.$$
$$\left.-\frac{2mn\alpha p}{n^2+p^2}\sinh\frac{n\pi}{p}\right], \quad\ldots\ldots\ldots\ldots\ldots\ldots\ldots\ldots\ldots\ldots(2)$$

where M is the mass of the column, g the acceleration of gravity, a the length AG, and α the angle $\angle GAB$, and $n^2=\frac{ag}{a^2+k^2}$, $m=\frac{a\varepsilon p^2}{a^2+k^2}$, in which k is the moment of inertia about G, ε and p are the amplitude and the frequency of the given ground motion.

Either overturning or non-overturning of the column due to any given ground motion may be deduced by comparing W_G with W_D. Namely, when $W_G>W_D$, the column is not to be overturned, but when $W_G<W_D$, the column is to be overturned.

2. Estimation of the Acceleration of the Imaichi Earthquake.

In case of the Imaichi Earthquake on Dec. 26, 1949, we could obtain the following data at two graveyards in Imaichi-Machi.

Table I.

Place		width × height	α	a	ratio
		cm. cm.		cm.	
Kawara-Machi, Imaichi-Machi. (A)	overturned	25 × 76	0.318	40.5	0.33
	non-overturned	36 × 128	0.274	66.4	0.28
The vicinity of Shimo-Imaichi Station. (B)	overturned	24 × 66	0.349	35.1	0.35
	non-overturned	36 × 120	0.291	62.6	0.30

These two places are shown in Fig. 2, and one of them is illustrated in Fig. 3.

We applied these values of a and α to the equation $W_G=W_D$, and giving the values of p, calculated the values of ε.

The relations between ε and p at the two places are shown in Figs. 4 and 5 respectively by curves I and II. Curve I is obtained from a and α of the overturned gravestone, and curve II from the non-overturned. When a ground motion expressed by the values of ε and p which correspond to the hatched parts surrounded by curves I and II is given, the high gravestone will not be overturned while the low one will be overturned by it.

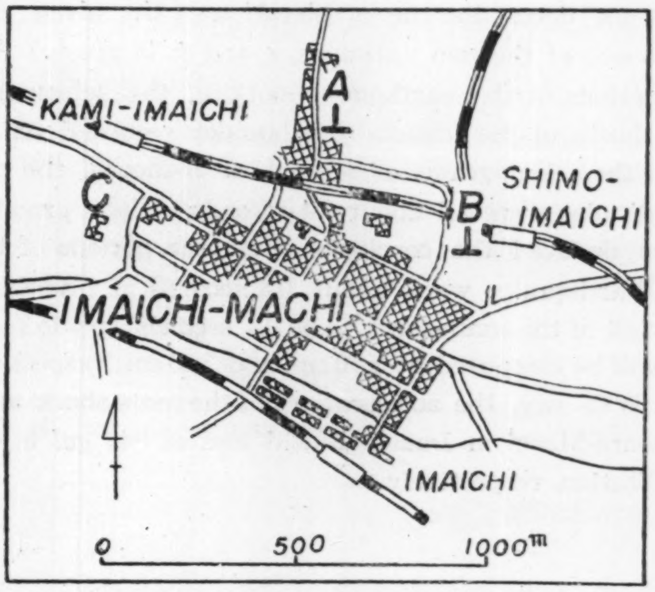
KAMI-IMAICHI
A
C
B
SHIMO-
IMAICHI
IMAICHI-MACHI
IMAICHI
0
500
1000m

Fig. 2. The map of Imaichi-Machi.

A: The graveyard at Kawara-Machi.
B: The graveyard in the vicinity of Shimo-Imaichi Station.
C: Observation Station of the after-shocks.

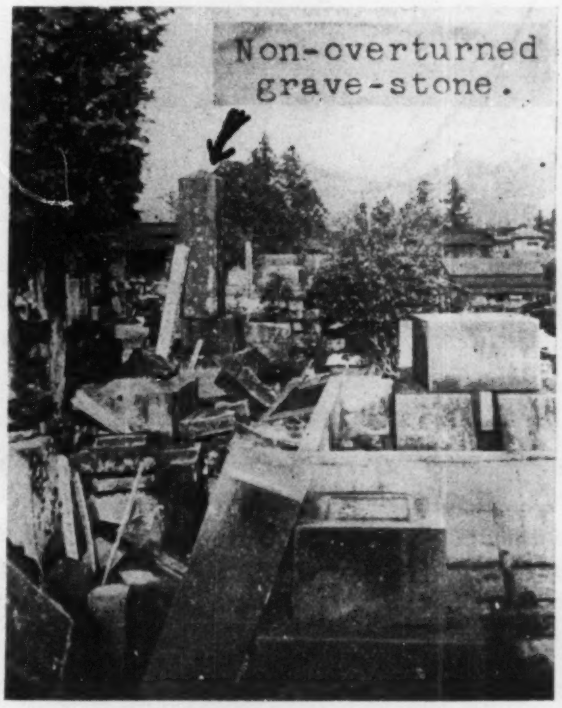
Non-overturned
grave-stone.

Fig. 3 Non-overturned gravestone, in the graveyard at Kawara-Machi (position A).

But we can not determine the acceleration of the given ground motion uniquely, unless one of the two variables, ε and p, is given. As a means of deducing the periods of the earthquake-motions, the seismograms obtained from the after-shocks of the Imaichi Earthquake recorded at Imaichi-Machi were used. In the seismograms of several after-shocks, the periods of the maximum amplitudes were all about 0.4 seconds. Upon grounds to be mentioned later we deduced the conclusion that the periods of the main-shock of the Imaichi Earthquake were about 0.4 seconds at Imaichi-Machi. If we assume the period of the main-shock to be 0.4 seconds ($p=15.7$), the values of the amplitude will be computed at 3.70 cm. and 3.85 cm. respectively from Figs. 4 and 5. That is to say, the accelerations of the main-shock are computed at 912 *gal* at Kawara-Machi in Imaichi-Machi and at 949 *gal* in the vicinity of Shimo-Imaichi Station, respectively.

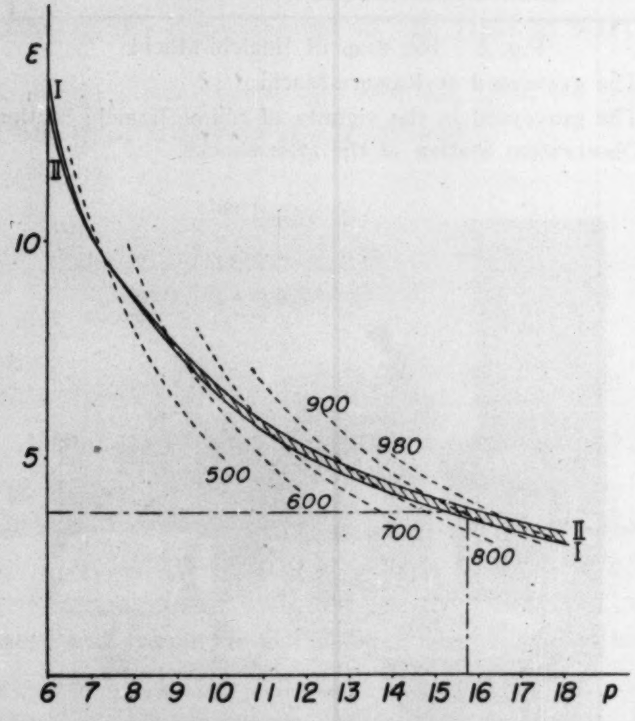

Fig. 4. Curves I and II show the limits of overturning and non-overturning of the gravestone at Kawara-Machi, Imaichi-Machi (position A). Dotted line shows curve of equal acceleration in gal.

Judging from the disaster suffered at Imaichi-Machi, these values of the acceleration may be considered to be overstimated, but the doubt will be dispelled by the following discussion.

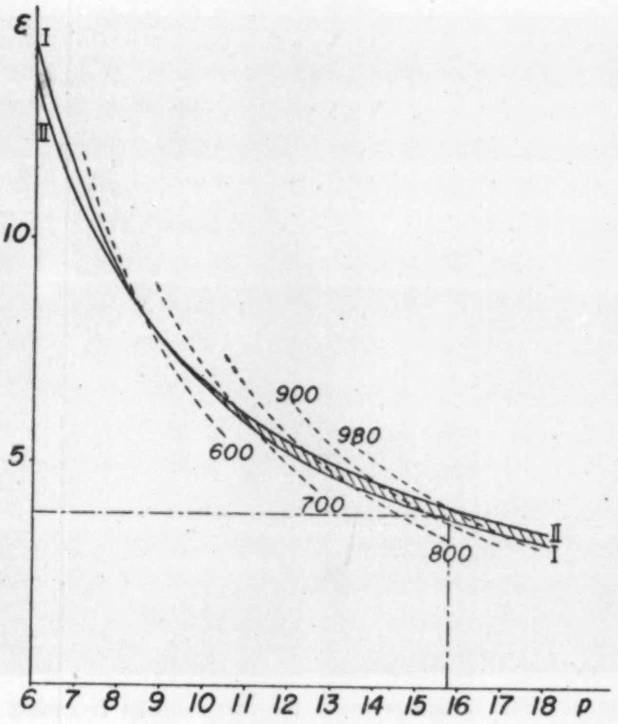

Fig. 5. Curves obtained from the data in the vicinity of Shimo-Imaichi Station (position B).

3. Discussion of the Results.

i) Application of our equations to the data of the Imaichi Earthquake.

Judging from the materials obtained by our field investigations of the Imaichi Earthquake, it seems probable that only one large amplitude or two of the ground motions continued and were damped very rapidly.

If we may consider that the after-shocks of the Imaichi Earthquake had a characteristic in common with the main-shock, we shall be able to identify the characteristic of the seismograms of the after-shocks observed at Imaichi-Machi with this above-mentioned characteristic of the main-shock. By way of illustration, we will show the characteristic in Fig. 6. As recognized from Fig. 6, after the P-phase lasted for a short time, the S-phase with the large amplitude appeared suddenly and repeated only once or twice before they decreased very rapidly. This characteristic of the ground motions accurately corresponds to the assumption in our theory, and we believe that our equations would have applied more precisely to the data of the Imaichi Earthquake than to the data of the Nankai Earthquake.

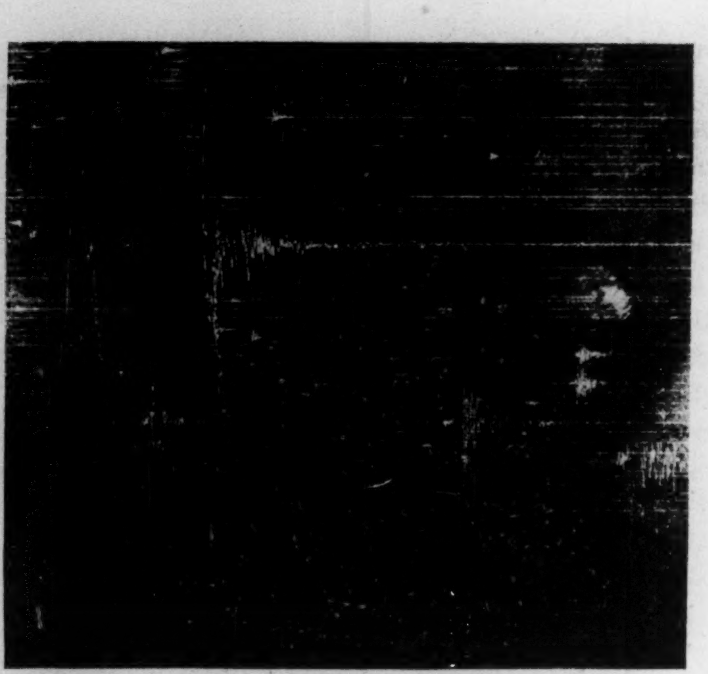

Fig. 6. The seismogram of the after-shocks recorded at Imaichi-Machi (position C).

ii) The doubt on the overestimation of the accelerations.

It was reported as the conclusive results of the field investigations of the Imaichi Earthquake by many investigators that there were scarcely any damages done to wooden houses, but many stone buildings which had been built with piled Ôya-ishi (Tertiary tuff quarried at Ôya, Tochigi Prefecture), were destroyed, which indorses the fact that the periods of the ground motions were rather short and the vibrations of the large amplitudes damped out rapidly. Damage would have been done to many wooden houses, if the ground motions of long periods and large amplitudes had continued for long time, and even in case the ground motions were of large acceleration, unless they continued long, the wooden houses would not be destroyed. Namely, it is probably not unfit to estimate that the maximum acceleration of the Imaichi Earthquake was very large.

iii) A few suggestions for future investigations.

A) It is not a complete estimation to deduce the intensity of earthquakes only from the ratio between the height and width of a gravestone. In case of the Imaichi Earthquake, the ratios of height to width of the overturned gravestones were 0.33 and 0.35, and if we deduce the acceleration as we used to hitherto, the estimated acceleration will be 0.33 g or 0.35 g. That is to say, we are in danger of underestimating, if the acceleration is deduced only from the ratio. We want to emphasize the necessity to take into account the dimensions of the gravestones in case of determining the acceleration of an earthquake motion.

B) In the past, the intensity of earthquake motion at a certain place was expressed by the value of the acceleration of the ground motion there. But to judge from the above-mentioned fact, we think that the intensity of earthquake at any place can be expressed only incompletely by the value of acceleration. In case of the Imaichi Earthquake, though the deduced accelerations were near gravity, the damages were confined only to stone-buildings. We can deduce from this fact that in spite of the high value of the acceleration, the amplitudes of the ground motions at Imaichi-Machi were small (namely, the periods were short) and the duration of that acceleration was comparatively short.

We think that in future, to estimate the intensity of an earthquake, the amplitude (or the period) of the ground motion and the duration of the acceleration as well as the value of the acceleration must be taken into account at any place.

---

9. 昭和24年12月26日今市地震に於ける墓石顚倒より推定した地震動の加速度

地震研究所 池上良平
地震研究所 岸上冬彦

従來大地震の際の加速度推定の資料として顚倒した墓石等を用ひて，その巾と高さの比から推定する事がしばしば行なはれて來た．然し加速度の推定を唯單に墓石の巾と高さとの比のみから行ふ事は不十分であると考へる．即ち大地震後の現地調査にあたつて，我々は比の値が大でもその墓石自身の大きさが小さいために顚倒し，逆に比の値が小であるにも係らずその大きさが大であるために顚倒しなかつた例をしばしば發見するのである．

昭和21年12月21日の南海地震の際にもこの例を海南市と木本市に於て發見し，これを解決する一つの方法を發表した.1)

今回の今市地震に於ても今市町内の2ヶ所（第2圖 A, B）に於てこの例を見出し，前回の方法と同様な取扱ひによつて加速度を推定した．その結果として本震の週期を0.4秒とすると加速度は夫々2ヶ所で912ガル及び949ガルとなつた．これらの値は被害程度から考へて一見過大のようであるが，然し次の理由から必ずしもそうでないと考へる．即ち加速度の値が大であつても，振

幅が小（週期が短）であつて且つその加速度を持つた振動が長く續かなければ，木造家屋のような建造物には大して被害はなくてすむと考へられる．事實野外調査の結果今回の地震は大振幅の振動は比較的早く減衰したらしい，又被害を受けた建造物は“大谷石”で積み上げたものや，又は石貼の石造建物が大多數であつて，木造家屋の被害は殆どなかつた事を考へ合せると以上の推定が甚しくは間違つてゐないと考へられる．

以上の事から考へて將來大地震の加速度の推定にあたつては，墓石等の比のみから行ふ事は過小に推定する危險があるから，その墓石自身の大きさも考へに入れて行ふ必要があると考へる．又ある地點での加速度の大きさのみを問題とせず，その繼續時間とか，振幅（又は週期）の大きさ迄も考慮に入れるべきであると考へる．

---

10. Change of the Ground-water Level due to the Imaichi Earthquake.

By Daisuke SHIMOZURU,

Earthquake Research Institute.

(Read Feb. 21, 1950.—Received May 30, 1950.)

Preface.

Soon after the earthquake of 26th of Dec. 1949, which occurred in Imaichi district, Tochigi Prefecture, the writer went there principally to investigate the time variation of the ground-water level. For this purpose, he asked several suitable persons to observe, during January this year, the water-level of their wells once every morning before they bail water out of them. Dotted marks in Fig. 1 indicate the position of those wells, but, to the writer's regret, the results of the observation could not be obtained from all of them.

Change of level just after the earthquake.

The area where the ground-water level had been disturbed by the main shock covers the region including the towns of Nikko and Imaichi, and the villages of Toyo-oka, Shinden, Yamakubo, Ōsawa, Okurugawa and Itaga. The water of the wells decreased or dried up everywhere in this region, with the exception of the western half of Itaga, where it increased. The increase of water in the well or spouting of sand and water such as was observed at Fukui alluvial plain in the case of Fukui Earthquake did not occur at the fan of Daiya River. Fig. 2 shows the change of water-level at Itaga village.

Time-variation of ground-water level after the earthquake.

Fig. 3 shows the results of the observation of water-level referred to above. These curves have many features common to each other. That is, after the earthquake, the water-level fell down until it reached a minimum point, and then gradually rose up, but the water-level has not yet attained the level prior to the earthquake. At Nagahata, the place nearest to the epicentre, the water-level became stationary earlier than at other places. A similar change was reported in the case of Fukui Earthquake, 28th of June 1948. In the present case, it is obvious if we consider the data of rain-fall and barometric pressure, that these meteorological conditions did not play an important rôle. Then what could be the main cause of these changes of

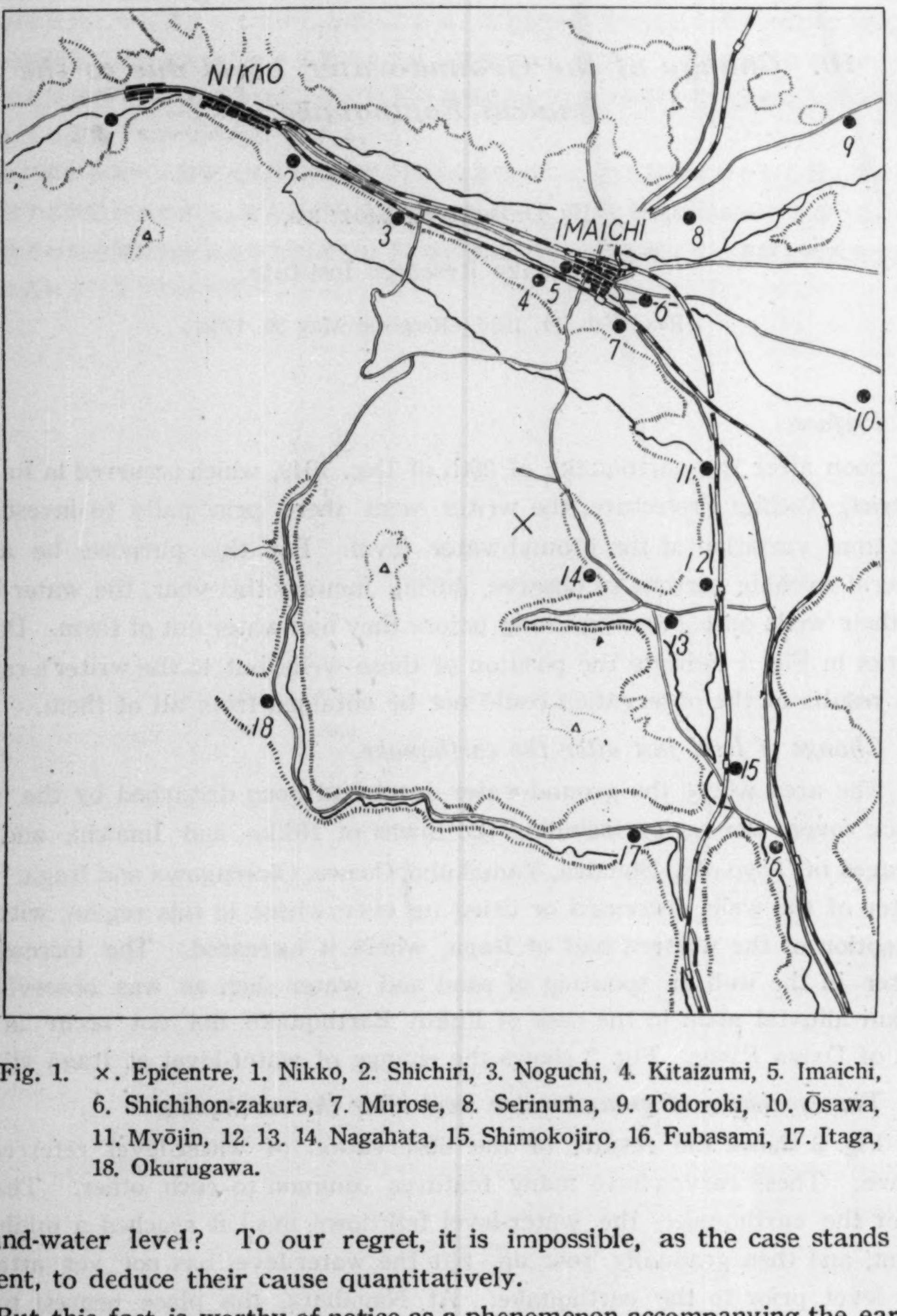

Fig. 1. ×. Epicentre, 1. Nikko, 2. Shichiri, 3. Noguchi, 4. Kitaizumi, 5. Imaichi, 6. Shichihon-zakura, 7. Murose, 8. Serinuma, 9. Todoroki, 10. Ōsawa, 11. Myōjin, 12. 13. 14. Nagahata, 15. Shimokojiro, 16. Fubasami, 17. Itaga, 18. Okurugawa.

ground-water level? To our regret, it is impossible, as the case stands at present, to deduce their cause quantitatively.

But this fact is worthy of notice as a phenomenon accompanying the earthquake.

Some other particular changes.

a) In the case of a well in a lumber mill at the southern end of Imaichi town, they could not use the pump from the middle of November 1949 due

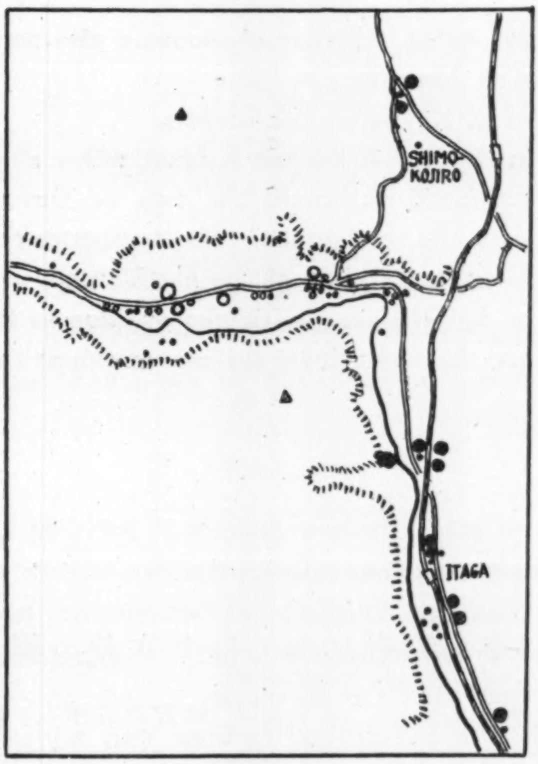

Fig. 2. Change of the ground-water level at Itaga village.

● Level fell down more than 2 feet. ○ Level rose above more than 2 feet.

• „ 1-2 feet. ∘ „ 1-2 feet.

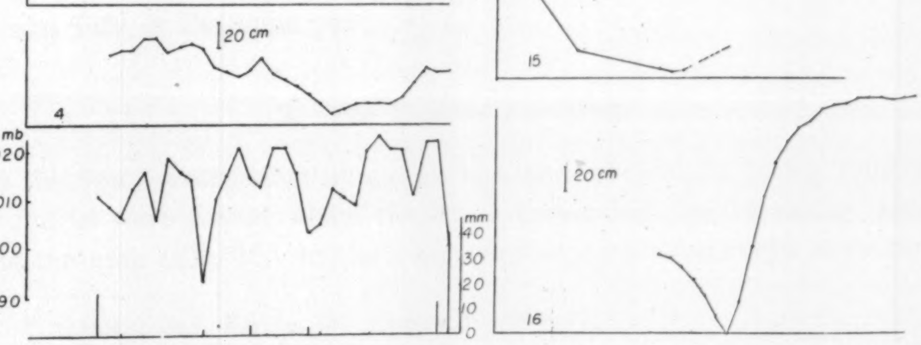

Fig. 3. Time-variation of the ground-water level at 2, 3, 4, 13, 15, 16 in Fig. 1. Rain fall and barometric pressure at Utsunomiya city are shown at the bottom of the left side.

to the decrease in the water. Similar phenomena also occurred at Shichihonzakura, Kissawa and at Murose.

b) Sakura hotel at Kinugawa hot springs.

They say that in the middle of last August, silver ring became black due to the spouting of sulpheric substance for two or three days. The same occurred at the time of the earthquake. The temperature of the hot springs has risen by 2°C-3°C from the time of the earthquake.

In conclusion, the writer's sincere thanks are due to those men who took the trouble to observe the water-level for one month at the writer's request.

---

10. 今市地震に依る地下水位の變化

地震研究所　下鶴大輔

福井地震の際に地下水位の時間的變化に興味ある點を見出したので，今回の今市地震の時は地下水位の時間的變化を主に調査した．十數箇所の井戸水位の1月間の毎日1回の觀測を依頼してその結果に就いて調べると，板荷村の西半分を除いていづれも地震に依つて水位がぐんぐん減少し，ある極小値に達してから又次第に水位が恢復しつゝある事が判つた．此の結果を定量的に解析する事は不可能であるけれども，もつと徹底的に調べれば，地震に伴つた現象としてその價値を發揮するかもしれない．

11. Precise Leveling at the Eastern Foot of Volcano Usu.

By Syun'itiro OMOTE,

Earthquake Research Institute.

(Read Apr. 18 1944, Sep. 19, 1944.—Received May 31, 1950.)

1. Introduction.

The eruption of Mt. Usu in Hokkaido which began in July 1910[1] resulted in the formation of 45 new craters on the northern plains of the volcano. After that it stopped activity and lay dormant for many years. Then, on Dec. 27, 1943, the inhabitants at the foot of Mt. Usu were frightened at the occurrence of a large number of earthquakes. The frequency of felt earthquakes increased day by day, until at last on Jan. 4 of the next year more than 300 earthquakes were felt in one whole day at the northwestern foot of the mountain, and it was feared that might be heralding an eruption. The seismic activities in these regions decreased quickly in February, but by this time it became clear that, in the wake of very shallow earthquakes, a remarkable crustal deformation, namely the elevation movement of land, was proceeding on the eastern plains of the mountain. There ran from north to south across this elevating area a road, a water drain for irrigation, a railway line and the River Osaru, and these were all cut at many points as the result of the rising of ground that had now taken place. The present author[2] visited the scene of disturbance with Dr. T. Minakami[3] in March 1944 to make precise measurements, and also conducted the second and third surveys in April and July of the same year.

2. The Precise Leveling.

In the first investigation made at the end of March, seven temporary bench marks were placed along the road traversing the elevating area as seen in the map (Fig. 1). In the second investigation resurveys were carried

---

1) F. OMORI, *Bull. Earthq. Inv. Comm.*, 5 (1911), 1.

2) S. OMOTE, *Spec. Bull. Earthq. Res. Inst.*, 3 (1944), 23.

3) T. MINAKAMI, *Spec. Bull. Earthq. Res. Inst.*, 3 (1944), 1. *Bull. Earthq. Res. Inst.*, **25** (1947), 65, 71; **27** (1949), 123, 129.

out with these bench marks to find the amounts of their upheaval during the interval of a month. From the result represented by curve A in Fig. 2, we know that BM-5 had elevated more than 5 meters within a month. The upheaval movement of this area was so conspicuous that the daily changes in the altitude of these bench marks could be measured. The amounts of upheaval of the bench marks within a whole day, from April 17th to 18th and from 18th to 19th, are given in Fig. 3-A. In this figure the movement at BM-5 is found to have been the most active, the upheaval velocity amounting to 30 cm. per day. Dividing the amount of upheaval of each bench mark during the period between the first and the second surveys by the number of days in the same period, we get the average daily amount of upheaval during that period. The average daily changes in the respective bench marks are shown in Fig. 3-B. This curve closely resembles the curves in Fig. 3-A, which show the actual daily changes in the altitude of the bench marks. The similarity of these two groups of curves in Fig. 3

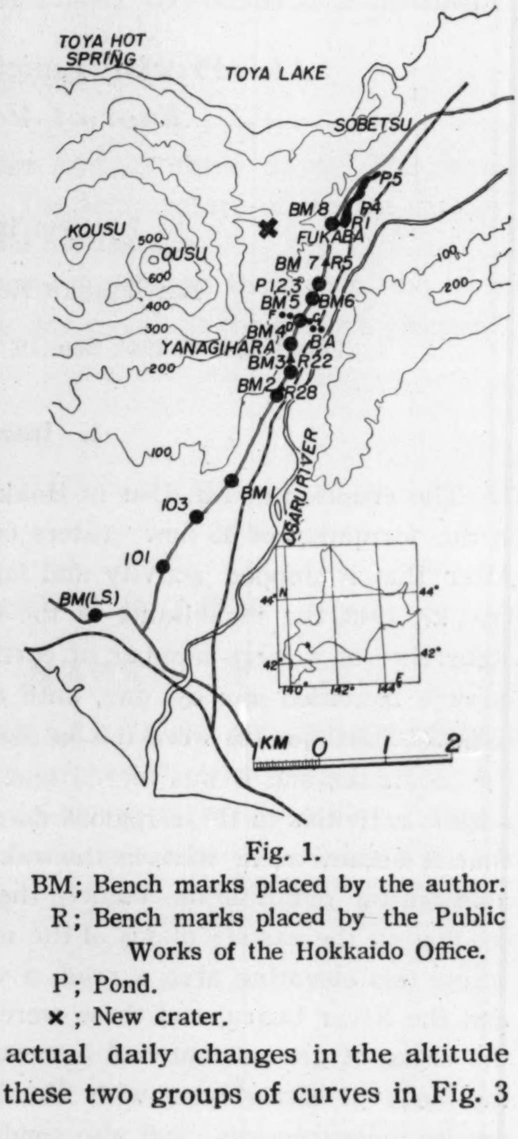
TOYA HOT SPRING
TOYA LAKE
SOBETSU
P5
BM 8
R4
R1
FUKABA
KOUSU
500
OUSU
600
400
300
BM 7
R5
P1,2,3
BM 5
BM6
F
C
BM 4
D
YANAGIHARA
B
A
BM3
R22
200
BM2
R28
100
OSARU RIVER
BM1
103
101
BM(LS.)
100
200
44°
N
42°
140°
142°
144°
E
KM 0 1 2

Fig. 1.

BM; Bench marks placed by the author.
R; Bench marks placed by the Public Works of the Hokkaido Office.
P; Pond.
×; New crater.

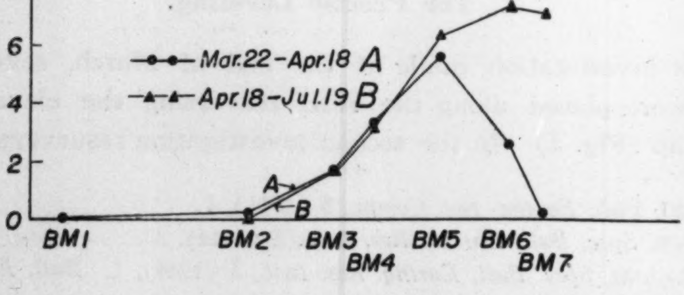

Fig. 2. Changes in the altitude difference of bench marks.

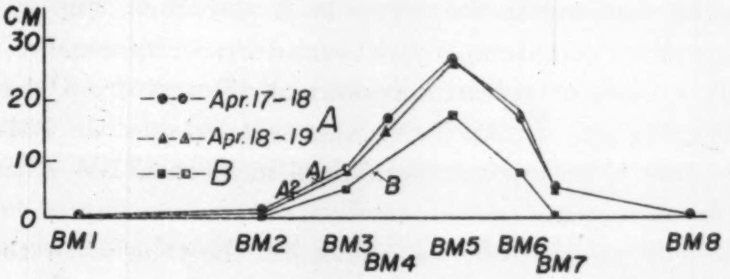

Fig. 3. Changes in the altitude difference of bench marks.
A; Changes within a whole day.
B; Averaged amount of change per day.

may indicate that the upheaval had continued with an almost constant velocity day by day from March to April, which is a very remarkable fact concerning the mechanism of the upheaval phenomena.

The third leveling survey was carried out in July after the explosions had begun at the newly formed crater. Changes in the altitude of bench marks during the three months that had elapsed after April are shown in Fig. 2-B. In this case too, as in the second survey, the amount of upheaval of each bench mark during the whole day from July 16th to 17th has been measured. The result is to be seen in a curve in Fig. 4-A. Also, as we did in the second survey, we calculated from Fig. 2-B the average daily change in the altitude of each bench mark during the period from April to July. The result is shown by a curve in Fig. 4-B. If we compare these two curves, A and B in Fig. 4,

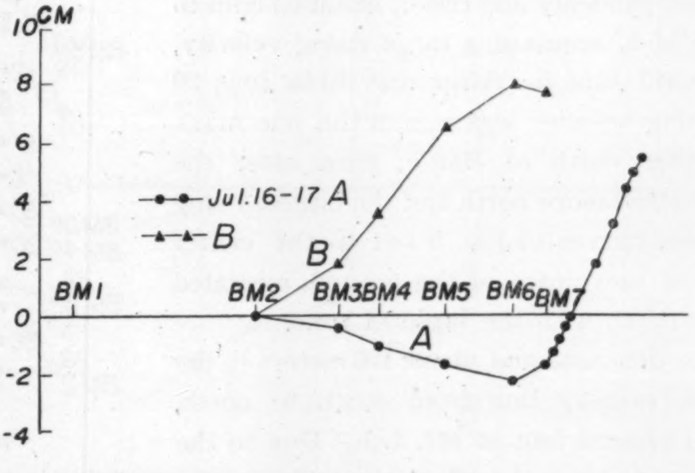

Fig. 4. Changes in the altitude difference of bench marks.
A; Changes within a whole day.
B; Averaged amount of change per day.

we at once notice that, unlike the curves in A and B of Fig. 3, these two curves in Fig. 4 differ considerably from each other in appearance. This tells us that in July a mode of upheaval movement different from that in March and April was going on. In April the upheaval velocity at BM-5 was the largest, but in July it became very small, and in its stead BM-7 came to show the most active movement.

From these curves, however, we cannot tell the time when the rising of BM-5 became less active and that of BM-7 became conspicuous.

Fortunately, at the end of April temporary bench marks of wooden piles were set up by the Bureau of Public Works of the Hokkaido Office along the same road along which our bench marks, BM-1 to 7, had been installed. The geographic distribution of these pile marks will be seen in the map of Fig. 1. It will be observed that some of the pile marks were installed very near to the author's bench marks. After April levelings were repeatedly carried out with these pile marks. The curves in Fig. 5 show the altitude of the respective bench marks at different times. From these curves we may infer the mode of the velocity change in the upheaval movement of each pile mark throughout the whole period from April to July. To facilitate comparison the level changes in the author's bench marks are given with open circles in the same figure. From Fig. 5, then, we see that the rising velocity was the largest at BM-5 in the period from April to May 23, after which date the activity of BM-5 decreased suddenly and BM-7, installed 60 m to the north of BM-5, acquired a large rising velocity, which lasted until June 5. After that up to June 20 the largest rising velocity was seen at the pile mark 5, a pile further north of BM-7; then after the pile marks situated more north had the largest rising velocity. These curves in Fig. 5 tell us the center of the upheaval movement of the ground migrated from south to north with the lapse of time.

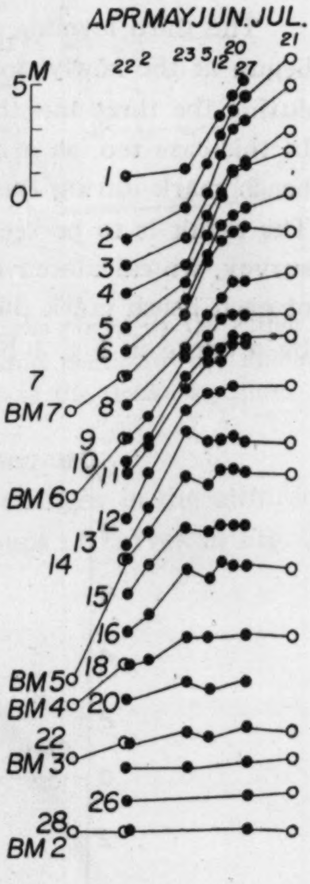

Fig. 5.

Altitude change of pile bench marks as compared with B. Ms. 2~7.

Parallel to this road and about 100 meters to the east runs the railway line from south to north, traversing the eastern foot of Mt. Usu. Due to the topographic changes just described the railway also suffered serious damages. Detailed leveling surveys along the railway were carried out by the Department of Railways, and the results were laid at the author's disposal through the courtesy of the authorities. The changes in the altitude of the bench marks distributed along the railway will be seen in Fig. 6. We notice in it that, although the amount of upheaval of the railway bench marks was certainly less than that of the pile marks along the road, the manner in which the upheaval movement proceeded in the two cases was much alike.

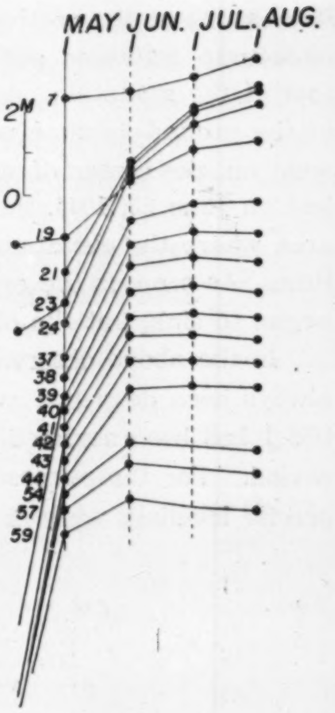

Fig. 6. Altitude changes along the rail-way.

The leveling routes surveyed above all ran from south to north; in other words, the routes ran parallel to the concentric arc of Mt. Usu. So in the second survey a leveling route A, B, ···F, that runs in the radial direction of the mountain and joins the route I at BM-5, was selected. The leveling surveys were made along this route three times on April 21, 22 and July 20 (Fig. 7, A & B). The changes in the level became smaller and smaller to the east, or in other words the lower marks were less elevated than the higher ones, and it appears probable that the center of the upheaval lay on the west side of the road.

These several evidences afforded by leveling surveys made us infer that the activities of Mt. Usu, which began on Dec. 27, progressed in the following

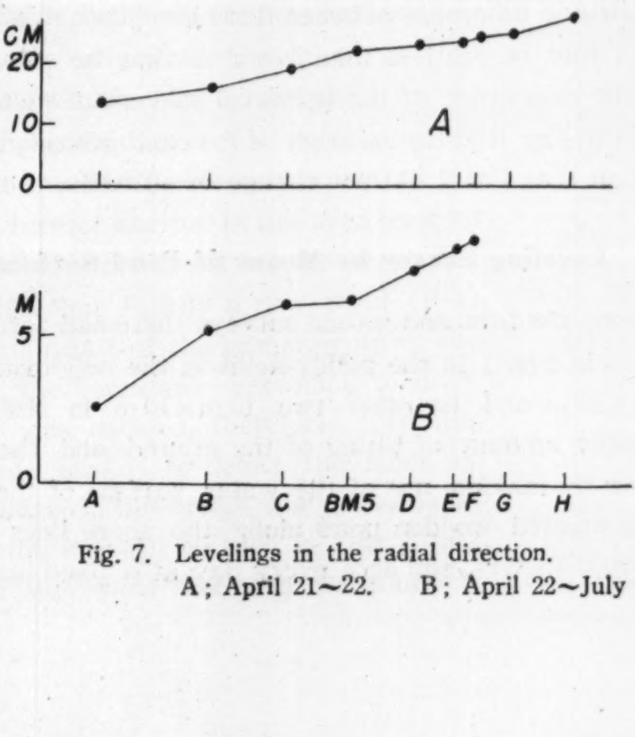

Fig. 7. Levelings in the radial direction.
A; April 21~22. B; April 22~July 22.

way: (1) in the first stage of activities, earthquakes began to be felt by the inhabitants at the northwest foot of Mt. Usu; (2) two months later, the center of seismic activities shifted to Yanagihara, a village situated at the eastern foot of the mountain, and at the same time a conspicuous upheaval movement of the ground became noticeable in the epicentral region; (3) then as time went on, the center of elevation migrated gradually northward, and (4) at last on June 23, 1944, the first eruption broke out near Fukaba village, the area where the elevation velocity is supposed to have been the largest at that time. As soon as the eruptions began certain places remote from the crater began to sink, but the observed amount of subsidence did not exceed 20 cm.

In the above observation, the altitude of the author's bench marks has always been described with reference to that of BM-1, and the altitude of BM-1 has been assumed to have remained unchanged throughout the whole period. For the purpose of discovering any change in the altitude of BM-1, precise levelings were carried out twice between our BM-1 and BM-345 of the Land Survey, which was situated at 3.5 km to the south of BM-1. The change in the altitude difference between these two bench marks in the period from April 19 to July 14 was less than 5 mm, as may be seen in Fig. 8.

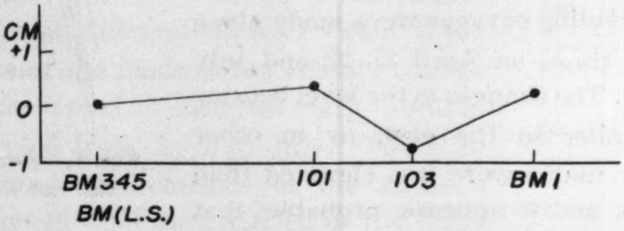

Fig. 8. Change in the altitude difference of BM 1 compared with the BM 345 of the Land Survey.

In view of the magnitude of the upheaval movement we are dealing with, it would be safe to say that the accuracy of the conclusions will not be affected by the assumption that BM-1 did not change in altitude.

3. Leveling Survey by Means of Pond Surfaces.

At the time of the first and second surveys there had formed three ponds P-1, P-2 and P-3 in Fig. 1 in the paddy-fields in the neighbourhood of BM-6, P-1 being 60 m×80 m and the other two 10 m×10 m in size. We tried to ascertain the daily amount of tilting of the ground and the azimuth of its maximum tilting by making use of the water surface of these ponds. For this purpose we erected wooden poles along the shore lines of the ponds at intervals of several meters, and once every day at a fixed hour the height of the water surface at each pole was read off. As these ponds happened to be in the region where the crustal deformation was going on most actively, the relative level change of the water surface with respect to two poles widest apart in the direction of maximum tilt exceeded 4 cm in a whole day. This convinces us that the amount of the tiltings observed in this way can be taken as sufficiently reliable. The result obtained is given in Table I. The amount of tiltings in Table I is so large that one might say it is extremely rare that such a great crustal deformation should be caught and observed in the course of its progress. In the calculation of tiltings the sine curve method was employed. Some examples of such curves are shown in Fig. 9. At the time of the third survey the center of upheaval lay in the neighbourhood of BM-7 and it was found necessary to extend the leveling route further north. In this area leveling surveys were rendered difficult by the heavy fall of volcanic ashes, but luckily a new pond (P-4) had formed as a result of the damming-up of the River Sobetsu, the backwater extending to more than 1 km. It was decided, therefore, that this should be made use of to detect the mode of topographic changes in this area. The position and the tiltings of the P-4 will be seen in Figs. 1 and 10. From the survey of this pond we found a

Table I. Tilting of the ground revealed from the survey by means of the pond surface. I; maximum angle of tilting. Z; azimuth of maximum tilting.

P—1			P—2			P—3		
Period	I	Z	Period	I	Z	Period	I	Z
April	′ ″	N W	April	′ ″	N W	April	′ ″	N W
13~14	3 50	85°	17~18	3 05	83°	17~18	2 25	71°
15~16	4 40	81	18~19	2 40	80	18~19	2 43	71
16~17	4 40	82	19~20	2 30	81	19~20	2 40	71
17~18	5 00	84	20~21	2 20	71	20~21	2 56	71
18~19	5 00	84	21~22	2 20	75	21~22	2 50	68
20~21	2 40	78	22~23	2 30	75	22~23	3 37	67
21~22	4 10	79						

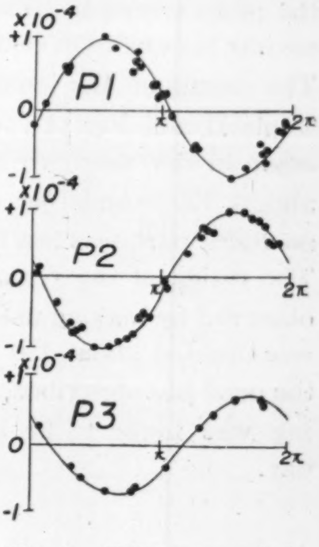

Fig. 9. Tiltings revealed by pond surface.

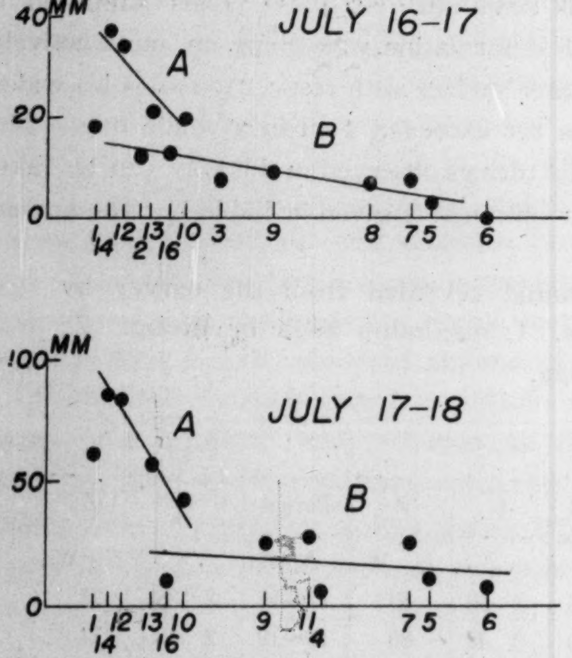

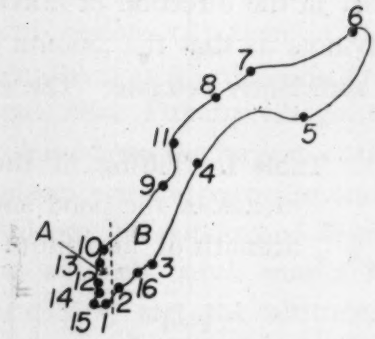

Fig. 10-II.

Fig. 10-I. Tilting of ground revealed by the survey of Pond-4. Location of dots corresponding to respective figures in Fig.10-I are seen in the map of Fig. 10-II. The amount of tilt in the A-part is definitely larger than the B-part.

distinct difference in the mode of crustal deformation between the southern part and northern part of the pond, as to be seen from the two curves, A and B, in Fig. 10. The boundary between the two parts exactly corresponded to the place where the Takinoue lava and the somma lava were in contact in geological ages. The result of the analysis will be seen in Table II and Fig. 11, A & B. The tilting angle in the southern part of the pond was almost 100 seconds per day, while that of the northern part was less than 10 seconds a day. The tilting of the region further north was observed by making use of a small pond which was situated about 100 meters to the north of the pond just described, and the angle of tilting was found to be less than 1 second per day.

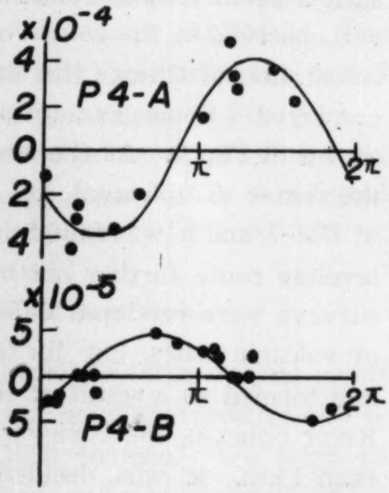

Fig. 11. Tilting of the Pond-4. The amount of tilting of the A-part is larger than the B-part.

Table II. The angle and azimuth of maximum tilt of the Pond-4.

Period	$I \times 10^{-4}$	Z
July 12~13	4·6	N 125° W
13~14	4·0	145
14~15	3·4	165
15~16	4·2	60
16~17	3·6	135
17~18	4·3	117
18~19	4·6	140
19~20	4·6	105

4. Leveling Surveys by Means of the Water Surface of Lake Toya.

In connection with the activity of Mt. Usu, it was considered an important study to know how far the phenomena of crustal deformation due to the present activity extended. It is almost impossible, however, to carry out a precise leveling over the vast area, so the Lake Toya situated to the north of the active area has been used for that purpose.

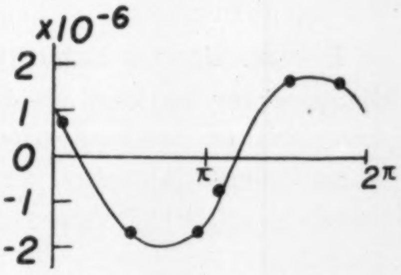

Fig. 12. Tilting of the Lake Toya.

Table III. Leveling survey by means of the water surface of Lake Toya.

No. of Bench Mark	T-1	T-2	T-3	T-4
Location	Toya Hot Spring	Nakano-Shima Is.	Muko-Toya	Takinoue
II. Observed date	July 20	July 20	July 19	July 19
Hour	13h	9h	16h	10h
Temperature	24°C	25°C	25°C	22°C
Wind	gentle	gentle	none	none
H' (cm)	231.37		214.36	106.54
△H' (cm)	−1.12		−0.25	0.00
H (cm)	232.49		214.61	106.54
I. Observed date	Apr. 22		Apr. 22	Apr. 22
H (cm)	342.71		324.14	217.68
Difference(II-I) (cm)	110.22		109.53	111.14

In the second survey, bench marks were placed at four points along the lake shore, namely, Takinoue, Toya Hot Spring, Muko-toya and Nakanoshima. The height difference between each benchmark and the surface of the water was measured as carefully as possible. Fortunately the weather was extremely calm and the water smooth when the survey was made, and we believe the probable errors involved in the observed values are less than 2 mm. The resurvey took place in July, and on that occasion a mercury manometer and a Y-level were used for greater accuracy. Among the four bench marks that of Muko-toya was the most distant from the active area, and we assumed that the altitude of this mark remained unchanged for the three months from April to July. By referring to this mark, the amounts of upheaval of the bench marks of Takinoue and Toya Hot Spring were measured as 16.1 mm and 6.9 mm respectively. The angle of tilting in the lake region calculated from these surveys was 20×10^{-4} and azimuth of maximum tilting was N 12° E.

In conclusion the author wishes to express his cordial thanks to Dr. T. Minakami for his kind advices in the course of the field surveys.

11. 有珠山の活動と精密水準測量

地震研究所　表　俊一郎

北海道有珠火山は明治43年大活動を行つて以來靜穏な狀態をつづけてきたが，昭和18年暮より再び活動を開始し，12月27日より多數の地震の發生していることが北麓で感知せられるやうになり，次で翌年1月には東側の山麓で著るしい土地の隆起運動が認められるようになつた．この隆起地帶は次第に北へと移行しついに6月23日フカバ附近に新火口を生じて噴火を行うようになつた．このような著るしい地殼變動現象がその進行の過程に於て捉へられて調査が行われることは極めて興味あることであるので著者は昭和19年3月，4月及び7月の3回にわたり現地に赴き精密水準測量を實施し，主として噴火を始める迄の期間に有珠山麓で如何なる地殼變動が行われたかを明らかにするために調査を行つたのでそれらの結果がこの報告に於てのべられている．

12. *Recent Activities of Volcano Usu (V). Topographical Deformations During the 1943–1945 Eruption.*

By Takeshi MINAKAMI,

Earthquake Research Institute.

(Read Dec. 20, 1949.—Received May 31, 1950.)

1. Introduction.

The marked topographical deformations which appeared in connection with explosive activities were brought to light in a number of volcanoes on the basis of resurveys made by means of precise levellings and triangulations. For example, in the cases of the volcanic activities of Usu(1) in 1910, Sakurazima(2) in 1914 and 1946, Komagadake(3) in 1929, Miyake-sima(4) in 1940, and Asama(5) in 1935–1937, upheavals and subsidences or horizontal displacements were made clear on and around those volcanoes, though the scales of deformation and the affected area varied according to the natures and magnitudes of eruptions.

However, these topographical deformations were usually elucidated by two series of surveys, of which the first was mostly carried out several years before, and the second just after the eruption. Therefore, we can not distinguish clearly whether they occurred prior to or in the midst of the eruption.

Since the recent outstanding eruption of Usu was preceded by about half a year of the pre-volcanic stage, in which the topographical deformations accompanying numerous perceptible earthquakes were in fact remarkable, levelling surveys(6) together with seismic observations(7) were carried out not only in the course of the paroxysmal eruption but also in the pre-volcanic stage. As the

---

1) F. ŌMORI, *Bull. Imp. Earthq. Inv. Comm.*, 5 (1911), 1 and 9 (1920), 41.

2) N. MIYABE, *Bull. Earthq. Res. Inst.*, 12 (1934), 471, C. TSUBOI, *Jap. Jour. Astr. Geophy.*, 10 (1933), 93. Y. HARADA, *Bull. Geogr. Surv. Bur.*, 1 (1948) 9.

3) C. TSUBOI, *Bull. Earthq. Res. Inst.*, 8 (1930), 298.

4) S. OMOTE, *Bull. Earthq. Res. Inst.*, 19 (1941), 389.

5) E. R. I., *Bull. Earthq. Res. Inst.*, 18 (1940), 463.

6) T. MINAKAMI, *Spec. Bull. Earthq. Res. Inst.*, 3 (1944), 1. *Bull. Earthq. Res. Inst.*, 25 (1947), 65, 71, S. OMOTE, *Spec. Bull. Earthq. Res. Inst.*, 3 (1944), 22.

7) T. MINAKAMI, *Bull. Earthq. Res. Inst.*, 27 (1949), 123, 129.

result of that, we could throw light on the modes of the crustal deformations and their developments in the various stages of the recent activity.

Judging from natures of volcanic phenomena, the recent activity of Volcano Usu during the period from December 28, 1943 to October 1945, are divided into the following three stages which accord essentially with the classification made by T. Ishikawa,[8] though he subdivided them into finer details.

1) Pre-volcanic stage:

This stage including the period from occurrence of the first earthquake to the day preceding the first explosion, is characterized by numerous perceptible earthquakes on and around Usu and remarkable rise of the ground at the eastern foot of the mountain forming cracks and fissures of various scales. The stage lasted six months from December 28, 1943 to June 22, 1944.

2) Stage of paroxysmal eruption:

The second stage includes the four months during paroxysmal explosions, forming seven craterlets newly opened at the central area of rise, namely the period from June 23 to October 31, 1944.

3) Stage during birth and development of lava-dome:

The third stage falls on the period in which a lava-dome appeared at the centre of the craterlets which opened in the second stage. Toward September 1945, the lava-dome being completly formed, the recent remarkable eruption came to an end. Accordingly, this stage includes the period from directly after the last paroxysmal eruption on October 31 to the end of the recent activity.

Although the division into these three stages just mentioned was made mainly from the view-point of volcanic phenomena, they harmonize well with the characteristics of earthquakes and topographical deformations.

2. Developments of the Rising Movements at the Eastern Base of Mt. Usu.

The cracks and fissures newly formed on the roads, canals, banks and corn fields between villages Kami-Osaru and Yanagihara, seem to indicate that the rising movements of the land at the eastern skirt of the volcano began to develop already towards the end of January, 1944. However, after the upheaval of the mentioned area lasted for about a month, the movement shifted immediately 1 km north to village Yanagihara.

On March 25, 1944, the writer in co-operation with the Civil Engineering Section of the Hokkaido Prefecture planned the levellings along the civil road passing through the rising area including villages Kami-Osaru, Yanagihara, Hukaba and Sōbetu. During March 28–April 4, 1944, the levellings along the route from Kami-Osaru to Hukaba were carried out daily or semi-daily to determine the mode of the uplifting movement. Thereafter, levellings were carried out twenty four times on the same route in order to elucidate the topographical deformations throughout the whole period of the eruption described above.

---

[8] T. ISHIKAWA, Read at the Pacific Sci. Cong. of 1948.

Although the topographical deformations based on those levellings were partly reported in the previous paper, the phenomena are here reviewed with respect to another particular.

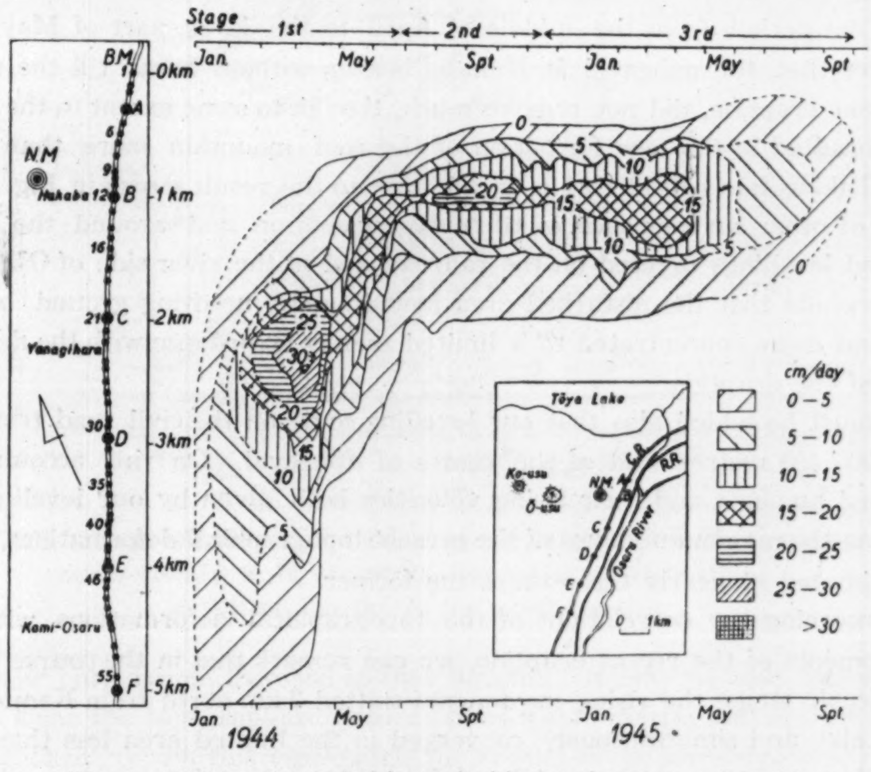

Fig. 1. Development of rising velocities at the eastern foot of Mt. Usu, during the period from March 1944 to September 1945.

As mentioned already, along the route of 5 km in length from Kami-Osaru to the southern part of Sōbetu, including 55 bench marks which were established at 100 m intervals, our levellings were made 30 times in the total or at intervals of two weeks on the average of surveys during the period from March 29, 1944, to May 22, 1945. From the results of those levellings, it was made clear that the vertical deformations developed in the form of dome throughout the three stages, amounting to 30–20 cm per day in the maximum rising velocity on this route. In order to examine the variations of the rising movements through the three stages mentioned, daily rising velocities of those bench marks are illustrated on the diagram of Fig. 1, on the basis of these levellings. Since our levellings did not cover the period before March 28, 1944 and after July 1945, approximate estimations concerning the rising velocities on this route before and after our surveys were made by means of available results of other surveys such as levellings on the railroad at the initial stage and tilt measurments of land by making use of the dammed water at the final stage, which was temporarily formed by marked upheaval at the bed of River Sōbetu. Aided by this figure, it will be clearly recognized that the centre of rising movements at Yanagihara shifted again nearly 1 km to Hukaba during the period from the middle of April to the later part of May, 1944, and after that, the upheaval at Hukaba lasting without break till the end of the recent eruption, did not remove much, though to some extent to the north, which resulted in the new formation of the roof mountain more than 200 m high. Taking into consideration, in addition to the result shown in Fig. 1, the results of other surveys such as tilt measurments on and around the rising area and levellings covered on the railroad and at the river side of Osaru, we may conclude that the disturbed area including the uplifting ground became more and more concentrated to a limited area in accordance with the developments of the eruption.

It must be added also that our levelling route on the civil road traversed about 300–400 metres east of the centre of upheaval. On this account, the upheaved amounts and their rising velocities both given by our levellings do not show the maximum values of the present topographical deformations, which are estimated at nearly three times the former.

Concerning the correlations of the topographical deformations with the developments of the recent eruption, we can remark that in the course of the pre-volcanic stage, the rising movements shifted 2 km north from Kami-Osaru to Hukaba and simultaneously converged in the limited area less than 1 km in its diametre toward the middle of June, 1944, when the paroxysmal stage began to start. During the birth of the lava dome and its rapid development, the rising area with velocities over 15 cm per day was enlarged conspicuously and subsequently the ground deformations were decreasing in their velocity as well as in their affected area up to September 1945 when those new formations were completely built.

To make everything precise, the phenomena are examined by movements of several bench marks which seem to represent their general modes. For the purpose, the movements and their daily velocitses with respect to the bench marks Nos. 6, 9, 12, 16 and 21 of which the locations are shown on the map in Fig. 1, are illustrated in Fig. 2 by taking time in abscissa. As will be seen in this figure, each bench mark rose with variable velocities according to the developments of the recent activity, though displacement curves in the

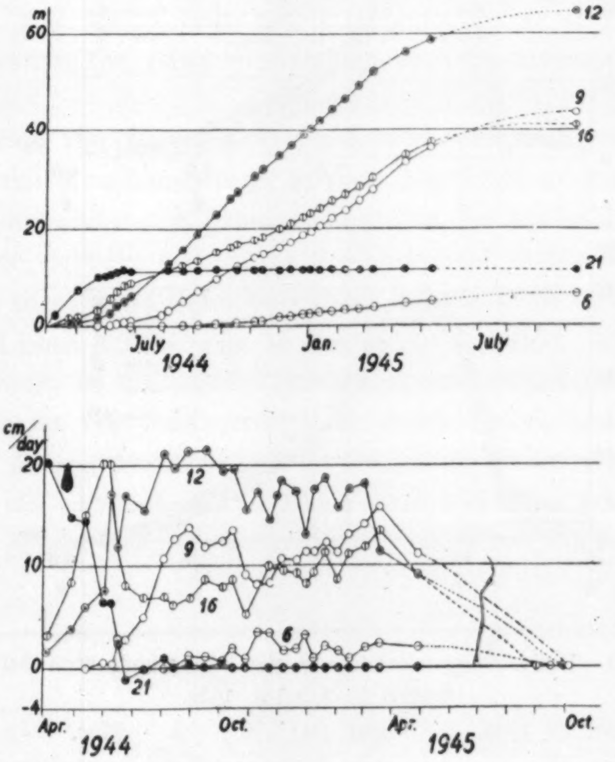

Fig. 2. Modes of upheaval and rising velocity of the representative bench marks (Nos. 6, 9, 12, 16 and 21) situated at the eastern foot of Volcano Usu during the recent eruption.

figure show only simple increase in their heights. It may be also interesting to make clear the topographical deformations within shorter period than those just mentioned. From this view-point, the results of the levellings which were carried out semi-daily at the initial stage from March 29 to April 4, 1944, are shown on the map in Fig. 3, in the form of daily velocity. By a glance at this diagram, we can conclude that the daily movements of the area during the seven days presented a considerable similarity as if those bench marks uplifted with constant velocities respectively.

It is, however, worthy of note that tilts on a small area changed their directions frequently, notwithstanding the fact that the area ~~on~~ which tilt measurements were continuously made, was rising with nearly constant velocity during the period. Therefore, it will be reasonable to infer that the tilts at an extremely limited area, such as several square metres, are not simple

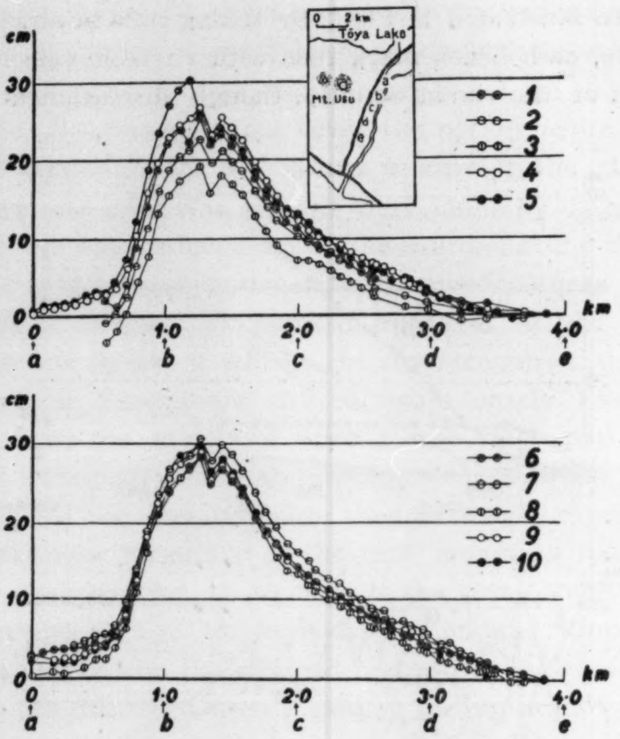

Fig. 3. Daily rising velocities at the Yanagihara area during March 29-April 4, 1944.

1……Mar. 29, 1944. 2……Mar. 30 (a. m.). 3……Mar. 30 (p. m.).
4 ……Mar. 31. 5……Apr. 1 (a. m.). 6 ……Apr. 1 (p. m.).
7……Apr. 2 (a. m.). 8……Apr. 2 (a. m.). 9……Apr. 4 (a. m.).
10 ……Apr. 4 (p. m.).

with respect to either their areal distribution or their time variations, even when the vertical movement of that area takes place in a simple manner. The foregoing relations between the topographical deformations and their differential quantities concerning time and space hold true with the results of tilt observations at Volcano Asama[9] which have been carried out continuously since 1934.

3. Horizontal Displacements on the Rising Area.

Measurements[10] for determining the horizontal displacements of the rising ground had been occasionally made during the recent eruption, though these surveys were not carried out so systematically as in the case of the vertical movements mentioned above. Generally speaking, however, the horizontal deformations throughout the eruption developed always in the outward or radial direction from the active craterlets which were all located on the central part of the uplifted area. As the result of that, the civil road and the railroad running 500 m and 650 m east respectively of those craters, both shifted exceedingly toward the eastern direction during development of the new mountain.

---

[9] T. MINAKAMI, *Bull. Earthq. Res. Inst.*, 20 (1942), 431.

[10] A. ZITSUKAWA and T. NAGATA, *Zisin*, 14 (1944), 1, S. MIYAMURA, *Spec. Bull. Earthq. Res. Inst.*, 3 (1944), 37.

To determine the mechanism of the new formations, namely, the roof mountain and the lava dome, it is, in fact, important to make clear not only the vertical deformations of ground, but also its horizontal displacements. For this purpose, surveys concerning the horizontal displacements were made in the summer of 1949, at those two roads on the basis of the topographical map which had been drawn prior to the recent eruption. In other words, the total displacements at the eastern flank and base of the new mountain were given by comparing the positions of these roads before and after the ground deformations. As the result of this investigation, it was made clear that the civil road and the railroad shifted about 60 m and 20 m respectively in their most affected points toward east or radial direction from the centre of the

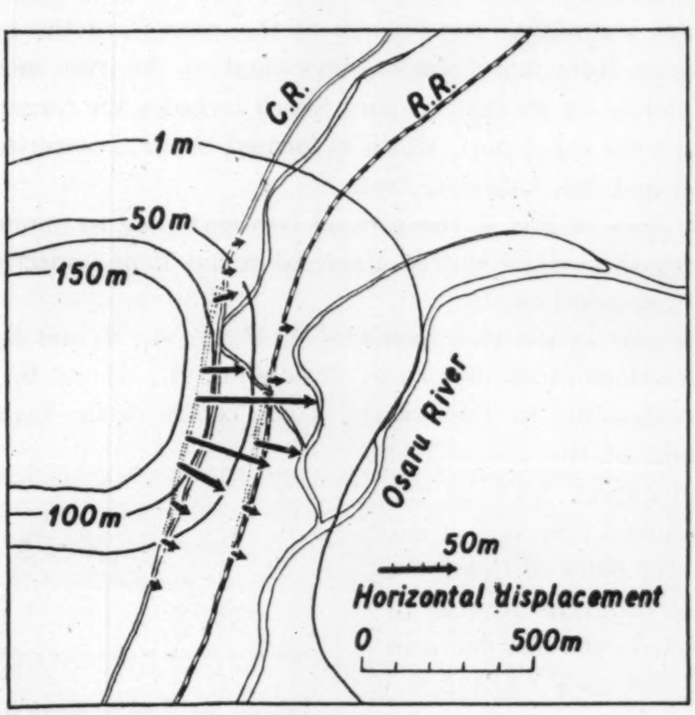

Fig. 4. Horizontal displacements at the eastern base of the newly formed mountain.

new mountain. Since these two points just mentioned were uplifted simultaneously nearly 70 m and 20 m respectively, the topographical deformations of this area were of quite the same amount in both vertical and horizontal directions. Fig. 4 shows the horizontal displacements of the civil road and the railroad together with the total upheaval of the area.

It must be remarked that, so far as the horizontal displacement is concerned, it underwent its greatest development at the final stage of the eruption. It is, however, quite natural that at the initial stage when lava had been intruding in the deep-seated vent, the vertical movements were decidedly superior to the horizontal deformations, and in converse the latter phenomena became exceedingly predominant according as viscous lava approached or came up to the earth's surface.

4. Mechanism of Development of Front Mountain.

Towards the middle of July, 1944, when the paroxysmal eruption was at its height, it was noticeable that the ground around the base of the new mountain began to rise abnormally and developed rapidly according as the lava dome grew and the horizontal displacements in the radial direction accelerated. In May 1945, a hill in the form of a ring or a half-ring, which is called the front mountain, was formed at the margin of the roof mountain (Fig. 6). Judging from morphological investigation, the front mountain is built up more completely at its eastern part which includes the former rice-field of soft soil than at the other part, which is formed by firm materials such as the Usu lava-flows and the Takinoue lava.

As will be seen in Fig. 4, the ground corresponding to the inner and outer sides of the ring-shaped hill shifted about 55 m and 15 m respectively outwards from the original positions.

In a small part of the ring formation in Fig. 5, A_1, A_2 and B_1, B_2 represent the original positions of the inner and outer sides, A_1', A_2' and B_1', B_2' the shifted positions corresponding to the former, O the centre of the lava-dome newly formed, θ, angle of the sector and r_1, r_2, r_1', r_2', distances between the original and shifted positions at the inner and outer sides of the front mountain. To compare lengths of the segments A_1A_2 etc. and the arcs A_1B_1 etc. and the area $(A_1A_2B_1B_2)$ with those after the deformations, the following ratios are made:

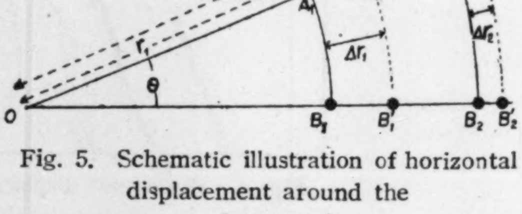

Fig. 5. Schematic illustration of horizontal displacement around the roof mountain.

$$\frac{A_1'A_2'}{A_1A_2} \text{ or } \frac{B_1'B_2'}{B_1B_2} = \frac{r_2+\Delta r_2-r_1-\Delta r_1}{r_2-r_1} = 0.733\,,$$

$$\frac{\Delta r_2-\Delta r_1}{r_2-r_1} = -2.7\times 10^{-1} \text{ ......contraction}\,,$$

$$\frac{\widehat{A_1'B_1'}}{\widehat{A_1B_1}} = \frac{\theta\,.\,(r_1+\Delta r_1)}{\theta\,.\,r_1} = 1.11\,,$$

$$\frac{\Delta r_1}{r_1} = 1.1\times 10^{-1} \text{ ......elongation}\,,$$

$$\frac{\widehat{A_2'B_2'}}{\widehat{A_2B_2}} = \frac{\theta\,.\,(r_2+\Delta r_2)}{\theta\,.\,r_2} = 1.02\,,$$

$$\frac{\Delta r_2}{r_2} = 2.3\times 10^{-2} \text{ ......elongation}\,,$$

$$\frac{\text{area } \widehat{A_1'B_1'}\ \widehat{A_2'B_2'}}{\text{area } \widehat{A_1B_1}\ \widehat{A_2B_2}} = \frac{1/2\,.\,\theta.\ \{(r_2+\Delta r_2)^2-(r_1+\Delta r_1)^2\}}{1/2\,.\,\theta.(r_2^2-r_1^2)} = 0.778\,,$$

$$\frac{2r_2\Delta r_2+\Delta r_2^2-2r_1\Delta r_1-\Delta r_1^2}{r_2^2-r_1^2} = -2.2\times 10^{-1} \text{ ......contraction}\,,$$

where $r_1=500$ m, $r_2=650$ m, $\Delta r_1=55$ m, $\Delta r_2=15$ m.
As the above results show manifestly, the line sides in the radial direction were considerably contracted, and on the other hand the arc sides were elongated along the co-radial direction. As the result of that, the area in question shows remarkable contraction amounting to 2.2×10^{-1}. It is thus obvious that the hill of ring form was built by considerable pressure acting laterally from the centre of disturbance owing to intrusion and extrusion of viscous lava and resulted in abnormal upheaval nearly 20 m high, retaining the original surface of ground. At gullies formed in the front mountain, we can observe remarkable warpings, foldings and thrusts of rather small sizes caused in the manner just mentioned. (Fig. 7).

Although the front mountain is a swelling of ground formed by mainly lateral pressure, tensional forces might act upon this area in the co-radial direction in the course of rapid development of the new formations.

On the other hand, cracks and fissures newly formed on the rising area were varing in their sizes as well as in their running directions. However, the fact that those of a comparatively larger scale were mainly running in the radial direction, suggests close relations with the tensional forces due to

the outward movements of ground. At all events, the mechanism concerning the formation of the front mountain are to be explained satisfactorily only by introducing the horizontal movements of the area and enormous lateral pressure which were both produced by invasion of viscous lava of large volume more or less solidified.

12. 最近の有珠山の活動(其の5) 噴火中(1944–1945)に現はれた地形變動

地震研究所 水上 武

既に報告した第1, 第2報に於て, 1943年12月28日にはじまる今回の有珠山の噴火に伴つた地震活動及びその後間もなく明かになつた東山麓の隆起について述べ, 更に昭和新山に成長するまでの經過の概略を報告した. また第3, 第4報に爆發的噴火及び熔岩丘の成長に伴つた地震の2, 3.の性質について述べた.

本文には同火山東麓の隆起の進行について水準測量の結果を綜合し, 地形變動の進展と噴火現象との關聯について報告してある. 特に1944年3月下旬より4月上旬に柳原部落を中心とする隆起を7日間に亘る毎日2回の測量結果を示し, この短い期間に於ける地形變動の模様を明かにし, この期間の隆起の速度, 隆起の地域が互に極めて類似する事を示した.

今回の活動によつて生じた所謂“昭和新山”の周邊の水平移動を調査した. その結果新山の中心より外方え向つて土地が放射狀に著しく移動している事が明かになつた. 粘性の大きい熔岩の噴出による横壓に原因するものと考えられる. この測定結果を用いて, 新山の周邊に環狀に形成された前山 (Front mountain) の生成機構を考究した.

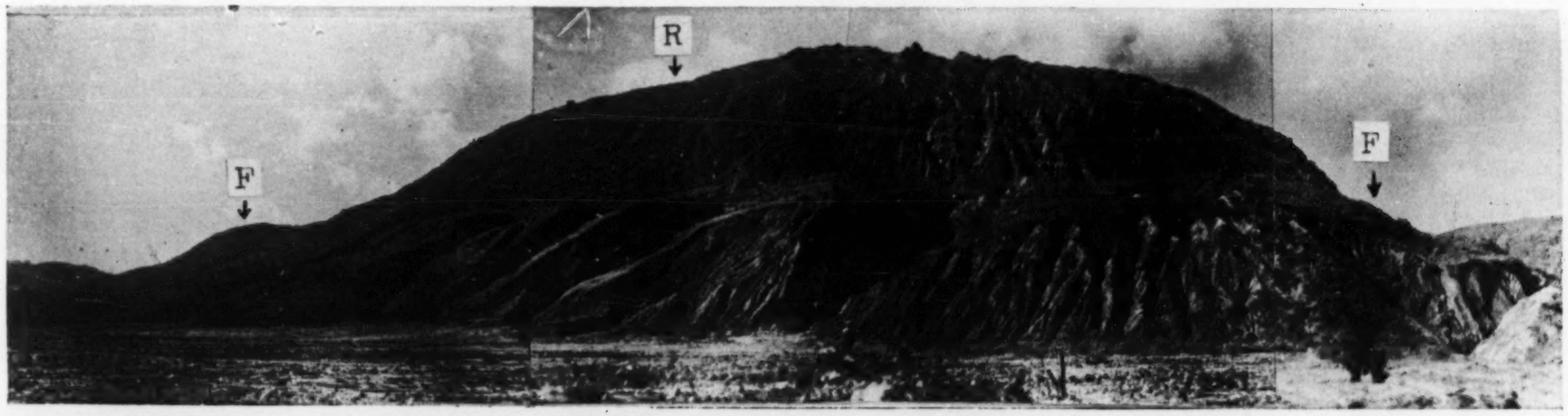

Fig. 6. The roof mountain and front mountain formed in the course of the recent eruption.
R; Roof mountain. F; Front mountain.

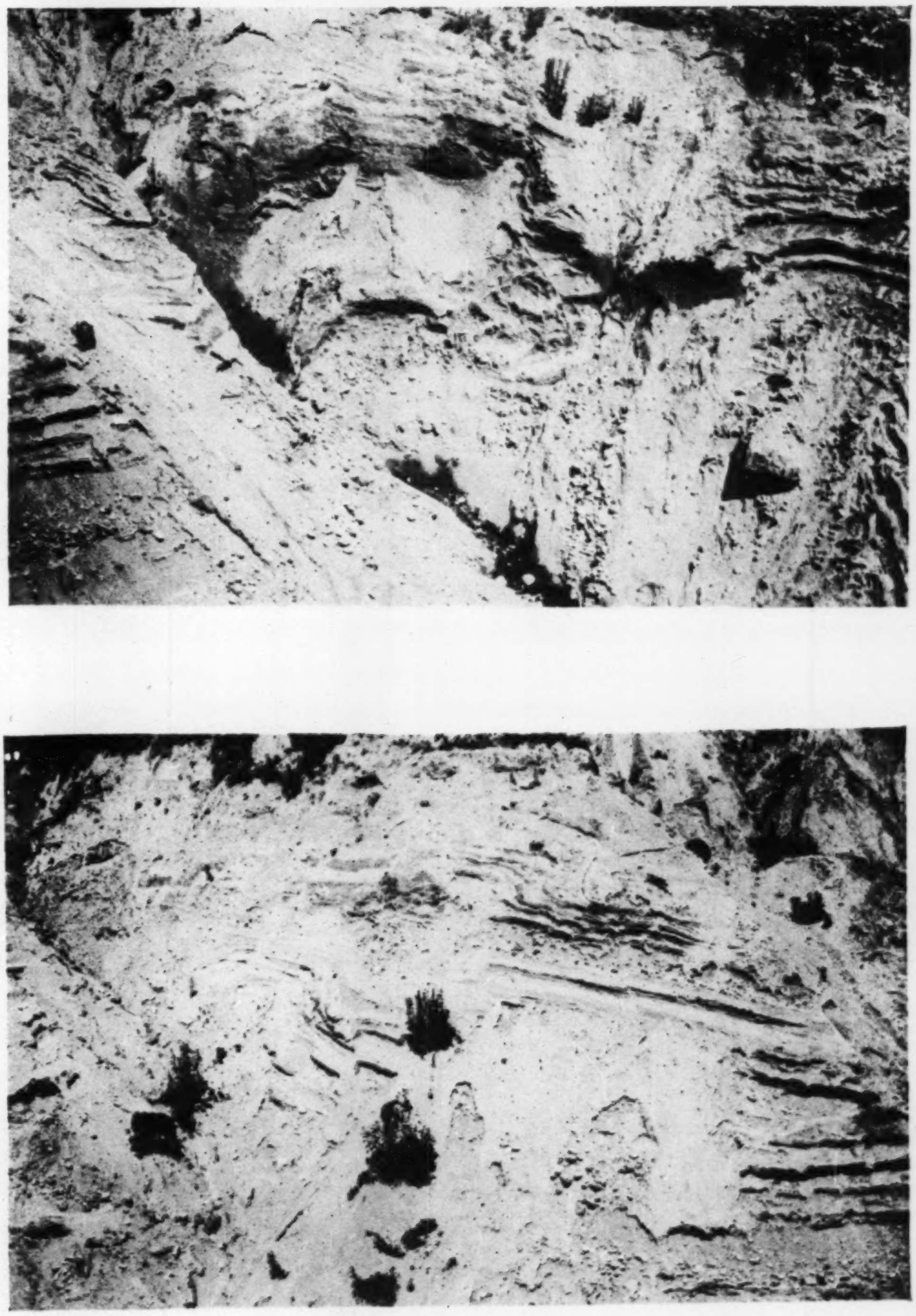

Fig. 7. Warpings and foldings of small size seen in gullies on the front mountain.

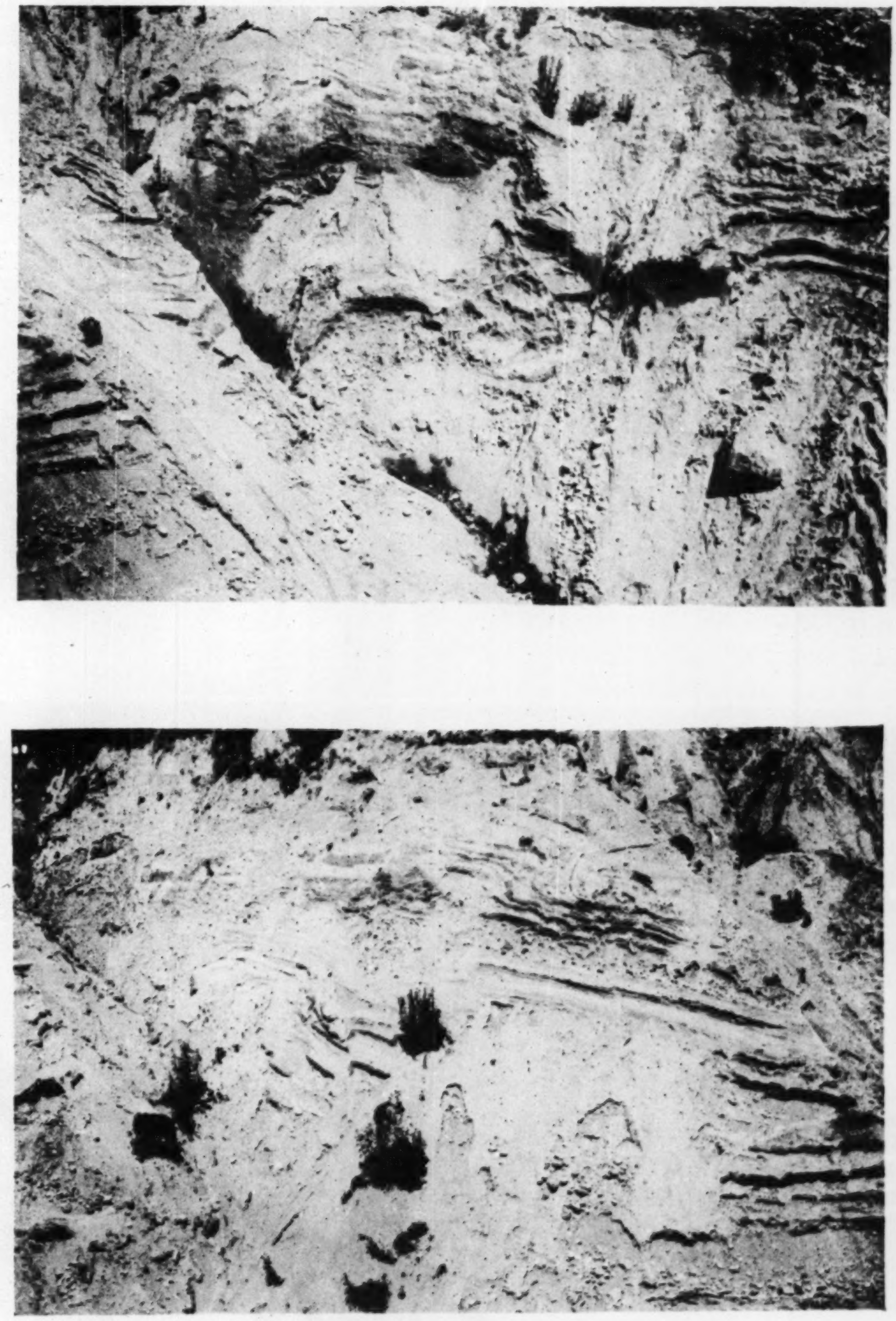

Fig. 7. Warpings and foldings of small size seen in gullies on the front mountain.

（震研彙報　第二十八號　圖版　水上）

13. *Recent Activities of Volcanō Usu (VI). Precise Levelling Around Mt. Usu in 1949.*

By

Takeshi MINAKAMI and Shûzô SAKUMA,

Earthquake Research Institute,

and Atsushi OKADA,

Geophysical Institute, Tokyo University.

(Read December 20, 1949.—Received May 31, 1950.)

1. Introduction.

As reported in the previous papers,[1] the remarkable upheaval at the eastern base of Volcano Usu and extrusion of viscous lava on the former formation resulted in the birth of a new mountain higher than 200 m. From the morphological viewpoint, this new formation falls into three main parts; the first or the roof mountain, including a conical platform lacking its top part, measures about 250 m and 500 m in its upper and base diameters respectively and is 150-200 m higher than the area surrounding it. The second is composed of a conical lava dome 100 m high which is situated on the westward summit of the former formation. The third or the front mountain includes the hill of half-ring form which lies on the eastern margin of the roof mountain (Fig. 5).

On the basis of numerous levelling surveys and other kinds of measurements, the developments of those formations were brought to light, the results of which have been reported in this Bulletin.[2]

According to reports from American volcanologists,[3] about the same time of the recent outstanding eruption of Usu, or to be more exact, during the period covering several years from February 5, 1943, outflows of fresh lava resulted in the birth of a new volcano in the village of Paricutin in Micohacan, Mexico.

---

[1] T. MINAKAMI, *Bull. Earthq. Res. Inst.*, 25 (1947), 65, 71; 28 (1950).

[2] *loc. cit.* 1)

[3] J. GONZALEZ and W. F. FORSHAG, *Smithonian Rep.*, 3878 (1946), 223.
R. E. WILCOX, *Trans. Ame. Geophy. Union,* 28 (1947), 559, 567, 725, 29 (1948), 69, 355, 877.

Those two newly formed volcanoes are exactly same, i.e., they were both given birth to by extrusion of lava through newly opened craters on level cultivated land. But in respect of the mechanism of formation and structures they differ entirely. The new volcano at Paricutin is, as is usually the case, a stratified or strato volcano produced by the accumulation of volcanic ejecta, such as lava-flows, fragments of rocks and volcanic ash etc., while the newly formed mountain at Volcano Usu was found, as has been dealt with in the same Bulletin, by the upward movements of viscous lava towards the earth's surface, which heaved up the ground around the craters newly in action, forming a dome-shaped mountain there. Thus in the process of formation the two volcanoes present extremely different characteristics.

2. Precise Levelling along the Western and Southern Foot of Mt. Usu.

Although the investigations of the topographical deformations made during the recent eruption were examined by means of various methods, the surveys covered only the eastern region of this volcano and no available information was given with respect to the land deformations, if any, at the western and southern area of this mountain.

Judging from the fact that an upheaved mountain 200 m high was newly formed during the period 1944–1945, it will be quite natural to expect vertical movements of the land around the Usu volcano, though their amounts are unknown. From this viewpoint, the writers planned the redetermination of the heights of the first order bench marks on the route along the western foot of Usu and along the north-eastern coast of the Utiura Bay, that is, the southern base of the volcano. In the summer of 1949, precise levellings were carried out for the purpose, and to compare with the former survey in 1919, the bench mark No. 6604 located at the north-western corner of Lake

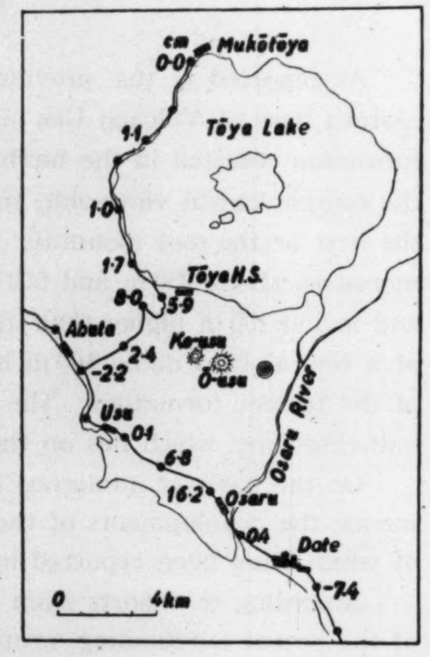

Fig. 1. Distribution of topographical deformation around Mt. Usu during 1919–1949.

Tōya (Dōya) was assumed as the fixed height during the period of those two surveys.

In Table I, are given the heights and their changes at the seventeen bench marks obtained by the former and present levellings. In order to investigate the general trend of rise and sink of these bench marks, their geographical distribution is indicated on the map of Fig. 1. In the table and the figure, we can find conspicuous rise at two groups of the bench marks, the first of which includes those at the western foot of Mt. Usu and the other at the southern skirt, being 8.0 cm for the former and 16.2 cm for the latter both in the maximum rise. Judging from the developments of the recent activity, it will be reasonable to infer that those remarkable upheavals at the two localities are extended towards the newly upheaved mountain at the eastern base of this volcano, though we have no information concerning the topographical deformations in the middle of the new formation and the bench marks.

Table I. Comparison of the results of precise levellings made in 1919 and 1949.
H_1; height of bench mark in 1919.
H_2; height of bench mark in 1949.
$\Delta H_1 = H_2 - H_1$; change in height.

B. M. No.	H_1	H_2	ΔH_1
	m	m	cm
6604	85.5009	85.5009 (fixed)	0.0
6603	86.2597	/	/
6602	86.8103	86.8217	1.1
6601	86.1558	/	/
6600	88.6848	88.6945	1.0
6599	86.3540	86.3709	1.7
6598	95.3932	95.4525	5.9
6597	150.5235	150.6039	8.0
6596	50.2057	50.2296	2.4
J. 4	3.9027	3.8804	−2.2
7193	9.7671	/	/
7194	3.9282	3.9288	0.1
7195	30.1495	30.2171	6.8
7196	6.5458	6.7081	16.2
7197	4.2710	4.2752	0.4
7198	5.5040	/	/
7199	14.0026	13.9284	−7.4

In case of volcanic eruptions, it is rather an usual mode of land deformations that the area near the active craters rises and contrariwise the region more distant subsides. As will be seen in Fig. 1, the present land deformations are of the same mode as just mentioned. On the other hand, the remarkable rise at the southern and western roots of this mountain agrees well with the epicentral area of the earthquakes which occurred 2–5 km deep in the course of the recent activity, with which the preceeding papers[4] dealt.

On the basis of these facts mentioned above and taking into consideration the usual mode of land deformations made clear in many other volcanoes, we do not hesitate to conclude that the greater part of the topographical deformations elucidated by the present levelling should be directly connected with the recent catastrophic eruption of Usu.

To permit ready comparison between the mode of the land deformations undergone at the time of the 1910 activity with that of the recent eruption, changes[5] of height appeared during 1905–1912 and 1919–1949 are given on the diagram in Fig. 2, both times making use of the same bench marks.

From these tables and figures, it is worthy of note that notwithstanding the fact that the present bench marks used for the two series of levellings are situated at nearly equal distances from the two upheaved mountains formed in 1910 and in 1944–1945, their amounts of rise in the former activity were almost ten or several times those in the latest one.

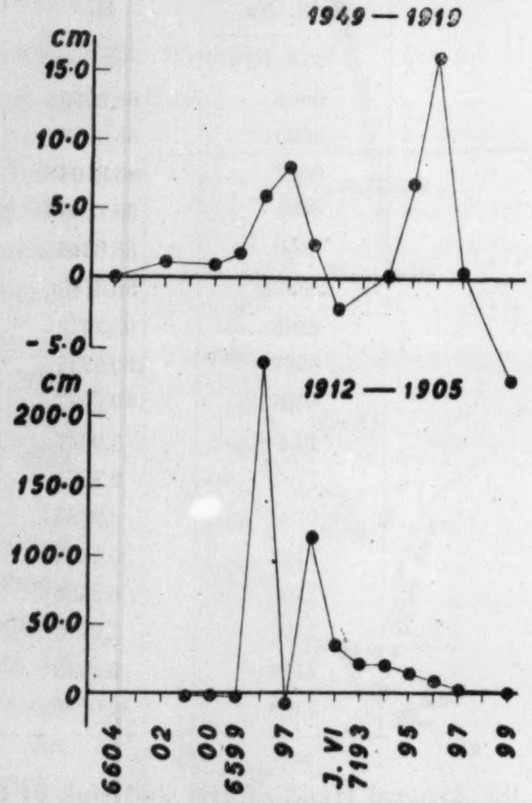

Fig. 2. Modes of upheaval and subsidence around Mt. Usu during 1919–1949, and 1905–1912.

In the 1910 activity, over 20 craterlets newly opened and were distributed over an area extending nearly 3 km from the northwestern foot of the volcano to the northeastern, while in the latest case, seven craterlets opened close to one another. However, so far as the upheaved mountains formed in

---

[4] T. MINAKAMI, *Bull. Earthq. Res. Inst.*, 25 (1947), 71.

[5] F. ŌMORI, *Bull. Imp. Earthq. Inv. Comm.*, 9 (1918–1921), 41.

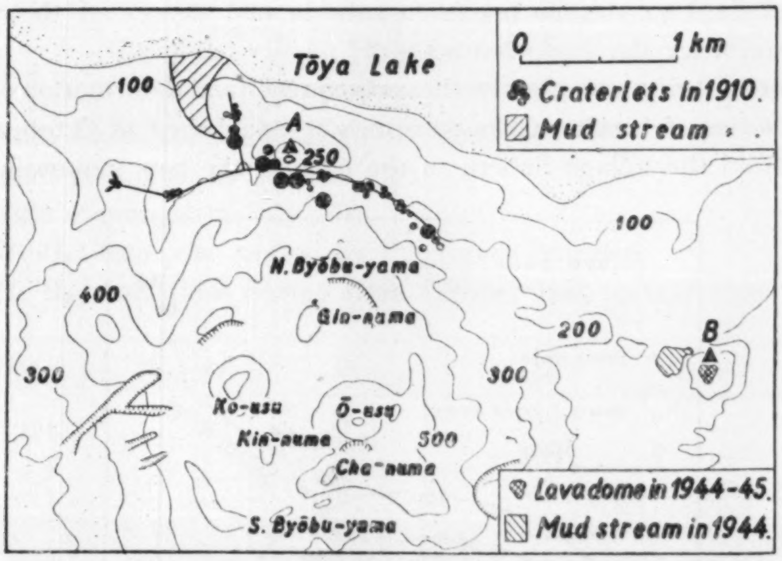
Tōya Lake
0 1 km
Craterlets in 1910.
Mud stream " .
100
A
250
100
N. Byōbu-yama
400
Gin-numa
200
B
300
300
Ko-usu
Ō-usu
Kin-numa
500
Cho-numa
S. Byōbu-yama
Lava dome in 1944-45.
Mud stream in 1944.

Fig. 3. Localities of the 1910 craterlets and the new mountains formed in 1910 and in 1944-1945.

A, the 1910 mountain.
B, the 1944-1945 mountain.

1910 and in 1944-1945 are concerned, they are quite similar in their height as well as in their volume. On the other hand, in the former case, no fresh lava extruded to the earth's surface, while in the recent eruption, fresh lava formed a lava dome partly covered by tuffaceous material on the upheaved mountain.

On the basis of comparisons of the volcanic phenomena just mentioned, it may be said that if the seismic activities followed were put out of question, the 1910 eruption was of greater scale, at least, in respect of the interior activity of the volcano which resulted in more remarkable land deformation in its affected area as well as in its amounts of rise than that in the latest case. At all events, it will be without doubt that the land deformations and the seismic activities accompanied with those eruptions were caused by intrusion or extrusion of the subterranean magma.

3. Precise Levellings on the New Mountain and at Its Northern Base.

As already mentioned, the recent activity of the Usu volcano came to an end towards October 1945, when the newly formed mountain with the lava dome on its summit had been completely built. In the case of the 1910 eruption, however, the mountain newly formed at the time together with the upheaved land around the Usu volcano began to subside and decreased their uplited amounts soon after the explosive activity.

In order to bring out clearly the subsequent land deformation of the 1945 mountain, series of bench marks were newly established in October 1948 on the route from the village Sōbetu to the base of the new mountain. At the same time, precise levelling on this route was carried out and re-examined in July 1949 both by the writers. At the occassion of the latter survey, several bench marks were newly added on the flank and summit of the roof mountain, with a view to accurately determining their heights and their promising changes. As the result, at various positions on the roof mountain, the total amounts of rise caused in the course of the eruption were determined on the basis of comparison with the topographical map made prior to the recent activity.

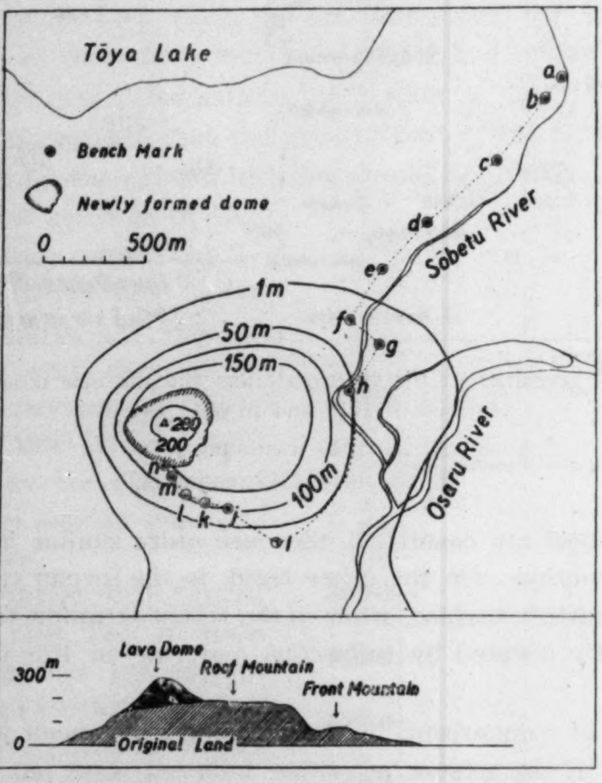
Tōya Lake
Bench Mark
Newly formed dome
0
500m
1m
50m
150m
100m
200
280
a
b
c
d
e
f
g
h
i
j
k
l
m
n
Sōbetu River
Osaru River
Lava Dome
Roof Mountain
Front Mountain
300m
0
Original Land

Fig. 4. Total amounts of upheaval of the new mountain, and locality of the bench marks newly established.

Simultaneously, along the route running through the village Sōbetu to the base of the new mountain, 2 km south of the former, the two series of levelling surveys made clear the changes in heights of those bench marks, which took place during the nine months between the two times of levelling.

Table II. The results of the precise levellings on the route from the village Sōbetu to the base of the new lava dome.

H_5; height above sea-level before the eruption.
H_6; height examined in October 1948.
H_7, height examined in July 1949.
$\varDelta H_2=H_7-H_5$; total rise caused by the recent eruption.
$\varDelta H_3=H_7-H_6$; variations during from October 1948 to July 1949.

B. M. No.	H_5	H_7	H_6	$\varDelta H_2$	$\varDelta H_3$
		m +55.21	m +55.21		
	m	m	m	m	mm
(a)	55.21	0.0000	0.0000	0.0	0.0
(b)	55.44	0.2376	0.2386	0.0	−1.0
(c)	61.77	6.5644	6.5650	0.0	−0.6
(d)	55.15	−0.0436	−0.0441	0,0	0.5
(e)	54.10	−1.0785	−1.0777	0.0	0.2
(f)	53.50	−1.4088	−1.4051	0.3	−2.7
(g)	53.70	2.1952	2.1932	3.7	3.0
(h)	52.50	56.8996		59.6	
(i)	102.0	83.2906		36.5	
(j)	105.0	146.7626		97.0	
(k)	108.5	155.3727		102.1	
(l)	110.3	166.4349		111.3	
(m)	113.5	180.3841		122.1	
(n)	115.0	200.3921		140.6	

It must be, however, added that the total amounts of rise and their changes mentioned above both are determined by the following assumption; the bench mark No. (a) situated at the village Sobetu has been fixed in its height throughout the whole period in question. If we take into account the facts that the total uplift of the summit of the new formation amounts to more than 200 m and the subsequent variations in height may be dependent on the total amount of rise, such as in the case of 1910, the above assumption will not seriously affect the result, though the fixed bench mark is located near the new mountain, only 2.0 km distant.

The results of levellings are given in Table II together with the approximate heights above the sea-level of these bench marks prior to the recent activity. Positions of these bench marks and their total amounts of upheaval caused during 1943–1949, are illustrated on the map of Fig. 4.

As will be seen in the table, no marked change in height concerning these bench marks took place during the nine months after October 1948.

In conclusion, the writers wish to express their sincere thanks to Mr. K. Ikeda, director of Civil Engineering Section, Hokkaido Prefecture, for facilities and courtesy given them throughout the levelling surveys including the 1944-1949 surveys.

Most of the expense necessary for this study was defrayed from the Funds for Scientific Research of the Department of Education.

---

13. 最近の有珠山の活動(其の6)
有珠山周邊の精密水準測量

地震研究所 { 水上 武
佐久間修三
東大地球物理教室 岡田 惇

今迄に報告した最近の有珠山の活動に伴つた地形變動は專ら同火山の東麓地域の隆起現象即ち新山の成長の經過に關するものであつた．本文は火山の西北，西及び南の山麓を通る既設の一等水準點を改測し，今回の著しい噴火に伴つたやゝ廣い地域に亘る水準變化の模樣を明かにせんと試みたものである．前回1919年の測量結果との比較から變動を求めたので，この30年間に亘つて生じた水準變化をその中に含むものであるが今回の測量で明かにされた隆起，沈下の分布から判斷して，その大部分は今回の噴火に伴つたものと推定される．それにしても最も著しい變動は同火山の南側（有珠部落附近）の僅か16糎の隆起を示すに過ぎなかつた．一方その北方約6粁に200米に及ぶ隆起によつて新山が形成された事を考えると，著しい變動は極めて限られた地域である事が判る．また，火山の南側及び西側の山麓の隆起地域は前に報告したA型地震（震源の深さ2-5粁）の震央域と一致している．

1948年10月新山の東北2粁の位置にある瀧の町部落より新山中腹に至る區間に約10個の水準點を新しく設け，第1回の精密水準測量を行つた．その後1950年7月に改測した結果によるとこの9ケ月に殆んど水準變化を示さなかつた．

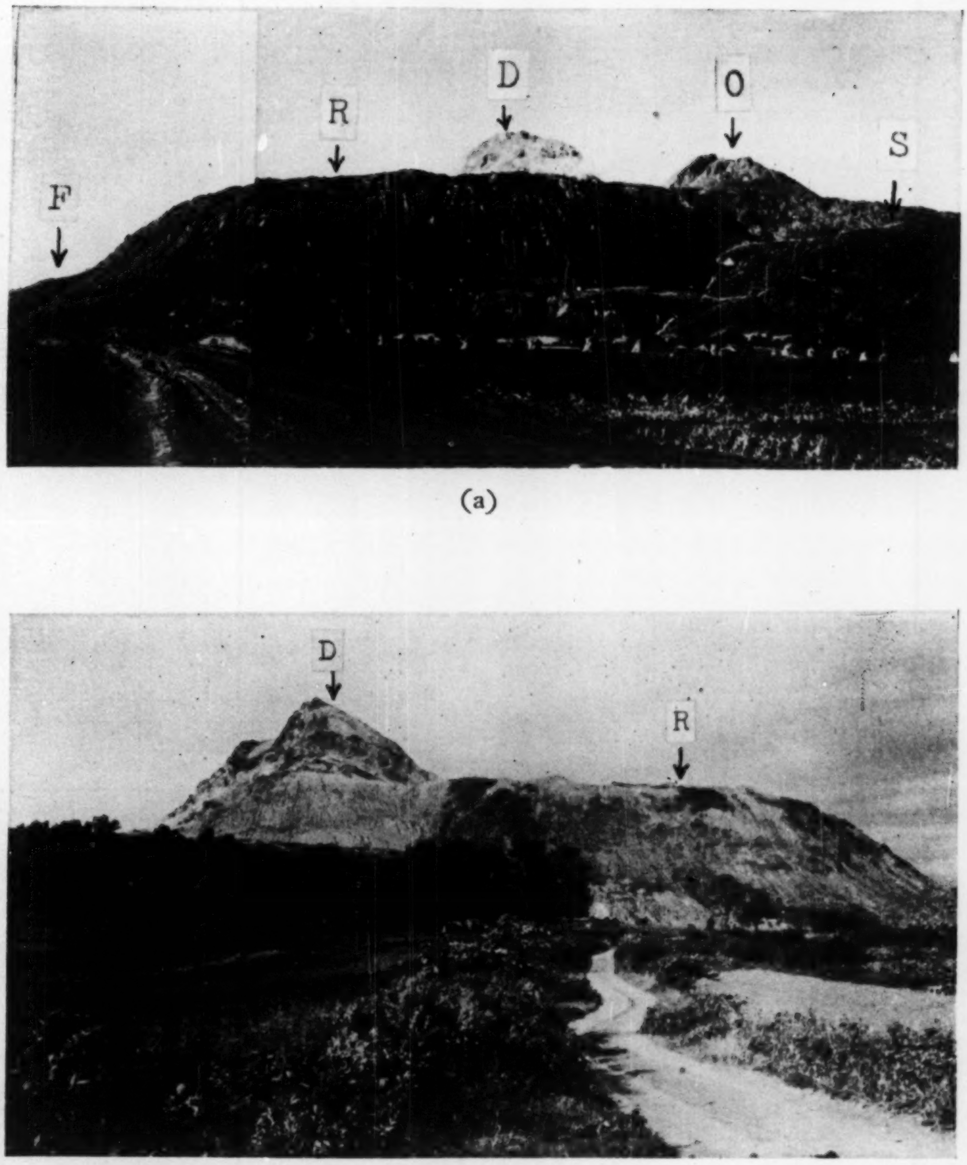

(a)

(b)

Fig. 5. The new mountain (Syowa-sinzan or Showa-shinzan) viewed from north (a) and south (b).

D, Lava dome. R, Roof mountain. F, Front mountain.

O, Ō-usu (old lava dome, summit of Usu). S, Somma of Usu.

（震研彙報 第二十八號 圖版 水上・佐久間・岡田）

14. *A Method of Determining the Stiffness of Each Storey of a n-storied Building.*

By Kiyoshi KANAI,

Earthquake Research Institute.

(Read Nov. 15, 1949.—Received May 31, 1950.)

A simple formula of finding out experimentally the stiffness of resistance to horizontal vibrations of each storey of a n-storied building has been obtained, by using the theoretical results of the previous paper,[1] as follows;

$$E_sI_s=K\frac{l_s^3\left(\frac{2\pi}{T}\right)^2\sum_{r=s}^{n} m_r y_r}{y_s-y_{s-1}},\ [s=1,\ 2,\ldots\ldots,\ n]\ldots\ldots\ldots\ldots \qquad (1)$$

in which

n=number of floors,
s=number of storey of which the stiffness is sought for,
E=Young's modulus,
I=total sum of the moments of inertia of sections,
l=the height between the s-1th and sth floors,
m=concentrated mass at floor,
y=horizontal displacement at floor,
T=vibration period,
K=constant determined by the fixing conditions of columns.

That is, in case the columns are clamped at the floors as well as at the base; K is 1/12, and in case the columns are clamped at the floors and hinged at the base; K is 1/12 at $s\geq 2$ and 1/3 at $s=1$.

In this equation, for simplicity, the effect of dissipation has been omitted.

In case of vibrational experiments of actual buildings by means of the vibrator, by using the equation (1) it is possible to find out the stiffness of each storey by measuring the horizontal displacements of each floor in the resonance condition as well as in the resonance period.

Two examples using this formula shall be given:—

(I) The case of an actual two-storied *precast* reinforced concrete building.

---

[1] K. SEZAWA and K. KANAI, "Some New Problem of Forced Vibrations of a Structure", *Bull. Earthq. Res. Inst.*, 12 (1934), 823-853.

The column heights l_1, l_2 and the mass concentrated at each floor m_1, m_2 of this building are 3.0 m, 3.3 m and 15.0 ton, 15.8 ton respectively. The results observed experimentally are shown in Table I.

Table I.

Resonance condition	Displacement (mm)		Resonance period (sec)
	First floor	Roof floor	
Fundamental	0.41	0.92	0.49
Second	−0.23	0.18	0.21

Substituting these data into the equation (1) with the two fixing conditions of columns, namely, (i) clamped at the floors as well as at the base, (ii) clamped at the floors and hinged at the base, it is possible to get easily the effective stiffness of each storey as follows;

(i) from the fundamental resonance condition

$$E_1I_1=1.9\times10^{16}\ (\text{C. G. S.}),\ E_2I_2=1.4\times10^{16}\ (\text{C. G. S.}),$$

from the second resonance condition

$$\underline{E_1I_1=0.54\times10^{16}\ (\text{C. G. S.})},\ E_2I_2=1.8\times10^{16}\ (\text{C. G. S.}),$$

(ii) from the fundamental resonance condition

$$\underline{E_1I_1=7.6\times10^{16}\ (\text{C. G. S.})},\ E_2I_2=1.4\times10^{16}\ (\text{C. G. S.}),$$

from the second resonance condition

$$E_1I_1=2.2\times10^{16}\ (\text{C. G. S.}),\ E_2I_2=1.8\times10^{16}\ (\text{C. G. S.}).$$

It will be seen that in the above results, the values of *EI* underlined differ clearly from those of the others. These facts tell us that the basements of this building are in clamped condition in the relatively longer vibrational period, but are rather in hinged condition than clamped condition in the shorter vibration period.

(II) The case of an actual two-storied brick-wall reinforced concrete building.

Table II.

Direction of vibration	Displacement (mm)		Resonance period (sec)
	First floor	Roof floor	
Beam (10 m) direction	0.045	0.082	0.37
Girder (56 m) direction	0.014	0.019	0.355

The column height l_1, l_2 and the mass concentrated at each floor m_1, m_2 of this building are 4.2 m, 6.3 m and 1030 ton, 1010 ton, respectively. The observed results under the fundamental resonance condition are shown in Table II.

Substituting these data into the equation (1) with the condition that the columns has been clamped at the floors as well as the base, we get the effective stiffness of each storey as follows;

(i) beam direction

$$E_1I_1=5.1\times10^{17}\ (\text{C.G.S.}),\quad E_2I_2=13.5\times10^{17}\ (\text{C.G.S.}),$$

(ii) girder direction

$$E_1I_1=4.6\times10^{17}\ (\text{C.G.S.}),\quad E_2I_2=25.3\times10^{17}\ (\text{C.G.S.}).$$

The above results show that the stiffness of every storey were nearly the same for both directions, but the displacements in the case of beam (10 m) direction were about three times larger than those of girder (56 m) direction. This fact may be interpreted as follows. The vibrational properties of the brick-walls are then much more prominent in diminishing the resonance amplitudes through its inner damping resistance than in raising the stiffness of the building.

At all events, from the above-cited examples we may say that the equation (1) will be usefull not only in determining the stiffness of each storey of a n-storied building but in examining many kinds of the vibrational characters of actual buildings.

---

14. *n* 層建實在建物の各階の水平剛度を調べる一つの方法

地震研究所　金井　清

n 層の實在建物の振動試驗結果から，各階の水平剛度を求める理論式が，質量はすべて各階の床のところに集中しているという假定のもとで，次のような簡單な形に導き出された．

$$E_sI_s=K\frac{l_s^3\left(\frac{2\pi}{T}\right)\sum_{r=s}^{n}m_ry_r}{y_s-y_{s-1}},\ [s=1,\ 2,\ldots\ldots,\ n]\ldots\ldots\ldots\ldots\ldots\ldots\ldots \quad (1)$$

(1) 式において，n は層數，s は剛度を求めんとする層番，E はヤング率，I は柱の慣性能率の總和，l は階高，m は床に集中した質量，y は床のところの振動變位，T は振動周期である．なお，K は節點の條件できまる常數で，剛節點固定脚の場合は $K=1/12$，剛節點で基礎支持の狀態の場合には 2 階以上 ($s\geq 2$) については $K=1/12$，1 階 ($s=1$) については $K=1/3$ である．本文中には，實際の建物について行つた振動試驗結果から (1) 式を利用して各階の効果的の水平剛度を求めると同時にその建物の振動性能を推定した例が 2 つあげてある．

15. *A Short Note on Kanai's Formula.*

By Ryutaro TAKAHASI,

Earthquake Research Institute.

(Read Dec. 20, 1949.—Received May 31, 1950.)

When a building with rigid floors is vibrating with a period T, we have, concentrating the mass of pillars at the floors,

$$\left.\begin{aligned} m_n\ddot{y}_n &= E_nI_ny''', \\ m_{n-1}\ddot{y}_{n-1} &= E_{n-1}I_{n-1}y''' - E_nI_ny''', \\ &\dots\dots\dots\dots \\ m_s\ddot{y}_s &= E_sI_sy''' - E_{s+1}I_{s+1}y''', \end{aligned}\right\} \qquad (1)$$

where $\ddot{y}_s$'s are accelerations, and E_sI_sy''' the shearing force in the pillar between m_s and m_{s-1}, of which the length is l_s.

Summing up (1), we have

$$\sum_{r=s}^{n} m_r\ddot{y}_r = E_sI_sy'''. \qquad (2)$$

Since $\ddot{y}_r = -4\pi^2 y_r/T^2$, we can write (2)

$$-y''' = 4\pi^2 \sum_{r=s}^{n} m_ry_r/E_sI_sT^2 \equiv S, \qquad (3)$$

which assumes a constant value, say S, for the pillar between m_s and m_{s-1}.

We assume for the same pillar,

$$\left.\begin{aligned} l_sy'' &= -ky' && \text{at } x=l_s, \\ l_sy'' &= hy' && \text{at } x=0, \\ y &= y_s - y_{s-1} && \text{at } x=l_s, \\ y &= 0 && \text{at } x=0, \end{aligned}\right\} \qquad (4)$$

taking the origin temporarily at m_{s-1}. Then from (3) and (4) we obtain after a simple calculation

$$S = \frac{12\,(h+k+hk)}{(12+4h+4k+hk)} \cdot \frac{y_s - y_{s-1}}{l_s^3}. \qquad (5)$$

Eliminating S from (3) and (5), we get finally

$$E_sI_s=\frac{12+4h+4k+hk}{3\,(h+k+hk)}\cdot\frac{\pi^2 l_s^3\sum_{r=s}^{n} m_r y_r}{T^2\,(y_s-y_{s-1})}\,, \qquad \text{(6)}$$

which is Kanai's formula generalized.[1]

For the clamped end of pillars, put h or k in the formula equal to ∞, and for the hinged end h or $k=0$.

Values of $\dfrac{12+4h+4k+hk}{3\,(h+k+hk)}$

		Upper End of Pillar		
		Clamped	Elastic	Hinged
Lower End of Pillar.	Clamped	$1/3$	$(4+k)/3(1+k)$	$4/3$
	Elastic	$(4+h)/3(1+h)$	$\dfrac{(12+4h+4k+hk)}{3(h+k+hk)}$	$4(3+h)/3h$
	Hinged	$4/3$	$4(3+k)/3k$	∞

---

[1] Kiyoshi KANAI, *Monthly Coll. Earthq. Res. Inst., Tokyo Univ.* Nov. 15, 1949.

---

15. 金井式小引

地震研究所 高橋龍太郎

建物の振動實驗の結果から各階の柱の剛性を求める金井清氏の式の擴張として

$$E_sI_s=\frac{12+4h+4k+hk}{3(h+k+hk)}\cdot\frac{\pi^2 l_s{}^3\sum_{s=s}^{n} m_r y_r}{T^2(y_s-y_{s-1})}$$

なる式を得た．此處に k 及び h は夫々柱の上及び下の節點の條件による常數で，剛節の場合 ∞ に，鉸節の場合 0 に取るべきものである．他の記號は金井式の場合と同樣である．

16. 日本における建物に震害を受けた度數の分布

地震研究所 金井　清
吉澤靜代

（昭和23年4月19日，7月19日發表—昭和25年5月31日受理）

日本において，有史以來の地震によつて，どの土地が何回建物被害を受けたかという分布圖を作つてみた．これらの圖の作り方は日本地圖の中に緯度經度共に10′間隔の線を引き，一つの地震で，網目の中の一つの土地でも震害を受けた記録があれば，その網目に1點を與え，所要の期間中についての集計をしたものである．

使用した主な記録資料は，大日本地震史料，震災豫防調査會報告，地震研究所彙報，

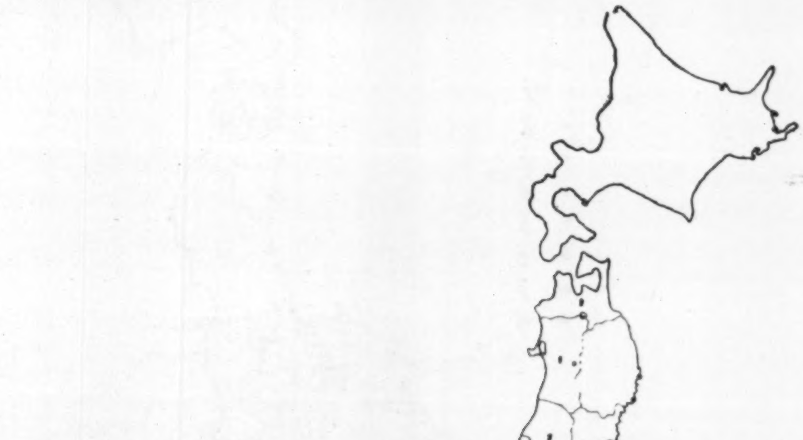

第1圖　599〜1191の593年間，地震數29回．

氣象要覽，建築雜誌である.

記錄の粗密の度合によつて，年代を次のように4分し，夫々の期間についての分布圖を第圖1～5に示す.

第1期； 599～1191の593年間，地震數29回（第1圖).

この期間は推古7年“大和國地震い”の最初の記錄から鎌倉幕府ができるまでである．この期間の記錄に出てくる土地名は大和の國式の國の名か又は京都というふうな都の名である.

第2期；1192～1687の496年間，地震數51回（第2圖).

この期間は鎌倉幕府ができたときから元祿時代の前までである．この期間に出てくる土地名は村名，郡名，寺名などであるが，稀に國名のみのものがある.

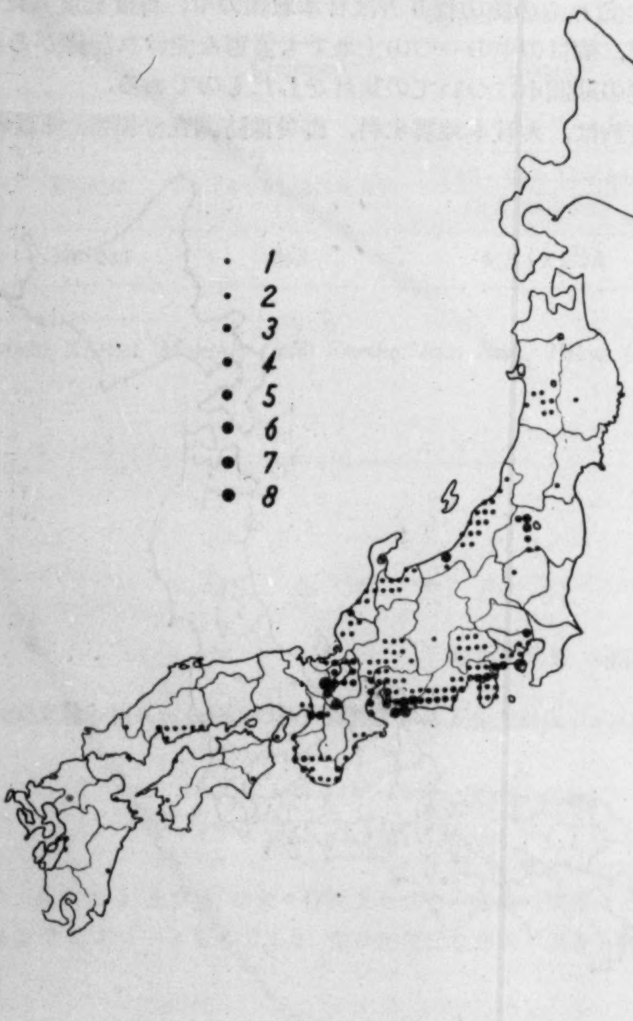

第2圖　1192～1687の496年間，地震數51回.

第3期；1688～1871の184年間，地震数51回（第3圖）.

この期間は元祿時代の始めから明治4年（濱田地震の前年）までである．この期間に出る土地名は村名，郡名，町名などであるが，記錄は餘程明確になり，近年のものに，かなり近い．

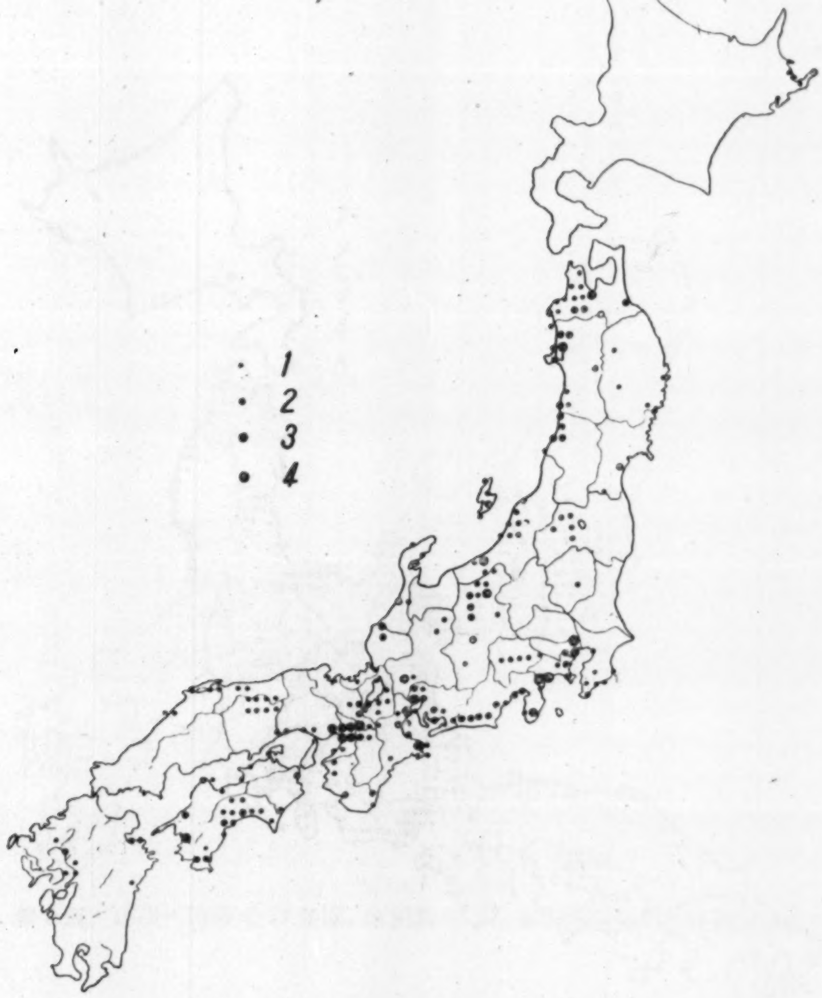

第3圖　1688～1871の184年間，地震数51回.

第4期；1872〜1948の77年間，地震數35回．

この期間には明治5年濱田地震から昭和23年福井地震までの地震が含まれる．この期間は記錄が非常に詳細であるから，被害指數約1%以上のもの（第4圖）と，被害の記錄さえあれば1回と數えたもの（第5圖）との2種類にした．こゝに被害指數とは(全潰+$^{1}/_{2}$半潰)/總戸數である．

記錄の極めて不明確な第1期を除き，第2〜4期の1192〜1948の757年間，地震數137回の分布圖を第6圖に示す．たゞし，第4期については1%以上のものをとつた．

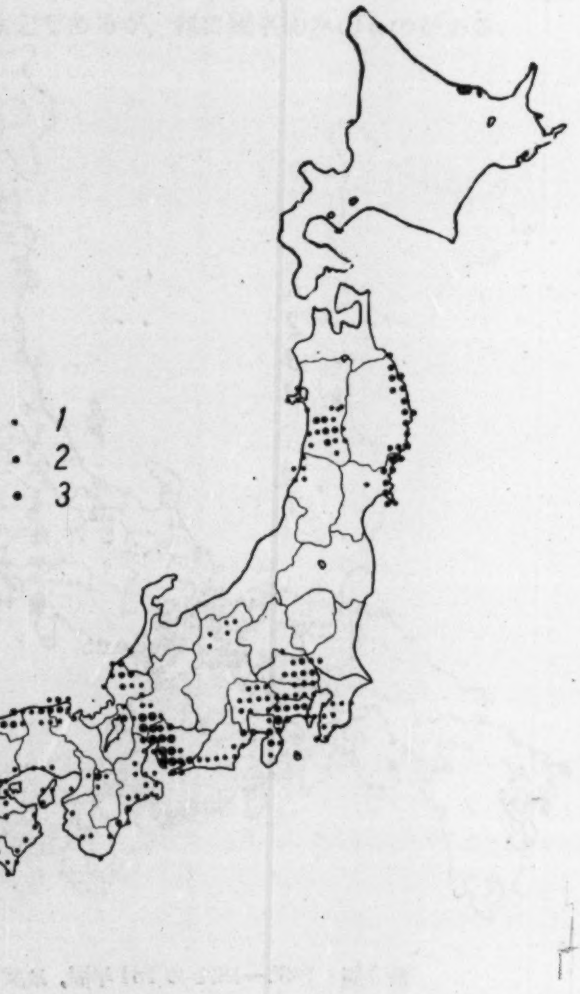

第4圖　1872〜1948の77年間，地震數35回，被害率1%以上の場合．

第1，2圖を見て直ちにわかることは，第1期には京都附近が特に度々被害を受け，第2期になると鎌倉附近の被害を受けた度數が急に増していることである．　この事は，古い時代の記録が政治文化の中心地域にかたよつていることを意味するものであろう．

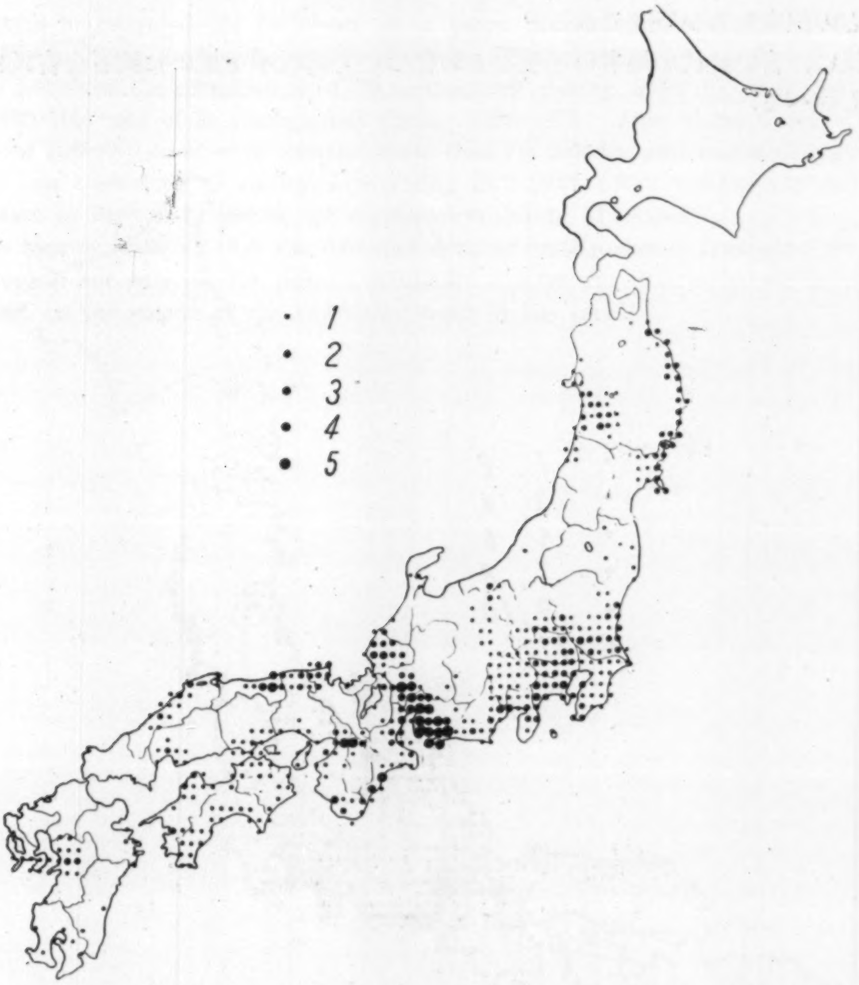

第5圖　1872～1948 の77年間，地震數62回，被害率に制限をおかない場合．

只今の震害を受けた度數の分布圖と受震指數の分布圖1) とを比較すると，豫想通り，舊來の日本式枘仕ロの木造家屋がいわゆる軟弱地盤上で震害を受け易いことが見られる．なお，この分布圖は建物に耐震的補强を施す際に土地に緩急の順位をきめる主な基準にはなるが，新式の建物設計にあたり各土地について工學的の震度をきめるための參考にはどの程度なるか疑問である.2)

最後に，古い時代の地名の不明なものについて御教示を戴いた武者金吉氏に厚く御禮を申し述べる.

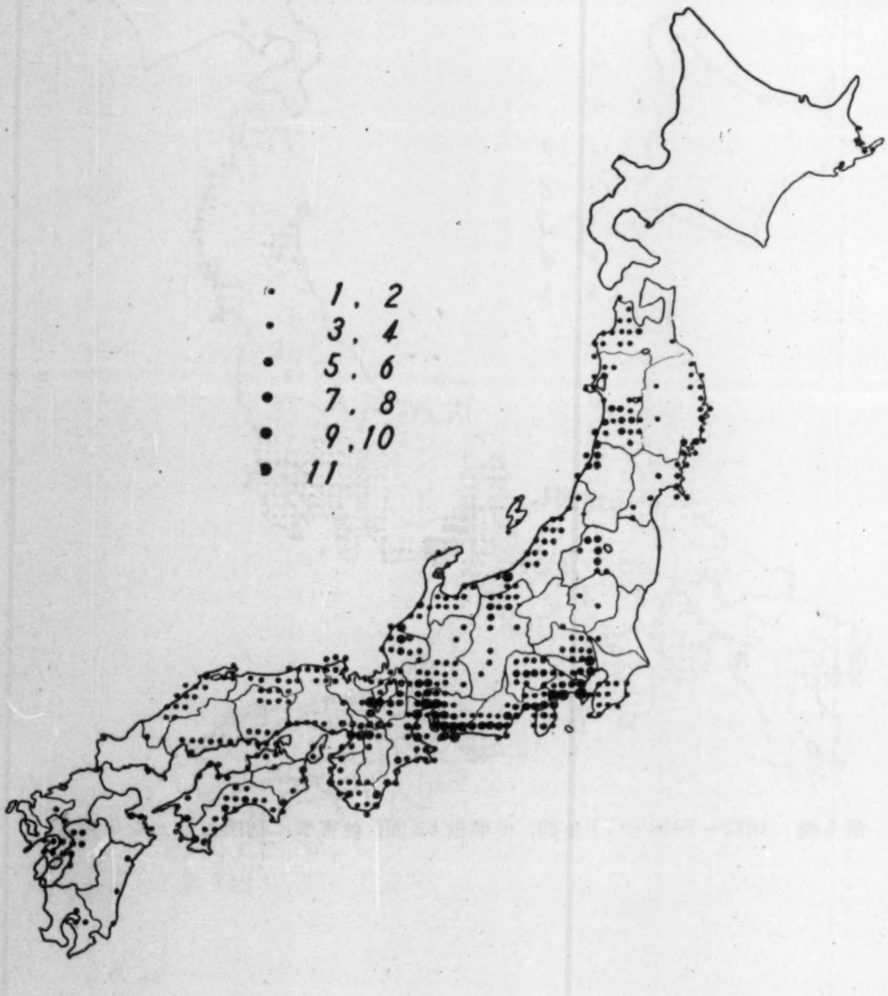

第6圖 1192～1948 の 757 年間，地震數 137 回，(第2～4圖の總和).

---

1) C. Tsuboi, *Geophs. Notes, Geophys. Inst., Tokyo Univ.*, No. 12 (1948), **2** (1949) No. 2. K. Kanai, *Zishin (Earthquakes)*, **1** (1948), 17.

2) K. Kanai, *Bull. Earthq. Res. Inst.*, **28** (1950).

16. *Distribution of Suffered Frequency of Earthquake Damage to House in Japan.*

By Kiyoshi KANAI and Shizuyo YOSHIZAWA,

Earthquake Research Institute.

We have investigated the frequency at a place of damages inflicted on houses by earthquakes in Japan during the 1350 years from 599 to 1948.

Figs. 1-3 show the distribution of 29 earthquakes during 599-1191, of 51 earthquakes during 1192-1687 and of 51 earthquakes during 1688-1871. Figs. 4 and 5 show the distribution of suffered number of damage more than 1% damage rate and of damage including slight one caused by 35 earthquakes during 1872-1948. Fig. 6 shows the distribution of total sum of Figs. 2-4, that is, 137 earthquakes during 1192-1948.

These figures show us that the damages done by earthquakes to Japanese-style wooden houses depend not only on the passive seismicity number for destructive earthquakes but also largely on the nature of the superficial layer of the earth.

75. Distribution of Seismic Frequency of Earthquake Causing Damage in Japan.

By [illegible]

[illegible] Research Institute.

We have investigated the frequency of a place [illegible] indicated in figures by earthquakes in Japan during the past years from [illegible] to 1948.

Figs. 1–3 show the distribution of [illegible] earthquakes during [illegible], of 51 earthquakes during [illegible] and of [illegible] earthquakes during [illegible]. Figs. 4 and 5 show the distribution of [illegible] number of damage more than 1% damage rate and of damage including [illegible] caused by [illegible] earthquakes during [illegible]. Fig. 6 shows the distribution of [illegible] of Figs. 1–5, that is, [illegible] earthquakes during [illegible].

These figures show us that the damage done by earthquakes to Japanese style wooden houses depend not only on the [illegible] number for destructive earthquakes but [illegible] on the nature of the [illegible] of the earth.

[illegible]

[illegible]

—所　報—

◎談話會記事

第263回談話會（昭和25年1月17日）

1. 地下450米における地震觀測結果（序報）	田中貞二 吉澤靜代 金井清
2. 建物振動に伴う土地の震動の測定結果（第1報）	金井清 鈴木富三郎 長田甲斐男
3. 福井地震餘震觀測報告（第2報）	表俊一郎 伊藤貞子
4. 第3紀の山嶽及火山生成	長岡半太郎
5. 今市地震の通信調査について（速報）	河角廣 佐藤泰夫
6. 今市地震概報	河角廣
7. 今市地震に伴つた地變に就て	河角廣 森本良平
8. 今市地震の建物被害について	金井清 田中貞二
9. 今市地震の餘震による建物振動測定結果	金井清 鈴木富三郎

追加

1. 今市，丸岡兩地震の關係に就き	長岡半太郎
2. 今市地震と鬼怒川地震帶	武者金吉

第264回談話會（昭和25年2月21日）

1. 立川市における地下水の汚染に就て	野口喜三雄 井口昭
2. 今市地方地下水位の變動に就て	下鶴大輔 野口喜三雄 西條八束 上野精一
3. 今市地震に於ける墓石顚倒より推定した震度	池上良平 岸上冬彦
4. 今市地震餘震の栃木縣鹽谷郡船生村における觀測結果（第1報）	宮村攝三 秋間哲夫 千喜良利雄 納本君子 田島廣一
5. 今市地震餘震觀測概報	地震研究所調査班
6. 大平洋周邊の火山系（第1）地球の核心と大洋の創成	長岡半太郎
7. 地磁氣異常分布とその磁氣中心（其の1）	力武常次郎
8. 郡中及び今治の驗潮記錄より見た地盤沈下	表俊一郎

9. 昭和24年9月7日の板橋火薬庫爆發の通信調査について	河角廣 佐藤泰夫
10. 地震斷層の運動（其の2）濃尾斷層について	那須信治

第265回談話會（昭和25年3月20日）

1. スターリング型の三次元內挿式	谷本勉之助 （西村所員紹介）
2. 堆積層中の凝灰岩の出現狀態について	村井勇
3. 二上山含柘榴石熔岩について（補遺）	森本良平
4. 地磁氣異常分布とその磁氣中心（其の2）	力武常次
5. 星霧狀態より地球核心と外部の構成　深發地震　水分の上昇	長岡半太郎
6. 濃尾地震と三河地震との關係	那須信治
7. 地盤の硬度と高層建築の震害 附 東京下町の震度分布	北澤五郎 （金井技官紹介）
8. 今市地震の餘震による建物振動測定結果（補遺）	金井清 鈴木富三郎
9. 非木造建物の震害（續報）	金井清 吉澤靜代
10. 今市地震の際の微小地震に就いて	淺田敏 鈴木次郎 （松澤所員紹介）
11. 今市地震餘震觀測概報（補遺）	地震研究所調査班
12. 今市地震後における落合村內水準測量の結果（第1報）	高橋龍太郎 平能金太郎 相田勇

第266回談話會（昭和25年4月18日）

1. 今市地震地域の地質（序報）	森本良平
2. 濃尾地震及び三河地震との關係（補足）	那須信次
3. 地震の縱波は地球の核を通過するも橫波は遮斷せらるゝ理由	長岡半太郎
4. 圓柱の倒れに關する實驗（第2報）	秋間哲夫 納本君子
5. 地盤の硬度と鐵筋コンクリート建造物の震害	北澤五郎 （河角所員紹介）

第267回談話會（昭和25年5月16日）

1. 提案の階差法による田澤湖及び猪苗代湖の靜振の計算	谷本勉之助
2. 房總半島勝浦町附近に發達する節理と斷層	村井勇
3. 迷走電流による電氣探鑛法の研究	岸上冬彦
4. 地球の核心	長岡半太郎
5. 大阪市內試錐資料より見た地盤の良否と震度豫想	河角廣
6. 今市地方第3回水準測量の結果	高橋龍太郎 平能金太郎 田勇

第268回談話會（昭和25年6月20日）

1.	二，三の n 次元内挿式	谷本勉之助
2.	表面波の研究（第5報） 層内に節をもつ表面波の振幅	佐藤泰夫
3.	今市地震の餘震	笠原慶一
4.	福井地震の餘震について（第2報）	表俊一郎
5.	地核の變動より地質時代の變化を論じ得べきか	長岡半太郎
6.	今市地震後落合村において行つた地殼變動の觀測	萩原尊禮 力武常次 齋藤貞夫
7.	地球内部の電氣的性質（其の8） 27日週期變化による考察	力武常次
8.	四國松山における地殼變動の觀測	萩原尊禮 力武常次 山田重平

昭和25年10月15日印刷
昭和25年10月20日發行

東京都文京區本富士町一番地
東京大學構內
編纂兼發行者　東京大學地震研究所

東京都港區芝浦一丁目一番地
印刷者　富田元

東京都港區芝浦一丁目一番地
印刷所　株式會社ヘラルド社

東京都千代田區神田一ツ橋通
賣捌所　岩波書店

東京都中央區日本橋二丁目六番地
丸善株式會社

Sold by
Iwanami Shoten,
Hitotsubashi dôri, Chiyoda, Tôkyô,
and
Maruzen Co., Ltd.,
Nihonbashi dôri, Chûô-ku, Tôkyô.
Price of this copy: 550 Yen. (Postage exclusive.)

BULLETIN OF
THE EARTHQUAKE RESEARCH INSTITUTE
TOKYO UNIVERSITY
Vol. XXVIII, Parts 1-2. Jan.~June, 1950.

Contents.

Papers and Reports.

Page
1. Y. SATÔ, Transformations of Wave-functions Related to the Transformations of Coordinates Systems. I. (in English) 1
2. Y. SATÔ, Rayleigh Waves Propagated along the Plane Surface of Horizontally Isotropic and Vertically Aeolotropic Elastic Body. (in English) 23
3. K. KANAI, The Effect of Solid Viscosity of Surface Layer on the Earthquake Movements. (in English) 31
4. T. TAKAHASHI and Y. SATÔ, On the Theory of Elastic Waves in Granular Substance. II. (in English) 37
5. T. RIKITAKE, Electromagnetic Induction within the Earth and Its Relation to the Electrical State of the Earth's Interior. Part I (1) (in English) 45
6. R. MORIMOTO, Petrogenic Meaning of the Occurrence of Spinel in Xenoliths. (in English) 101
7. F. KISHINOUYE and M. KOTAKA, A Statistical Investigation of Conspicuous Earthquakes in Japan during the Period 1933-1943. (in English) 109
8. R. IKEGAMI and F. KISHINOUYE, A Study on the Propagation of Microseismic Waves. Part II. (in English) 115
9. R. IKEGAMI and F. KISHINOUYE, The Acceleration of Earthquake Motion Deduced from Overturning of the Gravestones in Case of the Imaichi Earthquake on Dec. 26, 1949. (in English) 121
10. D. SHIMOZURU, Change of the Ground-water Level due to the Imaichi Earthquake. (in English) 129
11. S. OMOTE, Precise Leveling at the Eastern Foot of Volcano Usu. (in English) ... 133
12. T. MINAKAMI, Recent Activities of Volcano Usu (V). Topographical Deformations During the 1943-1945 Eruption. (in English) 143
13. T. MINAKAMI, S. SAKUMA and A. OKADA, Recent Activities of Volcano Usu (VI). Precise Levelling Around Mt. Usu in 1949. (in English) 153
14. K. KANAI, A Method of Determining the Stiffness of Each Storey of a n-storied Building. (in English) 161
15. R. TAKAHASI, A Short Note on Kanai's Formula. (in English) 165
16. K. KANAI and S. YOSHIZAWA, Distribution of Suffered Frequency of Earthquake Damage to House in Japan. (in Japanese) 167

Institute Notes.

(For the papers written in Japanese or in occidental languages, the abstracts are given in occidental languages or in Japanese respectively.)

BULLETIN OF THE EARTHQUAKE RESEARCH INSTITUTE,
TOKYO UNIVERSITY. Vol. XXVIII, Parts 3-4. July～Dec., 1950.

東京大學
地震研究所彙報

第28號　第3～4冊

昭和25年7～12月

目　次

論文及報告

頁
17. 坐標變換にともなふ波動方程式の解の變換 II (英文) ………………… 佐藤泰夫 175
18. 地球内の電磁感應およびその地球内部の電氣的性質との關係 第1報 (2) (英文) ………… 力武常次 219
19. 地球内の電磁感應およびその地球内部の電氣的性質との關係 第2報 (英文) ………… 力武常次 263
20. 地震動の尾部について (其の5) (英文) ………… 表俊一郎 285
21. 福井地震の余震について (英文) ………… 表俊一郎 311
22. 北海道有珠岳新側火山發生にともなつた地表變形の測定 (邦文) ….. 宮村攝三 321
23. 振動臺による圓柱の轉倒に關する實驗について (英文) ………… 秋間哲夫 333
24. 非健全家屋の振動試驗 (英文) ………… 那須信治 349
25. 今市地震概說 (英文) ………… 河角廣 355
26. 今市地震の計測 (英文) ………… 越川善明 369
27. 栃木縣今市町附近の地質 (その一) (英文) ………… 森本良平 379
28. 今市地震餘震觀測報告 (英文) ………… 地震研究所 387
29. 今市地震の餘震 (英文) ………… 萩原尊禮・笠原慶一 393
30. 西大芦村で觀測された今市地震の餘震 (英文) ………… 表俊一郎 401
31. 今市地震の際の微少地震に就て (英文) ………… 淺田敏・鈴木次郎 415
32. 今市地震余震の栃木縣船生村における觀測について (邦文) ………… 宮村攝三・秋間哲夫 421
33. 今市地震の震央附近における土地伸縮および傾斜變化の觀測 (英文) 萩原尊禮・力武常次 435
34. 今市地震の震央地域における精密水準測量結果 (概要) (英文) …… 高橋龍太郎・平能金太郎・相田勇 443
35. 井戸調査から知られた今市地方の地層の様辷りについて (英文)….. 本田孝雄 449
36. 今市地震によつて起された地辷りの器械觀測 (英文) ………… 岸上冬彦 457
37. 昭和24年12月26日今市地震の建物被害について (英文) ………… 金井清・田中貞二 461
38. 今市地震の余震による建物振動の觀測結果 (英文) ………… 金井清・鈴木富三郎 465
39. 昭和24年12月26日今市地震の觀測資料 (英文) ………… 地震研究所 471

所報
索引

(The titles in occidental languages are given on the back cover.)

本彙報ハ年４回（但シ第１號ヨリ第６號マデハ不定期ニ，第７號ハ３冊トシテ發行セリ），彙報別冊ハ不定期ニ發行ス．

本彙報掲載ノ論文及ビ報告ノ內容ニ關シテハ著者ノミニ其責任アルモノトス．

本彙報ニ關スル照會通信ハ東京大學地震研究所長ヘ宛テラレタシ．

The Bulletin is published quarterly. (Vols. I–VI were published at irregular intervals and Vol. VII consisted of three parts.)

Supplementary Volume is published at irregular interval.

The authors of the papers alone are responsible for the statements and opinions contained in their respective papers.

All communications relating to this Bulletin should be addressed to the Director of the Earthquake Research Institute, Tokyo University.

Errata of Bull. Earthq. Res. Inst., 28 (1950), 3~4.

Page	Line			
462	Table II.	$\frac{\text{Up (Hard) lands}}{\text{Plain (Soft) lands}}$	Read	$\frac{\text{Plain (Soft) lands}}{\text{Up (Hard) lands}}$
463	Fig. 2.	*A, B, C, D*	„	*A, D, C, B*

Errata of Bull. Earthq. Res. Inst. 27 (1949), 1

Boundary Conditions in the Problem of Generation of Elastic Waves. By Yasuo SATÔ.

Page	Line		
3	3	: $\mathfrak{B}'$	Read $\mathfrak{B}$
5	10	: $\frac{1}{\sin\theta}\frac{d}{d\theta}\{\sin\theta\, W^m\}-mV^{m'}$	,, $\frac{1}{\sin\theta}\left[\frac{d}{d\theta}\{\sin\theta\, W^m\}-mV^{m'}\right]$
5 6	13, 16, 23 1	: $\left[\frac{1}{\sin\theta}\frac{d}{d\theta}\{\cdots\cdots\right.$	,, $\frac{1}{\sin\theta}\left[\frac{d}{d\theta}\{\cdots\cdots\right.$
6	1	: $\frac{2n+1}{2n(n+1)}$	,, $-\frac{2n+1}{2n(n+1)}$
7	26	: $\mathfrak{E}$	,, $\mathfrak{E}'$

17. *Transformation of Wave-functions related to the Transformation of Coordinates Systems. II.*

By Yasuo SATÔ,

Earthquake Research Institute.

(Read July 16, 1946.—Received Sept. 20, 1950.)

Part III Three-dimensional Problem—(2)

Transformation of Surface Harmonics related to the Rotation of Polar Coordinates System.

8. **Rotation of polar coordinates system.**

Hitherto we have studied several kinds of transformations[1] of wave functions, and now we will proceed to the next problem related to the rotation of axes of polar coordinates.

The most general kind of transformation between two coordinates systems in three dimensional space is the case as shown in Fig. 11, of different origins and directions of three coordinate-axes. This is carried out by two steps, viz. the translation of origin in the direction of z-axis, and the rotation of axes around its own origin. Since the first step has been already treated in the previous articles, we shall only consider here the second procedure, omitting the description of the full process for simplicitiy's sake. In this case, however, the distance R of any point from the origin remains constant, so that function $(hR)^{-\frac{1}{2}}H^{(2)}_{n+\frac{1}{2}}(hR)$ is an invariant in this transformation and we have only to pay attention to the part of

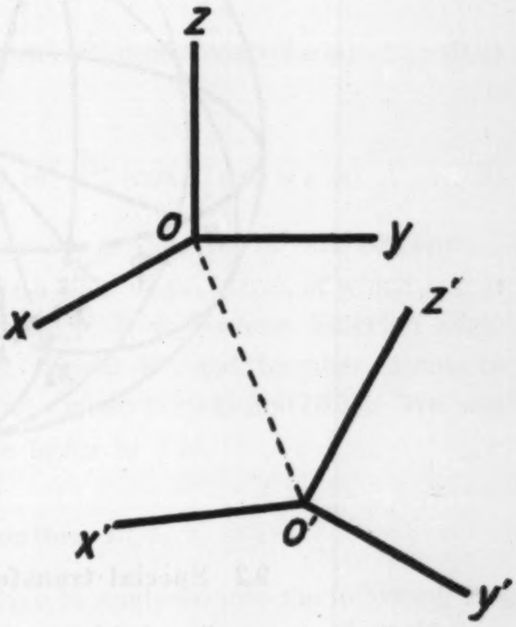

Fig. 11

---

[1] Y. SATÔ, *Bull. Earthq. Res. Inst.*, 28 (1950) 1.

spherical surface harmonics $\overline{P}{}_n^m(\cos\theta)\genfrac{}{}{0pt}{}{\cos}{\sin} m\varphi$, which appears not only in wave functions but also in potential functions and in solutions of heat conduction etc. Thus the formulae obtained in this paper are also applicable to the discussion of relations between geographical and geomagnetic coorninates in the theory of geomagnetism.

9. Analysis into elementary transformations.

9.1 Relation between two coordinates systems.

At first take two systems (x_0, y_0, z_0) and (x, y, z), then the Eulerian angle ϕ, χ, ψ connecting two systems is defined as is shown in Fig. 12 and the direction cosines between two systems in terms of Eulerian angles are found in every text-book on mechanics.[2] (Cf. Fig. 12)

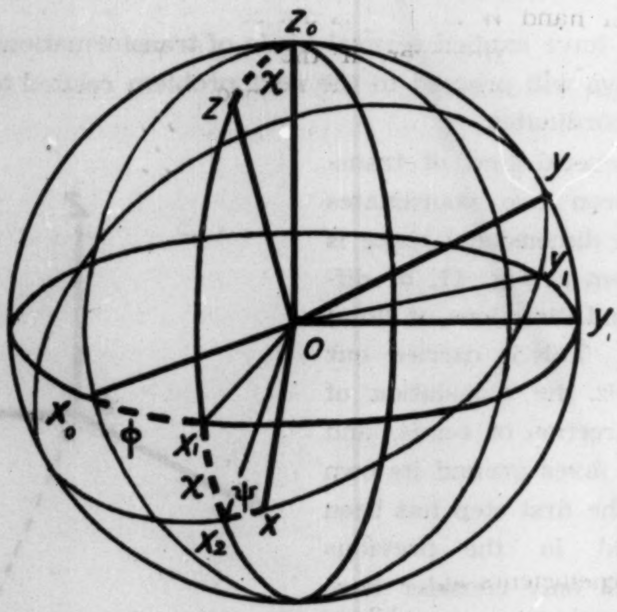

Fig. 12.

9.2 Special transformations $\varPhi$, W and W'.

Next, for convenience' sake, we will consider the following several fundamental transformations, or operations.

---

2) e.g. WHITTAKER, *Analytical Dynamics*, 4th ed. (1937) p. 10. TAMARU, *Rikigaku* I (1938) p. 226. T. SAKAI, *Ippan-Rikigaku* (1948) p. 12.

1° When χ and ψ vanish and only ϕ exists, we name this transformation as operation Φ.

2° When ϕ vanishes and $\chi=\psi=\pi/2$ we name this as operation W.

3° When ψ vanishes and $\phi=\chi=-\pi/2$ we name this as operation W'.

By slight kinematical considerations we may prove that any transformation whose Eulerian angle is represented by (ϕ, χ, ψ) can be analysed into the above three kinds of elementary operations, but we will postpone its description for the present and examine the nature of each elementary operation separately.

Φ is a very simple operation representing the rotation of the coordinates system around z-axis by an angle ϕ, consequently it only causes a variation of azimuthal angle; the relation between the old and new azimuthal angle φ and φ_1 is $\varphi=\varphi_1+\phi$, thus

$$\overline{P}_n^m(\cos\theta)\exp(im\varphi)=\exp(im\phi)\,\overline{P}_n^m(\cos\theta)\exp(im\varphi_1) \quad \text{............(9.1)}$$

On the other hand W and W' is not so simple, and the result cannot be written down at once. However, if the result may be complicated surface harmonics of order n must be transformed to a kind of surface harmonics whose order is also n. Therefore formulae of the following type must exist.

By operation W;

$$\overline{P}_n^m(\cos\theta^*)\exp(im\varphi^*)=\sum_{\kappa=-n}^{n} w_\kappa(n,m)\;\overline{P}_n^\kappa(\cos\theta)\exp(i\kappa\varphi) \quad \text{......(9.2)}$$

By operation W';

$$\overline{P}_n^m(\cos\theta^\dagger)\exp(im\varphi^\dagger)=\sum_{\kappa} w'_\kappa(n,m)\;\overline{P}_n^\kappa(\cos\theta)\exp(i\kappa\varphi) \quad \text{......(9.3)}$$

in which θ and φ are new coordinates and θ^*, φ^* and $\theta^\dagger$, $\varphi^\dagger$ are old ones.

Now, our subject has been reduced to a pair of problems, of which one is how to analyse a general transformation $T[\phi, \chi, \psi]$—whose Eulerian angle is ϕ, χ, ψ—into elementary operations Φ, W and W', and the other is how to determine the coefficients $w_\kappa(n, m)$ and $w'_\kappa(n, m)$ in (9.2) and (9.3). We will treat the former problem in § 9.3 and the latter in § 10.

9.3 General transformation $T[\phi, \chi, \psi]$.

General transformation $T[\phi, \chi, \psi]$ may be analysed into the following elementary transformations, as will be seen from slight kinematical considerations. (We shall denote the original coordinates as x_0, y_0, z_0 or R_0, θ_0, φ_0 and the spherical surface harmonics of order n as $Y_n(\theta_0, \varphi_0)$ and the latter new coordinates as x, y, z or $R(=R_0)$, θ, φ and the same surface harmonics referred to the new coordinates as $Y_n'(\theta, \varphi)$.

Process I; $T[\phi, 0, 0]$ (Operation Φ).

Rotate the (x_0, y_0, z_0)-system arround z_0-axis by the angle ϕ, and take new y-axis in xy-plane. We denote the new coordinates as $(x_{\rm I}, y_{\rm I}, z_{\rm I})$-system, where $z_{\rm I}=z$. Transformation of $Y_n(\theta_0, \varphi_0)$ due to the above process is as follows:

$$\theta \to \theta_{\rm I}, \qquad \varphi \to \varphi_{\rm I}+\phi$$

$$Y_n(\theta_0, \varphi_0)=\bar{P}_n^m(\cos\theta_0)\exp(im\varphi_0)$$

$$\to {}_{\rm I}Y_n(\theta_{\rm I}, \varphi_{\rm I})=\exp(im\phi)\,\bar{P}_n^m(\cos\theta_{\rm I})\exp(im\varphi_{\rm I}) \quad\text{......(9.4)}$$

Process II; $T[-\pi/2, -\pi/2, 0]$. (Operation W')

We interchange the coordinates axes and let new axes $x_{\rm II}$, $y_{\rm II}$, $z_{\rm II}$ coincide with the old ones as follows

$$x_{\rm I}\to y_{\rm II}, \qquad y_{\rm I}\to z_{\rm II}, \qquad z_{\rm I}\to x_{\rm II}$$

New colatitudinal and azimuthal angle are assumed to be $\theta_{\rm II}$ and $\varphi_{\rm II}$, and the transformation due to the above interchange is formally written down as follows:

$${}_{\rm I}Y_n(\theta_{\rm I}, \varphi_{\rm I})\to {}_{\rm II}Y_n(\theta_{\rm II}, \varphi_{\rm II})$$

$$=\exp(im\phi)\sum_{\kappa=-n}^{n} w'_\kappa(n, m)\,\bar{P}_n^\kappa(\cos\theta_{\rm II})\exp(i\kappa\varphi_{\rm II}) \quad\text{.........(9.5)}$$

Process III; $T[\chi, 0, 0]$

Rotate the $(x_{\rm II}, y_{\rm II}, z_{\rm II})$-system arround $z_{\rm II}$ axis by an angle χ, and make the new $x_{\rm III}$-axis coincide with the z-axis. By this operation, we have

$$\theta_{\rm II}\to\theta_{\rm III}, \qquad \varphi_{\rm II}\to\varphi_{\rm III}+\chi$$

$${}_{\rm II}Y_n(\theta_{\rm II}, \varphi_{\rm II})\to {}_{\rm III}Y_n(\theta_{\rm III}, \varphi_{\rm III})$$

$$=\exp(im\phi)\sum_{\kappa=-n}^{n}\exp(i\kappa\chi)\,w'_\kappa(n, m)\,\bar{P}_n^\kappa(\cos\theta_{\rm III})\exp(i\kappa\varphi_{\rm III}) \quad\text{...(9.6)}$$

Process IV; $T[0, \pi/2, \pi/2]$. (Operation W)

In process II, we have interchanged three coordinates axes, and by the present process we return to the original state; that is to say

$$x_{\rm III}\to z_{\rm IV}, \quad y_{\rm III}\to x_{\rm IV}, \quad z_{\rm III}\to y_{\rm IV},$$

and the transformation due to this process is

$${}_{\rm III}Y_n(\theta_{\rm III}, \varphi_{\rm III})\to {}_{\rm IV}Y_n(\theta_{\rm IV}, \varphi_{\rm IV})=\exp(im\phi)$$

$$\cdot\sum_{\kappa=-n}^{n}\exp(i\kappa\chi)\,w'_\kappa(n, m)\sum_{\gamma=-n}^{n} w_\gamma(n, \kappa)\,\bar{P}_n^\gamma(\cos\theta_{\rm IV})\exp(i\gamma\varphi_{\rm IV}) \quad\text{......(9.7)}$$

Process V; $T[\psi, 0, 0]$

In the last stage, we rotate the system arround z_{IV}-axis by the angle ψ, and make the new three axes coincide with x, y, z-axes. Thus we have completed the general transformation.

$$\theta_{\mathrm{IV}} \to \theta, \quad \varphi_{\mathrm{IV}} \to \varphi+\psi; \quad x_{\mathrm{IV}} \to x, \quad y_{\mathrm{IV}} \to y, \quad z_{\mathrm{IV}} \to z.$$

$$_{\mathrm{IV}}Y_n(\theta_{\mathrm{IV}}, \varphi_{\mathrm{IV}}) \to Y'_n(\theta, \varphi) = \exp(im\phi) \sum_{\kappa} \exp(i\kappa\chi)\, w'_\kappa(n, m)$$

$$\cdot \sum_{\gamma=-n}^{n} \exp(i\gamma\psi)\, w_\gamma(n, \kappa)\, \overline{P}_n^\gamma(\cos\theta) \exp(i\gamma\varphi)$$

$$= \exp(im\phi) \sum_{\gamma=-n}^{n} \overline{P}_n^\gamma(\cos\theta)\ \exp\{i\gamma(\varphi+\psi)\}$$

$$\cdot \sum_{\kappa=-n}^{n} \exp(i\kappa\chi)\, w'_\kappa(n, m)\, w_\gamma(n, \kappa) \quad \text{......} (9.8)$$

By (9.8), the most general kind of transformation is expressed. We will proceed to the next step, i.e. how to get the coefficients $w_\kappa'(n, m)$ and $w_\gamma(n, \kappa)$ in the following articles.

10. Operation *W*.

First we will consider how to express the surface harmonics

$$Y_n(\theta^*, \varphi^*) \equiv \overline{P}_n^m(\cos\theta^*) \exp(im\varphi^*). \quad \text{......} (10.1)$$

We can obtain the next expression without difficulty.

$$Y_n(\theta^*, \varphi^*) = (x^* + iy^*)^m R^{-m} P_n^{(m)}(z^*/R) \quad \text{......} (10.2)$$

where $\quad P_n^{(m)}(\zeta) \equiv d^m P_n(\zeta)/d\zeta^m$

Obviously
$$\begin{cases} x^* = R\sin\theta^*\cos\varphi^* \\ y^* = R\sin\theta^*\sin\varphi^* \\ z^* = R\cos\theta^* \end{cases}$$

Now, the operation W is the interchange of axes such as

$$x^* \to z, \quad y^* \to x, \quad z^* \to y,$$

where x, y and z are the new coordinates, therefore

$$\begin{cases} x^* = z = R\cos\theta \\ y^* = x = R\sin\theta\cos\varphi \\ z^* = y = R\sin\theta\sin\varphi \end{cases}$$

Using these relations, we can express $Y_n(\theta^*, \varphi^*)$ as a function of θ and φ.

$$Y_n(\theta^*, \varphi^*) = (\cos\theta + i\sin\theta\cos\varphi)^m P_n^{(m)}(\sin\theta\sin\varphi) \quad \text{......} (10.3)$$

10.11 $(\cos\theta + i\sin\theta\cos\varphi)^m$

From the well known formula3)

$$(z+\sqrt{(z^2-1)}\cdot\cos\varphi)^m = P_m(z) + 2\sum_{\gamma=1}^{m}\frac{m!}{(m+\gamma)!}P_m^\gamma(z)\cos\gamma\varphi \quad \dots(10.4)$$

we may obtain a slightly modified expression ; i. e. putting $z=\cos\theta$

$$(\cos\theta + i\sin\theta\cos\varphi)^m = \sum_{\gamma=-m}^{m}\frac{m!}{(m+\gamma)!}i^\gamma\,\overline{P}_m^\gamma(\cos\theta)\exp(i\gamma\varphi) \dots(10.5)$$

Next, we must transform $P_n^{(m)}(\sin\theta\sin\varphi)$ into a more convenient from.

10.12 $(d/d\cos\omega)^m\cos\gamma\omega$

First we consider the differential equation satisfied by $u=\cos\gamma\omega$ when the independent variable is $c=\cos\omega$;

$$(1-c^2)\frac{d^2u}{dc^2} - c\frac{du}{dc} + \gamma^2 u = 0 \quad \dots\dots\dots\dots\dots\dots(10.6)$$

Differentiating m times with respect to c we have

$$(1-c^2)\frac{d^{m+2}u}{dc^{m+2}} - (2m+1)c\frac{d^{m+1}u}{dc^{m+1}} + (\gamma^2-m^2)\frac{d^m u}{dc^m} = 0 \dots\dots\dots(10.7)$$

or, writing $d^m u/dc^m = w$

$$(1-c^2)\frac{d^2w}{dc^2} - (2m+1)c\frac{dw}{dc} + (\gamma^2-m^2)w = 0 \quad \dots\dots\dots\dots(10.8)$$

We will again change the independent variable from c to ω, then the above equation takes the following form.

$$\sin\omega\frac{d^2w}{d\omega^2} + 2m\cos\omega\frac{dw}{d\omega} + (\gamma^2-m^2)\sin\omega\cdot w = 0 \quad \dots\dots\dots(10.9)$$

where $w = (d/d\cos\omega)^m u$.

In the following calculation we will expand this function into a Fourier series. Assuming w as $w=\sum a_s\cos s\omega$, we introduce this expression into (10.9) and we obtain the next recurrence formula.

$$\varepsilon_{s-2}\,a_{s-2}(\gamma+m+s-2)(\gamma-m-s+2) + a_s(\gamma+m-s)(-\gamma+m-s) = 0 \dots(10.10)$$

where $\varepsilon_N \equiv \begin{cases} 2 \dots \text{ when } N=0 \\ 1 \dots \quad " \quad N\neq 0 \end{cases}$

---

3) HOBSON, *Spherical and Ellipsoidal Harmonics.* p. 97. This famous text-book will be cited as HOBSON. TERAZAWA, *Sûgaku-gairon.* p. 485.

Since $\cos\gamma\omega$ is a polynomial of $\cos\omega$ of γ-th degree, w is a polynomial of $(\gamma-m)$-th degree. Moreover, the terms of $(\gamma-m-2\kappa-1)$-th degree (where κ is an interger) vanish. Thus putting $s=\gamma-m-2\kappa$, we have

$$\varepsilon_{\gamma-m-2\kappa-2}\, a_{\gamma-m-2\kappa-2} = \frac{(m+\kappa)(\gamma-m-\kappa)}{(\kappa+1)(\gamma-1-\kappa)}\, a_{\gamma-m-2\kappa} \quad \dots\dots\dots\dots\dots\dots\dots\dots(10.11)$$

On the other hand we know the formula[4]

$$\cos\gamma\omega = 2^{\gamma-1}\cos^{\gamma}\omega + \cdots\cdots$$

Introducing this relation into (10.9), we can obtain the following relation that determines the first coefficient

$$\varepsilon_{\gamma-m}\, a_{\gamma-m} = 2^m\{\gamma\,!/(\gamma-m)\,!\} \quad \dots\dots\dots\dots\dots\dots\dots\dots\dots\dots(10.12)$$

By combining the above two formulae, we can get the explicit form of any coefficient;

$$\varepsilon_{\gamma-m-2\kappa}\, a_{\gamma-m-2\kappa} = 2^m\gamma\cdot\frac{(m)_\kappa(\gamma-1-\kappa)\,!}{\kappa\,!\,(\gamma-m-\kappa)\,!} \quad \dots\dots\dots\dots\dots\dots(10.13)$$

in which $(m)_\kappa = m\,(m+1)\dots\dots(m+\kappa-1)$, $(m)_0=1$, $m\neq 0$.

Therefore

$$\begin{aligned} w &= (d/d\cos\omega)^m\cos\gamma\omega \\ &= \sum_{\kappa=0}^{\langle\gamma-m\rangle}\frac{2^m\gamma}{\varepsilon_{\gamma-m-2\kappa}}\cdot\frac{(m)_\kappa(\gamma-1-\kappa)\,!}{\kappa\,!\,(\gamma-m-\kappa)\,!}\cos(\gamma-m-2\kappa)\omega \quad \dots\dots\dots(10.14) \end{aligned}$$

where $$\langle N\rangle \equiv \begin{cases} N/2 & \dots \text{ when } N \text{ is even} \\ (N-1)/2 \dots & \quad ,, \quad\quad \text{odd} \end{cases}$$

By just considering the domain of summation we can easily get the following result.

$$\left(\frac{d}{d\cos\omega}\right)^m\cos\gamma\,\omega = 2^{m-1}\gamma\sum_{\kappa=0}^{\gamma-m}\frac{(m)_\kappa(\gamma-1-\kappa)\,!}{\kappa\,!\,(\gamma-m-\kappa)\,!}\exp[i\,(\gamma-m-2\kappa)\omega]$$

$$\dots\dots\dots(10.15)$$

10.13 $P_n^{(m)}(\sin\theta\sin\varphi)$

From the well known addition theorem of zonal harmonics, we have[5]

---

4) BROMWICH, *Theory of Infinite Series* 2nd ed. (1926) p. 202.

5) HOBSON, p. 143.

$$P_n(\cos\gamma)=P_n(\cos\theta)\,P_n(\cos\chi)+2\sum_{r=1}^{n}\frac{(n-r)\,!}{(n+r)\,!}\,\bar{P}_n^r(\cos\theta)\,\bar{P}_n^r(\cos\chi)\cos r\omega \qquad \text{.........(10.16)}$$

where $\cos\gamma=\cos\theta\cos\chi+\sin\theta\sin\chi\cos\omega$.

Differentiating this expression m times with respect to $\cos\omega$, we have

$$\left(\frac{d}{d\cos\omega}\right)^m P_n(\cos\gamma)=2\sum_{r=m}^{n}\frac{(n-r)\,!}{(n+r)\,!}\,\bar{P}_n^r(\cos\theta)\,\bar{P}_n^r(\cos\chi)$$

$$\cdot\left(\frac{d}{d\cos\omega}\right)^m\cos r\omega \qquad \text{..................(10.17)}$$

The last factor has just been obtained in § 10.12. On the other hand, the same function is written down in the following form

$$\left(\frac{d}{d\cos\omega}\right)^m P_n(\cos\gamma)=\left(\frac{d\cos\gamma}{d\cos\omega}\cdot\frac{d}{d\cos\gamma}\right)^m P_n(\cos\gamma)$$

$$=(\sin\theta\sin\chi)^m\,P_n^{(m)}(\cos\gamma) \qquad \text{...............(10.18)}$$

Thus, equating the two expressions (10.17) and (10.18), we arrive at the next relation.

$$(\sin\theta\sin\chi)^m\,P_n^{(m)}(\cos\gamma)=2\sum_{r=m}^{n}\frac{(n-r)\,!}{(n+r)\,!}\sin^r\theta\,P_n^{(r)}(\cos\theta)$$

$$\cdot\sin^r\chi\,P_n^{(r)}(\cos\chi)\cdot 2^{m-1}\,r\sum_{\kappa=0}^{r-m}\frac{(m)_\kappa\,(r-\kappa-1)\,!}{\kappa\,!\,(r-\kappa-m)\,!}\exp[i(r-m-2\kappa)\omega]$$

Putting $\chi=-\pi/2$, $\omega=\varphi+\pi/2$ we have

$$P_n^{(m)}(\sin\theta\sin\varphi)=\sum_{r=m}^{n}\frac{(n-r)\,!}{(n+r)\,!}\sin^{r-m}\theta\,P_n^{(r)}(\cos\theta)\,(-)^{r-m}\,P_n^{(r)}(0)$$

$$\cdot 2^m r\sum_{\kappa=0}^{r-m}\frac{(m)_\kappa\,(r-\kappa-1)\,!}{\kappa\,!\,(r-\kappa-m)\,!}\exp[i\,(r-m-2\kappa)\,(\varphi+\pi/2)] \text{...(10.19)}$$

10.14 $P_n^{(r)}(0)$

Next we will calculate the value of $P_n^{(r)}(0)$ in (10.19).

Since $P_n(z)$ is an even function when n is even, and an odd function when n is odd, $P_n^{(r)}(0)$ vanishes when $(n-r)$ is odd. Therefore we will conisder the case when r is expressed as $n-2$p.

$$P_n^{(n-2p)}(0)=\left[\left(\frac{d}{dz}\right)^{n-2p}\sum_{s=0}^{\langle n\rangle}(-)^s\frac{(2n-2s)\,!}{2^n s\,!\,(n-s)\,!\,(n-2s)\,!}\,z^{n-2s}\right]_{z=0}$$

$$= (-)^{p} \frac{(2n-2p)\,!}{2^{n}\, p\,!\,(n-p)\,!} \quad \ldots\ldots\ldots\ldots\ldots\ldots\ldots\ldots\ldots\ldots\ldots\ldots (10.20)$$

10.2 Explicit expression of operation *W*.

With the above preparation we can write down the explicit form of $P_n^{(m)}(\sin\theta\sin\varphi)$.

Into the expression (10.19) we introduce a notation p, which is defined by $r=n-2p$, and combing it with (10.20) we have

$$P_n^{(m)}(\sin\theta\sin\varphi)=i^{-n+m}2^{-n+m}\sum_{p=0}^{\langle n-m\rangle}\sum_{\kappa=0}^{n-m-2p}(-)^{\kappa}\frac{(2p)\,!}{p\,!\,(n-p)\,!}(n-2p)$$
$$\cdot\frac{(m)_{\kappa}\,(n-2p-\kappa-1)\,!}{\kappa\,!\,(n-m-2p-\kappa)\,!}\cdot\sin^{n-m-2p}\theta\, P_n^{(n-2p)}(\cos\theta)$$
$$\cdot\exp\left[i(n-m-2p-2\kappa)\,\varphi\right]\ldots\ldots\ldots\ldots\ldots\ldots\ldots\ldots\ldots\ldots\ldots\ldots (10.21)$$

Using an integer $q=p+\kappa$ and changing the summation with regard to κ into that of q, we have (cf. Fig. 13).

$$P_n^{(m)}(\sin\theta\sin\varphi)=i^{-n+m}2^{-n+m}\sum_{p=0}^{\langle n-m\rangle}\sum_{q=p}^{n-m-p}(-)^{p+q}$$
$$\cdot\frac{(2p)\,!\,(n-2p)\cdot(m)_{-p+q}\,(n-p-q-1)\,!}{p\,!\,(n-p)\,!\,(-p+q)\,!\,(n-m-p-q)\,!}\cdot\sin^{n-m-2p}\theta$$
$$\cdot P_n^{(n-2p)}(\cos\theta)\exp\left[i(n-m-2q)\,\varphi\right]\ldots\ldots\ldots\ldots\ldots\ldots\ldots\ldots (10.22)$$

Fig. 13.

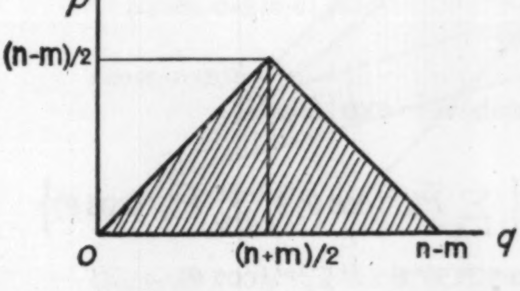

Fig. 14.

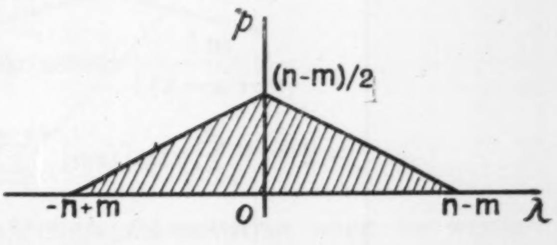

Further, we employ another notation $\lambda=n-m-2q$, and change the above summation into that of p and λ (cf. Fig. 14).

$$P_n^{(m)}(\sin\theta\sin\varphi)=i^{-n+m}2^{-n+m}\sum_{p=0}^{\langle n-m\rangle}\sum_{\lambda=-n+m+2p}^{n-m-2p}e(n+m+\lambda)\,(-)^{p+(n-m-\lambda)/2}$$

$$\cdot \frac{(2p)!\,(n-2p)}{p!\,(n-p)!} \cdot \frac{(m)_{-p+(n-m-\lambda)/2}\,(n-p-(n-m-\lambda)/2-1)!}{(-p+(n-m-\lambda)/2)!\,(n-p-(n-m-\lambda)/2-m)!}$$

$$\cdot \sin^{n-m-2p}\theta\, P_n^{(n-2p)}(\cos\theta)\exp[i\lambda\varphi] \quad\ldots\ldots\ldots\ldots(10.23)$$

in which the newly introduced function $e(\ )$ means

$$e(N)\equiv\begin{cases}1 \ \ldots\ldots\ \text{when } N \text{ is even}\\ 0 \ \ldots\ldots\ \quad\text{,,}\quad\ \text{odd.}\end{cases} \quad\ldots\ldots\ldots(10.24)$$

This is the expression at which we have aimed in the last part of § 10.11.

Combining the above formula with that of § 10.11, we have an explicit expression of $Y_n(\theta^*, \varphi^*)$ which we will state in the next article.

10.21 Fourier series representation of $Y_n(\theta^*, \varphi^*)$ with regard to φ.

From (10.3), (10.5) and (10.23), we have

$$Y_n(\theta^*, \varphi^*) = 2^{-n+m}\sum_{p=0}^{\langle n-m\rangle}\ \sum_{\lambda=-n+m+2p}^{n-m-2p}\ \sum_{r=-m}^{m} e(n+m+\lambda)\, i^{r-\lambda+2p}\sin^{n-m-2p}\theta$$

$$\cdot \overline{P}_m^r(\cos\theta)\cdot P_r^{(n-2p)}(\cos\theta)$$

$$\cdot\frac{m!}{(m+r)!}\left[\frac{(2p)!\,(n-2p)}{p!\,(n-p)!}\ \frac{(m)_{\frac{1}{2}n-\frac{1}{2}m-\frac{1}{2}\lambda-p}\,(\frac{1}{2}n+\frac{1}{2}m+\frac{1}{2}\lambda-p-1)!}{(\frac{1}{2}n-\frac{1}{2}m-\frac{1}{2}\lambda-p)!\,(\frac{1}{2}n-\frac{1}{2}m+\frac{1}{2}\lambda-p)!}\right]$$

$$\cdot\exp[i(\lambda+r)\varphi] \quad\ldots\ldots\ldots\ldots(10.25)$$

Introducing another variable $\kappa=\lambda+r$, change the summation with regard to r into that of χ, then

$$Y_n(\theta^*, \varphi^*) = 2^{-n+m}\sum_{p=0}^{\langle n-m\rangle}\ \sum_{\lambda=-n+m+2p}^{n-m-2p}\ \sum_{\kappa=\lambda-m}^{\lambda+m} e(n+m+\lambda)\, i^{\kappa-2\lambda+2p}\sin^{n-m-2p}\theta$$

$$\cdot \overline{P}_m^{\kappa-\lambda}(\cos\theta)\, P_m^{(n-2p)}(\cos\theta)$$

$$\cdot\frac{m!}{(m+\kappa-\lambda)!}[\text{same with above}]\cdot\exp[i\kappa\varphi]$$

$$=2^{-n+m}\sum_{\kappa=-n}^{n}\exp[i\kappa\varphi]\sum_{p=0}^{\langle n-m\rangle}\left\{\sum_{\lambda \text{ in } K+}\overline{P}_m^{\kappa-\lambda}(\cos\theta)+\sum_{\lambda \text{ in } K-}\overline{P}_m^{\kappa-\lambda}(\cos\theta)\right\}$$

$$\cdot e(n+m+\lambda)\, i^{\kappa-2\lambda+2p}\sin^{n-m-2p}\theta\cdot P_n^{(n-2p)}(\cos\theta)$$

$$\cdot\frac{m!}{(m+\kappa-\lambda)!}[\text{same with above}] \quad\ldots\ldots\ldots\ldots(10.26)$$

The domain of summation will be clear by the figures 14, 15 and 16. In K^+, $\kappa>\lambda$ and in K^-, $\kappa<\lambda$.

Fig. 15.

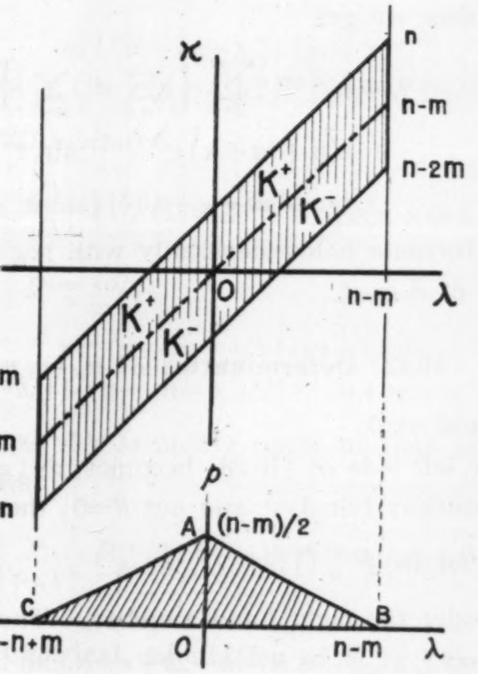
κ
n
n-m
n-2m
K⁺
K⁻
O
n-m
λ
K⁺
K⁻
-n+2m
-n+m
-n
p
A
(n-m)/2
C
B
-n+m
O
n-m
λ

Fig. 16

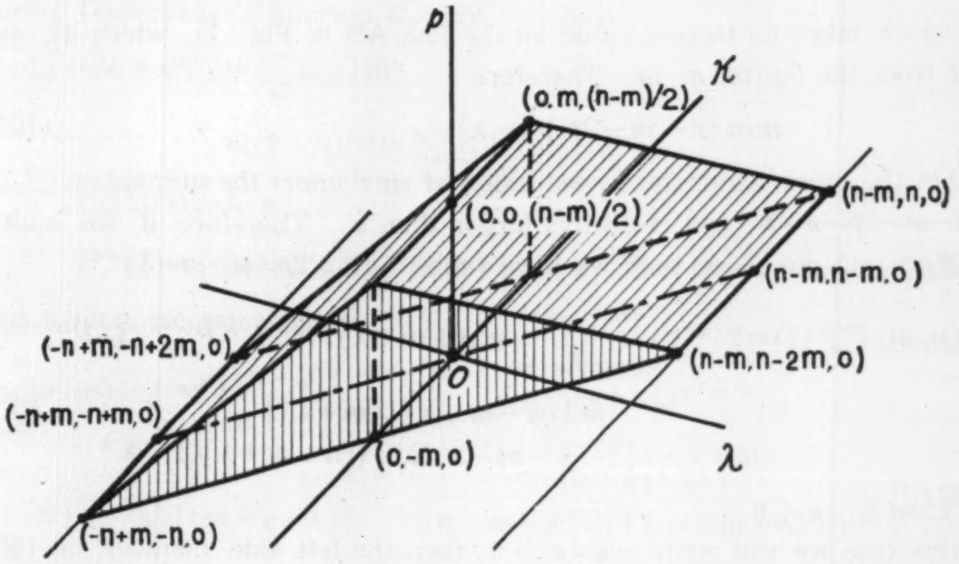
p
κ
(o,m,(n-m)/2)
(n-m,n,o)
(o,o,(n-m)/2)
(n-m,n-m,o)
(-n+m,-n+2m,o)
(n-m,n-2m,o)
O
(-n+m,-n+m,o)
(o,-m,o)
λ
(-n+m,-n,o)

Generally any spherical surface harmonics of order n must be written down as the linear combination of $\overline{P}_n^{\kappa}(\cos\theta)\exp[i\kappa\varphi]$, therefore $Y_n(\theta^*, \varphi^*)$ may be expressed as

$$Y_n(\theta^*, \varphi^*) = \sum_{\kappa=-n}^{n} w_\kappa(n, m)\, \overline{P}_n^{\kappa}(\cos\theta)\exp[i\kappa\varphi]. \quad \dots\dots\dots\dots\dots\dots(10.27)$$

On the other hand, the above function must be equal to the right hand member of (10.26), thus we get

$$w_\kappa(n,m)\,\overline{P}{}^\kappa_n(\cos\theta)=2^{-n+m}\sum_{p=0}^{<n-m>}\Big\{\sum_{\lambda\text{ in }K+}+\sum_{\lambda\text{ in }K-}\Big\}$$

$$\cdot\, e(n+m+\lambda)\,i^{\kappa-2\lambda+2p}\sin^{n-m-2p}\theta\, P^{(n-2p)}_n(\cos\theta)$$

$$\cdot\,\{m!/(m+\kappa-\lambda)!\}\,[\text{same with above}]\ldots\ldots(10.28)$$

Besides, the above formula holds identically with regard to θ, therefore we may put any value of θ in it.

10.22 Determination of $w_\kappa(n, m)$.

Case 1; $\kappa>0$ and $\kappa=0$.

In this case the left side of (10.28) becomes $w_\kappa(n,m)\sin^\kappa\theta\;P_n^{(\kappa)}(\cos\theta)$. Therefore, if we multiply $(\sin\theta)^{-\kappa}$ and put $\theta=0$, then we have

$$w_\kappa(n,m)\,P^{(\kappa)}_n(1)\quad\ldots\ldots\ldots\ldots\ldots\ldots\ldots\ldots\ldots\ldots\ldots\ldots\ldots(10.29)$$

We must next consider the right hand member. The power index of $\sin\theta$ under the summation $\Sigma_{\lambda\text{ in }K+}$ is $n-m-2p+\kappa-\lambda$ and the smallest value of it is

$$\min(n-m-2p+\kappa-\lambda)=n-m-\max(2p+\lambda)+\kappa\,,$$

and $2p+\lambda$ takes its largest value on the line AB in Fig. 15, which is, as is clear from the figure, $n-m$. Therefore

$$\min(n-m-2p+\kappa-\lambda)=\kappa\quad\ldots\ldots\ldots\ldots\ldots\ldots\ldots\ldots\ldots\ldots\ldots(10.30)$$

On the other hand, the power index of $\sin\theta$ under the summation $\Sigma_{\lambda\text{ in }K-}$ is $n-m-2p-\kappa+\lambda$, and is always larger than κ. Therefore if we multiply $(\sin\theta)^{-\kappa}$ and put $\theta=0$, then we have (substituting $2p=n-m-\lambda$)

$$w_\kappa(n,m)\,P^{(\kappa)}_n(1)=2^{-n+m}\sum_{\lambda=\max(0,\kappa-m)}^{\min(n-m,\kappa)}e(n+m+\lambda)\,i^{n-m+\kappa+\lambda}\,P^{(\kappa-\lambda)}_m(1)\,P^{(m+\lambda)}_n(1)$$

$$\cdot\,\frac{m!\,(n-m-\lambda)!\,(m+\lambda)!}{(m+\kappa-\lambda)!\,\{(n-m-\lambda)/2\}!\,\{(n+m+\lambda)/2\}!\,\lambda!}\ \ldots(10.31)$$

Case 2; $\kappa<0$

In this case we will write $-\kappa=\kappa'>0$, then the left side member of (10.28) becomes

$$w_{-\kappa'}(n,m)\,(-)^{\kappa'}\frac{(n-\kappa')!}{(n+\kappa')!}\sin^{\kappa'}\theta\,P^{(\kappa')}_n(\cos\theta)\ \ldots\ldots\ldots\ldots(10.32)$$

As for the right hand member under the summation $\Sigma_{\lambda\text{ in }K-}$, the smallest power index of $\sin\theta$ is obtained on the line AC in Fig. 15, and its value is κ'. Putting $-\kappa=\kappa'$ and $-\lambda=\lambda'$, $2p=n-m-\lambda'$ into (10.28), the term of the lowest power of $\sin\theta$ is

$$\sin^{\kappa'}\theta\cdot 2^{-n+m}\sum_{\lambda'}e(n+m+\lambda')\,i^{n-m+\kappa'-\lambda'}\,P_m^{(\kappa'-\lambda')}(\cos\theta)\,P_n^{(m+\lambda')}(\cos\theta)$$

$$\cdot\frac{m\,!\,(n-m-\lambda')\,!\,(m+\lambda')\,!}{(m+\kappa'-\lambda')\,!\,\{(n-m-\lambda')/2\}\,!\,\{(n+m+\lambda')/2\}\,!\,\lambda'\,!}$$

Comparing this with (10.32) we have

$$w_{-\kappa'}(n,m)\,(-)^{\kappa'}\frac{(n-\kappa')\,!}{(n+\kappa')\,!}\,P_n^{(\kappa')}(1)=2^{-n+m}\sum_{\lambda'}e(n+m+\lambda')\,i^{n-m+\kappa'-\lambda'}$$

$$\cdot P_m^{(\kappa'-\lambda')}(1)\,P_n^{(m+\lambda')}(1)$$

$$\cdot\frac{m\,!\,(n-m-\lambda')\,!\,(m+\lambda')\,!}{(m+\kappa'-\lambda')\,!\,\{(n-m-\lambda')/2\}\,!\,\{(n+m+\lambda')/2\}\,!\,\lambda'\,!}\quad\ldots(10.33)$$

The summation in the right side is nearly equal to that of (10.31) and we can write (10.33) as follows

$$w_{-\kappa}(n,m)\,(-)^{\kappa}\frac{(n-\kappa)\,!}{(n+\kappa)\,!}\,P_n^{(\kappa)}(1)=(-)^{n-m+\kappa}\,\overline{w_\kappa(n,m)}\,P_n^{(\kappa)}(1)\quad\ldots(10.34)$$

10.23 Numerical calculation of $w_\kappa(n,m)$.

At first we will show a lemma useful for calculating (10.31).

Using Gegenbauer's function $C_n^\nu(z)$[6], we have

$$(1-2h+h^2)^{-\nu}=\sum_n C_n^\nu(1)h^n$$

$$=(1-h)^{-2\nu}=\sum\{(2\nu)_n/n\,!\}h^n$$

$$\therefore C_n^\nu(1)=(2\nu)_n/n\,!$$

$$P_n^{(\kappa)}(1)=\{(2\kappa)\,!/2^\kappa\kappa\,!\}C_{n-\kappa}^{\kappa+\frac{1}{2}}(1)=\{(n+\kappa)\,!/2^\kappa\kappa\,!\,(n-\kappa)\,!\}\quad\ldots\ldots(10.35)$$

By this lemma, we can simplify (10.31).

$$w_\kappa(n,m)=2^{-n}\frac{\kappa\,!\,(n-\kappa)\,!}{(n+\kappa)\,!}\sum_{\lambda=max(0,\kappa-m)}^{min(n-m,\kappa)}e(n+m+\lambda)\,i^{n-m+\kappa+\lambda}$$

$$\cdot\frac{1}{\lambda\,!\,(\kappa-\lambda)\,!\,(m-\kappa+\lambda)\,!}\cdot\frac{(n+m+\lambda)\,!}{\{(n-m-\lambda)/2\}\,!\,\{(n+m+\lambda)/2\}\,!}\quad(10.36)$$

The results of calculations are tabulated in Tab. 1.

10.3 Formulae expressing $w_\kappa(n,m)$ when m or κ is negative.

Hitherto we have studied the computation of $w_\kappa(n,m)$ in which n, m, κ are all positive. But in the transformation formula (9.8) there appear some

---

[6] WHITTAKER and WATSON, *Modern Analysis*. 4th ed. (1925) p. 329.

Table 1. $w_\kappa(n, m)$

n	m \ κ	0	1	2	3	4	5	6	7
1	0	0	$-i/2$						
	1	1	$i/2$						
2	0	$-1/2$	0	$-1/2^3$					
	1	0	$-i/2$	$1/2^2$					
	2	3	i	$-1/2^2$					
3	0	0	$i/2^3$	0	$i/2^4\cdot 3$				
	1	$-3/2$	$-i/2^3$	$-1/2^3$	$-i/2^4$				
	2	0	$-i5/2^2$	$1/2$	$i/2^3$				
	3	$3\cdot 5$	$i3\cdot 5/2^2$	$-3/2^2$	$-i/2^3$				
4	0	$3/2^3$	0	$1/2^4\cdot 3$	0	$1/2^7\cdot 3$			
	1	0	$i3/2^3$	$-1/2^3\cdot 3$	$i/2^4\cdot 3$	$-1/2^5\cdot 3$			
	2	$-3\cdot 5/2$	$-i3/2^2$	$-1/2^2$	$-i/2^3$	$1/2^5$			
	3	0	$-i3\cdot 7/2^2$	$7/2^2$	$i3/2^3$	$-1/2^4$			
	4	$3\cdot 5\cdot 7$	$i3\cdot 7$	$-7/2$	$-i/2$	$1/2^4$			
5	0	0	$-i/2^4$	0	$-i/2^7\cdot 3$	0	$-i/2^8\cdot 3\cdot 5$		
	1	$3\cdot 5/2^3$	$i/2^4$	$1/2^4$	$i/2^7$	$1/2^7\cdot 3$	$i/2^8\cdot 3$		
	2	0	$i7/2^2$	$-1/2^2$	$i/2^5$	$-1/2^4\cdot 3$	$-i/2^6\cdot 3$		

	3	$-3\cdot5\cdot7/2$	$-i3\cdot7/2^2$	$-3/2^2$	$-i13/2^5$	$3/2^5$	$i/2^6$		
	4	0	$-i3^2\cdot7/2$	3^2	$i3^3/2^4$	$-1/2^2$	$-i/2^5$		
	5	$3^3\cdot5\cdot7$	$i3^2\cdot5\cdot7/2$	$-3^2\cdot5/2$	$-i3^2\cdot5/2^4$	$5/2^4$	$i/2^5$		
6	0	$-5/2^4$	0	$-1/2^7$	0	$-1/2^8\cdot3\cdot5$	0	$-1/2^{10}\cdot3^2\cdot5$	
	1	0	$-i5/2^4$	$1/2^6$	$-i/2^7$	$1/2^6\cdot3\cdot5$	$-i/2^8\cdot3\cdot5$	$1/2^9\cdot3\cdot5$	
	2	$3\cdot5\cdot7/2^3$	$i5/2^3$	$17/2^6$	$i3/2^6$	$1/2^7\cdot3$	$i/2^7\cdot3$	$-1/2^9\cdot3$	
	3	0	$i3^2\cdot5/2^2$	$-3^3/2^4$	$i/2^5$	$-1/2^4$	$-i/2^6$	$1/2^7\cdot3$	
	4	$-3^3\cdot5\cdot7/2$	$-i3^2\cdot5$	$-3^2\cdot5/2^4$	$-i3\cdot5/2^3$	$13/2^5$	$i/2^4$	$-1/2^7$	
	5	0	$-i3^2\cdot5\cdot11/2$	$3^2\cdot5\cdot11/2^3$	$i3\cdot5\cdot11/2^4$	$-11/2^3$	$-i5/2^5$	$1/2^6$	
	6	$3^3\cdot5\cdot7\cdot11$	$i3^3\cdot5\cdot11$	$-3^3\cdot5\cdot11/2^3$	$-i3\cdot5\cdot11/2^3$	$3\cdot11/2^4$	$i3/2^4$	$-1/2^6$	
7	0	0	$i5/2^7$	0	$i/2^8\cdot5$	0	$i/2^{10}\cdot3^2\cdot5$	0	$i/2^{11}\cdot3^2\cdot5\cdot7$
	1	$-5\cdot7/2^4$	$-i5/2^7$	$-5/2^7$	$-i3/2^8\cdot5$	$-1/2^8\cdot5$	$-i/2^{10}\cdot3^2$	$-1/2^{10}\cdot3^2\cdot5$	$-i/2^{11}\cdot3^2\cdot5$
	2	0	$-i3^3\cdot5/2^6$	$5/2^5$	$-i19/2^7\cdot5$	$1/2^5\cdot5$	$-i/2^9\cdot3\cdot5$	$1/2^8\cdot3\cdot5$	$i/2^{10}\cdot3\cdot5$
	3	$3^3\cdot5\cdot7/2^3$	$i3^4\cdot5/2^6$	$5\cdot19/2^6$	$i3\cdot13/2^7$	$-1/2^7$	$i11/2^9\cdot3$	$-1/2^9$	$-i/2^{10}\cdot3$
	4	0	$i3^3\cdot5\cdot11/2^4$	$-5\cdot11/2^2$	$-i11/2^5$	$-1/2^2$	$-i5^2/2^7\cdot3$	$1/2^5\cdot3$	$i/2^8\cdot3$
	5	$-3^3\cdot5\cdot7\cdot11/2$	$-i3^3\cdot5^2\cdot11/2^4$	$-3\cdot5\cdot11/2^4$	$-i3\cdot11^2/2^5$	$3\cdot5^2/2^5$	$i43/2^7$	$-5/2^7$	$-i/2^8$
	6	0	$-i3^3\cdot5\cdot11\cdot13/2^3$	$3\cdot5\cdot11\cdot13/2^2$	$i3^2\cdot11\cdot13/2^4$	$-3\cdot13/2^2$	$-i5\cdot13/2^6$	$3/2^5$	$i/2^7$
	7	$3^3\cdot5\cdot7\cdot11\cdot13$	$i3^3\cdot5\cdot7\cdot11\cdot13\cdot/2^3$	$-3\cdot5\cdot7\cdot11\cdot13/2^3$	$-i3\cdot7\cdot11\cdot13/2^4$	$3\cdot7\cdot13/2^4$	$i7\cdot13/2^6$	$-7/2^6$	$-i/2^7$

$w_\kappa(n, m)$ where m and κ are not always positive. Thus we must prepare formulae applicable to these cases.

From (10.31) we know

$$\overline{w_\kappa(n, m)} = (-)^\kappa\, w_\kappa(n, m) \quad \text{.................................(10.37)}$$

Therefore using (10.34) we obtain

$$w_{-\kappa}(n, m) = (-)^{n+m+\kappa}\, \frac{(n+\kappa)\,!}{(n-\kappa)\,!}\, w_\kappa(n, m) \text{.........} (n \geqq m > 0) \quad \text{...(10.38)}$$

Now that we have obtained $w_\kappa(n, m)$ and $w_{-\kappa}(n, m)$ $(m > 0)$, we must proceed to the calculation of $w_\kappa(n, -m)$ and $w_{-\kappa}(n, -m)$.

By the operation W, the surface harmonics of order n are transformed into

$$\overline{P}{}_n^m(\cos\theta^*)\exp(im\varphi^*) = \sum_\kappa w_\kappa(n, m)\, \overline{P}{}_n^\kappa(\cos\theta)\exp(i\kappa\varphi)$$

Therefore

$$\overline{P}{}_n^{-m}(\cos\theta^*)\exp(-im\varphi^*) = (-)^m\, \frac{(n-m)\,!}{(n+m)\,!} \cdot \overline{P}{}_n^m(\cos\theta^*)\exp(-im\varphi^*)$$

$$= (-)^m\, \frac{(n-m)\,!}{(n+m)\,!} \{\text{Conjugate complex of } \sum w_\kappa(n, m)\overline{P}{}_n^\kappa(\cos\theta)\exp[i\kappa\varphi]\}$$

Substituting (10.37)

$$\overline{P}{}_n^{-m}(\cos\theta^*)\exp(-im\varphi^*)$$

$$= (-)^m\, \frac{(n-m)\,!}{(n+m)\,!} \sum (-)^\kappa w_\kappa(n, m)\overline{P}{}_n^\kappa(\cos\theta) \cdot \exp[-i\kappa\varphi]$$

$$= (-)^m\, \frac{(n-m)\,!}{(n+m)\,!} \sum w_{-\kappa}(n, m) \cdot \frac{(n-\kappa)\,!}{(n+\kappa)\,!}\, \overline{P}{}_n^\kappa(\cos\theta)\exp[i\kappa\varphi] \text{...(10.39)}$$

On the other hand, the left side member will be transformed, as is clear from the above expression, into

$$\sum_\kappa w_\kappa(n, -m)\, \overline{P}{}_n^\kappa(\cos\theta)\exp[i\kappa\varphi]$$

Comparing the two expressions just obtained, we have a formula showing the relation between $w_\kappa(n, -m)$ and $w_{-\kappa}(n, m)$

$$w_\kappa(n, -m) = (-)^m\, \frac{(n-m)\,!}{(n+m)\,!}\, \frac{(n-\kappa)\,!}{(n+\kappa)\,!}\, w_{-\kappa}(n, m)$$

in which κ may take any value of integer. However the following type of expression is convenient;

$$\text{when} \quad \kappa \geq 0\,, \quad w_\kappa(n, -m) = (-)^{n+\kappa} \frac{(n-m)\,!}{(n+m)\,!} w_\kappa(n, m), \; (m>0,\ \kappa \geq 0) \quad (10.40)$$

when $\kappa < 0$, putting $\kappa \rightarrow -\kappa$

$$w_{-\kappa}(n, -m) = (-)^m \frac{(n-m)\,!}{(n+m)\,!} \frac{(n+\kappa)\,!}{(n-\kappa)\,!} w_\kappa(n, m)\,, \; (m>0\,,\ \kappa>0) \quad (10.41)$$

10.31 When *m* is zero.

Formulae of $w_\kappa\,(n, m)$ obtained in the previous article do not hold when m is zero, for when we obtained (10.15) in § 10.12 we assumed m to be positive. To get rid of this restriction we will go back and repeat the transformation of $P_n\,(\cos\theta^*)$ separately.

By the operation W zonal harmonics is transformed as follows;

$$Y_n(\theta^*, \varphi^*) = P_n(\cos\theta^*) = P_n(\sin\theta\sin\varphi) \quad \ldots\ldots\ldots\ldots\ldots(10.42)$$

On the other hand from the addition theorem

$$P_n(\cos\gamma) = P_n(\cos\theta)\, P_n(\cos\chi) + 2\sum_{\nu=1}^{n} \frac{(n-\nu)\,!}{(n+\nu)\,!} \overline{P}{}_n^\nu(\cos\theta) \cdot \overline{P}{}_n^\nu(\cos\chi) \cos\nu\omega$$

$$\text{where} \quad \cos\gamma = \cos\theta\cos\chi + \sin\theta\sin\chi\cos\omega\,.$$

Putting $\chi = -\pi/2$ and $\omega = \varphi + \pi/2$ we have

$$P_n(\sin\theta\sin\varphi) = P_n(\cos\theta)\, P_n(0) + 2\sum_{p=0}^{\langle n-1\rangle} \frac{(2p)\,!}{(2n-2p)\,!} \overline{P}{}_n^{n-2p}(\cos\theta)$$

$$\cdot\, (-)^n P_n^{(n-2p)}(0) \cos\left[(n-2p)\left(\varphi + \frac{\pi}{2}\right)\right]$$

$$= \sum_{p=0}^{n} \overline{P}{}_n^{n-2p}(\cos\theta) \cdot i^{-n} \frac{(2p)\,!}{2^n p\,!\,(n-p)\,!} \exp\{i\,(n-2p)\,\varphi\}$$

Changing the suffix from p to κ defined by $n-2p=\kappa$

$$P_n(\sin\theta\sin\varphi) = \sum_{\kappa=-n}^{n} w_\kappa(n, 0)\, \overline{P}{}_n^\kappa\,(\cos\theta) \exp[i\kappa\varphi]$$

$$\text{where} \quad w_\kappa\,(n, 0) = e\,(n+\kappa)\, i^{-n}[(n-\kappa)\,!/\{2^n\,(\tfrac{1}{2}n - \tfrac{1}{2}\kappa)\,!\,(\tfrac{1}{2}n + \tfrac{1}{2}\kappa)\,!\}] \quad (10.43)$$

The results of the calculation are included in Tab. 1.

Although, in the above formula, κ may take any integral value, the next expression is more convenient when the suffix is negative.

$$w_{-\kappa}\,(n, 0) = \frac{(n+\kappa)\,!}{(n-\kappa)\,!} w_\kappa\,(n, 0) \ldots\ldots\ldots\ldots\ldots\ldots\ldots\ldots\ldots\ldots(10.44)$$

11. Operation W'.

We have studied the operation W, and in this article we will take up the other operation W', which is, as is easily shown, an inverse operation of W. In the present operation we have

$$\begin{cases} x^\dagger = y = R \sin\theta \sin\varphi \\ y^\dagger = z = R\cos\theta \\ z^\dagger = x = R\sin\theta\cos\varphi \end{cases} \qquad \dots\dots\dots\dots(11.1)$$

From the formulae (10.2) and (11.1) we have

$$\begin{aligned} Y_n(\theta^\dagger, \varphi^\dagger) &= (x^\dagger + iy^\dagger)^m R^{-m} P_n^{(m)}(z^\dagger/R) \\ &= (\sin\theta\sin\varphi + i\cos\theta)^m P_n^{(m)}(\sin\theta\cos\varphi) \quad \dots\dots\dots(11.2) \end{aligned}$$

On the other hand we have obtained in (10.3) and (10.27)

$$(\cos\theta + i\sin\theta\cos\varphi)^m P_n^{(m)}(\sin\theta\sin\varphi) = \sum_{\kappa=-n}^{n} w_\kappa(n,m)\, \overline{P}_n^\kappa(\cos\theta)\exp[i\kappa\varphi] \quad (11.3)$$

Here, put $\varphi \rightarrow \varphi + \pi/2$ into (11.3), then we have

$$\begin{aligned} &(\sin\theta\sin\varphi + i\cos\theta)^m P_n^{(m)}(\sin\theta\cos\varphi) \\ &\qquad = \sum_\kappa i^{m+\kappa} w_\kappa(n,m)\, \overline{P}_n^\kappa(\cos\theta)\exp[i\kappa\varphi] \quad \dots\dots\dots(11.4) \end{aligned}$$

Comparing this with (9.3), we have the relation connecting $w_\kappa'(n,m)$ and $w_\kappa(n,m)$

$$w'_\kappa(n,m) = i^{m+\kappa} w_\kappa(n,m) \quad \dots\dots\dots\dots(11.5)$$

where κ may take any integral value.

11.1 Formulae expressing $w_\kappa'(n,m)$ when κ is negative.

Just as in § 10.3 we prepared formulae for $w_\kappa(n,m)$ when κ takes negative value, we will discuss in this article the value of $w'_{-\kappa}(n,m)$

From (11.5) and (10.38) we can immediately get the following formula.

$$\begin{aligned} w'_{-\kappa}(n,m) &= i^{m-\kappa} w_{-\kappa}(n,m) \\ &= i^{2n-m+\kappa} \frac{(n+\kappa)!}{(n-\kappa)!} w_\kappa(n,m) \quad \dots\dots\dots(11.6) \end{aligned}$$

12. Modification of the transformation formula.

Formally we have already obtained a transformation formula in (9.8), that is;

$$Y_n(\theta_0, \varphi_0) = \bar{P}_n^m(\cos\theta_0)\exp[im\varphi_0] = \exp(im\phi)$$

$$\cdot\sum_{\gamma=-n}^{n}\bar{P}_n^\gamma(\cos\theta)\cdot\exp\{i\gamma(\varphi+\psi)\}\sum_{\kappa=-n}^{n}\exp(i\kappa\chi)\,w'_\kappa(n,m)\,w_\gamma(n,\kappa)\ldots(12.1)$$

However, κ and γ involved in this expression is not always positive; so that it is desirable for us to modify this formula so that all the suffixes involved may become non-negative. From (12.1) we have

$$Y_n(\theta_0, \varphi_0) = \exp(im\phi)\Bigg[\sum_{\gamma=1}^{n}(-)^\gamma\frac{(n-\gamma)!}{(n+\gamma)!}\bar{P}_n^\gamma(\cos\theta)\cdot\exp\{-i\gamma(\varphi+\psi)\}$$

$$\cdot\Bigg\{\sum_{\kappa=1}^{n}\exp(-i\kappa\chi)\,w'_{-\kappa}(n,m)\,w_{-\gamma}(n,-\kappa)+w'_0(n,m)\,w_{-\gamma}(n,0)$$

$$+\sum_{\kappa=1}^{n}\exp(i\kappa\chi)\,w'_\kappa(n,m)\,w_{-\gamma}(n,\kappa)\Bigg\}$$

$$+P_n(\cos\theta)\Bigg\{\sum_{\kappa=1}^{n}\exp(-i\kappa\chi)\,w'_{-\kappa}(n,m)\,w_0(n,-\kappa)+w'_0(n,m)\,w_0(n,0)$$

$$+\sum_{\kappa}\exp(i\kappa\chi)\,w'_\kappa(n,m)\,w_0(n,\kappa)\Bigg\}$$

$$+\sum_{\gamma=1}^{n}\bar{P}_n^\gamma(\cos\theta)\exp\{i\gamma(\varphi+\psi)\}$$

$$\cdot\Bigg\{\sum_{\kappa}\exp(-i\kappa\chi)\,w'_{-\kappa}(n,m)\,w_\gamma(n,-\kappa)+w'_0(n,m)\,w_\gamma(n,0)$$

$$+\sum_{\kappa}\exp(i\kappa\chi)\,w'_\kappa(n,m)\,w_\gamma(n,\kappa)\Bigg\}\Bigg]\quad\ldots\ldots\ldots\ldots\ldots\ldots\ldots\ldots(12.2)$$

or using new notations

$$Y_n(\theta_0, \varphi_0) = \exp\left\{im\left(\phi+\frac{\pi}{2}\right)\right\}$$

$$\cdot\Bigg[\sum_{\gamma=1}^{n}\bar{P}_n^\gamma(\cos\theta)\exp\left\{-i\gamma\left(\varphi+\psi+\frac{\pi}{2}\right)\right\}$$

$$\cdot\left\{\sum_{\kappa=1}^{n}\exp(-i\kappa\chi)\cdot[--]+[0-]+\sum_{\kappa=1}^{n}\exp(i\kappa\chi)\cdot[+-]\right\}$$

$$+P_n(\cos\theta)\cdot\left\{\sum_{\kappa}\exp(-i\kappa\chi)\cdot[-0]+[00]+\sum_{\kappa}\exp(i\kappa\chi)\cdot[+0]\right\}$$

$$+\sum_{\gamma=1}^{n}\bar{P}_n^\gamma(\cos\theta)\exp\left\{i\gamma\left(\varphi+\psi+\frac{\pi}{2}\right)\right\}$$

$$\cdot\left\{\sum_{\kappa}\exp(-i\kappa\chi)\cdot[-+]+[0+]+\sum_{\kappa}\exp(i\kappa\chi)\cdot[++]\right\}\Bigg]\ldots\ldots(12.3)$$

in which

$$\left\{\begin{aligned}
[--]&=i^{-m+\gamma}\cdot(-)^{\gamma}\frac{(n-\gamma)!}{(n+\gamma)!}w'_{-\kappa}(n,m)\,w_{-\gamma}(n,-\kappa)\\
&\qquad\qquad=(-)^{n+m+\kappa+\gamma}\cdot C_{\kappa\gamma}(n,m)\\
[0-\ ]&=i^{-m+\gamma}\cdot(-)^{\gamma}\frac{(n-\gamma)!}{(n+\gamma)!}w'_{0}(n,m)\,w_{-\gamma}(n,0)=(-)^{\gamma}\cdot C_{0\gamma}(n,m)\\
[+-]&=i^{-m+\gamma}\cdot(-)^{\gamma}\frac{(n-\gamma)!}{(n+\gamma)!}w'_{\kappa}(n,m)\,w_{-\gamma}(n,\kappa)=(-)^{n+\kappa}\cdot C_{\kappa\gamma}(n,m)\\
[-0]&=i^{-m}\cdot\quad w'_{-\kappa}(n,m)\,w_{0}(n,-\kappa)=(-)^{m}\cdot C_{\kappa 0}(n,m)\\
[\ 00\ ]&=i^{-m}\cdot\quad w'_{0}(n,m)\,w_{0}(n,0)=\cdot C_{00}(n,m)\\
[+0]&=i^{-m}\cdot\quad w'_{\kappa}(n,m)\,w_{0}(n,\kappa)=\cdot C_{\kappa 0}(n,m)\\
[-+]&=i^{-m-\gamma}\cdot\quad w'_{-\kappa}(n,m)\,w_{\gamma}(n,-\kappa)=(-)^{m}\cdot C_{\kappa\gamma}(n,m)\\
[0+\ ]&=i^{-m-\gamma}\cdot\quad w'_{0}(n,m)\,w_{\gamma}(n,0)=(-)^{\gamma}\cdot C_{0\gamma}(n,m)\\
[++]&=i^{-m-\gamma}\cdot\quad w'_{\kappa}(n,m)\,w_{\gamma}(n,\kappa)=(-)^{\gamma}\cdot C_{\kappa\gamma}(n,m)
\end{aligned}\right. \qquad \ldots\ldots\ldots\ldots(12.4)$$

$$\text{where}\quad C_{\kappa\gamma}(n,m)=i^{\kappa+\gamma}\,w_{\kappa}(n,m)\,w_{\gamma}(n,\kappa)\quad\ldots\ldots\ldots\ldots(12.5)$$

Before proceeding further, we will prove that all [ ] are real quantities. For, judging from the expressions (10.36) or (10.37), we notice that $w_\kappa(n,m)$ when multiplied by i^κ, take real values. Introducing this relation into (12.4) we find easily that all [ ] take real value (including the case $m=0$; cf. (10.43)).

Using these functions, (12.3) can be transformed as follows:

$$\begin{aligned}
Y_n(\theta_0,\varphi_0)=\exp&\left\{im\left(\phi+\frac{\pi}{2}\right)\right\}\Bigg[\sum_{\gamma=1}^{n}\bar{P}_n^{\gamma}(\cos\theta)\Bigg(\cos\gamma\left(\varphi+\psi+\frac{\pi}{2}\right)\\
&\cdot\left\{\sum_{\kappa=1}^{n}\cos\kappa\chi\cdot(++++)+(0++)+i\sum_{\kappa=1}^{n}\sin\kappa\chi\cdot(--++)\right\}\\
&+\sin\gamma\left(\varphi+\psi+\frac{\pi}{2}\right)\\
&\cdot\left\{\sum_{\kappa}\cos\kappa\chi\cdot(-+-+)+(0-+)+i\sum_{\kappa}\sin\kappa\chi\cdot(+--+)\right\}\Bigg)\\
&+P_n(\cos\theta)\\
&\cdot\left\{\sum_{\kappa}\cos\kappa\chi\cdot(++0)+[0\,0]+i\sum_{\kappa}\sin\kappa\chi\cdot(-+0)\right\}\Bigg]\quad\ldots\ldots\ldots\ldots(12.6)
\end{aligned}$$

in which

$$\left\{\begin{aligned}
(++++)&\equiv\ [--]+[-+]+[+-]+[++]\\
(--++)&\equiv-[--]-[-+]+[+-]+[++]
\end{aligned}\right.$$

$$\left\{\begin{array}{lcl}(-+-+) & \equiv & -[--]+[-+]-[+-]+[++]\\ (+--+) & \equiv & \ \ [--]-[-+]-[+-]+[++]\\ (0++) & \equiv & \ \ [0-]+[0+]\\ (0-+) & \equiv & -[0-]+[0+]\\ (++0) & \equiv & \ \ [-0]+[+0]\\ (-+0) & \equiv & -[-0]+[+0]\end{array}\right. \qquad\ldots\ldots(12.7)$$

Putting the relation (12.4) into (12.7) and using the function $e(\ \ )$ previously difined by (10.24),

$$\left\{\begin{array}{l}(++++)=4\,e(m+\gamma)\quad e(n+\kappa+\gamma)\quad(-)^{m}\ C_{\kappa\gamma}(n,m)\\ (--++)=4\,e(m+\gamma+1)\,e(n+\kappa+\gamma)\quad(-)^{m+1}C_{\kappa\gamma}(n,m)\\ (-+-+)=4\,e(m+\gamma)\quad e(n+\kappa+\gamma+1)\,(-)^{m}\ C_{\kappa\gamma}(n,m)\\ (+--+)=4\,e(m+\gamma+1)\,e(n+\kappa+\gamma+1)\,(-)^{m+1}C_{\kappa\gamma}(n,m)\end{array}\right. \qquad\ldots\ldots(12.8)$$

Similarly we have

$$\left\{\begin{array}{l}(0++)=2\,(-)^{\gamma}\quad C_{0\gamma}(n,m)\\ (0-+)=0\\ (++0)=2e(m)\quad C_{\kappa 0}(n,m)\\ (-+0)=2e(m+1)\,C_{\kappa 0}(n,m)\end{array}\right. \qquad\ldots\ldots(12.9)$$

To obtain formulae conveniently applicable for our practical purpose, we must calculate the expressions shown in (12.8) and (12.9) numerically.

13. Separation of real and imaginary parts.

We have been treating $\overline{P}_n^m(\cos\theta)\exp(im\varphi)$ in the previous articles. Now, however, we will separate the real and the imaginary parts as we have written in § 8.

From (12.6) we have

$$\left\{\begin{array}{l}\overline{P}_n^m(\cos\theta_0)\cos m\varphi_0=\cos m\left(\phi+\dfrac{\pi}{2}\right)\mathfrak{A}_n^m-\sin m\left(\phi+\dfrac{\pi}{2}\right)\mathfrak{B}_n^m\\ \overline{P}_n^m(\cos\theta_0)\sin m\varphi_0=\cos m\left(\phi+\dfrac{\pi}{2}\right)\mathfrak{B}_n^m+\sin m\left(\phi+\dfrac{\pi}{2}\right)\mathfrak{A}_n^m\end{array}\right. \qquad\ldots(13.1)$$

in which $\mathfrak{A}_n^m$ and $\mathfrak{B}_n^m$ are, using (12.8) and (12.9)

$$\left\{\begin{aligned}
\mathfrak{A}_n^m = & \sum_{\gamma=1}^{n} \bar{P}_n^\gamma(\cos\theta) \\
& \cdot\Big[\cos\gamma\Big(\varphi+\psi+\frac{\pi}{2}\Big)\Big\{\sum_{\kappa=1}^{n}\cos\kappa\chi\cdot 4e(m+\gamma)\,e(n+\kappa+\gamma) \\
& \qquad\qquad \cdot(-)^m C_{\kappa\gamma}(n,m) \\
& \qquad\qquad +2(-)^\gamma C_{0\gamma}(n,m)\Big\} \\
& \quad -\sin\gamma\Big(\varphi+\psi+\frac{\pi}{2}\Big)\Big\{\sum_{\kappa}\sin\kappa\chi\cdot 4e(m+\gamma+1)\,e(n+\kappa+\gamma+1) \\
& \qquad\qquad \cdot(-)^m C_{\kappa\gamma}(n,m)\Big\}\Big] \\
& \quad +P_n(\cos\theta)\ \Big\{\sum_{\kappa}\cos\kappa\chi\cdot 2e(m)\,C_{\kappa 0}(n,m)+C_{00}(n,m)\Big\} \\
\mathfrak{B}_n^m = & \sum_{\gamma=1}^{n} \bar{P}_n^\gamma(\cos\theta) \qquad \qquad \qquad \qquad \ldots\ldots\ldots(13.2) \\
& \cdot\Big[\sin\gamma\Big(\varphi+\psi+\frac{\pi}{2}\Big)\Big\{\sum_{\kappa}\cos\kappa\chi\cdot 4e(m+\gamma)\,e(n+\kappa+\gamma+1) \\
& \qquad\qquad \cdot(-)^m C_{\kappa\gamma}(n,m)\Big\} \\
& \quad +\cos\gamma\Big(\varphi+\psi+\frac{\pi}{2}\Big)\Big\{\sum_{\kappa}\sin\kappa\chi\cdot 4e(m+\gamma+1)\,e(n+\kappa+\gamma) \\
& \qquad\qquad \cdot(-)^{m+1} C_{\kappa\gamma}(n,m)\Big)\Big\}\Big] \\
& \quad +P_n(\cos\theta)\ \Big\{\sum_{\kappa}\sin\kappa\chi\cdot 2e(m+1)\,C_{\kappa 0}(n,m)\Big\}
\end{aligned}\right.$$

Now we will adopt a new notation $\varepsilon_{\kappa\gamma}$ defined by

$$\varepsilon_{\kappa\gamma}=\begin{cases} 4\cdots\cdots\kappa\neq 0\,,\ \gamma\neq 0 \\ 2\cdots\cdots\kappa=0\,,\ \gamma\neq 0\,,\ \text{or}\ \kappa\neq 0\,,\ \gamma=0\,. \\ 1\cdots\cdots\kappa=\gamma=0 \end{cases} \qquad \ldots\ldots\ldots\ldots\ldots\ldots(13.3)$$

and simplify the above formulae.

After giving a little consideration to the property of $C_{\kappa\gamma}(n,m)$ or $w_\kappa(n,m)$, we can write the above expression of $\mathfrak{A}_n^m$ as follows

$$\begin{aligned}
\mathfrak{A}_n^m = & (-)^m \sum_{\gamma=0}^{n}\bar{P}_n^\gamma(\cos\theta) \\
& \cdot\Big[e(m+\gamma)\cos\gamma\Big(\varphi+\psi+\frac{\pi}{2}\Big)\Big\{\sum_{\kappa=0}^{n} e(n+m+\kappa)\cdot\varepsilon_{\kappa\gamma}\,C_{\kappa\gamma}(n,m)\cdot\cos\kappa\chi\Big\} \\
& +e(m+\gamma+1)\sin\gamma\Big(\varphi+\psi+\frac{\pi}{2}\Big)\Big\{\sum_{\kappa=1}^{n} e(n+m+\kappa)\cdot\varepsilon_{\kappa\gamma}\,C_{\kappa\gamma}(n,m)\cdot\sin\kappa\chi\Big\}\Big]
\end{aligned}$$

$$\ldots\ldots\ldots(13.4)$$

Similarly

$$\mathfrak{B}_n^m=(-)^m\sum_{\gamma=0}^{n}\overline{P}_n^{\gamma}(\cos\theta)$$
$$\cdot\Big[e(m+\gamma)\sin\gamma\Big(\varphi+\psi+\frac{\pi}{2}\Big)\Big\{\sum_{\kappa=1}^{n}e(n+m+\kappa+1)\cdot\varepsilon_{\kappa\gamma}C_{\kappa\gamma}(n,m)\cdot\cos\kappa\chi\Big\}$$
$$-e(m+\gamma+1)\cos\gamma\Big(\varphi+\psi+\frac{\pi}{2}\Big)\Big\{\sum_{\kappa=1}^{n}e(n+m+\kappa+1)\cdot\varepsilon_{\kappa\gamma}C_{\kappa\gamma}(n,m)\cdot\sin\kappa\chi\Big\}\Big] \qquad \text{.........(13.5)}$$

Further, if we treat separately the case when m is even and when m is odd, we can write the above two expressions still more simply.

i) When m is even;

$$\left\{\begin{aligned}\mathfrak{A}_n^m=&\sum_{\gamma=0}^{n}\overline{P}_n^{\gamma}(\cos\theta)\cos\gamma(\varphi+\psi)\\&\cdot\Big[e(\gamma)(-)^{\gamma/2}\Big\{\sum_{\kappa=0}^{n}e(n+\kappa)\cdot\varepsilon_{\kappa\gamma}C_{\kappa\gamma}(n,m)\cdot\cos\kappa\chi\Big\}\\&+e(\gamma+1)(-)^{(\gamma-1)/2}\Big\{\sum_{\kappa=1}^{n}e(n+\kappa)\cdot\varepsilon_{\kappa\gamma}C_{\kappa\gamma}(n,m)\cdot\sin\kappa\chi\Big\}\Big]\\\mathfrak{B}_n^m=&\sum_{\gamma=1}^{n}\overline{P}_n^{\gamma}(\cos\theta)\sin\gamma(\varphi+\psi)\\&\cdot\Big[e(\gamma)(-)^{\gamma/2}\Big\{\sum_{\kappa=1}^{n}e(n+\kappa+1)\cdot\varepsilon_{\kappa\gamma}C_{\kappa\gamma}(n,m)\cdot\cos\kappa\chi\Big\}\\&+e(\gamma+1)(-)^{(\gamma-1)/2}\Big\{\sum_{\kappa=1}^{n}e(n+\kappa+1)\cdot\varepsilon_{\kappa\gamma}C_{\kappa\gamma}(n,m)\cdot\sin\kappa\chi\Big\}\Big]\end{aligned}\right. \qquad \text{......(13.6)}$$

ii) When m is odd;

$$\left\{\begin{aligned}\mathfrak{A}_n^m=&\sum_{\gamma=1}^{n}\overline{P}_n^{\gamma}(\cos\theta)\sin\gamma(\varphi+\psi)\\&\cdot\Big[e(\gamma+1)(-)^{(\gamma-1)/2}\Big\{\sum_{\kappa=0}^{n}e(n+\kappa+1)\cdot\varepsilon_{\kappa\gamma}C_{\kappa\gamma}(n,m)\cdot\cos\kappa\chi\Big\}\\&+e(\gamma)(-)^{\gamma/2+1}\Big\{\sum_{\kappa=1}^{n}e(n+\kappa+1)\cdot\varepsilon_{\kappa\gamma}C_{\kappa\gamma}(n,m)\cdot\sin\kappa\chi\Big\}\Big]\\\mathfrak{B}_n^m=&\sum_{\gamma=0}^{n}\overline{P}_n^{\gamma}(\cos\theta)\cos\gamma(\varphi+\psi)\\&\cdot\Big[e(\gamma+1)(-)^{(\gamma+1)/2}\Big\{\sum_{\kappa=1}^{n}e(n+\kappa)\cdot\varepsilon_{\kappa\gamma}C_{\kappa\gamma}(n,m)\cdot\cos\kappa\chi\Big\}\\&+e(\gamma)(-)^{\gamma/2}\Big\{\sum_{\kappa=1}^{n}e(n+\kappa)\cdot\varepsilon_{\kappa\gamma}C_{\kappa\gamma}(n,m)\cdot\sin\kappa\chi\Big\}\Big]\end{aligned}\right. \qquad \text{......(13.7)}$$

14. Numerical expressions.

In the previous articles we have obtained the expressions of $\mathfrak{A}_n^m$ and $\mathfrak{B}_n^m$. However they are not sufficient for practical purposes since the numerical values of coefficients are not yet given explicitly. In this article, we will give these values.

First we will recall the important expression (13.1), which takes different form according as m is even or odd.

i) When m is even;

$$\left\{\begin{aligned}\overline{P}_n^m(\cos\theta_0)\cos m\varphi_0&=(-)^{m/2}[\cos m\phi\cdot\mathfrak{A}_n^m-\sin m\phi\cdot\mathfrak{B}_n^m]\\ \overline{P}_n^m(\cos\theta_0)\sin m\varphi_0&=(-)^{m/2}[\cos m\phi\cdot\mathfrak{B}_n^m+\sin m\phi\cdot\mathfrak{A}_n^m]\end{aligned}\right. \quad\ldots\ldots\ldots(14.1)$$

ii) When m is odd.

$$\left\{\begin{aligned}\overline{P}_n^m(\cos\theta_0)\cos m\varphi_0&=(-)^{(m+1)/2}[\sin m\phi\cdot\mathfrak{A}_n^m+\cos m\phi\cdot\mathfrak{B}_n^m]\\ \overline{P}_n^m(\cos\theta_0)\sin m\varphi_0&=(-)^{(m+1)/2}[\sin m\phi\cdot\mathfrak{B}_n^m-\cos m\phi\cdot\mathfrak{A}_n^m]\end{aligned}\right. \quad\ldots\ldots(14.2)$$

Next, we will practically write down the expressions of $\mathfrak{A}_n^m$ and $\mathfrak{B}_n^m$ in the following part.

(In the following expressions, $P_n\equiv P_n(\cos\theta)$, $P_n^\gamma\equiv\overline{P}_n^\gamma(\cos\theta)$, $\cos\gamma(\ \ )\equiv\cos\gamma(\varphi+\psi)$ and $\sin\gamma(\ \ )\equiv\sin\gamma(\varphi+\psi)$.

When the coefficients are needed in fractional form, one may calculate $\varepsilon_{\kappa\gamma}\,C_{\kappa\gamma}(n,m)$ from Tab. 1.))

$$\begin{array}{ll}
\mathfrak{A}_1^0=P_1\qquad\cdot\cos\chi\ , & \mathfrak{B}_1^0=0\\
\quad+P_1^1\cos(\ \ )\cdot(-\sin\chi) & \\
\mathfrak{A}_1^1=\qquad\qquad , & \mathfrak{B}_1^1=P_1\qquad\cdot(-\sin\chi)\\
\quad P_1^1\sin(\ \ ) & \quad+P_1^1\cos(\ \ )\cdot(-\cos\chi)\\
\mathfrak{A}_2^0=P_2\qquad\cdot(0{\cdot}25+0{\cdot}75\cos 2\chi)\, , & \mathfrak{B}_2^0=0\\
\quad+P_2^1\cos(\ \ )\cdot(\quad-0{\cdot}5\sin 2\chi) & \\
\quad+P_2^2\cos 2(\ \ )\cdot(0{\cdot}125-0{\cdot}125\cos 2\chi) & \\
\mathfrak{A}_2^1=\qquad\qquad , & \mathfrak{B}_2^1=P_2\qquad(-1{\cdot}5\sin 2\chi)\\
\quad P_2^1\sin(\ \ )\cdot\cos\chi & \quad+P_2^1\cos(\ \ )\cdot(-\cos 2\chi)\\
\quad+P_2^2\sin 2(\ \ )\cdot(-0{\cdot}5\sin\chi) & \quad+P_2^2\cos 2(\ \ )\cdot(+0{\cdot}25\sin 2\chi)\\
\mathfrak{A}_2^2=P_2\qquad\cdot(-1{\cdot}5+1{\cdot}5\cos 2\chi)\, , & \mathfrak{B}_2^2=\\
\quad+P_2^1\cos(\ \ )\cdot(\quad-\sin 2\chi) & \quad P_2^1\sin(\ \ )\cdot(-2\sin\chi)\\
\quad+P_2^2\cos 2(\ \ )\cdot(-0{\cdot}75-0{\cdot}25\cos 2\chi) & \quad+P_2^2\sin 2(\ \ )\cdot(-\cos\chi)
\end{array}$$

$$\begin{aligned}
\mathfrak{A}_3^0 &= P_3 && \cdot(+0.375\cos\chi + 0.625\cos 3\chi) \qquad \mathfrak{B}_3^0 = 0\\
&+ P_3^1 \cos\ (\quad) && \cdot(-0.0625\sin\chi - 0.3125\sin 3\chi)\\
&+ P_3^2 \cos 2(\quad) && \cdot(+0.0625\cos\chi - 0.0625\cos 3\chi)\\
&+ P_3^3 \cos 3(\quad) && \cdot(-0.03125\sin\chi + 0.01041667\sin 3\chi)
\end{aligned}$$

$$\begin{aligned}
\mathfrak{A}_3^1 &= &&\\
&P_3^1 \sin\ (\quad) && \cdot(+0.375 + 0.625\cos 2\chi)\\
&+ P_3^2 \sin 2(\quad) && \cdot(\qquad -0.25\sin 2\chi)\\
&+ P_3^3 \sin 3(\quad) && \cdot(+0.0625 - 0.0625\cos 2\chi)
\end{aligned}$$

$$\begin{aligned}
\mathfrak{B}_3^1 &= P_3 && (-0.375\sin\chi - 1.875\sin 3\chi)\\
&+ P_3^1 \cos\ (\quad) && \cdot(-0.0625\cos\chi - 0.9375\cos 3\chi)\\
&+ P_3^2 \cos 2(\quad) && \cdot(-0.0625\sin\chi + 0.1875\sin 3\chi)\\
&+ P_3^3 \cos 3(\quad) && \cdot(-0.03125\cos\chi + 0.03125\cos 3\chi)
\end{aligned}$$

$$\begin{aligned}
\mathfrak{A}_3^2 &= P_3 && (-3.75\cos\chi + 3.75\cos 3\chi),\\
&+ P_3^1 \cos\ (\quad) && \cdot(+0.625\sin\chi - 1.875\sin 3\chi)\\
&+ P_3^2 \cos 2(\quad) && \cdot(-0.625\cos\chi - 0.375\cos 3\chi)\\
&+ P_3^3 \cos 3(\quad) && \cdot(+0.3125\sin\chi + 0.0625\sin 3\chi)
\end{aligned}$$

$$\begin{aligned}
\mathfrak{B}_3^2 &= &&\\
&P_3^1 \sin\ (\quad) && \cdot(-2.5\sin 2\chi)\\
&+ P_3^2 \sin 2(\quad) && \cdot(-\qquad \cos 2\chi)\\
&+ P_3^3 \sin 3(\quad) && \cdot(+0.25\sin 2\chi)
\end{aligned}$$

$$\begin{aligned}
\mathfrak{A}_3^3 &= &&\\
&P_3^1 \sin\ (\quad) && \cdot(-3.75 + 3.75\cos 2\chi)\\
&+ P_3^2 \sin 2(\quad) && \cdot(\qquad -1.5\sin 2\chi)\\
&+ P_3^3 \sin 3(\quad) && \cdot(-0.625 - 0.375\cos 2\chi)
\end{aligned}$$

$$\begin{aligned}
\mathfrak{B}_3^3 &= P_3 && (+11.25\sin\chi - 3.75\sin 3\chi)\\
&+ P_3^1 \cos\ (\quad) && \cdot(+1.875\cos\chi - 1.875\cos 3\chi)\\
&+ P_3^2 \cos 2(\quad) && \cdot(+1.875\sin\chi + 0.375\sin 3\chi)\\
&+ P_3^3 \cos 3(\quad) && \cdot(+0.9375\cos\chi + 0.0625\cos 3\chi)
\end{aligned}$$

$$\begin{aligned}
\mathfrak{A}_4^0 &= P_4 && (+0.140625 + 0.3125\cos 2\chi + 0.546875\cos 4\chi)\\
&+ P_4^1 \cos\ (\quad) && \cdot(\qquad -0.0625\sin 2\chi - 0.21875\sin 4\chi)\\
&+ P_4^2 \cos 2(\quad) && \cdot(+0.015625 + 0.0208333\cos 2\chi - 0.03645833\cos 4\chi)\\
&+ P_4^3 \cos 3(\quad) && \cdot(\qquad -0.01041667\sin 2\chi + 0.00520833\sin 4\chi)\\
&+ P_4^4 \cos 4(\quad) && \cdot(+0.001953125 - 0.0026041667\cos 2\chi + 0.0006510417\cos 4\chi)
\end{aligned}$$

$$\mathfrak{B}_4^0 = 0$$

$$\begin{aligned}
\mathfrak{A}_4^1=P_4^1\sin\;(\quad)&\cdot(+0{\cdot}5625\cos\chi+0{\cdot}4375\cos3\chi)\\
+P_4^2\sin2\,(\quad)&\cdot(-0{\cdot}0625\sin\chi-0{\cdot}1458333\sin3\chi)\\
+P_4^3\sin3\,(\quad)&\cdot(+0{\cdot}03125\cos\chi-0{\cdot}03125\cos3\chi)\\
+P_4^4\sin4\,(\quad)&\cdot(-0{\cdot}015625\sin\chi+0{\cdot}005208333\sin3\chi)
\end{aligned}$$

$$\begin{aligned}
\mathfrak{B}_4^1=P_4\qquad\quad\;&\;\;(-0{\cdot}625\sin2\chi-2{\cdot}1875\sin4\chi)\\
+P_4^1\cos\;(\quad)&\cdot(-0{\cdot}125\cos2\chi-0{\cdot}875\cos4\chi)\\
+P_4^2\cos2\,(\quad)&\cdot(-0{\cdot}0416667\sin2\chi+0{\cdot}1458333\sin4\chi)\\
+P_4^3\cos3\,(\quad)&\cdot(-0{\cdot}02083333\cos2\chi+0{\cdot}02083333\cos4\chi)\\
+P_4^4\cos4\,(\quad)&\cdot(+0{\cdot}005208333\sin2\chi-0{\cdot}002604167\sin4\chi)
\end{aligned}$$

$$\begin{aligned}
\mathfrak{A}_4^2=P_4\qquad\quad\;&\;\;(-2{\cdot}8125-3{\cdot}75\cos2\chi+6{\cdot}5625\cos4\chi)\\
+P_4^1\cos\;(\quad)&\cdot(\qquad\qquad+0{\cdot}75\sin2\chi-2{\cdot}625\sin4\chi)\\
+P_4^2\cos2\,(\quad)&\cdot(-0{\cdot}3125-0{\cdot}25\cos2\chi-0{\cdot}4375\cos4\chi)\\
+P_4^3\cos3\,(\quad)&\cdot(\qquad\qquad+0{\cdot}125\sin2\chi+0{\cdot}0625\sin4\chi)\\
+P_4^4\cos4\,(\quad)&\cdot(-0{\cdot}0390625+0{\cdot}03125\cos2\chi+0{\cdot}0078125\cos4\chi)
\end{aligned}$$

$$\begin{aligned}
\mathfrak{B}_4^2=P_4^1\sin\;(\quad)&\cdot(-1{\cdot}125\sin\chi-2{\cdot}625\sin3\chi)\\
+P_4^2\sin2\,(\quad)&\cdot(-0{\cdot}125\cos\chi-0{\cdot}875\cos3\chi)\\
+P_4^3\sin3\,(\quad)&\cdot(-0{\cdot}0625\sin\chi+0{\cdot}1875\sin3\chi)\\
+P_4^4\sin4\,(\quad)&\cdot(-0{\cdot}03125\cos\chi+0{\cdot}03125\cos3\chi)
\end{aligned}$$

$$\begin{aligned}
\mathfrak{A}_4^3=P_4^1\sin\;(\quad)&\cdot(-7{\cdot}875\cos\chi+7{\cdot}875\cos3\chi)\\
+P_4^2\sin2\,(\quad)&\cdot(+0{\cdot}875\sin\chi-2{\cdot}625\sin3\chi)\\
+P_4^3\sin3\,(\quad)&\cdot(-0{\cdot}4375\cos\chi-0{\cdot}5625\cos3\chi)\\
+P_4^4\sin4\,(\quad)&\cdot(+0{\cdot}21875\sin\chi+0{\cdot}09375\sin3\chi)
\end{aligned}$$

$$\begin{aligned}
\mathfrak{B}_4^3=P_4\qquad\quad\;&\;\;(+26{\cdot}25\sin2\chi-13{\cdot}125\sin4\chi)\\
+P_4^1\cos\;(\quad)&\cdot(+5{\cdot}25\cos2\chi-5{\cdot}25\cos4\chi)\\
+P_4^2\cos2\,(\quad)&\cdot(+1{\cdot}75\sin2\chi+0{\cdot}875\sin4\chi)\\
+P_4^3\cos3\,(\quad)&\cdot(+0{\cdot}875\cos2\chi+0{\cdot}125\cos4\chi)\\
+P_4^4\cos4\,(\quad)&\cdot(-0{\cdot}21875\sin2\chi-0{\cdot}015625\sin4\chi)
\end{aligned}$$

$$\begin{aligned}
\mathfrak{A}_4^4=P_4\qquad\quad\;&\;\;(+39{\cdot}375-52{\cdot}5\cos2\chi+13{\cdot}125\cos4\chi)\\
+P_4^1\cos\;(\quad)&\cdot(\qquad\qquad+10{\cdot}5\sin2\chi-5{\cdot}25\sin4\chi)\\
+P_4^2\cos2\,(\quad)&\cdot(+4{\cdot}375-3{\cdot}5\cos2\chi-0{\cdot}875\cos4\chi)\\
+P_4^3\cos3\,(\quad)&\cdot(\qquad\qquad+1{\cdot}75\sin2\chi+0{\cdot}125\sin4\chi)\\
+P_4^4\cos4\,(\quad)&\cdot(+0{\cdot}546875+0{\cdot}4375\cos2\chi+0{\cdot}015625\cos4\chi)
\end{aligned}$$

$$\begin{aligned}
\mathfrak{B}_4^4=P_4^1\sin\;(\quad)&\cdot(\qquad\qquad+31{\cdot}5\sin\chi-10{\cdot}5\sin3\chi)\\
+P_4^2\sin2\,(\quad)&\cdot(\qquad\qquad+3{\cdot}5\cos\chi-3{\cdot}5\cos3\chi)\\
+P_4^3\sin3\,(\quad)&\cdot(\qquad\qquad+1{\cdot}75\sin\chi+0{\cdot}75\sin3\chi)\\
+P_4^4\sin4\,(\quad)&\cdot(\qquad\qquad+0{\cdot}875\cos\chi+0{\cdot}125\cos3\chi)
\end{aligned}$$

$$\begin{aligned}
\mathfrak{A}_5^0 = {} & P_5 \quad (+0{\cdot}234375 \cos \chi + 0{\cdot}2734375 \cos 3\chi + 0{\cdot}4921875 \cos 5\chi) \\
& + P_5^1 \cos (\quad) \cdot (-0{\cdot}015625 \sin \chi - 0{\cdot}0546875 \sin 3\chi - 0{\cdot}1640625 \sin 5\chi) \\
& + P_5^2 \cos 2 (\quad) \cdot (+0{\cdot}015625 \cos \chi + 0{\cdot}0078125 \cos 3\chi - 0{\cdot}0234375 \cos 5\chi) \\
& + P_5^3 \cos 3 (\quad) \cdot (-0{\cdot}001953125 \sin \chi - 0{\cdot}004231773 \sin 3\chi + 0{\cdot}0029296875 \sin 5\chi) \\
& + P_5^4 \cos 4 (\quad) \cdot (+0{\cdot}0006510417 \cos \chi - 0{\cdot}0009765625 \cos 3\chi + 0{\cdot}0003255208 \cos 5\chi) \\
& + P_5^5 \cos 5 (\quad) \cdot (-0{\cdot}0003255208 \sin \chi + 0{\cdot}0001627604 \sin 3\chi - 0{\cdot}00003255208 \sin 5\chi)
\end{aligned}$$

$$\mathfrak{B}_5^0 = 0$$

$$\begin{aligned}
\mathfrak{A}_5^1 = {} & P_5^1 \sin (\quad) \cdot (+0{\cdot}234375 + 0{\cdot}4375 \cos 2\chi + 0{\cdot}328125 \cos 4\chi) \\
& + P_5^2 \sin 2 (\quad) \cdot (\qquad - 0{\cdot}0625 \sin 2\chi - 0{\cdot}09375 \sin 4\chi) \\
& + P_5^3 \sin 3 (\quad) \cdot (+0{\cdot}009765625 + 0{\cdot}0078125 \cos 2\chi - 0{\cdot}017578125 \cos 4\chi) \\
& + P_5^4 \sin 4 (\quad) \cdot (\qquad - 0{\cdot}005208333 \sin 2\chi + 0{\cdot}002604167 \sin 4\chi) \\
& + P_5^5 \sin 5 (\quad) \cdot (+0{\cdot}0009765625 - 0{\cdot}001302083 \cos 2\chi + 0{\cdot}0003255208 \cos 4\chi)
\end{aligned}$$

$$\begin{aligned}
\mathfrak{B}_5^1 = {} & P_5 \quad (-0{\cdot}234375 \sin \chi - 0{\cdot}8203125 \sin 3\chi - 2{\cdot}4609375 \sin 5\chi) \\
& + P_5^1 \cos (\quad) \cdot (-0{\cdot}015625 \cos \chi - 0{\cdot}1640625 \cos 3\chi - 0{\cdot}8203125 \cos 5\chi) \\
& + P_5^2 \cos 2 (\quad) \cdot (-0{\cdot}015625 \sin \chi - 0{\cdot}0234375 \sin 3\chi + 0{\cdot}1171875 \sin 5\chi) \\
& + P_5^3 \cos 3 (\quad) \cdot (-0{\cdot}001953125 \cos \chi - 0{\cdot}012695312 \cos 3\chi + 0{\cdot}01464844 \cos 5\chi) \\
& + P_5^4 \cos 4 (\quad) \cdot (-0{\cdot}000651042 \sin \chi + 0{\cdot}0029296875 \sin 3\chi - 0{\cdot}001627604 \sin 5\chi) \\
& + P_5^5 \cos 5 (\quad) \cdot (-0{\cdot}0003255208 \cos \chi + 0{\cdot}0004882812 \cos 3\chi - 0{\cdot}0001627604 \cos 5\chi)
\end{aligned}$$

$$\begin{aligned}
\mathfrak{A}_5^2 = {} & P_5 \quad (-6{\cdot}5625 \cos \chi - 3{\cdot}28125 \cos 3\chi + 9{\cdot}84375 \cos 5\chi) \\
& + P_5^1 \cos (\quad) \cdot (+0{\cdot}4375 \sin \chi + 0{\cdot}65625 \sin 3\chi - 3{\cdot}28125 \sin 5\chi) \\
& + P_5^2 \cos 2 (\quad) \cdot (-0{\cdot}4375 \cos \chi - 0{\cdot}09375 \cos 3\chi - 0{\cdot}46875 \cos 5\chi) \\
& + P_5^3 \cos 3 (\quad) \cdot (+0{\cdot}0546875 \sin \chi + 0{\cdot}05078125 \sin 3\chi + 0{\cdot}05859375 \sin 5\chi) \\
& + P_5^4 \cos 4 (\quad) \cdot (-0{\cdot}018229167 \cos \chi + 0{\cdot}01171875 \cos 3\chi + 0{\cdot}006510417 \cos 5\chi) \\
& + P_5^5 \cos 5 (\quad) \cdot (+0{\cdot}009114583 \sin \chi - 0{\cdot}001953125 \sin 3\chi - 0{\cdot}0006510417 \sin 5\chi)
\end{aligned}$$

$$\begin{aligned}
\mathfrak{B}_5^2 = {} & P_5^1 \sin (\quad) \cdot (-1{\cdot}75 \sin 2\chi - 2{\cdot}625 \sin 4\chi) \\
& + P_5^2 \sin 2 (\quad) \cdot (-0{\cdot}25 \cos 2\chi - 0{\cdot}75 \cos 4\chi) \\
& + P_5^3 \sin 3 (\quad) \cdot (-0{\cdot}03125 \sin 2\chi + 0{\cdot}140625 \sin 4\chi) \\
& + P_5^4 \sin 4 (\quad) \cdot (-0{\cdot}02083333 \cos 2\chi + 0{\cdot}020833333 \cos 4\chi) \\
& + P_5^5 \sin 5 (\quad) \cdot (+0{\cdot}005208333 \sin 2\chi - 0{\cdot}0026041667 \sin 4\chi)
\end{aligned}$$

$$\begin{aligned}
\mathfrak{A}_5^3 = {} & P_5^1 \sin (\quad) \cdot (-6{\cdot}5625 - 5{\cdot}25 \cos 2\chi + 11{\cdot}8125 \cos 4\chi) \\
& + P_5^2 \sin 2 (\quad) \cdot (\qquad + 0{\cdot}75 \sin 2\chi - 3{\cdot}375 \sin 4\chi) \\
& + P_5^3 \sin 3 (\quad) \cdot (-0{\cdot}2734375 - 0{\cdot}09375 \cos 2\chi - 0{\cdot}6328125 \cos 4\chi) \\
& + P_5^4 \sin 4 (\quad) \cdot (\qquad + 0{\cdot}0625 \sin 2\chi + 0{\cdot}09375 \sin 4\chi) \\
& + P_5^5 \sin 5 (\quad) \cdot (-0{\cdot}02734375 + 0{\cdot}015625 \cos 2\chi + 0{\cdot}01171875 \cos 4\chi)
\end{aligned}$$

$$\mathfrak{B}_5^3 = P_5 \quad (+19{\cdot}6875 \sin \chi + 42{\cdot}65625 \sin 3\chi - 29{\cdot}53125 \sin 5\chi)$$

$$+P_5^1\cos\ (\quad)\cdot(+1{\cdot}3125\cos\chi+8{\cdot}53125\cos 3\chi-9{\cdot}84375\cos 5\chi)$$
$$+P_5^2\cos 2(\quad)\cdot(+1{\cdot}3125\sin\chi+1{\cdot}21875\sin 3\chi+1{\cdot}40625\sin 5\chi)$$
$$+P_5^3\cos 3(\quad)\cdot(+0{\cdot}1640625\cos\chi+0{\cdot}66015625\cos 3\chi+0{\cdot}17578125\cos 5\chi)$$
$$+P_5^4\cos 4(\quad)\cdot(+0{\cdot}0546875\sin\chi-0{\cdot}15234375\sin 3\chi-0{\cdot}01953125\sin 5\chi)$$
$$+P_5^5\cos 5(\quad)\cdot(+0{\cdot}02734375\cos\chi-0{\cdot}025390625\cos 3\chi-0{\cdot}001953125\cos 5\chi)$$

$$\mathfrak{A}_5^4=P_5\qquad(+118{\cdot}125\cos\chi-177{\cdot}1875\cos 3\chi+59{\cdot}0625\cos 5\chi)$$
$$+P_5^1\cos\ (\quad)\cdot(-7{\cdot}875\sin\chi+35{\cdot}4375\sin 3\chi-19{\cdot}6875\sin 5\chi)$$
$$+P_5^2\cos 2(\quad)\cdot(+7{\cdot}875\cos\chi-5{\cdot}0625\cos 3\chi-2{\cdot}8125\cos 5\chi)$$
$$+P_5^3\cos 3(\quad)\cdot(-0{\cdot}984375\sin\chi+2{\cdot}7421875\sin 3\chi+0{\cdot}3515625\sin 5\chi)$$
$$+P_5^4\cos 4(\quad)\cdot(+0{\cdot}328125\cos\chi+0{\cdot}6328125\cos 3\chi+0{\cdot}0390625\cos 5\chi)$$
$$+P_5^5\cos 5(\quad)\cdot(-0{\cdot}1640625\sin\chi-0{\cdot}10546875\sin 3\chi-0{\cdot}00390625\sin 5\chi)$$

$$\mathfrak{B}_5^4=P_5^1\sin\ (\quad)\cdot(+63\sin 2\chi-31{\cdot}5\sin 4\chi)$$
$$+P_5^2\sin 2(\quad)\cdot(+9\cos 2\chi-9\cos 4\chi)$$
$$+P_5^3\sin 3(\quad)\cdot(+1{\cdot}125\sin 2\chi+1{\cdot}6875\sin 4\chi)$$
$$+P_5^4\sin 4(\quad)\cdot(+0{\cdot}75\cos 2\chi+0{\cdot}25\cos 4\chi)$$
$$+P_5^5\sin 5(\quad)\cdot(-0{\cdot}1875\sin 2\chi-0{\cdot}03125\sin 4\chi)$$

$$\mathfrak{A}_5^5=P_5^1\sin\ (\quad)\cdot(+118{\cdot}125-157{\cdot}5\cos 2\chi+39{\cdot}375\cos 4\chi)$$
$$+P_5^2\sin 2(\quad)\cdot(\qquad+22{\cdot}5\sin 2\chi-11{\cdot}25\sin 4\chi)$$
$$+P_5^3\sin 3(\quad)\cdot(+4{\cdot}921875-2{\cdot}8125\cos 2\chi-2{\cdot}109375\cos 4\chi)$$
$$+P_5^4\sin 4(\quad)\cdot(\qquad+1{\cdot}875\sin 2\chi+0{\cdot}3125\sin 4\chi)$$
$$+P_5^5\sin 5(\quad)\cdot(+0{\cdot}4921875+0{\cdot}46875\cos 2\chi+0{\cdot}0390625\cos 4\chi)$$

$$\mathfrak{B}_5^5=P_5\qquad(-590{\cdot}625\sin\chi+295{\cdot}3125\sin 3\chi-59{\cdot}0625\sin 5\chi)$$
$$+P_5^1\cos\ (\quad)\cdot(-39{\cdot}375\cos\chi+59{\cdot}0625\cos 3\chi-19{\cdot}6875\cos 5\chi)$$
$$+P_5^2\cos 2(\quad)\cdot(-39{\cdot}375\sin\chi+8{\cdot}4375\sin 3\chi+2{\cdot}8125\sin 5\chi)$$
$$+P_5^3\cos 3(\quad)\cdot(-4{\cdot}921875\cos\chi+4{\cdot}5703125\cos 3\chi+0{\cdot}3515625\cos 5\chi)$$
$$+P_5^4\cos 4(\quad)\cdot(-1{\cdot}640625\sin\chi-1{\cdot}0546875\sin 3\chi-0{\cdot}0390625\sin 5\chi)$$
$$+P_5^5\cos 5(\quad)\cdot(-0{\cdot}8203125\cos\chi-0{\cdot}17578125\cos 3\chi-0{\cdot}00390625\cos 5\chi)$$

$$\mathfrak{A}_6^0=P_6\qquad(+0{\cdot}09765625+0{\cdot}205078125\cos 2\chi+0{\cdot}24609375\cos 4\chi+0{\cdot}451171875\cos 6\chi)$$
$$+P_6^1\cos\ (\quad)\cdot(\qquad-0{\cdot}01953125\sin 2\chi-0{\cdot}046875\sin 4\chi-0{\cdot}12890625\sin 6\chi)$$
$$+P_6^2\cos 2(\quad)\cdot(+0{\cdot}0048828125+0{\cdot}00830078125\cos 2\chi+0{\cdot}0029296875\cos 4\chi-0{\cdot}01611328125\cos 6\chi)$$
$$+P_6^3\cos 3(\quad)\cdot(\qquad-0{\cdot}00146484375\sin 2\chi-0{\cdot}001953125\sin 4\chi+0{\cdot}0017903646\sin 6\chi)$$

$$\begin{aligned}
&+P_6^4\cos 4(\quad)\cdot(+0{\cdot}0^{3}16276042+0{\cdot}0^{4}8138021\cos 2\chi-0{\cdot}0^{3}42317708\cos 4\chi\\
&\qquad\qquad\qquad\qquad\qquad\qquad\qquad\qquad\qquad+0{\cdot}0^{3}17903646\cos 6\chi)\\
&+P_6^5\cos 5(\quad)\cdot(\qquad\qquad-0{\cdot}0^{4}8138021\sin 2\chi+0{\cdot}0^{4}6510417\sin 4\chi\\
&\qquad\qquad\qquad\qquad\qquad\qquad\qquad\qquad\qquad-0{\cdot}0^{4}16276042\sin 6\chi)\\
&+P_6^6\cos 6(\quad)\cdot(+0{\cdot}0^{4}13563368-0{\cdot}0^{4}2034505\cos 2\chi+0{\cdot}0^{5}8138021\cos 4\chi\\
&\qquad\qquad\qquad\qquad\qquad\qquad\qquad\qquad\qquad-0{\cdot}0^{5}13563368\cos 6\chi)
\end{aligned}$$

$$\mathfrak{B}_6^0=0$$

$$\begin{aligned}
\mathfrak{A}_6^1=&P_6^1\sin\ \ (\quad)\cdot(+0{\cdot}390625\cos\chi+0{\cdot}3515625\cos 3\chi+0{\cdot}2578125\cos 5\chi)\\
&+P_6^2\sin 2(\quad)\cdot(-0{\cdot}01953125\sin\chi-0{\cdot}052734375\sin 3\chi-0{\cdot}064453125\sin 5\chi)\\
&+P_6^3\sin 3(\quad)\cdot(+0{\cdot}009765625\cos\chi+0{\cdot}0^{2}9765625\cos 3\chi-0{\cdot}0107421875\cos 5\chi)\\
&+P_6^4\sin 4(\quad)\cdot(-0{\cdot}0013020833\sin\chi-0{\cdot}001953125\sin 3\chi+0{\cdot}00143229165\sin 5\chi)\\
&+P_6^5\sin 5(\quad)\cdot(+0{\cdot}0^{3}3255208\cos\chi-0{\cdot}0^{3}48828125\cos 3\chi+0{\cdot}0^{3}162760415\cos 5\chi)\\
&+P_6^6\sin 6(\quad)\cdot(-0{\cdot}0^{3}16276042\sin\chi+0{\cdot}0^{4}8138021\sin 3\chi-0{\cdot}0^{4}162760415\sin 5\chi)
\end{aligned}$$

$$\begin{aligned}
\mathfrak{B}_6^1=&P_6\qquad\qquad\qquad(-0{\cdot}41015625\sin 2\chi-0{\cdot}984375\sin 4\chi-2{\cdot}70703125\sin 6\chi)\\
&+P_6^1\cos\ \ (\quad)\cdot(-0{\cdot}0390625\cos 2\chi-0{\cdot}1875\cos 4\chi-0{\cdot}7734375\cos 6\chi)\\
&+P_6^2\cos 2(\quad)\cdot(-0{\cdot}0166015625\sin 2\chi-0{\cdot}01171875\sin 4\chi+0{\cdot}0966796875\sin 6\chi)\\
&+P_6^3\cos 3(\quad)\cdot(-0{\cdot}0029296875\cos 2\chi-0{\cdot}0078125\cos 4\chi+0{\cdot}0107421875\cos 6\chi)\\
&+P_6^4\cos 4(\quad)\cdot(-0{\cdot}0^{3}162760415\sin 2\chi+0{\cdot}0016927083\sin 4\chi\\
&\qquad\qquad\qquad\qquad\qquad\qquad\qquad\qquad\qquad-0{\cdot}00107421875\sin 6\chi)\\
&+P_6^5\cos 5(\quad)\cdot(-0{\cdot}0^{3}162760415\cos 2\chi+0{\cdot}0^{3}2604167\cos 4\chi-0{\cdot}0^{4}9765625\cos 6\chi)\\
&+P_6^6\cos 6(\quad)\cdot(+0{\cdot}0^{4}40690104\sin 2\chi-0{\cdot}0^{4}3255208\sin 4\chi+0{\cdot}0^{5}8138021\sin 6\chi)
\end{aligned}$$

$$\begin{aligned}
\mathfrak{A}_6^2=&P_6\qquad\qquad\qquad(-4{\cdot}1015625-6{\cdot}97265635\cos 2\chi-2{\cdot}4609375\cos 4\chi\\
&\qquad\qquad\qquad\qquad\qquad\qquad\qquad\qquad\qquad+13{\cdot}53515625\cos 6\chi)\\
&+P_6^1\cos\ \ (\quad)\cdot(\qquad\qquad+0{\cdot}6640625\sin 2\chi+0{\cdot}46875\sin 4\chi-3{\cdot}8671875\sin 6\chi)\\
&+P_6^2\cos 2(\quad)\cdot(-0{\cdot}205078125-0{\cdot}2822265625\cos 2\chi-0{\cdot}029296875\cos 4\chi\\
&\qquad\qquad\qquad\qquad\qquad\qquad\qquad\qquad\qquad-0{\cdot}4833984375\cos 6\chi)\\
&+P_6^3\cos 3(\quad)\cdot(\qquad\qquad+0{\cdot}04980469\sin 2\chi+0{\cdot}01953125\sin 4\chi\\
&\qquad\qquad\qquad\qquad\qquad\qquad\qquad\qquad\qquad+0{\cdot}0537109375\sin 6\chi)\\
&+P_6^4\cos 4(\quad)\cdot(-0{\cdot}0068359375-0{\cdot}002766927\cos 2\chi+0{\cdot}004231771\cos 4\chi\\
&\qquad\qquad\qquad\qquad\qquad\qquad\qquad\qquad\qquad+0{\cdot}00537109375\cos 6\chi)\\
&+P_6^5\cos 5(\quad)\cdot(\quad+0{\cdot}002766927\sin 2\chi-0{\cdot}0^{3}65104167\sin 4\chi-0{\cdot}0^{3}48828125\sin 6\chi)\\
&+P_6^6\cos 6(\quad)\cdot(-0{\cdot}0^{3}56966146+0{\cdot}0^{3}6917318\cos 2\chi-0{\cdot}0^{4}8138021\cos 4\chi\\
&\qquad\qquad\qquad\qquad\qquad\qquad\qquad\qquad\qquad-0{\cdot}0^{4}40690104\cos 6\chi)
\end{aligned}$$

$$\begin{aligned}
\mathfrak{B}_6^2=&P_6^1\sin\ \ (\quad)\cdot(-0{\cdot}78125\sin\chi-2{\cdot}109375\sin 3\chi-2{\cdot}578125\sin 5\chi)\\
&+P_6^2\sin 2(\quad)\cdot(-0{\cdot}0390625\cos\chi-0{\cdot}31640625\cos 3\chi-0{\cdot}64453125\cos 5\chi)\\
&+P_6^3\sin 3(\quad)\cdot(-0{\cdot}01953125\sin\chi-0{\cdot}005859375\sin 3\chi+0{\cdot}107421875\sin 5\chi)
\end{aligned}$$

$$+P_6^4\sin 4(\quad)\cdot(-0{\cdot}002604167\cos\chi-0{\cdot}01171875\cos 3\chi+0{\cdot}014322917\cos 5\chi)$$

$$+P_6^5\sin 5(\quad)\cdot(-0{\cdot}0^{2}6510417\sin\chi+0{\cdot}0029296875\sin 3\chi-0{\cdot}0016276042\sin 5\chi)$$

$$+P_6^6\sin 6(\quad)\cdot(-0{\cdot}0^{3}3255208\cos\chi+0{\cdot}0^{3}48828125\cos 3\chi-0{\cdot}0^{3}16276042\cos 5\chi)$$

$$\mathfrak{A}_6^3=P_6^1\sin\;(\quad)\cdot(-14{\cdot}0625\cos\chi-1{\cdot}40625\cos 3\chi+15{\cdot}46875\cos 5\chi)$$

$$+P_6^2\sin 2(\quad)\cdot(+0{\cdot}703125\sin\chi+0{\cdot}2109375\sin 3\chi-3{\cdot}8671875\sin 5\chi)$$

$$+P_6^3\sin 3(\quad)\cdot(-0{\cdot}3515625\cos\chi-0{\cdot}00390625\cos 3\chi-0{\cdot}64453125\cos 5\chi)$$

$$+P_6^4\sin 4(\quad)\cdot(+0{\cdot}046875\sin\chi+0{\cdot}0078125\sin 3\chi+0{\cdot}0859375\sin 5\chi)$$

$$+P_6^5\sin 5(\quad)\cdot(-0{\cdot}01171875\cos\chi+0{\cdot}001953125\cos 3\chi+0{\cdot}009765625\cos 5\chi)$$

$$+P_6^6\sin 6(\quad)\cdot(+0{\cdot}005859375\sin\chi-0{\cdot}0^{3}3255208\sin 3\chi-0{\cdot}0^{3}9765625\sin 5\chi)$$

$$\mathfrak{B}_6^3=P_6\qquad(+44{\cdot}296875\sin 2\chi+59{\cdot}0625\sin 4\chi-54{\cdot}140625\sin 6\chi)$$

$$+P_6^1\cos\;(\quad)\cdot(+4{\cdot}21875\cos 2\chi+11{\cdot}25\cos 4\chi-15{\cdot}46875\cos 6\chi)$$

$$+P_6^2\cos 2(\quad)\cdot(+1{\cdot}79296875\sin 2\chi+0{\cdot}703125\sin 4\chi+1{\cdot}93359375\sin 6\chi)$$

$$+P_6^3\cos 3(\quad)\cdot(+0{\cdot}31640625\cos 2\chi+0{\cdot}46875\cos 4\chi+0{\cdot}21484375\cos 6\chi)$$

$$+P_6^4\cos 4(\quad)\cdot(+0{\cdot}017578125\sin 2\chi-0{\cdot}1015625\sin 4\chi-0{\cdot}021484375\sin 6\chi)$$

$$+P_6^5\cos 5(\quad)\cdot(+0{\cdot}017578125\cos 2\chi-0{\cdot}015625\cos 4\chi-0{\cdot}001953125\cos 6\chi)$$

$$+P_6^6\cos 6(\quad)\cdot(-0{\cdot}00439453125\sin 2\chi+0{\cdot}001953125\sin 4\chi+0{\cdot}0^{3}16276042\sin 6\chi)$$

$$\mathfrak{A}_6^4=P_6\qquad(+147{\cdot}65625+73{\cdot}828125\cos 2\chi-383{\cdot}90625\cos 4\chi$$

$$+162{\cdot}421875\cos 6\chi)$$

$$+P_6^1\cos\;(\quad)\cdot(\qquad-7{\cdot}03125\sin 2\chi+73{\cdot}125\sin 4\chi-46{\cdot}40625\sin 6\chi)$$

$$+P_6^2\cos 2(\quad)\cdot(+7{\cdot}3828125+2{\cdot}9882813\cos 2\chi-4{\cdot}5703125\cos 4\chi$$

$$-5{\cdot}80078125\cos 6\chi)$$

$$+P_6^3\cos 3(\quad)\cdot(\qquad-0{\cdot}527343758\sin 2\chi+3{\cdot}046875\sin 4\chi+0{\cdot}64453125\sin 6\chi)$$

$$+P_6^4\cos 4(\quad)\cdot(+0{\cdot}24609375+0{\cdot}029296875\cos 2\chi+0{\cdot}66015625\cos 4\chi$$

$$+0{\cdot}064453125\cos 6\chi)$$

$$+P_6^5\cos 5(\quad)\cdot(\qquad-0{\cdot}029296875\sin 2\chi-0{\cdot}1015625\sin 4\chi$$

$$-0{\cdot}005859375\sin 6\chi)$$

$$+P_6^6\cos 6(\quad)\cdot(+0{\cdot}0205078125-0{\cdot}00732421875\cos 2\chi-0{\cdot}0126953125\cos 4\chi$$

$$-0{\cdot}0^{3}48828125\cos 6\chi)$$

$$\mathfrak{B}_6^4=P_6^1\sin\;(\quad)\cdot(+56{\cdot}25\sin\chi+84{\cdot}375\sin 3\chi-61{\cdot}875\sin 5\chi)$$

$$+P_6^2\sin 2(\quad)\cdot(+2{\cdot}8125\cos\chi+12{\cdot}65625\cos 3\chi-15{\cdot}46875\cos 5\chi)$$

$$+P_6^3\sin 3(\quad)\cdot(+1{\cdot}40625\sin\chi+0{\cdot}234375\sin 3\chi+2{\cdot}578125\sin 5\chi)$$

$$+P_6^4\sin 4(\quad)\cdot(+0{\cdot}1875\cos\chi+0{\cdot}46875\cos 3\chi+0{\cdot}34375\cos 5\chi)$$

$$+P_6^5\sin 5(\quad)\cdot(+0{\cdot}046875\sin\chi-0{\cdot}1171875\sin 3\chi-0{\cdot}0390625\sin 5\chi)$$

$$+P_6^6\sin 6(\quad)\cdot(+0{\cdot}0234375\cos\chi-0{\cdot}01953125\cos 3\chi-0{\cdot}00390625\cos 5\chi)$$

$$\mathfrak{A}_6^5=P_6^1\sin\;(\quad)\cdot(+309{\cdot}375\cos\chi-464{\cdot}0625\cos 3\chi+154{\cdot}6875\cos 5\chi)$$

$$+P_6^2\sin 2(\quad)\cdot(-15{\cdot}46875\sin\chi+69{\cdot}609375\sin 3\chi-38{\cdot}671875\sin 5\chi)$$

$$\begin{aligned}
&+P_6^3 \sin 3(\quad)\cdot(+7{\cdot}734375 \cos \chi -1{\cdot}2890625 \cos 3\chi -6{\cdot}4453125 \cos 5\chi)\\
&+P_6^4 \sin 4(\quad)\cdot(-1{\cdot}03125 \sin \chi +2{\cdot}578125 \sin 3\chi +0{\cdot}859375 \sin 5\chi)\\
&+P_6^5 \sin 5(\quad)\cdot(+0{\cdot}2578125 \cos \chi +0{\cdot}64453125 \cos 3\chi +0{\cdot}09765625 \cos 5\chi)\\
&+P_6^6 \sin 6(\quad)\cdot(-0{\cdot}12890625 \sin \chi -0{\cdot}107421875 \sin 3\chi -0{\cdot}009765625 \sin 5\chi)
\end{aligned}$$

$$\begin{aligned}
\mathfrak{B}_6^5=P_6 &\qquad (-1624{\cdot}21875 \sin 2\chi +1299{\cdot}375 \sin 4\chi -324{\cdot}84375 \sin 6\chi)\\
&+P_6^1 \cos\ (\quad)\cdot(-154{\cdot}6875 \cos 2\chi +247{\cdot}5 \cos 4\chi -92{\cdot}8125 \cos 6\chi)\\
&+P_6^2 \cos 2(\quad)\cdot(-65{\cdot}7421875 \sin 2\chi +15{\cdot}46875 \sin 4\chi +11{\cdot}6015625 \sin 6\chi)\\
&+P_6^3 \cos 3(\quad)\cdot(-11{\cdot}6015625 \cos 2\chi +10{\cdot}3125 \cos 4\chi +1{\cdot}2890625 \cos 6\chi)\\
&+P_6^4 \cos 4(\quad)\cdot(-0{\cdot}64453125 \sin 2\chi -2{\cdot}234375 \sin 4\chi -0{\cdot}12890625 \sin 6\chi)\\
&+P_6^5 \cos 5(\quad)\cdot(-0{\cdot}64453125 \cos 2\chi -0{\cdot}34375 \cos 4\chi -0{\cdot}01171875 \cos 6\chi)\\
&+P_6^6 \cos 6(\quad)\cdot(+0{\cdot}16113281 \sin 2\chi +0{\cdot}04296875 \sin 4\chi +0{\cdot}0^39765625 \sin 6\chi)
\end{aligned}$$

$$\begin{aligned}
\mathfrak{A}_6^6=P_6 &\qquad (-3248{\cdot}4375 +4872{\cdot}65625 \cos 2\chi -1949{\cdot}0625 \cos 4\chi\\
&\qquad\qquad +324{\cdot}84375 \cos 6\chi)\\
&+P_6^1 \cos\ (\quad)\cdot(\qquad -464{\cdot}0625 \sin 2\chi +371{\cdot}25 \sin 4\chi -92{\cdot}8125 \sin 6\chi)\\
&+P_6^2 \cos 2(\quad)\cdot(-162{\cdot}421875 +197{\cdot}2265625 \cos 2\chi -23{\cdot}203125 \cos 4\chi\\
&\qquad\qquad -11{\cdot}6015625 \cos 6\chi)\\
&+P_6^3 \cos 3(\quad)\cdot(\qquad -34{\cdot}8046875 \sin 2\chi +15{\cdot}46875 \sin 4\chi +1{\cdot}2890625 \sin 6\chi)\\
&+P_6^4 \cos 4(\quad)\cdot(-5{\cdot}4140625 +1{\cdot}93359375 \cos 2\chi +3{\cdot}3515625 \cos 4\chi\\
&\qquad\qquad +0{\cdot}12890625 \cos 6\chi)\\
&+P_6^5 \cos 5(\quad)\cdot(\qquad -1{\cdot}93359375 \sin 2\chi -0{\cdot}515625 \sin 4\chi\\
&\qquad\qquad -0{\cdot}01171875 \sin 6\chi)\\
&+P_6^6 \cos 6(\quad)\cdot(-0{\cdot}451171875 -0{\cdot}4833984375 \cos 2\chi -0{\cdot}064453125 \cos 4\chi\\
&\qquad\qquad -0{\cdot}0^39765625 \cos 6\chi)
\end{aligned}$$

$$\begin{aligned}
\mathfrak{B}_6^6=P_6^1 &\sin\ (\quad)\cdot(-1856{\cdot}25 \sin \chi +928{\cdot}125 \sin 3\chi -185{\cdot}625 \sin 5\chi)\\
&+P_6^2 \sin 2(\quad)\cdot(-92{\cdot}8125 \cos \chi +139{\cdot}21875 \cos 3\chi -46{\cdot}40625 \cos 5\chi)\\
&+P_6^3 \sin 3(\quad)\cdot(-46{\cdot}40625 \sin \chi +2{\cdot}578125 \sin 3\chi +7{\cdot}734375 \sin 5\chi)\\
&+P_6^4 \sin 4(\quad)\cdot(-6{\cdot}1875 \cos \chi +5{\cdot}15625 \cos 3\chi +1{\cdot}03125 \cos 5\chi)\\
&+P_6^5 \sin 5(\quad)\cdot(-1{\cdot}546875 \sin \chi -1{\cdot}2890625 \sin 3\chi -0{\cdot}1171875 \sin 5\chi)\\
&+P_6^6 \sin 6(\quad)\cdot(-0{\cdot}7734375 \cos \chi -0{\cdot}21484375 \cos 3\chi -0{\cdot}01171875 \cos 5\chi)
\end{aligned}$$

$$\begin{aligned}
\mathfrak{A}_7^0=P_7 &\qquad (+0{\cdot}17089844 \cos \chi +0{\cdot}18457031 \cos 3\chi +0{\cdot}2255859 \cos 5\chi\\
&\qquad\qquad +0{\cdot}4189453 \cos 7\chi)\\
&+P_7^1 \cos\ (\quad)\cdot(-0{\cdot}006103516 \sin \chi -0{\cdot}019775390 \sin 3\chi -0{\cdot}04028320 \sin 5\chi\\
&\qquad\qquad -0{\cdot}10473633 \sin 7\chi)\\
&+P_7^2 \cos 2(\quad)\cdot(+0{\cdot}006103516 \cos \chi +0{\cdot}004638672 \cos 3\chi +0{\cdot}0^38951824 \cos 5\chi\\
&\qquad\qquad -0{\cdot}011637369 \cos 7\chi)
\end{aligned}$$

$$\begin{aligned}
&+P_7^3\cos 3(\quad)\cdot(-0{\cdot}0^{3}3662109\sin\chi-0{\cdot}0^{3}9521484\sin 3\chi-0{\cdot}0^{3}9847005\sin 5\chi\\
&\qquad+0{\cdot}001163737\sin 7\chi)\\
&+P_7^4\cos 4(\quad)\cdot(+0{\cdot}0^{3}12207031\cos\chi-0{\cdot}0^{4}244140625\cos 3\chi-0{\cdot}0^{3}2034505\cos 5\chi\\
&\qquad+0{\cdot}0^{3}10579427\cos 7\chi)\\
&+P_7^5\cos 5(\quad)\cdot(-0{\cdot}0^{4}16954210\sin\chi-0{\cdot}0^{4}22379557\sin 3\chi+0{\cdot}0^{4}2916124\sin 5\chi\\
&\qquad-0{\cdot}0^{5}8816189\sin 7\chi)\\
&+P_7^6\cos 6(\quad)\cdot(+0{\cdot}0^{5}3390842\cos\chi-0{\cdot}0^{5}6103516\cos 3\chi+0{\cdot}0^{5}3390842\cos 5\chi\\
&\qquad-0{\cdot}0^{6}6781684\cos 7\chi)\\
&+P_7^7\cos 7(\quad)\cdot(-0{\cdot}0^{5}1695421\sin\chi+0{\cdot}0^{5}10172526\sin 3\chi-0{\cdot}0^{6}3390842\sin 5\chi\\
&\qquad+0{\cdot}0^{7}4844060\sin 7\chi)
\end{aligned}$$

$$\mathfrak{B}_7^0=0$$

$$\begin{aligned}
\mathfrak{A}_7^1=\;&P_7^1\sin\;(\quad)\cdot(+0{\cdot}1708985+0{\cdot}3295899\cos 2\chi+0{\cdot}2900391\cos 4\chi\\
&\qquad+0{\cdot}2094726\cos 6\chi)\\
&+P_7^2\sin 2(\quad)\cdot(\qquad-0{\cdot}02441406\sin 2\chi-0{\cdot}04296876\sin 4\chi\\
&\qquad-0{\cdot}04654948\sin 6\chi)\\
&+P_7^3\sin 3(\quad)\cdot(+0{\cdot}003417968+0{\cdot}004638672\cos 2\chi-0{\cdot}001074219\cos 4\chi\\
&\qquad-0{\cdot}006982420\cos 6\chi)\\
&+P_7^4\sin 4(\quad)\cdot(\qquad-0{\cdot}0^{3}9765624\sin 2\chi-0{\cdot}0^{3}78125\sin 4\chi\\
&\qquad+0{\cdot}0^{3}8463540\sin 6\chi)\\
&+P_7^5\sin 5(\quad)\cdot(+0{\cdot}0^{4}9494358+0{\cdot}0^{4}2034506\cos 2\chi-0{\cdot}0^{3}2034505\cos 4\chi\\
&\qquad+0{\cdot}0^{4}8816192\cos 6\chi)\\
&+P_7^6\sin 6(\quad)\cdot(\qquad-0{\cdot}0^{4}4069012\sin 2\chi+0{\cdot}0^{4}3255208\sin 4\chi\\
&\qquad-0{\cdot}0^{5}8138020\sin 6\chi)\\
&+P_7^7\sin 7(\quad)\cdot(+0{\cdot}0^{5}6781684-0{\cdot}0^{4}1017253\cos 2\chi+0{\cdot}0^{5}4069012\cos 4\chi\\
&\qquad-0{\cdot}0^{6}6781684\cos 6\chi)
\end{aligned}$$

$$\begin{aligned}
\mathfrak{B}_7^1=\;&P_7\qquad(-0{\cdot}1708985\sin\chi-0{\cdot}5537110\sin 3\chi-1{\cdot}127930\sin 5\chi\\
&\qquad-2{\cdot}932618\sin 7\chi)\\
&+P_7^1\cos\;(\quad)\cdot(-0{\cdot}006103516\cos\chi-0{\cdot}05932616\cos 3\chi-0{\cdot}2014160\cos 5\chi\\
&\qquad-0{\cdot}7331544\cos 7\chi)\\
&+P_7^2\cos 2(\quad)\cdot(-0{\cdot}006103516\sin\chi-0{\cdot}01391602\sin 3\chi-0{\cdot}004475912\sin 5\chi\\
&\qquad+0{\cdot}08146156\sin 7\chi)\\
&+P_7^3\cos 3(\quad)\cdot(-0{\cdot}0^{3}3662109\cos\chi-0{\cdot}002856444\cos 3\chi-0{\cdot}004923504\cos 5\chi\\
&\qquad+0{\cdot}008146156\cos 7\chi)\\
&+P_7^4\cos 4(\quad)\cdot(-0{\cdot}0^{3}1220703\sin\chi+0{\cdot}0^{4}7324220\sin 3\chi+0{\cdot}001017253\sin 5\chi\\
&\qquad-0{\cdot}0^{3}7405600\sin 7\chi)\\
&+P_7^5\cos 5(\quad)\cdot(-0{\cdot}0^{4}1695421\cos\chi-0{\cdot}0^{4}6713868\cos 3\chi+0{\cdot}0^{3}1458062\cos 5\chi\\
&\qquad-0{\cdot}0^{4}6171332\cos 7\chi)
\end{aligned}$$

$$
\begin{aligned}
&+P_7^6\cos 6(\quad)\cdot(-0{\cdot}0^5 3390842\sin\chi+0{\cdot}0^4 1831055\sin 3\chi-0{\cdot}0^4 1695421\sin 5\chi\\
&\qquad\qquad+0{\cdot}0^5 474718\sin 7\chi)\\
&+P_7^7\cos 7(\quad)\cdot(-0{\cdot}0^5 1695421\cos\chi+0{\cdot}0^5 3051758\cos 3\chi-0{\cdot}0^5 1695421\cos 5\chi\\
&\qquad\qquad+0{\cdot}0^6 3390842\cos 7\chi)
\end{aligned}
$$

$$
\begin{aligned}
\mathfrak{A}_7^2=P_7\quad&(-9{\cdot}228516\cos\chi-7{\cdot}013672\cos 3\chi-1{\cdot}353516\cos 5\chi\\
&\qquad\qquad+17{\cdot}59570\cos 7\chi)\\
&+P_7^1\cos(\quad)\cdot(+0{\cdot}3295899\sin\chi+0{\cdot}7514648\sin 3\chi+0{\cdot}2416992\sin 5\chi\\
&\qquad\qquad-4{\cdot}398926\sin 7\chi)\\
&+P_7^2\cos 2(\quad)\cdot(-0{\cdot}3295899\cos\chi-0{\cdot}1762695\cos 3\chi-0{\cdot}005371096\cos 5\chi\\
&\qquad\qquad-0{\cdot}4887692\cos 7\chi)\\
&+P_7^3\cos 3(\quad)\cdot(+0{\cdot}01977539\sin\chi+0{\cdot}03618162\sin 3\chi+0{\cdot}005908204\sin 5\chi\\
&\qquad\qquad+0{\cdot}04887692\sin 7\chi)\\
&+P_7^4\cos 4(\quad)\cdot(-0{\cdot}006591796\cos\chi+0{\cdot}0^3 9277344\cos 3\chi+0{\cdot}001220703\cos 5\chi\\
&\qquad\qquad+0{\cdot}004443360\cos 7\chi)\\
&+P_7^5\cos 5(\quad)\cdot(+0{\cdot}0^3 9155276\sin\chi+0{\cdot}0^3 8504232\sin 3\chi-0{\cdot}0^3 1749674\sin 5\chi\\
&\qquad\qquad-0{\cdot}0^3 3702800\sin 7\chi)\\
&+P_7^6\cos 6(\quad)\cdot(-0{\cdot}0^3 1831055\cos\chi+0{\cdot}0^3 2319336\cos 3\chi-0{\cdot}0^4 2034505\cos 5\chi\\
&\qquad\qquad-0{\cdot}0^4 2848307\cos 7\chi)\\
&+P_7^7\cos 7(\quad)\cdot(+0{\cdot}0^4 9155276\sin\chi-0{\cdot}0^4 3865561\sin 3\chi+0{\cdot}0^5 2034505\sin 5\chi\\
&\qquad\qquad+0{\cdot}0^5 2034505\sin 7\chi)
\end{aligned}
$$

$$
\begin{aligned}
\mathfrak{B}_7^2=&P_7^1\sin(\quad)\cdot(-1{\cdot}318360\sin 2\chi-2{\cdot}3203124\sin 4\chi-2{\cdot}513672\sin 6\chi)\\
&+P_7^2\sin 2(\quad)\cdot(-0{\cdot}09765624\cos 2\chi-0{\cdot}34375\cos 4\chi-0{\cdot}5585936\cos 6\chi)\\
&+P_7^3\sin 3(\quad)\cdot(-0{\cdot}01855469\sin 2\chi+0{\cdot}008593752\sin 4\chi+0{\cdot}03378904\sin 6\chi)\\
&+P_7^4\sin 4(\quad)\cdot(-0{\cdot}0^3 390625\cos 2\chi-0{\cdot}00625\cos 4\chi+0{\cdot}01015625\cos 6\chi)\\
&+P_7^5\sin 5(\quad)\cdot(-0{\cdot}0^4 8138024\sin 2\chi+0{\cdot}001627604\sin 4\chi-0{\cdot}001057943\sin 6\chi)\\
&+P_7^6\sin 6(\quad)\cdot(-0{\cdot}0^3 1627605\cos 2\chi+0{\cdot}0^3 2604167\cos 4\chi-0{\cdot}0^4 9765624\cos 6\chi)\\
&+P_7^7\sin 7(\quad)\cdot(+0{\cdot}0^4 4069012\sin 2\chi-0{\cdot}0^4 3255208\sin 4\chi+0{\cdot}0^5 813802\sin 6\chi)
\end{aligned}
$$

$$
\begin{aligned}
\mathfrak{A}_7^3=&P_7^1\sin(\quad)\cdot(-9{\cdot}228517-12{\cdot}524416\cos 2\chi+2{\cdot}900391\cos 4\chi\\
&\qquad\qquad+18{\cdot}85254\cos 6\chi)\\
&+P_7^2\sin 2(\quad)\cdot(\qquad+0{\cdot}9277344\sin 2\chi-0{\cdot}4296876\sin 4\chi\\
&\qquad\qquad-4{\cdot}189452\sin 6\chi)\\
&+P_7^3\sin 3(\quad)\cdot(-0{\cdot}1845703-0{\cdot}1762695\cos 2\chi-0{\cdot}01074219\cos 4\chi\\
&\qquad\qquad-0{\cdot}6284180\cos 6\chi)\\
&+P_7^4\sin 4(\quad)\cdot(\qquad+0{\cdot}03710938\sin 2\chi-0{\cdot}0078125\sin 4\chi\\
&\qquad\qquad+0{\cdot}07617188\sin 6\chi)
\end{aligned}
$$

$$+P_7^5 \sin 5(\quad)\cdot(-0{\cdot}005126954 - 0{\cdot}0^3773112 \cos 2\chi - 0{\cdot}002034505 \cos 4\chi$$
$$+0{\cdot}007934572 \cos 6\chi)$$

$$+P_7^6 \sin 6(\quad)\cdot(\qquad +0{\cdot}001546224 \sin 2\chi + 0{\cdot}0^3 3255208 \sin 4\chi$$
$$-0{\cdot}0^3732422 \sin 6\chi)$$

$$+P_7^7 \sin 7(\quad)\cdot(-0{\cdot}0^3 3662110 + 0{\cdot}0^3 3865561 \cos 2\chi + 0{\cdot}0^4 4069012 \cos 4\chi$$
$$-0{\cdot}0^4 6103516 \cos 6\chi)$$

$$\mathfrak{B}_7^3 = P_7 \qquad (+27{\cdot}68555 \sin \chi + 71{\cdot}98244 \sin 3\chi + 74{\cdot}44336 \sin 5\chi$$
$$-87{\cdot}97853 \sin 7\chi)$$

$$+P_7^1 \cos\ (\quad)\cdot(+0{\cdot}9887696 \cos \chi + 7{\cdot}712400 \cos 3\chi + 13{\cdot}29346 \cos 5\chi$$
$$-21{\cdot}99463 \cos 7\chi)$$

$$+P_7^2 \cos 2(\quad)\cdot(+0{\cdot}9887696 \sin \chi + 1{\cdot}809082 \sin 3\chi + 0{\cdot}2954103 \sin 5\chi$$
$$+2{\cdot}443848 \sin 7\chi)$$

$$+P_7^3 \cos 3(\quad)\cdot(+0{\cdot}05932616 \cos \chi + 0{\cdot}3713377 \cos 3\chi + 0{\cdot}3249512 \cos 5\chi$$
$$+0{\cdot}2443848 \cos 7\chi)$$

$$+P_7^4 \cos 4(\quad)\cdot(+0{\cdot}01977539 \sin \chi - 0{\cdot}009521488 \sin 3\chi - 0{\cdot}06713868 \sin 5\chi$$
$$-0{\cdot}02221680 \sin 7\chi)$$

$$+P_7^5 \cos 5(\quad)\cdot(+0{\cdot}002746583 \cos \chi + 0{\cdot}008728028 \cos 3\chi - 0{\cdot}009623208 \cos 5\chi$$
$$-0{\cdot}001851400 \cos 7\chi)$$

$$+P_7^6 \cos 6(\quad)\cdot(+0{\cdot}0^3 5493164 \sin \chi - 0{\cdot}002380371 \sin 3\chi + 0{\cdot}001118978 \sin 5\chi$$
$$+0{\cdot}0^3 1424154 \sin 7\chi)$$

$$+P_7^7 \cos 7(\quad)\cdot(+0{\cdot}0^3 2746583 \cos \chi - 0{\cdot}0^3 3967286 \cos 3\chi + 0{\cdot}0^3 1118978 \cos 5\chi$$
$$+0{\cdot}0^4 1017253 \cos 7\chi)$$

$$\mathfrak{A}_7^4 = P_7 \qquad (+406{\cdot}0548 \cos \chi - 81{\cdot}21094 \cos 3\chi - 676{\cdot}7578 \cos 5\chi$$
$$+351{\cdot}9141 \cos 7\chi)$$

$$+P_7^1 \cos\ (\quad)\cdot(-14{\cdot}50196 \sin \chi + 8{\cdot}701172 \sin 3\chi + 120{\cdot}8496 \sin 5\chi$$
$$-87{\cdot}97852 \sin 7\chi)$$

$$+P_7^2 \cos 2(\quad)\cdot(+14{\cdot}50196 \cos \chi - 2{\cdot}041016 \cos 3\chi - 2{\cdot}685548 \cos 5\chi$$
$$-9{\cdot}775391 \cos 7\chi)$$

$$+P_7^3 \cos 3(\quad)\cdot(-0{\cdot}8701172 \sin \chi + 0{\cdot}4189452 \sin 3\chi + 2{\cdot}954102 \sin 5\chi$$
$$+0{\cdot}9775391 \sin 7\chi)$$

$$+P_7^4 \cos 4(\quad)\cdot(+0{\cdot}2900390 \cos \chi + 0{\cdot}01074219 \cos 3\chi + 0{\cdot}6103516 \cos 5\chi$$
$$+0{\cdot}08886719 \cos 7\chi)$$

$$+P_7^5 \cos 5(\quad)\cdot(-0{\cdot}04028320 \sin \chi + 0{\cdot}009847004 \sin 3\chi - 0{\cdot}08748372 \sin 5\chi$$
$$-0{\cdot}007405600 \sin 7\chi)$$

$$+P_7^6 \cos 6(\quad)\cdot(+0{\cdot}008056640 \cos \chi + 0{\cdot}002685547 \cos 3\chi - 0{\cdot}01017253 \cos 5\chi$$
$$-0{\cdot}0^3 5696616 \cos 7\chi)$$

$$+P_7^7 \cos 7(\quad)\cdot(-0{\cdot}004028320 \sin \chi -0{\cdot}0^{3}4475912 \sin 3\chi +0{\cdot}001017253 \sin 5\chi$$
$$+0{\cdot}0^{4}4069012 \sin 7\chi)$$

$$\mathfrak{B}_7^4 = P_7^1 \sin (\quad)\cdot(+116{\cdot}0156 \sin 2\chi +92{\cdot}81252 \sin 4\chi -100{\cdot}5469 \sin 6\chi)$$
$$+P_7^2 \sin 2(\quad)\cdot(+8{\cdot}593748 \cos 2\chi +13{\cdot}75 \cos 4\chi -22{\cdot}34374 \cos 6\chi)$$
$$+P_7^3 \sin 3(\quad)\cdot(+1{\cdot}632812 \sin 2\chi -0{\cdot}34375 \sin 4\chi +3{\cdot}351562 \sin 6\chi)$$
$$+P_7^4 \sin 4(\quad)\cdot(+0{\cdot}34375 \cos 2\chi +0{\cdot}25 \cos 4\chi +0{\cdot}40625 \cos 6\chi)$$
$$+P_7^5 \sin 5(\quad)\cdot(+0{\cdot}007161456 \sin 2\chi -0{\cdot}06510416 \sin 4\chi -0{\cdot}04231772 \sin 6\chi)$$
$$+P_7^6 \sin 6(\quad)\cdot(+0{\cdot}01432292 \cos 2\chi -0{\cdot}01041667 \cos 4\chi -0{\cdot}00390625 \cos 6\chi)$$
$$+P_7^7 \sin 7(\quad)\cdot(-0{\cdot}003580729 \sin 2\chi +0{\cdot}001302083 \sin 4\chi +0{\cdot}0^{3}3255208 \sin 6\chi)$$

$$\mathfrak{A}_7^5 = P_7^1 \sin (\quad)\cdot(+406{\cdot}0546 +87{\cdot}01172 \cos 2\chi -870{\cdot}1172 \cos 4\chi$$
$$+377{\cdot}0507 \cos 6\chi)$$
$$+P_7^2 \sin 2(\quad)\cdot(\qquad -6{\cdot}445312 \sin 2\chi +128{\cdot}9063 \sin 4\chi$$
$$-83{\cdot}7890 \sin 6\chi)$$
$$+P_7^3 \sin 3(\quad)\cdot(+8{\cdot}121094 +1{\cdot}224610 \cos 2\chi +3{\cdot}222656 \cos 4\chi$$
$$-12{\cdot}56836 \cos 6\chi)$$
$$+P_7^4 \sin 4(\quad)\cdot(\qquad -0{\cdot}2578125 \sin 2\chi +2{\cdot}34375 \sin 4\chi$$
$$+1{\cdot}523438 \sin 6\chi)$$
$$+P_7^5 \sin 5(\quad)\cdot(+0{\cdot}2255860 +0{\cdot}005371092 \cos 2\chi +0{\cdot}6103516 \cos 4\chi$$
$$+0{\cdot}1586914 \cos 6\chi)$$
$$+P_7^6 \sin 6(\quad)\cdot(\qquad -0{\cdot}01074219 \sin 2\chi -0{\cdot}09765624 \sin 4\chi$$
$$-0{\cdot}01464844 \sin 6\chi)$$
$$+P_7^7 \sin 7(\quad)\cdot(+0{\cdot}01611328 -0{\cdot}002685547 \cos 2\chi -0{\cdot}01220704 \cos 4\chi$$
$$-0{\cdot}001220703 \cos 6\chi)$$

$$\mathfrak{B}_7^5 = P_7 \qquad (-2030{\cdot}274 \sin \chi -2679{\cdot}962 \sin 3\chi +3492{\cdot}070 \sin 5\chi$$
$$-1055{\cdot}743 \sin 7\chi)$$
$$+P_7^1 \cos (\quad)\cdot(-72{\cdot}50980 \cos \chi -287{\cdot}1387 \cos 3\chi +623{\cdot}5840 \cos 5\chi$$
$$-263{\cdot}9356 \cos 7\chi)$$
$$+P_7^2 \cos 2(\quad)\cdot(-72{\cdot}50980 \sin \chi -67{\cdot}35350 \sin 3\chi +13{\cdot}85742 \sin 5\chi$$
$$+29{\cdot}32617 \sin 7\chi)$$
$$+P_7^3 \cos 3(\quad)\cdot(-4{\cdot}350588 \cos \chi -13{\cdot}82520 \cos 3\chi +15{\cdot}24317 \cos 5\chi$$
$$+2{\cdot}932615 \cos 7\chi)$$
$$+P_7^4 \cos 4(\quad)\cdot(-1{\cdot}450195 \sin \chi +0{\cdot}3544922 \sin 3\chi -3{\cdot}149414 \sin 5\chi$$
$$-0{\cdot}2666016 \sin 7\chi)$$
$$+P_7^5 \cos 5(\quad)\cdot(-0{\cdot}2014160 \cos \chi -0{\cdot}3249512 \cos 3\chi -0{\cdot}4514160 \cos 5\chi$$
$$-0{\cdot}0222168 \cos 7\chi)$$
$$+P_7^6 \cos 6(\quad)\cdot(-0{\cdot}0402832 \sin \chi +0{\cdot}08862304 \sin 3\chi +0{\cdot}05249024 \sin 5\chi$$
$$+0{\cdot}001708984 \sin 7\chi)$$

$$+P_7^7\cos 7\,(-0{\cdot}0201416\cos\chi+0{\cdot}01477051\cos 3\chi+0{\cdot}005249024\cos 5\chi$$
$$+0{\cdot}0^31220703\cos 7\chi)$$

$$\mathfrak{A}_7^6=P_7\qquad(-10557{\cdot}42\cos\chi+19003{\cdot}36\cos 3\chi-10557{\cdot}42\cos 5\chi$$
$$+2111{\cdot}486\cos 7\chi)$$
$$+P_7^1\cos\ (\ )\cdot(+377{\cdot}0508\sin\chi-2036{\cdot}074\sin 3\chi+1885{\cdot}254\sin 5\chi$$
$$-527{\cdot}8712\sin 7\chi)$$
$$+P_7^2\cos 2\,(\ )\cdot(-377{\cdot}0508\cos\chi+477{\cdot}5976\cos 3\chi-41{\cdot}89456\cos 5\chi$$
$$-58{\cdot}65232\cos 7\chi)$$
$$+P_7^3\cos 3\,(\ )\cdot(+22{\cdot}62305\sin\chi-98{\cdot}03320\sin 3\chi+46{\cdot}08400\sin 5\chi$$
$$+5{\cdot}865232\sin 7\chi)$$
$$+P_7^4\cos 4\,(\ )\cdot(-7{\cdot}541016\cos\chi-2{\cdot}513672\cos 3\chi+9{\cdot}521484\cos 5\chi$$
$$+0{\cdot}5332032\cos 7\chi)$$
$$+P_7^5\cos 5\,(\ )\cdot(+1{\cdot}047363\sin\chi-2{\cdot}304199\sin 3\chi-1{\cdot}364746\sin 5\chi$$
$$-0{\cdot}0444336\sin 7\chi)$$
$$+P_7^6\cos 6\,(\ )\cdot(-0{\cdot}2094726\cos\chi-0{\cdot}6284180\cos 3\chi-0{\cdot}1586914\cos 5\chi$$
$$-0{\cdot}003417969\cos 7\chi)$$
$$+P_7^7\cos 7\,(\ )\cdot(+0{\cdot}1047363\sin\chi+0{\cdot}1047364\sin 3\chi+0{\cdot}01586914\sin 5\chi$$
$$+0{\cdot}0^32441406\sin 7\chi)$$

$$\mathfrak{B}_7^6=P_7^1\sin\ (\ )\cdot(-4524{\cdot}608\sin 2\chi+3619{\cdot}688\sin 4\chi-904{\cdot}9219\sin 6\chi)$$
$$+P_7^2\sin 2\,(\ )\cdot(-335{\cdot}1562\cos 2\chi+536{\cdot}25\cos 4\chi-201{\cdot}0938\cos 6\chi)$$
$$+P_7^3\sin 3\,(\ )\cdot(-63{\cdot}67969\sin 2\chi-13{\cdot}40625\sin 4\chi+30{\cdot}16406\sin 6\chi)$$
$$+P_7^4\sin 4\,(\ )\cdot(-13{\cdot}40625\cos 2\chi+9{\cdot}75\cos 4\chi+3{\cdot}65625\cos 6\chi)$$
$$+P_7^5\sin 5\,(\ )\cdot(-0{\cdot}2792968\sin 2\chi-2{\cdot}539062\sin 4\chi-0{\cdot}3808595\sin 6\chi)$$
$$+P_7^6\sin 6\,(\ )\cdot(-0{\cdot}5585936\cos 2\chi-0{\cdot}40625\cos 4\chi-0{\cdot}03515625\cos 6\chi)$$
$$+P_7^7\sin 7\,(\ )\cdot(+0{\cdot}1396484\sin 2\chi+0{\cdot}05078125\sin 4\chi+0{\cdot}002929688\sin 6\chi)$$

$$\mathfrak{A}_7^7=P_7^1\sin\ (\ )\cdot(-10557{\cdot}42+15836{\cdot}13\cos 2\chi-6334{\cdot}453\cos 4\chi$$
$$+1055{\cdot}742\cos 6\chi)$$
$$+P_7^2\sin 2\,(\ )\cdot(\qquad -1173{\cdot}047\sin 2\chi+938{\cdot}4376\sin 4\chi$$
$$-234{\cdot}6093\sin 6\chi)$$
$$+P_7^3\sin 3\,(\ )\cdot(-211{\cdot}1484+222{\cdot}8789\cos 2\chi+23{\cdot}46094\cos 4\chi$$
$$-35{\cdot}19140\cos 6\chi)$$
$$+P_7^4\sin 4\,(\ )\cdot(\qquad -46{\cdot}92188\sin 2\chi+17{\cdot}0625\sin 4\chi$$
$$+4{\cdot}265624\sin 6\chi)$$
$$+P_7^5\sin 5\,(\ )\cdot(-5{\cdot}865236+0{\cdot}9775388\cos 2\chi+4{\cdot}443360\cos 4\chi$$
$$+0{\cdot}4443360\cos 6\chi)$$
$$+P_7^6\sin 6\,(\ )\cdot(\qquad -1{\cdot}955078\sin 2\chi-0{\cdot}7109376\sin 4\chi$$
$$-0{\cdot}04101563\sin 6\chi)$$

$$\begin{aligned} &+P_7^7 \sin 7(\quad)\cdot(-0{\cdot}4189454 -0{\cdot}4887696 \cos 2\chi -0{\cdot}0886719 \cos 4\chi \\ &\qquad\qquad\qquad\qquad\qquad\qquad\qquad\qquad -0{\cdot}003417969 \cos 6\chi) \end{aligned}$$

$$\begin{aligned} \mathfrak{B}_7^7 = P_7 \qquad &(+73901{\cdot}96 \sin \chi -44341{\cdot}18 \sin 3\chi +14780{\cdot}39 \sin 5\chi \\ &\qquad\qquad\qquad\qquad\qquad\qquad -2111{\cdot}486 \sin 7\chi) \end{aligned}$$

$$\begin{aligned} &+P_7^1 \cos\ (\quad)\cdot(+2639{\cdot}357 \cos \chi -4750{\cdot}840 \cos 3\chi +2639{\cdot}355 \cos 5\chi \\ &\qquad\qquad\qquad\qquad\qquad\qquad\qquad\qquad -527{\cdot}8712 \cos 7\chi) \end{aligned}$$

$$\begin{aligned} &+P_7^2 \cos 2(\quad)\cdot(+2639{\cdot}357 \sin \chi -1114{\cdot}394 \sin 3\chi +58{\cdot}65234 \sin 5\chi \\ &\qquad\qquad\qquad\qquad\qquad\qquad\qquad\qquad +58{\cdot}65234 \sin 7\chi) \end{aligned}$$

$$\begin{aligned} &+P_7^3 \cos 3(\quad)\cdot(+158{\cdot}3614 \cos \chi -228{\cdot}744 \cos 3\chi +64{\cdot}51758 \cos 5\chi \\ &\qquad\qquad\qquad\qquad\qquad\qquad\qquad\qquad +5{\cdot}865234 \cos 7\chi) \end{aligned}$$

$$\begin{aligned} &+P_7^4 \cos 4(\quad)\cdot(+52{\cdot}787112 \sin \chi +5{\cdot}865234 \sin 3\chi -13{\cdot}33008 \sin 5\chi \\ &\qquad\qquad\qquad\qquad\qquad\qquad\qquad\qquad -0{\cdot}5332032 \sin 7\chi) \end{aligned}$$

$$\begin{aligned} &+P_7^5 \cos 5(\quad)\cdot(+7{\cdot}331544 \cos \chi -5{\cdot}376464 \cos 3\chi -1{\cdot}910644 \cos 5\chi \\ &\qquad\qquad\qquad\qquad\qquad\qquad\qquad\qquad -0{\cdot}04443359 \cos 7\chi) \end{aligned}$$

$$\begin{aligned} &+P_7^6 \cos 6(\quad)\cdot(+1{\cdot}466309 \sin \chi +1{\cdot}466309 \sin 3\chi +0{\cdot}2221680 \sin 5\chi \\ &\qquad\qquad\qquad\qquad\qquad\qquad\qquad\qquad +0{\cdot}003417969 \sin 7\chi) \end{aligned}$$

$$\begin{aligned} &+P_7^7 \cos 7(\quad)\cdot(+0{\cdot}7331544 \cos \chi +0{\cdot}2443848 \cos 3\chi +0{\cdot}02221680 \cos 5\chi \\ &\qquad\qquad\qquad\qquad\qquad\qquad\qquad\qquad +0{\cdot}0^32441406 \cos 7\chi) \end{aligned}$$

15. Appendix I—Expression of $\overline{P}_n^m(\cos\theta)$ in sine and cosine-functions of multiples of θ.

Addition theorem of zonal harmonics is known in the form of (10.16), while our formula takes the form of (13.6 a). Therefore, comparing the two formulae we have the expression of Legendre's associated functions in sine and cosine-functions of multiples of θ. The results are as follows:[7]

$$\overline{P}_1^1(\cos\theta) = \sin\theta$$

$$\overline{P}_2^1(\cos\theta) = \frac{3}{2}\sin 2\theta$$

$$\overline{P}_2^2(\cos\theta) = \frac{3}{2}(-\cos 2\theta + 1)$$

$$\overline{P}_3^1(\cos\theta) = \frac{3}{2^3}(5\sin 3\theta + \sin\theta)$$

---

[7] Formulae corresponding to the case $n \leq 4$ are found in JAHNKE-EMDE's famous "*Funktionentafeln,*" p. 177.

$$\overline{P}_3^2(\cos\theta)=\frac{3\cdot5}{2^2}(-\cos 3\theta+\cos\theta)$$

$$\overline{P}_3^3(\cos\theta)=\frac{3\cdot5}{2^2}(-\sin 3\theta+3\sin\theta)$$

$$\overline{P}_4^1(\cos\theta)=\frac{5}{2^4}(7\sin 4\theta+2\sin 2\theta)$$

$$\overline{P}_4^2(\cos\theta)=\frac{3\cdot5}{2^4}(-7\cos 4\theta+4\cos 2\theta+3)$$

$$\overline{P}_4^3(\cos\theta)=\frac{3\cdot5\cdot7}{2^3}(-\sin 4\theta+2\sin 2\theta)$$

$$\overline{P}_4^4(\cos\theta)=\frac{3\cdot5\cdot7}{2^3}(\cos 4\theta-4\cos 2\theta+3)$$

$$\overline{P}_5^1(\cos\theta)=\frac{3\cdot5}{2^7}(21\sin 5\theta+7\sin 3\theta+2\sin\theta)$$

$$\overline{P}_5^2(\cos\theta)=\frac{3\cdot5\cdot7}{2^5}(-3\cos 5\theta+\cos 3\theta+2\cos\theta)$$

$$\overline{P}_5^3(\cos\theta)=\frac{3\cdot5\cdot7}{2^5}(-9\sin 5\theta+13\sin 3\theta+6\sin\theta)$$

$$\overline{P}_5^4(\cos\theta)=\frac{3\cdot5\cdot7\cdot9}{2^4}(\cos 5\theta-3\cos 3\theta+2\cos\theta)$$

$$\overline{P}_5^5(\cos\theta)=\frac{3\cdot5\cdot7\cdot9}{2^4}(\sin 5\theta-5\sin 3\theta+10\sin\theta)$$

$$\overline{P}_6^1(\cos\theta)=\frac{3\cdot7}{2^8}(33\sin 6\theta+12\sin 4\theta+5\sin 2\theta)$$

$$\overline{P}_6^2(\cos\theta)=\frac{3\cdot5\cdot7}{2^8}(-33\cos 6\theta+6\cos 4\theta+17\cos 2\theta+10)$$

$$\overline{P}_6^3(\cos\theta)=\frac{5\cdot7\cdot9}{2^6}(-11\sin 6\theta+12\sin 4\theta+9\sin 2\theta)$$

$$\overline{P}_6^4(\cos\theta)=\frac{3\cdot5\cdot7\cdot9}{2^6}(11\cos 6\theta-26\cos 4\theta+5\cos 2\theta+10)$$

$$\overline{P}_6^5(\cos\theta)=\frac{3\cdot5\cdot7\cdot9\cdot11}{2^5}(\sin 6\theta-4\sin 4\theta+5\sin 2\theta)$$

$$\overline{P}_6^6(\cos\theta)=\frac{3\cdot5\cdot7\cdot9\cdot11}{2^5}(-\cos 6\theta+6\cos 4\theta-15\cos 2\theta+10)$$

$$\overline{P}_7^1(\cos\theta)=\frac{7}{2^{10}}(429\sin 7\theta+165\sin 5\theta+81\sin 3\theta+25\sin\theta)$$

$$\overline{P}_7^2(\cos\theta)=\frac{7\cdot9}{2^9}(-143\cos 7\theta+11\cos 5\theta+57\cos 3\theta+75\cos\theta)$$

$$\overline{P}_7^3(\cos\theta)=\frac{5\cdot7\cdot9}{2^9}(-143\sin 7\theta+121\sin 5\theta+117\sin 3\theta+45\sin\theta)$$

$$\overline{P}_7^4(\cos\theta)=\frac{5\cdot7\cdot9\cdot11}{2^7}(13\cos 7\theta-25\cos 5\theta-3\cos 3\theta+15\cos\theta)$$

$$\overline{P}_7^5(\cos\theta)=\frac{3\cdot5\cdot7\cdot9\cdot11}{2^7}(13\sin 7\theta-43\sin 5\theta+33\sin 3\theta+25\sin\theta)$$

$$\overline{P}_7^6(\cos\theta)=\frac{3\cdot5\cdot7\cdot9\cdot11\cdot13}{2^6}(-\cos 7\theta+5\cos 5\theta-9\cos 3\theta+5\cos\theta)$$

$$\overline{P}_7^7(\cos\theta)=\frac{3\cdot5\cdot7\cdot9\cdot11\cdot13}{2^6}(-\sin 7\theta+7\sin 5\theta-21\sin 3\theta+35\sin\theta)$$

Appendix II—Notations used in this paper.

$\mathfrak{A}_n^m$ and $\mathfrak{B}_n^m$	Defined in (13.2), (13.6) and (13.7), and included in the expressions (14.1) and (14.2).
$e(N)$	$\begin{cases}=1 \text{ when } N \text{ is even}\\ =0 \quad \text{,,} \quad \text{odd}.\end{cases}$
ε_N	$\begin{cases}=2 \text{ when } N=0\\ =1 \quad \text{,,} \quad N\neq 0.\end{cases}$
$\varepsilon_{\kappa\gamma}$	$\begin{cases}=4 \text{ when } \kappa\neq 0,\ \gamma\neq 0\\ =2 \quad \text{,,} \quad \kappa=0,\ \gamma\neq 0 \text{ or } \kappa\neq 0,\ \gamma=0\\ =1 \quad \text{,,} \quad \kappa=0,\ \gamma=0\end{cases}$
$\langle N\rangle$	$\begin{cases}=N/2 \quad \text{when } N \text{ is even}\\ =(N-1)/2 \quad \text{,,} \quad \text{odd},\end{cases}$
$\theta_0, \varphi_0;\ \theta, \varphi$	Colatitudinal and azimuthal angle of original and transformed polar coordinates, respectively.
$\overline{P}_n^m(\zeta)$	Associated Legendre function in Ferrers' definition.
$P_n^m(\zeta)$	Associated Legendre function in Hobson's definition.
$P_n^{(m)}(\zeta)$	$=(d/d\zeta)^m P_n(\zeta)$
ϕ, χ, ψ	Eulerian angle (cf. Fig. 12).

Résumé

In this paper, the transformation of surface harmonics $Y_n(\theta_0, \varphi_0) = \overline{P}_n^m(\cos\theta_0)\exp(im\varphi_0)$ related to the rotation of coordinates system around its own origin is discussed, and the coefficients in the results are numerically computed, for the cases $n \leq 7$.

First, we considered a general transformation $T[\phi, \chi, \psi]$, in which the Eulerian angles are represented by ϕ, χ and ψ, and analysed it into elementary operations Φ, W and W' (§ 9).

Φ is a very simple operation representing the rotation of coordinate-axes arround z axis, and the result is obtained easily (§ 9.2). On the other hand, operation W is not so simple. By this rotation original axes x^*, y^*, z^* are transformed so that $x^* \rightarrow z$, $y^* \rightarrow x$, $z^* \rightarrow y$, and the surface harmonics $Y_n(\theta^*, \varphi^*)$ referred to (x^*, y^*, z^*) system, is expressed by the new coordinates θ, φ as follows;

$$Y_n(\theta^*, \varphi^*) = \sum_{\kappa=-n}^{n} w_\kappa(n, m)\, \overline{P}_n^\kappa(\cos\theta)\exp(i\kappa\varphi)\,.$$

The necessary procedure to obtain the coefficients $w_\kappa(n, m)$ are described in § 10, and the expressions obtained are (10.36), (10.38), (10.40), (10.41), (10.43) and (10.44), and the numerical values are tabulated in Tab. 1 for the cases $n \leq 7$.

W' is an inverse operation of W, and since we have already discussed W, we can easily get necessary formulae (§ 11).

With these calculations, the essential part of our study is completed. However, for convenience of practical application, we somewhat modified our transformation formulae (§ 12).

Next we separated the real and the imaginary parts (§ 13).

The results of numerical calculations are expressed in the next section (§ 14).

As appendices, expressions of Legendre's associated functions by means of sine- and cosine-functions of the multiples of θ, which are by-products of our study, are given (Appendix I). The notations used in this investigation are also to be found (Appendix II).

Our present task is composed of three parts, of which the first two parts were published as the first report. The whole contents are divided into the sections as shown below.

1 Introduction.
Part I Two-dimensional problem.
2 Transformation from polar to cartesian coordinates.

3 Translation of origin of polar coordinates.
4 Rotation of polar coordinates.
Part II Three-dimensional problem……(1).
5 Transformation from polar to cartesian coordinates.
5.1 Reduction of integration.
5.11 When $n-m$ is odd.
5.12 When $n-m$ is even.
6 Transformation from polar to cylindrical coordinates.
7 Translation of origin of polar coordinates.
Part III Three-dimensional problem……(2).
Transformation of surface harmonics related to the rotation of polar coordinates.
8 Rotation of polar coordinates.
9 Analysis into elementary transformations.
9.1 Relation between two coordinates systems.
9.2 Special transformation Φ, W and W'.
9.3 General transformation $T[\phi, \chi, \psi]$.
10 Operation W.
10.11 $(\cos\theta + i\sin\theta\cos\varphi)^m$.
10.12 $(d/d\cos\omega)^m\cos\gamma\omega$.
10.13 $P_n^{(m)}(\sin\theta\sin\varphi)$.
10.14 $P_n^{(r)}(0)$.
10.2 Explicit expression of operation W.
10.21 Fourier series representation of $Y_n(\theta^*, \varphi^*)$ with regard to φ.
10.22 Determination of $w_\kappa(n, m)$.
10.23 Numerical calculation of $w_\kappa(n, m)$.
10.3 Formulae expressing $w_\kappa(n, m)$ when m or κ is negative.
10.31 When m is zero.
11 Operation W'.
11.1 Formulae expressing $w_\kappa'(n, m)$ when κ is negative.
12 Modification of transformation formula.
13 Separation of real and imaginary parts.
14 Numerical expressions.
15 Appendix.

The writer is very much obliged to Mr. T. Takahashi who kindly read through the manuscript and pointed out some defects. It was also made known by him that the same problem had already been treated from the stand-point of the theory of rotation group. Since surface harmonics is the base of unitary representation, it is evident that the said treatment may also

be made use of in our problem. But the result has not yet been expressed in a form which may be easily used in our practical problems, although the fundamental theory is to be found in some books on the theory of groups.[8] Further, the writer wishes to offer his heartiest thanks to Prof. H. Kawasumi for his incessant instructions and encouragement.

---

17. 坐標變換にともなふ波動方程式の解の變換 II

地震研究所 佐藤泰夫

境界値問題をとく場合に我我が普通にとる方法は，問題の境界面上で坐標の一つが一定値をとるやうな坐標系をえらび，これによつて基本方程式の解を表はす，といふやり方である．所が，例へば一點より發生する彈性波動をあらはすには，この點を原點とする極坐標による解を採るのが便利であるが，この波に對するある平面の影響を求めようとすれば，上の解をカルト坐標によつて表現することが望ましい．このやうな理由から表題にあげた問題が，我我に密接な關係を持つて來るのである．

我我はかうした種類の問題を統一的，且綜合的に扱ふことを目的として，まづ第一報においては，第一部で

二次元の極坐標からカルト坐標へ（§2）
二次元極坐標の原點の移動（§3）
二次元極坐標の回轉（§4）

を，第二部では

球坐標よりカルト坐標へ（§5）
球坐標より圓壔坐標へ（§6）
球坐標の原點の移動（§7）

を扱つたのであつた．

本報告はその第三部をなすものであつて，球坐標の回轉によつて波動函數がいかに變換されるかが取扱はれてゐる．この場合原點よりの距離には變化がないから，波動函數とはいつても，要するに表面球函數 $\bar{P}_n^m(\cos\theta)\,{}^{\cos}_{\sin}\,m\phi$ の變換といふことになる．（§8）

もつとも一般的な回轉は，オイラーの角 ϕ, χ, ψ が勝手な値をとるものであるが，これを $T[\phi, \chi, \psi]$ であらはせば，$T[\phi, \chi, \psi]$ は簡單な基本的變換 Φ, W, W' にわけて考へることができる．ここに Φ は z 軸のまはりの單純な回轉を示すものであり，W は $x\rightarrow z$, $y\rightarrow x$, $z\rightarrow y$ とかはるやうな坐標軸の交換，W' はその逆變換を表してゐる．（§9.1〜9.2）

---

[8] e.g. H. WEYL, *Gruppentheorie und ihre Anwendungen auf die Quantenmechanik der Atomspektren* (1931).

T. YAMANOUCHI, *Kaiten-gun oyobi sono Hyôgen-ron* (1948) (In Japanese).

我我の當面の問題は $T[\phi, \chi, \psi]$ をいかにして Φ, W, W' に分解するか，といふ事と，基本的變換の性質を求める事，の二種類に分たれる．前者は §9.3 に，後者は §10 以下に扱はれてゐる．

球函數に關する一般的定理によつて，表面球函數はその軸をいかに回轉しても常にその位數が一定であることはよくしられているから，變換 W を行ふ前の天頂角および方位角を θ^*, ϕ^* とし，變換後のものを θ, ϕ とすれば

$$\overline{P}_n^m(\cos\theta^*)\exp(im\varphi^*)=\sum_{\kappa=-n}^{n} w_\kappa(n,m)\,\overline{P}_n^\kappa(\cos\theta)\exp(i\kappa\varphi)$$

と書くことができる．我我はいくらかの解析的なとり扱いによつて（§10.11〜§10.31）上の係數 $w_\kappa(n, m)$ を決定した（Tab. 1）

W' に關する公式は上の結果を變形すれば容易に求めることができる（§11).

以上によつて原理的には問題はとかれたわけであるが，實際的な取扱ひの便利のために公式の形を少しかへ（§12)，實數部と虚數部をわけて示した（§13).

最後の結果は m が偶數の場合と奇數の場合では形が少しことなり

$$m\text{ 偶數の時；}\begin{cases}\overline{P}_n^m(\cos\theta_0)\cos m\varphi_0=(-)^{m/2}\left[\cos m\phi\cdot\mathfrak{A}_n^m-\sin m\phi\cdot\mathfrak{B}_n^m\right]\\ \overline{P}_n^m(\cos\theta_0)\sin m\varphi_0=(-)^{m/2}\left[\cos m\phi\cdot\mathfrak{B}_n^m+\sin m\phi\cdot\mathfrak{A}_n^m\right]\end{cases}\qquad\ldots\ldots\ldots(14.1)$$

$$m\text{ 奇數の時；}\begin{cases}\overline{P}_n^m(\cos\theta_0)\cos m\varphi_0=(-)^{(m+1)/2}\left[\sin m\phi\cdot\mathfrak{A}_n^m+\cos m\phi\cdot\mathfrak{B}_n^m\right]\\ \overline{P}_n^m(\cos\theta_0)\sin m\varphi_0=(-)^{(m+1)/2}\left[\sin m\phi\cdot\mathfrak{B}_n^m-\cos m\phi\cdot\mathfrak{A}_n^m\right]\end{cases}\qquad\ldots\ldots\ldots(14.2)$$

となる．ここに $\mathfrak{A}_n^m$, $\mathfrak{B}_n^m$ は χ, ψ をパラメータとして含む表面球函數であり，その形は §14 に $n\leq 7$, $m\leq n$ の凡ての場合に對してあげてある．

なほつけたりとして $\overline{P}_n^m(\cos\theta)$ 函數を θ の倍角の sin, cos で表はした式を示す．

本論文は高橋健人氏の教示に負ふ所多く，河角廣教授にも亦懇切な御指導を給はつた．厚く感謝する次第である．

18. Electromagnetic Induction within the Earth and Its Relation to the Electrical State of the Earth's Interior. Part 1 (2)*

By Tsuneji RIKITAKE,

Earthquake Research Institute.

(Read Mar. 18, Apr. 16 and Sept. 16, 1947.—Received Sept. 18, 1947.)

CHAPTER VI. ELECTROMAGNETIC INDUCTION BY MAGNETIC VARIATION CONNECTED WITH SOLAR ERUPTION.

1. Radio fade-outs and magnetic variations connected with solar chromospheric eruptions.

On the basis of many data collected in the years 1935 and 1936, Dellinger[52] showed that sudden fade-outs of radio signals reflected from the ionosphere (the so-called Dellinger-effect) used to be accompanied by magnetic effects of special character. Meanwhile, according to solar observations, it was reported that many bright chromospheric eruptions were accompanied by the fade-outs reported by Dellinger. It is very likely, that, at the time of solar eruption, H-alpha light sent from the sun causes remarkable changes in the ionization of the ionosphere, especially in or just below the E-layer, and consequently the absorption of electric waves and variation in the earth's magnetic field both take place.

Although it is beyond the scope of this paper to discuss the general aspects of solar eruption and its allied phenomena, a brief description of the magnetic effect will be given here.

The magnetic effects connected with solar eruptions are of different type from the other magnetic disturbances such as bay-type disturbance, pulsation and sudden commencement of magnetic storm. According to magnetographic records accumulated up to this time, the disturbance begins suddenly reaching its maximum within several or scores of *minutes* and then decreases gradually.

---

*) Being continued from p. 98 of the Bulletin Vol. 28 parts 1-2 (1950).

[52] J. H. DELLINGER, *Terr. Mag.* 42 (1937), 49.

Its maximum magnitude usually amounts to scores of *gammas*. It seldom lasts over one *hour*. Changes in vertical intensity are generally small compared with that of the horizontal components.

As to the distribution of the disturbing forces, examination of the records from many observatories shows that nothing takes place at observatories situated in the dark hemisphere while magnetic effects at observatories situated in the sun-lit hemisphere are considerable. According to Fleming[53] and McNish[54], [55] who investigated the atmospheric current-systems by which the magnetic effect may be caused, it was established that the direction of this change roughly agreed with those of the diurnal variation expected at that time and the magnitude was roughly proportional to the magnitude of the diurnal variation departure. McNish showed clearly this character in several figures concluding that the magnetic effect accompanying the solar eruption is an augumentation of S_q. It is reasonable, when we bear the "dynamo"-theory of S_q in mind, that the increase in the electric conductivity of the ionosphere due to the abnormal ionization caused by the solar eruption permits an increase in the electric current-intensity then flowing.

Although the mechanism of occurrence of the magnetic effects accompanying the solar eruption was investigated rather lately, the existence of such magnetic variations was already known at the early period of this century. Birkeland[39] showed a kind of magnetic disturbance called "Cyclo-median storm." The magnetograms from many observatories showed clearly the same character as mentioned above. In spite of the fact that the relations to the solar phenomena and the fade-out were unknown at that time, we may presume that Birkeland's "Cyclo-median storm" was a magnetic effect associated with the solar eruption.

2. The analysis of the magnetic variation accompanied by solar eruption.

Since the disturbing forces of the magnetic variation caused by a solar eruption are not measurable in the dark hemisphere, while they increase towards the sub-solar point in the other hemisphere, it is obvious that a large number of spherical harmonics is needed to make an approximation of the field with a spherical harmonic expansion. In that case, accordingly, we must have more complete data from well-distributed observatories to make a spherical harmonic analysis than in the case of S_q in which we could express the field fairly well with only a few harmonic functions.

---

53) J. A. FLEMING, *Terr. Mag.* 41 (1936), 404.

54) A. G. MCNISH, *Terr. Mag.* 42 (1937), 109.

55) A. G. MCNISH, *Nature* 139 (1937), 244.

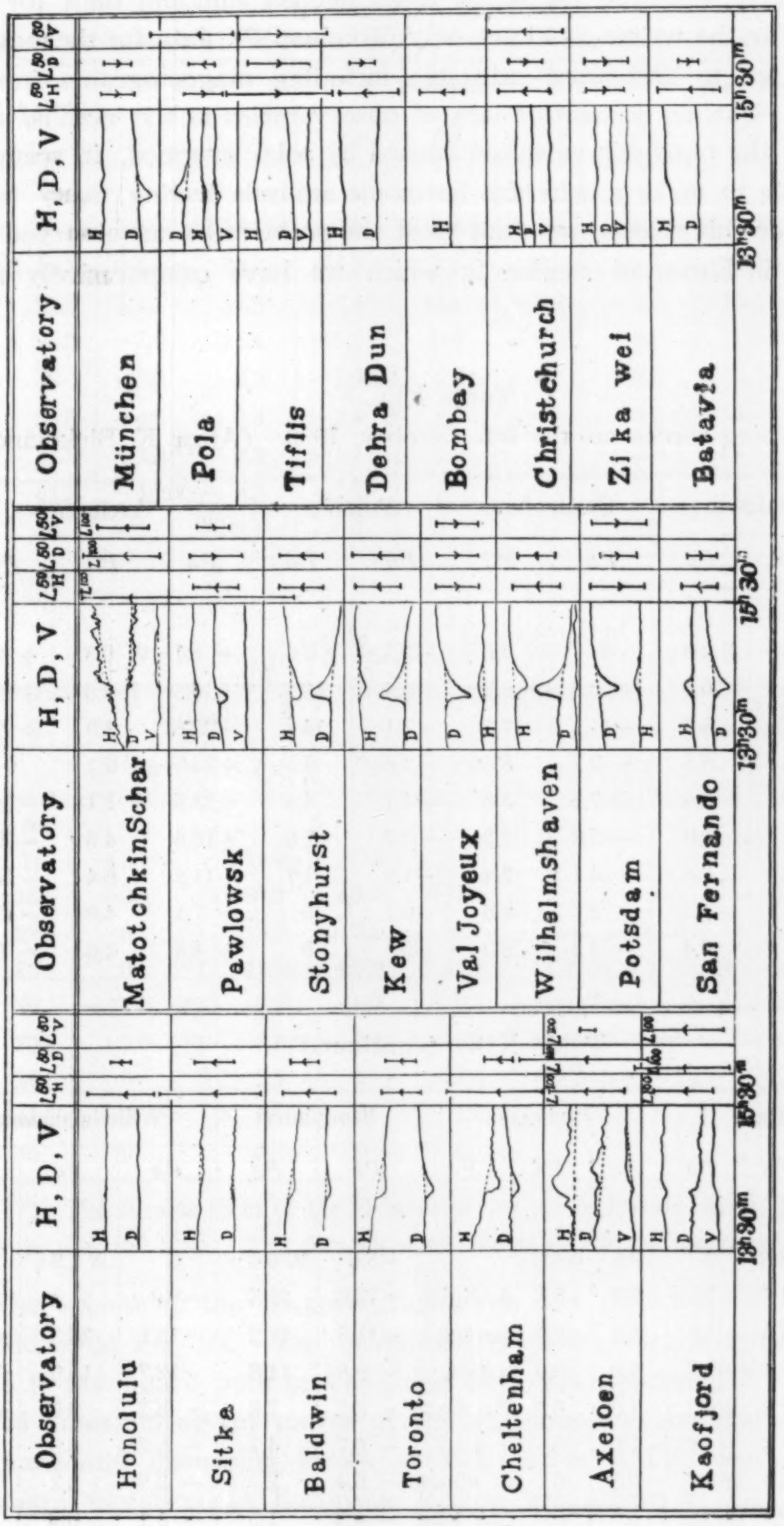

Fig. 25. The disturbance of Oct. 6, 1902. The scale value is given graphically by lines placed at the end of each curve. At the head of the column are the signs L_h^n, L_d^n and L_v^n, which indicate the length of a deflection in **H**, **D** and **V** respectively, corresponding to direction of increasing horizontal intensity, increasing westerly declination, and increasing vertical intensity. (After Birkeland)

Unfortunately, however, the writer could not get sufficient data for that purpose. So far the writer could get, only Birkeland's[39] data for the magnetic variation of Oct. 6, 1902 were utilizable including magnetograms from 23 observatories. But, on account of lack of observatories in the oceans, as in other cases of the magnetic variation caused by solar eruption, it seems almost impossible to make a spherical harmonic analysis having many higher harmonics. For this reason, we shall treat the problem as one observed on a plane surface in European Region in which we have comparatively many stations.

Table XIX.

The perturbing forces on the 6th October, 1902. (After K. Birkeland)

G.M.T.	Baldwin		Cheltenham		Toronto		Axeloren		
	Ph	*Pd*	*Ph*	*Pd*	*Ph*	*Pd*	*Ph*	*Pd*	*Pv*
h m									
14 15	−1.6 γ	E 3.9 γ	0	W 0.6 γ	−2.2 γ	E 0.6 γ	+ 8.1 γ	W 0.3 γ	+ 2.4 γ
18.8	−3.5	10.2	− 6.0 γ	E 6.5	−6.4	12.3	+16.5	E 0.6	+19.7
22.5	−4.4	8.7	−11.1	12.7	−7.1	14.4	+22.5	2.0	+17.2
26.3	−3.4	6.5	− 9.7	8.6	−2.6	8.5	+24.5	0.1	0
30	−2.0	5.0	− 7.5	5.6	−4.7	4.8	+23.5	W 1.1	−14.8
33.8	−1.1	3.0	− 5.9	5.2	−3.2	2.6	+16.4	4.6	−19.7
37.5	−0.6	2.5	− 4.1	2.4	−1.9	1.7	+11.2	6.4	−14.8
41.3	−0.1	1.3	− 2.7	0.8	−0.7	0	+ 7.1	4.9	−12.3
45	0	0.4	− 1.3	0.2	0	0	+ 4.5	2.6	− 9.8

Table XIX (continued)

G.M.T.	Kaafjord			Pawlowsk			Stonyhurst		Wilhelmshaven		
	Ph	*Pd*	*Pv*	*Ph*	*Pd*	*Pv*	*Ph*	*Pd*	*Ph*	*Pd*	*Pv*
h m											
14 15	−2.9 γ	W 3.3 γ	0	−0.5 γ	W 5.5 γ		−5.6 γ	W 9.4 γ	0	W 1.9 γ	0
18.8	−3.1	5.5	+1.1 γ	−5.5	5.5	A slight perturbation; *Pv* max = +3.7γ at about 14*h* 24*m*	−13.0	23.5	−6.2 γ	31.3	0
22.5	−1.9	0.5	+5.0	−5.0	2.8		−11.8	17.2	−13.1	28.3	−3.0 γ
26.3	+0.7	E 1.4	+7.2	−2.0	0.9		− 9.8	11.8	−12.7	16.6	−5.5
30	+1.0	2.2	+6.2	−1.0	0.5		− 8.2	7.8	− 8.2	9.6	−4.0
33.8	+1.2	3.0	+6.2	−1.0	0		− 6.7	4.7	− 5.2	4.9	0
37.5	+1.0	2.8	+6.2	−0.5	0		− 5.4	2.7	− 2.9	2.2	0
41.3	+0.2	2.7	+5.5	0	0		− 4.5	1.5	− 1.1	0.4	0
45	0	1.5	+1.0	0	0		− 3.9	0.8	− 0.6	0	0

Table XIX (continued)

G. M. T.	Kew		Potsdam			Val Joyeux		
	Ph	*Pd*	*Ph*	*Pd*	*Pv*	*Ph*	*Pd*	*Pv*
h *m*								
14 15	0	W16.1 γ	−0.6 γ	W10.4 γ	−0.6 γ	−2.1 γ	W 8.2 γ	
18.8	−4.4 γ	24.3	−4.4	25.5	0	−3.2	16.2	Perhaps a slight neg. deflection. The curve somewhat indistinct.
22.5	−7.1	17.3	−5.8	16.2	+0.6	−3.5	14.4	
26.3	−7.5	11.4	−5.1	9.6	+0.6	−3.5	7.9	
30	−6.2	8.2	−3.6	4.9	0	−3.3	5.3	
33.8	−4.8	5.4	−2.3	2.6	0	−3.1	3.4	
37.5	−4.4	3.8	−1.7	1.0	0	−2.5	2.1	
41.3	−4.1	2.8	−1.1	0	0	−2.3	1.4	
45	−3.5	2.1	−0.7	0	0	−1.8	0.8	

Table XIX (continued)

G. M. T.	Münich		Pola			San Fernando	
	Ph	*Pd*	*Ph*	*Pd*	*Pv*	*Ph*	*Pd*
h *m*							
14 15	+2.0 γ	W15.0 γ	+0.4 γ	0		0	0
18.8	+2.5	30.0	+1.8	W13.1 γ		+10.4 γ	W 27.2 γ
22.5	0 (*)	19.5	+3.9	22.7	From 14 *h* 16 *m* to 14 *h* 28 *m* a slight perturbation in V. At 14 *h* 20 *m* *Pv* max. = −2.1.	+10.3	25.9
26.3	0 (*)	11.3	+3.0	15.1		+ 4.5	14.9
30	+11.0 (*)	7.5	+0.4	9.3		+ 1.2	9.9
33.8	+3.0 (*)	3.8	+0.2	5.2		+ 0.5	6.2
37.5	0	2.2	0	2.6		0	3.2
41.3	0	0	0	1.0		0	1.5
45	0	0	0	0	.	0	0.7

(*) The curious form of the H-curve is due to a certain work going on in the Observatory at the time. The corresponding values of *Ph* are therefore rather uncertain.

The copies of the magnetographic records collected by Birkeland are reproduced in Fig. 25. The deviations from the normal curves which are shown in the figure with broken lines were also obtained by Birkeland at several times during the course of the variation as tabulated in Table XIX. The horizontal disturbing forces at 14 *h* 22.5 *m* GMT (nearly the time of maximum variation) in European Region are shown in Fig. 26 while the magnitudes in vertical intensity were reported from only five observatories, Kaafjord, Pawlowsk, Wilhelmshaven, Potsdam and Pola as shown in Fig. 28.

Taking into account the similarity of the field-distribution to that of S_q, we may draw equal variation line of X and Z as illustrated in Figs. 27 and 28.

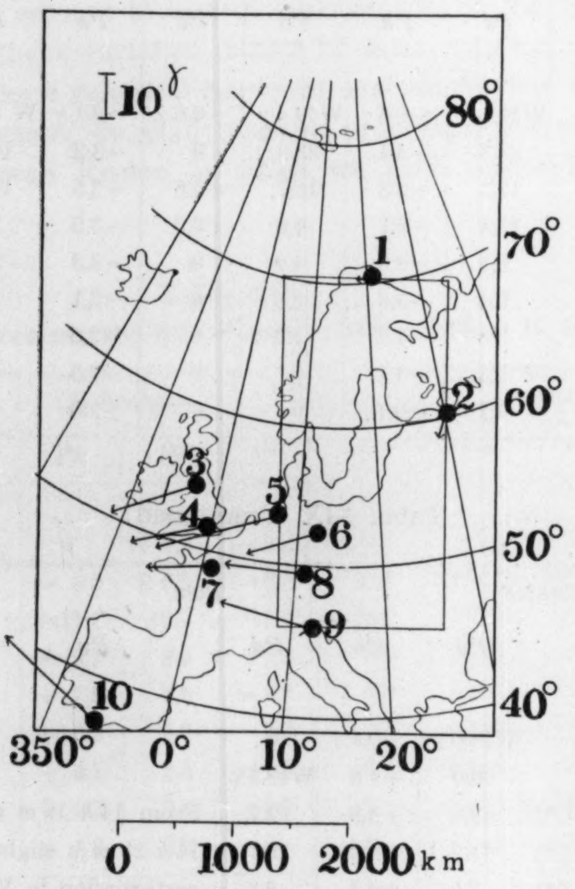

Fig. 26. The horizontal disturbing forces at 14 *h* 22.5 *m*. 1. Kaafjord. 2. Pawlowsk. 3. Stonyhurst. 4. Kew. 5. Wilhelmshaven. 6. Potsdam. 7. Val-Joyeux. 8. Münich. 9. Pola. 10 San Fernand.

In order to include five stations from which variation in the vertical intensity was reported, we shall study the rectangular area, as also shown in Fig. 26, with sides approximately 3000×1500 *km*. Owing to the shortage, however, of available data we shall merely estimate the first harmonic by means of Fourier analysis or practically least squares.

The magnetic potential of the variation is generally expressed as follows;

$$W=\sum_m\sum_n (e_{mm}e^{-kz}+i_{mm}e^{kz})\begin{matrix}\cos\\ \sin\end{matrix}\, mx\,\begin{matrix}\cos\\ \sin\end{matrix}\, ny\,, \quad\text{......................}(2.1)$$

where

$$k^2=m^2+n^2\ \text{..................................}(2.2)$$

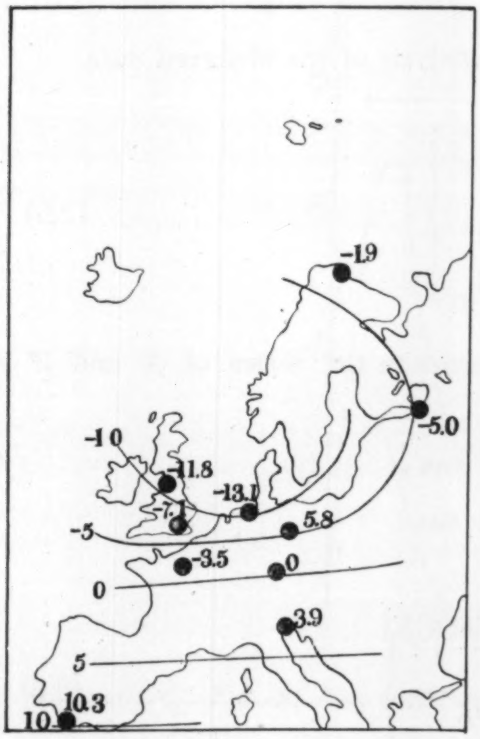

Fig. 27. Equal variation line for the north component at 14 *h* 22.5 *m*. (Unit: γ)

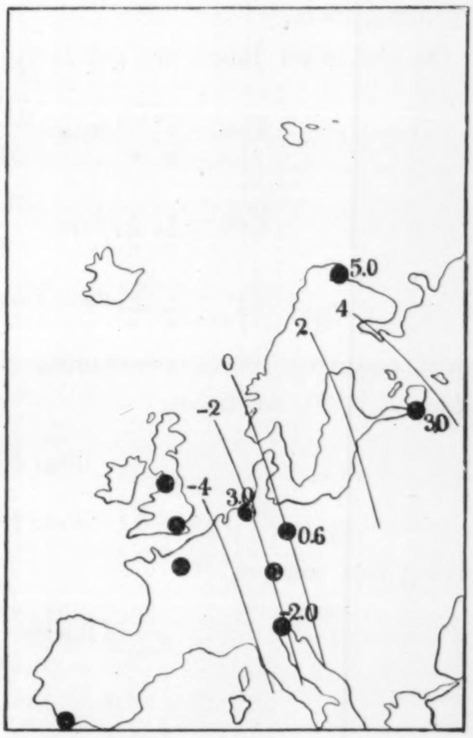

Fig. 28. Equal variation line for the vertical component at 14 *h* 22.5 *m*. (Unit: γ)

If we take x, y and z to the directions north-, east- and downwards, the terms involving negative indices of exponential correspond to the potential originating above the earth and positive indices to that within the earth. In that case, the components of the magnetic field are given by

$$\left.\begin{aligned} X &= -\sum_m \sum_n (e_{mn}e^{-kz} + i_{mn}e^{kz}) \frac{\partial V_{mn}}{\partial x}, \\ Y &= -\sum_m \sum_n (e_{mn}e^{-kz} + i_{mn}e^{kz}) \frac{\partial V_{mn}}{\partial y}, \\ Z &= -\sum_m \sum_n k(-e_{mn}e^{-kz} + i_{mn}e^{kz}) V_{mn}, \end{aligned}\right\} \quad \dots\dots\dots\dots\dots(2.3)$$

writing V_{mn} in place of the harmonic functions in (2.1). Then we get on the earth's surface

$$\left.\begin{aligned} X &= -\sum_m \sum_n (e_{mn} + i_{mn}) \frac{\partial V_{mn}}{\partial x}, \\ Y &= -\sum_m \sum_n (e_{mn} + i_{mn}) \frac{\partial V_{mn}}{\partial y}, \\ Z &= -\sum_m \sum_n k(-e_{mn} + i_{mn}) V_{mn}, \end{aligned}\right\} \quad \dots\dots\dots\dots\dots\dots\dots\dots(2.4)$$

by putting $z=0$.

On the other hand, we get from the analysis of the observed data

$$\left.\begin{aligned} X&=-\sum_m\sum_n a_{mn}\frac{\partial V_{mn}}{\partial x}, \\ Y&=-\sum_m\sum_n b_{mn}\frac{\partial V_{mn}}{\partial y}, \\ Z&=-\sum_m\sum_n c_{mn}V_{mn}. \end{aligned}\right\} \qquad \text{(2.5)}$$

Hence, equating the corresponding coefficients in the series of X and Z in (2.4) and (2.5), we have

$$e_{mn}+i_{mn}=a_{mn},$$

$$k(-e_{mn}+i_{mn})=c_{mn}.$$

Solving this we get

$$\left.\begin{aligned} e_{mn}&=\frac{a_{mn}-c_{mn}/k}{2}, \\ i_{mn}&=\frac{a_{mn}+c_{mn}/k}{2}. \end{aligned}\right\} \qquad \text{(2.6)}$$

Thus we can separate the coefficients of the magnetic potential into the external and internal parts. The same determination can also be done combining Y and Z.

In the case of the magnetic variation concerned here, the coefficients of $\frac{L}{\pi}\sin\frac{\pi}{L}x$ in Y and $\frac{L}{\pi}\cos\frac{\pi}{L}x$ in Z are determined at nine times during the course of the variation. L denotes the length of the sides parallel to x axis. Applying, then, the above mentioned theory, the coefficients of the magnetic potential are obtained as shown in Table XX and Fig. 29. As pointed out by Birkeland himself, since the variation at Kaafjord seemed to be affected by local irregularities during later periods in which $\triangle Z$ at Kaafjord amounted to several *gammas* while $\triangle Z$ was not measurable at other stations, the determined coefficients after 14 *h* 30 *m* seem to be less reliable.

Table XX. The coef. of the magnetic potential.

Time / Coef.	14*h*15*m*	18·8 *m*	22·5 *m*	26·3 *m*	30 *m*	33·8 *m*	37·5 *m*	41·3 *m*	45 *m*
$-e$	−0·4γ	3·2	6·6	6·5	4·3	2·7	2·5	1·6	0·4
$-i$	−0·5	2·1	2·8	2·0	0·8	0·1	−0·2	−0·8	0·0

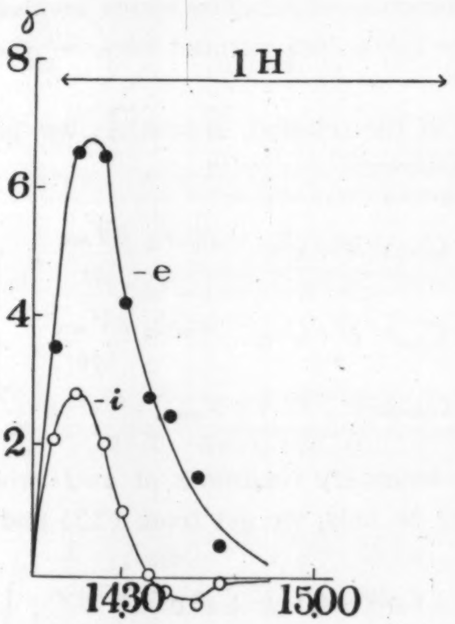

Fig. 29. The coefficients of the magnetic potential.

3. Theory of plane-earth induction and its relation to the electrical state of the earth's interior.

We shall discuss the electromagnetic induction within the plane-earth as shown in Fig. 30 where the superficial layer with thickness D is non-conducting while the deeper region has specific conductivity σ.

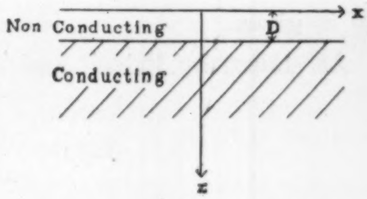

Fig. 30.

In the non-conducting region, the magnetic potential exists as is given by (2.1) having the components of the magnetic field expressed by (2.3). Meanwhile, we have vector potential $\vec{A}$ in the conducting region which satisfies in quasi-stationary state

$$\nabla^2\vec{A}=4\,\pi\sigma\,\frac{\partial\vec{A}}{\partial t}\,,\qquad\qquad(3.1)$$

provided $\mu=1$. Putting p in place of $\partial/\partial t$, (3.1) becomes in operational form

$$(\nabla^2-\kappa^2)\,\vec{A}=0\,,\qquad \kappa^2=4\,\pi\sigma p\qquad\qquad(3.2),\ (3.3)$$

The solution of (3.2) which is sufficient for the present problem is given by

$$\vec{A}=C_{mn}e^{-\sqrt{k^2+\kappa^2}\,z}\,[\,\vec{r}\ \mathrm{grad}\ V_{mn}]\,,\qquad\qquad(3.4)$$

where C_{mn} denotes a function of p. The terms involving positive indices of expotential must not be taken into account because they become infinite at $z \to \infty$.

Then with the aid of the relation $\overrightarrow{B} = \mathrm{rot}\,\overrightarrow{A}$, we get the components of the magnetic field as follows;

$$\left.\begin{aligned} X &= -C_{mn}\sqrt{k^2+\kappa^2}\, e^{-\sqrt{k^2+\kappa^2}\,z}\,\frac{\partial V_{mn}}{\partial x}, \\ Y &= -C_{mn}\sqrt{k^2+\kappa^2}\, e^{-\sqrt{k^2+\kappa^2}\,z}\,\frac{\partial V_{mn}}{\partial y}, \\ Z &= C_{mn}k^2\, e^{-\sqrt{k^2+\kappa^2}\,z}\, V_{mn}. \end{aligned}\right\} \qquad \ldots\ldots\ldots\ldots\ldots(3.5)$$

In order to satisfy the boundary conditions at $z=D$ where the continuity in the magnetic field must be held, we get from (2.3) and (3.5)

$$\left.\begin{aligned} \boldsymbol{e}\, e^{-kD} + \boldsymbol{i}\, e^{kD} &= C\sqrt{k^2+\kappa^2}\, e^{-\sqrt{k^2+\kappa^2}\,D}, \\ \boldsymbol{e}\, e^{-kD} - \boldsymbol{i}\, e^{kD} &= Cke^{-\sqrt{k^2+\kappa^2}\,D}. \end{aligned}\right\} \qquad \ldots\ldots\ldots\ldots\ldots\ldots(3.6)$$

abbreviating suffices m and n. Solving (3.6) we have

$$\boldsymbol{i}(t) = I(p)\, \boldsymbol{e}(t), \qquad I(p) = e^{-2kD}\,\frac{\sqrt{k^2+\kappa^2}-k}{\sqrt{k^2+\kappa^2}+k} \qquad \ldots\ldots\ldots\ldots\ldots\ldots(3.7)$$

by which we can estimate the change in the induced field when the inducing field is given.

As shown by Price[7] and already used in the previous chapter, we have

$$\begin{aligned} \boldsymbol{i}(t) &= \frac{d}{dt}\int_0^t \boldsymbol{e}(t-u)\, h(u)\, du \\ &= \boldsymbol{e}(t)\, h(0) + \int_0^t \boldsymbol{e}(t-u)\, h'(u)\, du \end{aligned} \qquad \ldots\ldots\ldots\ldots\ldots(3.8)$$

where $h(t)$ corresponds to $\boldsymbol{i}(t)$ when $\boldsymbol{e}(t)=0$ $(t<0)$ and $=1$ $(t>0)$. $h(u)$, then, is given by the contour integration

$$h(u) = \frac{1}{2\pi i}\int_L e^{pu}\, I(p)\,\frac{dp}{p} \qquad \ldots\ldots\ldots\ldots\ldots\ldots\ldots\ldots(3.9)$$

where L is Bromwich's path of integration having all sigularities in its left-hand-side on the complex plane.

At present, there is only one branch-point at $-\dfrac{k^2}{4\pi\sigma}$, real and negative. Then, the integration along L is equivalent to that as is shown in Fig. 31 in

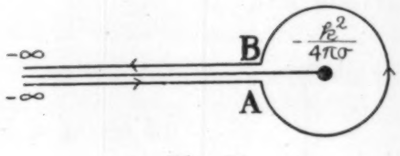

Fig. 31.

which a cut is made in the Riemann surface with straight line from $-\frac{k^2}{4\pi\sigma}$ to $-\infty$. With this convention the integrand is one-valued and analytic. Hence the integrals along $(-\infty)A$ and $B(-\infty)$ become respectively

$$\int_{(-\infty)A} = e^{-2kD}\int_{\infty}^{\frac{k^2}{4\pi\sigma}} e^{-qu}\frac{\sqrt{k^2-4\pi\sigma q}+k}{\sqrt{k^2-4\pi\sigma q}-k}\frac{dq}{q},$$

$$\int_{B(-\infty)} = e^{-2kD}\int_{\frac{k^2}{4\pi\sigma}}^{\infty} e^{-qu}\frac{\sqrt{k^2-4\pi\sigma q}-k}{\sqrt{k^2-4\pi\sigma q}+k}\frac{dq}{q},$$

and consequently

$$\int_{(-\infty)A} + \int_{B(-\infty)} = \frac{k}{\pi\sigma}e^{-2kD}\int_{\frac{k^2}{4\pi\sigma}}^{\infty}\frac{\sqrt{k^2-4\pi\sigma q}}{q^2}e^{-qu}\,dq.$$

Writing then β^2 in place of $q-\frac{k^2}{4\pi\sigma}$, we get

$$\int_{(-\infty)A} + \int_{B(-\infty)} = i8a\,e^{-2kD-\frac{k^2}{4\pi\sigma}u}\int_0^{\infty} e^{-u\beta^2}\frac{\beta^2 d\beta}{(\beta^2+\frac{k^2}{4\pi\sigma})^2}.\left(a^2=\frac{k^2}{4\pi\sigma}\right)$$

Meanwhile, the integral round the small circle AB vanishes when the radius of the circle reaches zero. Thus we get

$$h(u)=\frac{4a}{\pi}e^{-2kD-\frac{k^2}{4\pi\sigma}u}\int_0^{\infty} e^{-u\beta^2}\frac{\beta^2 d\beta}{(\beta^2-\frac{k^2}{4\pi\sigma})^2}. \text{ ....(3.10)}$$

By this expression, we can calculate $h(u)$ at any value of u with the aid of numerical integration.

On the other hand, however, we have more convenient expression for small value of u. Expanding $I(p)$ in a series of descending power of p, we obtain

$$I(p)=e^{-2kD}\left(1-2\sqrt{\frac{k^2}{4\pi\sigma}}\,p^{-\frac{1}{2}}-2\frac{k^2}{4\pi\sigma}p^{-1}......\right) \text{ ......(3.11)}$$

whence

$$h(u)=e^{-2kD}\left(1-\frac{2k}{\pi\sqrt{\sigma}}\sqrt{u}-\frac{k^2}{\pi\sigma}u\text{ ......}\right) \text{ ....(3.12)}$$

for small value of u.

For instance, $h(u)$ is obtained in four case, $D=200$ *km* $\sigma=5\times10^{-12}$*emu*, $D=200$ *km* $\sigma=10^{-13}$*emu*, $D=400$ *km* $\sigma=5\times10^{-12}$*emu* and $D=400$ *km* $\sigma=10^{-13}$*emu* as shown in Fig. 32.

$i(t)$, then may be obtained by integrating numerically (3.8). But, to a fair degree of approximation, $h'(u)$ is regarded as a constant for the small value of u when the process of calculation becomes easier. $i(t)$ which corresponds to $e(t)$ given by Table XX are calculated in the four cases mentioned above being shown in Fig. 33 together with the values obtained from the analysis. As easily seen in the figure, the cases in which D is assumed to be 200 *km* give larger values in the maximum amplitude than the values obtained from the observation while the cases in which D is assumed to be 400 *km* give roughly suitable values in their maximum magnitudes, decaying, however, more rapidly in the case $\sigma=10^{-13}$ *emu* and more slowly in the case $\sigma=5\times10^{-12}$ *emu*. Then we may approximately consider that D amounts to about 400 *km* and σ amounts to the order of 10^{-12}*emu* to make the results of theory agree with those of the analysis.

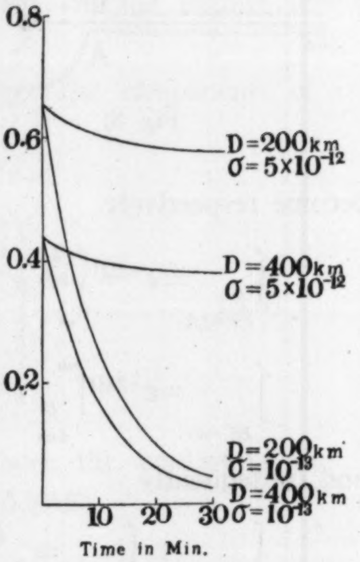

Fig. 32. $h(t)$ for various cases.

It is very interesting that the study of the magnetic variation which accompanies solar eruption shows us nearly the same electrical structure in the earth's interior which was already obtained in the cases of S_q, S_D, D_{st} and bay-type disturbance.

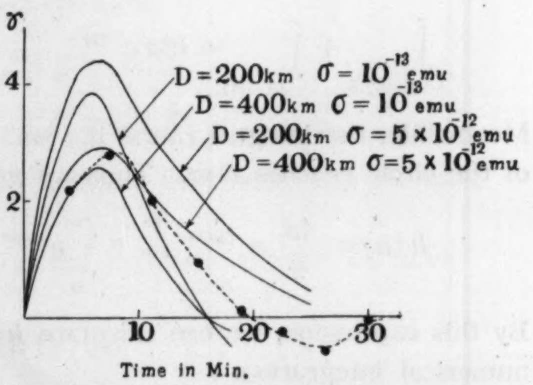

Fig. 33. The induced field expected from theory in various cases and the result from analysis (broken line).

Although in the present study the conductivity in the conducting region seems rather low, when compared with that obtained in the case of S_q, discussions about such detail will prove fruitless because we have only one example in this chapter and consequently can say nothing about the accuracy of the determination of the coefficients. Hence the present study merely shows that there are no serious objections to the electrical state of the earth's interior which was previously studied, leaving for the future more accurate research on the induction by the magnetic variation connected with solar eruption.

4. The distribution of the induced currents.

As the relation between the current-density $\overrightarrow{c}$ and the vector potential $\overrightarrow{A}$ is given by

$$\overrightarrow{c} = -\sigma \frac{\partial \overrightarrow{A}}{\partial t}, \qquad \text{.................................(4.1)}$$

substituting (3.4) in (4.1), we have in operational form

$$\overrightarrow{c} = -\sigma p C(p)\, e^{-\sqrt{k^2+\kappa^2}z}\, e(t)\, [\overrightarrow{r}\,\mathrm{grad} V_{mn}], \qquad \text{...........(4.2)}$$

where $C(p)$ is given by the solution of the simultaneous equations (3.6) as

$$C(p) = \frac{2e^{-(k-\sqrt{k^2+\kappa^2})D}}{k+\sqrt{k^2+\kappa^2}} \qquad \text{. ....(4.3)}$$

Taking into consideration, then, that $e(t)$ in Fig. 31 is expressible, to a fair degree of approximation, by

$$e(t) = Ate^{-\omega t}\,(t>0), \qquad =0\,(t<0)$$

preferring suitable values for A and ω $(A=-5{\cdot}1\times10^{-2}\,\gamma,\ \omega=2{\cdot}8\times10^{-3}\,sec^{-1})$. The operational form of $e(t)$ is given by

$$e(t) = \frac{Ap}{(p+\omega)^2} H(t), \qquad \text{........................(4.4)}$$

where $H(t)$ denotes Heaviside's unit function.

Hence the coefficient of $[\overrightarrow{r}$ grad $V_{mn}]$ in (4.2) can be written as follows;

$$c(t) = -2A\sigma e^{-kD} \frac{e^{-\sqrt{k^2+\kappa^2}(z-D)}}{k+\sqrt{k^2+\kappa^2}} \frac{p^2}{(p+\omega)^2} H(t) \qquad \text{...............(4.5)}$$

The solution of the operational equation (4.5), as often studied in the previous chapters, is given by a contour integral of the type

$$c(t) = -\frac{A\sigma e^{-kD}}{\pi i}\int_L \frac{e^{-\sqrt{k^2+\kappa^2}(z-D)}}{k+\sqrt{k^2+\kappa^2}} \frac{p}{(p+\omega)^2} e^{pt}\, dp, \qquad \text{............(4.6)}$$

where L is Bromwich's path of integration having all singularities on its left-hand-side. Then, taking into consideration the fact that we have a branch-point at $-\frac{k^2}{4\pi\sigma}$ and a double pole at $-\omega$, both real and negative ($\omega > \frac{k^2}{4\pi\sigma}$ in this case), the integration along L becomes equivalent with that along a contour, as shown in Fig. 34, where, making a cut with a straight line connecting $-\infty$ to the branch-point, the integrand is one-valued and analytic.

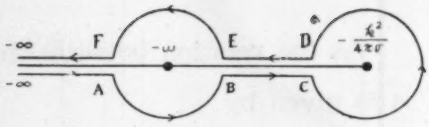

Fig. 34.

For the sake of brevity, however, we shall neglect to describe in detail the process of integration. Taking into consideration that $\int_{CD}$ vanishes when the radius attains to zero while $\int_{AB}+\int_{EF}$ does not, we get

$$c(t)=-A\sigma e^{-kD}\left[\left\{\frac{d}{dp}\frac{e^{pt-\sqrt{k^2+4\pi\sigma p}\,(z-D)}}{k+\sqrt{k^2+4\pi\sigma p}}\right\}_{p=-\omega}\right.$$

$$\left.-\frac{e^{-\frac{k^2t}{4\pi\sigma}}}{\pi^2\sigma}\int_0^\infty\frac{k\sin\sqrt{4\pi\sigma}\,(z-D)\,\beta+\sqrt{4\pi\sigma}\,\beta\cos\sqrt{4\pi\sigma}\,(z-D)\,\beta}{\left(\beta^2+\dfrac{k^2}{4\pi\sigma}-\omega\right)^2}e^{-t\beta^2}\beta d\beta\right] \qquad \ldots\ldots\ldots\ldots(4.7)$$

A more convenient expression for small value of t is also obtained in a similar way with (4.12) and (4.13), Chapter V. As to large value of p we get from (4.5)

$$c(t)\simeq-A\sqrt{\frac{\sigma}{\pi}}\,e^{-kD}(1/\sqrt{p}\,)\,e^{-(z-D)\sqrt{4\pi\sigma p}}\,H(t)\,.\ldots\ldots\ldots(4.8)$$

Solving (4.8), we have

$$c(t)\simeq-2\sigma Ae^{-kD}\left\{\frac{1}{\pi}\sqrt{\frac{t}{\sigma}}\,e^{-\frac{\pi\sigma(z-D)^2}{t}}-(z-D)\left(1-\text{erf.}\,(z-D)\sqrt{\frac{\pi\sigma}{t}}\right)\right\} \qquad \ldots\ldots\ldots\ldots(4.9)$$

56)

Taking, then, $\sigma=10^{-12}emu$, $t=360\ sec$, $D=400\ km$ and $k=\frac{\pi}{L}=1.05\times10^{-8}\ cm^{-1}$, the change in the current-density with depth is calculated as shown in Fig. 35 on an arbitrary scale. As seen in the figure the decay of the induced currents is so rapid that they become practically zero at the depth of 100 *km* beneath the surface of the core.

At the depth of z, consider, a current-sheet of infinitesimal thickness. The intensity of its own magnetic field just outside its surface is determined solely by the value and distribution of current-density $\vec{c}$ in the sheet. The magnetic field at any depth z_0 varies as $e^{-k(z-z_0)}$. Hence at the earth's surface the magnetic field

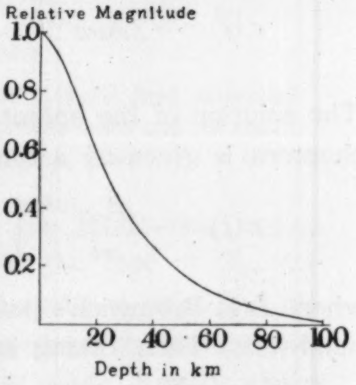

Fig. 35. The distribution of the induced currents in the earth.

---

56) See footnote (18), Chapter V.

due to the current-sheet is proportional to $|\overrightarrow{c}|e^{-kz}$. Thus we calculate the contribution of the currents of various depth to the magnetic field at the earth's surface, being expressed by almost the same curve with the current-distribution shown in Fig. 35 because the range of the depth in which the currents are flowing is comparatively small compared with its depth measured from the earth's surface.

In short, we may say that the determined conductivity corresponds to that just below the surface of the uniform core.

CHAPTER VII ELECTROMAGNETIC INDUCTION BY SUDDEN COMMENCEMENT OF MAGNETIC STORM.

1. The world-wide distribution of sudden commencements.

It is well known that magnetic storms often begin abruptly with an increase in horizontal intensity. In almost all cases, sudden changes stop within several minutes. Thus, it is of interest to study electromagnetic induction by such rapid variation in order to make clear the electrical state of the earth's interior in conjunction with slower variations already studied in the preceding chapters.

According to the investigations[57], [58], [59], [60], [61], [62], [63], [64], up to this time, sudden commencement occurs almost simultaneously all over the earth with an increase in horizontal intensity, while the changes in vertical intensity and declination depend on circumstances. On the basis of data collected by Bauer[58], as reproduced in Tables XXI, XXII and XXIII, some characters of this sudden commencement will be subsequently examined.

In the first place, we find as a whole that the order of magnitudes of increases in horizontal intensity or ΔH is roughly maintained throughout all storms, that is to say, the increases in horizontal intensity at some stations where the increases are larger or smaller than at other stations in case of storm seem

---

[57] L. A BAUER, *Terr. Mag.* 16 (1911), 85 and 163.

[58] L. A. BAUER, *Terr. Mag.* 15 (1910), 9 and 219.

[59] L. A. BAUER, and W. J. PETERS, *Terr. Mag.* 30 (1925), 45.

[60] L. RODÉS, *Terr. Mag.* 27 (1922) 161.

[61] G. ANGENHEISTER, *Nachrichten Ges. Wiss. Göttingen, Math.-Phys. Klasse,* 4 (1913) 565.

[62] R. L. FARIS, *Terr. Mag.* 15 (1910) 93, 213 and 16 (1911), 109.

[63] A. TANAKADATE, *Assemblée de Lisbonne* (1933), *Int. Geod. Geophys. Union, Associaiton Magn. Electr. Terr.* p. 149.

[64] W. ELLIS, *Proc. Roy. Soc. London* 102 (1892) 191.

Table XXI ΔH in γ (After L. A. Bauer)

Observatory	Geomagn. Latitude	Geomagn. Longitude	No. 1	No. 2	No. 3	No. 4	No. 5	No. 6	No. 7	No. 8	No. 9	No. 10	No. 11	No. 12	No. 13	No. 14	No. 15
Sitka	60·0	275·4	−12·9	12·9	27·3	23·0	19·1	16·5	—	47·2	29·3	105·5	37·2	—	113·0	10·9	64·2
Stonyhurst	57·0	82·5	57	25	40	50	30	25	—	45	—	150	10	78	85	−17	—
Copenhagen	55·7	98·6	—	—	—	—	45	—	—	—	6	136	−25	62	—	17	—
Greenwich	54·2	83·8	65	24	45	63	35	6	—	41	11	130	6	79	37	22	—
Kew	54·0	83·3	57	22	35	42	41	10	53	38	8	112	7	75	72	20	−420
Falmouth	54·0	77·9	50	19	34	55	20	10	34	37	6	100	6	60	65	19	—
Uccle	52·7	87·8	40	18	36	32	34	8	48	32	−6	110	−8	49	57	15	−354
Potsdam	52·5	97·1	−6	4	61	50	40	5	61	32	5	147	−14	64	55	12	21
Cheltenham	50·1	350·5	−23·5	8·7	10·0	23·2	18·0	17·7	−23·7	49·6	23·7	15·5	25·2	74·2	97·5	3·9	—
Baldwin	48·9	328·5	36·9	6·3	50·1	18·0	15·8	25·9	15·8	47·2	26·0	6·8	31·1	41·0	97·8	9·1	−150
Ekaterinburg	48	40	40	19	45	32	9	10	58	10	—	—	−6	35	15	5	17
München	48	93	39	14	43	22	26	13	31	30	5	90	4	47	51	9	−261
Pola	45·1	94·4	32·5	15·0	45·0	20·0	35·0	17·5	40·7	30·5	—	101·8	5·1	45·8	61·0	15·3	−262·1
Porto Rico	29·6	3·9	22·1	3·1	17·2	7·0	7·1	13·8	12·0	13·9	4·9	16·5	13·5	26·1	72·0	2·1	114
Helwan	27·2	106·4	—	—	—	—	25	25	35	29	19	115	26	45	72	26	86
Honolulu	21·1	266·5	19·4	8·6	42·3	18·5	18·4	14·1	15·1	18·6	19·0	21·7	22·0	30·2	55·0	2·5	95
Zi-ka-wei	19·9	189·5	24	12	63	34	34	20	—	19	22	93	16	34	68	21	143
Bombay	9·5	143·6	26	7	65	19	29	22	32	15	20	119	18	23	67	22	101
Samoa	−16·0	260·2	19·2	6·0	32·4	19·2	—	14·9	13·4	18·8	15·1	23·0	19·6	25·3	—	—	—
Batavia	−18·0	175·6	35	9	13	48	37	25	37	22	25	53	21	36	—	25	—
Pilar	−20·2	4·6	—	—	66	38	25	24	−28	8	16	50	22	57	35	25	54
Mauritius	−26·6	122·4	22	7	49	9	17	17	11	18	14	16	60	8	23	42	47

Table XXII ΔZ in γ (After L. A. Bauer)

Observatory	No. 1	No. 2	No. 3	No. 4	No. 5	No. 6	No. 7	No. 8	No. 9	No. 10	No. 11	No. 12	No. 13	No. 14	No. 15
Sitka	6·2	−0·6	8·7	0	7·9	4·7	—	5·1	3·7	20·3	3·8	—	34·5	3·0	—
Stonyhurst	—	—	—	—	—	—	—	—	—	—	—	—	—	—	—
Copenhagen	—	—	—	—	10	—	—	—	—	31	−7	14	—	—	—
Greenwich	9	0	0	17	0	4	9	4	−4	17	−4	13	9	4	—
Kew	10	5	—	10	0	6	20	6	0	0	0	0	10	0	—
Falmouth	8	0	4	8	2	1	18	5	−2	14	−2	6	4	2	—
Uccle	—	—	—	15	—	—	—	—	—	11	—	12	18	12	—
Potsdam	2	−1	−7	−2	−5	−5	−5	−5	−1	−27	−2	−7	−7	−3	−27
Cheltenham	−2·5	−1·6	2·9	−4·5	−4·8	1·9	−5·4	−1·6	1·2	6·0	0·9	−4·3	−5·5	0	−14·7
Baldwin	−3·4	−2·0	−3·0	3·0	−2·0	0	−11·2	7·6	−1·0	10·6	—	−5·0	−2·4	−1·2	−39
Ekaterinburg	2	5	−3	1	3	0	0	1	—	—	−3	−3	1	1	−9
München	—	—	—	—	—	—	—	—	—	—	—	—	—	—	—
Pola	—	—	—	9·6	—	9·6	—	−4·4	—	4·4	−24·0	9·6	−19·2	—	−16·9
Porto Rico	—	−2·5	15·4	−16·3	7·1	6·1	11·0	7·1	6·2	5·7	14·7	—	28·0	4·2	56·3
Helwan	—	—	—	—	−9	−12	−12	−12	−9	−39	−12	—	−24	−9	—
Honolulu	3·7	4·4	4·2	5·1	8·4	4·8	8·4	5·3	6·2	11·2	6·4	13·4	16·9	—	6·5
Zi-ka-wei	−2	−1	—	−10	—	−3	—	—	—	—	−3	−6	−7	−2	−26
Bombay	−4	0	−12	−1	−5	−4	−6	−2	−3	−14	−2	−3	−15	−2	−20
Samoa	—	—	—	—	4·5	4·7	—	—	2·9	5·8	3·0	4·0	—	—	—
Batavia	3	2	—	—	—	—	5	—	—	0	−7	2	—	3	36
Pilar	—	—	−2·8	−9·7	−1·0	−1·0	1·0	0·3	0·8	−1·0	−0·7	0·8	1·3	0·6	4·0
Mauritius	−9	−1	−13	−3	—	—	—	−2	−14	—	−6	−7	—	—	−50

Table XXIII Δt in *min.* (After L. A. Bauer)

Observatory	No. 1	No. 2	No. 3	No. 4	No. 5	No. 6	No. 7	No. 8	No. 9	No. 10	No. 11	No. 12	No. 13	No. 14	No. 15
Sitka	2·0	1·2	1·2	0·8	1·5	3·0	—	3·6	3·6	—	3·3	—	—	—	—
Stonyhurst	1·5	4	0·5	1	1	2	—	4	—	—	2	2	6	—	—
Copenhagen	—	—	—	—	—	—	—	—	—	—	—	—	—	—	—
Greenwich	—	7	4	—	—	—	—	—	—	—	—	—	5	—	—
Kew	2	7	4	2	4	1	12	5	1	—	1	1	5	—	—
Falmouth	2	10	3	1	1	1	3	3·5	0·5	—	—	4	6	—	—
Uccle	3	5·4	3·1	1·2	5·4	5·0	—	4·6	3·1	—	1·0	1·9	7·7	—	—
Potsdam	0·8	1·5	4·5	3·0	1·2	0·6	4·5	3·6	0·8	—	1·5	1·5	6·0	—	—
Cheltenham	0·5	1·5	0·6	0·8	0·8	2·4	0·8	3·7	3·6	—	2·4	3·0	9·0	—	—
Baldwin	3·0	1·2	1·8	0·8	1·0	3·6	0·6	4·5	3·9	—	3·6	4·5	6·0	—	—
Ekaterinburg	2·5	2·7	3·8	1·2	0·8	0·8	1·6	0·7	—	—	0·0	0·4	0·8	—	—
München	3·0	9·0	7·5	2·0	1·3	7·0	4·5	5·5	3·0	—	0·1	2·8	7·0	—	—
Pola	1·5	6·0	4·0	3·0	4·5	8·0	12·0	3·0	—	—	1·0	0·5	8·0	—	—
Porto Rico	0·9	2·1	1·5	0·8	0·9	4·5	1·5	2·4	3·6	—	4·5	1·8	9·9	—	—
Helwan	—	—	—	—	2	2	5	3	2	—	8	2	6	—	—
Honolulu	4·5	3·0	2·0	1·8	1·8	3·0	2·1	4·5	2·2	—	5·1	0·6	9·6	—	—
Zi-ka-wei	5	3	10	2	7	5	—	5	2	—	2	1	13	—	—
Bombay	4·0	2·5	9·2	1·8	6·3	6·8	3·8	4·0	3·5	—	6·3	1·5	10·7	—	—
Samoa	7	5	2	1	—	4	1	3	3	—	6	1	—	—	—
Batavia	3·9	2·4	3·0	4·0	4·0	4·0	3·6	4·2	3·6	—	2·4	3·0	—	—	—
Pilar	—	—	1·6	1·2	4·0	6·8	4·8	2·0	6·5	—	5·2	2·0	6·0	—	—
Mauritius	1	6	3	2	8	6	9	8	4	—	2	1	8	—	—

to be always larger or smaller at any time than those of the respective stations. For instance, taking the increase of No. 4 as abscissa and those of Nos. 2 and 13 as ordinate, we find that the relations mentioned above hold good in the main as shown respectively in Figs. 36 and 37.

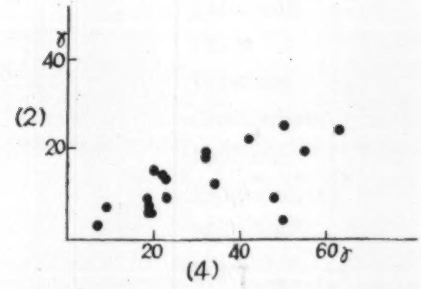

Fig. 36. Abscissa: ΔH for No. 4.
Ordinate: ΔH for No. 2.

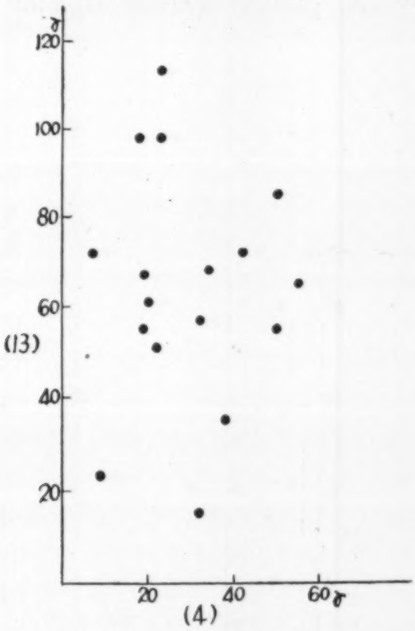

Fig. 37. Abscissa: ΔH for No. 4.
Ordinate: ΔH for No. 13.

In the second place, similar tendency is found in the changes in vertical intensity or ΔZ as shown in Figs. 38 and 39.

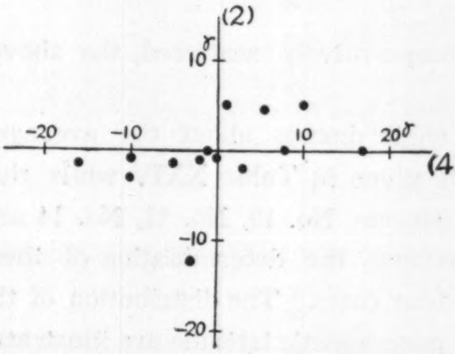

Fig. 38. Abscissa: ΔZ for No. 4.
Ordinate: ΔZ for No. 2.

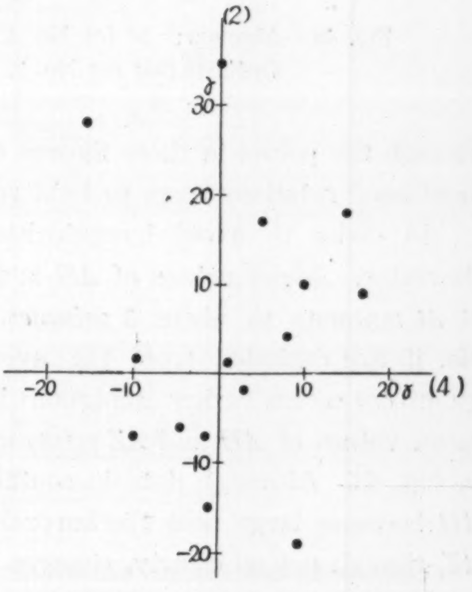

Fig. 39. Abscissa: ΔZ for No. 4.
Ordinate: ΔZ for No. 13.

In the third place, the duration-time of sudden commencements or Δt measured from the beginning to the first turning point is rather long in some storms in all the stations while in other storm it is comparatively short. Such relations, for instance, are shown in Figs. 40 and 41 in which Δt's of No. 2 and No. 13 are plotted against that of No. 4 with respect to each observatory.

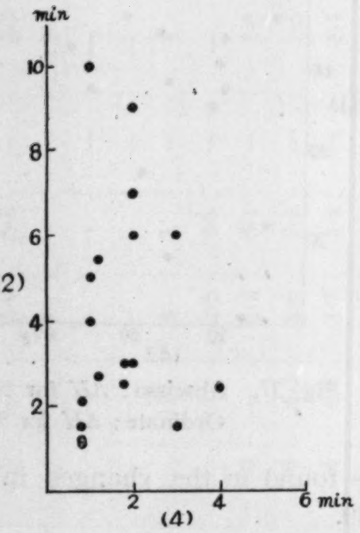

Fig. 40. Abscissa: Δt for No. 4.
Ordinate: Δt for No. 2.

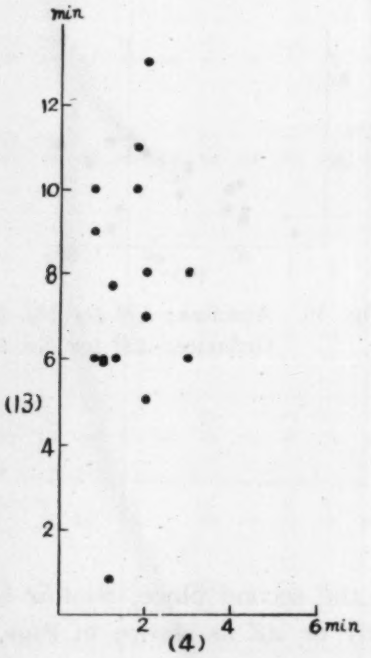

Fig. 41. Abscissa: Δt for No. 4.
Ordinate: Δt for No. 13.

Though the points in these figures seem comparatively scattered, the above-mentioned relations seem to hold roughly.

In order to avoid irregularities, we shall discuss about the averaged character. Mean values of ΔH and ΔZ are given in Table XXIV while that of Δt amounts to about 3 ***minutes***. The storms No. 10, No. 11, No. 14 and No. 15 are excluded from the average because the determination of these quantities seems rather ambiguous in these four cases. The distribution of the mean values of ΔH and ΔZ referred to the geomagnetic latitude are illustrated in Fig. 42. Although data in southern hemisphere are scarce, it seems that ΔH becomes large near the auroral zones and the geomagnetic equator, while ΔZ, though not so clearly, changes its sign at the geomagnetic equator. As fully studied in the investigation on the main phase of magnetic storm, these characters suggest that the sudden commencement is caused by the effect

Table XXIV. Mean value of ΔH and ΔZ.

Observatory	ΔH (γ)	ΔZ (γ)
Sitka	39	7
Stonyhurst	46	—
Copenhagen	38	6
Greenwich	37	5
Kew	38	6
Falmouth	33	4
Uccle	28	—
Potsdam	30	−4
Cheltenham	25	−2
Baldwin	34	−2
Ekaterinburg	24	1
München	27	—
Pola	32	−6
Porto Rico	18	7
Honolulu	23	7
Zi-ka-wei	31	−5
Bombay	29	−5
Samoa	18	4
Batavia	28	1
Pilar	26	−1
Mauritius	21	7

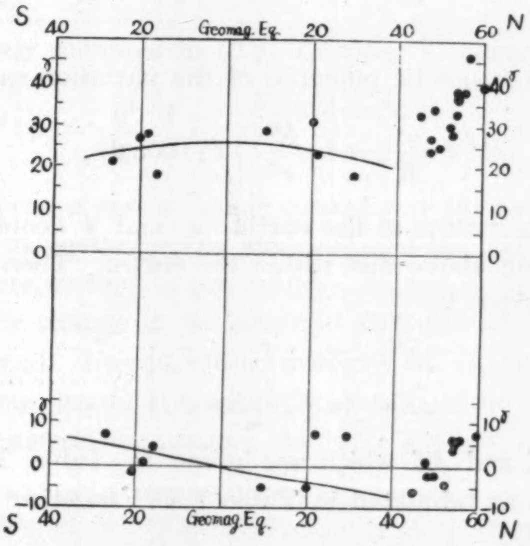

Fig. 42. The distribution of mean values of ΔH (upper) and ΔZ (lower) referred to geomagnetic coordinate. The curves show the first harmonic components in the low and middle latitude.

equivalent to the electric current concentrating above the auroral zones and the equator.

2. The analysis of sudden commencements.

As shown in Fig. 42, the greatest part of the magnetic potential of the variation can be expressed with the term including $P_1(\cos\theta)$, where θ denotes geomagnetic colatitude, the high latitudes being excluded. Limitting our discussions to the low and middle latitudes, we shall estimate the coefficients of the components of the magnetic field as follows. Taking into consideration the fact that the changes in declination are usually small, we may approximately regard $\varDelta H$ as the changes in geomagnetic north component $\varDelta X$. Using the data from observatories distributed between 30°N and 30°S except Honolulu and Porto Rico[65], the coefficients of $\sin\theta$ and $\cos\theta$ respectively in $\varDelta X$ and $\varDelta Z$ are obtained by means of least squares in every storm being shown in Table XXV.

Table XXV Coefficients in γ.

Storm Coef.	No. 1	No. 2	No. 3	No. 4	No. 5	No. 6	No. 7	No. 8	No. 9	No. 11	No. 12	No. 13
$-\Delta H$	26	8·2	47	26	26	21	25	19	19	26	34	61
$-\Delta Z$	6·1	3·2	25	15	11	10	8·7	3·2	4·5	9·5	11	17

In that case, the magnetic potential of the variation can be expressed by

$$R\left(e\frac{r}{R}+i\frac{R^2}{r^2}\right)P_1(\cos\theta),$$

where R denotes the radius of the earth. e and i denote respectively the coefficients originating above and within the earth. Then the magnetic field at the surface are given by

$$\left.\begin{aligned}\varDelta X&=-(e+i)\sin\theta,\\ \varDelta Z&=(e-2i)\cos\theta.\end{aligned}\right\}\quad\ldots\ldots\ldots\ldots\ldots\ldots\ldots\ldots(2.1)$$

Thus combining $\varDelta X$ and $\varDelta Z$ which are given in Table XXV, e and i are obtained from (2.1) as tabulated in Table XXVI together with the ratio e/i.

---

[65] The changes at both observatories are remarkably different from the general tendency, especially in vertical intensity. According to the writer's opinion, this may be due to the influence of the sea as will be studied later.

Table XXVI Coef. of the external and internal parts in γ.

Storm	No. 1	No. 2	No. 3	No. 4	No. 5	No. 6	No. 7	No. 8	No. 9	No. 11	No. 12	No. 13
$-e$	19	6·5	40	22	21	17	20	14	14	21	26	46
$-i$	6·7	1·7	7·3	3·7	5·0	3·7	5·3	5·3	4·7	5·3	7·7	15
e/i	2·8	3·8	5·5	5·9	4·2	4·6	3·8	2·6	3·0	4·0	3·4	3·1

Thus the most probable value of e/i becomes 3.9 ± 0.2. It is to be noted that e/i is considerably large when compared with that of any other variation studied before.

3. The relation to the electrical state of the earth's interior.

According to the theories of electromagnetic induction within a uniformly conducting sphere, the coefficient of the n-th order harmonics of the magnetic potential i_n originating within that sphere, as already studied in the previous chapters, is given by the operational equation of the type

$$i_n = I(p)\, e_n(t)\,, \qquad \text{(3.1)}$$

where e_n denotes the corresponding coefficient of the inducing field originating out of the sphere.

$I(p)$ was already obtained in (3.3), Chapter V, being given as

$$I(p) = \frac{q^3}{2}\left\{1 - \frac{F_1(\sqrt{4\pi\sigma p q a})}{F_0(\sqrt{4\pi\sigma p q a})}\right\} \qquad \text{(3.2)}$$

in the case $n=1$ where a and q denote respectively the radius of the sphere on whose surface the magnetic field is observed and the ratio of the radius of the conducting sphere to that of the former. F_0 and F_1 were already known[66].

The mode of the change in the external part differs from each other in every storm concerned. However, the gradient of change is steeper at the beginning, decreasing gradually with the lapse of time. For the sake of mathematical convenience, we assume that $e(t)$ goes on as

$$\left.\begin{aligned} e(t) &= A(1-e^{-\alpha t}) \quad (t>0)\,, \\ &= 0 \qquad\qquad\quad\; (t<0)\,. \end{aligned}\right\} \qquad \text{(3.3)}$$

---

[66] See the footnote on p. 95.

Preferring a suitable value to α, the course of assumed $e(t)$ is shown in Fig. 43. Writing (3.3) in operational form, we get

$$e(t) = \frac{A\alpha}{p+\alpha} H(t) \text{..........................} (3.4)$$

where $H(t)$ denotes Heaviside's unit function. Accordingly, we have an operational equation

$$i(t) = A \frac{\alpha I(p)}{p+\alpha} H(t)\,, \text{.....................} (3.5)$$

substituting (3.4) in (3.1).

Hence, in the same way as in the studies on the solutions of operational equations in Chapters IV, V and VI, we get the solution of (3.5) as follows;

$$i(t) = A \frac{q^3}{2} \Big[-\Big\{ 1 + \frac{3}{4\pi\sigma\alpha q^2 a^2} (\sqrt{4\pi\sigma\alpha}\,qa \coth \sqrt{4\pi\sigma\alpha}\,qa - 1) \Big\} e^{-\alpha t} + \frac{6\alpha}{\pi^2} \sum_{s=1}^{\infty} \frac{1}{s^2} \frac{e^{-\alpha_s t}}{\alpha - \alpha_s} \Big], \text{..............................} (3.6)$$

where α_s's are the successive roots of $\sin\sqrt{4\pi\sigma p}\,qa = 0$ except zero. A more convenient expression for the small value of t is also obtained as follows. Taking into consideration the asymptotic expansion of F_0/F_1 given in (3.15), Chapter II, (3.5) can be written as

$$\begin{aligned} i(t) &\simeq \alpha A \frac{q^3}{2} \Big\{ 1 - \frac{3}{\sqrt{4\pi\sigma}\,qa} p^{-\frac{1}{2}} + \frac{3}{4\pi\sigma q^2 a^2} p^{-1} \ldots \Big\} (p+\alpha)^{-1} H(t) \\ &\simeq A \frac{q^3}{2} \Big\{ \frac{\alpha}{p+\alpha} + \frac{3}{4\pi\sigma q^2 a^2} \Big(\frac{1}{p} - \frac{1}{p+\alpha} \Big) \\ &\qquad - \frac{3}{\sqrt{4\pi\sigma}\,qa} (\alpha p^{-\frac{3}{2}} - \alpha^2 p^{-\frac{5}{2}} + \ldots) \Big\} H(t)\,. \end{aligned}$$

Then the solution of this operational equation becomes

$$i(t) \simeq A \frac{q^3}{2} \Big[1 - e^{-\alpha t} - \frac{3}{4\pi\sigma\alpha q^2 a^2} (1 - \alpha t - e^{-\alpha t}) - \frac{4}{\sqrt{4\pi\sigma\alpha}\,qa} \sqrt{\frac{\alpha^3 t^3}{\pi}} \Big\{ 1 - \frac{2}{5} \alpha t + \ldots\ldots \Big\} \Big] \text{.........} (3.7)$$

for the small value of t.

With the aid of (3.6) or (3.7), $i(t)$ is estimated for several values of σ as shown in Fig. 43 whereas A is assumed to be 21 *gammas* corresponding to the mean magnitude of sudden commencements given in Table XXIV. It was assumed, besides, that $a = 6400\,km$, $\alpha = 0.04\,sec.^{-1}$ and $q = 1$.

As seen in the figure, the decay in the internal part becomes faster with decrease in conductivity, while the maxima in $e+i$ or ΔH occur 2 or 3 *minutes* after the beginnig. The ratio e/i amounts to about 4, 2.5 and less for $\sigma=10^{-15}$, 10^{-14} and 10^{-13} *emu* respectively at that moment. Comparing these values to that obtained from the analysis, it is reasonable to conclude that the conductivity in the earth approximately amounts to the order of 10^{-15} *emu.* Even if we take $q=0.9$, which is smaller than the determined value of q in the studies on the electromagnetic induction by various variations, σ hardly amounts to more than 10^{-14} *emu* for the explanation of the ratio.

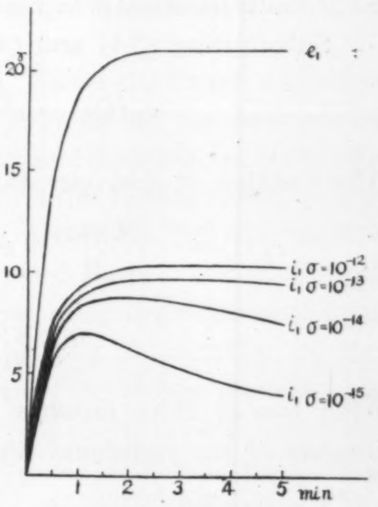

Fig. 43. The inducing and induced field for various cases.

The discrepancy between the electrical state of the earth obtained in the previous chapters in which σ amounts to $10^{-12}\sim10^{-13}$ *emu* below the depth of a few hundred *kilometers* and that obtained here is considerable, so that, taking into consideration the fact that the slower the change is the deeper the induced currents penetrate, we may presume the electrical conductivity near the earth's surface to be rather small because the greatest part of currents induced by sudden commencements flow in shallower zone than the induced currents in the cases of any other variation studied before. Hence, even in the superficial non-conducting layer reported in the studies of S_q, S_D, D_{st}, bay and magnetic variation connected with Dellinger effect, it is better to consider that the conductivity, though very low, has a finite value comparable with that of usual rock found on the earth's surface.

4. The distribution of the induced currents in the earth.

In order to examine the extent to which the induced currents penetrate, we shall study the distribution of the induced currents in the earth. The process of the calculation is just the same with Chapman and Prices'[8] investigation in the case of induction by D_{st} in which the components of the current-density are given by

$$c_r=0\,,\ c_\theta=0\,,\ c_\phi=-\sigma a\rho p C(p)\,F_1(k\rho a)\,e(t)\,P_1(\cos\theta)\,, \quad \ldots\ldots(4.1)$$

where

$$\rho=r/a$$

and

$$C(p)=\frac{1}{2}\,\frac{1}{F_0(kqa)} \quad \ldots\ldots\ldots\ldots\ldots\ldots\ldots\ldots\ldots(4.2)$$

as already mentioned in Section 4, Chapter V.

Substituting (3.4) and (4.2) in (4.1), we get

$$c_\phi(t) = -\frac{A\sigma a\alpha\rho}{2}\frac{p}{p+\alpha}\frac{F_1(k\rho a)}{F_0(kqa)}H(t)\,. \qquad \text{............}(4.3)$$

The solution of this operational equation is easily obtained as follows;

$$c_\phi(t) = -\frac{A\sigma a\alpha\rho}{2}\Bigg[e^{-\alpha t}\left\{\frac{F_1(k\rho a)}{F_0(kqa)}\right\}_{p=-\alpha}$$

$$+2\sum_{s=1}^{\infty}(-1)^{s+1}\frac{\alpha_s e^{-\alpha_s t}}{\alpha-\alpha_s}\{F_1(k\rho a)\}_{p=-\alpha_s}\Bigg] \qquad \text{.........}(4.4)$$

After two or three ***minutes*** past from the beginning the first term in the bracket of the righthand side of (4.4) almost decays out getting

$$c_\phi(t) = \frac{3A}{4\pi a\rho}\sum_{s=1}^{\infty}(-1)^s\frac{\alpha}{\alpha-\alpha_s}\left(\cos\sqrt{4\pi\sigma\alpha_s}\rho a - \frac{\sin\sqrt{4\pi\sigma\alpha_s}\rho a}{\sqrt{4\pi\sigma\alpha_s}\rho a}\right)e^{-\alpha_s t}\,.$$

$$\text{..................}(4.5)$$

Taking $t=180$ ***sec.*** and $\sigma=10^{-15}$ ***emu*** the distribution of the induced currents are shown in Fig. 44 against depth in arbitrary unit. $\rho^3|c_\phi|$, which is proportional to the contribution of the currents in an infinitesimally thin layer of radius ρa to the magnetic field at the earth's surface, is also shown in Fig. 45. As shown

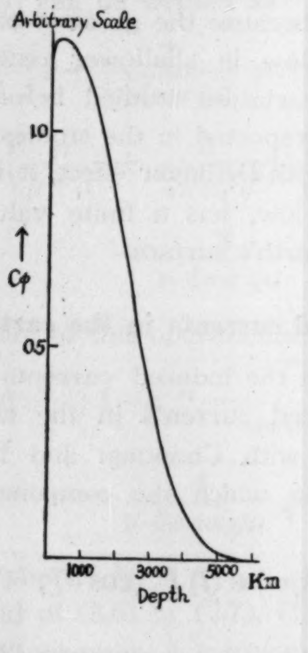

Fig. 44. The distribution of the induced currents in the earth.

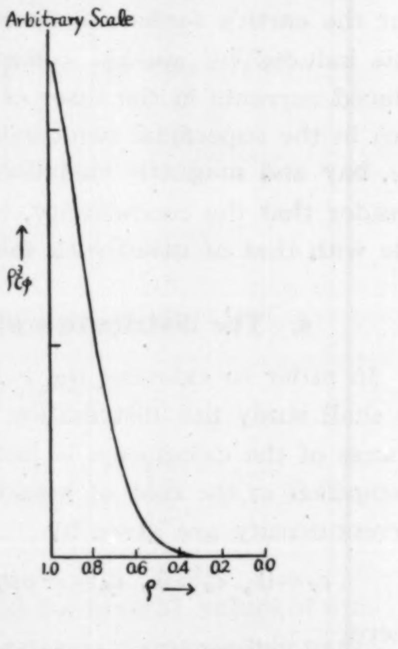

Fig. 45. The contribution of the induced currents to the magnetic field at the earth's surface.

in the figure, the contribution of the currents flowing in great depth is very small.

As will be discussed in the following Section, however, rapid variation such as sudden commencement is affected rather seriously by the presence of sea. Especially, in case of the distribution of the induced currents, we naturally presume that a considerable part may concentrate in the high conducting sea-water and consequently the remaining part which penetrates into the earth's interior becomes smaller than the estimate as mentioned above. Unfortunately, however, exact study is impossible owing to the irregular distribution of land and sea. In order to get some knowledge on the degree of partition of the induced currents in sea-water and the earth's interior, the writer assumes, as already done by Chapman, Price and Lahiri, that the earth is surrounded by a sea of uniform depth. In that case, regarding the sea as a thin, conducting shell having conductivity σ_0, depth D and radius a, the current-function J, as already obtained in (1.4), Chapter II, satisfies the next differential equation

$$\frac{1}{\sin\theta}\left\{\frac{\partial}{\partial\theta}\left(\sin\frac{\partial}{\partial\theta}\right)+\frac{1}{\sin\theta}\frac{\partial^2}{\partial\phi^2}\right\}J=a^2D\sigma_0\frac{\partial B_r}{\partial t}, \quad \text{............(4.6)}$$

where B_r denotes the normal component of magnetic induction. When J and B_r can be expressed by series involving spherical surface harmonic $S_n{}^m$ such as

$$\left.\begin{aligned} J&=\sum_n\sum_m K_n^m(t)\,S_n^m,\\ B_r&=\sum_n\sum_m M_n^m(t)\,S_n^m,\end{aligned}\right\} \quad \text{............................(4.7)}$$

we get from (4.6) by equating the corresponding terms of both sides

$$K_n^m=-\frac{a^2D\sigma_0}{n(n+1)}\frac{dM_n^m}{dt}. \quad \text{......................(4.8)}$$

In the case $n=1$, $m=0$, it becoms

$$K_1^0=-\frac{a^2D\sigma_0}{2}\frac{dM_1^0}{dt} \quad \text{..............................(4.9)}$$

and using (1.3), Chapter II, the components of current-density are given by

$$c_\theta=0, \quad c_\phi=\frac{aD\sigma_0}{2}\frac{dM_1^0}{dt}P_1(\cos\theta). \quad \text{..................(4.10)}$$

Meanwhile the magnetic potential due to this shell is given by

$$\left.\begin{aligned} W_e&=\ \ 4\pi\sum_n\sum_m\frac{n}{2n+1}K_n^m S_n^m,\\ W_i&=-4\pi\sum_n\sum_m\frac{n+1}{2n+1}K_n^m S_n^m,\end{aligned}\right\} \quad \text{......................(4.11)}$$

respectively just out- and inside of the shell. Putting (4.8) in (4.11), we get for $n=1$, $m=0$

$$\left.\begin{aligned} W_e &= -\frac{2}{3}\pi a^2 D\sigma_0 \frac{dM_1^0}{dt}, \\ W_i &= \frac{4}{3}\pi a^2 D\sigma_0 \frac{dM_1^0}{dt}. \end{aligned}\right\} \quad \text{.........................(4.12)}$$

Hence, taking into consideration that the magnetic potential of the variation is composed of the one due to this current-sheet and that due to the currents flowing inner region, we get for the case $n=1$, $m=0$

$$\left.\begin{aligned} ae &= ae' - W_i, \\ ai &= ai' + W_e, \end{aligned}\right\} \quad \text{.........................(4.13)}$$

where e and i denote, as often used in this paper, the coefficients of the magnetic potential originating out- and inside of the suface and e' and i' the respective coefficients just below the sea considered. As shown by (2.1), since $M_1^0 = -(e-2i)$, (4.13) can be written as

$$\left.\begin{aligned} e' &= e - \frac{4\pi a D\sigma_0}{3}\frac{d}{dt}(e-2i), \\ i' &= i - \frac{2\pi a D\sigma_0}{3}\frac{d}{dt}(e-2i). \end{aligned}\right\} \quad \text{.......................(4.14)}$$

Then considering (3.1) and (3.2), e' is given by the operational equation as follows;

$$e'(t) = \left[1 - \frac{4}{3}\pi a D\sigma_0 p\{1-2I(p)\}\right] e(t). \quad \text{.........(4.15)}$$

Further, taking into account (3.4), we get

$$e'(t) = \frac{A\alpha}{p+\alpha}\left[1 - \frac{4}{3}\pi\alpha D\sigma_0 p\{1-2I(p)\}\right] H(t). \quad \text{......(4.16)}$$

Then the current-density becomes for the inner region

$$c_{\phi\text{earth}} = -\sigma a\rho p C(p)\left[1 - \frac{4}{3}\pi a D\sigma_0 p\{1-2I(p)\}\right] \times \frac{A\alpha}{p+\alpha} F_1(k\rho a) H(t) P_1, \quad \text{....................(4.17)}$$

using e' in place of e in (4.1), while we also get for our sea from (4.10)

$$c_{\phi\text{sea}} = -\frac{aD\sigma_0 p}{2}\{1-2I(p)\}\frac{A\alpha}{p+\alpha} H(t) P_1. \quad \text{......(4.18)}$$

By solving the operational equations (4.17) and (4.18), we get the whole distribution of the induced currents.

The solution for the small value of t is obtained as follows. Putting $q=1$, the coefficients of P_1 in (4.17) and (4.18) for the large value of p are written respectively

$$c_{\text{sea}}\ (t) \simeq -\frac{\alpha A}{4}\frac{3}{\sqrt{\pi\sigma}}(p^{-\frac{1}{2}}-\alpha p^{-\frac{3}{2}}\ldots)\,H(t)\,, \qquad \text{.......................(4.19)}$$

$$c_{\text{earth}}(t) \simeq -\frac{\alpha A}{4}\frac{3}{\sqrt{\pi\sigma}}\frac{a}{\rho}\,p^{-\frac{1}{2}}e^{-\sqrt{4\pi\sigma}\,a(1-p)p^{\frac{1}{2}}}\left(1-2\sqrt{\frac{\pi}{\sigma}}\,D\sigma_0 p^{\frac{1}{2}}\ldots\right)H(t)\,.$$

$$\text{.......................(4.20)}$$

Applying the formulae of operational calculus, the solution of these equations are easily obtained for small t getting

$$c_{\text{sea}}\ (t) \simeq -\frac{\alpha A}{2}\frac{3}{\pi\sqrt{\sigma}}D\sigma_0 t^{\frac{1}{2}}\,, \qquad \text{..(4.21)}$$

$$c_{\text{earth}}(t) \simeq -\frac{\alpha A}{2}\frac{3}{\pi\sqrt{\sigma}}\frac{a}{\rho}\,\sigma\left\{t^{\frac{1}{2}}\,e^{-\frac{\pi\sigma a^2(1-\rho)^2}{t}}\right.$$

$$\left.-\pi\sqrt{\sigma}a(1-\rho)\left(1-\text{erf.}\,\frac{\sqrt{\pi\sigma}a(1-\rho)}{t^{\frac{1}{2}}}\right)\right\}. \qquad \text{.........(4.22)}$$

Roughly speaking, then, the current-density in the sea is σ_0/σ times larger compared with that in the earth at $\rho=1$. As σ_0/σ amounts to as much as the order of 10^4, we know that the greatest part of the induced currents are flowing in sea-water. For illustration, current-distribution and its contribution to the field at the surface are shown in Figs. 46 and 47 for the case $\sigma=10^{-15}$ ***emu***,

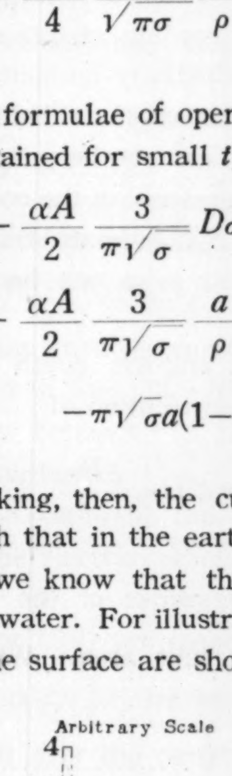

Fig. 46. The partition of the induced currents in the idealized sea and in the earth.

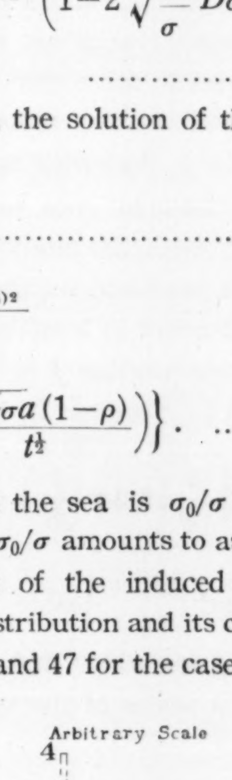

Fig. 47. The contribution of the induced currents in the idealized sea and in the earth to the magnetic field.

$\sigma_0=4\times 10^{-11}$ *emu* and $t=3$ *minutes.* Although the present calculation seems to be an over-estimate on acount of its neglect of ocean boundaries, we may say that the conductivity obtained in this chapter is reliable as regards the shallow part of the earth.

5. The influences of the oceans.

Since, in the case of sudden commencement of magnetic storm, the rate of time-change in the earth's magnetic field is considerably larger than in the cases of any other variations treated in the preceding chapters, the electric currents induced in sea-water in which the conductivity amounts to the order of 10^{-11} *emu* will become more intense than the currents induced by more slower variations. In order to study, to what extent the magnetic field of sudden commencement may be affected by the presence of the oceans, we shall, in similar way with the study in the case of S_q, estimate the order of the magnetic field produced by the currents flowing in a sea bounded by two meridians $\pi/2$ apart in longitude.

The current-function J in such a sea with uniform depth D is already obtained in (1.4), Chapter II, being given by the solution of

$$\frac{1}{\sin\theta}\left\{\frac{\partial}{\partial\theta}\left(\sin\theta\frac{\partial}{\partial\theta}\right)+\frac{1}{\sin\theta}\frac{\partial^2}{\partial\phi^2}\right\}J=a^2D\sigma_0\frac{\partial B_r}{\partial t}\,, \quad\text{.............(5.1)}$$

where a, σ_0 and $\frac{\partial B_r}{\partial t}$ denote respectively the radius of the earth, specific conductivity of sea-water and flux-change per unit area. When J can be expressed by a series of the type

$$J=\sum_n\sum_m K_n^m S_n^m\,, \quad\text{............................(5.2)}$$

where $S_n{}^m$ denotes spherical surface harmonic and $K_n{}^m$ a function of time, we have

$$-\sum_n\sum_m K_n^m n(n+1)S_n^m=a^2D\sigma_0 f'(t)P_1\,, \quad\text{..................(5.3)}$$

where it is assumed

$$B_r=f(t)P_1(\cos\theta)\,, \quad\text{.............................(5.4)}$$

taking into consideration the distribution of the field of sudden commencement. Meanwhile, the normal component of the electric currents must vanish at the boundries, namely $i_\phi=0$ at $\phi=0$ and $\phi=\pi/2$. This condition is satisfied by taking $P_n{}^{2m}\sin 2m\phi$ in place of $S_n{}^m$. Then expanding P_1 into a series of the type

$$P_1=\sum_n\sum_m \gamma_{n,\,m}\,P_n^{2m}\sin 2m\phi \quad (0<\phi<\pi/2) \;\ldots\ldots\ldots\ldots\ldots(5.5)$$

where
$$\gamma_{n,\,m}=\frac{2n+1}{\pi}\int_{\theta=0}^{\pi}\int_{\phi=0}^{\pi/2}P_1\,P_n^{2m}\sin 2m\phi\sin\theta\,d\theta d\phi\,, \;\ldots\ldots(5.6)$$

we get $K_n{}^m$ by comparing the corresponding coefficients of both sides of (5.3) as follows;

$$K_{2k+1}^{2l+1}=-\,a^2D\sigma_0 f'(t)\,\frac{\gamma_{2k+1,\,2l+1}}{(2k+1)(2k+2)} \;\ldots\ldots\ldots\ldots\ldots\ldots(5.7)$$

because $\gamma_{2k,\,2l+1}$, $\gamma_{2k,\,2l}$ and $\lambda_{2k+1,\,2l}$ are all zero. $\gamma_{2k+1,\,2l+1}$ is easily calculated from (5.6). Substituting, then, (5.7) in (5.2), the current function can be expressed by

$$J=-a^2D\sigma_0 f'(t)\sum_{k=1}^{\infty}\sum_{l=0}^{l\leq\frac{k-1}{4}}\frac{\gamma_{2k+1,2l+1}}{(2k+1)(2k+2)}\,P_{2k+1}^{2(2l+1)}\sin 2(2l+1)\phi\,, \;(5.8)$$

or taking main term we have

$$J=-a^2D\sigma_0 f'(t)\{(0.0925\,P_3^2+0.0232\,P_5^2+\ldots)\sin 2\phi+\ldots\} \;\ldots\ldots\ldots\ldots(5.9)$$

by which we can draw the current-lines in our ocean as shown in Fig. 48. The amount of the current-flow between two adjacent lines in the figure is constant.

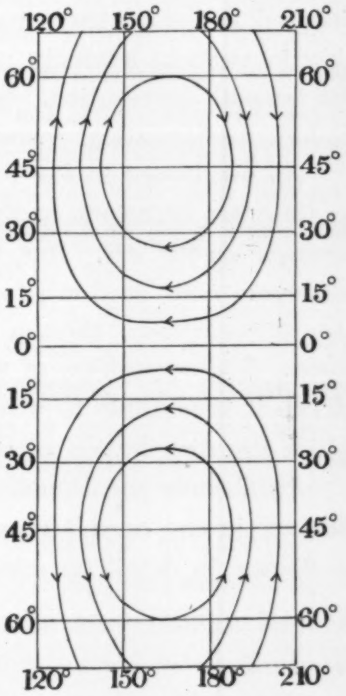

Fig. 48. The induced currents in the ocean.

In order to estimate the magnetic field produced by the electric currents shown in the figure, let us use an approximate method. Though (5.8) or (5.9) are merely available in the region $0<\phi<\frac{\pi}{2}$, we assume that they are effective all over the earth neglecting the magnetic field produced by the currents flowing in the rgeions except $0<\phi<\pi/2$, whence the magnetic potential due to these currents flowing in a spherical shell is given by

$$W=4\pi\sum_n\frac{n}{2n+1}J_n\,(a/r)^{n+1}\ldots\ldots\ldots(5.10)$$

out of the earth, where J_n denotes the term of the current-function having order n.
Thus, differentiating W with respect to the respective directions, the components of the magnetic field at $r=a$ are approximately given as follows;

$$X=1.49\,aD\sigma_0 f'\,(X_3^2+0.443\,X_5^2+\dots)\sin 2\phi\,,\ \dots\dots\dots\dots(5.11)$$

$$Z=1.98\,aD\sigma_0 f'\,(P_3^2+0.400\,P_5^2+\dots)\ \sin 2\phi\,.\ \dots\dots\dots\dots(5.12)$$

Hence the magnetic field on $\phi=45°$ meridian becomes as shown in Fig. 49 in which the increase in Z near the centre of eddies in Fig. 48 is remarkable.

As an accurate estimate is difficult to get owing to the ambiguity of the determination of the flux-change or $f'(t)$, we shall estimate very roughly the order of the field-intensity. Taking $a=6400\,km$, $D=4000\,m$, $\sigma_0=4\times10^{-11} emu$ and $f'=10^{-3}\gamma/sec$, Z near the centres of eddies amounts to about 20 *gammas*, downwards or upwards respectively in the northern or southern hemispheres, while H amounts to about 8 *gammas*, northwards, on the equator.

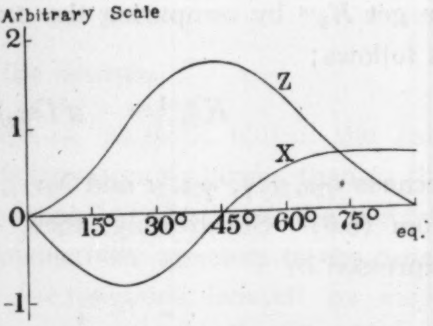

Fig. 49. The magnetic field produced by the induced currents in the ocean.

With such effect of ocean in mind, it may fairly be presumed that Honolulu, situated in the northern part of the central Pacific Ocean, is affected remarkably in vertical intensity as shown in Fig. 42 deviating about 10 *gammas* from the normal distribution. Such effect is likely to exist in the case of Porto Rico though mathematical investigation is more difficult to carry out.

As mentioned in the well known book "*Geomagnetism*",67) the sign of ΔZ on different occasions at the same station is roughly constant, though not so constant as for ΔH. But, the opposition of sign between the values of ΔZ at relatively near stations, for example Greenwich and Paris, is striking and almost invariable, though in ΔH and ΔD the movements are generally the same. The opposition of sign is only observable in the case of sudden change. Hence it is possible to attribute such phenomena to the local characters of which the distribution of sea is probably the most important factor.

As already mentioned in this section, the influences of sea on sudden changes in the earth's magnetic field are sometimes striking, but it is difficult to discuss in detail on account of the irregular distribution of land and sea.

---

67) CHAPMAN and BARTELS, *loc. cit.* Vol. I, p. 297.

SUMMARY AND CONCLUSION

In Chapter I, brief outlines of the investigations carried out up to this time on the magnetic permeability in the earth were described. These studies, both physical and geophysical, proved the ferromagnetic state in the earth to be impossible. Although the results of these studies are not always applicable to the actual earth, we may consider, at the present stage of investigation, that the magnetic permeability does not differ materially from unity. For this reason, the writer assumed $\mu=1$ throughout this study.

In the first part of Chapter II, the influences of oceans on the diurnal variation on quiet days were discussed. Since the specific conductivity of sea-water amounts to the order of 10^{-11} *emu*, about 10,000 times larger than that of usual rocks found on the earth's surface, the electric currents induced by magnetic variation in deep ocean will become appreciably intense. In practice, the magnetic field produced by the oceanic-current will be of complicated distribution corresponding to the irregular distribution of land and sea. Owing to mathematical difficulties, only a few investigations on the effect of world-wide ocean of uniform depth spread all over the earth were hitherto carried out. The writer, intending to study the possible effect of oceans, such as the Pacific and the Atlantic, investigated to what extent S_q might be affected by the presence of a sea of uniform depth bounded by two meridians $\pi/2$ apart in longitude. The results indicated that S_q might not be so affected by the ocean that the field due to induced currents in the ocean occupies the main part. Accordingly, the internal part of S_q obtained from spherical harmonic analysis in which it was assumed that S_q depends solely on local time could be on the whole considered for that was produced by the induced currents flowing in the inner part of the earth. Further, on certain assumptions, though not quite accurate, the effect of the Pacific Ocean was abstracted which agreed roughly with what was expected from the theory. As to the layer of moist soil covering the land area, its influence is negligible because its conductivity is less than 1/100 of sea-water and its thickness does not exceed 1000 *m*.

In the succeeding sections of Chapter II, electromagnetic induction by S_q was studied with the aid of a newly made analysis. As Nagata pointed out, the analyses made by Hasegawa and Benkova seem to be more reliable than the well known Chapman's analysis which has been hitherto used to study electromagnetic induction by S_q. Taking into consideration the discontinuity at the depth of 2900 *km*, the writer attempted to determine the electrical state out- and inside of this boundary separately. Unfortunately, however, the induced currents do not always penetrate into great depth, and the determined conductivity for the inner core was ambiguous though we got a value about ten times larger than the outer part or mantle. Hence, the result agreed with that obtained in the case of uniform core model. We get, as already obtained by Nagata, $\sigma=5.0\times10^{-12}$ *emu* and the depth of non-conducting layer $D=400$ ***km*** on the basis of Benkova's analysis while Chapman has obtained $\sigma=3.6\times10^{-13}$ ***emu*** and $D=260$ ***km*** from his own analysis. It is of interest that the conductivity obtained from the newly made analysis becomes about ten times larger than that obtained from Chapman's old one.

Recent accumulation of magnetic data shows clearly that there were, on the average, daily variation of definite type on disturbed days called solar daily disturbance variation or S_D. As shown empirically by Chapman and theoretically by the preseht writer, the distribution of S_D differs very much from that of S on quiet days or S_q. In order to check the electrical state of the earth's interior obtained from the study of S_q, electromagnetic induction by S_D was studied in Chapter III. Though it was impossible to make an accurate determination on account of the shortage of available data, we found out that the electrical state for S_q was approximately applicable to the electromagnetic induction by S_D.

In Chapter IV, electromagnetic induction by storm-time variation or D_{st} within the earth-model consisting of superficical non-conducting layer, mantle and inner core, was studied with a view to getting some knowledge about the electrical state in deeper region. Since the conductivity amounts to 5×10^{-12} ***emu*** in Benkova's model, the discrepancy between the studies on S_q and D_{st} which was hitherto taken into account seriously by Chapman and his colleagues was almost overcome leaving little difference. Although, the remaining difference was vanished by introducing high conducting inner core as obtained in the case of S_q, the value of the conductivity was less reliable because only a minor part of the induced currents penetrates into such region of great depth.

With the aid of Hatakeyama's excellent data, the writer treated the electromagnetic induction by bay-type disturbance in Chapter V. Separation of the external part from the internal one was carried out after the same method as in the case of D_{st}. With the idealized feature of the atmospheric current-systems obtained both empirically and theoretically in mind, only the coefficients of $Q_1^1(\cos\theta)$, which was the most predominant in the magnetic potential in the low and middle latitudes, were studied. Roughly speaking, the results supported the view obtained in the studies on S_q. The electrical conductivity must increase below the depth of a few hundred ***kilometers*** from the earth's surface amounting at least to the order of 10^{-12} ***emu.*** The extent to which the induced currents penetrate was also studied, the conclusion being that they become practically zero at the depth of several hundred *kilometers* measured from the earth's surface. Considering the duration-time of bay-type disturbances which amounts to 1~5 *hours*, the obtained conductivity should be reliable as to regions shallower than those in the case of S_q and of course D_{st}.

Moreover, we have a type of variation of shorter duration. That is the magnetic effect connected with solar eruption and consequently with radio fade-out or Dellinger effect. Electromagnetic induction by magnetic variation of this type was studied in Chapter VI. As has been made clear recently, since the magnetic effects accompanying the solar eruption are an augumentation of diural variation departure having no effect in the dark hemisphere, a larger number of observed data from well-distributed observatories are needed for spherical harmonic analysis. However, we lack sufficient data for the purpose. Then, the writer treated the problem as an induction within plane-earth in the European Region where the distribution of observatories is comparatively dense.. Constructing the theory of plane-earth induction, the writer investigated the electrical state of the earth's interior inferred from the variation and found out that the conductivity increased below the depth of 400 *km* amounting to 10^{-12} *emu* while the outer layer must be non-conducting. Though only an example from Birkeland's data was available and we could say nothing about the accuracy of determination, it was of interest to note that the result agreed with the view in the cases of various variation treated in the previous chapters. The induced currents decrease very sharply with the increase of depth, the determined conductivity corresponding to that just below the boundary between the non-conducting and conducting regions.

In Chapter VII, induction by sudden commencement of magnetic storm, one of the most rapid variation in the earth's magnetic field, was discussed. As shown in the last section, since sudden commencement are apt to be affected by the complicated influence of sea, the discussions seem to be rather rough. Treating in the same way as in the study in previous chapters, however, we got, on the average, the ratio of the coefficient of the external potential to that of the internal one amounting to as much as 3.9 for $P_1(\cos\theta)$. Such a large value was hardly to be expected from the earth-model in the cases of the variations treated before. A plausible explanation was furnished by taking the conductivity of the earth to be as small as 10^{-15} *emu* agreeing with that of usual rocks found on the earth's surface. Hence, taking into consideration the sharp decrease of the induced currents with the increase of depth, especially concentration in sea, we concluded that even in the non-conducting region obtained in the studies on S_q, D_{st}, bay and variation connected with solar eruption the conductivity took a finite value of the order of 10^{-15} *emu.*

Table XXVII Summarization of the

Variation	Period or approximate duration-time	Researcher	Data	*e*/*i* at maximum variation
Diurnal variation on quiet days (S_q)	**24 and 12 *h*. (Auxiliary 8 and 6 *h*.)**	**Chapman and Price**	**Chapman**	**2·8 for P_2^1, 2·2 for P_3^2**
		Lahiri and Price	**„**	—
		Terada	**„**	—
		Nagata	**Hasegawa**	**2·30 for P_2^1, 2·43 for P_3^2**
		Nagata	**Benkova**	**2·34 for P_2^1, 2·30 for P_3^2**
		Rikitake	**Chapman**	—
		Rikitake	**Benkova**	—
Solar daily disturbance variation (S_D)	**24 *h*.**	**Rikitake**	**Vestine**	**3·7 for P_2^1, 2·3 for P_4^1**
Storm-time variation (D_{st})	**2~3 *days***	**Chapman and Price**	**Chapman**	**2·4 for P_1**
		Lahiri and Price	**„**	—
		Nagata	**„**	—
		Rikitake	**„**	—
Bay-type disturbance	**1~3 *h*.**	**Rikitake**	**Hatakeyama**	**2·2 for Q_1^1**
Variation connected with solar eruption	**30 *min*.**	**Rikitake**	**Birkeland**	**2·4 for wave length approximately 6000 *km*.**
Sudden commencement of magnetic storm	**3 *min*. (average)**	**Rikitake**	**Bauer**	**3·9 for P_1**

electrical state of the earth's interior.

Electrical state		Effective depth (*km*)	Remark
Depth (*km*)	Conductivity (*emu*)		
250	$3{\cdot}6\times10^{-13}$	700*)	
Conductivity increases with increases of depth.		—	Non-uniform earth
	„	—	Non-uniform earth
400	$1{\cdot}5\times10^{-12}$	850*)	
400	$5{\cdot}1\times10^{-12}$	850*)	
200	$3{\cdot}0\times10^{-13}\left(\begin{array}{l}3\times10^{-11}\text{ for}\\ \text{inner core}\end{array}\right)$	—	Earth-model consisting of mantle and inner core
400	$5{\cdot}0\times10^{-12}\left(\begin{array}{l}5\times10^{-11}\text{ for}\\ \text{inner core}\end{array}\right)$	850*)	„
Roughly agrees with S_q.		—	
400	$4{\cdot}4\times10^{-12}$	1100	
700	more than 10^{-11}	—	Non-uniform earth
400	$5{\cdot}1\times10^{-12}$	1100	
400	$5{\cdot}0\times10^{-12}\left(\begin{array}{l}5\times10^{-11}\text{ for}\\ \text{inner core}\end{array}\right)$	1100	Earth-model consisting of mantle and inner core
260	at least 10^{-12}	320	
400	10^{-12}	420	Plane-earth
0~500	10^{-15}	30**)	Accurate determination for both depth and conductivity is unable.

*) Mean for P_2^1 and P_3^2.

**) It was assumed that the earth was covered by world-wide sea, a few thousand *meters* in depth.

Toward the end of this chapter, possible influence of any ocean on sudden commencement was discussed to obtain results for a reasonable explanation of abnormality in vertical intensity at observatories situated in ocean. According to the writer's opinion, sudden changes in the earth's magnetic field are sometimes affected considerably by the presence of sea though exact investigation is of great difficulty to carry out on account of the irregular distribution of land and sea.

In addition to various variations treated in this paper, we have a kind of magnetic variation of special type called pulsation. Unfortunately, however, as the writer has no data available yet, the electromagnetic induction by pulsation will be left untouched till he can get sufficient data.

Summarization of the results of this paper is shown in Table XXVII together with those hitherto obtained by many researchers. The depth and conductivity tabulated in this Table were obtained with respect to the uniform core model excepting the studies done by Lahiri and Price, and Terada.

The writer introduced a convenient concept "effective depth" in order to get the distribution of the electrical conductivity in the earth. As mentioned in the respective sections of all chapters, we know the distribution of the induced currents in the conducting region and consequently the contribution

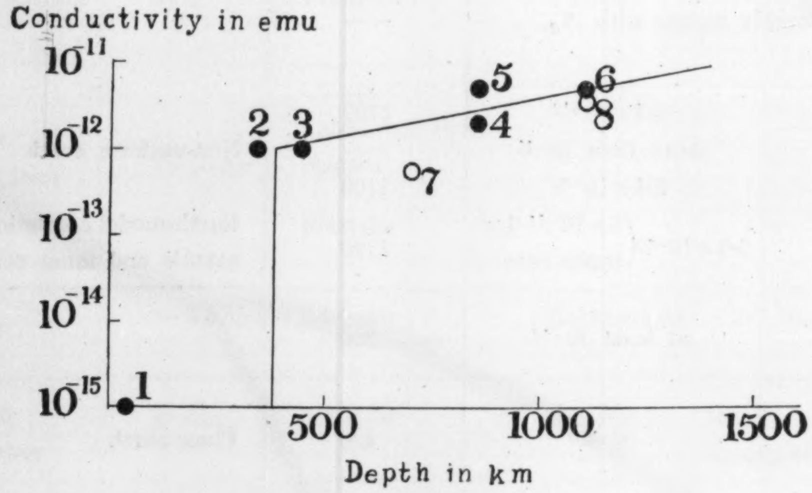

Fig. 50. The conductivity-distribution in the earth.

1. Sudden commencement.
2. Bay-type disturbance.
3. Variation connected with solar eruption.
4. S_q (Hasegawa).
5. S_q (Benkova).
6. D_{st} (Chapman-Benkova).
7. S_q (Chapman).
8. D_{st} (Chapman).

of current flowing at any depth to the magnetic field at the earth's surface as a function of depth denoted by $\varphi(D)$ or $\varphi(\rho)$ in the spherical case. We shall define the most effective depth that coresponds to the determined conductivity by $\int D\varphi(D)\,dD \Big/ \int \varphi(D)\,dD$ or $\int_0^1 \rho\varphi(\rho)\,d\rho \Big/ \int_0^1 \varphi(\rho)\,d\rho$ in the spherical case. With the aid of these expressions, the writer calculated "effective depth" in each case as shown in Table XXVII. Hence the conductivity can be plotted against depth, though not exactly, as shown in Fig. 50. Taking into consideration the fact that the conductivity of usual rocks found on the earth's surface amounts to the order of as small as 10^{-15} *emu*, the increase of the conductivity must be so steep, almost discontinuous, down to the depth of about 400 *km*. Then the rate of increase becomes small. The electrical state in great depth, more than 1500 *km*, can not be accurately determined though it seems advantageous for the explanation of the electromagnetic induction by D_{st} that the greater the depth the higher the conductivity.

It is beyond the scope of the present paper to investigate into the reason why the conductivity increases enormously below the depth of a few hundred *kilometers*. It must be discussed from the physical stand-point. The writer hopes that studies on the properties of matter under high pressure and high temperature will give, in the near future, some suggestions for the interpretation of the results given in the present study.

ACKNOWLEDGEMENT

In the course of this study, the writer was encouraged by his senior colleagues, among whom to Professor C. Tsuboi and Dr. T. Nagata especially the writer wishes to express his cordial thanks for their kind advices and helpful suggestions. At the same time the writer also wishes to express his hearty thanks to Professor F. Kishinouye, Professor T. Hagiwara and Professor T. Minakami who gave him the chance to carry out this study and offered him helpful criticisms. He also cordially expresses thanks to Dr. H. Hatakeyama for his kind suggestions on magnetic data.

Throughout the numerical work, Miss K. Sano always assisted the writer and to her the writer's hearty thanks are also due. A part of this study was done with the financial aid of research grant from the Department of Education and sincere thanks are also due to the Department.

APPENDIX

When the writer studied magnetic effect connected with solar eruption or Dellinger effect, it was treated as plane-earth induction owing to the shortage of well-distributed data. Though it is not unusual to regard a part of the earth's surface as a plane in potential problem of geophysics, the influence of the neglect of the earth's curvature should be taken into account for the present problem because the induced currents which produce the internal part of the magnetic potential concentrate at the depth of several hundred *kilometers* which amounts to about one tenth of the earth's radius. From this point of view, the difference between the spherical and plane induction will be discussed here.

Taking the uniform core model, in the first place, the relations between the coefficients of spherical surface harmonics are obtained as follows. In general, the potential of the magnetic field can be expressed by

$$W=a\sum_{n=1}^{\infty}\sum_{m=0}^{n}\{e^m_{n,\,a}\,\rho^n+i^m_{n,\,a}\,\rho^{-n-1})\cos m\phi+$$

$$(e^m_{n,\,b}\,\rho^n+i^m_{n,\,b}\,\rho^{-n-1})\sin m\phi\}P^m_n$$

in polar coordinate where a, ρ, e and i denote respectively the earth's radius, radial distance divided by a, the coefficients of the potential originated above the earth and those originated in the earth. When, by means of spherical harmonic analysis, the northward and downward components of the magnetic field may be expressed as

$$X=\sum_{n=1}^{\infty}\sum_{m=0}^{n}(a^m_n\cos m\phi+b^m_n\sin m\phi)\,X^m_n\,,$$

$$Z=\sum_{n=1}^{\infty}\sum_{m=0}^{n}(\tilde{a}^m_n\cos m\phi+\tilde{b}^m_n\sin m\phi)\,P^m_n\,,$$

we have the well-known relations

$$a^m_n=n(e^m_{n,\,a}+i^m_{n,\,a})\,,\qquad \tilde{a}^m_n=ne^m_{n,\,a}-(n+1)\,i^m_{n,\,a}\,,$$

$$b^m_n=n(e^m_{n,\,b}+i^m_{n,\,b})\,,\qquad \tilde{b}^m_n=ne^m_{n,\,b}-(n+1)\,i^m_{n,\,b}\,.$$

These relations can also be obtained from the combination of the eastward and downward components.

Meanwhile, according to the induction theory, the coefficients of internal origin are given by the operational equation

$$i^m_n(t)=I(p)\,e^m_n(t)$$

where $$I(p)=\frac{nq^{2n+1}}{n+1}\left\{1-\frac{F_n(k^2q^2a^2)}{F_{n-1}(k^2q^2a^2)}\right\},\quad k^2=4\pi\sigma p\,.$$

In the expressions, σ and q denote respectively the electrical conductivity and the radius of the conducting core. Magnetic permeability is assumed to be unity while F_n is a transcendental function which was already studied in detail by S. Chapman and A. T. Price[8]. In the case of periodic induction of period $2\pi/\alpha$, we have $i_n{}^m$ corresponding to $e_n{}^m = E_n{}^m \cos \alpha t$ as follows

$$i_n^m = \frac{nq^{2n+1}}{n+1} E_n^m \left\{ \left(1 - \frac{A}{A^2+B^2}\right) \cos \alpha t - \frac{B}{A^2+B^2} \sin \alpha t \right\},$$

where

$$A = \frac{\beta}{2n+1} \left\{ 1 + \frac{n}{\beta} + \frac{n(n+1)}{4\beta^2} \cdots \right\},$$

$$B = \frac{\beta}{2n+1} \left\{ 1 - \frac{n(n+1)}{4\beta^2} - \frac{n(n+1)}{4\beta^3} \right\}, \qquad \beta^2 = 4\pi^2 \sigma q^2 a^2 .$$

Thus we get

$$a_n^m = nE_{n,a}^m \left[\left\{ 1 + \frac{nq^{2n+1}}{n+1} \left(1 - \frac{A}{A^2+B^2} \right) \right\} \cos \alpha t - \frac{nq^{2n+1}}{n+1} \frac{B}{A^2+B^2} \sin \alpha t \right],$$

$$\tilde{a}_n^m = nE_{n,a}^m \left[\left\{ 1 - q^{2n+1} \left(1 - \frac{A}{A^2+B^2} \right) \right\} \cos \alpha t + q^{2n+1} \frac{B}{A^2+B^2} \sin \alpha t \right], \text{ etc.}$$

Hence, we can calculate the magnetic forces at the earth's surface corresponding to any magnetic potential of external origin.

Next, the magnetic forces are analysed in a rectangular area as shown in Fig. 51. We obtain $A_{\mu\nu}$ and $\tilde{A}_{\mu\nu}$ as the coefficients of $\sin \frac{\mu\nu}{L} x \cos \frac{\nu\pi}{L'} y$ in X and $\cos \frac{\mu\pi}{L} x \cos \frac{\nu\pi}{L'} y$ in Z. Meanwhile, as mentioned in Chapter VI, we have

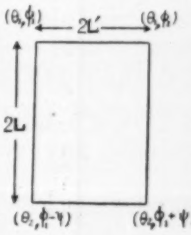

Fig. 51.

$$e_{\mu\nu} = \frac{1}{2} \left\{ \frac{L}{\mu\pi} A_{\mu\nu} + \frac{1}{\pi \left\{ \left(\frac{\mu}{L}\right)^2 + \left(\frac{\nu}{L'}\right)^2 \right\}^{\frac{1}{2}}} \tilde{A}_{\mu\nu} \right\},$$

$$i_{\mu\nu} = \frac{1}{2} \left\{ \frac{L}{\mu\pi} A_{\mu\nu} - \frac{1}{\pi \left\{ \left(\frac{\mu}{L}\right)^2 + \left(\frac{\nu}{L'}\right)^2 \right\}^{\frac{1}{2}}} \tilde{A}_{\mu\nu} \right\}.$$

Then the coefficients of external and internal parts can be calculated in the case of plane-earth from the external potential given for spherical case.

On the other hand, according to the plane-earth induction theory studied in Chapter VI, the coefficients of internal origin $i'_{\mu\nu}$ are given by

$$i'_{\mu\nu}(t) = I'(p)\, e_{\mu\nu}(t),$$

where

$$I'(p) = e^{-2\pi \left\{ \left(\frac{\mu}{L}\right)^2 + \left(\frac{\nu}{L'}\right)^2 \right\}^{\frac{1}{2}} D} \times \frac{\left\{ \pi^2 \left[\left(\frac{\mu}{L}\right)^2 + \left(\frac{\nu}{L'}\right)^2 \right] + 4\pi\sigma p \right\}^{\frac{1}{2}} - \pi \left\{ \left(\frac{\mu}{L}\right)^2 + \left(\frac{\nu}{L'}\right)^2 \right\}^{\frac{1}{2}}}{\left\{ \pi^2 \left[\left(\frac{\mu}{L}\right)^2 + \left(\frac{\nu}{L'}\right)^2 \right] + 4\pi\sigma p \right\}^{\frac{1}{2}} + \pi \left\{ \left(\frac{\mu}{L}\right)^2 + \left(\frac{\nu}{L'}\right)^2 \right\}^{\frac{1}{2}}}.$$

In the expression, D denotes the depth of the non-conducting layer. When $e_{\mu\nu} = P\cos\alpha t + Q\sin\alpha t$, we get

$$i'_{\mu\nu}(t) = \frac{e^{-2uD}}{2\sqrt{u^4+v^2}+u^2+2u\sqrt{\sqrt{u^4+v^2}u^2}}$$

$$\times\left[\left\{P(2\sqrt{u^4+v^2}-u^2)+2Qu\sqrt{\sqrt{u^4+v^2}-u^2}\right\}\cos\alpha t\right.$$

$$\left.-\left\{2Pu\sqrt{\sqrt{u^4+v^2}-u^2}-Q(2\sqrt{u^4+v^2}-u^2)\right\}\sin\alpha t\right],$$

where $$u=\pi\left\{\left(\frac{\mu}{L}\right)^2+\left(\frac{\nu}{L'}\right)^2\right\}^{\frac{1}{2}} \text{ and } v=4\pi\alpha\sigma.$$

To discuss the influence of plane-earth treatment, then, will be reduced to compare $i_{\mu\nu}$ to $i'_{\mu\nu}$.

For instance, a comparison in the case of induction by variation associated with solar eruption, will be approximately made as follows.

As is well known, the atmospheric current-systems of that variation closely resemble those of S_q in the sunlit hemisphere. For this reason, we may assume that the potential of the inducing field is given by

$$W=K\{7{\cdot}7\,P_2^1\cos(\phi+24^\circ)+4{\cdot}4\,P_3^2\cos(2\phi+202^\circ)$$
$$+2{\cdot}2\,P_4^3\cos(3\phi+35^\circ)+0{\cdot}7\,P_5^4\cos(4\phi+232^\circ)\}$$

that is proportional to the S_q current-systems obtained by Chapman as the equinoctial mean for the year 1905. Further, we assume that the field is periodic, say $K=K_0\cos\alpha t$, for the sake of mathematical simplicity. Thus calculating a_n^m and $\tilde{a}_n^m$, we get

$$X=K_0\cos\alpha t\{22{\cdot}6\,X_2^1\cos(\phi+24^\circ)+19{\cdot}3\,X_3^2\cos(2\phi+202^\circ)$$
$$+12{\cdot}6\,X_4^3\cos(3\phi+35^\circ)+4{\cdot}8\,X_5^4\cos(4\phi+232^\circ)\}$$
$$-K_0\sin\alpha t\{0{\cdot}3\,X_2^1\cos(\phi+24^\circ)+0{\cdot}3\,X_3^2\cos(2\phi+202^\circ)$$
$$+0{\cdot}3\,X_4^3\cos(3\phi+35^\circ)+0{\cdot}1\,X_5^4\cos(4\phi+232^\circ)\},$$
$$Z=K_0\cos\alpha t\{4{\cdot}6\,P_2^1\cos(\phi+24^\circ)+5{\cdot}2\,P_3^2\cos(2\phi+202^\circ)$$
$$+4{\cdot}1\,P_4^3\cos(3\phi+35^\circ)+1{\cdot}9\,P_5^4\cos(4\phi+232^\circ)\}$$
$$+K_0\sin\alpha t\{0{\cdot}4\,P_2^1\cos(\phi+24^\circ)+0.5\,P_3^2\cos(2\phi+202^\circ)$$
$$+0{\cdot}3\,P_4^3\cos(3\phi+35^\circ)+0{\cdot}1\,P_5^4\cos(4\phi+232^\circ)\},$$

where it is assumed that $\sigma=10^{-12}$ *emu*, $q=0.94$ and the period is 1 *hour*. Then neglecting the term involving $\sin\alpha t$ in which the coefficients are less than one tenth compared to the term involving $\cos\alpha t$, e_{10} and i_{10} are calculated with

respect to the meridian $\phi=165°$ that passes the centre of the current-systems. i_{10}/e_{10} is shown in Fig. 52 being plotted against L, half wave-length, that measured from $\theta=20°$ to the lower latitudes. i'_{10}/e_{10} is also calculated for $D=400\ km$ being also shown in Fig. 52. As seen in the figure, the discrepancy between i and i' becomes considerable as L becomes small. Hence it is dangerous to analyse in a region whose range does not exceed much the depth of the non-conducting layer. However, it seems likely that the treatment in Chapter VI, in which $L=3000\ km$ will be, to a rough approximation, correct.

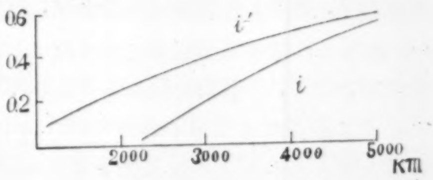

Fig. 52.

18. 地球內の電磁感應およびその地球內部の電氣的性質との關係 第1報 (2)

地震研究所 力武常次

太陽面爆發に伴う地磁氣變化（デリンジヤー現象に伴う變化）はまた極めて特徴のある變化の型式を示し，その分布は夜間の半球では變化を示さず，晝間の半球では日變化磁場を增大するような變化をすることがよく知られているが，第6章に於て Birkeland の集めた資料によつて，上述の各章に於けると同樣の考察を行つた．この場合球函數分析を行うためには高次の球函數をも考慮せねばならず，數少い觀測資料を使うためにやむをえず比較的觀測點の多いヨーロツパ地方に就いて，地球を平面的に取扱つた．方法は地球を球とした場合と同じであつて，波長 6000 *km* の調和函數に就いて內外磁場を分離した．この內外磁場間の關係はやはり絕緣的な表面層の深さを 400 *km*, それより下の部分では $\sigma=10^{-12}\ emu$ とすると都合よく說明出來る．

灣型變化では變化の繼續時間は 1〜3 時間，太陽面爆發に伴う變化では 30 分程度である．これに對し磁氣嵐の急始に於ては水平分力の飛躍は平均として 2〜3 分程度で終了する．第7章は磁氣嵐の急始を取扱つたもので，資料は Bauer の集めたものによつた．*Dst* の場合と同樣中低緯度に於て P_1 の係數を求めた．この場合外および內側に原因を有する磁場のポテンシヤルの比は 3.9 程度となり，今迄扱つた變化のそれに比して著しく內部磁場が小さい．したがつて地球の最も外側に近い部分の σ が小さい（$10^{-15}\ emu$ 程度）ために短週期の變化ではこのようにあらわれるのではないかと考えられる．またこのようなはやい變化に對しては，海水の高電導性が問題となり，それについて若干の議論を行つた．

上述の各種の變化の資料の精度は一定ではなく，したがつて決定された電氣的性質の信頼度も一定でなく，誤差の評價も困難であるが一應かなりはやい變化からおそい變化迄を含んでいるか

ら，いろいろな深さについて σ の分布が如何樣であるかの目安を近似的につくることが可能と思われる．一般に誘導電流の深さに對する分布したがつて任意の深さを流れる電流の表面磁場に對する寄與を計算することが出來るから筆者は最も有効な深さとして $\int D\varphi(D)\,dD/\int\varphi(D)\,dD$ で與えられる量をとつた．茲に $\varphi(D)$ は D なる深さのところを流れる電流の表面に於ける磁場に對する寄與を表わす．球として取扱つた場合は，$\int_0^1\rho\varphi(\rho)\,d\rho/\int_0^1\varphi(\rho)\,d\rho$ $(\rho=r/a$，a は地球の半徑$)$ としてよい．卽ちこれ等の式で定義される深さの電氣的性質が決定された σ に對して最も有効であると考えるのであつて，一義的に決めることが不可能な以上この程度の近似的な考え方で滿足せざるを得ない．その結果は本文中の最後の圖に示したような σ の分布となつて，地表下 400 *km* 附近に殆ど不連續と考えられるような飛躍を考えねばならない．もし σ が岩石中のようにイオン傳導度によるとすると溫度の增加は σ を增し壓力の增大は σ を減少させる方向に働くと考えられるが，定量的なことは物理學的な物性に關する理論および高溫高壓下の實驗をまつて說明されるべきことがらであり，本報文に於ては單に地磁氣變化の研究より得られた結果を述べるにとゞめる．

またこのように σ の大體の分布を求め得たからには，第二の近似として σ がこのような分布をするモデルを考えて各種の地磁氣變化から分布型式をさらに精密に決定することが望ましいが，それは次の機會に實行したいと考える．

19. *Electromagnetic Induction within the Earth and Its Relation to the Electrical State of the Earth's Interior. Part II.*

By Tsuneji RIKITAKE,

Earthquake Research Institute.

(Read Dec. 16, 1947—Received Dec. 18, 1947.)

1. Introduction.

In Part I[1] of this paper, the writer studied electromagnetic induction by geomagnetic variation of various types—diurnal variation on quiet days (S_q), solar daily disturbance variation (S_D), storm-time variation (D_{st}), bay-type disturbance, variation connected with solar eruption or Dellinger effect and sudden commencement of magnetic storm. In order to explain the relation between part of external origin and that of internal origin, the writer took "unform core model" for the first approximation. Since the period or approximate duration-time of these variations ranged from a few minutes to a few days, the extent of penetration of induced currents in the earth differed in each case. Hence, introducing a convenient concept "effective depth" the writer approximately determined the distributiou of the electrical conductivity in the earth as reproduced in Fig. 1. As seen in the figure, the outermost part of the earth, down to the depth of about 400 *km*, seems to be almost non-conducting where the conductivity is of the same order with rock or dry soil found on the earth's surface amounting to the order of 10^{-15} *emu*. At the depth of about 400 *km*, the conductivity increases discontinuously reaching the order of 10^{-12} *emu*. Then it increases exponentially with the increase in depth below this level.

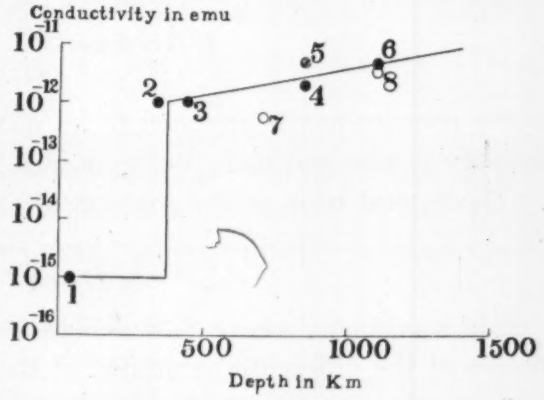

Fig. 1.

---

[1] T. RIKITAKE, *Bull. Earthq. Res. Inst.* **28** (1950), 45 and 219.

Strictly speaking, the conductivity distribution shown in Fig. 1 which was obtained by introducing "effective depth" must be considered as an approximation by which we may get a rough knowldge on the conductivity-distribution in the earth. As to the second approximation, we shall then study electromagnetic induction within an earth-model in which

$$\begin{aligned}\sigma&=\sigma' \text{ for } 1>\rho>q \\ &=\sigma_0\rho^{-l} \text{ for } q>\rho>0\end{aligned} \qquad (\rho=r/a) \;\ldots\ldots\ldots\ldots\ldots(1)$$

where a and r denote respectively the earth's radius and radial distance from the centre of the earth and q, σ', σ_0 and l are constants. Giving suitable values to σ', σ_0 and l, the conductivity-distribution shown in Fig. 1 may be fairly represented by (1). In the manner we determined σ and q in Part I, we will here determine σ', σ_0, q and l through which the relations between the external and internal parts of various vaniations in the earth's magnetic field can be explained.

2. Electromagnetic induction within non-uniform earth and determination of the conductivity-distribution.

Mathematical theory of electromagnetic induction in a sphere in which the electrical conductivity-distribution is given by (1) is easily constructed in like manner with the previous studies carried out by Chapman, Price, Lahiri and the writer.

In conducting medium, we have vector potential $\overrightarrow{A}$ which satisfies the relation

$$\nabla^2\overrightarrow{A}=4\pi\sigma\frac{\partial\overrightarrow{A}}{\partial t}\,, \;\ldots\ldots\ldots\ldots\ldots\ldots\ldots\ldots\ldots\ldots\ldots(2)$$

for the phenomenon is assumed to be quasi-stationary. Here, magnetic permeability is assumed to be unity as well as in Part I.

The typical term of the solution of (2) is given by

$$\overrightarrow{A_n^m}=af_n(t,\rho)\,[\overrightarrow{r}\text{ grad } S_n^m] \;\ldots\ldots\ldots\ldots\ldots\ldots\ldots(3)$$

in polar coordinate, where $S_n{}^m$ denotes spherical surface harmonic. f_n is a solution of the differential equation of the next type

$$\frac{\partial}{\partial\rho}\left(\rho^2\frac{\partial f_n}{\partial\rho}\right)=\{n(n+1)+4\pi a^2\sigma\rho^2\partial/\partial t\}\,f_n\,. \;\ldots\ldots\ldots\ldots\ldots(4)$$

As the r, θ and ϕ components of $\overrightarrow{A_n{}^m}$ in (3) become respectively

$$0, \ -af_n \frac{\partial S_n^m}{\sin\theta\partial\phi} \ \text{and} \ af_n \frac{\partial S_n^m}{\partial\theta}, \qquad \text{.......................(5)}$$

we get the components of the magnetic field as follows.

$$\left.\begin{aligned} H_r &= -\frac{1}{\rho}\, n(n+1) f_n S_n^m, \\ H_\theta &= -\frac{1}{\rho}\frac{\partial}{\partial\rho}(\rho f_n)\frac{\partial S_n^m}{\partial\theta}, \\ H_\phi &= -\frac{1}{\rho}\frac{\partial}{\partial\rho}(\rho f_n)\frac{\partial S_n^m}{\sin\theta\partial\phi}. \end{aligned}\right\} \qquad \text{.........................(6)}$$

On the other hand, there is, outside the earth, magnetic potential of which typical term is given by

$$W_n^m = a\{\boldsymbol{e}_n(t)\rho^n + \boldsymbol{i}_n(t)\rho^{-n-1}\}S_n^m \qquad \text{.....................(7)}$$

by which we get the components of the magnetic field as follows.

$$\left.\begin{aligned} H_r &= -\{n\,\boldsymbol{e}_n\rho^{n-1} - (n+1)\,\boldsymbol{i}_n\rho^{-n-2}\}S_n^m, \\ H_\theta &= -(\boldsymbol{e}_n\rho^{n-1} + \boldsymbol{i}_n\rho^{-n-2})\frac{\partial S_n^m}{\partial\theta}, \\ H_\phi &= -(\boldsymbol{e}_n\rho^{n-1} + \boldsymbol{i}_n\rho^{-n-2})\frac{\partial S_n^m}{\sin\theta\partial\phi}. \end{aligned}\right\} \qquad \text{.....................(8)}$$

Putting p in place of $\partial/\partial t$, (4) becomes in the outermost shell

$$\left\{\frac{d^2}{d\rho^2} + \frac{2(n+1)}{\rho}\frac{d}{d\rho} - k^2a^2\right\} f_{n,1} = 0. \qquad (k^2 = 4\pi\sigma' p) \qquad \text{.........(9)}$$

The solution of (9) is given by

$$f_{n,1}(p,\rho) = C_1\rho^n F_n(p,\rho) + D_1\rho^{-n-1}G_n(p,\rho) \qquad \text{...............(10)}$$

as already studied in Chapter II, Part I. C_1 and D_1 are functions of time. Meanwhile we get in the region $\rho < q$

$$\frac{d}{d\rho}\left(\rho^2\frac{d}{d\rho}\right) f_{n,2} = \{n(n+1) + 4\pi a^2\sigma_0\rho^{-l+2}p\} f_{n,2} \qquad \text{..........(11)}$$

As already studied by Lahiri and Price[2], the solution of (11) is given by

$$f_{n,2}(p,\rho) = C_2\rho^{-\frac{1}{2}} K_\nu(z) \qquad \text{..........................(12)}$$

for $l > 2$, where

$$\rho^{1-\frac{1}{2}l} = \frac{l-2}{2\zeta}\, z, \quad \nu = \frac{2n+1}{l-2}, \quad \zeta^2 = 4\pi a^2\sigma_0 p \qquad \text{...................(13)}$$

---

[2] B. N. LAHIRI and A. T. PRICE, *Phil. Trans. Roy. Soc. London*, A 237 (1939), 509.

and C_2 is a function of time. The solution for the cases $l \leqq 2$ are also obtained by them, but is not important for the present problem.

At the boundaries of the earth-model shown in Fig. 2, say at $\rho=1$ and $\rho=q$, the components of the magnetic field must be continuous. Hence, we get from (6) and (8)

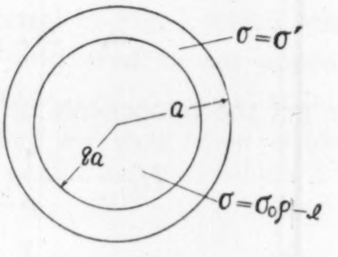

Fig. 2.

$$\left.\begin{aligned} &n(n+1)f_{n,1}(p,1)=n\boldsymbol{e}_n-(n+1)\boldsymbol{i}_n\,,\\ &f_{n,1}(p,1)+\left[\frac{d}{d\rho}f_{n,1}(p,\rho)\right]_{\rho=1}=\boldsymbol{e}_n+\boldsymbol{i}_n\,,\\ &\qquad\qquad f_{n,1}(p,q)=f_{n,2}(p,q)\,,\\ &f_{n,1}(p,q)+\left[\frac{d}{d\rho}f_{n,1}(p,q)\right]_{\rho=q}=f_{n,2}(p,q)+\left[\frac{d}{d\rho}f_{n,2}(p,\rho)\right]_{\rho=q}. \end{aligned}\right\} \tag{14}$$

Taking into consideration (10), (12) and recurrence formulae for F_n, G_n and K_ν, we get by solving the simultaneous equations (14)

$$\boldsymbol{i}_n(t)=I(p)\,\boldsymbol{e}_n(t) \quad \ldots\ldots\ldots\ldots\ldots\ldots\ldots\ldots\ldots(15)$$

where

$$I(p)=-\frac{n}{n+1}\,\frac{\left(\frac{z_1}{2\nu}K_{\nu-1}(z_1)G_n(q)+K_\nu(z_1)G_{n+1}(q)\right)\left(F_n(1)-F_{n-1}(1)\right)+q^{2n+1}\left(K_\nu(z_1)F_{n-1}(q)-\frac{z_1}{2\nu}K_{\nu+1}(z_1)F_n(q)\right)G_{n+1}(1)}{\left(\frac{z_1}{2\nu}K_{\nu-1}(z_1)G_n(q)+K_\nu(z_1)G_{n+1}(q)\right)F_{n-1}(1)+q^{2n+1}\left(K_\nu(z_1)F_{n-1}(q)-\frac{z_1}{2\nu}K_{\nu+1}(z_1)F_n(q)\right)\left(G_n(1)-G_{n+1}(1)\right)}. \tag{16}$$

Here, for the sake of simplicity, we write z_1 in place of $z_{\rho=q}$ and also $F_n(1)$, $F_n(q),\cdots$ respectively in place of $F_n(p,1)$, $F_n(p,q),\cdots$.

When the inducing field is periodic with period $2\pi/\alpha$, the amplitude ratio, say $\boldsymbol{i}_n/\boldsymbol{e}_n$, and the phase difference, say $\iota_n-\mathrm{e}_n$, of the field at $r=a$ are given by

$$\boldsymbol{i}_n/\boldsymbol{e}_n=\mathrm{mod}\,I(i\alpha)\,,\qquad \iota_n-\mathrm{e}_n=\arg I(i\alpha)\,.\ldots\ldots\ldots\ldots\ldots\ldots(17)$$

In the case of aperiodic field, $\boldsymbol{i}_n(t)$ is given by solving the operational equation (15). According to the theorems of operational calculus, we have

$$\boldsymbol{i}_n(t)=\frac{d}{dt}\int_0^t \boldsymbol{e}_n(t-u)\,h(u)\,du\,,\ \ldots\ldots\ldots\ldots\ldots\ldots\ldots(18)$$

where $$h(u)=\frac{1}{2\pi i}\int_L e^{pu}\,I(p)\,\frac{dp}{p}\,,\ \ldots\ldots\ldots\ldots\ldots\ldots\ldots\ldots(19)$$

the path of integration L being the well known Bromwich's one. As easily seen, the function $h(t)$ is the value of $\boldsymbol{i}_n(t)$ when $\boldsymbol{e}_n(t)$ is equal to Heaviside's unit function defined by $H(t)=0$ when $t\leqq 0$, $H(t)=1$ when $t>0$.

Using these theorems, we can theoretically solve the problems of the electromagnetic induction concerned here. Unfortunately, however, $I(p)$ is so complicated that a rigorous treatment is very difficult, so we must do with suitable approximation for $I(p)$.

In the first place, an approximate expression of $I(p)$ when t is small is obtained as follows.

When p tends to $+\infty$, we have from the definitions of F_n and G_n as already given in Part I,

$$F_n(q) \simeq \frac{(2n+1)!}{2^n n!} \frac{e^{kqa}}{2(kqa)^{n+1}}$$
$$\times \left\{1 - \frac{n(n+1)}{2kqa} + \frac{(n-1)n(n+1)(n+2)}{8(kqa)^2} \cdots\right\}, \quad G_n(q) \simeq 0 .$$

Thus, it becomes

$$I(p) \simeq \frac{n}{n+1} \frac{F_{n-1}(1) - F_n(1)}{F_{n-1}(1)}$$
$$\simeq \frac{n}{n+1}\left\{1 - \frac{2n+1}{2\sqrt{\pi\sigma'}a} p^{-\frac{1}{2}} + \frac{n(2n+1)}{4\pi\sigma' a^2} p^{-1} + \ldots\right\} \ldots\ldots\ldots(20)$$

from which we know that $I(p)$ is equal to that for a shere having the same radius and uniform conductivity σ'. To state physically, as the induction-effect penetrates from the surface, the electrical property of the outermost part is the most effective one just after the beginning of variation whatever the conductivity in deeper part may be. When $I(p)$ is given by (20) and $e_n(t) = \frac{A}{p+\alpha} H(t)$, the solution of the operational equation (15) becomes just the same type with (3.7), Chapter VII, Part I by which we discussed the relation between the external and internal parts of sudden commencement of magnetic storm. Hence σ' is determined to be the order of 10^{-15} *emu* as well as in Part I.

Meanwhile, as already shown in Part I, the outermost shell of the present earth-model can be regarded to be almost non-conducting for slower variations. In that case, F_n and G_n are expanded in ascending powers of σ' as

$$F_n(q) = 1 + \frac{(kqa)^2}{2(2n+3)} + \frac{(kqa)^4}{2\cdot4\cdot(2n+3)(2n+5)} + \ldots ,$$

$$G_n(q) = e^{-kqa}\left\{1 + kqa + \frac{2(n-1)}{2!(2n-1)}(kqa)^2\right.$$
$$\left. + \frac{2^2(n-2)(n-1)}{3!(2n-2)(2n-1)}(kqa)^3 + \ldots\right\} ,$$

excepting large p or small t. Hence we get

$$\begin{aligned} I(p)= \frac{n}{n+1}\, q^{2n+1} \frac{K_{\nu-1}(z_1)}{K_{\nu+1}(z_1)} \Bigg[1 - \Bigg\{ & \frac{1}{2(2n+1)} - \frac{2n-1}{2(2n+1)}\, q^2 \\ & - \frac{q^2}{2}\left(\frac{1}{2n+1}\, \frac{K_\nu(z_1)}{K_{\nu-1}(z_1)} - \frac{z_1}{2\nu}\, \frac{1}{2n+3}\, \frac{K_{\nu+1}(z_1)}{K_{\nu-1}(z_1)} \right) \\ & + q^2 \left(\frac{z_1}{2\nu}\, \frac{n-1}{2n-1}\, \frac{K_{\nu-1}(z_1)}{K_{\nu+1}(z_1)} + \frac{n}{2n+1}\, \frac{K_\nu(z_1)}{K_{\nu+1}(z_1)} \right) \\ & - \frac{q^{-2n-1}}{(2n+1)(2n+3)}\, \frac{K_{\nu+1}(z_1)}{K_{\nu-1}(z_1)} + \frac{q^{2n+1}}{(2n-1)(2n+1)}\, \frac{K_{\nu-1}(z_1)}{K_{\nu+1}(z_1)} \Bigg\} k^2 a^2 \\ & + \ldots \Bigg] \quad \ldots\ldots\ldots(21) \end{aligned}$$

or neglecting σ' wholly we get

$$I(p)= \frac{n}{n+1}\, q^{2n+1} \frac{K_{\nu-1}(z_1)}{K_{\nu+1}(z_1)} \quad \ldots\ldots\ldots\ldots\ldots\ldots\ldots\ldots(22)$$

which is just the same expression as obtained by Lahiri and Price[3]. In order to investigate into the contribution of the outermost layer, which is so thin that its thickness amounts to only several percent of the earth's radius, we shall calculate the relation between the external and internal parts, denoted respectively by e_n' and i_n', just below this layer.

As shown by Lahiri and Price, we have

$$\left. \begin{aligned} e_n' &= e_n - \frac{c_n}{n}\, \frac{d}{dt} \{ n e_n - (n+1) i_n \} \quad , \\ i_n' &= i_n - \frac{c_n}{n+1}\, \frac{d}{dt} \{ n e_n - (n+1) i_n \} \quad , \end{aligned} \right\} \ldots\ldots\ldots\ldots\ldots(23)$$

where

$$c_n = \frac{4\pi\sigma' \bar{a} \delta}{2n+1} \, . \quad \ldots\ldots\ldots\ldots\ldots\ldots\ldots\ldots(24)$$

$\bar{a}$ and δ denote respectively the mean radius of the shell and the thickness. Thus we regard the shell equivatent to a thin shell of conductivity $\sigma'\delta$.

In the case of periodic induction with period $2\pi/\alpha$, we replace d/dt by $i\alpha$ and e_n by $Ee^{i\alpha t}$ etc. in (23). Taking then $\sigma'=10^{-15}\,emu$, $\bar{a}=6{\cdot}2\times 10^8\,cm$, $\delta=4{\cdot}0\times 10^7\,cm$, we get for the case $n=2$, $m=1$

$$\begin{aligned} E' &= E - i0{\cdot}0023\,(2E-3I)\,, \\ I' &= I - i0{\cdot}0015\,(2E-3I)\,, \end{aligned}$$

---

3) B. N. LAHIRI and A. T. PRICE, *loc. cit.*

and also for the case $n=3$, $m=2$

$$E'=E-i0{\cdot}0021\,(3E-4I)\,,$$

$$I'=E-i0{\cdot}0016\,(3E-4I)\,.$$

Hence, the influences of the outer layer are so small that they only amount to the order of one thousandth. Taking into account the accuracy of spherical harmonic analysis of S_q, we can say that the coefficients of magnetic potential just outside the surface $\rho=q$ are practically the same with those obtained at the earth's surface.

Next, in the case of bay-type disturbance, we assume, as studied in Section 4, Chapter V, Part I, that $e_1=Ate^{-\omega t}$ ($\omega=0{\cdot}28\times10^{-3}\,sec^{-1}$) and $i_1=0{\cdot}42e_1$ whence we easily estimate the effect of the layer. For the same values of σ', $\bar{a}$ and δ given above, assuming the maximum value of e_1 is $10\,\gamma$, the effects of the layer or the second terms in (23) were found to be less than $0.1\,\gamma$ except near the beginning of disturbance. As to the induction by D_{st} that changes more slowly than bay-type disturbance, it is obviously seen that the effects becomes lesser. In short, the effects of the outermost layer are practically negligible for the induction by S_q, D_{st}, and bay-type disturbance. From this point of view, we may discuss our present problem, excepting sudden commencement of magnetic storm, on the basis of (22) that corresponds to the earth-model in which the outermost layer is regarded to be non-conducting.

In the first place, we shall get the combinations of q, σ_0 and l by which the relation between the external and internal parts of S_q, is explained. Taking into consideration (17), we put

$$z_1=x\sqrt{i}\,,\quad x=\frac{4a\sqrt{\pi\sigma_0\alpha}}{|\,l-2\,|}\,,\quad \alpha=\frac{2\pi m}{86400}\,,\qquad\ldots\ldots\ldots\ldots\ldots\ldots(25)$$

whence $x>1$ for the cases in which σ_0 is the order of $10^{-12}\,emu$ and $l<30$. Thus an expansion in a descending series of x is available. With the aid of asymptotic expansion of modified Bessel function, we have

$$\left.\begin{aligned} \iota_n-\epsilon_n&=\tan^{-1}\frac{\mu_{\nu-1}}{\lambda_{\nu-1}}-\tan^{-1}\frac{\mu_{\nu+1}}{\lambda_{\nu+1}}\,,\\ i_n/e_n&=\frac{n}{n+1}\,q^{2n+1}\sqrt{\frac{\lambda_{\nu-1}{}^2+\mu_{\nu-1}{}^2}{\lambda_{\nu+1}{}^2+\mu_{\nu+1}{}^2}}\,, \end{aligned}\right\}\qquad\ldots\ldots\ldots\ldots\ldots(26)$$

where

$$\lambda_{\nu-1}=1+\frac{4\,(\nu-1)^2-1}{8\sqrt{2}\,x}+\ldots\,,$$

$$\mu_{\nu-1}=-\frac{4\,(\nu-1)^2-1}{8\sqrt{2}\,x}-\frac{\{4\,(\nu-1)^2-1\}\,\{4\,(\nu-1)^2-9\}}{128x^2}-\ldots\,,$$

$$\lambda_{\nu+1}=1+\frac{4(\nu+1)^2-1}{8\sqrt{2}\,x}+\dots,$$

$$\mu_{\nu+1}=-\frac{4(\nu+1)^2-1}{8\sqrt{2}\,x}-\frac{\{4(\nu+1)^2-1\}\{4(\nu+1)^2-9\}}{128x^2}-\dots.$$

Thus e_2^1/i_2^1 are calculated with respect to three cases $q=0{\cdot}90$, $0{\cdot}94$ and $0{\cdot}98$ as shown in Fig. 3a, while $\iota_2^1-\epsilon_2^1$ is almost the same throughout three cases as shown in Fig. 3b, In the calculation, the formulae in uniform core model are used for $l=2$ and some expressions obtained by Lahiri and Price are taken into account for $l<2$.

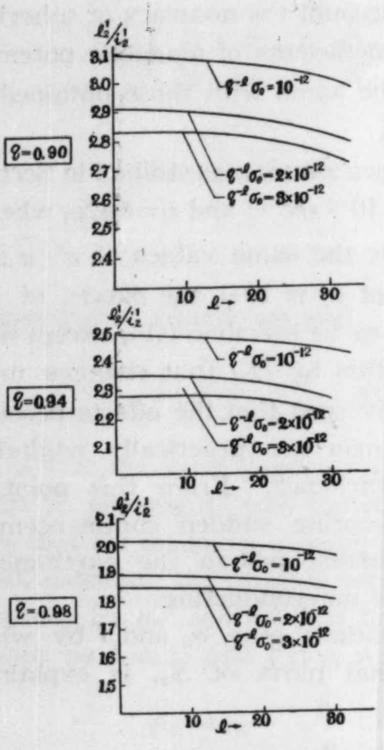

Fig. 3a. Amplitude ratio.

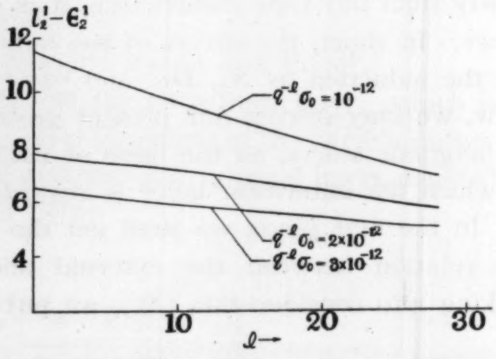

Fig. 3b. Phase difference in degree.

It is easily seen from the figures that the combination $q^{-l}\sigma_0=2{\cdot}0\times10^{-12}$ *emu* or $\sigma_0=1{\cdot}0\times{}^{-12}$ *emu*, $q=0{\cdot}94$ and $l=11$, giving $e_2^1/i_2^1=2{\cdot}34$ and $\iota_2^1-\epsilon_2^1=7{\cdot}0°$, is the most preferrable for the explanation of e_2^1/i_2^1 and $\iota_2^1-\epsilon_2^1$ obtained from the analysis. In fact, Hasegawa got 2·30 and 9°, Benkova 2·34 and 5° and then the mean values are 2·32 and 7°. Taking the combination of σ_0, q and l, besides, we get $e_3^2/i_3^2=2{\cdot}35$, $\iota_3^2/\epsilon_3^2=7{\cdot}4°$ and $e_4^3/i_4^3=2{\cdot}51$, $\iota_4^3-\epsilon_4^3=7{\cdot}7°$ which approximately agree with the results of Hasegawa's and Benkova's analyses. In the next place, we shall investigate how well the relations between the external and internal parts are explained by taking the above determined conductivity-distribution in the cases of D_{st} and bay-type disturbance.

As fully discussed by Lahiri and Price, $h(t)$ in (18) and (19) is given by

$$h(t)=\frac{nq^{2n+1}}{n+1}\frac{8\nu}{\pi^2}\int_0^\infty e^{-v^2t/\tau}\frac{1}{J_{\nu+1}^2(v)+Y_{\nu+1}^2(v)}\frac{dv}{v^3}\quad\dots\dots\dots\dots\dots\dots(27)$$

for $l > 2$, where

$$\tau = 16\pi a^2 \sigma_0/(l-2)^2 \text{ ....(28)}$$

Alternative expressions for $h(t)$, which is more convenient for numerical calculation, can be obtained as follows.
When t/τ is small, we have

$$h(t) = \frac{nq^{2n+1}}{n+1}\left\{1 + \frac{c_2 t}{\tau} + \frac{c_4 t^2}{2!\,\tau^2} + \dots \right.$$
$$\left. + \sqrt{\frac{t}{\pi\tau}}\left(2c_1 + \frac{2^2 c_3 t}{3\tau} + \frac{2^3 c_5 t^2}{3\cdot 5\tau^2} + \dots\right)\right\}, \text{ ....(29)}$$

where

$$c_s = a_s(\nu - 1) - \sum_{r=0}^{s-1} c_r a_{s-r}(\nu+1), \quad c_0 = 1;$$
$$a_s(\nu) = \frac{(4\nu^2-1)(4\nu^2-3^2)\dots\{4\nu^2-(2s-1)^2\}}{8^s\, s!}. \text{ ....(30)}$$

For larger values of t, we have

$$h(t) \simeq \frac{nq^{2n+1}}{(n+1)\,\Gamma(1+\nu)}\left\{\left(\frac{4t}{\tau}\right)^{-\nu} - 2\left(\frac{4t}{\tau}\right)^{-1-\nu}\right.$$
$$+ \frac{(3-2\nu)(1+\nu)}{\nu(1-\nu)}\left(\frac{4t}{\tau}\right)^{-2-\nu} + \dots$$
$$\left. + \frac{2\{\Gamma(1-\nu)\}^2}{\Gamma(2+\nu)\,\Gamma(1-2\nu)}\left(\frac{4t}{\tau}\right)^{-1-2\nu} + \dots\right\}. \text{ ......(31)}$$

Corresponding to the values of σ_0, q and l determined in the preceding paragraph, we get $h(t)$ for $n=1$ as shown in Fig. 4. Then, $i_1(t)$ is found by integrating (18) numerically. In the case of the bay-type disturbances, for example those of Feb. 24, 1933 and Apr. 10, 1933, which were treated in Chapter V, Part I, we estimate i_a, e_b as shown by broken lines in Figs. 5 and 6 together with the coefficients of the inducing field. As easily seen in the figures, the calculated curves approximately agree with those obtained by the analyses as in the case of uniform core model studied in Part I.

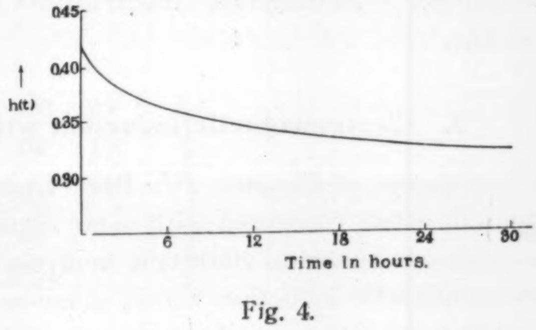

Fig. 4.

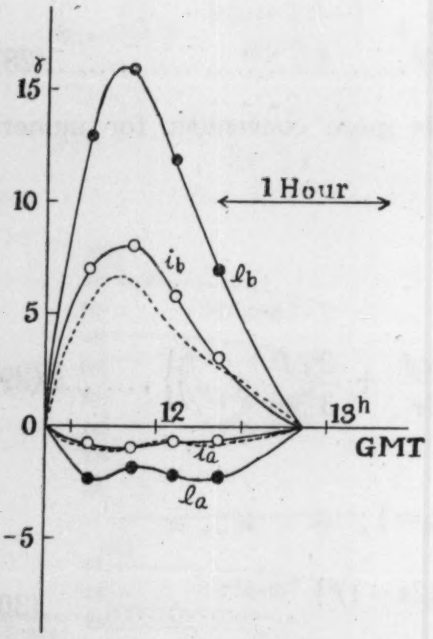

Fig. 5. The bay-type disturbance on Feb. 24, 1933.

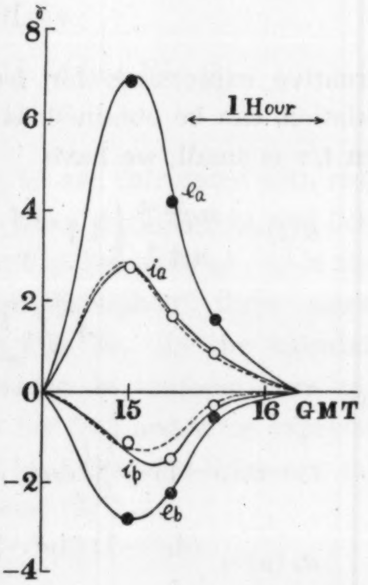

Fig. 6. The bay-type disturbance on Apr. 10, 1933.

Meanwhile, $i_1(t)$ for D_{st} is calculated as shown in Fig. 7 together with the results of the analysis. In the figure, small circles denote the observed values. The agreement of the calculated values and the observed ones seems to be good.

Hence, we conclude that the conductivity-distribution determined in the studies of S_q is also approximately compatible with bay-type disturbance and D_{st}.

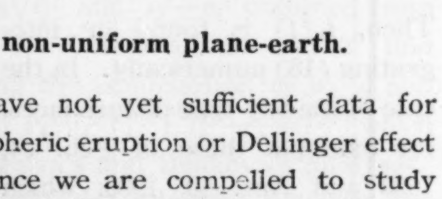

Fig. 7.

3. Electromagnetic induction within non-uniform plane-earth.

As shown in Chapter IV, Part I, we have not yet sufficient data for magnetic effect connected with solar chromospheric eruption or Dellinger effect to carry out spherical harmonic analysis. Hence we are compelled to study electromagnetic induction within plane-earth as we did in Part I.

Let us consider semi-infinite, non-uniform earth covered by a superficial layer with thickness D. x and y axes are taken in the surface-plane of this layer and z axis taken to be positive downwards. As already studied in the former section, the outermost part of the earth is regarded to be non-conducting except for rapid variations such as the sudden commencement of magnetic storm. For this reason, we may assume $\sigma=0$ in the superficial layer and, taking into consideration the most probable conductivity-distribution obtained in Section 2, $\sigma(z)=c_1+c_2z^2$ which can fairly represent the distribution if we take $c_1=1{\cdot}2\times10^{-12}$ *emu* and $c_2=5{\cdot}2\times10^{-28}$ *emu/cm* for z smaller than about 1500 *km*.

In the conducting region, vector potential $\overrightarrow{A}$ satisfies

$$\{\nabla^2-4\pi\sigma(z)\,p\}\,\overrightarrow{A}=0 \qquad\text{.............................(32)}$$

where we write p in place of $\partial/\partial t$.

The solution becomes

$$\overrightarrow{A}=C_{mn}g(z)\,[\,\overrightarrow{r}\ \mathrm{grad}\ V] \qquad\text{.............................(33)}$$

where V denotes harmonic function of x and y and

$$\frac{d^2g}{dz^2}-(\alpha^2+\beta^2z^2)\,g=0\,,\qquad \alpha^2=4\pi c_1p+k^2\,,$$

$$\beta^2=4\pi c_2p\,,\qquad k^2=m^2+n^2\,. \qquad\text{......(34)}$$

It is difficult to find an accurate solution for the differential equation (34). Fortunately, however, since $c_1\gg c_2\,z^2$ and consequently $\alpha^2\gg\beta^2\,z^2$ for z less than 100 *km*, we get, neglecting the higher order of β^2z^2/α^2, the solution as follows.

$$g(z)=\left(1-\frac{\beta^2}{8\alpha^4}-\frac{\beta^2}{4\alpha^3}\,z^2-\frac{\beta^2}{4\alpha^2}\,z^2-\frac{\beta^2}{6\alpha}\,z^3\right)e^{-\alpha z} \qquad\text{............(35)}$$

where another solution involving $e^{\alpha z}$ is not taken into account because it becomes infinity as z tends to infinity.

Taking into account the relation $\overrightarrow{H}=\mathrm{rot}\ \overrightarrow{A}$, the components of the magnetic field are given by

$$\left.\begin{aligned} X&=C_{mn}\,\frac{dg}{dz}\,\frac{\partial V}{\partial x}\,,\\ Y&=C_{mn}\,\frac{dg}{dz}\,\frac{\partial V}{\partial y}\,,\\ Z&=C_{mn}\,k^2gV\,. \end{aligned}\right\} \qquad\text{...........................(36)}$$

Meanwhile, in the non-conducting region, we have magnetic potential W whose typical term is given by

$$W=(e_{mn}\,e^{-kz}+i_{mn}\,e^{kz})V \qquad\text{...........................(37)}$$

from which we have

$$\left.\begin{aligned} X &= -(\boldsymbol{e}_{mn}\,e^{-kz}+\boldsymbol{i}_{mn}\,e^{kz})\,\frac{\partial V}{\partial x}\,, \\ Y &= -(\boldsymbol{e}_{mn}\,e^{-kz}+\boldsymbol{i}_{mn}\,e^{kz})\,\frac{\partial V}{\partial y}\,, \\ Z &= k\,(\boldsymbol{e}_{mn}\,e^{-kz}-\boldsymbol{i}_{mn}\,e^{kz})\,V\,. \end{aligned}\right\}\quad\text{.........................}(38)$$

By the continuity of the magnetic field at the boundary $z=D$, we have

$$\left.\begin{aligned} \boldsymbol{e}e^{-kD}+\boldsymbol{i}e^{kD} &= C\alpha\Big(1+\frac{\beta^2}{8\alpha^4}+\frac{\beta^2}{4\alpha^3}D \\ &\qquad +\frac{\beta^2}{4\alpha^2}D^2-\frac{\beta^2}{6\alpha}D^3\Big)e^{-\alpha D}\,, \\ \boldsymbol{e}e^{-kD}-\boldsymbol{i}e^{kD} &= Ck\Big(1-\frac{\beta^2}{8\alpha^4}-\frac{\beta^2}{4\alpha^3}D \\ &\qquad -\frac{\beta^2}{4\alpha^2}D^2-\frac{\beta^2}{6\alpha}D^3\Big)e^{-\alpha D}\,. \end{aligned}\right\}\quad\text{.........}(39)$$

where, for the sake of simplicity, the suffices m and n are not written.

Solving the simultaneous equations (39), we get an operational equation

$$\boldsymbol{i}(t)=I(p)\,\boldsymbol{e}(t)$$

where

$$I(p)=e^{-2kD}$$
$$\times\frac{(\alpha-k)\Big(1-\dfrac{\beta^2}{6\alpha}D^3\Big)+(\alpha+k)\dfrac{\beta^2}{4\alpha^2}\Big(\dfrac{1}{2\alpha^2}+\dfrac{D}{\alpha}+D^2\Big)}{(\alpha+k)\Big(1-\dfrac{\beta^2}{6\alpha}D^3\Big)+(\alpha-k)\dfrac{\beta^2}{4\alpha^2}\Big(\dfrac{1}{2\alpha^2}+\dfrac{D}{\alpha}+D^2\Big)}\quad\text{......}(40)$$

or, neglecting the higher order of β^2D^2/α^2,

$$I(p)=e^{-2kD}\,\frac{\alpha-k}{\alpha+k}\Big\{1+\frac{k\beta^2}{\alpha}\,\frac{1}{\alpha^2-k^2}\Big(\frac{1}{2\alpha^2}+\frac{D}{\alpha}+D^2\Big)\Big\}\,.\quad\text{.........}(41)$$

Hence with the aid of (18) and (19), we can find $\boldsymbol{i}(t)$ which corresponds to any $\boldsymbol{e}(t)$. But, as was often done in the previous studies, more convenient procedure for numerical calculation is available as follows. Expanding $I(p)$ in a descending series of p, we get

$$\begin{aligned} I(p)={}^{-2kD}\Big[1+\frac{c_2}{c_1}\gamma D^2-\Big\{2\gamma+\frac{c_2}{c_1}\gamma D\Big(2\gamma D-\frac{1}{\sqrt{4\pi c_1}}\Big)\Big\}p^{-\frac{1}{2}} \\ -\Big\{2\gamma^2+\frac{c_2}{c_1}\gamma\Big(\frac{5}{2}\gamma^2D^2+\frac{2\gamma D}{\sqrt{4\pi c_1}}-\frac{2}{8\pi c_1}\Big)\Big\}p^{-1} \end{aligned}$$

$$-\left\{\gamma^3+\frac{c_2}{c_1}\gamma\left(\frac{3\gamma D}{\sqrt{4\pi c_1}}+\frac{1}{4\pi c_1}\right)\right\}p^{-\frac{3}{2}}+\ldots\Big] \qquad \ldots\ldots\ldots\ldots(42)$$

and interpreting term by term, we obtain

$$h(t)=e^{-2kD}\Big[1+\frac{c_2}{c_1}\gamma D^2-\frac{2}{\sqrt{\pi}}\left\{2\gamma+\frac{c_2}{c_1}\gamma D\left(2\gamma D-\frac{1}{\sqrt{4\pi c_1}}\right)\right\}t^{\frac{1}{2}}$$

$$-\left\{2\gamma^2+\frac{c_2}{c_1}\gamma\left(\frac{5}{2}\gamma^2D^2+\frac{2\gamma D}{\sqrt{4\pi c_1}}-\frac{1}{8\pi c_1}\right)\right\}t$$

$$-\frac{4}{3\sqrt{\pi}}\left\{\gamma^3+\frac{c_2}{c_1}\gamma\left(\frac{3\gamma D}{\sqrt{4\pi c_1}}+\frac{1}{4\pi c_1}\right)\right\}t^{\frac{3}{2}}+\ldots\Big] \qquad \ldots\ldots(43)$$

where $$\gamma^2=\frac{k^2}{4\pi c_1}.$$

Taking the most probable combination of D, c_1 and c_2 which was deduced from the result obtained in Section 2, say giving 380 *km*, $1{\cdot}2\times10^{-12}$ ***emu*** and $5{\cdot}2\times10^{-28}$ ***emu/cm***^{2} to D, c_1 and c_2 respectively, $h(t)$ is calculated as shown in Fig. 8. Applying this to the estimate of $i(t)$ which corresponds to $e(t)$ obtained in the analysis of Birkeland's data in Chapter VI, Part I, $i(t)$ is calculated as shown in Fig. 9 together with the observed results. As seen in the figure,

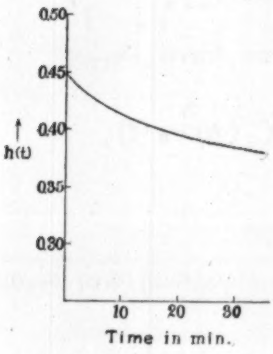

Fig. 8.

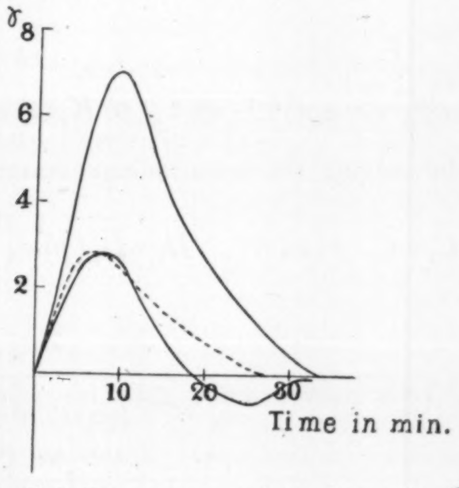

Fig. 9. Full lines correspond to observed e (upper) and i (lower). Broken line denotes i calculated here.

the calculated values decrease more slowly than the observed ones with the lapse of time. Taking into consideration, however, the accuracy of the analysis, we may say that the calculated values agree roughly with the observed ones. In order to make the agreement better, c_1 becomes smaller than the values cited above, c_1 amounting to about 5×10^{-13} *emu*, while D must not be altered. As to the value of c_2, precise determination is impossible because the induced currents decay rapidly with the increasing depth. We must study much slower variation to determine c_2.

In short, the present study shows that the conductivity-distribution determined from the studies on S_q, D_{st} and bay-type disturbance is also approximately applicable to the electromagnetic induction by magnetic variation connected with solar eruption or Dellinger effect. Although there remains small disagreement, we can not judge whether it is true or due to the errors in the analysis.

4. The distribution of the induced currents.

It is well known that current-density is given by

$$\vec{c} = -\sigma \frac{\partial \vec{A}}{\partial t} . \qquad \text{......................(44)}$$

Hence the current-density in the outer layer and the inner high conducting region become respectively

$$\left.\begin{aligned} \vec{c}^{\,m}_{n,1} &= -\sigma' ap\{\overline{C}_1(p)\,\rho^n F_n(\rho) + \overline{D}_1(p)\,\rho^{-n-1} G_n(\rho)\} \\ &\qquad\qquad \times\; e_n(t)\,[\,\vec{r}\,\mathrm{grad}\, S^m_n\,] , \\ \vec{c}^{\,m}_{n,2} &= -\sigma_0 \rho^{-l-\frac{1}{2}}\; ap\,\overline{C}_2(p)\, K_\nu(z)\, e_n(t)\,[\,\vec{r}\,\mathrm{grad}\, S^m_n\,] , \end{aligned}\right\} \text{...(45)}$$

where, by solving the simultaneous equations (14), we have

$$C_1 = \overline{C}_1(p)\, e_n(t) , \quad D_1 = \overline{D}_1(p)\, e_n(t) , \quad C_2 = \overline{C}_2(p)\, e_n(t) ,$$

and

$$\left.\begin{aligned} \overline{C}_1(p) &= \frac{1}{n+1} \frac{\frac{z_1}{2\nu} K_{\nu-1}(z_1) G_n(q) + K_\nu(z_1) G_{n+1}(q)}{\left\{\frac{z_1}{2\nu} K_{\nu-1}(z_1) G_n(q) + K_\nu(z_1) G_{n+1}(q)\right\} F_{n-1}(1) + q^{2n+1}\left\{K_\nu(z_1) F_{n-1}(q) - \frac{z_1}{2\nu} K_{\nu+1}(z_1) F_n(q)\right\}\{G_n(1) - G_{n+1}(1)\}} , \\ \overline{D}_1(p) &= \frac{q^{2n+1}}{n+1} \frac{K_\nu(z_1) F_{n-1}(q) - \frac{z_1}{2\nu} K_{\nu+1}(z_1) F_n(q)}{''} , \\ \overline{C}_2(p) &= \frac{q^{2n+1}}{n+1} \frac{F_{n-1}(q) G_n(q) - F_n(q) G_n(q) + F_n(q) G_{n+1}(q)}{''} . \end{aligned}\right\} \text{(46)}$$

In order to calculate the distribution of the current-density in the cases of aperiodic field, expansions in ascending powers of p are obtained as follows. With the aid of the asymptotic expansion of F_n, G_n and K_ν, we have

$$\left.\begin{aligned}
\overrightarrow{c_{n,1}^{m}} &= -\frac{1}{2}\sqrt{\frac{\sigma'}{\pi}}\,\frac{2n+1}{n+1}\,\rho^{-n}\,[\overrightarrow{r}\ \mathrm{grad}\ S_n^m]\,c_1(t)\,,\\
\overrightarrow{c_{n,2}^{m}} &= -\frac{q^{\frac{3}{4}l-1}}{2}\sqrt{\frac{\sigma_0}{\pi}}\,\frac{2n+1}{n+1}\,\rho^{\frac{1}{2}-\frac{1}{4}l}[\overrightarrow{r}\,\mathrm{grad}\,S_n^m]\,c_2(t)\,.
\end{aligned}\right\}\ldots\ldots(47)$$

in which

$$\left.\begin{aligned}
c_1(t) &= e^{-\sqrt{4\pi\sigma'}\,a\,(1-\rho)\,p^{\frac{1}{2}}}\,p^{\frac{1}{2}}\,(1+A_1p^{-\frac{1}{2}}+B_1p^{-1}+\ldots)\,e_n(t)\,,\\
c_2(t) &= e^{-\sqrt{4\pi}\,a\,\left\{(1-q)\sqrt{\sigma'}+\frac{2}{l-2}\sqrt{\sigma_0}\,(\rho^{1-\frac{1}{2}l}-q^{1-\frac{1}{2}l})\right\}p^{\frac{1}{2}}}\\
&\qquad\qquad \times\ p^{\frac{1}{2}}(1+A_2p^{-\frac{1}{2}}+B_2p^{-1}+\ldots)\,e_n(t)\,,
\end{aligned}\right\}\ldots(48)$$

where

$$\left.\begin{aligned}
A_1 &= \frac{n}{4\sqrt{\pi\sigma'}\,a}\left(n-1-\frac{n+1}{\rho}\right),\\
B_1 &= \frac{n}{32\pi\sigma' a^2}\left\{(n-1)(n^2-n+2)-\frac{2n(n^2-1)}{\rho}\right.\\
&\qquad\qquad\left.+\frac{(n+2)(n^2-1)}{\rho^2}\right\}\ldots,\\
A_2 &= \frac{1}{4\sqrt{\pi}a}\left[\left\{n(n-1)-\frac{3(n+1)}{q}\right\}\frac{1}{\sqrt{\sigma'}}\right.\\
&\qquad\left.+\frac{l-2}{8}\left\{(4\nu^2-1)\,\rho^{-1+\frac{1}{2}l}-(4\nu^2-8\nu+3)\,q^{-1+\frac{1}{2}l}\right\}\frac{1}{\sqrt{\sigma_0}}\right],\\
B_2 &= \frac{1}{32\pi a^2}\left[\left\{-n^2+3n+2+\frac{2(n+1)(n^2-4n+2)}{q}\right.\right.\\
&\qquad\left.-\frac{(n+1)(n^2-3n-6)}{q}\right\}\frac{1}{\sigma'}\\
&\qquad+\frac{(l-2)^2}{64}\{(4\nu^2-1)(4\nu^2-9)\rho^{-2+l}\\
&\qquad-2(4\nu^2-1)(4\nu^2-8\nu+3)\,(\rho q)^{-1+\frac{1}{2}l}\\
&\qquad+(4\nu^2-8\nu+3)\,(4\nu^2-8\nu+1)\,q^{-2+l}\}\,\frac{1}{\sigma_0}\\
&\qquad+\left\{\frac{l-2}{4}\left\{n(n-1)-\frac{3(n+1)}{q}\right\}\right\{(4\nu^2-1)\,\rho^{-1+\frac{1}{2}l}\\
&\qquad\left.\left.-(4\nu^2-8\nu+3)\,q^{-1+\frac{1}{2}l}\right\}\frac{1}{\sqrt{\sigma'\sigma_0}}\right],\\
&\ldots\ldots\ldots\ldots\ldots\ldots\ldots\ldots\ldots\ldots\ldots\ldots\ldots\ldots
\end{aligned}\right\}(49)$$

Then, corresponding to the idealized inducing field of sudden commencement, bay-type disturbance and later part of D_{st}, we have

$$\left.\begin{array}{l}
\text{1) sudden commencement}\\
\qquad e_n(t)=A\dfrac{\alpha}{p+\alpha}H(t)\,,\ n=1\,,\ \alpha=0{\cdot}04\,sec^{-1}\\
\qquad c_1(t)=A\alpha\{\varphi_2(t)+A_1\varphi_3(t)+(B_1-\alpha)\,\varphi_4(t)+\dots\}\,,\\
\qquad c_2(t)=A\alpha\{\psi_2(t)+A_2\psi_3(t)+(B_2-\alpha)\,\psi_4(t)+\dots\}\,,\\
\text{2) bay-type disturbance}\\
\qquad e_n(t)=A\dfrac{p}{(p+\alpha)^2}H(t)\,,\ n=1\,,\ \alpha=0{\cdot}28\times10^{-3}\,sec^{-1}\\
\qquad c_1(t)=A\{\varphi_0(t)+A_1\varphi_1(t)+(B_1-2\alpha)\,\varphi_2(t)+\dots\}\,,\\
\qquad c_2(t)=A\{\psi_0(t)+A_2\psi_1(t)+(B_2-2\alpha)\,\psi_2(t)+\dots\}\,,\\
\text{3) later part of } D_{st}\\
\qquad e_n(t)=A\dfrac{p}{p+\alpha}H(t)\,,\ n=1\,,\ \alpha=3{\cdot}2\times10^{-6}\,sec^{-1}\\
\qquad c_1(t)=A\{\varphi_0(t)+A_1\varphi_1(t)+(B_1-\alpha)\,\varphi_2(t)+\dots\}\,,\\
\qquad c_2(t)=A\{\psi_0(t)+A_2\psi_1(t)+(B_2-\alpha)\,\psi_2(t)+\dots\}\,,\\
\text{where}\\
\qquad \left.\begin{array}{l}\psi_0(t)\\ \varphi_0(t)\end{array}\right\}=\dfrac{2}{\pi}\displaystyle\int_0^\infty e^{-tx^2}\cos\begin{array}{c}k_\psi\\ k_\varphi\end{array}x\,dx\,,\\
\qquad \left.\begin{array}{l}\psi_1(t)\\ \varphi_1(t)\end{array}\right\}=\dfrac{2}{\pi}\displaystyle\int_0^\infty \dfrac{e^{-tx^2}}{x}\sin\begin{array}{c}k_\psi\\ k_\varphi\end{array}x\,dx\,,\\
\text{and}\qquad\qquad \cdots\cdots\cdots\cdots\cdots\cdots\cdots\cdots\cdots\cdots\\
\quad k_\psi=\sqrt{4\pi}\,a\left\{(1-q)\sqrt{\sigma'}+\dfrac{2}{l-2}\sqrt{\sigma_0}\,(\rho^{1-\frac{1}{2}l}-q^{1-\frac{1}{2}l})\right\},\\
\quad k_\varphi=\sqrt{4\pi\sigma'}\,a\,(1-\rho)\,.
\end{array}\right\}\quad(50)$$

The first three of the infinite integrals in (50) are easily obtained as follows.

$$\left.\begin{array}{l}\psi_0(t)\\ \varphi_0(t)\end{array}\right\}=\frac{e^{-k^2/4t}}{\sqrt{\pi t}}\,,\quad \left.\begin{array}{l}\psi_1(t)\\ \varphi_1(t)\end{array}\right\}=1-\text{erf.}\,\frac{k}{2\sqrt{t}}\,,$$

$$\left.\begin{array}{l}\psi_2(t)\\ \varphi_2(t)\end{array}\right\}=2\sqrt{\frac{t}{\pi}}\,e^{-k^2/4t}-k\left(1-\text{erf.}\,\frac{k}{2\sqrt{t}}\right). \quad (51)$$

φ_3, φ_4,$\cdots$ and ψ_3, ψ_4,$\cdots$ are obtained by numerical integration, but not important for numerical calculation. As the convergency of these series which appeared in (50) are very rapid, numerical calculation of $c_1(t)$ and $c_2(t)$ are comparatively easy. Giving the values determined in the previous sections, then, the relative magnitude of the current-density for each case are calculated as shown in Figs. 10, 11 and 12, the distribution being calculatad for $t=\mathbf{T}$ as also shown in the figures respectively.

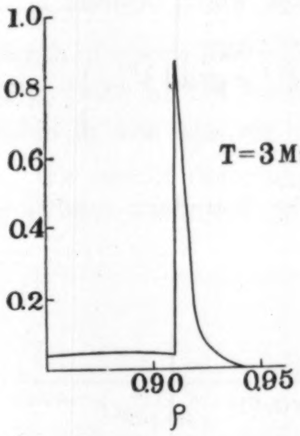

Fig. 10. The distribution of the induced currents for sudden commencement.

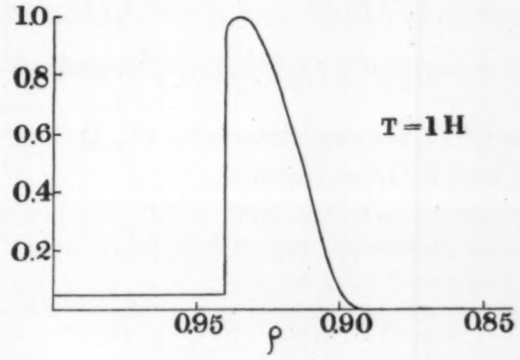

Fig. 11. The distribution of the induced currents for bay-type disturbance.

In the case of periodic induction, we can obtained the expression for the current-density by putting $p=i\alpha$ and $e(t)=Ee^{i\alpha t}$ in (45). The expression can be evaluated by means of various formulae already given in the calculation of amplitude ratio and phase difference. The relative distribution of the current-density for the harmonic P_2^1, diurnal term of S_q, is calculated in regard to our earth-model being shown in Fig. 13. Strictly speaking, the phase of the induced currents differ from each other with different depths. But its difference is neglected here as in Chapter II, Part I. The distribution for P_3^2 is also calculated being almost the same with that for P_2^1.

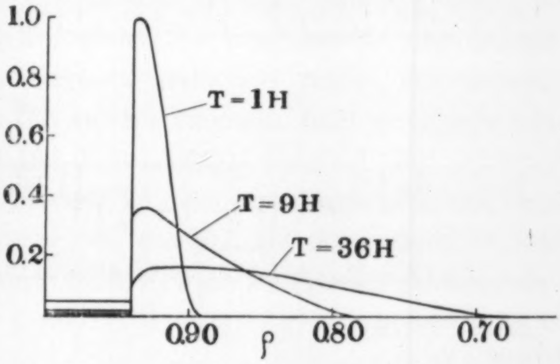

Fig. 12. The distribution of the induced currents for later part of D_{st}.

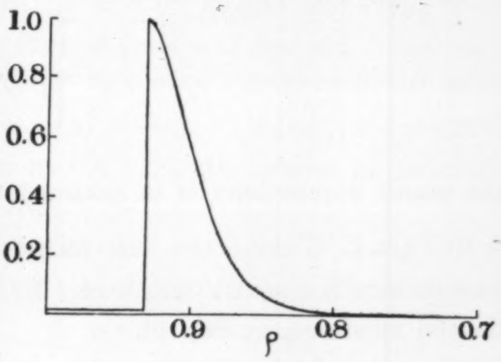

Fig. 13. The distribution of the induced currents for diurnal and semi-diurnal components of S_q.

In the next place, we shall

evaluate the distribution in the case of magnetic effect which is associated with Dellinger-effect. We have vector potential $\overrightarrow{A_1}$ and $\overrightarrow{A_2}$ respectively for the superficial layer and the inner high conducting region, which become

$$\left.\begin{aligned}\overrightarrow{A_1}&=\{C_1(p)\,e^{-\sqrt{4\pi\sigma' p+k^2}\,z}+D_1(p)\,e^{\sqrt{4\pi\sigma' p+k^2}\,z}\}\,e(t)\,[\overrightarrow{r}\,\mathrm{grad}\,V],\\ \overrightarrow{A_2}&=C_2(p)\,g(p,z)\,e(t)\,[\overrightarrow{r}\,\mathrm{grad}\,V].\end{aligned}\right\}\ \ldots(52)$$

Meanwhile we can determine C_1, D_1 and C_2 from the boundary conditions at $z=0$ and $z=D$ as follows.

$$\left.\begin{aligned}&\left.\begin{matrix}C_1(p)\\ D_1(p)\end{matrix}\right\}=\frac{1}{2}e^{\pm\sqrt{4\pi\sigma' p+k^2}\,z}\left\{g(p,D)\pm\frac{g'(p,D)}{\sqrt{4\pi\sigma' p+k^2}}\right\}C_2(p),\\ &C_2(p)=\frac{4}{(k+\sqrt{4\pi\sigma' p+k^2})\left(g(p,D)-\frac{g'(p,D)}{\sqrt{4\pi\sigma' p+k^2}}\right)e^{\sqrt{4\pi\sigma' p+k^2}\,D}+(k-\sqrt{4\pi\sigma' p+k^2})\left(g(p,D)+\frac{g'(p,D)}{\sqrt{4\pi\sigma' p+k^2}}\right)e^{-\sqrt{4\pi\sigma' p+k^2}\,D}},\end{aligned}\right\}(53)$$

Hence the current-density is obtained by (52). Corresponding to large p, we have

$$\left.\begin{aligned}\overrightarrow{c_1}&=-A\sigma'\frac{2}{\sqrt{\pi\sigma'}}p^{-\frac{1}{2}}\left\{1-\gamma' p^{-\frac{1}{2}}+\left(\frac{\gamma'^2}{2}-2\omega\right)p^{-1}+\ldots\right\}\\ &\qquad\times e^{-\sqrt{4\pi\sigma' p}\,z}[\overrightarrow{r}\,\mathrm{grad}\,V]\,H(t),\\ \overrightarrow{c_2}&=-A\sigma(z)\frac{2p^{-\frac{1}{2}}}{\sqrt{\pi}(\sqrt{\sigma'}+\sqrt{c_1})}\left\{1+\left(\frac{\beta^2}{6}\frac{1}{\sqrt{4\pi c_1}}-\gamma'\right)p^{-\frac{1}{2}}\right.\\ &\qquad\left.+(K-2\omega)p^{-1}+\ldots\right\}e^{-\sqrt{4\pi p}\{\sqrt{\sigma'}D+\sqrt{c_1}(z-D)\}}[\overrightarrow{r}\,\mathrm{grad}\,V]\,H(t),\end{aligned}\right\}(54)$$

where

$$\gamma'^2=\frac{k^2}{4\pi\sigma'},\ \gamma^2=\frac{k^2}{4\pi c_1},\ K=\frac{\gamma'^2}{2}-\frac{\gamma'\beta^2}{6\sqrt{4\pi c_1}}-\frac{1}{\sqrt{\sigma'}+\sqrt{c_1}}\times\left\{\frac{\sqrt{\sigma'}\gamma'^2+\sqrt{c_1}\gamma^2}{2}-\frac{\beta^2}{4}\frac{D^2(\sqrt{\sigma'}-\sqrt{c_1})}{4\pi c_1}\right\}.$$

In the above expressions, it is assumed that $e(t)=\dfrac{Ap}{(p+\omega)^2}H(t)$ as already done in Part I. Taking the first terms of (54), we get the expressions of the current-density for small values of t by which the relative magnitude can be evaluated as shown in Fig. 14.

As seen in the figures, Figs. 10~14, almost all the induced currents concentrate in the upper part of the high conducting region as well as in the case of the uniform core model studied in Part I. It is clearly shown that the slower the variation is the deeper the currents penetrate into the earth. Hence the determined values of σ_0, q and l in this paper are responsible for the electrical state down to the depth of about 1000～1500 *km* to that depth the magnitude of the induced current is appreciable in the slowest variation concerned here. We cannot determine the electrical property in deeper part until slower variation become available.

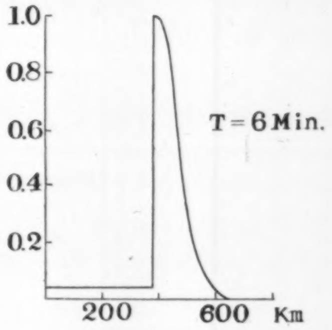

Fig. 14. The distribution of the induced currents for solar flare effect.

5. Summary and conclusion.

On the basis of the approximate knowledge on the electrical conductivity studied in Part I, the writer assumed an analytical expression for the conductivity-distribution as given by (1) by which, when we give suitable values to the constants involved, we can well represent the conductivity distribution obtained in Part I. Then the electromagnetic induction within the present earth-model by various variations in the eatrh's magnetic field are studied in Part II. In order to explain the relation between the external and internal parts of potential of magnetic field observed at the earth's surface, the constants of the analytical expression, say σ', σ_0, q and l, are determined. Combining the studies on various variations, from the one with period or duration-time of a few minutes to the one of a few days, the most preferrable values are determined to be $\sigma'=10^{-15}$ *emu*, $\sigma_0=1{\cdot}0\times10^{-12}$ *emu*, $q=0{\cdot}94$ and $l=11$. Thus the upper part of the earth, down to the depth of about 400 *km*, seems to be almost non-conducting. The conductivity in this region amounts to only 10^{-15} *emu* that is the same order with that of rock and dry soil found on the earth's surface. However, the conductivity increases discontinuously at this level amounting to the order of as much as 10^{-12} *emu*. Then its rate of increase becomes somewhat small in proportion to the eleventh power of inverse of the radial distance from the earth's centre.

As to the errors of the determination of the constants, σ', σ_0, q and l, it is difficult to discuss exactly because the errors included in the analyses of the actual data are not clearly known. A rough estimate of the errors is effected in the main on the basis of the analyses of S_q which are repeatedly subjected to spherical harmonic analysis. According to Hasegawa's and Benkova's analyses of S_q, which are believed to be the most reliable, the amplitude ratio and the phase difference of main harmonics are given as shown in Table I.

Table I.

		Hasegawa		Benkova		Mean	
n	m	e/i	$\iota-\epsilon$	e/i	$\iota-\epsilon$	e/i	$\iota-\epsilon$
2	1	2·30	9°	2·34	5°	2·32	7°
3	2	2·43	10°	2·30	5°	2·37	8°
4	3	2·25	14°	—	—	—	—

Hence the probable errors of the mean values of both analyses amount to about ±2° in phase difference and ±0·03 in amplitude ratio. Taking into consideration these errors, we know the errors of q must not exceed about ±0·01, otherwise the amplitude ratio will protrude far from the range of the errors of the analyses. As to the range of σ_0 and l, as shown in Fig. 15, we know the maximum of σ_0, that is $2{\cdot}4\times10^{-12}$ *emu*, occurs when $l=0$ and σ_0 decreases to $0{\cdot}6\times10^{-12}$ *emu* as l increases to 20, while values of l larger than 20 are not appropriate.

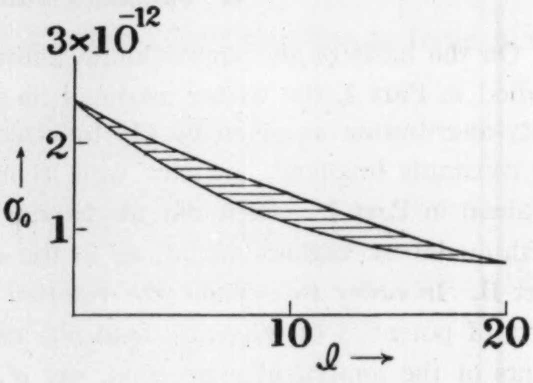

Fig. 15.

If there exist errors of $\pm1\gamma$ in the analyses of the other variations, roughly speaking, any combination of q, σ_0 and l within the range of errors cited above gives in the main reasonable results for the explanation of the relation between inducing and induced field. To sum up, though the most probable distribution of the conductivity is given by (1) with $\sigma'=10^{-15}$*emu*, $\sigma_0=1{\cdot}0\times10^{-12}$ *emu*, $q=0{\cdot}94$ and $l=11$ as shown

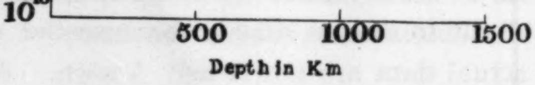

Fig. 16. The second approximation for the conductivity-distribution in the earth.

in Fig. 16, the accuracy of these values are somewhat less as mentioned above. A more sufficient accumulation of magnetic data is needed to make the determination more accurate.

In conclusion, the writer wishes to express his deep appreciations of the kind advices and helpful suggestions rendered him by Dr. T. Nagata. He also wishes to express his hearty thanks to Professor T. Hagiwara for his general encouragement. This study was made with the financial aid of research grant from the Department of Education. The writer wishes to express his sincere thanks to the Department of Education for the grant received.

---

19. 地球内の電磁感應およびその地球内部の電氣的性質との關係 第2報

地震研究所 力武常次

筆者は第1報に於いて，種々の地磁氣變化の解析より地球內部の電氣傳導度の分布が近似的に推定できることを示したが，本報文に於いては第1報に於いて便宜的に求めた分布を analytical な形で近似し，そのような電氣傳導度の分布をもつ地球內部の電磁感應を數學的にとりあつかい，常數に適當な値を採用することによつて，磁氣嵐の急始，デリンジャー現象に伴う變化，灣型變化，日變化および磁氣嵐の主相等の內外磁場の關係がほゞ滿足すべき程度に說明出來ることを示した．

即ち

$$\begin{aligned} \sigma &= \sigma' & 1 > \rho > q \\ &= \sigma_0 \rho^{-l} & q > \rho > 0 \end{aligned} \qquad (\rho = r/a)$$

なる形で電氣傳導度の分布があたえられるものとし，內外磁場の關係が滿足されるように，σ', q, l 等の値を決定するのである．計算は第1報でのべた uniform core model の場合にくらべてはるかに面倒となるが，原理的には全く同じである．かくして常數のもつとも適當な値として

$$\sigma' = 10^{-15}\,emu, \quad \sigma_0 = 1.0 \times 10^{-12}\,emu, \quad q = 0.94, \quad l = 11$$

がえられた．したがつて電氣傳導度は地表から深さ約 400 *km* 迄の間は 10^{-15} *emu* 程度であり，そこで不連續的に增加して 2.0×10^{-12} *emu* となり，それより深いところでは地球中心からの半徑の逆數の 11 乘に比例して增加することとなる．この決定に對する誤差の吟味は嚴密に行うことは困難であるが，もつとも信頼出來ると考えられる日變化の解析結果をもととして若干の議論を行つた．

電流の分布も計算したが，そのほとんど大部分が高電導領域の上部に集中し，深さ 1500 *km* 以上の內部のことはもつとおそい變化を解析しなければ，何も言えないことになる．

20. *On the Coda Waves of Earthquake Motions.* (*Part* 5)

By Syun'itiro OMOTE,

Earthquake Research Institute.

(Read Oct. 10, 1946 and Feb. 19, 1947.—Received Sept. 20, 1950.)

Chapter 6. Analysis of the Period of Coda Oscillations by Takahasi-Husimi's Method.[1]

§ 21. Takahasi-Husimi's Method of Analysis.

Takahasi-Husimi's[2] method of analysis aims at finding the two characteristic constants of a vibrating system, p and ϵ, namely, the coefficient of damping and the circular frequency, from a curve recorded by the motion of the vibrating system when it is exposed to irregular external forces. This new method of analysis devised by K. Takahasi will be made use of in our study here, since it seems to be highly fitted for our present purpose of analysing the coda oscillations of earthquake motions.

In our present study, however, the external forces mean the energies that are conveyed as seismic waves. These seismic waves have to be reflected and refracted many times when they reach the surface of the earth or as they pass through some discontinuities within the earth. Therefore it is not to be denied that the seismic waves are likely to have the character of irregular impulsive waves when they are observed by seismometers installed on the earth's surface. But at the same time it is to be expected that regular periodic waves also are to be detected in the records on the same seismometers. It is our aim, therefore, to expand Takahasi's method to cover the case where the external force consists not only of irregular impulses but also of regular periodic waves, and to see what results are derived from the analysis of the records made by the vibrating system in such a case.

---

[1] S. OMOTE, *Bull. Earthq. Res. Inst.*, 21 (1943), 458. 22 (1944), 140. 23 (1945), 47. 28 (1950), 49.

[2] K. TAKAHASI and K. HUSIMI, *Geophys. Mag.*, 9 (1935), 29.

§ 22. The Expansion of Takahasi's Method.

When the external force that affects the vibrating system is supposedly made up of a regular and an irregular part, the equation of motion of the vibrating system, according to usual notations, will be given by

$$\frac{d^2x}{dt^2} + 2\epsilon\frac{dx}{dt} + n^2x = f(t) \quad \ldots\ldots\ldots\ldots\ldots\ldots(22.1)$$

where $f(t)$ is an external force. Whence can be set up the equation

$$f(t) = \varphi(t) + Le^{-\alpha t}\sin pt \quad \ldots\ldots\ldots\ldots\ldots\ldots(22.2)$$

in which $\varphi(t)$ is the term representing the wholly irregular motions, and the second term represents the periodic motions of a simple harmonic type with damping.

In the case when $n > \epsilon$, the solution of the equation (22.1) is given by

$$x = c_1e^{-\varepsilon t}\cos\sigma t + c_2e^{-\varepsilon t}\sin\sigma t - \frac{e^{-\varepsilon t}\cos\sigma t}{\sigma}\int f(t)\,e^{\varepsilon t}\sin\sigma t\,dt$$

$$+\frac{e^{-\varepsilon t}\sin\sigma t}{\sigma}\int f(t)\,e^{\varepsilon t}\cos\sigma t\,dt \quad \ldots\ldots\ldots\ldots\ldots\ldots(22.3)$$

$$\sigma = \sqrt{n^2-\varepsilon^2} \quad \ldots\ldots\ldots\ldots\ldots\ldots(22.4)$$

That this $\varphi(t)$ is a wholly irregular disturbance, according to Takahasi's assumption, is to be interpreted to mean

(1) That $\varphi(t)$ is not related either with x or dx/dt.

(2) That the mean value of $\varphi(t)$ is zero.

(3) That $\int_{t_1}^{t_2}\varphi(t)\,dt$ has nothing to do with $\int_{t_1'}^{t_2'}\varphi(t)\,dt$ so long as (t_1, t_2) and (t_1', t_2') do not have a common domain.

Now, if we put

$$\varphi(t) = \varphi_0(t-\delta_0) + \varphi_1(t-\delta_1) + \cdots + \varphi_n(t-\delta_n) + \cdots \quad \ldots\ldots(22.5)$$

where

$$\left.\begin{array}{ll} t-\delta_i < 0\,, & \varphi_i(t-\delta_i) = 0 \\ 0 < t-\delta_i < +\Delta t_i\,, & \varphi_i(t-\delta_i) \neq 0 \\ t-\delta_i > +\Delta t_i\,, & \varphi_i(t-\delta_i) = 0 \end{array}\right\} \quad \ldots\ldots\ldots\ldots\ldots\ldots(22.6)$$

$$\left.\begin{array}{l} \delta_{i-1} < \delta_i \\ i = 0,\ 1,\ 2,\cdots \end{array}\right\} \quad \ldots\ldots\ldots\ldots\ldots\ldots(22.7)$$

then, in such a case, the aspect in which one after another of the free oscillations of a vibrating system is stimulated will be shown in the form

$$x=\sum[e^{-\varepsilon(t-\delta i)}\{c_{1i}\cos\sigma(t-d_i)+c_{2i}\sin\sigma(t-d_i)\}]$$
$$+\frac{Le^{-\alpha t}}{\sqrt{(\alpha^2-2\alpha\varepsilon+n^2-p^2)+4p^2(\alpha-\varepsilon)^2}}\sin p(t-\tau)$$
$$-\frac{e^{-\varepsilon t}\cos\sigma t}{\sigma}\int\varphi(t)e^{\varepsilon t}\sin\sigma t\,dt+\frac{e^{-\varepsilon t}\sin\sigma t}{\sigma}\int\varphi(t)e^{\varepsilon t}\cos\sigma t\,dt. \qquad \text{............(22.8)}$$

With respect to the equation (22.8), if we pick up from among the values of x observed at certain intervals of time those whose deviation from the mean value of x is positive, and arrange in vertical column the portions of the curve beginning with t_s where x is positive, in orden to work out the mean of these partial curves, what sort of a curve is to be obtained, provided that we have had a great many such x_s?

To make the matter simple, we will divide the motion of x into two parts, x', x'', and put

$$x=x'+x'' \qquad \text{.....................................(22.9)}$$

where x' represents a part that oscillates simply harmonically and x'' the part that oscillates irregularly.

To begin with, let us consider the x' parts only. If we assume that the sole irregular external force φ_0 worked on the vibrating system, the motion of x' under the influence of this force, to be given by x'_0, will have the form

$$x'_0=e^{-\varepsilon t}\{c_1\cos\sigma t+c_2\sin\sigma t\}$$
$$+\frac{Le^{-\alpha t}}{\sqrt{(\alpha^2-2\alpha\varepsilon+n^2-p^2)^2+4p^2(\alpha-\varepsilon)^2}}\sin p(t-\tau) \quad \text{...(22.10)}$$

(where δ_0 is treated as zero).

The equation (22.10) can be rearranged into a simpler form. In the following form the phase difference between the first and second terms of the right-hand side of the equation (22.10) is represented by Δ, since it can be given any quite arbitrary values:—

$$x'_0=ae^{-\varepsilon t}\sin\sigma t+be^{-\alpha t}\sin\{p(t-\tau)+\Delta\}. \quad \text{..................(22.11)}$$

Now we will make $x'_0(t_0)\cdots\cdots x'_0(t_n)$ represent the various values which x'_0 has at regular intervals of time, or at $t_0=0$, $t_1=k$, $t_2=t_1+k$, $\cdots\cdots$ (22.12), (k being a certain unit of time), and assume that ε and α of x'_0 are equal and so small that the oscillations will last a sufficiently long time. We will further assume that at a certain definite hour, t_s in (22.12), the first term of the right-hand side of the equation (22.11) had a certain positive value h. In such a case, the second term must be greater than $(-h)$ to make $x'_0(t_s) > 0$. If we make a equal to b, the above conditions will be satisfied by

$$\pi+\gamma > p(t_s-\tau)+\varDelta$$

or

$$2\pi-\gamma < p(t_s-\tau)+\varDelta$$

and from this we see that the probabitity P_+ that makes $x'_0(t_s) > 0$ when the first term of the right-hand side in the equation (22.10) is equal to $+h$, will be given by

$$P_+ = \frac{1}{2} + \frac{\gamma}{\pi}.$$

In the same way, in the case of $a \sin\gamma = -h$, the probability P_- that makes $x'_0(t_s) > 0$ will be given by

$$P_- = \frac{1}{2} - \frac{\gamma}{\pi}.$$

Generally speaking, under these assumptions, at any time-point defined by the equation (22.12), when the first term of the right-hand side of (22.10) is positive, the probability that makes $x'_0 > 0$ is larger than when it is negative. This probability becomes still larger as the absolute value of the first term increases. Now if we make up the summation of

$$\sum\{x'_0(t_s)\} \qquad\qquad (22.13)$$

with regard to a very long period of time—of the values of x_0 at the t_s that makes $x_0(t_s) > 0$—the terms that are small in their absolute values are likely to be cancelled, since there will occur as many of them in the positive as in the negative, while the terms that are large in their absolute values will remain uncancelled in $\Sigma\{x'_0(t_s)\}$ for the lack of their negative values to offset them.

What we have considered above about the first term of the right-hand side of the equation (22.10) is also perfectly applicable to the second term of the same equation. With respect to the second term too, we can easily see that terms with the large positive values are added together in $\Sigma\{x'_0(t_s)\}$.

In general, the maximum amplitudes a and b of the first and the second terms are not equal to each other, but even here it will be easily seen that terms with larger positive values are added together.

In the second place, we will consider the case where the free oscillation of the vibrating system is stimulated by one after another of the successive external forces. What modifications will it be necessary to make in the above statement?

Let us make $x'(t_0)$, $x'(t_1)$ ········ represent the values of x' of the equation

(22.9) at the time-points $t_1, t_2, \cdots\cdots t_n$, defined in (22.12), and assume $x'(t_s) > 0$ at the time-point t_s. In such a case too, when the free oscillations of that vibrating system are being stimulated in the form $e^{-\varepsilon(t_s-\delta_i)}\{c_1 \cos\sigma(t_s-\delta_i) + c_2 \sin\delta(t_s-\delta_i)\}$, it will be easily suspected that the term that has a large amplitude has a high probability to make $x'(t_s) > 0$. Similarly, with respect to the oscillations of a simple harmonic type due to an external force that is denoted as $[Le^{-\alpha t}/\{(\alpha^2-2\varepsilon+n^2-p^2)^2+4p^2(\alpha-\varepsilon)^2\}^{\frac{1}{2}}] \sin p(t-\tau)$ the same statement will hold good.

Next, we will compare

$$\sum x'(t_s) \quad \ldots\ldots\ldots\ldots\ldots\ldots\ldots\ldots\ldots\ldots\ldots (22.14)$$

with

$$\sum x'(t_s+k). \quad \ldots\ldots\ldots\ldots\ldots\ldots\ldots\ldots\ldots\ldots (22.15)$$

The former is the summation of all the values of x' at the time-point t_s that make $x'(t_s) > 0$, and the latter is the summation of all the values of x' at the time-point of (t_s+k), namely, after the lapse of one unit time k from the respective t_s used in the former summation. From the definition of (22.14) it is not to be expected that all of the values of $x'(t_s+k)$ should also be positive and it is reasonable to expect that some of the values of $x'(t_s+k)$ will be negative. Then, statistically, we shall have to put

$$\sum x'(t_s) > \sum x'(t_s+k).$$

These results will lead us to the following conjecture; if we pick up every positive $x'(t_s)$ and put the value of $x'(t_s)$ as x_0, and also assume that time as the point of commencement, then the curve of the values of x after t_s may be drawn. In this manner, we can draw many curves of x'_0 that begin with the different positive values of x'_0, and finally we can calculate their mean value and draw a mean curve of them all. Such a mean curve will make a damping oscillatory curve with its maximum value at the beginning. The mean curve thus obtained is composed of two independent simple harmonic oscillations not in any way mutually connected either with regard to their periods or with regard to the phases, so that if x' is at its maximum at the beginning, this means that these two curves also have their maximum values at $t=0$. The mean curve will be shown by

$$\overline{x'}_+ = \overline{a^{(+)}} e^{-\varepsilon t} \cos\sigma t + \overline{b^{(+)}} e^{-\alpha t} \cos pt \quad \ldots\ldots\ldots\ldots\ldots\ldots (22.16)$$

where $\overline{x'}_+$ means the average of all the values of x' that make $x' > 0$, and $\overline{a^{(+)}}$ and $\overline{b^{(+)}}$ mean the average amplitudes of the first and the second terms of the equation (22.11) when x' has the $+$ sign. This, however, does not mean that all the terms of $\overline{a^{(+)}}$ and $\overline{b^{(+)}}$ are positive in their signs.

Next, we will consider the amplitude x which is expressed by $x=x'+x''$ where x' is a term due to the simple harmonic motions considered above, and x'' is a term due to irregular external forces. In this expression, even if $x'>0$, it does not necessarily follow that $x>0$. But we can pick up a very large number of positive x and draw curves that begin each with such a positive x, and calculate and draw an average curve of them all. In this average curve the positive and negative values of x'' will occur in equal numbers, so that the positive and negative effects of x'' will cancel each other, as a result of which the same conclusions will be derived statistically as we get in the case of the curve x'.

Therefore, if we denote such an average value by $\overline{x_+}$, then, $\overline{x_+}$ probably has the same nature as $\overline{x'_+}$ and, similar to the equation (22.16), it will be given by

$$\overline{x}_+=\overline{A}^{(+)}e^{-\varepsilon t}\cos pt+\overline{B}^{(+)}e^{-\alpha t}\cos pt \quad \text{.................}(22.17)$$

where $\overline{A}^{(+)}$ and $\overline{B}^{(+)}$ are both constant terms.

Hitherto, we have solely discussed the cases when the deviation of x from the average is positive. In precisely the same manner, when the deviation is negative, we can fined the average $\overline{x_-}$ of all the negative values of x, and the following equation will be derived.

$$\overline{x}_-=\overline{A}^{(-)}e^{-\varepsilon t}\cos \sigma t+\overline{B}^{(-)}e^{-\alpha t}\cos pt \quad \text{..............}(22.18)$$

where $\overline{A}^{(-)}$ and $\overline{B}^{(-)}$ are the average of the maximum amplitudes of the first and second terms when the sign of x is negative.

These irregular external disturbances will imply positive and negative motions occurring with equal frequency, and the simple harmonic motion will be distributed symmetrically from its zero line, so that as a whole the average of a great many values of x, $\overline{x_+}$ will be the same as $\overline{x_-}$ in their absolute value and have the opposite signs.

As the consequence of this, we have

$$\overline{x}_+ + (-\overline{x}_-)=|\overline{A}|\,e^{-\varepsilon t}\cos \sigma t+|\overline{B}|\,e^{-\alpha t}\cos pt\text{......}(22.19)$$

The first term of the right-hand side of this equation represents the free oscillation of the vibrating system, and the second the damping sine waves due to the external forces.

Now if in some way this curve is analysed into its two component curves, we shall be able to find out the damping constants and the periods of the two oscillatory motions. And thanks to Takahasi's method of analysis, we now have the way to determine from seismographs not only the damping constant and the period of a vibrating system but also the damping constants and the periods of the external forces provided that they contain periodical forces.

Table I. Earthquake and it's portion that the Takahasi-Husimi's analysis were resorted to.

A	B	C	D	h	E	A	B	C	D	h	E
				s	m m					s	m m
16-1	16	Siwoyasaki	E-W	1	10- 12	37-4	73	New-Guinea	E-W	2	71- 72
16-2	,,	,,	,,	,,	12- 14	37-5	,,	,,	,,	,,	72- 73
16-3	,,	,,	,,	,,	16- 17	37-6	,,	,,	,,	,,	82- 84
19-1	19	Kesenuma	N-S	2	14- 15	37-7	,,	,,	,,	,,	93- 95
20-1	20	Koti-Yamato	E-W	1	15- 17	37-8	,,	,,	,,	,,	100-102
						37-9	,,	,,	,,	,,	102-104
20-2	,,	,,	N-S	,,	11- 13	49- 1	49	Mexico	,,	,,	69- 71
20-3	,,	,,	,,	,,	14- 16	49- 2	,,	,,	,,	,,	71- 72
54-1	54	Kagi	,,	1	30- 32	49- 3	,,	,,	,,	,,	72- 73
34-1	34	Celebes Sea	E-W	2	40- 42	49- 4	,,	,,	,,	,,	73- 74
36-1	36	Celebes	,,	2	40- 41	49- 5	,,	,,	,,	,,	82- 84
36-2	,,	,,	,,	,,	41- 42	49- 6	,,	,,	,,	,,	84- 85
36-3	,,	,,	,,	,,	42- 43	49- 7	,,	,,	,,	,,	90- 92
36-4	,,	,,	,,	,,	43- 44	49- 8	,,	,,	,,	,,	92- 94
36-5	,,	,,	,,	,,	50- 51	49- 9	,,	,,	,,	2	99-101
36-6	36	Celebes	E-W	2	51- 52	49-10	,,	,,	,,	,,	101-103
36-7	,,	,,	,,	,,	60- 62	51- 1	51	Peru	E-W	,,	56- 58
36-8	,,	,,	,,	,,	62- 64	51- 2	,,	,,	,,	,,	58- 60
36-9	,,	,,	,,	,,	71- 73	51- 3	,,	,,	,,	2	71- 73
37-1	37	New-Guinea	E-W	2	50- 52	51- 4	,,	,,	,,	,,	77- 79
37-2	,,	,,	,,	,,	53- 55	51- 5	,,	Peru	E-W	2	79- 81
37-3	,,	,,	,,	,,	69- 71	51- 6	,,	,,	,,	,,	122-124

(to be continued)

(continued)

A	B	C	D	h	E	A	B	C	D	h	E
				s	m m					s	m m
51- 7	51	Peru	N-S	2	56- 58	52-10	52	Chili	E-W	2	121-122
51- 8	„	„	„	„	58- 59	52-11	„	„	„	„	122-123
51- 9	„	„	„	„	59- 61	52-12	„	„	„	„	138-139
51-10	„	„	„	„	70- 72	52-13	„	„	„	„	139-140
51-11	„	„	„	„	72- 74	52-14	„	„	„	„	140-141
51-12	„	„	„	„	80- 82	52-15	„	„	„	„	62- 63
51-13	„	„	„	„	82- 84	52-16	„	„	„	„	63- 64
51-14	„	Chili	E-W	„	150-151	52-17	„	„	N-S	2	66- 67
51-15	„	„	„	„	151-153	52-18	„	„	„	„	67- 68
52- 1	52	Chili	„	„	66- 68	52-19	„	„	„	„	80- 81
52- 2	„	„	„	„	68- 70	52-20	„	„	„	„	82- 83
52- 3	„	„	„	2	80- 81	52-21	„	„	„	„	83- 84
52- 4	„	„	„	„	81- 83	52-22	„	„	„	„	115-117
52- 5	„	„	„	„	83- 85	52-23	„	„	„	„	117-119
52- 6	„	„	„	„	105-107	52-24	„	„	„	„	130-131
52- 7	„	„	„	„	107-108	52-25	„	„	„	„	131-132
52- 8	„	„	„	„	108-110	52-26	„	„	„	„	132-133
52- 9	„	„	„	„	120-121	52-27	„	„	„	„	133-134

A: Curve No. B: Earthquake No. C: Epicenter.
D: Component. E: Portion in which the analysis was made.

Table II. Numerical values of oscillation curves calculated by means of Takahasi-Husimi's method.

Figures in each heading is curve number in Table I.

	16 1	16-2	16-3	19-1	20-1	20-2	20-3	54-1	34 1
1	+154.2	+132.7	+78.2	+65.6	+183.3	+229.1	+206.0	+158.3	+507.5
2	+102.6	+63.5	+52.3	+36.5	+70.7	+176.6	+169.8	+124.7	+350.5
3	−29.1	−46.4	−10.9	+5.9	−25.6	+18.3	+48.2	+26.7	+101.1
4	−102.2	−117.5	−58.6	−29.7	−79.9	−114.9	−65.4	−91.4	−161.4
5	−83.4	−122.2	−58.2	−56.5	−73.1	−135.1	−141.1	−159.9	−335.9
6	−18.6	−33.0	−21.1	−45.1	−47.2	−50.6	−130.4	−140.2	−367.6
7	+34.9	+51.6	+29.1	−0.5	−21.1	+70.0	−70.6	−39.9	−256.6
8	+68.2	+89.7	+52.5	+21.5	−20.1	+133.3	−3.0	+85.1	−63.7
9	+67.2	+67.9	+46.5	+39.4	−30.1	+99.5	+13.3	+161.7	+112.1
10	+18.7	−1.5	+14.8	+22.5	−29.1	+6.1	+35.6	+145.7	+234.8
11	−47.1	−55.5	−21.0	+8.7	+8.1	−87.6	+40.8	+37.0	+256.8
12	−69.3	−73.2	−42.1	−15.2	+61.6	−117.6	+45.4	−88.5	+176.0
13	−43.3	−35.8	−33.6	−25.6	+68.7	−44.3	+6.0	−168.2	+47.2
14	−9.4	+31.2	−4.0	−12.3	+36.9	+39.1	+8.5	−161.5	−67.3
15	+32.9	+71.5	+21.4	+1.1	−23.7	+61.6	−77.1	−67.6	−117.8
16	+74.2	+61.8	+32.5	+6.4	−68.1	+29.1	−58.0	+68.3	−106.8
17	+68.9	+2.5	+25.6	+10.0	−84.5	−38.4	+5.9	+162.1	−50.1
18	+4.5	−54.0	−4.9	+6.3	−52.6	−84.1	+23.9	+169.3	+10.6
19	−71.4	−74.1	−19.6	−2.5	+10.7	−72.5	−44.1	+86.5	+32.0
20	−96.8	−42.9	−35.6	−6.0	+58.6	−17.4	+45.8	−39.5	−12.2

	36-1	36-2	36-3	36-4	36-5	36-6	36-7	36-8	36-9	37-1
1	+618.0	+812.1	+757.1	+359.8	+359.8	+334.7	+182.1	+121.5	+118.2	+122.0
2	+509.4	+553.0	+509.5	+147.7	+229.4	+249.0	+136.7	+97.0	+66.7	+99.4
3	+144.6	+303.0	+141.7	−37.3	+103.5	+36.6	+51.8	+39.7	+4.7	+44.3
4	−196.1	−184.9	−204.5	−159.1	−8.2	−180.3	−42.0	−48.9	−60.5	−16.6
5	−423.2	−521.5	−324.0	−94.8	−150.1	−264.5	−73.8	−107.6	−83.9	−61.9
6	−391.2	−711.6	−377.0	−105.1	−142.1	−168.6	−42.0	−137.1	−65.0	−91.6
7	−211.8	−573.4	−265.6	−45.5	−74.8	+36.8	+3.9	−104.8	−26.2	−94.8
8	−8.9	−300.9	−60.4	+90.6	+39.3	+213.9	+40.6	−53.9	+20.2	−69.1
9	+39.9	+54.0	+95.5	+107.2	+118.9	+240.7	+63.6	+9.8	+52.3	−11.7
10	+106.8	+222.9	+177.8	+75.5	+49.5	+132.2	+60.4	+76.3	+42.6	+40.4
11	+122.4	+552.4	+196.6	+1.9	+10.7	−33.3	+39.0	+130.0	+39.0	+76.1
12	+136.2	+642.8	+180.7	−118.8	−56.9	−146.1	−17.6	+164.8	+1.1	+70.4
13	+17.9	+618.8	+104.3	−145.3	−103.5	−147.4	−74.0	+150.3	−43.8	+60.5
14	+25.4	+272.6	−60.8	−111.2	−37.6	−47.1	−98.4	+87.4	−55.1	+36.3
15	−231.2	−17.3	−253.8	−45.8	+15.9	+102.0	−73.5	−21.5	−32.9	+17.9
16	−173.9	−381.0	−286.5	−75.2	+79.8	+176.4	−11.4	−96.0	−9.8	−28.7
17	+17.7	−574.4	−197.3	−76.8	+92.1	+127.5	+46.1	−130.0	+11.6	−47.8
18	+71.7	−589.9	−55.8	−93.9	+35.3	−6.9	+56.9	−134.1	+8.0	−69.5
19	−132.3	−444.9	+58.9	−93.4	−8.1	−150.8	+26.1	−111.8	+19.9	−82.1
20	+137.3	−235.8	+301.6	+19.5	−31.9	−190.2	−11.2	−71.1	+39.4	−63.2

(to be continued)

(continued)

	37-2	37-3	37-4	37-5	37-6	37-7	37-8	37-9	49-1	49-2
1	+108.7	+95.8	+121.7	+88.7	+82.2	+52.9	+83.7	+77.4	+159.4	+118.0
2	+86.8	+69.5	+88.8	+52.1	+45.3	+39.2	+66.5	+58.0	+127.9	+81.4
3	+27.1	+7.3	+5.2	+1.5	−15.1	+7.4	+28.4	+9.7	+50.3	+24.3
4	−30.4	−51.6	−56.1	−22.2	−52.1	−20.3	−11.4	−25.4	−38.8	−22.7
5	−72.9	−75.8	−66.7	−29.6	−42.9	−22.7	−36.2	−43.8	−85.4	−54.0
6	−88.4	−56.5	−51.6	−27.4	−6.4	−14.4	−21.2	−53.7	−81.1	−45.3
7	−64.4	+1.4	−35.2	−12.1	+25.6	−4.1	+8.6	−32.5	−37.2	−5.6
8	−22.6	+37.3	+10.8	+7.9	+39.2	−4.7	+35.3	+43.0	−0.8	+31.5
9	+20.9	+63.9	+56.4	+13.4	+20.2	+5.7	+41.2	+17.4	+8.7	+49.9
10	+48.1	+50.4	+51.2	+12.7	−1.5	+18.8	+26.2	+15.1	−17.6	+41.9
11	+53.8	−10.1	+9.9	−8.6	−25.4	+24.6	−7.1	−10.8	−38.2	+30.1
12	+39.9	−59.6	−64.6	−0.7	−41.0	+14.5	−34.2	−37.6	−30.7	+5.9
13	+18.6	−72.1	−88.5	+13.7	−33.7	−6.0	−50.2	−37.9	+7.0	+10.3
14	−11.5	−28.7	−40.6	+45.9	−10.9	−27.9	−35.9	−24.5	+48.2	−16.9
15	−34.9	+34.5	+27.5	+45.6	+14.2	−34.1	−4.1		+70.8	−17.7
16	−45.2	+80.5	+59.0	+20.2	+29.2	−25.4	+20.6		+49.7	−8.5
17	−37.3	+84.4	+57.4	−26.9	+18.0	−5.0	+29.0		−9.6	−20.2
18	−20.6	+38.4	+44.3	−49.3	−1.3	+10.0	+10.5		−75.1	−38.5
19	+3.7	−28.1	+12.5	−52.0	−18.1	+9.4	−21.4		−104.4	−42.3
20	+34.0	−77.9	−32.2	−23.9	−15.9	+5.7	−41.4		−66.7	−45.3

	49-3	49-4	49-5	49-6	49-7	49-8	49-9	49-10	51-1	51-2
1	+113.0	+346.7	+228.1	+253.4	+241.9	+233.9	+179.6	+127.1	+286.7	+236.6
2	+103.8	+288.0	+179.6	+190.9	+172.4	+176.9	+79.2	+99.1	+228.7	+196.6
3	+77.5	+159.7	+61.5	+61.2	+34.8	+62.7	−33.6	+28.8	+108.8	+85.6
4	+29.8	+11.6	−59.8	−42.4	−58.8	−69.8	−113.3	+20.9	−17.0	−24.9
5	−26.0	−98.6	−119.5	−83.4	−119.5	−166.4	−129.5	−103.4	−92.2	−151.9
6	−50.3	−139.8	−88.1	−32.6	−113.3	−161.0	−80.8	−108.0	−121.8	−168.5
7	−35.3	−119.1	+9.0	+46.9	−39.1	−57.8	−37.6	−63.2	−56.4	−114.6
8	−0.5	−43.9	+132.1	+109.3	+46.2	+80.9	+51.7	+7.7	+19.7	−15.5
9	+25.0	+18.0	+216.2	+96.0	+78.5	+182.9	+144.0	+64.4	+74.3	+65.2
10	+25.5	+33.0	+204.2	+30.6	+42.4	+215.3	+122.9	+90.0	+77.3	+87.3
11	−2.8	+18.2	+95.4	−48.1	−9.9	+153.6	+34.5	+70.2	+17.5	+44.4
12	−51.3	−25.7	−54.6	−94.8	−69.5	+5.0	−42.8	+18.6	−83.1	−24.3
13	−83.6	−55.3	−80.1	−57.7	−96.4	−125.4	−86.0	−37.0	−175.7	−61.4
14	−91.8	−76.0	−154.1	−14.8	−80.0	−164.5	−64.5	−76.2	−211.7	−112.5
15	−60.3	−87.6	−66.7	+35.8	−32.1	−89.1	+5.6	−74.8	−168.1	+0.6
16	−5.9	−99.8	+74.6	+58.5	+8.3	+2.0	+106.1	−38.9	−62.2	+107.3
17	+25.9	−124.7	+175.4	+34.5	+19.0	+92.5	+203.6	+12.2	+57.7	+176.3
18	+47.8	−127.7	+193.3	+13.9	−52.8	+138.2	+220.8	+47.3	+140.9	+169.2
19	+52.1	−98.2	+83.3	−46.9	−103.4	+84.7	+142.0	+55.1	+153.1	+90.4
20	+45.3	−40.9	−55.4	−40.4	−101.1	−15.9	−23.7	+30.6	+99.3	−54.9

(to be continued)

(continued)

	51-3	51-4	51-5	51-6	51-7	51-8	51-9	51-10	51-11	51-12
1	+144.5	+214.9	+200.8	+115.0	+803.4	+749.7	+209.1	+140.9	+73.9	+257.4
2	+98.2	+182.9	+137.0	+89.0	+593.7	+582.3	+147.7	+106.7	+53.5	+212.3
3	+5.6	+96.4	+19.1	+17.4	+282.1	+140.9	+9.1	+27.6	+9.8	+79.4
4	−95.7	−7.7	−98.7	−60.8	−44.8	−366.5	−147.5	−62.7	−39.5	−73.8
5	−134 4	−90.1	−156.6	−101.9	−368.8	−630.1	−224.2	−122.4	−70 3	−188.1
6	−108.8	−125.0	−131.2	−89.7	−549.3	−654.0	−201,5	−124.0	−66.9	−233.1
7	−34.7	−110.9	−36.0	−29.2	−479.4	−361.9	−77.0	−69.1	−31.6	−177.2
8	+57.1	−42.1	+57.9	+39.5	−126.6	+63.8	+92.5	+11.9	+15.3	−46.5
9	+113.5	+34.8	+112.5	+86.5	+286.2	+409.8	+206.1	+73.9	+43.2	+95.3
10	+111.1	+75.9	+105.9	+85.2	+556.8	+550.1	+243.0	+108.1	+58.3	+199.7
11	+56.5	+73.0	+36.5	+37.7	+585.7	+457.5	+161,0	+80.4	+34.0	+281.5
12	−23.4	+24.4	−37.2	−26.5	+383.1	+102.8	+2.0	+14.0	−7.2	+167.7
13	−89.1	−15.0	−93.0	−69.7	−47.4	−289.3	−148.2	−52.3	−41.1	+35.6
14	−99.3	−39.9	−102.0	−75.0	−447.0	−534.8	−248.9	−98.7	−61.4	−94.1
15	−62.0	−35.5	−67.7	−37.6	−687.6	−551.2	−224.2	−68.6	−24.4	−184.9
16	+0.6	−2.9	+7.4	+22.6	−632.6	−241.1	−97.3	−12.6	+15.3	−212.2
17	+57.2	+35.5	+60.7	+67.2	−259.8	+204.8	+75.9	+53.9	+51.7	−151.4
18	+81.2	+65.4	+94.8	+75.3	+210.5	+535.4	+195.1	+94.8	+66.1	−32.9
19	+51.0	+81.3	+67.3	+43.7	+546.3	+596.0	+236.2	+92.4	+50.7	+84.2
20	−9.4	+71.4	+14.3	−12.3	−662.0	+406.2	+163.9	+26.1	−6.8	+163.5

	51-13	51-14	51-15	52-1	52-2	52-3	52-4	52-5	52-6	52-7
1	+282 6	+78.5	+71.4	+639.2	+512.5	+635.2	+473.2	+440.6	+444.6	+329.6
2	+219.9	+51.4	+50.8	+453.4	+383.1	+564.7	+393.2	+380.2	+280.3	+273.0
3	+43.5	+5.6	+5.0	+134.5	+138.9	+356.2	+171.2	+144.1	+20.0	+76.0
4	−146.6	−46.2	−36.4	−122.8	−132.3	+82.8	−49.9	−91.5	−211.4	−130.5
5	−267.5	−76.8	−43.1	−291.8	−373.7	−132.4	−303.9	−248.4	−363.6	−242.9
6	−238.6	−62.4	−52.1	−359.0	−373.0	−245.0	−337.1	−234.3	−364.7	−208.8
7	−88.0	−14.0	−12.9	−293.1	−323.5	−235.4	−229.2	−122.7	−233.5	−74.4
8	+96.0	+43.8	+40.5	−51.7	−74.2	−103.5	−31.1	+2.2	−70.4	+29.4
9	+211.5	+78.4	+59.8	+209.5	+168.7	+50.4	+130.4	+83.5	+111.2	+87.3
10	+197.9	+69.4	+56.1	+237.5	+342.4	+108.6	+174.5	+48.8	+227.8	+60.2
11	+95.8	+18.7	+20.7	+153.9	+416.6	+24.4	+88.8	−69.4	+244.6	−8.6
12	−32.7	−41.6	−19.9	+33.2	+213.0	−171.8	−48.7	−180.6	+121.7	−40.7
13	−131.7	−76.5	−53.4	−168.5	−68.3	−334.3	−122.8	−283.7	+60.9	−32.7
14	−134.7	−68.6	−58.9	−249.5	−300.3	−365.2	−225.0	−272.2	−2.9	+31.9
15	−80.7	−21.1	−30.3	−147.4	−399.9	−246.1	+1.2	−57.5	−98.5	+75.6
16	+83.8	+39.1	+15.6	+51.3	−268 3	−5.3	+214.7	+155.6	−162.5	+44.1
17	+168.9	+77.0	+46.2	+162.9	−44.3	+268.9	+352.7	+374.8	−185.6	−17.8
18	+142.6	+73.6	+59.7	+168.1	+251.5	+495.2	+338.4	+448.7	−162.5	−87.7
19	−5.6	+20.9	+37.0	+114.2	+434.7	+591.6	+180.8	+338.9	−90.5	−112.5
20	−142.9	−31.7	−6.0	+12.1	+393.3	+507.1	−109.9	+173.4	+5.2	−69.8

(to be continued)

(continued)

	52-8	52-9	52-10	52-11	52-12	52-13	52-14	52-15	52-16	52-17
1	+275.9	+110.2	+107.9	+83.8	+103.4	+127.8	+121.7	+771.2	+896.1	+248.5
2	+202.2	+72.5	+68.9	+47.7	+89.3	+92.5	+90.9	+525.2	+645.1	+179.7
3	+38.7	+24.5	+31.1	-4.1	+31.5	+13.3	+23.8	+39.0	+111.3	+91.2
4	-105.1	-41.2	-2.4	-58.8	-35.8	-68.7	-33.0	-430.3	-462.8	-111.5
5	-184.8	-72.2	-45.0	-67.7	-90.6	-106.7	-54.3	-702.7	-818.4	-207.5
6	-143.7	-57.4	-42.7	-44.2	-81.7	-80.1	-27.9	-650.6	-816.0	-204.8
7	-41.2	-13.3	-22.4	-9.3	-37.5	-12.8	+15.2	-282.2	-357.4	-118.7
8	+71.9	+22.6	+11.8	+33.7	+20.2	+57.9	+55.3	+202.4	+181.8	+18.3
9	+124.6	+31.0	+35.6	+44.5	+60.8	+100.3	+55.8	+596.9	+697.0	+144.0
10	+109.1	+21.3	+14.9	+34.3	+53.2	+69.6	+12.4	+738.4	+914.6	+206.8
11	+47.1	-14.5	+3.2	+9.9	+21.4	+14.4	-47.2	+561.7	+805.5	+189.2
12	-43.8	-21.5	-17.1	-15.5	-14.2	-59.1	-85.6	+119.1	+205.6	+57.8
13	-103.6	-12.4	-31.1	-24.3	-34.3	-112.6	-91.0	-365.3	-307.6	-73.1
14	-146.4	+0.8	-11.3	-20.6	-23.8	-100.9	-56.1	-691.4	-719.4	-201.6
15	-103.7	+16.8	+4.8	-7.9	-4.5	-39.8	+1.3	-684.6	-798.9	-237.3
16	-22.8	+12.3	+23.9	+4.0	+18.1	+48.5	+37.4	-383.7	-465.5	-175.4
17	+55.6	+15.7	+27.6	+14.1	+28.4	+101.2	+38.7	+94.7	+35.4	-38.3
18	+119.2	+14.2	+10.6	+5.4	+16.1	+101.5	+13.3	+503.4	+512.8	+116.8
19	+98.4	+9.7	-2.4	-9.5	-19.1	+46.6	-18.7	+678.6	+681.2	+183.1
20	+41.4	-11.5	-9.5	-11.2	-42.3	-33.8	-30.4	+540.1	+563.8	+234.2

	52-18	52-19	52-20	52-21	52-22	52-23	52-24	52-25	52 26	52-27
1	+299.3	+105.6	+107.9	+138.2	+155.3	+184.4	+185.9	+189.3	+111.9	+164.2
2	+248.5	+81.9	+92.8	+135.4	+116.4	+135.2	+89.1	+122.0	+52.2	+80.3
3	+105.9	+27.3	+52.6	+75.0	+40.4	+16.6	+0.6	-2.7	+14.3	+4.3
4	-63.8	-34.9	-4.7	+13.0	-35.4	-93.6	-113.9	-119.9	-20.2	-98.9
5	-189.5	-82.4	-61.5	-40.6	-94.2	-140.7	-139.7	-167.7	-45.1	-137.7
6	-230.5	-100.8	-93.9	-76.0	-72.0	-111.4	-102.9	-106.5	+14.6	-92.4
7	-175.7	-85.4	-84.7	-68.0	-21.0	-22.9	-7.6	-2.0	+20.7	-9.8
8	-61.8	-49.4	-56.4	-19.2	+0.9	+64.5	+79.5	+120.9	+66.9	+74.2
9	+51.4	-4.4	-7.5	-1.9	+25.9	+108.6	+125.4	+165.7	+44.8	+138.1
10	+116.9	+29.4	+38.3	+1.3	+10.4	+83.5	+116.7	+144.5	+45.1	+107.4
11	+119.6	+40.6	+64.1	+13.4	-17.2	+20.8	+39.9	-2.4	+5.3	+61.0
12	+72.2	+26.8	+59.2	-3.4	-13.0	-45.2	-28.5	-86.1	-6.1	-74.5
13	+0.1	-0.6	+19.7	-46.1	+5.2	-73.6	-91.4	-171.2	-4.2	-152.4
14	-55.7	-30.1	-22.4	-79.1	+23.2	-64.4	-107.1	-122.4	-20.9	-171.7
15	-74.9	-46.6	-56.9	-83.9	+47.0	-24.7	-68.7	-32.9	+21.4	-95.0
16	-58.4	-41.2	-70.8	-58.2	+31.1	+24.4	-10.4	+85.0	-4.8	-2.2
17	-27.2	-17.0	-48.7	-22.2	-18.2	+54.1	+86.3	+149.4	+38.9	+122.5
18	-5.9	+18.6	-15.3	-6.9	-44.5	+44.5	+114.7	+106.8	-19.5	+151.8
19	-15.9	+50.9	+26.1	+13.0	-74.4	+16.6	+89.8	+31.4	+9.1	+139.0
20	-41.4	+68.5	+58.6	+3.1	-63.6	-19.0	+24.6	-70.9	-25.6	+53.1

§ 23. Analysis of the Seismograph.

The earthquakes and the portions of their coda oscillations analysed by Takahasi's method are tabulated in Table I. The oscillation curves obtained as the result of the analyses are given in Table II and Figs. 1–7. Of these oscillation curves, some have a distinct periodicity which at once convinces us that they are composed of a single sine curve, while others are not so simple and are supposed to be composed of two sine curves of the damping nature.

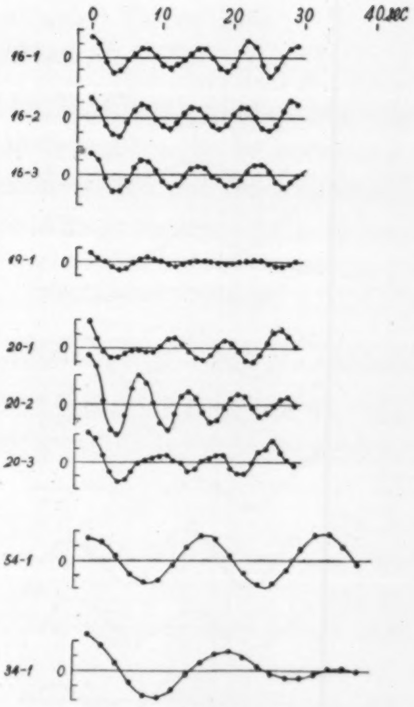

Fig. 1. Oscillation curve.

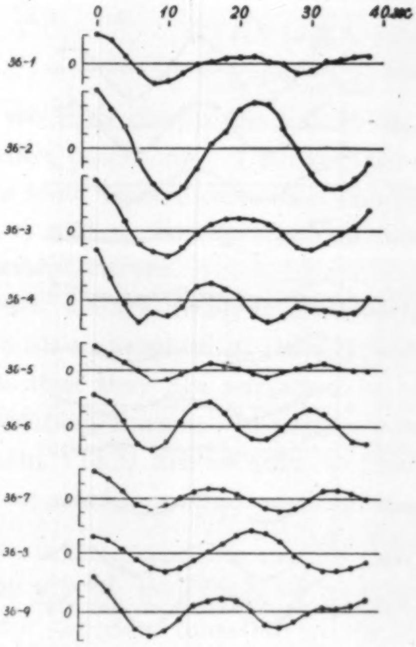

Fig. 2. Oscillation curve (Celebes earthquake).

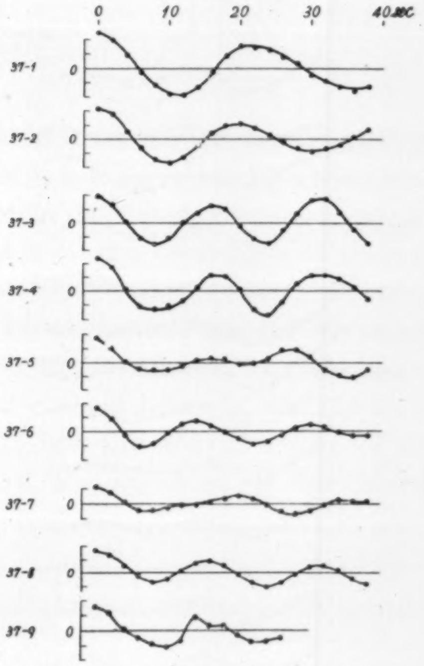

Fig. 3. Oscillation curve (New Guinea earthquake).

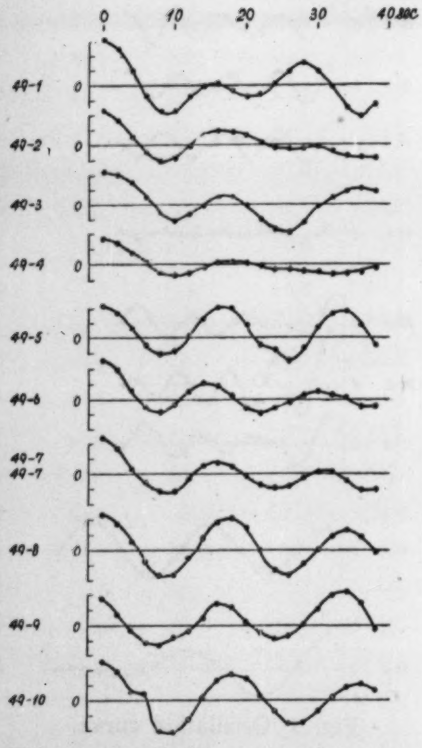

Fig. 4. Oscillation curve (Mexico earthquake).

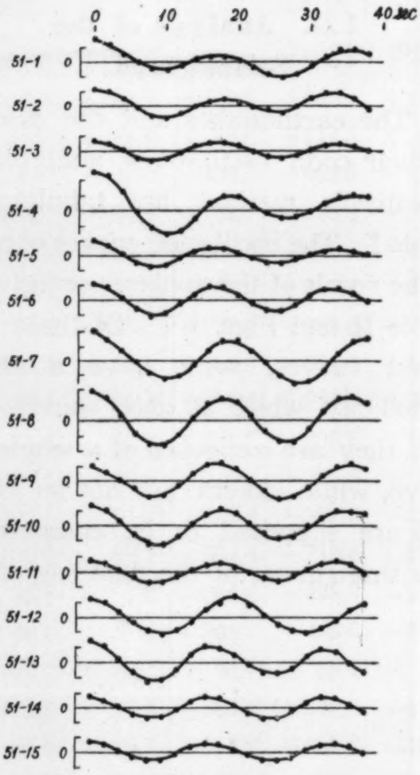

Fig. 5. Oscillation curve (Peru earthquake).

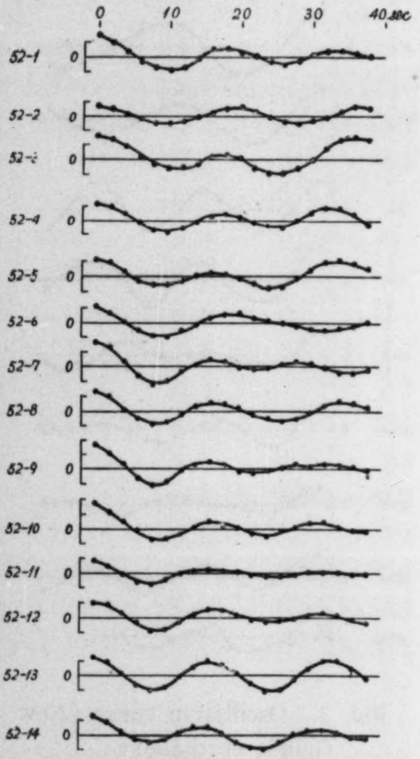

Fig. 6. Oscillation curve (Chili earthquake E-W comp.).

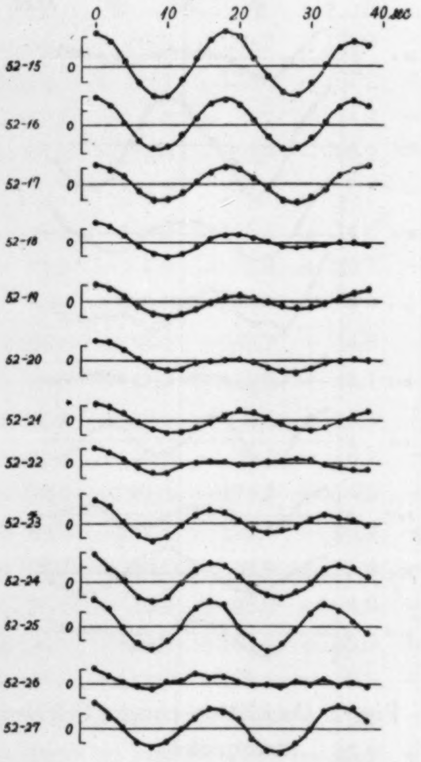

Fig. 7. Oscillation curve (Chili earthquake N-S comp.).

§ 24. Decomposition of an Oscillation Curve into its Component Curves.

As most of the oscillation curves obtained by Takahasi's method of analysis are composed of two sine curves of the damping nature, it is necessary to decompose them into their two component curves. If we put the amplitude of the oscillation curve corresponding to the time t as y, then y will be given by

$$y=Ae^{-\varepsilon t}\sin n\,(t-\tau_1)+Be^{-\alpha t}\sin p\,(t-\tau)\ \ldots\ldots\ldots\ldots\ldots\ldots\ldots\ldots(24.1)$$

which is written as

$$y=\alpha_1\,e^{\beta_1 t}+\alpha_2 e^{\beta_2 t}+\alpha_3 e^{\beta_3 t}+\alpha_4 e^{\beta_4 t}\ {}^{3)}\ldots\ldots\ldots\ldots\ldots\ldots\ldots\ldots(24.2)$$

where α and β are complex numbers. As the value of y is given at certain intervals of time (and these intervals of time are given by $t_\gamma=t_1+\gamma h$, $\gamma=1, 2, \cdots$) y_γ will be written as

$$y_\gamma=\alpha_1 e^{\beta_1(t_1+\overline{\gamma-1}h)}+\alpha_2 e^{\beta_2(t_1+\overline{\gamma-1}h)}+\alpha_3 e^{\beta_3(t_1+\overline{\gamma-1}h)}+\alpha_4 e^{\beta_4(t_1+\overline{\gamma-1}h)}\ \ldots\ldots(24.3)$$

Now, putting

$$z_1=e^{\beta_1 h},\quad z_2=e^{\beta_2 h},\quad z_3=e^{\beta_3 h},\quad z_4=e^{\beta_4 h}\ \ldots\ldots\ldots(24.4)$$

z_1, z_2, z_3 and z_4 are to be obtained as the set of four roots of the fourth order equation

$$z^4+s_1z^3+s_2z^2+s_3z+s_4=0\ ,\ \ldots\ldots\ldots\ldots\ldots\ldots\ldots\ldots(24.5)$$

provided

$$\left.\begin{aligned} s_1&=-(z_1+z_2+z_3+z_4)\\ s_2&=z_1z_2+z_2z_3+z_3z_4+z_4z_1\\ s_3&=(z_1z_2z_3+z_2z_3z_4+z_3z_4z_1+z_4z_1z_2)\\ s_4&=z_1z_2z_3z_4 \end{aligned}\right\}\ ,\ \ldots\ldots\ldots(24.6)$$

then we shall obtain the values of ε, n, α and p from the solution of the observation equations. Then replace them in (24.2) and carry out the calculation of the least square once more, and we shall obtain the remaining four constants A, B, τ_1 and τ. In short, we thus come to know all the coefficients of the two component curves.

Now we are going to analyse the oscillation curves in Figs. 1–7 by means of the above method of analysis, but some of the oscillation curves are so simple that they are supposed to be composed each of a single sine curve of the damping nature. In such a case, the third and the fourth terms of the equation (24.2) are lacking, so that, instead of the equation of the fourth order of (24.5), a quadratic equation

$$z^2+s_1z+s_2=0\ \ldots\ldots\ldots\ldots\ldots\ldots\ldots\ldots\ldots(24.7)$$

will be solved and a set of conjugate complex roots of the equation will be used for the determination of the sine curve.

---

3) C. RUNGE und H. KÖNIG, "Vorlesungen über Numerischen Rechnen," Berlin (1924), 231.

§ 25. Analysis of Oscillation Curves.

We picked up ten curves out of the Figs. 1–7 which were supposed to be composed of two sine curves, and executed the calculation explained in the last paragraph with the results given in Table III. These calculated curves are compared with the observed ones in Fig. 8, in which I is the oscillation curve obtained by Takahasi's method of analysis, II the calculated curve, III and IV the two component sine curves into which curve I was decomposed. In all the cases in Fig. 8, the observed curves agree fairly well with the calculated ones but some curves in III and IV differ from each other by π in

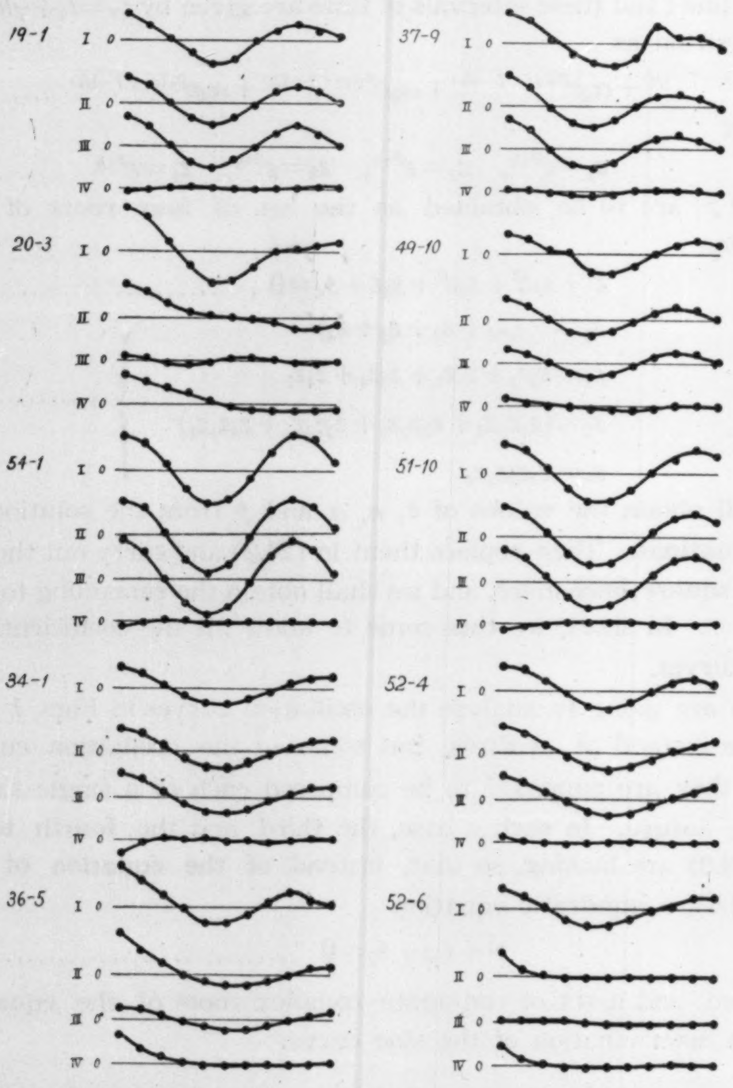

Fig. 8. I; Oscillation curve. III, IV; curves decomposed the curve I into it's elementary two curves. II; III+IV.

their phases, so that some have the negative value at the beginning. Anyhow, with respect to these two component curves, we notice that the curve that has a large damping coefficient affects the curve II only slightly while the curve that has a small damping largely determines the shape of the oscillation curve.

Table III. Constants of damping sine curves obtained
by solving the 4th equation.

Curve No.	ε	α	n	p	T_n	T_p	A	B
19- 1	−0.0707	−0.5383	44°45′	56°29′	16.08	6.4	+ 34.51	− 3.77
20- 3	−0.0311	−0.1577	61°41′	19°31′	5.9	36.88	+ 9.79	+ 67.58
54- 1	−0.0115	−0.6712	44°01′	67°33′	16.36	10.66	+ 89.05	− 12.62
34- 1	−0.0899	−0.9502	36°22′	54°46′	19.84	13.14	+282.28	− 31.94
36- 5	−0.0364	−0.5728	33°10′	23°50′	21.70	30.25	+ 54.78	+127.81
37- 9	−0.0942	−0.3995	45°14′	46°55′	15.92	15.46	+ 35.03	+ 4.09
49-10	−0.0145	−0.3234	43°57′	42°25′	16.40	17.00	+ 33.06	+ 18.63
51-10	−0.0348	−0.5204	40°33′	38°14′	17.76	19.00	+ 72.92	− 1.35
52- 4	−0.0588	−0.9333	34°34′	38°26′	20.84	18.74	+200.74	+ 44.42
52- 6	−0.0565	−0.8378	23°41′	39°13′	30.49	18.38	+ 4.30	+241.94

Table IV. Constants of a damping sine curve obtained
by solving the quadratic equation.

Curve No.	ε	n	T	A	Curve No.	ε	n	T	A
		° ′	sec				° ′	sec	
16-1	0.168	51 23	7.01	395.644	51- 1	0.197	41 06	17.56	642.659
16-2	0.049	49 01	7.34	273.748	51- 6	0.025	43 20	16.62	239.972
20-2	0.099	51 53	6.94	477.396	51-14	0.001	43 34	16.52	157.160
54-1	0.010	44 23	16.22	364.714	51-15	0.052	43 30	16.56	221.358
36-6	0.050	47 19	15.21	692.202	52- 1	0.138	39 27	18.26	711.766
37-2	0.063	36 33	19.70	204.716	52- 2	0.042	39 20	18.30	1051.983
37-3	0.079	44 03	16.34	213.030	52- 3	0.267	36 47	19.56	1530.230
37-4	0.083	48 29	14.86	226.346	52- 9	0.156	44 38	16.14	2578.848
37-5	0.262	43 14	16.66	197.462	52-10	0.280	42 47	16.84	280.259
37-6	0.102	48 23	14.88	154.754	52-12	0.077	44 24	16.28	258.741
37-7	0.196	45 14	15.92	133.194	52-13	0.01	43 49	16.44	232.288
49-1	0.181	42 11	17.08	360.774	52-15	0.005	39 27	18.26	1513.130
49-2	0.153	40 03	17.98	258.493	52-19	0.064	34 24	20.94	239.822
49-3	0.136	37 33	19.18	223.619	52-21	0.235	40 00	18.00	378.014
49-4	0.196	36 30	19.72	736.259	52-23	0.069	44 10	16.28	389.700
49-5	0.022	40 11	17.90	415.161	52-25	0.035	43 41	16.50	384.975
49-9	0.091	43 33	16.72	420.052					

Secondly, we picked up some curves of the simple form from Figs.1~7, and calculated their periods and damping coefficients by solving a quadratic equation (24.7). The results are seen in Table IV and in Fig. 9. In the figure the values obtained by means of Takahasi's method are shown by small dots for comparison. As will be seen in Fig. 9 these calculated and observed values resemble each other losely.

These 32 oscillation curves here analysed are such fine sine curves that their periods are easily determined from their graphs by inspection. For comparison's sake the periods determined by inspection and by calculation are shown in the T' and T columns in Table V. The difference between the two periods obtained by calculation and by inspection is extremely small, the probable error of their difference amounting to only ±0.3 sec. For this reason, with all the rest of the curves not analysed by the method explained in § 24, we determined their periods by inspection.

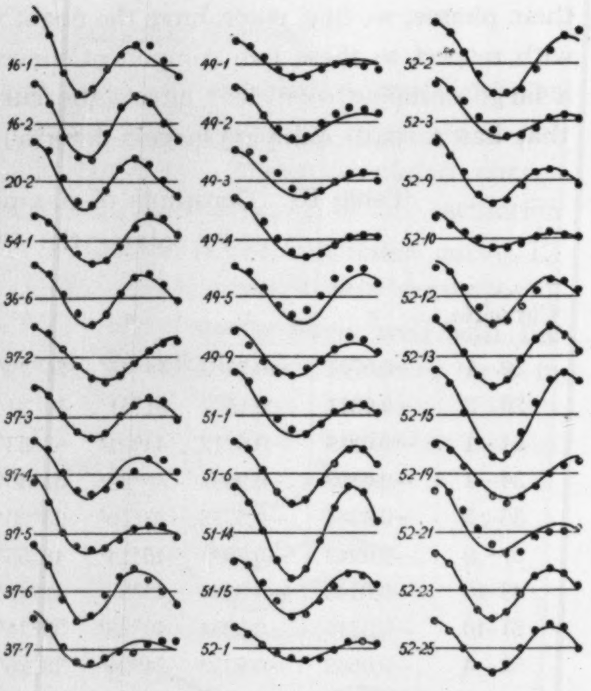

Fig. 9. • ; Amplituds obtained by means of the Takahasi-Husimi's method.
Full line ; Calculated curves obtained by solving the quadratic equation.

Apropos of this, the errors of these theoretical curves will be shown in Table VI. From the observation equations given by (24.3), normal equations are formed. By solving the normal equations, s_i will be obtained, and when the values of s_i are replaced in (24.3), the residual v for each observation equation is given by

$$y_\gamma s_4 + y_{\gamma+1} s_3 + y_{\gamma+2} s_2 + y_{\gamma+3} s_1 + y_{\gamma+4} = v$$

From this v the probable error for each observation equation will be calculated. If we denote the probable error of y as r_y and put $r_y = r/\sqrt{1+\sum s_i^2}$ we shall be able to get some rough estimation of the errors. The r and r_y will be seen in Table VI-A. The values of r_y in Table VI-A are very small in comparison with the values of y in Table II, showing that the calculated results are fairly reliable. The values of r and r_y obtained by solving quadratic equations are given in column B of the same Table. The amount of errors they bring about in the calculated periods will be seen in the last column of the same table.

Table V. Comparison of T and T'.

T; Periods obtained from calculation.
T'; Periods obtained graphically, $T' = \frac{1}{2}(Ta+2Ti)$.
Ti; Half periods of sine curves in Figs. 1~7.
Ta; One Periods of sine curves in Figs. 1~7.

Curve No	Ti	Ta	T'	T	Curve No.	Ti	Ta	T'	T
36-5	8.6	16.4	16.8	16.80	51-11	8.4	16.8	16.8	16.22
36-6	7.4	15.4	15.1	15.21	51-14	8.4	16.6	16.7	16.52
37-2	9.8	19.4	19.5	19.70	51-15	8.4	16.6	16.7	16.56
37-3	8.2	16.6	16.5	16.34	52- 1	9.2	17.6	18.0	18.25
37-4	7.6	15.4	15.3	14.86	52- 2	9.2	18.8	18.6	18.30
37-5	8.4	16.8	16.8	16.70	52- 3	10.4	16.8	18.8	19.56
37-6	7.2	14.6	14.5	14.88	52- 9	8.4	16.2	16.5	16.14
49-1	8.8	16.8	17.2	17.08	52-10	8.6	16.4	16.8	16.80
49-2	8.8	17.2	17.4	17.98	52-12	8.4	16.4	16.6	16.28
49-3	9.6	17.8	18.5	19.18	52-13	8.4	16.2	16.5	16.44
49-4	10.2	18.8	19.6	19.72	52-15	8.8	18.4	18.0	18.26
49-5	9.0	17.4	17.7	17.92	52-18	9.6	19.2	19.2	19.06
49-9	8.4	16.8	16.8	16.72	52-19	10.4	20.2	20.5	20.94
51-1	9.0	17.2	17.6	17.56	52-21	9.6	18.6	18.9	18.00
51-6	8.2	16.6	16.5	16.62	52-23	8.2	16.4	16.4	16.28
51-9	8.8	17.6	17.6	17.84	52-25	8.2	16.4	16.4	16.50

Table VI. Errors of oscillation curves.

A			B			
Curve No.	r	r_y	Curve No.	r	r_y	r_T sec.
19- 1	4.80	3.70	16- 1	8.93	5.24	1.60
20- 3	11.92	6.61	20- 2	8.38	5.18	1.21
54- 1	3.80	2.31	54- 1	3.20	1.58	1.49
34- 1	7.86	2.83	36- 6	3.35	2.50	1.72
36- 5	17.81	10.06	37- 2	3.07	1.50	2.84
37- 9	16.30	14.20	49- 1	4.67	2.69	3.02
49-10	11.71	9.00	51- 6	1.78	0.90	1.08
51-10	4.62	3.74	51-14	2.25	1.28	1.16
52- 4	18.95	12.55	52- 1	4.10	2.23	0.78
52- 6	22.38	12.01	52-23	3.11	1.21	1.62

§ 26. Periods of Oscillation Curves.

Now that oscillation periods have been calculated with regard to all the curves in Figs. 1–7, we shall proceed to the consideration of each of them.

The first three curves in Fig. 1 are those of the Sioyazaki earthquake. The next 19–1 is that of the Kesenuma earthquake (No. 19), composed of two curves of periods 6.4 sec. and 8.0 sec. respectively. The curves 20–1, 2, 3 belong to the Koti-Yamato earthquake (No. 20), and we obtain the periods of 6.8 sec. from 1 and 2, and 5.8 sec. and 18.5 sec. from 3. We obtain two periods of $T_1=$ 10.7 sec. and $T_2=16.4$ sec. from the curve 54–1 of the Kagi earthquake (No. 54), and two also from the Celebes Sea earthquake (No. 34), $T_1=13.1$ sec. and $T_2=19.8$ sec. With regard to the curves of the Celebes earthquake (No. 36), we obtain the period of about 20 sec. from the curves 36–1, 2, 3 analysed in the portion between 40 and 50 minutes, and the period of about 15 sec. from the curves 36–6∼9 in the portion between 50 and 70 minutes. If we decompose 36–5 into two curves we have $T_1=15.1$ sec, $T_2=21.7$ sec. In the Celebes earthquake two different periods seen to be present, namely $T_1=15.4\pm0.10$ sec. and $T_2=20.3\pm0.47$ sec. In the New Guinea earthquake (No. 37) we observe a period of 20 sec. at about 50 minutes and another of 15 sec. in the later portion, and in the still later portion, at about 70 min. from the P commencement, there are apparently two periods of about 16 sec. and 15 sec. Inclusive of tow periods appearing at about 50 minutes, we find three types of period in the New Guinea earthquake. The oscillation curves of the Mexico earthquake (No. 49) are shown in Fig. 4. A great majority of these curves have a period of 17 sec., but there exists the period of 20 sec. in 49-3, 4, and those of 16.4 sec. and 17.0 sec. in the neighbourhood of 100 minutes, that is, near the end portion. The oscillation curves of the Peru earthquake (No. 51) are seen in Fig. 5. Between 50 and 80 min. there exist two waves of 16.5 sec. and 19.5 sec., and in the later portions beyond 100 min., the waves with the period of 16.6 sec. are predominant. Figs. 6 and 7 are the results of the Chili earthquake (No. 52). In the portion of 50–80 min. there appear two periods of $T_1=18.3$ sec. and $T_2=20.2$ sec. Waves in this portion were named the first coda waves in Chapters 1–3, but then the mean periods in this part could not be decided accurately owing to the large fluctuation of the respective periods. Contrary to this, in the portion which we named the second coda, namely the part beyond 100 minutes, the mean values of the one-minute periods were fairly uniform according to the calculation performed in Chapters 1–3. With regard to this portion the period $T_3=16.4$ sec. has been obtained both through the calculations performed and through Takahasi's method of analysis. All the periods obtained from the respective oscillation curves are shown in Table VII.

Table VII. Periods of oscillation curves.

Curve No.	*T*	Curve No.	*T*	Curve No.	*T*
	sec.		sec.		sec.
16-1	7.0	49- 1	17.1	52- 3	18.7, 19.6
16-2	7.3	49- 2	17.9	52- 4	20.8
16-3	7.1	49- 3	19.2	52- 5	18.0
19-1	6.4	49- 4	19.7	52- 6	18.2
20-1	6.8	49- 5	17.9	52- 7	16.3
20-2	6.9	49- 6	16.6	52- 8	16.6
20-3	5.9, 18.5	49- 7	17.3	52- 9	16.1
54-1	10.7, 16.4	49- 8	17.5	52-10	16.8
34-1	13.1, 19.8	49- 9	16.7	52-11	16.4
36-1	18.8	49-10	17.0, 16.4	52-12	16.3
36-2	21.7	51- 1	17.6	52-13	16.4
36-3	19.4	51- 2	17.8	52-14	16.3
36-4	15.9	51- 3	17.3	52-15	18.3
36-5	15.1, 21.7	51- 4	17.5	52-16	18.2
36-6	15.2	51- 5	17.4	52-17	18.3
36-7	15.6	51- 6	16.6	52-18	19.1
36-8	21.2	51- 7	19.8	52-19	20.9
36-9	15.3	51- 8	19.0	52-20	20.1
37-1	20.8	51- 9	17.8	52-21	18.0
37-2	19.7	51-10	17.8, 19.0	52-22	16.4
37-3	16.3	51-11	17.6	52-23	16.3
37-4	14.9	51-12	20.0	52-24	16.3
37-5	19.2, 16.7	51-13	17.4	52-25	16.5
37-6	19.7	51-14	16.5	52-26	16.2
37-7	15.9	51-15	16.6	52-27	16.4
37-8	15.6, 15.9	52- 1	18.3		
37-9	15.5	52- 2	18.3		

§ 27. Relations between the Epicentral Distance and the Coda Periods Revealed by Takahasi's Method.

If we divide the periods in Table VII into adequate groups with regard to each earthquake and make the mean of the respective groups, we are able to find the predominant periods of coda oscillations of the respective earthquakes, as are shown in Table VIII. From the table it appears that two or three sorts of waves of different periods are likely to exist in the coda oscillations of the respective earthquake. These are denoted by T_1, T_2 and T_3,

Table VIII. Predominant period determined by means of Takahasi-Husimi's method.

Earthq. No.	Epicenter	Comp.	Epicental distance	T_1	T_2	T_3
16	Siwoya-Saki	E-W	295 km	7.1 sec	— sec	— sec
19	Kesenuma	N-S	380	6.4	—	—
20	Koti-Yamato	E-W & N-S	391	6.5	19.6	—
54	Kagi	N-S	2,230	10.7	—	16.4
34	Celebes Sea	E-W	4,110	13.1	19.8	—
36	Celebes	E-W	4,470	15.4	20.3	—
37	New Guinea	E-W	4,550	15.4	20.3	16.3
49	Mexico	E-W	11,600	17.3	19.5	16.6
51	Peru	E-W	14,900	17.5	—	16.6
,,	,,	N-S	,,	17.6	19.5	16.6
52	Chili	E-W	16,800	18.3	20.2	16.4
,,	,,	N-S	,,	18.2	20.0	16.4

and the relations between these periods and the epicentral distances of the respective earthquakes are shown in Fig. 10. From the table we notice at once that the T_1 period agrees very well with the predominant period determined in the preceding chapters, and from the figure we see that as the epicentral distance increases T_1 also increases. On the contrary, the T_2 and

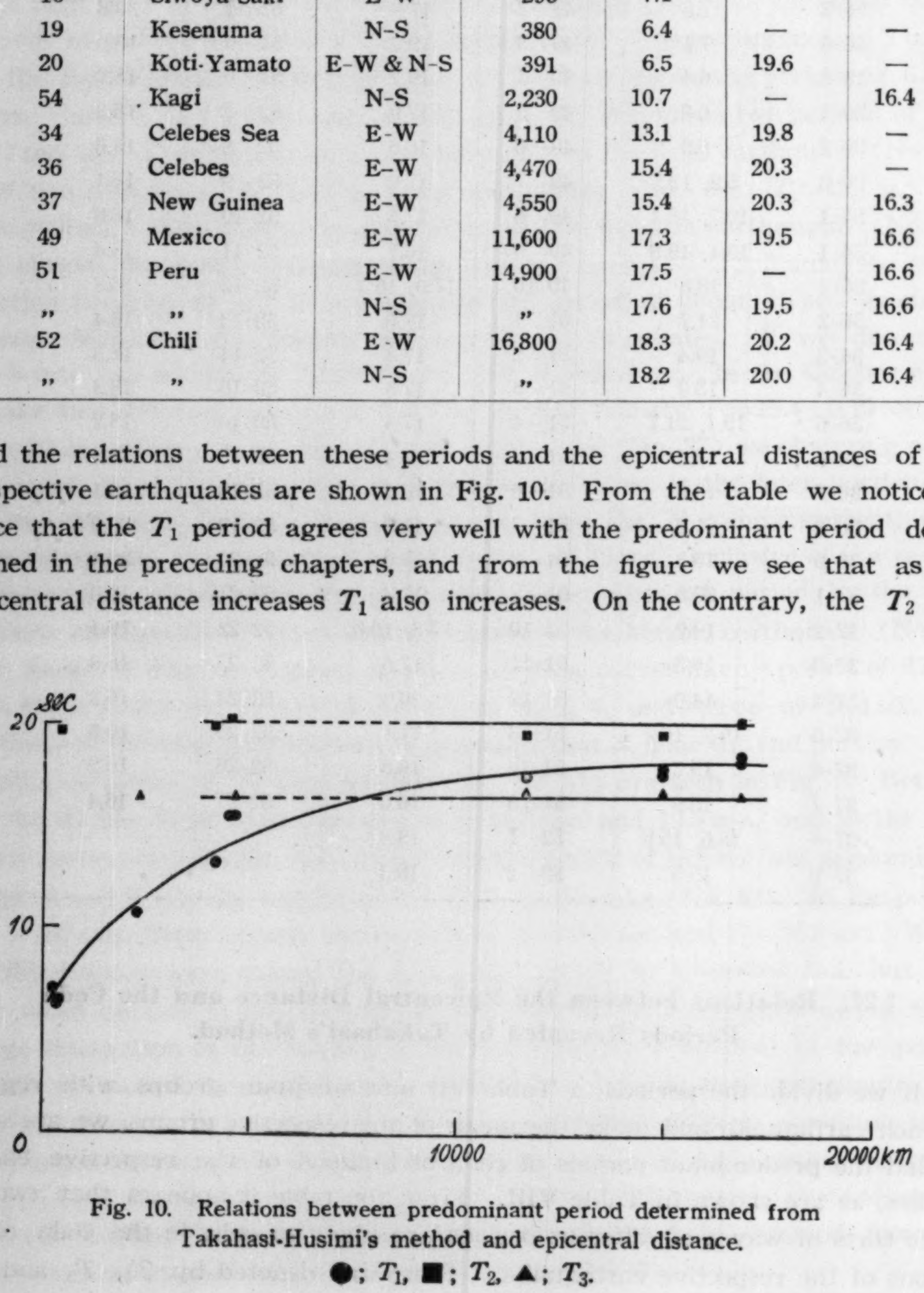

Fig. 10. Relations between predominant period determined from Takahasi-Husimi's method and epicentral distance.

●; T_1, ■; T_2, ▲; T_3.

T_3 apparently have the same values in all the earthquakes irrespective of the differences of their epicentral distances, T_2 being roughly 20 sec. and T_3 roughly 16 sec. In the predominant period obtained from the mean periods in the preceeding chapters too, the period 16 sec. was found in the second coda waves of the earthquakes with the epicentral distances upwards of 10,000 km. Here, also, the period T_3 was found mostly in the second coda waves of the earthquakes with long epicentral distances. It is also to be found in the first coda oscillations of New Guinea and Kagi earthquakes that have medium epicentral distances.

The T_2 period has been observed in the first coda waves of the Mexico, Peru and Chili earthquakes, but as it existed mixed up with the oscillations of 17–18 sec. periods, its existence was not demonstrated until we had succeeded in separating these two periods by the method of analysis explained in the last paragraph. With respect to the earthquakes of Celebes, New Guinea and Celebes Sea too, the T_2 period is seen to exist in the beginning part of the first coda oscillation.

Of these three types of periods that exist in the coda oscillations of earthquake motions, T_2 and T_3 have constant values in all the earthquakes without regard to their different epicentral distances. So it will not be unreasonable to assume that these represent the free oscillation periods of the vibrating system, while the T_1 period that increases with epicentral distances is the period of external forces that reach the vibrating systems, namely, the period of the propagative seismic waves. However, the fact that we have adopted Takahasi's method of analysis presupposes that we are assuming the existence of some vibrating system. Therefore the question we have to consider is this:—What types of vibrating systems is it most proper for us to assume to exist?

As the free oscillation period of the seismometer used for recording earthquake motions has been kept up at about 60 sec., that observed period T_2 can by no means be the free oscillation period of this seismometer. Another probable assumption is that the earth's surface layers upon which the seismometer is installed may constitute a vibrating system.

There have been repeated discussions regarding the possibility of occurrence of free vibrations in a surface layer, but if we assume its possibility in common with the prevailing opinions, we can find in it a convenient explanation for the three periods here observed.

During the period within which the sine type external waves stimulate the vibrating system, the system will continue forced oscillations and will display a T_1 period, but as the periodicity of the external disturbance fades away and external forces come to have a nature of random stimulation to the vibrating system, it will be expected that the free oscillation periods T_2 and T_3 will be observed. The study of the free oscillations of the surface layer will also afford an apt explanation to the phenomenon of T_1 period appearing in one section of the first coda oscillations, and T_2 in another, as in the case of the oscillatory curves here analysed.

In order that such a free oscillation might be maintained for a long time, the damping coefficient of the vibrating system will require some consideration. The damping coefficients of the respective waves of different periods are seen in Table IX. As seen in the table the dampings of the waves of free oscil-

Table IX. Damping constant *h* for respective oscillation curves.

Curve No.	T_1	h	Curve No.	T_2	h	Curve No.	T_3	h
	sec			sec			sec	
16- 1	7.0	0.0866	34- 1	19.8	0.1212	54- 1	16.4	0.0119
16- 2	7.3	0.0439	36- 1	18.8	0.1676	37- 3	16.3	0.0814
19- 1	6.4	0.3358	36- 5	21.7	0.0556	37- 5	16.7	0.2690
20- 2	6.9	0.0778	37- 2	19.7	0.0848	37- 9	15.9	0.0930
54- 1	10.7	0.2673	37- 7	20.0	0.2273	49- 9	16.6	0.0960
34- 1	13.1	0.5573	49- 3	19.5	0.1741	49-10	16.4	0.0156
36- 6	15.2	0.0461	49- 4	19.7	0.2565	51- 6	16.6	0.0272
37- 4	14.9	0.0734	51-10	19.0	0.5511	51-14	16.5	0.0002
37- 6	14.9	0.0907	52- 3	19.6	0.2674	51-15	16.6	0.0552
37- 9	15.5	0.3501	52-18	19.7	0.0992			
49- 1	17.1	0.1959	52-19	20.9	0.0936			
49- 2	17.9	0.1790						
49- 5	17.9	0.0402						
49-10	17.0	0.3337						
51- 1	17.6	0.2211						
51- 3	17.3	0.0538						
51- 4	17.5	0.0943						
51- 9	17.8							
51-10	17.8	0.0406						
52- 1	18.3	0.0522						
52- 2	18.3	0.0522						
52- 4	18.7	0.0850						
52- 6	18.2	0.7161						
52-15	18.3	0.0066						
52-21	18.0	0.2704						

lation are smaller than those of the waves that propagate, and the waves of T_3 period display particularly small damping coefficients.

As to the free oscillation in the surface layer, E. Wiechert[4] advanced the theory of a stationary wave that has a node at the lower end of the surface layer and a loop at the surface of the layer. If we take up such a model, the thickness of the layer d will be represented by $d=\frac{1}{4}VT$, where V is the velocity of the elastic shear waves that pass through the layer, and T the period of the stationary waves. Now if we give to d and V in the upper and middle layers the values $d_1=4.5$ km, $d_2=16$ km, $V_1=1.1$ km/sec and $V_2=3.2$ km/sec respectively, according to the result of T. Matuzawa,[5] we shall be able to expect the periods of the stationary waves to be $T_3=16$ sec., and $T_2=20$ sec. These, however, are quite rough estimations, and we will discuss them in detail in the following chapters.

In concluding this chapter the author wishes to express his cordial thanks to Professors T. Hagiwara and Ch. Tsuboi for their kind advices and continuous encouragement throughout the course of this study.

20. 地震動の尾部について (其の 5)

地震研究所 表俊一郎

第6章 高橋伏見の方法による地震動の尾部の週期解析.

高橋伏見の方法により震央距離の異る9個の地震について尾部の振動の週期解析を行つた結果をのべた. まず始めに高橋伏見の方法により解析を行へば得られる振動曲線は2つの減衰性正弦波が重ね合せられたものとなることをのべ次に之を夫々の component curve に分解して夫々の曲線の減衰率と週期とを求める方法を述べた. このようにして53個の振動曲線より70本の正弦曲線を求め尾部の週期を解析した所, 前章迄では正確な週期を見出すことの出來なかつた第1尾部の部分についても充分正確に解析を進めることが出來地震動の尾部には3つの種類の週期の群が見られることが明らかになつた. 之等を T_1, T_2 及び T_3 と名付けた. T_1 は震央距離の大きい地震程大きな値を示す週期であり T_2 及び T_3 は之に反して震央距離の如何に拘はらず常に一定の値を示すものであり T_2 は主として第1尾部, T_3 は第2尾部の振動の中に見られその値は略々 $T_2=20$ 秒 $T_3=16$ 秒となることを知ることが出來た.

---

4) E. Wiechert und K. Zöppritz, "Über Erdbeben Wellen" Göttingen, 1907, 54.
5) T. Matuzawa, *Bull. Earthq. Res. Inst.*, 6 (1929), 177.

21. *On the Aftershocks of the Fukui Earthquake.* (*Part 2*)

By Syun'itiro OMOTE,

Earthquake Research Institute.

(Read June 20, 1950.—Received Sep. 20, 1950.)

1. Introduction.

The severe Fukui earthquake which shook the Echizen Plain at 18 h 50 m on June 28, 1948, was accompanied by a great many aftershocks. The present author hurried to the seismic area with many collaborators and the observations of aftershocks were carried out by a temporary network of seismological stations from July 5 to August 10.[1] As the result of such observations it was found that the epicenters of the aftershocks were distributed all over the Echizen Plain and over the adjacent hilly regions on its east and northeast. In the course of observations we made some new attempts in recording these aftershocks: 1) With a view to knowing the exact time of the commencement of the tremors at each station, we placed time-marks on the seismograms at several stations and hoped to get time-distance curves due to the arrival times of the seismic waves of aftershocks. 2) With a view to making some studies on the distribution of the first impulsions, two horizontal motion seismometers were installed at each of the five stations. In the following two sections these two subjects will be discussed.

I. TIME-DISTANCE CURVES OF AN AFTERSHOCK.

2. The commencement times at each station.

The study of near earthquakes directed our attention to the necessity of establishing the time-distance curves in regions very near the focus of a shock. For this purpose it seemed desirable to draw time-distance curves due to aftershocks observed by a more or less small network of observation points. First it was necessary to measure the accurate commencement time of an aftershock at as many stations as possible. We selected five stations, Daishoji, Yamanaka, Shioya, Maruoka and Fukui, and on the seismograms of these stations time-marks were placed at every one minute by means of a clock and at every one hour by the time broadcast by radio. The time-marks in these manners of recording, however, will not give a highly accurate commencement time of a shock, but supposing a shock has happened very near the radio time-mark, the commencement time at the respective stations of such a shock will have a fairly reliable value. Fortunately enough we had such a shock, and it was recorded at all the five observation stations though it was the only case out of the 500 recorded aftershocks to satisfy this condition. This shock took place at about 16 h 01 m of July 29 and had the intensity I due to the Japanese scale at the nearest station, Daishoji. Seismograms obtained at the respective station are reproduced in the Plate. The position of the epicenter of this shock, reported on in the previous paper, is shown in Fig. 1 by a double circle. The commencement time of this shock was recorded at the respective stations as listed in the last column of Table I. Since, with respect to this table, the accuracy of the figures in the last cloumn concerns us most, the processes by which these figures were derived and the probable errors in the materials used are given

---

[1] S. OMOTE and others, *Rep. Fukui Earthq.* (1950 Tokyo), 37.

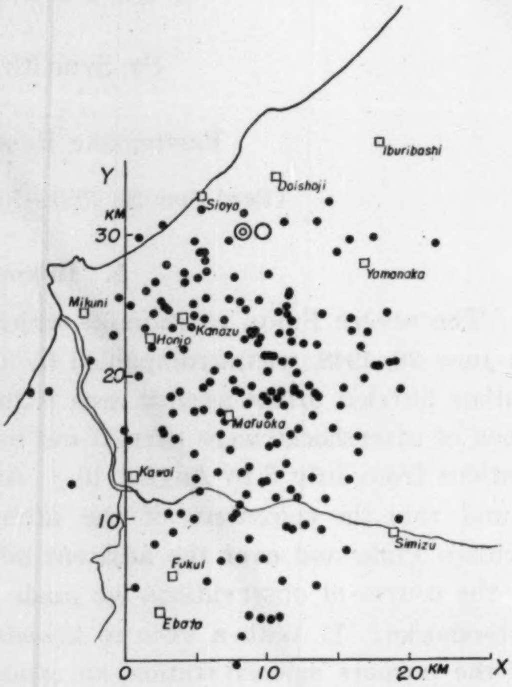

Fig. 1. Distribution of foci of aftershocks.
◎; epicenter of the shock determined in the previous report.
○; revised epicenter.

Table I. Commencement times at observation stations.

	Length of one minute mark	Time of two marks	AB	RB	BP	Commencement time			
								P	S
	mm mm	sec	mm	mm		h	m	sec	sec
Daishoji	73·0±0·064	59·91	73·3	64·4	10·5	16	01	2·78	4·89
Shioya	60·4±0·063	60·37	60·89	0·18	2·3	16	01	2·79	4·90
Maruoka	63·5±0·051	60·42	63·9	7·8	59·0	16	01	3·61	6·28
Yamanaka	63·3±0·054	60·08	60·1	26·5	37·1	16	01	2·96	5·22
Fukui	26·9±0·054	—	—	—	10·1	16	01	5·56	9·57

in preceding columns in the same table. The notations in Table I refer to the corresponding letters in Fig. 2. As shown in the table the shock occurred in less than 61 seconds after the radio time mark of 16 h 00 m, so that the accuracy of the commencement time observed at the stations will be trusted to within ±1.0 second, and further, considering that the revolution of the recording drums was not very irregular at that time, the commencement times will be accurate even to ±0.1 sec. The length of the record between two successive minute-marks observed at Shioya Station is plotted and shown in Fig. 3 as an example. From this figure we shall be able to infer the degree of uniformity of the revolution of the recording drum and the accuracy of the minute marks of the clock.

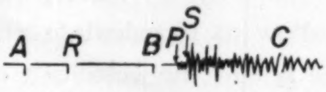

Fig. 2. An example of a seismograph with time marks. R is radio mark A, B and C are minute marks.

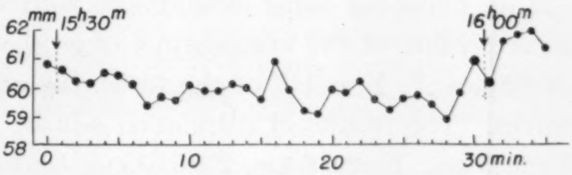

Fig. 3. Variation of the length of time mark of every one minute at Shioya station.

3. Determination of the focus.

In order to determine the focus of this shock three different methods were applied.

i) The focus of the shock calculated from the times of arrival of waves.

The orthogonal co-ordinates X, Y were placed in the positions shown in Fig. 1, and Z was taken vertically downward with its origin at the earth's surface. Now take the co-ordinates of the focus as X, Y, Z, the origin time of the shock as T_0, and the velocity of P and S waves as V and v respectively. Though the velocity distributions within the earth are not yet known, for the sake of simplicity, we assumed that P and S waves were uniform in velocity throughout the whole area, and that the wave paths were straight lines from focus to station. These assumptions, to be sure, may not be strictly applicable, but some evidences seem to indicate that the granitic layer exists very near the earth's surface and the depth of focus is not over 15 km, so that it may be safe to assume a uniform velocity and a straight path of seismic waves. As discussed in the previous paper the value of the Omori constant k was calculated as $k=7.2$. With the earthquakes in regions along the Sea of Japan, k always has a large value, and it appears probable that in these regions the uppermost layer which Matuzawa(1) found in the Kwanto District

---

1) T. MATUZAWA, *Bull. Earthq. Res. Inst.*, 7 (1329), 241.

is supposedly very thin if it exists at all, and the second layer (granitic layer) stretches very near the thin superficial sedimentary layer. In this way we have five unknown quantities and five observed values due to five stations, and these unknown quantities will be solved easily as follows:

$X=9.59$km, $Y=28.65$ km, $Z=1.40$ km, $T=16$ h 01 m 1.83 sec., $V=6.33$ km/sec.

ii) The focus of the shock calculated from the commencement times of S waves.

If we make the same assumptions with S waves as with P waves, the observed value of the arrival time of S waves will allow us to calculate the co-ordinates X, Y and Z of the focus, the origin time t_0 and the velocity v of S waves. The results of calculation will be as follows:

$X=9.53$ km, $Y=29.00$ km, $Z=5.03$ km, $t_0=16$ h 01 m 2.75 sec., $v=3.58$ km/sec.

iii) The focus of the shock calculated from P–S times.

P–S times (duration time of preliminary tremor) at the respective stations are easily known from the commencement times of P and S waves observed by them, and from these P–S times the focus and the Omori constant k will be calculated. The result obtained in this way is as follows:—

$X=9.57$ km, $Y=29.77$ km, $Z=14.21$ km, $k=7.15$.

If we compare the values obtained in i), ii) and iii) with each other we at once see the close proximity of the figures of the co-ordinates X, Y of the epicenter. These two values, therefore, are certainly reliable, but the other values derived above have such unreasonable figures that our next question is how to find out the most reasonable values for the position of the focus, the origin time and the velocities of P and S waves.

4. The focus of the shock.

First of all we will concentrate our attention on the determination of the position of the epicenter of the shock. For that purpose we will begin by assuming that

$V=5.1$ km/sec., $T_0=0.16$ sec.,

in this, V is the velocity of the P waves and T_0 is the value wich will satisfy

16 h 01 m$+T_0=$origin time of waves

then the focus will by the least square method, be:—

$X=9.83\pm0.907$ km,

$Y=29.67\pm0.145$ km,

$Z=12.30\pm0.065$ km,

Taking these as the first approximation values, the correction values were calculated as:—

$\delta X=+0.053$ km, $\delta Y=-0.201$ km, $\delta Z=+0.086$ km.

With respect to S waves, in the same way as with P, the velocity and origin time of S waves will be assumed to be :—

$v=3.0$ km/sec., $t_0=-0.11$ sec.,

then the focus will be :—

$X=9.79\pm0.090$ km,
$Y=30.02\pm0.043$ km,
$Z=13.45\pm0.020$ km,

and the correction terms :—

$\delta X=+0.058$ km, $\delta Y=-0.135$ km, $\delta Z=+0.051$ km.

As to the P-S time, we assume $k=7.4$, whence :

$X=9.87\pm0.792$ km,
$Y=30.52\pm0.375$ km,
$Z=14.98\pm0.168$ km,
$\delta X=-0.18$ km, $\delta Y=-0.71$ km, $\delta Z=-0.11$ km.

5. Determination of the velocities and origin times of P and S waves.

Besides the notations used in the preceding paragraphs, we introduce here d_i, P_i and S_i, where d_i being the distance from the focus to the station i, P_i and S_i being the commencement times of P and S waves at the station i. We then have[1] :—

for P waves: $d_i/V+T_0=P_i$, $i=1, 2, 3, 4, 5$.
for S waves: $d_i/v+t_0=S_i$, $i=1, 2, 3, 4, 5$.

The two groups of unknowns $(1/V, T_0)$ and $(1/v, t_0)$ can be solved severally by the least square method from the above two pairs of equations, and we get :—

$V=5.071\pm0.002$ km/sec., $T=+0.061\pm0.038$ sec,
and $v=3.015\pm0.003$ km/sec., $t_0=+0.321\pm0.054$ sec.

According to this result the time of origin of S waves seems to have been a little later than that of P waves, but it will still be too rash to discuss from this result the problem which waves, P or S, were generated first.

6. Residuals.

The focus of the shock, the time of origin and the velocities of P and S waves have all been measured by the above calculations. And therefore, if we assume that a seismic wave had started from the focus thus determined at the time corresponding to the origin time of P or S wave and spread with the velocity of P or S thus determined, we shall be able to calculate the arrival times of P and S waves at each station. The difference between the two arrival times, the observed and the calculated, at the respective stations will be seen in the A and C columns in Table II.

---

[1] P. G GANE, A. L HALES & H. O. OLIVER, *Bull. Seis. Soc. Amer.*, **36** (1946), 49.

This difference is less than 0.2 seconds at any observation station with respect to both P and S waves. If we shift the origin time of P or S wave slightly, namely 0.10 sec. for P and -0.17 sec. for S, the values of the residuals will become fairly small. (See B and D columns in Table II). On the whole these are very satisfactory results, but closer examination of the Table reveals that residuals at Maruoka and Fukui stations are somewhat larger than those of the other stations. This may indicate the existence of a thicker layer of alluvium underneath these regions, but the amount of the residuals is so small that it will be of little use if we are to calculate the thickness of the alluvium from these data.

Table II: Residuals of observed minus calculated origin time.

Station	P		S		P~S	
	A	B	C	D	E	F
	$t_i - t$ cal	$t_i - t$ cal	$t_i - t$ cal	$t_i - t$ cal	$(P\sim S)_{ob}$	$(P\sim S)_{cal}$
	$T_0=0.06$	$T_0=0.16$	$t_0=0.32$	$t_0=0.15$	I*	II*
Daishoji	+0.13	+0.03	−0.09	+0.08	+0.04	−0.04
Shioya	+0.06	−0.04	−0.21	−0.04	−0.02	−0.13
Yamanaka	+0.08	−0.02	−0.19	−0.02	0.00	0.00
Maruoka	+0.12	+0.02	−0.18	−0.01	−0.03	−0.03
Fukui	+0.09	−0.01	−0.16	+0.01	+0.01	−0.02

* I; forcus is assumed at $X=9.87$, $Y=30.52$, $Z=14.98$ and
II at $X=10.84$, $Y=29.81$, $Z=15.47$.

7. Time-distance curves.

The results obtained in this Section will be summarized as follows:—

The focus of the shock: $X=9.81$ km, $Y=29.72$ km, $Z=13.79$ km,
The origin time: $T_0=16$ h 01 m 0.06 sec, $t_0=16$ h 01 m 0.32 sec.
Velocities: $V=5.07$ km/sec, $v=3.02$ km/sec.

The arrival times of P and S waves plotted with reference to their respective epicentral distances determined from the above results are shown in Fig. 4. Incidentally, the time-distance curve due to hypocentral distance is given in Fig. 5.

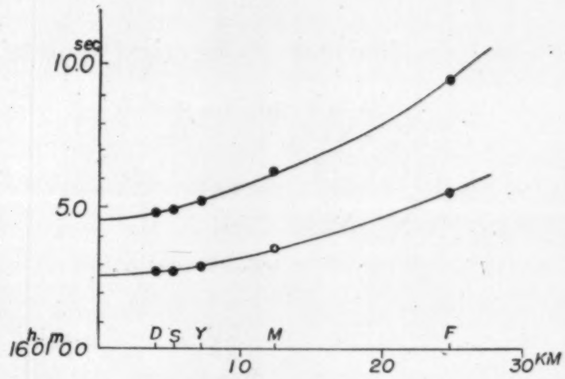

Fig. 4. Time distance curves. D, Daishoji; S, Shioya; Y, Yamanaka; M, Maruoka; F, Fukui.

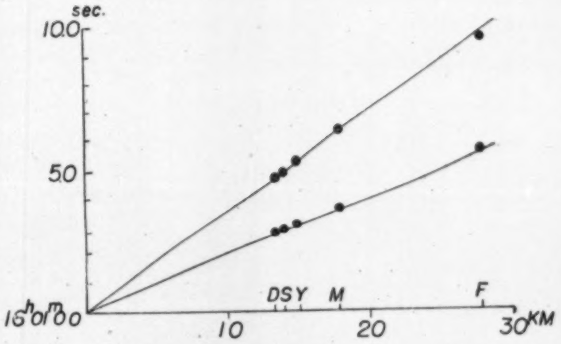

Fig. 5. Commencement times of P and S waves plotted to the hypocentral distances. D, Daishoji; S, Shioya; Y, Yamanaka; M, Maruoka; F, Fukui.

II. DISTRIBUTION OF THE FIRST IMPULSIONS OF AFTERSHOCKS.

8. Observation of the first impulsions.

The observation of aftershocks was carried out at eleven stations. Of these eleven stations five were equipped with two horizontal motion seismometers to conduct the study of the first impulsions of aftershocks. These five were stations at Fukui, Ebata, Maruoka, Shioya and Daishoji, and at the last named (Daishoji) station a vertical motion seismograph was also installed. The records obtained at Fukui were not suitable for the study, the beginning of the motion not being clear enough in them, and the observation at Ebata station covered only a too brief period. It will be seen, then, that the number of observation points was too small to draw a distribution map of the first impulsions with respect to each individual aftershock.

9. The distribution map of the first impulsions.

As the first step to this study we assumed that all the aftershocks took place with the same mechanism and at the same depth. Next, we put the epicenter of an aftershock upon that of another, in this way piling up the epicenters of all the shocks at a single point in the map. We then drew an arrow at the spot corresponding to each observation point to indicate the direction of the first impulsion.

Such a map is the result of the observation of many aftershocks at one seismic station (the epicenters of the aftershocks being determined by the three- or four- station method), and consequently the meaning of this map is that:—It gives a diagram showing the distribution of the first impulsions of a seismic wave when an imaginary shock took place at the origin point in the map and obsevations of the first impulsion were carried out at all the points denoted by full or open circles in the map.

Fig. 6 is a map obtained from Daishoji station and Fig. 7 from Maruoka station. From these we at once notice that the above assumptions do not apply wholly well in these cases, but still, if we except some few shocks (shown by arrows in thin lines), we can see that the majority of the aftershocks are to be considered to have had the same mechanism of occurrence. The regions of the first condensation and rarefaction are to be divided into four quadrants.

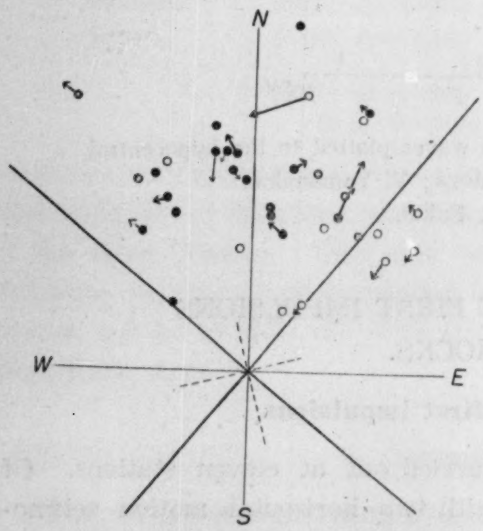

Fig. 6. Pull push distributions due to the Daishoji station. ●; push, ○; pull.

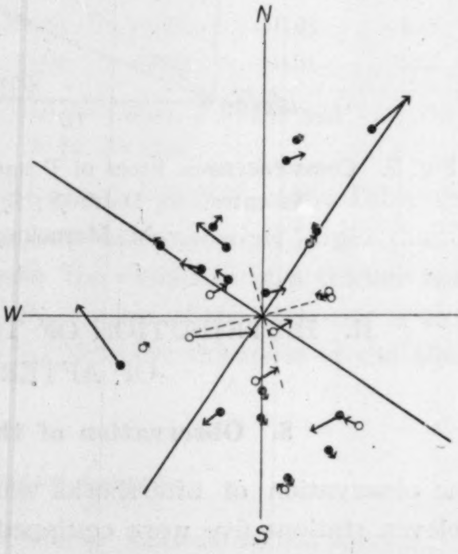

Fig. 7. Pull push distributions due to the Maruoka station. ●; push, ○; pull.

The distribution of the first impulsions of the main shock was studied by

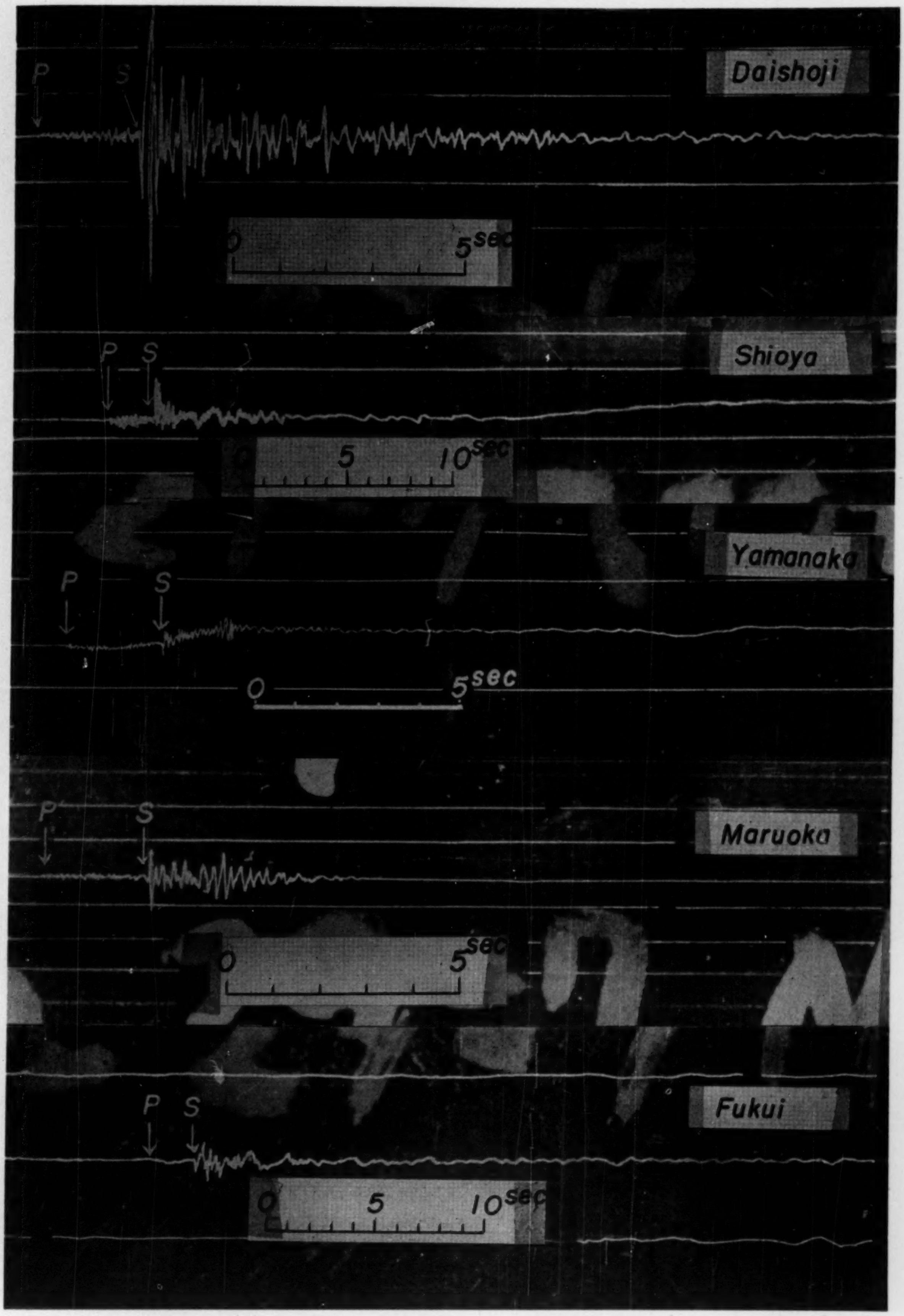

（震研彙報 第二十八號 圖版 表）

T. Hirono[1], who drew the two nodal lines intersecting each other at a right angle at a point near the epicenter of the main shock, one of them having the direction of *N* 20° *W*. According to the results here obtained by us the direction of the nodal lines due about 35 degrees counter-clockwise.

At Daishoji station a vertical motion seismograph had also been installed. If we examine Fig. 6 minutely we notice that with respect to three shocks observed at Daishoji the direction of the first impulsion determined from the two components of horizontal motion seismometers contradicts with the direction derived from the vertical motion seismometer.

This fact brings forward a serious problem to the study of the first impulsions. It cannot be denied that some unsatisfactory records of small amplitudes of aftershock had to be used in this study of the first impulsions, and that more strict examinations of these records are needed before accuracy of results is to be hoped for.

The author's thanks and appreciation are due to Mrs. T. Asada, Z. Suzuki and K. Tazime of the Geophysical Institute of the Tokyo University, for the co-operation they lent him in the observation of the Fukui aftershocks. A part of the expense of this study was defrayed by the Scientific Research Fund of the Ministry of Education.

---

21. 福井地震の余震について

地震研究所　表俊一郎

昭和23年6月28日の福地震の余震の震央分布については既に別に報告されてゐる．この福井地震の余震觀測の際余震の發震時を求めるための試みがなされ幸にして1つの余震については可なりの程度迄信用し得る發震時を測定し得たので，種々の方法によりその余震の震央を求めた．その結果P, Sの發震時から獨立に求められた震央も略々一致した價となること，P, Sの震源での發震時も略々同一の値となり，特にどちらかがたしかに早く震源を出發したと主張出來るやうな證據は認められなかつたことが注意された．P及びSの速度V及びvは夫々$V=5.2$ km/s, $v=3.0$ km/sとなり沖積層の下にすぐ所謂 granitic layer が來てゐるのではないかと思はせるものがあつた．各觀測點の發震時と，最後に求められた震央及 origin time 及び速度より計算によつて得られるP, Sの到達時刻との差から沖積層の厚さを求めようとしたが上述の差があまり小さくなつたために之は求め得なかつた．震央距離25 kmまでの發震時による走時曲線を圖に示した．次に余震の押引の分布を求めた結果本震の押引の分布とくらべ節線の位置が反時計的に35°回轉したと考へられるやうな分布を示すもののやうである．

---

[1] H. KAWASUMI and others, *Rep. Fukui Earthq.* (1950, Tokyo), 6.

22.　北海道有珠岳新側火山發生にともなつた地表變形の測定

地震研究所　　宮村攝三

（昭和19年11月21日發表—昭和21年3月1日受理）

§1. 昭和18年12月すえから，北海道洞爺（トウヤ）湖畔の有珠（ウス）岳（第1圖）附近に，有感地震が頻發し，翌19年1月すえには，その山のふもと壯瞥（ソウベツ）村の南部，伊達（ダテ）町との境界ちかくに，多數の龜裂ができ，その一帶が次第に隆起しはじめた．山麓一帶の有感地震はのち次第にへつていつたが，3月ごろからは壯瞥村柳原（ヤナギハラ）の隆起地域に局部的微震が發生しだした．5月下旬から隆起はだんだん北へうつつて，6月には隆起中心は壯瞥村フカバ附近になつた．そして，そこを中心とする局部的微震も次第に增加し，つひに6月23日にいたつて，フカバの通路西方約600 m，隆起中心點附近から噴火した．

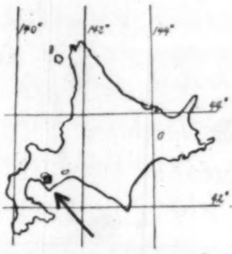

第1圖甲

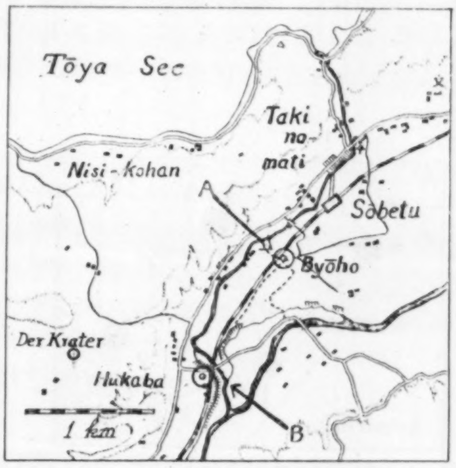

第1圖乙

水上博士，永田博士をはじめ，越川理學士，表理學士，實川顯氏らによつて，この隆起に關して，すでに各種の研究がおこなはれた.[1] 噴火は火山灰の噴出を主とするもので，熔岩の流出などはまつたくなかつたが，とにかくその後も，ますますはげしくなつてゆく狀態であつた．そして火口自身次第に隆起して，ひとつの側火山に生長しつゝあり，附近の地變もさかんに進行しつゝあつた．水上博士，表理學士はひきつゞき地震觀測，水準測量，傾斜其他種々の地形變動の觀測をおこなつてをられる．筆者は昭和19年7月下旬から8月はじめにかけて，地表變動の測定を，噴出點にちかい一二の箇所でおこなつた．かぎられた點での，きはめて短期間のしらべであり，ごく貧弱な，それだけ

---

1)　地震研究所研究速報　第3號（昭和19年9月）

としてはたゞ表土の性質についての若干の推論と，その短い期間における，一二の點での地變の傾向とをしめすものにすぎないが，水上博士其他の包括的研究にくりいれていたゞくなら，あるいはひとつの資料としてやくだちうるかともかんがへ，かきしるすことにした次第である．

§2. 地面の變形を，彈性論上の各種のひずみとして測定するには，三鷹（ミタカ）において，陸地測量部の手でおこなはれ，寺田，坪井兩博士らが，それについて種々地球物理的議論をされている，菱形邊長の測定が，一つの便利な方法であることは，よくしられている.[2] 永田博士，實川顯氏は，今度の有珠岳東麓の隆起地帶で，この方法による測定をおこない，興味ある結果を報告された.[3] 筆者は陸地測量部 30 m 鋼まき尺をもちい，有珠新噴火點ちかくで，同様の測定をくわだてた．

壯瞥村瀧ノ町室蘭（タキノマチムロラン）營林署苗甫內および同村フカバ鐵道鐵橋わきの畑地に，比較的平坦なところをえらび，一邊約 29 m の菱形をつくり，菱形の頂點には丈夫に杭をうちこんだ．（第1圖，第2圖）杭の丸太は，長さ 1,5–2 m，きりくちさしわたし 10–15 cm，ほとんど大部分を土中にうちこみ，杭頭が4本ほゞおなじ水平面上にあるようにし，おのおののきりくちのうへには，アルミニューム板に十字線をひいたものを，くぎづけし，その十字線にまき尺の目盛をあはせてよめるようにした．まき尺は第3圖にしめずようなぐあいに，一端は杭 P_A に固定し，他端は杭 P_B における滑車を通じておもり G（約1貫）をさけ，まき尺 M にくはは る張力を一定にし，菱形頂點の杭 P_1，P_2 のうへの十字線の交點の位置は，二人の觀測で，同時によみとる．一つの邊をはかるのに，それを5回くりかへし，その前後に溫度をよんだ．

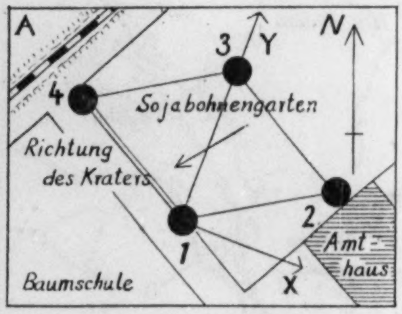
A
N
3
Y
4
Sojabohnengarten
Richtung
des Kraters
2
1
Amt-
haus
Baumschule
X

第2圖甲

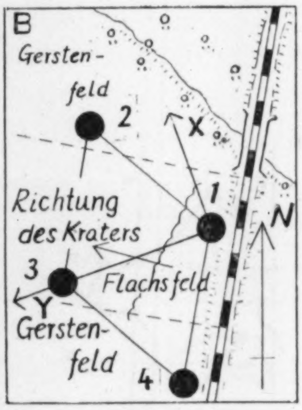
B
Gersten-
feld
2
X
1
Richtung
des Kraters
N
3
Y
Flachsfeld
Gersten-
feld
4

第2圖乙

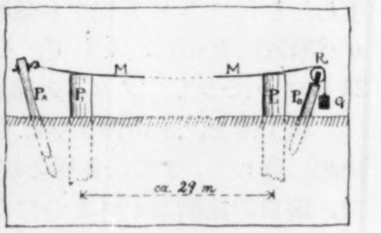
P_A
P_1
M
M
R
P_2
P_B
Q
ca. 29 m

第3圖

---

2) 寺田 *Proc. Imp. Acad.* 8 (1932); *Bull. E. R. I.* 10 (1932).
坪井 *Bull. E. R. I.* 8 (1930), 13 (1935) 19 (1941); *Proc. Imp. Acad.* 6 (1930), 7 (1931).
武藤・篠 *Bull. E. R. I.* 10 (1932).

3) 永田・實川 地震 16（昭和19年8月）No. 8

§3. 第4圖のごとく，右手系直交座標をとつて，菱形の頂點を 1 (X_1, Y_2), 2 (X_2, Y_2); 3 (X_3, Y_3), 4 (X_4, Y_4), 各頂點間の距離，すなはち菱形の邊長をそれぞれ $L_{12}=L_{21}$, $L_{23}=L_{32}$, $L_{31}=L_{13}$, $L_{14}=L_{41}$ とすると，

$$X_1=Y_1=0,\ X_3=0,\ Y_3=L_{13}.$$

邊長はみなほゞ 29 m で，一定であるから，$L=29\,\mathrm{m}$ とすると

$$Rij=L+lij\ (i\neq j,\ ij=1, 2, 3, 4)$$

とかけ，lij は Lにくらべて小さい量となる．また x_2, y_2, x_4, y_4 を L にくらべて小さい量として，

$$X_2=-(\sqrt{3}/2)\,L+x_2,\ Y_2=(1/2)\,L+y_2;$$

$$X_4=-(\sqrt{3}/2)\,L-x_4,\ Y_4=(1/2)\,L+y_4,$$

とかくことができる．

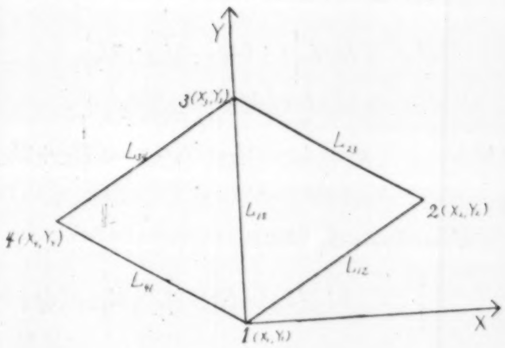

第4圖

Δ123, Δ143 の面積 S_1, S_4 はそれぞれ

$$S_1=\left\{P_2\,(P_2-L_{12})\,(P_2-L_{23})\,(P_2-L_{31})\right\}^{1/2},$$

$$S_4=\left\{P_4\,(P_4-L_{14})\,(P_4-L_{13})\,(P_4-L_{31})\right\}^{1/2},$$

たゞし

$$2P_2=L_{12}+L_{23}+L_{31}=3L+2p_2,\quad 2p_2=l_{12}+l_{23}+l_{31};$$

$$2P_4=L_1{}^4+L_{43}+L_{31}=3L+2p_4,\quad 2p_4=l_{14}+l_{43}+l_{31}.$$

である．よつて

$$P_2-L_{12}=L/2+p_2-l_{12},\quad P_2-L_{23}=L/2+p_2-l_{23},\quad P_2-L_{31}=L/2+p_2-l_{31},$$

したがつて，

$$\begin{aligned}S_2&=\left\{(3L/2+p_2)\,(L/2+p_2-l_{12})\,(L/2+p_2-l_{23})\,(L/2+p_2-l_{31})\right\}^{1/2}\\&=(\sqrt{3}/4)\,L^2\Big[\left\{1+(2p_2/3L)\right\}\left\{1+(2p_2-2l_1)/L\right\}\left\{1+(2p_2-3l_{23})/L\right\}\\&\qquad\qquad\left\{1+(2p_2-2l_{31})/L\right\}\Big]^{1/2}\\&\fallingdotseq(\sqrt{3}/4)\,L^2\left\{1+(8p_2/3L)\right\}^{1/2}\\&\fallingdotseq(\sqrt{3}/4)\,L^2\left\{1+(4p_2/3L)\right\}\\&=(\sqrt{3}/4)\,L^2+p_2L/\sqrt{3}.\end{aligned}$$

同樣に

$$S_4=(\sqrt{3}/4)\,L^2+p_4L/\sqrt{3}$$

よつて

$$\begin{aligned}X_2&=2S_2/L_{13}\\&=(\sqrt{3}/2)\,L^2\,(1+4p_2/3L)/L\,(1+l_{13}/L)\end{aligned}$$

$$\fallingdotseq(\sqrt{3}/2)\,L\,(1+4p_2/3L)\,(1-l_{13}/L)$$
$$\fallingdotseq(\sqrt{3}/2)L\left\{1+(4p_2-3l_{13})/3L\right\}$$
$$=(\sqrt{3}/2)\,L+(4p_2-3l_{13})/2\sqrt{3}\,.$$

すなはち　$x_2=(4p_2-3l_{13})/2\sqrt{3}=(2l_{12}+2l_{23}-l_{13})/2\sqrt{3}\,.$

また

$$Y_2=(L_{12}{}^2-X_2{}^2)^{1/2}$$
$$=\left[L^2(1+l_{12}/L)^2-(3/4)L^2\left\{4l_{12}-(4p_2-3l_{13})/3L\right\}^2\right]^{1/2}$$
$$\fallingdotseq L\left[(1+2l_1/L)-(3/4)\left\{1+2(4p_2-3l_{13})/3L\right\}\right]^{1/2}$$
$$=L\left[1/4+\left\{4l_{12}-(4p_2-3l_{13})\right\}/2L\right]^{1/3}$$
$$\fallingdotseq(L/2)\left[1+\left\{4l_{12}-(4l_{12}-3l_{13})\right\}/L\right]$$
$$=L/2+\left\{4l_{12}-(4p_2-3l_{13})\right\}/2\,.$$

すなはち　$y_2=\left\{4l_{12}-(4p_2-3l_{13})\right\}/2=(2l_{12}-2l_{23}+l_{13})/2\,.$

同様にして

$$X_3=-2S_4/L_{13}$$
$$=-(\sqrt{3}/2)\,L-(4p_4-3l_{31})/2\sqrt{3}\,.$$
$$x_4=(4p_4-3l_{31})/2\sqrt{3}=(2l_{14}+2l_{43}-l_{13})/2\sqrt{3}\,.$$

また

$$Y_4=L/2+\left\{4l_{14}-(4p_4-3l_{13})\right\}/2\,,$$
$$y_4=\left\{4l_{14}-(4p_4-3l_{13})\right\}/2=(2l_{14}-2l_{43}+l_{13})/2\,.$$

さて，變形の各頂點のずれの成分を．それぞれ u_1, v_1；u_2, v_2；u_3, v_3；u_4, v_4；とする．そして，いま，原點をうごかないと假定し，1-3 の方向もかはらないものとすると，

$$\begin{aligned}\delta X_1&=u_1=0, & \delta Y_1&=v_1=0;\\ \delta X_2&=u_2=\delta x_2, & \delta Y_2&=v_2=\delta y_2;\\ \delta X_3&=u_3=0, & \delta Y_3&=v_3=\delta l_{13};\\ \delta X_4&=u_4=-\delta x_4, & \delta Y_4&=v_4=\delta y_4.\end{aligned}$$

こゝで，各頂點のずれの成分が，それぞれその點の座標の一次式であらはされるものと假定する．すなはち

$$\left.\begin{aligned}u_i&=aX_i+bY_i+c,\\ v_i&=a'X_i+b'Y_i+c',\end{aligned}\right.\qquad (i=1,\ 2,\ 3)$$

とする．ひとつひとつをかくと，このばあいは

$$\begin{aligned}u_1&=aX_1+bY_1+c, & v_1&=a'X_1+b'Y_1+c'\\ u_2&=aX_2+bY_2+c, & v_2&=a'X_2+b'Y_2+c'\\ u_3&=aX_3+bY_3+c, & v_3&=a'X_3+b'Y_3+c'\\ u_4&=aX_4+bY_4+c, & v_4&=a'X_4+b'Y_4+c'\end{aligned}$$

これに u_1, v_1 等についての條件をいれると,

$$c=0, \qquad c'=0$$
$$u_2=aX_2, \qquad v_2=a'X_2+b'Y_2$$
$$b=0, \qquad u_3=b'Y_3$$
$$u_4=aY_4, \qquad v_4=a'X_4+b'Y_4$$

これから

$$a=u_2/X_2 \fallingdotseq u_2/(\sqrt{3}/2)\,L=\delta x_2/(\sqrt{3}/2)L=(2\delta l_{12}+2\delta l_{23}-\delta l_{12})/3L$$

または $$a=u_4/X_4 \fallingdotseq -u_v/(\sqrt{3}\ 2L=\delta x_4/(\sqrt{3}/2)L=(2\delta l_{04}+2\delta l_{43}-\delta l_{03}-\delta l_{03})/3L$$

また $$b'=v_3/Y_3 \fallingdotseq v_3/L=\delta y_3/L=\delta l_{23}/L$$

つぎに $$a' \fallingdotseq \left\{v_2-(v_3/L)\,(L/2)\right\} \Big/ (\sqrt{3}/2)L$$
$$\fallingdotseq \left\{(2/\sqrt{3})v_2-v_3/\sqrt{3}\right\}/L=\left\{(2/\sqrt{3}\ \delta y_2-\delta y_3/\sqrt{3}\right\} \Big/ L$$
$$=2(\delta l_{02}-\delta l_{23})/\sqrt{3}\,L$$

または $$a' \fallingdotseq \left\{v_4-(v_3/2)\ (L/2)\right\} \Big/ \left\{-(\sqrt{3}\ 2)/L\right\}$$
$$\fallingdotseq -\left\{(2/\sqrt{3})v_4-v_3/\sqrt{3}\right\}/L=-\left\{(2/\sqrt{3})\delta y_4-\delta y_3/\sqrt{3}\right\} \Big/ L$$
$$=2(\delta l_{04}-\delta l_{43})/\sqrt{3}\,L$$

さて $$\partial u/\partial X=a,$$
$$\partial u/\partial Y=b=0,$$
$$\partial v/\partial X=a',$$
$$\partial v/\partial Y=b',$$

であるから, ひずみとして面積膨脹率 (Ausdehnung) Δ, 廻轉 (Rotation) ω, すべり (Scherung) σ, 最大すべり (Maximalscherung) Σ, をかんがへると,

$$\Delta=(\partial u/\partial X)+(\partial v/\partial Y)=a+b',$$
$$\omega=\left\{(\partial u/\partial Y)-(\partial v/\partial X)\right\} \Big/ 2=(q-a')/2=-a'/2,$$
$$\sigma=(\partial u/\partial Y)+(\partial v/\partial Y)=b+a'=a',$$
$$\Sigma=\left[\left\{(\partial u/\partial x)-(\partial v/\partial Y)\right\}^2+\left\{(\partial v/\partial X)+(\partial u/\partial Y)\right\}^2\right]^{1/2}$$
$$=\left\{(a-b')^2+(a'+b)^2\right\}^{1/2}$$
$$=\left\{(a-b')^2+a'^2\right\}^{1/2}.$$

おもなひずみ (Hauptdeformation) はそれぞれ

$$\gamma_1,\ \gamma_2=(\partial u/\partial X)+(ev\partial Y)\pm\left[\left\{(\partial u/\partial X)-(\partial v/\partial Y)\right\}^2+\left\{(\partial v/\partial X)+(\partial u/\partial Y\right\}^2\right]^{1/2}$$
$$=a'+b'\pm\Sigma=a+b'\pm\left\{(a-b')^2+a'^2\right\}^{1/2},$$

その方向は, x 軸から反時計まわりにはかり,

$$\theta_1=\mathrm{arctg}\left[(\partial v/\partial Y)-(\partial u/\partial X)+\left\{\overline{(\partial u/\partial X)-(\partial v/\partial Y)^2+(\partial v/\partial X)+(vu/\partial Y)^2}\right\}^{1/2}\right]$$
$$\div\left\{(\partial u/\partial Y)+(\partial v/\partial X)\right\}$$
$$=\mathrm{arctg}\ [(b'-a+\Sigma)/a'],$$

$$\theta_2=\mathrm{arctg}\left[(\partial v/\partial Y)-(\partial u/\partial X)-\left\{\overline{(\partial u/\partial X)+(\partial v/\partial/\partial Y)}^2+\overline{(\partial v/\partial X)+(\partial u/\partial Y)}^2\right\}^{1/2}\right]$$

$$\div\left\{(\partial u/\partial Y)+(\partial v/\partial X)\right\}$$

$$=\mathrm{arctg}[(b'-a-\Sigma)/a'],$$

であらはされる．

§4 邊長の測定結果は第I表にしめすとほりで，うえの式にしたがつて計算した種々のひずみの數値は第II表にしめしてある．

邊長測定からひずみを計算した場合の誤差は普通の誤差傳播のかんがへで，つぎのやうにしてもとめられる．

第I表 菱形邊長測定値 (單位 cm. 溫度 C°.)

A. Byōho

Nr.	Datum	l_{14}	l_{34}	l_{31}	l_{23}	l_{12}
I	VII 21	−10.12±.05 (23.°4)	−7.38±.04 (22.°9)	−26.44±.16 (24.°2)	−20.05±.04 (20.°2)	+6.75±.02 (23.°0)
II	VII 22	− 8.45±.08 (23.°5)	−7.32±.03 (22.°1)	−25.60±.02 (22.°1)	−19.80±.05 (23.°2)	+6.93±.01 (22.°8)
III	VII 23	− 8.61±.05 (22.°3)	−7.27±.01 (23.°5)	−25.41±.03 (23.°0)	−19.44±.01 (24.°5)	+6.70±.06 (22.°6)
IV	VII 24	− 9.40±.04 (21.°5)	−7.10±.01 (24.°0)	−25.70±.04 (22.°5)	−19.44±.04 (21.°9)	+6.83±.00 (23.°0)
V	VII 30	− 9.40±.09 (28.°0)	−7.67±.02 (27.°8)	−25.91±.02 (28.°5)	−19.88±.02 (28.°4)	+6.40±.01 (28.°4)
VI	VIII 2	− 9.74±.04 (29.°0)	−7.90±.03 (29.°2)	−26.21±.03 (29.°3)	−20.04±.01 (28.°5)	+6.25±.01 (29.°4)

B. Hukaba

Nr.	Datum	l_{14}	l_{34}	l_{31}	l_{23}	l_{12}
I	VII 21	−6.67±.02 (20.°0)	− 3.71±.04 (19.5°)	−10.25±.08 (20.°7)	−6.94±.02 (19.°2)	−21.56±.05 (21.°6)
II	VII 22	−5.69±.09 (21.°9)	− 6.03±.04 (21.°5)	−11.73±.02 (21.°4)	−6.91±.01 (21.°5)	−22.56±.05 (21.°4)
III	VII 23	−6.38±.06 (22.°9)	− 8.20±.07 (24.°9)	−14.49±.04 (22.°3)	−7.17±.04 (24.°8)	−26.80±.04 (22.°8)
IV	VII 29	−9.16±.05 (29.3°)	−18.73±.05 (29.°8)	−25.30±.02 (28.°5)	−8.37±.02 (27.°0)	−41.67±.08 (29.°0)
V	VII 30	−9.43±.01 (29.°2)	−20.93±.04 (28.7°)	−27.58±.04 (30.°9)	−8.28±.01 (29.°2)	−45.12±.07 (29.°5)
IV	VIII 2	−9.73±.07 (27.°0)	−27.08±.02 (27.°0)	−33.11±.03 (27.°0)	−9.09±.01 (27.°0)	−53.66±.03 (27.°0)

第 II 表菱形邊長の變化（單位 cm. 溫度差 δt に対するなほしは 0.036 δt とす）

A. Byōho

Nr.	Datum	δl_{14}	δl_{34}	δl_{31}	δl_{23}	δl_{12}
II-I	VII21-VII22	$+1.67\pm0.09$	$+0.06\pm0.04$	$+0.76\pm0.16$	$+0.36\pm0.06$	$+0.17\pm0.02$
III-II	VII22-VII23	-0.20 ± 0.09	$+0.10\pm0.03$	$+0.26\pm0.04$	$+0.41\pm0.05$	-0.24 ± 0.07
IV-III	VII23-VII24	-0.79 ± 0.07	$+0.19\pm0.02$	-0.31 ± 0.05	-0.09 ± 0.04	$+0.13\pm0.09$
V-IV	VII24-VII30	$+0.23\pm0.10$	-0.43 ± 0.02	$+0.01\pm0.05$	-0.21 ± 0.04	-0.22 ± 0.00
VI-V	VII30-VIII2	-0.30 ± 0.10	-0.18 ± 0.04	-0.28 ± 0.04	-0.16 ± 0.03	-0.21 ± 0.01

B. Hukaba

Nr.	Datum	δl_{14}	δl_{34}	δl_{31}	δl_{23}	δl_{12}
II-I	VII21-VII22	$+1.05\pm0.09$	-2.25 ± 0.05	-1.45 ± 0.08	$+0.11\pm0.02$	-1.01 ± 0.05
III-II	VII22-VII23	-0.65 ± 0.11	-2.05 ± 0.09	-2.73 ± 0.05	-0.14 ± 0.04	-4.19 ± 0.06
IV-III	VII23-VII29	-2.55 ± 0.09	-10.35 ± 0.08	-10.59 ± 0.05	-1.12 ± 0.04	-14.65 ± 0.09
V-IV	VII29-VII30	-0.27 ± 0.06	-2.24 ± 0.06	-2.19 ± 0.05	$+0.17\pm0.02$	-3.43 ± 0.11
VI-V	VII30-VIII2	-0.38 ± 0.07	-6.21 ± 0.04	-5.67 ± 0.06	-0.73 ± 0.01	-8.63 ± 0.07

第 N 回における邊長 l_{ij} の測定で, 5 回の算術平均の標準偏差は

$$\sigma_{l_{ij}^N}=\sqrt{\frac{\Sigma\varepsilon^2}{5(5-1)}} \qquad i\neq j\ \ i,j=1,2,3,4;\ N=\mathrm{I},\mathrm{II},\ldots\mathrm{VI}$$

これが第 I 表の邊長測定結果に附記してある. つぎにこれをもととして, 計算したひずみの値の標準偏差をもとめる. まづ邊長の變化の標準偏差をもとめるに, たとへば第 II 回と第 I 回における l_{12} の測定の標準偏差を $\sigma_{l_{12}^{\mathrm{I}}}$, $\sigma_{l_{12}^{\mathrm{II}}}$ とすると, その差の標準偏差 $\sigma_{l_{12}^{\mathrm{III}}}$ は

$$\sigma_{\delta l_{12}^{\mathrm{II,I}}}=\left\{\sigma^2_{l_{12}^{\mathrm{II}}}+\sigma^2_{l_{12}^{\mathrm{I}}}\right\}^{\frac{1}{2}}.$$

である. 同樣にして

$$\sigma_{\delta l_{23}^{\mathrm{III,II}}}=\left\{\sigma^2_{l_{23}^{\mathrm{III}}}+\sigma^2_{l_{23}^{\mathrm{II}}}\right\}^{\frac{1}{2}} \qquad \text{etc.}$$

である. そこで $a=(\partial u/\partial X)$, $b=(\partial u/\partial Y)$, $a'=(\partial v/\partial X)$, $b'(\partial v/\partial Y)$ の標準偏差はそれぞれ

$$\sigma_a=\left\{2^2\sigma^2_{\delta l_{12}}+2^2\sigma^2_{\delta l_{23}}+\sigma^2_{\delta l_{13}}\right\}^{\frac{1}{2}}\Big/3L,$$

あるひは $$\sigma_a=\left\{2^2\sigma^2_{l_{14}}+2^2\delta^2_{l_{13}}+\sigma^2_{\delta'_{13}}\right\}^{\frac{1}{2}}\Big/3L;$$

$$\sigma_b=0;$$

$$\sigma_{a'}=2\left(\sigma^2_{\delta'_{12}}+\sigma^2_{\delta l_{23}}\right)^{\frac{1}{2}}\Big/\sqrt{3}\,L,$$

あるひは $$\sigma_{a'}=2\left(\sigma^2_{\delta l_{14}}+\sigma^2_{\delta'_{43}}\right)^{\frac{1}{2}}\Big/\sqrt{3}\,L,$$

および $$\sigma_{b'}=\sigma_{\delta l_{13}}/L,$$

となる.

よつてひずみの標準偏差は

$$\sigma_{\varDelta} = \left\{\sigma^2{}_{a'} + \sigma^2{}_{b'}\right\}^{\frac{1}{2}};$$

$$\sigma_{\omega} = \sigma_{a'}/2;$$

$$\sigma_{\sigma} = \sigma_{a'};$$

また

$$\sigma_{\Sigma} = \left\{\left(\frac{\partial\Sigma}{\partial a}\right)^2 \sigma^2{}_{a} + \left(\frac{\partial\Sigma}{\partial a'}\right)^2 \sigma^2{}_{a'} + \left(\frac{\partial\Sigma}{\partial b'}\right)\sigma^2{}_{b'}\right\}^{\frac{1}{2}},$$

$$\frac{\partial\Sigma}{\partial a} = 1\,\frac{(a-b')}{\{(a-b')^2+a'^2\}^{\frac{1}{2}}}, \quad \frac{\partial\Sigma}{\partial a'} = \frac{a'}{\{(a-b')^2+a'^2\}^{\frac{1}{2}}}, \quad \frac{\partial\Sigma}{\partial b'} = \frac{-(a-b')}{\{(a-b')^2+a'^2\}^{\frac{1}{2}}}$$

$$= \frac{a-b'}{\Sigma} \qquad = \frac{a'}{\Sigma} \qquad = -\frac{a-b'}{\Sigma}$$

$$\therefore \quad \sigma_{\Sigma} = \left\{(a-b')^2\sigma^2{}_{a} + a'^2\sigma^2{}_{a'} + (a-b')^2\sigma^2{}_{b'}\right\}^{\frac{1}{2}} \Big/ \Sigma;$$

$$= \left\{(a-b')^2\sigma^2{}_{\varDelta} + a'^2\sigma^2{}_{\sigma}\right\}^{\frac{1}{2}} \Big/ \Sigma$$

また

$$= \left\{\sigma^2{}_{a} + \sigma^2{}_{b'} + \sigma^2{}_{\Sigma}\right\}^{\frac{1}{2}} = \left\{\sigma^2{}_{\varDelta} + \sigma^2{}_{\Sigma}\right\}^{\frac{1}{2}}.$$

§5. 邊長の時間的變化は第5圖にしめすとおりになつた. 面積膨脹率 ($\varDelta$), 最大すべり (Σ), は第III表, 第6~7圖によつてみることができる.*

第III表 面積膨脹率と最大すべり (單位 10^{-4})

A. Byōho	Δ123				Δ143			
Datum	Δ	$\sigma_{\varDelta}$	Σ	σ_{Σ}	Δ	$\sigma_{\varDelta}$	Σ	σ_{Σ}
VII21-VII22	+3.0	0.6	2.9	0.6	+1.0	0.6	8.5	0.5
VII22-VII23	+1.0	0.3	1.3	0.3	+0.6	0.3	1.6	0.4
VII23-VII24	−0.6	0.3	1.6	0.3	−1.3	0.3	4.1	0.3
VII24-VII30	−1.0	0.2	1.0	0.4	+0.1	0.3	2.6	0.4
VII30-VIII2	−0.4	0.2	1.6	0.4	−0.2	0.3	1.8	0.3

B. Hukaba	Δ123				Δ143			
Datum	Δ	$\sigma_{\varDelta}$	Σ	σ_{Σ}	Δ	$\sigma_{\varDelta}$	Σ	σ_{Σ}
VII21-VII22	− 9.8	0.4	4.8	0.3	− 5.7	0.4	14.8	0.4
VII22-VII23	− 4.1	0.3	23.9	0.3	− 7.8	0.4	15.0	0.4
VII23-VII29	−18.1	0.3	85.3	0.1	−24.7	0.3	58.2	0.4
VII29-VII30	− 3.9	0.3	19.2	0.4	+10.5	0.3	30.0	0.3
VII30-VIII2	− 7.6	0.3	45.3	0.3	−14.0	0.9	39.0	0.3

邊長の變化は, 苗甫ではきはめてわづかである. フカバでは, 噴火口方向にほゞ直角な 14, 23 の邊は, やはり變化がすくないが, 12, 13, 34 の邊は大きく變化している. 變化はおおむね負, つまり短縮である.

---

* 圖の方はすべて温度のなほしをしてない値からかいてあるが大したちがひはない.

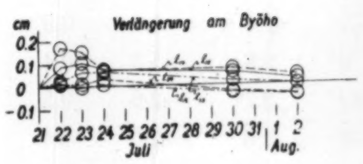

第５圖甲　邊長の變化（苗甫）

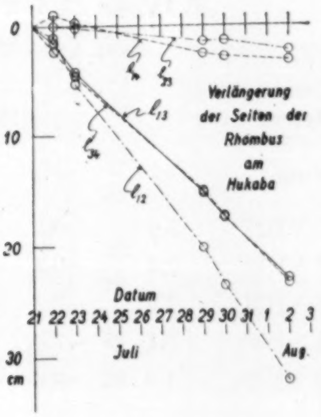

第５圖乙　邊長の變化（フカバ）

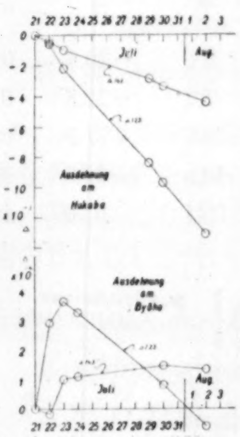

第６圖　面積膨脹率の變化
（上フカバ下苗甫）

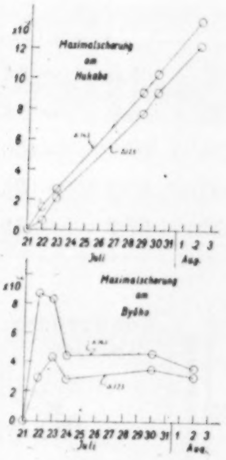

第７圖　最大すべりの變化
（上フカバ下苗甫）

面積膨脹率（Δ）と最大すべり（Σ）とをみると，苗甫とフカバではその量はひとけたちがい，苗甫は，Δは大體正（膨脹）で10^{-4}のけた，フカバは負（縮少）で10^{-3}のけたである．Σも苗甫は10^{-4}，フカバは10^{-3}のけたである．いづれにせよ時間的變化はフカバは簡單に線型であるが，苗甫の方ははじめすこし複雜に變化し，あとあまり變化しなくなつている．

おもなひずみの量とむきとを計算したのが第IV表であり，第8圖はその量の時間的變化をしめしている．第9圖にはその量とむき，測定點からの火口のむき，およびフカバにおいて，測定地點に23日～29日にできたわれめの方向をしめし，これらの關係をみやすくするようにしてある．苗甫ではΔ123はのびが主で，Δ143はのびとちゞみと同程度，いづれも10^{-4}のけたであり，むきもでたらめである．フカバの方はΔ123はちゞみが主であり，Δ143もちゞみが大きいが，のびもすこしある．量は10^{-3}～10^{-2}であり，10^{-2}に達した7月29日よりまへに破壊がおこつて，われめができたのである．壓縮による破壊であるから無論さけたのではなく，西の部分が東の部分をおしあげたよ

第IV表　おもなひずみの大きさ（單位 10^{-4}）と
方向（$+x$軸より反時計まはりの角度）

A. Byōho	Δ123				Δ143			
Datum	γ_1	γ_2	σ_γ	θ_1	γ_1	γ_2	σ_γ	θ_1
VII21-VII22	5.9	0.1	0.9	−71°	8.1	−9.0	0.8	−66°
VII22-VII23	2.3	−0.3	0.4	−65°	2.2	−1.0	0.5	+70°
VII23-VII24	1.0	−2.2	0.4	+ 9°	2.8	−5.3	0.4	+39°
VII24-VII30	0.1	−2.0	0.5	−89°	2.7	−2.6	0.5	−43°
VII30-VIII2	1.2	−2.0	0.5	+ 6°	1.6	−2.0	0.4	−51°

B. Hukaba	Δ123				Δ143			
Datum	γ_1	γ_2	σ_γ	θ_1	γ_1	γ_2	σ_γ	θ_1
VII21-VII22	5.0	− 14.6	0.5	−34°	9.1	−20.4	0.6	−33°
VII22-VII23	9.9	− 28.0	0.4	−21°	7.2	−22.8	0.5	−11°
VII23-VII29	67.2	−100.0	0.3	−20°	28.5	−77.9	0.5	−19°
VII29-VII30	15.3	− 23.0	0.5	−22°	40.5	−19.5	0.4	−14°
VII30-VIII2	37.7	− 52.8	0.4	−22°	25.1	−53.0	1.0	−19°

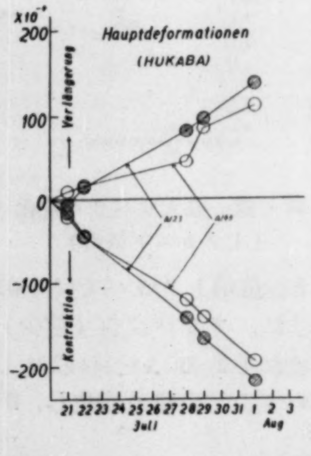

第8圖甲　おもなひずみの時間的
變化（フカバ）

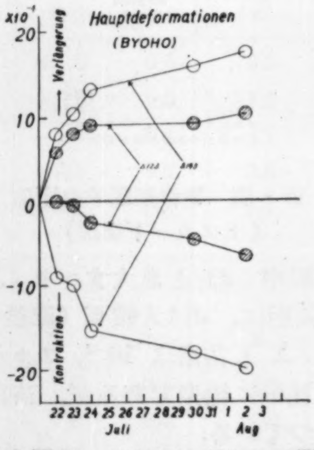

第8圖乙　おもなひずみの時間的
變化（苗甫）

うなかたちになつた．火口のむきにちゞんでいることも明瞭であり，火口の隆起にともなつて，外方へ地表がおされ一方壯瞥川の對岸は不動であつて，收縮を生じたものといへよう．この移動は鐵道線路を東へおす結果となり，問題になつていた．地表の土質は火山礫，火山灰のかたまつたものである．Terzaghi の教科書などでみると試驗片の實驗では粘土の破壞は 2×10^{-3}（黄粘土）〜7×10^{-3}（青粘土）くらいのひずみでおこることになつている．ひろい地表面の土もほゞ同程度のつよさであることがわかる．

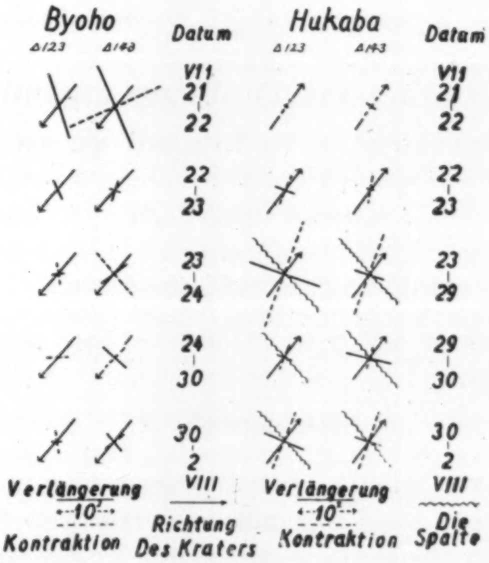
Byoho
Δ123
Δ143
Datum
Hukaba
Δ123
Δ143
Datum
VII
21
22
22
23
23
24
24
30
30
2
VIII
VII
21
22
22
23
23
29
29
30
30
2
VIII
Verlängerung
10'
Kontraktion
Richtung
Des Kraters
Verlängerung
10'
Kontraktion
Die
Spalte

第９圖　おもなひづみと火口のむき，フカバにできたわれめ．

§6.　をはりに，この測定に援助をあたへられた當時の陸地測量部武藤勝彦博士，また現地の官民各位の御厚意をしるし感謝の意を表したい．本所水上武博士には終始御指導をたまはつた．測定に協力された室蘭營林署壯瞥苗甫の三ノ宮秀起君の名も特にこゝにしるして感謝のしるしとしたい．

22. *Vermessung der Deformation der Erdoberflächen bei der Eruption eines neuen Flankenvulkans von Usu-dake, Hokkaido, 1944.*

Von Setumi Miyamura,
Institut für Erdbebenforschung.

(Vorgelegt am 21. November 1944. Eingegangen am 1. März, 1946)

Seit dem Ende 1943 wurden einige vulkanische Erdbeben und Bodendeformationen in der Umgebung von Usu-dake, Hokkaido, berichtet, und schliesslich am 23. Juni, 1944 brach ein Flankenvulkan am östlichen Fusse des Berges aus.

Der Verfasser führte dann die Vermessung der horizontalen Deformationen der Erdoberflächen in der Nähe des neuen Kraters aus. An zwei Orten legte er je einen kleinen Rhombus mit ca. 30 m langen Seiten auf dem Boden an und mass deren Seiten genau mit Stahlbandmass aus.

Auf einer der Messtellen an der Hukaba zeigte der Boden von vulkanischen Abschichtungen eine Zusammenziehung von ca. 2×10^{-2} in der Richtung des Kraters in 13 Tagen und bei Verschiebung weniger als 10^{-2} brach sie zusammen. Die letztere Zahlenwert entspricht ungefähr der experimentellen Druckfestigkeit des tonigen Bodens im Laboratorium nach Terzaghi.

23. *Experiments on the Overturnings of Circular Columns by the aid of a Shaking-Table.*

By Tetsuo AKIMA,

Earthquake Research Institute.

(Read April 18, 1950.—Received Sept. 20, 1950).

1. Introduction.

Approximate Maximum accelerations of ground motions at several places near the epicenter of destructive earthquake have been often estimated by observing the overturnings of grave-stones or many other bodies of similar shape. The phenomena of overturnings of such bodies due to ground vibrations are, however, very much complicated. Unlike the case of other ordinary oscillations, the natural periods of rocking motions depend much upon their amplitudes, and this makes the mathematical treatments of these phenomena quite tedious even if the external vibrations are assumed to be only horizontal and pure sinsoidal ones.

The ground motions due to actual earthquake vibrations containing not only vertical vibrations but also those due to many phases, the complete theoretical treatment of the overturnings phenomena of such bodies in these cases are almost impossible. Such being the case, the analytical studies on these phenomena have been made under quite simplified assumptions which may be quite different from the actual case.[1]

The practical estimation of the magnitudes of maximum ground accelerations due to earthquake vibrations by means of these phenomena is, as is well known, based upon West's formula $\alpha=dg/h$, where g is the acceleration due to gravity, 980 cm/sec^2, h and d are the height and width of an overturning grave-stone like column respectively. But this formula implies that the grave-stone begins to move without sliding when a constant acceleration α is given at its bottom. There remains therefore a doubt whether this formula is applicable to the case of the external acceleration which is not constant but periodic.

This problem has been experimentally studied by Dr. F. Ōmori[2] and recently by Dr. W. Inouye.[3] They reported that West's formula is only statistically and approximately applicable even when the external vibrations are horizontal and pure sinsoidal.

---

[1] H. KIMURA and K. IIDA, *Zishin*, 6, (1934), 125, 165.

[2] F. ŌMORI, "Fracturing and Overturning of Columns." (1899).

More recently, Dr. F. Kishinouye and Mr. R. Ikegami treated these phenomena mathematically, considering the work done by the external sinsoidal vibrations during its quarter period, and found the possibility of disoverturning of columns even when the maxmium accelerations due to the external vibrations exceed the value of α. They gave actual data observed on the Nankai Earthquake of Dec. 21st, 1946.[4]

The writer has made some experimental studies of this problem with many circular columns with various ratios of height to width. The columns are of steel, all 5 mm in diameter, with various heights, and these circular columns are erected on a circular levellable aluminium plates. (Fig. 1)

The bottoms of these circular columns are scooped like B in Fig. 1 in order to have the conditions at the bases of different circular columns as uniform and the frictions between the bases and the surface of the circular plate as large as possible.

This paper contains the results of experiments made by using a horizontal shaking-table in order to examine mainly the applicability of these circular columns as simple acceleration seismographs.

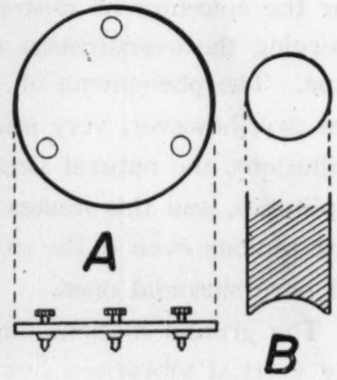

Fig. 1. The plate A and the circular column B.

2. Method.

The experiments were performed as follows. Place several horizontal plates on a shaking-table, erect a circular column mentioned above on the center of each plate, and shake the table gradually stronger. The maximum acceleration A, due to which any of these circular columns was overturned was measured. For one and the same circular column, experiments were repeated many times, for instance 100 times, and the frequency distribution of the maximum acceleration A's at which the column was overturned were investigated. As the amplitudes of the vibrations of this shaking-table could not be

---

3) W. INOUYE, *Zishin* 5 (1933), 750.

4) R. IKEGAMI and F. KISHINOUYE, *Bull. Earthq. Res. Inst.*, 25 (1947), 49.

changed continuously nor freely on account of its constructions, the accelerations were raised only by increasing the frequencies of vibrations.

The maximum acceleration due to the vibration of this shaking-table was calculated by measuring the frequencies and amplitudes of its vibrations which are recorded directly on a rotating drum. The form of the vibrations and the relation between frequencies～amplitudes and frequencies～maximum accelerations of the shaking-table are shown in Fig. 2 and 3.

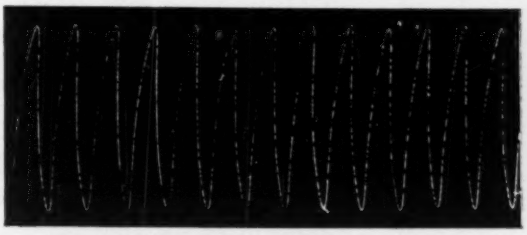

Fig. 2. The form of the vibrations of the shaking-table.

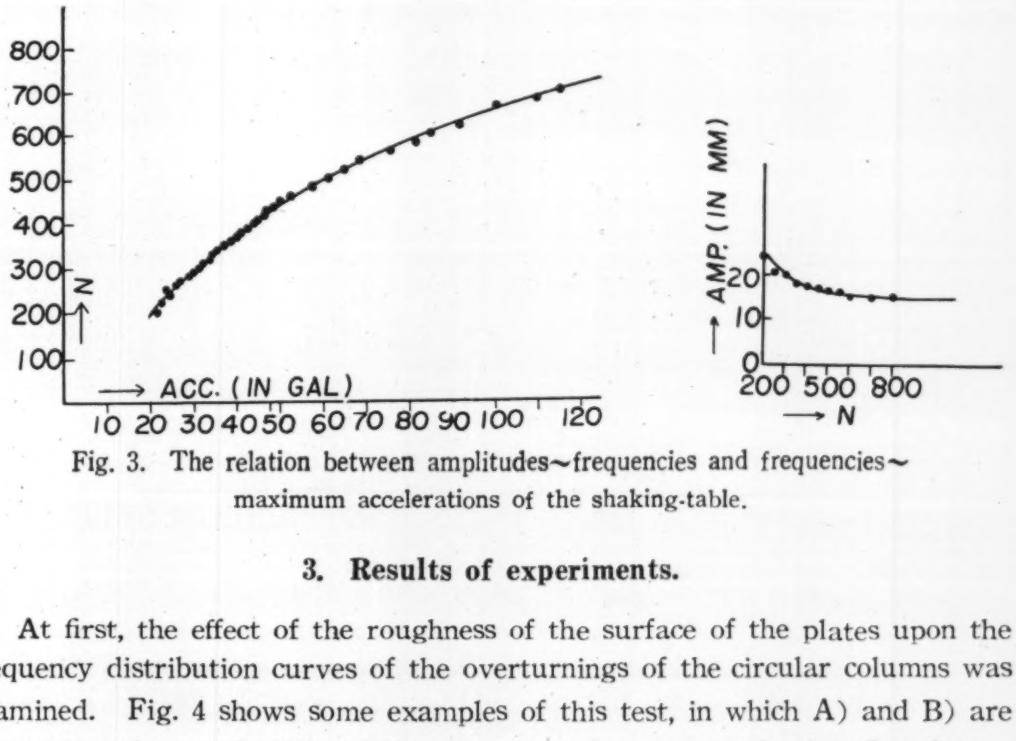

Fig. 3. The relation between amplitudes～frequencies and frequencies～maximum accelerations of the shaking-table.

3. Results of experiments.

At first, the effect of the roughness of the surface of the plates upon the frequency distribution curves of the overturnings of the circular columns was examined. Fig. 4 shows some examples of this test, in which A) and B) are the curves when a circular column was erected on a smooth plate I and on a rough plate II respectively. This figure shows that the smoothness of the surface of the plate makes the frequency distribution curves of overturnings of the circular columns sharper and the mean acceleration greater.

In the course of these experiments, it was noticed that some of the circular columns showed quite different features with regard both to their frequency distribution curves for the acceleration A and the overturning's directions, according to the inititial azimuth in which they were erected at the beginning of each experiment. This can be seen in Fig. 5 and 6, which shows the results obtained by keeping the azimuth of erection of the circular column in four

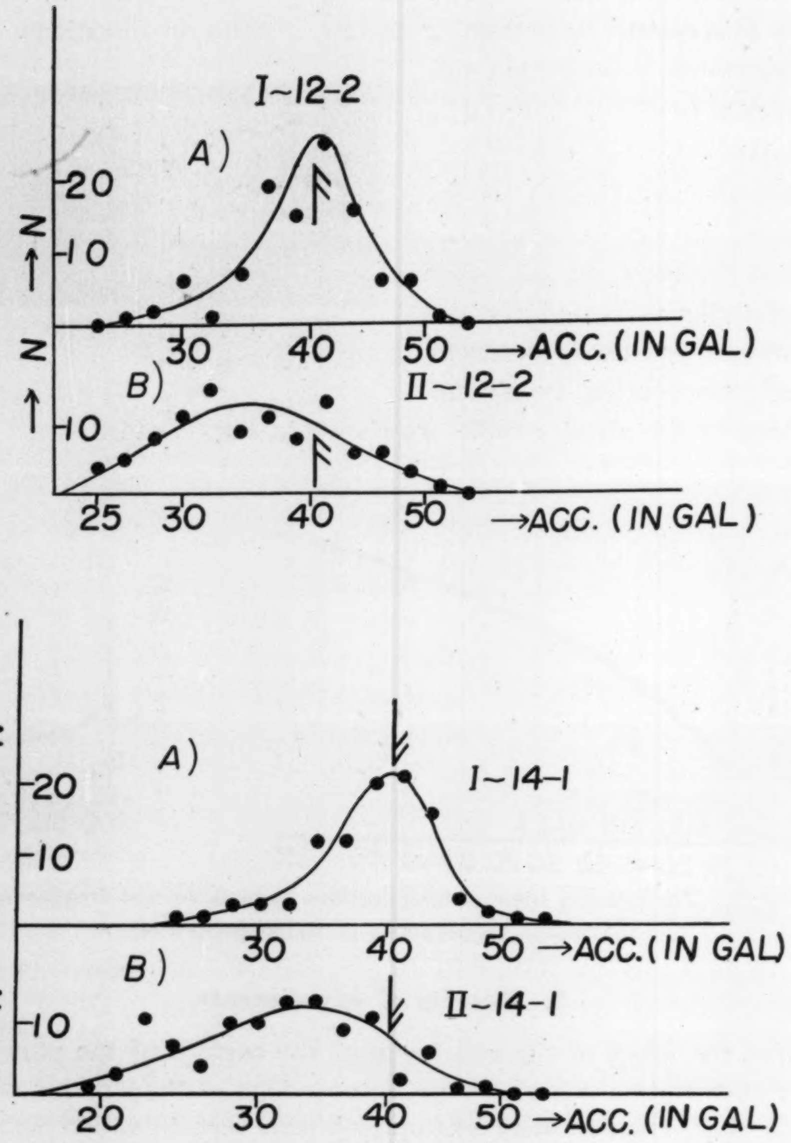

Fig. 4. Effect of the roughness of the plate.

definite directions as are shown in these figures, and performed 25 times for each azimuth.

These abnormal phenomena seem to have occurred owing to a slight inclination either of the circular column or of the plate or both of them towards a certain direction. For instance, in the case of the circular column 10-6 in Fig. 6, the result is clearly explained when this circular column and the plate are inclined to the direction as is indicated by the arrow in the same figure.

The third interesting result was that the rate of increase of the maximum

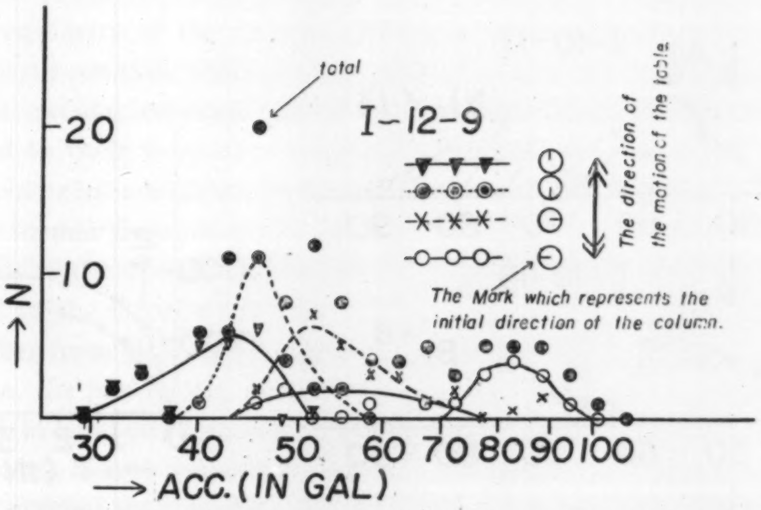

Fig. 5. The difference of frequency distribution curves by the initial azimuth for which the column was erected.

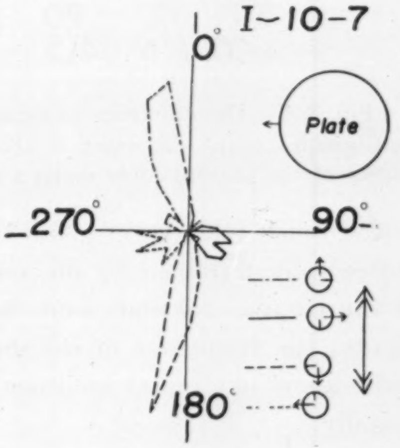

Fig. 6. The difference of directional distribution curves by the initial azimuth for which the column was erected.

acceleration of the sinsoidal horizontal vibrations given has a remarkable influence upon the mean value of our frequency distribution curves as is shown in Fig. 7-1. In this figure, A) and B) are the two curves obtained by such rates of maximum acceleration increase as are indicated by A) and B) in the following Fig. 7-2. In Fig. 7-1, the abnormal distribution curve of the last example concerning the circular column 10-7 is caused by the slight inclination of this column as was mentioned above.

In this figure, the numbers given on the right-side of the mark indicate the number of cases when the circular columns are not overturned in 100 experiments in spite of a quite rapid increase in the frequency of the shaking-table. The discussion of these phenomena will be given later.

By the results above obtained, the phenomena of overturnings of circular columns are found to be quite complicated, under the influence of many trivial factors such as the smoothness of the surface of the plate on which they are erected, the characteristics of the circular columns and the rate of frequency increase of the external vibrations, etc.

Considering the results obtained, the following experiments were performed

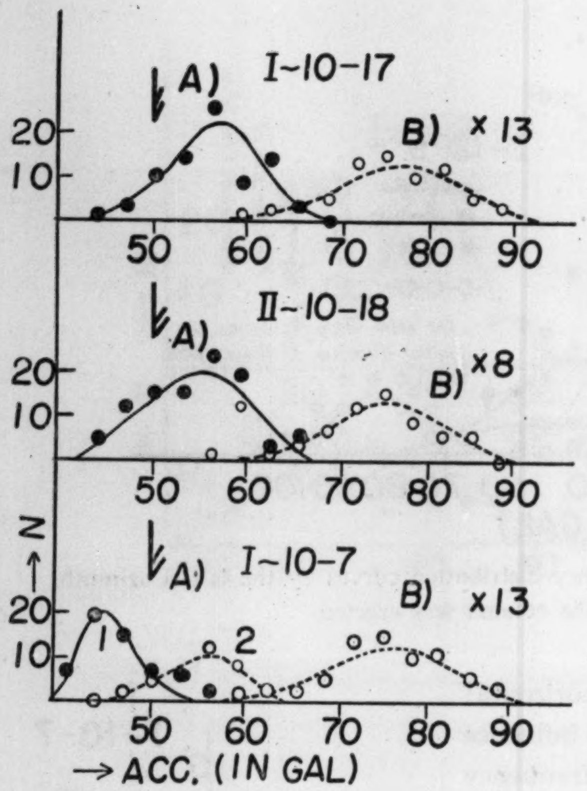

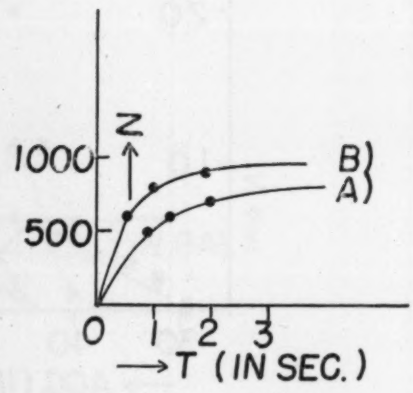

Fig. 7-1. The difference of mean value of frequency distribution curves according to the rate of frequency raising of the shaking-table under a constant amplitude.

Fig. 7-2. Two types of frequency raising.

under much more cares about the uniformity of conditions; the surfaces of the plates were flattened by file more throughly; the initial azimuth of erection of the circular columns were kept approximately the same for every experiments; the frequency of the shaking-table was raised as slowly as possible; the inclinations of circular columns and the levels of the plates were tested occassionally.

4. The dispersion of the frequency distributions or the separability of our circular columns for the external vibrational accelerations.

For the purpose of using these circular columns as simple acceleration seismographs and to apply them for studying the relation between the geographical or the topographical conditions and the maximum magnitudes of the ground's accelerations at many places due to earthquake vibrations, the first to be investigated experimentally is the frequency distribution of overturnings of many kinds of circular columns with various ratios of *d*/*h*, or the separability for the external vibrational accelerations.

For such purpose, the experiments were continued with much more care as to the regularity of the several conditions given above. The frequency distribution curves thus obtained were, however, not so sharp in general and some of the circular columns, moreover, showed still much different features with regard to their frequency distribution curves from other ordinary ones.

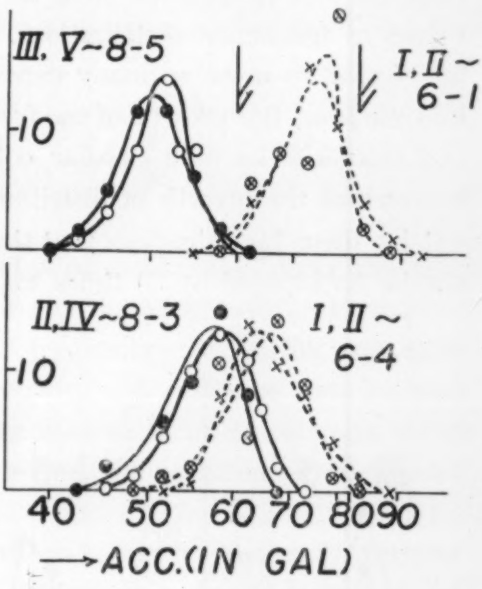

Fig. 8. Some examples of abnormal circular columns.

Such examples are shown in Fig. 8 and 9. The former shows how the mean accelerations of the frequency distribution curves of the circular columns 8-3 and 6-4 differ from that of 8-5 and 6-1 respectively. In this figure, and which is the same in any other figure, V~8-5, for instance, means the column 8 cm long No. 5 erected on the plate No. V. It may also be clear in the same figure that these differences are not due to the conditions of the plates but to the nature of circular columns themselves.

The latter figure shows the poor separability of our circular column for the external vibrational accelerations when these abnormal circular columns given above are included. These deviations of their mean accelerations of frequency distributions are considered to come from the small inclinations of these columns themselves or from the levels of plates or the slight curvature

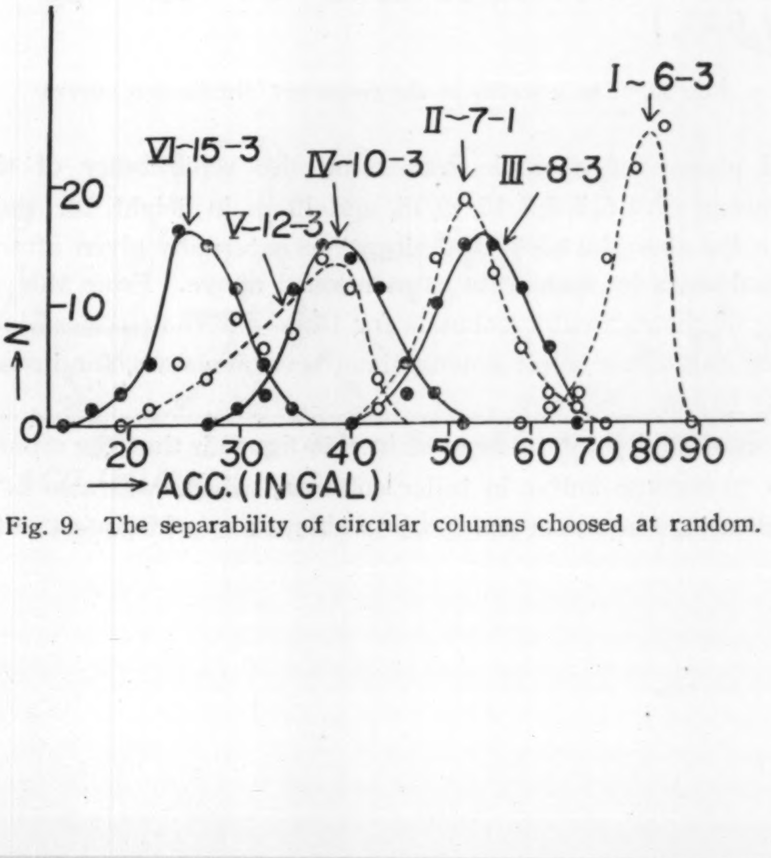

Fig. 9. The separability of circular columns choosed at random.

of the columns especially in taller ones which are too microscopic to be found out by simple methods.

Such being the case, the one method to remove such abnormal ones from our circular columns is to try to overturn them on a shaking-table, and to find out their mean acceleration of the frequency distribution curves of overturnings, which lead us to the problem of how many times of experiments on each circular column we have to perform in order to anticipate their mean values of frequency distributions. For, it is quite troublesome and takes a lot of time to make so many experiments as 100 times on each column. For this purpose, the growth of the frequency distribution curves in every 10 times was examined on each circular column already examined. Fig. 10 shows the features of the growth of distribution curves on some columns. It was found out by these investigations that the mean acceleration of frequency distribution can be anticipated by 30 times experiments at most.

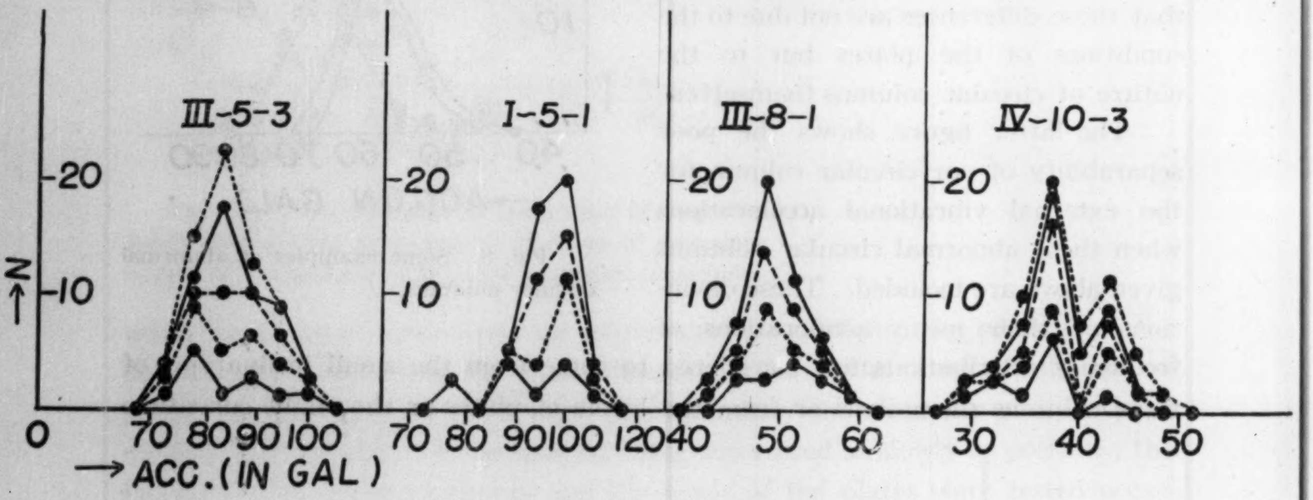

Fig. 10. The growths of the frequency distribution curves.

Fig. 11 shows an example concerning the separability of the normal circular columns of 4.5, 5, 6, 8, 10, 12, 15, and 19 cm in height, for the accelerations due to the sinsoidal horizontal vibrations externally given after removing the abnormal ones by such tests as mentioned above. From this figure, the separability of these circular columns for these external accelerations is found to be 10~25 gals if we select among them several classes, for instance, 4.5, 6, 8, 10, 15 and 19 cm.

The remarkable point to be seen in this figure is that the separability has a tendency to become better in taller columns, which will also be noticed in Table I indicating the mean and the probable errors of frequency distributions of overturnings on many circular columns.

Table I.

h (cm)	d/h	α (gal)	A (gal)			
4.5	0.11	109	105±4	102±5	103±5	103±5
5	0.1	98	93±5	92±5	94±6	94±6
6	0.083	82	72±8	73±5	78±4	74±5
8	0.062	61	55±5	51±5	50±4	53±4
10	0.05	49	39±3	40±2	40±3	42±3
12	0.041	40	36±4	35±3	37±2	35±2
15	0.033	33	28±2	25±2	26±2	25±3

In this table, the columns ***h***, ***d/h***, α and A represents the height, the ratio of height to diameter, the value of acceleration in West's formula and the mean acceleration and the probable error of frequency distribution curves of overturnings on each circular column respectively. A tendency may be seen in this table that the probable errors become smaller in taller columns, which fact shows that the taller columns are more sensible as acceleration seismograghs.

This table shows another fact that the mean values of frequency distributions are all smaller than the values of α. This fact is clearly indicated also in many figures following Fig. 8 already indicated. In these figures, the downward or the upward two feather-arrows show the positions of the values of α. In Fig. 11 the deviations of the mean values of frequency distribution curves from the values of α are indicated by lateral arrows. Before discussing the

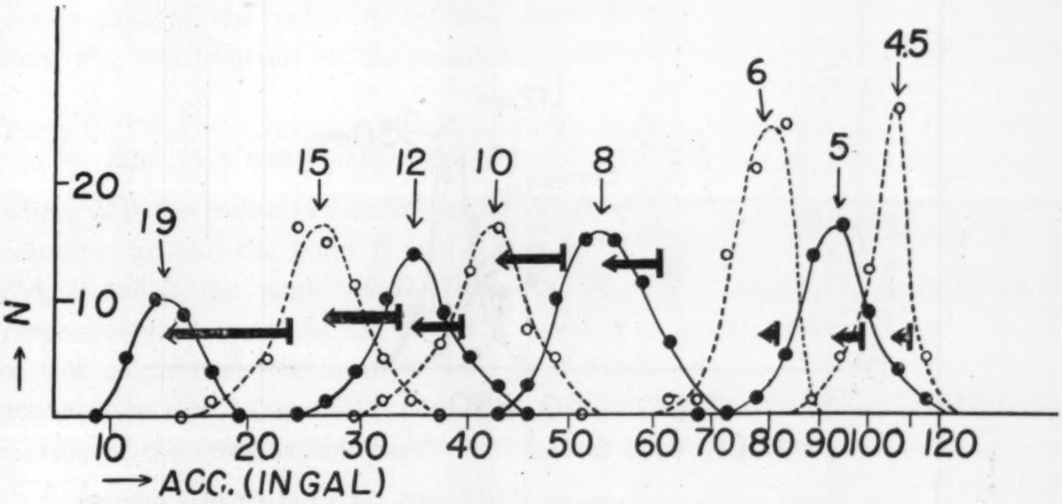

Fig. 11. The separability of the normal circular columns.

matter, the next experiments will be described here, the results of which may have some relations with the results given above.

These experiments were made in order to investigate the relation between the diameter of the circular columns and the amplitude of the external vibrations on the overturning phenomena.

The results are, as few examples, shown in Fig. 12–1, 2, 3, in which the numbers in the small circles represent the diameter of these circular columns *d* in mm. As the amplitude a of the vibrations of the shaking-table is approximately 1.5 mm in these regions of accelerations (See Fig. 2.), the ratios of

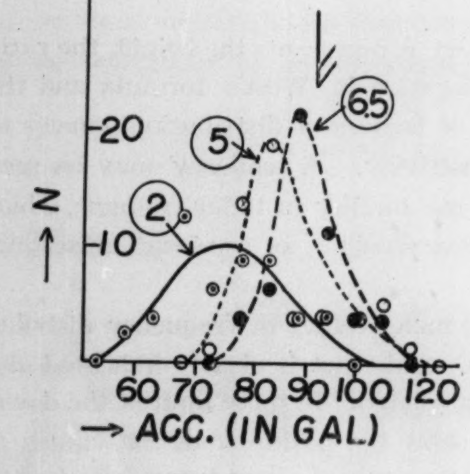

Fig. 12-1.

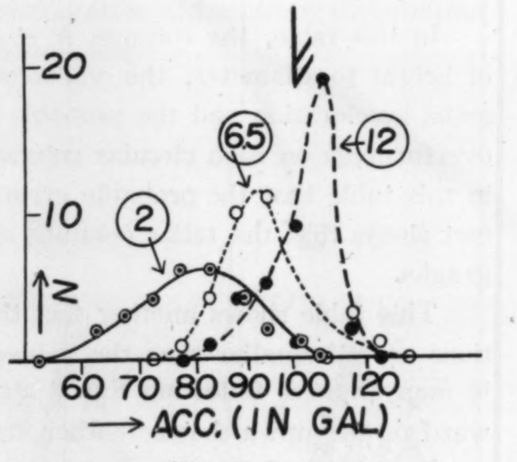

Fig. 12–2.

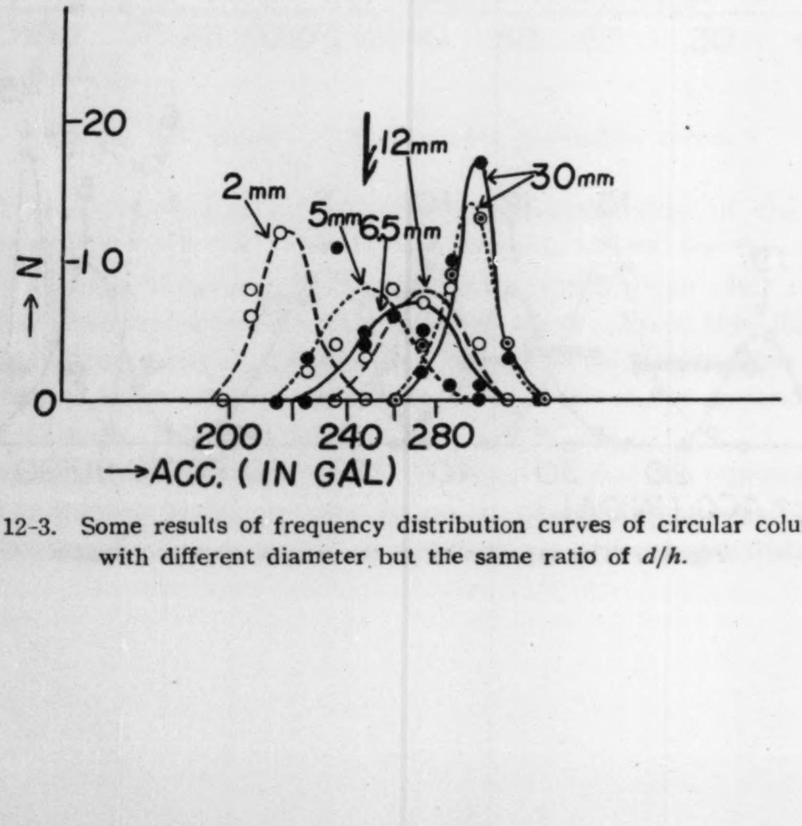

Fig. 12-3. Some results of frequency distribution curves of circular columns with different diameter but the same ratio of *d*/*h*.

corresponding to the circular columns with 2, 5, 6.5, 12 and 30 mm in diameter are 1.3, 3.3, 4.3, 8.0 and 20 respectively.

From these figures, it is obvious that the greater the ratios d/a, the greater becomes the mean accelerations of their frequency distribution curves. These results show that the phenomena of overturnings of columns by external vibrations depend not only upon the maximum acceleration due to external vibrations but upon their amplitudes relative to the sizes of the columns.

Another interesting phenomenon was also observed by these experiments, that is, the circular columns 30 cm in diameter ($d/a=20$) do not seem likely to overturn but only make rocking motions even when the maximum acceleration exceed the values of α.

In Fig. 12, therefore, the frequency distribution curves concerning these columns were obtained for the maximum accelerations by which they began to make rocking motions. The same phenomena were also observed sometimes in the case of 12 mm's ones. For instance, in Fig. 12–3, the times when they did not overturn but only made rocking motions and the times when they were at last overturned after continued rocking motions for some time were 6 and 8 in 40 times experiments respectively. From these results, we may say that the columns with larger values of d/a are more stable against the external vibrations.

Now, for the purpose of explaining this phenomenon given above, let us consider the natural periods of the rocking motions of our five kinds of circular columns with different values of d/a but with the same ratio of d/h. In the natural rocking motions of circular columns, the time taken by the circular columns rotate around the point A by the angle θ_0 (See Fig. 13) is given by the equation

$$t=\sqrt{\frac{R^2+c^2}{2gc}}\int_{\theta_0}^{0}\frac{d\theta}{\sqrt{\cos(\beta-\theta_0)-\cos(\beta-\beta)}},\quad\ldots(2)$$

where R is the radius of rotation of the circular columns around the point A, c the length of GA, β and θ_0 the angle of GAD and GAG_0 respectively where G_0 is the center of gravity of this column at which $d\theta/dt=0$, g is the acceleration due to gravity, and θ is the angle varying with the rocking motion of the circular columns.[5]

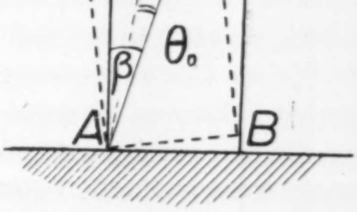

Fig. 13. The rocking motion of the columns.

---

[5] C. Tsuboi, 'Shindōron," 308. ("Theory of Oscillation (in Japanese)," Kawadeshobō, Tōkyō, 1942.)

The value of above expressed is calculated as follows.

$$\cos(\beta-\theta_0)=2\cos^2\frac{\beta-\theta_0}{2}-1, \qquad \cos(\beta-\theta)=2\cos^2\frac{\beta-\theta}{2}-1,$$

$$\therefore \int_{\theta_0}^{0}\frac{d\theta}{\sqrt{\cos(\beta-\theta_0)-\cos(\beta-\theta)}}=\frac{1}{\sqrt{2}}\int_{\theta_0}^{0}\frac{d\theta}{\sqrt{\cos^2\frac{\beta-\theta_0}{2}-\cos^2\frac{\beta-\theta}{2}}}.$$

Changing the variable θ into the new variable by the following equation

$$\cos\frac{\beta-\theta}{2}=\cos\frac{\beta-\theta_0}{2}\sin\varphi,$$

then

$$t=\sqrt{\frac{R^2+c^2}{4cg}}\int_{\theta_0}^{0}\frac{d\theta}{\sqrt{\cos^2\frac{\beta-\theta_0}{2}-\cos^2\frac{\beta-\theta}{2}}}$$

$$=\sqrt{\frac{R^2+c^2}{cg}}\int_{\frac{\pi}{2}}^{\varphi_0}\frac{d\varphi}{\sqrt{1-\cos^2\frac{\beta-\theta_0}{2}\sin^2\varphi}}$$

$$=\sqrt{\frac{R^2+c^2}{cg}}\int_{\frac{\pi}{2}}^{\varphi_0}\frac{d\phi}{\sqrt{1-k^2\sin^2\varphi}}, \quad \dots\dots\dots\dots\dots\dots(3)$$

where $k=\cos\left(\frac{\beta-\theta_0}{2}\right)$, and φ_0 is the value of φ correspond to $\theta=0$, that is,

$$\varphi_0=\sin^{-1}\left(\cos\frac{\beta}{2}\Big/\cos\frac{\beta-\theta_0}{2}\right).$$

As the integral expressed in (3) is the Elliptic Integral of the 1st kind, the value of t can be calculated by a mathematical table. The results of the calculations on five kinds of circular columns with the diameter of 30 mm, 12 mm, 6.5 mm, 5 mm, and 2 mm and with the same ratio of $d/h=4$ are shown in Fig. 14. As β is always 14° approximately for these circular columns, the period T become infinitive at $\beta=14°$.

On the other hand, as the value of α in West's formula which corresponds to the case of Fig. 12 is 980×1/4=245 gals, $ap^2=a(2\pi/T)^2=245$, where T is the period of the shaking-table. As the amplitude a is approximately 1.5 mm in our case, the value of T is calculated to be approximately 0.16 sec, which is also shown as a horizontal dotted line in Fig. 14.

This figure shows that the natural periods of the rocking motions of small-sized circular columns such as 5 mm and 2 mm in diameter come near to the period T of the vibration of the shaking-table, while those of the large-sized ones such as 12 mm and 30 mm in diameter deviate from it when about to overturn. As these columns do not overturned unless the rotating angle θ exceeds 14°, this fact may lead us to the conclusion that when the circular columns are about to overturn by external vibrations, the amplitude of the rocking motions of the small-sized columns are enhanced while those of the large ones are rather weakened or put out of order by the period of external vibrations.

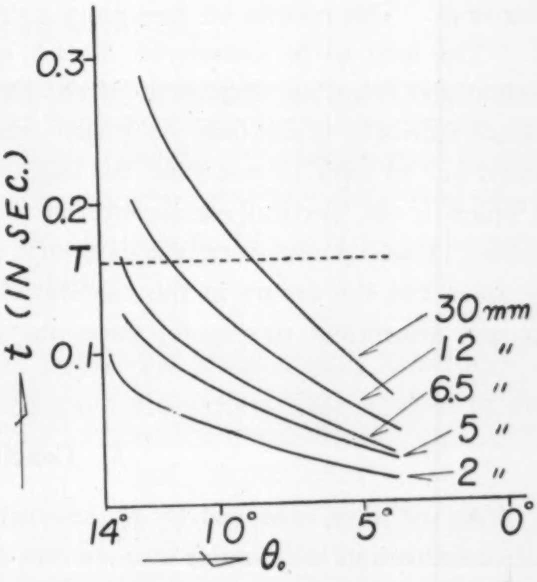

Fig. 14. The natural periods of the rocking motions.

The previousely reported phenomena that the circular columns become harder to be overturned by rapid maximum acceleration increase will also be explained from the same considerations as given above. That is to say, if the frequency of the external vibrations changes greatly before the center of gravity G of the column passes through the position G', the motion of the column which is about to be overturned is likely to be prevented.

Hitherto, the writer has investigated the phenomenon wherein the larger-sized circular columns do not overturn but only make rocking motions even when the maximum accelerations of external vibrations exceed the values of α. However, another phenomenon was also observed in the above experiments and remains to be discussed. That is to say, the mean values of frequency distribution curves were, at least when the diameter of the circular column d is smaller than the value of 4 a, all smaller than the value of α and moreover, this tendency is greater when the column's size become smaller compared with the amplitudes of external vibrations.

Considering the previousely reported results in this paper concerning the effect of the roughness of the plates upon the instability of the 5 mm's diameter columns against external vibrations, the writer presumes this same factor, that is, the roughness of the plate, to be the principal cause of the general tendency observed above. That is to say, the influence of these irregularities is larger upon the overturnings of the smaller-sized ones than upon that of the larger ones when external horizontal vibrations are applied. Of course, other causes may be given. The first to be considered is the minute inclinations of columns themselves and in the levels of plates. But, if these inclinations were the principal factor governing these phenomena, the influence must appear in the frequency distribution curves for the directions of overturnings. The results on this point were, however, negative.

The next to be considered is the errors in the maximum accelerations calculated from the displacement record of the shaking-table's vibrations. In other words, a doubt may be raised whether the actual values of accelerations are greater or not than the calculated ones owing to the existence of ripples or the vertical components in the vibrations of this horizontal shaking-table. These points were also examined recording them by acceleration seismographs, but the errors in the calculated values of accelerations were found to be too insufficient to explain these phenomena.

5. Conclusions.

As we have observed by the several results given hitherto, the phenomena of overturnings of circular clumns due to external vibrations are quite complicated even when the vibrations are purely sinsoidal and only horizontal. Of course, more important problems remain to be studied; for instance, what would become of our frequency distribution curves if we give vertical sinsoidal vibrations besides the horizontal ones, or raise maximum accelerations not by increasing the frequencies but by increasing the amplitudes or by increasing them both. These problems are certainly quite interesting and it is desired that they are studied not only from the seismological but from a purely physical point of view.

The former condition, adding vertical components to horizontal ones, will make the phenomena much more complicated. For, the phase relations between these two components must be a quite delicate factor for the overturning-phenomena of these circular columns even when these two components have both the same frequency. The latter condition is more similar to the feature of the vibrations due to actual earthquakes and the experiments under such conditions will yield undoubtedly some more interesting results for our present study. From this point of view, a shaking-table capable of being changed freely both in its frequency and amplitude of vibrations is quite desirable.

The present works, although they were restricted by the faculty of the shaking-table and should have been done more quantitatively with much more care to microscopic conditions, made clear, however, several factors which have great influence upon the overturnings of columns by external horizontal vibrations. It must be especially remarked here that the factors which govern the overturnings of the columns are not only a) the magnitude of the maximum acceleration of these external vibrations but there are two more important factors; that is, b) the amplitude of the external vibrations relative to the columns size and c) the rate of the change of frequencies, in another expression, the value of $\frac{d^3x}{dt^3}$ under a constant amplitude.

When we consider these circumstances, the separability of these circular columns as acceleration seismograghs in the case of actual earthquakes can not be easily anticipated from these experimental results. The writer thus intends to study these phenomena of overturnings statistically by comparing them with the acceleration seismographs in the after-shocks of any large earthquake which will eventually take place in the future.

In conclusion, the writer wishes to express his hearty thanks to Dr. K. Kanai who was so kind as to lend the writer his shaking-table for quite a long time, and to Mr. S. Miyamura who gave the writer many abvices in the course of these experiments.

---

23. 振動臺による圓柱の轉倒に關する實驗について

地震研究所　秋間哲夫

水平面上に垂直に立てられた柱狀物體の底面にある一定の加速度 α が與えられた時，その物體が滑らずに轉動し始める條件 $\alpha \geqq \frac{d}{h} g$ に基づいて，昔から大地震の際の各地の地震動の强さが墓石等の轉倒の觀察から近似的に推定されているが，果してこの式が，どの程度に實際の地震動による墓石等の轉倒に對してあてはまるかと云う點には，かなりの疑問がある．一方，若しもこの樣な柱狀物體の轉倒現象が，統計的にもせよ，相當の精度で地震動の强さの目安を與えうるものであるならば，同一の太さをもつた種々の長さの圓柱が，簡單な加速度計の役目を果たすことになる．そこで，このことを調べる目的で，手始めとして，太さ5mmの，いろいろの長さの圓柱を鋼鐵で作り，それをアルミニユーム製の臺に垂直に立てて，之等を振動臺でゆらせて何遍も繰返し轉倒させ，その時々の振動臺の最大加速度に對する轉倒回數の頻度分布を調べて見た．その結果，底面に加えられた振動による柱狀物體の轉倒と云う一つの物理現象には，實に種々の微視的な要素迄もが大きな影響を及ぼしていることが分つたが，その中で特に注目すべき點は，

1. 轉倒の頻度分布の山は，單に $\frac{d}{g} h$ だけではきまらず，他に
    a) 圓柱の太さと外部からの振動の振巾との比も關係すること．
    b) 加速度の時間的な變化の割合が關係すること．
2. 頻度分布曲線の確率誤差は數ガル程度であること．

等である．

勿論，以上の結果は，外部からの振動が單純な正弦波的の水平振動の場合であり，加速度のあげ方も，振動臺の機能上から，振巾は殆んど變化せずに振動數のみの極めて緩かな增加によつたと事う點を考慮せねばならず，從つて之等の結果をそのまま實際の地震動の際の圓柱の轉倒現象にまで適用させることは出來ないが，一つの物理現象の究明にはなつたと思われる．今後は，之等の圓柱を多數加速度計と同一場所に設置し，實際の地震動をうけた場合の轉倒につき，加速度計による地震動の强さと比較しつゝ統計的に調べてゆき度いと考えている．

24. *Vibration Tests of Defective Buildings.*

By Nobuji NASU,

Earthquake Research Institute.

(Read Sept. 19, 1950—Received Sept. 20, 1950.)

The principal purpose of this paper is to show the actual examples of buildings which have certain defects from the view point of earthquake-proof construction. As is well known, the fundamentals of satisfactory earthquake-proof design are symmetry of plan, mass and rigidity. If these conditions are not satisfied the house will not vibrate as a unit and the failure at the connexion of the parts of different characters will be the result. A defective footing is of course dangerous. The houses which are described in this paper were tested under a forced vibration which was caused by a vibrator. From the results of this test the behavior of the houses during an earthquake has been made clear. A brief note of the results will be given in the following.

(1) A reinforced concrete building of three stories which was reported1) to be considerably damaged in the Kwanto earthquake of 1923, was tested (Fig. 1). The vibrator and the seismographs were installed in the places as

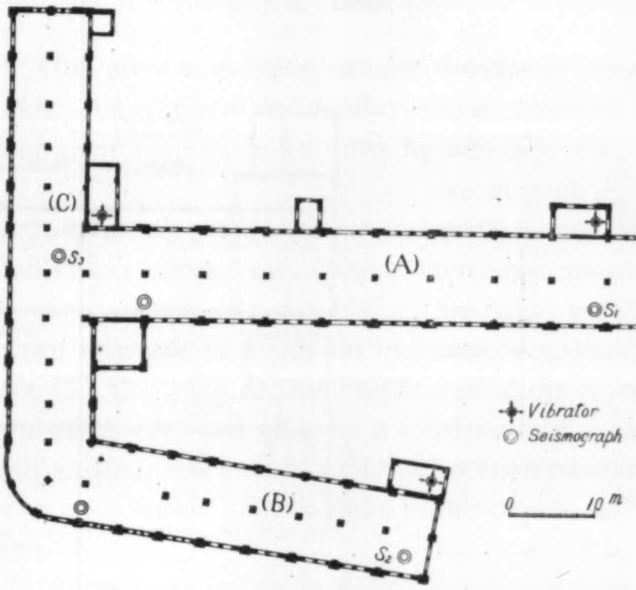

Fig. 1.

---

1) Yosiro NAGATA, *Report Earthq. Inv. Comm.*, II, No 100 C, 1926,

shown in this figure. In the transverse direction, three parts of the building (A), (B) and (C) showed a resonance with different periods, that is, 0.41 sec. at S_1, 0.39 sec. at S_2 and 0.26 sec. at S_3. In the longitudinal direction, 0.16 sec., 0.30 sec. and 0.22 sec, were the resonance-periods on these points respectively. Thus, we see that the three parts of this building have periods different from each other. The deflections in the transverse and the longitudinal diretions are shown in Fig. 2. A noteworthy fact is that the deflection of Part-(B) is particularly large as compared with those of (A) and (C), especially in the transverse direction. The curve in this case is similar to that of the column hinged at the base. This indicates that some of the columns in part-(B) are defective. Actually, the failure of the columns near the end of (B) was found after the 1923 earthquake and these damaged columns were repaired, but this repair-work is not effective at present. For these columns further improvements are being made so as to increase the area of the cross-section and joint the separate footings so as to form of a continuous footing.

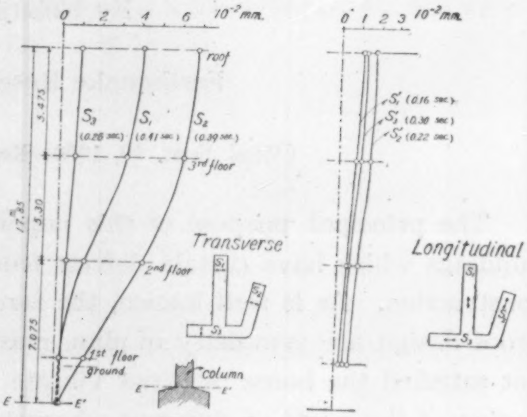

Fig. 2. Deflection.

(2) A reinforced two-storeyed building (Fig. 3) which was burnt by fire in 1923 and 1945 was tested. Although the columns and walls on the second floor have been temporarily repaired for the present, they are not strong enough to resist a violent shock, because large crack are still seen in them. Moreover, no repair-work has been done on the first storey. The plan of this building and the stiffness is not symmetrical; perhaps less stiffer in the middle and strongest near the water tank. The building will rotate about an axis lying near this strongest

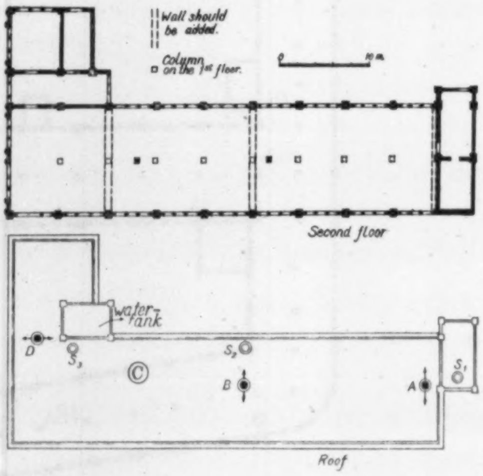

Fig. 3.

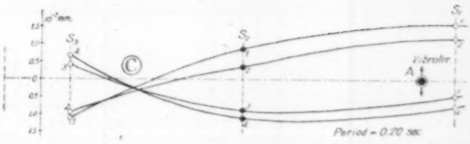

Fig. 4.

point. This motion is actually seen by the vibration test as shown in Fig. 4. The period in this case was 0.20 sec. Curves-1,-2,-3 and -4 show the rotation determined by the simultaneous observations at S_1, S_2 and S_3.

When this building was shaken at B by the vibrator in the transverse direction, a resonance occurred with a period of 0.37 sec. The largest amplitude was naturelly in the middle of the roof of the building. As in the previous example, the deflection curves, in Fig. 5 was similar to that of the column with a hinged end. This gives a warning against the danger of collapsing in case of an earthquake. All columns and walls must be repaired and at least three partition-walls of reinforced concrete must be added in the positions as shown in Fig. 3.

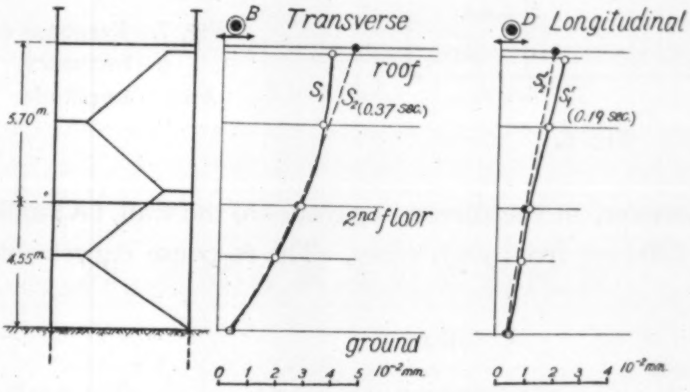

Fig. 5. Deflections.

In the longitudinal direction, the natural period was 0.19 sec. From the longitudinal deflections alone, the failure of the column is hardly to be detected.

(3) The third example is a wooden building of two stories which was recently completed. The plan of this building (Fig. 6) is rectangular, being divided into two parts, (A) and (B), by a reinforced concrete wall. In (A) no partition wall existed, whereas in (B) there were several partitions and the sizes of the room were small. Hence there must be some unbalance of stiffness betweed (A) and (B).

When the building was shaken in a direction perpendicualr to the concrete wall, all parts of the second floor moved as a unit. This proves that the wall is effective for the vibration normal to the wall. The response curve is shown

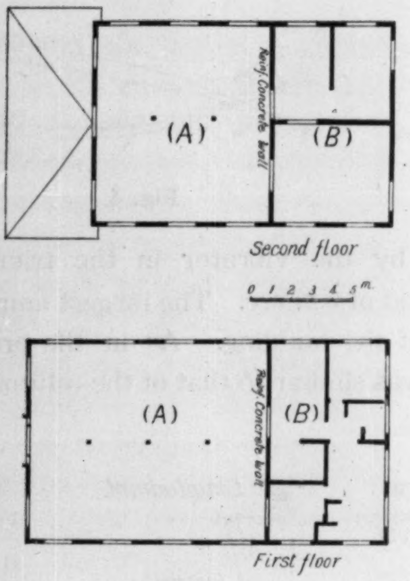

Fig. 6.

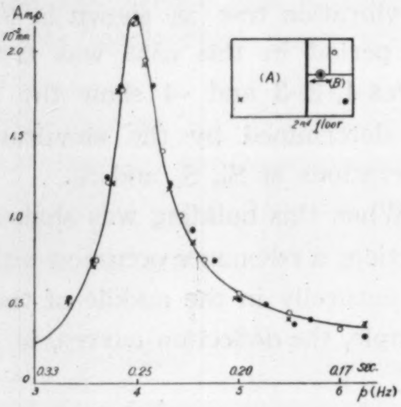

Fig. 7. Response curve,
p = frequency,
Amp. = amplitude.

in Fig. 7. However, in the direction parallel to the wall, (A) and (B) vibrated with periods different from each other. The response curves obtained (Fig. 8, left for (A), right for (B)) are not simple in this case, because of the relative motion of (A) and (B). This will cause the failure of the parts near the concrete wall when the shock becomes large. Further, the motion of (A) is restricted on one side by this wall and the amplitude is always larger at the other end than near the wall like a cantilever. A comparison showed that on the second floor the ratio of the amplitudes at 8 m. and 1 m. from the wall was 4.0 : 1. Fig. 9 shows the resonance curve at 1 m. In this case, the vibrator was installed in (A). Thus, the left end of this building vibrates with a larger amplitude than any other parts, and the end must be supported obliquely by

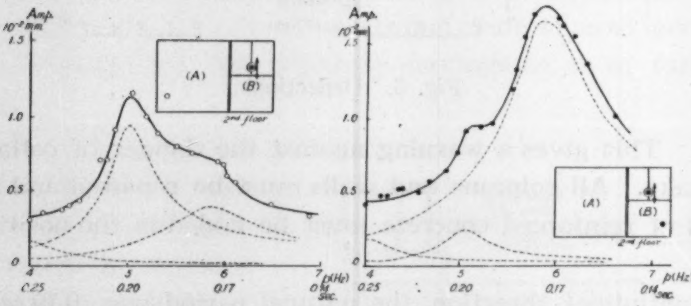

Fig. 8. Response curves of (A) (left) and (B) (right).

stays extending from the roof down to the ground.

Further, the ends of the beams of (A) and (B) should be jointed rigidly, for example, by means of metal-ties and bolts.

The study is continued also on structures outside of building through the Fund for the Science Research of the Ministry of Education for the year 1950.

I wish to express my sincere thanks to Prof. T. Naito of the Waseda University for his kind advice and guidance.

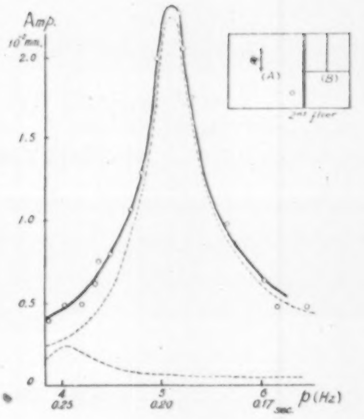

Fig. 9. Response curve of (A).

24. 非健全家屋の振動試驗

地震研究所　那須信治

火災のため相當ひどく破損したコンクリート建物及び新築の木造ではあるが，構造上缺點があると思われる建物の振動測定結果から補强對策の一例を述べた．

[illegible] Study of [illegible] Buildings [illegible]

[illegible] the [illegible]

[illegible]

[illegible] of [illegible]

[illegible]

The study is [illegible] of building [illegible] the [illegible] of the [illegible] for the year [illegible]

I wish to express my sincere thanks to [illegible] of the [illegible] for his kind advice and guidance.

[illegible]

[illegible]

[illegible]

[illegible]

25. *The Imaichi Earthquake of December 26th, 1949. General Description.*

By Hirosi KAWASUMI.

Earthquake Research Institute.

(Read Jan. 17, 1950.—Received Dec. 20, 1950.)

Introduction.

On the 26th of December 1949 about daybreak, at 6 h. 44 m. in the morning, most people in the Kwantō Plain were awakened from their sleep by a moderate earthquake originated in the south-western part of the Ibaraki Prefecture. Heralded however, by this non-destructive earthquake, severer shocks alarmed the district as well as the adjacent districts in less than two hours, at 8 h. 16 m. and 8 h. 25 m. respectively, the epicentral tracts of them being situated about 70 km. north-west of the first, near the northern border of the Kwantō Plain. Collapse of 299 dwelling houses and tremendous landslides took place taking a toll of 10 human lives and interrupting communication and railway lines in the neighbourhood of Imaichi Town, Tochigi Prefecture, which lies at 7 km. E. S. E. of the famous religious Town of Nikko.

As soon as the details of the earthquake were known, the Earthquake Research Institute organized a research party which started on the next morning for the disaster area. The party consisted of members who shared the work of inspections of general affairs, engineering aspects, geology, topographical and ground water changes and observations of aftershocks etc. respectively.

For these studies of our Institute, the Ministry of Education granted a sum of 100,000 yen from the Science Research Fund, by which our work was greatly promoted. Our thanks to the Ministry are hereby expressed gratefully. We must also mention with thanks the aids given by the official circles of the Prefectural Government and the inhabitants of the afflicted area, by which our work was much facilitated. Observational data at the Meteorological stations were also used, to which our thanks are also due.

Summarizing the results of these and other studies, general features of the present earthquake are described in the following.

Topography and Geology of the Epicentral Area.[1]

The present disaster area lies near the eastern margin of the Ashio mountain land, where the Chichibu (Permo-Carboniferous) system constitutes the back bone with many intrusions of biotite granite, granite-porphiry and quartz-porphiry. These paleozoic formations outcrop mainly in the southern part of the river Daiya which flows from the lake Chūzenji through the towns of Nikko and Imaichi and joins the river Kinu, a tributary of the Tone, at about 7 km. NE of Imaichi. Some remnants of the Tertiary volcanic activity such as green tuffs and some andesites are also seen in the south-eastern side of the district.

Around these hills develop fluviatile beds, consisting of rounded gravels of andesitic rocks cemented by fine volcanic materials. These fluviatile beds are covered by younger deposits of pumice and other volcanic ejecta, derived from a group of Diluvial volcanoes called the "Nikko Volcanic Group", which stand to the north of the lake Chūzenji and the Daiya River on the basement of the eroded older complex as we have seen in the southern area. Of the nine volcanoes, (1) Gassan (1,278 m), (2) Nyohō-Akanagi (2464 m), (3) Komanago (2,323 m), (4) Ōmanago (2,375 m), (5) Nantai (2484 m), (6) Tarō (2,368 m), (7) Sannōbōshi (2,073 m), (8) Mitsudake (1945 m), and (9) Shirane (2,578 m), the last and highest Shirane alone is known to have been active in historic times, the eruptions of which being recorded in 1625, 1649, 1872, 1873 and 1889. Among the rest extinct volcanoes, the Nantai, a beautiful conide standing by the side of the lake Chūzenji, was active to latest times and its ejecta are broadly deposited over the present district. The Shirane and the Nantai are respectively distant about 30 and 18 km. in the W by N direction from the Imaichi Town. These volcanoes together with the Akagi and Haruna in the SW and the Takahara, Nasu, Bandai, Azuma and Zaō etc. in the NE constitute the Nasu Volcanic Zone which extends as far north as to the Usu volcano in Hokkaidō. The readers are referred to the description of the topography and geology of the present area by R. Morimoto in the next article.

Seismic History.[2]

The earthquakes of these districts are recorded for 500 years almost perfectly in the diaries of the Buddhist temple Tōdera in the adjacent Aizu district and the Tōshōgu shrine at Nikko, as well as in the chronicles of the feudal government in Yedo. In the following table are tabulated remarkable shocks originating within a hundred km. together with those earthquakes in the adjacent area which were felt strongly and accompanied by some damage in the Nikko area.

---

[1] S. TSUBOI, & SUGI; Guide Book for the Excursion 1926.

[2] Table of Great Earthquakes in Japan since Historic Times, published by the Association for the Prevension of Earthquake Disasters.

F. OMORI. (*Rep. Imp. Earthq. Inv. Comm.*) 88 (C). (1920). 42.

Table I.

Historical Earthquakes Arround the Nikko Area.

1. 1433 XI 7 (Eikyō 5 IX 16) $M_k=3$.
   The Tōdera Hachiman shrine in the Aizu district was demolished. On the same day a great earthquake took place in Sagami Bay which caused demolition of temples and shrines at Kamakura and Ōyama, Sagami Province. It was accompanied by a tunami by which the river water of the Tone, then flowing into the Tokyo Bay, was compelled to flow upward.
2. 1555 IX 14 (Kōzi 1 VIII 19) $M_k=3$.
   Landslides and demolition of houses were caused in the lower reach of the river Tadami around Takidani village.
3. 1611 IX 27 (Keichō 16 VIII 21) $M_k=4$.
   Strongest earthquake ever recorded in the Aidzu district, by which most part of the district, about 50 km. in diameter, were badly shaken with heavy landslides and depression forming a lake which lasted about 30 years. About 20,000 houses were destroyed and more than 3,700 lives were lost.
4. 1644 IV (Shōho 1 III-) $M_k=2$.
   Stone walls of the Tōshōgu shrine were slightly destroyed.
5. 1646 VI 9 (Shōho 3 IV 26) $M_k=5$.
   An earthquake originated off the Pacific coast of the Rikuzen, which caused destruction of the castle in Sendai. Stone fences and walls were also damaged at Nikko.
6. 1649 VII 29 (Keian 2 VI 20) $M_k=4$.
   There was a severe earthguake in Yedo and it destroyed the stone walls and gates of the castle. Many houses in the city were destroyed causing loss of human lives. It was also strongly felt at Nikko and caused damage to stone walls etc.. Probably the epicentre was some 40 km north of Yedo. The volcano Shirane erupted in this year.
7. 1658 V 5 (Manji 1 IV 3) $M_k=2$.
   A slight damage was caused at Nikko.
8. 1659 IV 21 (Manji 2 II 30) $M_k=3$.
   309 houses collapsed with loss of 28 human lives in the Aizu district.

More than 100 houses were also destroyed at Nasu in Shimotsuke Province causing loss of 11 lives.

9. 1683 V 1 (Tenna 3 IV 5) $M_k=2$.

Fissures in the ground and some landslides were observed around Nikko.

10. 1683 VI 17 (Tenna 3 V 23) $M_k=3$.

The district around Nikko became seismically very active since the 11th of the month and on this day a strong shock occurred in the northern vicinity, accompanied by heavy landslides on the slope of the Volcano Akanagi. Stone walls and stone towers in the Tōshōgu shrine were badly destroyed.

11. 1683 VI 18 (Tenna 3 V 24) $M_k=4$.

A stronger shock than that of the previous day occurred in the same district causing more damage to the shrine so that the shrine had to be almost rebuilt. Dwelling houses at Nikko were badly shaken down while the shock was strong enough at Yedo to damage some houses within the castle.

12. 1683 X 20 (Tenna 3 IX 1) $M_k=3$.

The epicentre of this shock was about 20 km north of Nikko in the uppermost part of the river Kinu. Heavy landslides blocked the course of the rivers Kinu and the Inari, a tributary of the Daiya river which joins at Nikko. The Tōshōgū shrine which had hardly completed repairing was again damaged.

13. 1693 II 26 (Genroku 6 I 22) $M_k=2$.

The Tōshōgu shrine was slightly damaged.

14. 1703 XII 31 (Genroku 16 XI 23) $M_k=6.6$.

The great Kwantō earthquake which exceeded the 1923 earthquake in magnitude. The earthquake was only moderate at Nikko, and only the doors of the Tōshōgu shrine were shaken open, and some stone lanterns were overturned.

15. 1710 IX 13 (Hōei 7 VIII 20) $M_k=3$.

Some destruction of houses are recorded in the Aizu district, but details are lacking.

16. 1725 V 29 (Kyōho 10 IV 18) $M_k=3$.

Some stone lanterns and stone fences were overturned at Nikko.

17. 1735 IV 6 (Kyōho 20 III 14) $M_k=2$.

Only a small portion of stone walls at the Tōshōgu shrine were destroyed.

18. 1746 V 14 (Enkyō 3 III 24) $M_k=4$.

Some houses in Yedo were damaged, while at Nikko stone fences were overturned slightly. The hypocentre might have been nearer to Yedo with a depth of about 50 km.

19. 1755 IV 21 (Hōreki 5 III 10) $M_k=2$.
Three strong shocks took place at Nikko, and stone fences and stairs were badly shaken, and some stone and bronze lanterns were overturned, but buildings suffered little damage.
(The chronicles and diaries of Nikko after the year 1762 have not yet been published so that some moderate shocks which might have occurred since remain unknown. But it is certain that no severe earthquakes have originated there until the 1949 earthquake.)
20. 1821 XII 13 (Bunsei 4 XI 19) $M_k=2$.
A small local destructive shock afflicted the villages around the lake Numasawa. 130 houses were demolished and some human lives were lost. Heavy landslides and numerous aftershocks terrified all the people to leave their hamlets.
21. 1855 XI 11 (Ansei 2 X 2) $M_k=4$.
Demolition of 14346 houses and loss of 7000 human lives and great conflagration were caused in the city of Yedo. The epicentre was in the suburb NE of the City.
22. 1859 III (Ansei 6 II) $M_k=2$.
Castle at Iwatsuki in Musashi Province was damaged.
23. 1894 VI 20 (Meiji 27) $M_k=5$.
It originated in the north-eastern part of Musashi Province. 90 houses were levelled to the ground and 24 lives were lost.
24. 1923 IX 1 (Taishō 12) $M_k=6$.
The great Kwantō earthquake. It was accompanied with subversion of 128,266 houses and loss of 142,807 lives. Great conflagrations and tunami followed by which 447,128 houses were burnt and 868 washed away. In the present disaster area this earthquake was felt somewhat strongly, but no material damage was caused.
25. 1943 VIII 12 (Shōwa 18) $M_k=2$.
Landslides occurred and were accompanied by slight damage to the walls of houses around the town of Tazima, in Aizu district.

From the above table we see that the earthquakes which seem to have originated within the present area were Nos. 4 (1644), 7 (1658), 9, 10, 11 (1683), 13 (1693), 16 (1725), 17 (1735), and 19 (1755), of which only the earthquakes of 1683 and 1755 were strong enough to cause some damage to wooden buildings. F. Omori[3] pointed out in 1920 that those earthquakes originating in the Nikko region are volcanic in origin so that we have no need of expecting severer shocks than those of 1683 and 1755. This anticipation proved true so far as the present earthquake is concerned, although the hypothesis of the volcanic origin still remains destitute of crucial testimony. To this point we shall return later.

---

[3] F. OMORI: *loc. cit.*

Seismometrical features.

The epicentres of the first and second shocks were determined by Y. Koshikawa[4] from the arrival times of various phases by means of the least square method. The results were

1st shock

$\varphi=36°41.1\,\mathrm{N}$, $\lambda=139°39.9\,\mathrm{E}$; from $\bar{S}$,

2nd shock

$\varphi=36°43.6\,\mathrm{N}$, $\lambda=139°38.8\,\mathrm{E}$; from $\bar{P}$.

The values determined from P^* for the first shock were 1′ larger in longitude and latitude, while those for the second shock as determined from P^* were 0′.1 larger in latitude and 1′.1 larger in longitude than those determined from $\bar{P}$. At any rate the positions thus determined from time observations at remote stations are remarkably concordant with the macroseismic observations as described in the following. They also coincide with the area in which aftershocks originated as revealed from observations at near stations set up temporalily by our Institute.

The hypocentral depths of these shocks could not be determined by Koshikawa definitely, but was estimated tentatively by him to be about 15 km. for the first shock and 10 km. for the second one. The times of occurrences of these shocks worked out by Koshikawa were 8 h 17 m 29.1 s and 8 h 24 m 51.9 s on the 26 th day, in Japanese Civil Time or 23 h 17 m 29.1 s and 23 h 24 m 51.9 s on the 25 th day in G. M. T. respectively.

The first impulsions as observed at meteorological stations around the epicentres were rarefactional i. e. directed to the epicentre except at remote northern stations in both earthquakes. The distribution may be explained by the mechanism of conical type, in which the wave of condensational front is radiated within the cone surface. According to Hagiwara and Kasahara[5] the axis of the cone was inclined 30° southward and the apical angle was about 140°.

Foreshocks and aftershocks.

According to the naratives of the inhabitants in the afflicted area, they had heard sounds like explosions in mines occasionally since about five months, and at Nakai Hamlet, Ochiai Village it is said that they heard the same sounds two times at about 20 h. in the previous day and a sound in the morning of the calamitous day. These sounds were similar to the earthquake sounds which accompanied infallibly the aftershocks. It is therefore presumable that foreshocks had already existed for a few months.

---

[4] Y. KOSHIKAWA, *Bull. Earthq. Res. Inst.*, 28 (1925), 369.

[5] T. HAGIWARA and K. KASAHARA, *Bull. Earthq. Res. Inst.*, 28 (1950), 393.

Aftershocks were observed at temporal seismic stations, set up by our Institute[6] at Imaichi, Nikko, Kanuma, Funyū and Nishiōashi and later at Nagahata as well. The epicentres thus worked out cluster around the Keimei mountain situated at 6 km. S. W. of Imaichi Town within an area of about 100 sq. km. The hypocentres of these aftershocks were also confined to depths less than 10 km. The number of the earthquakes felt at the Utsunomiya Meteorological Station at about 24 km. from the epicentral tract declined regularly as shown in Fig. 1. Needless to say, the number at nearer points was much larger. We felt at Nikko 34 earthquakes in less than 14 hours from 19 h. on the 27 th to 9 h. on the next morning.

Moichirō Fukuda at Nagahata Taziri Hamlet of the Ochiai Village, the very centre of the epicentral tract, observed the aftershocks without aid of instrument since the 3rd of January and recorded 283 earthquakes in January, 182 in February, 80 in March, 41 in April, 26 in May, 16 in June, 4 in July and 14 in August. Even the above mentioned number amounts in the total to as much as 646, and if supplemented with those which occurred 8 days prior to the beginning of his observation, the total number in 2/3 year might have reached 1000. Compared with the total number 652 of felt aftershocks of the Fukui earthquake[7] in one ensuing year, the higher frequency of aftershocks of the present earthquake may be noteworthy.

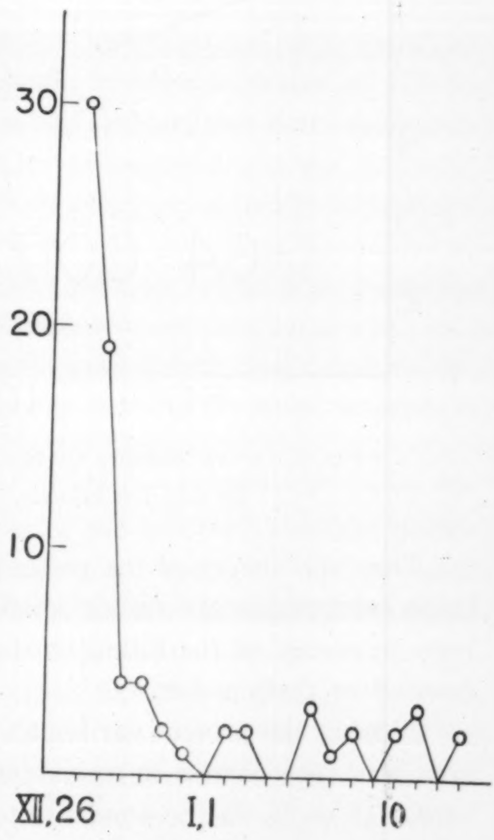

Fig. 1. Daily number of aftershocks felt at Utsunomiya of the Imaichi Earthquake, 1949.

---

6) *Earthq. Res. Inst. Bull. Earthq. Res. Inst.*, 28 (1950), 471.
7) S. OMOTE, *Rep. of Fukui Earthq.* (1950), 37.

Macroseismic features.

The intensity of these shocks as observed at the meteorological stations indicate that the magnitudes (M_k) in the writer's scale of the first and second shocks were about 2.8 and 3.2 respectively, while the mean intensity-distance curve deduced by the writer and Y. Satō from the replies gathered by the postcard method for the second larger shock was

$$I' = 6.4 - 0.0178\,\Delta \qquad (\Delta \text{ in km}),$$

where: I' is the intensity in the international scale in 12 degrees. (Fig. 2).

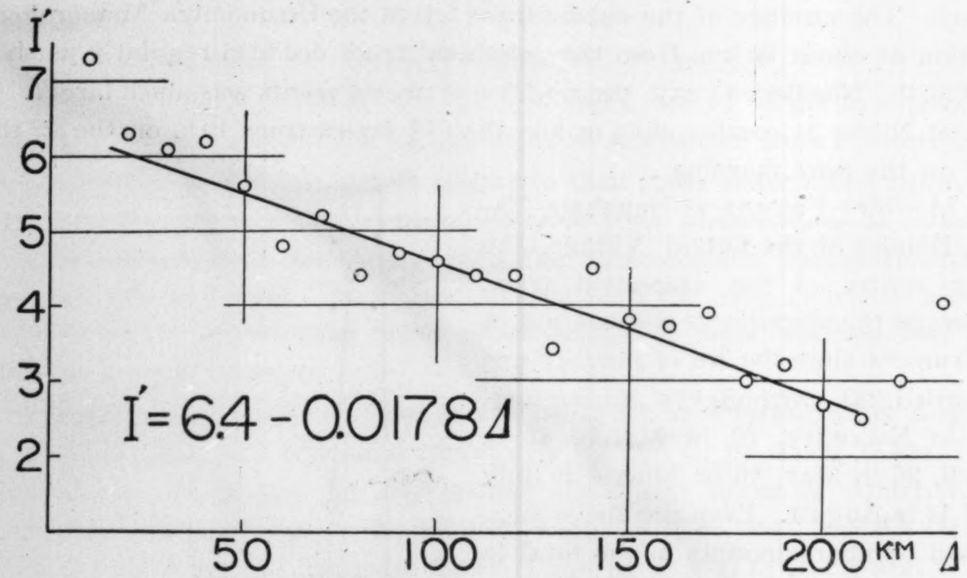

Fig. 2. Mean intensity-distance curve in the international scale of the Imaichi Earthquake. (After Kawasumi and Satō.)

Thus the energy of the present shocks as compared with the previous large earthquakes are rather small. They were about 1/100 and 1/30 respectively in energy of the Fukui earthquake of 1948, which ranked low among the destructive earthquakes.

Althoug the present earthquake was small in magnitude and the disaster area was very narrow in consequence, the intensity in the epicentral area was very high owing to the proximity to or shallowness of the hypocentre. A mine owner's wife residing at Nakai Hamlet, Ochiai Village, the very centre of the epicentral tract, observed that a stone implement, called "ishiusu" (Fig. 9 a Pl. XIII) in Japanese, which was about 50 cm. in diametre, and placed before her house, was tossed upward about 20 cm. a few times like a rebounding rubber ball. The shock, being accompanied by a very loud detonation, at this place was confined to vertical motion so that even objects upon the shelves did not fall at all. Therfore, she as well as her husband did not believe it to be an earthquake and went to her neighbour's to ask whether it was not the result of a bombardment or an explosion. It seems in itself wonderful that the house suffered no damage and tomb stones near by (Fig. 9 b) remained standing in the very centre of the epicentral tract, while the subversions of tombs at more distant places (Fig. 9 c) were as severe as in the epicentral tract of the Fukui earthquake[8] where acceleration of more than 0.6 times of gravity was observed. The writer was also informed that iron kettles were thrown off from hooks by which they were hung on fireplaces from the ceilings at Imaichi Town and Itabashi Hamlet in Ochiai Village. Moreover, it is said that at Shitone Hamlet in Toyooka Village a kettle placed on the ground was also overturned by the earthquake motion. These phenomena may be evidences of the fact that the acceleration of the earthquake motion in the epicentral tract was as large as that of gravity.

It is, therefore, no wonder that the fissures in the ground and landslides in the mountainous region within the disaster area were so severe as will be seen in the map to be presented by the writer and R. Morimoto in the following. But the writer, who had learned the landslides accompanied with the Calabrian earthquake of 1783 from Lyell's Principle of Geology, could really understand the severity of the landslides in Italy when he saw the large landslides at places where the slopes before the earthquake were as low as 7 or 8 degrees in the present earthquake district. (See Figs. 6, 7 & 8.)

The landslides in the present disaster area were greatly facilitated, on the other hand, by the existence of a very slippery stratum of much weathered white pumice which was ejected from the Nantai Volcano.

It was also found out that the strata of about 6 m in thickness above the slippery pumice layer which formed the base of the Imaichi Town slid bodily about 6 cm. eastward relative to the substratum. The fact was revealed from the discontinuity of the vertical walls of the wells throughout the town. The ground surface in the town was inclined only about 1 degree eastward from the horizon. Although such a phenomenon like this might have been of rare occurrence, the fact itself has an important bearing to the geodesy as well as the geophysics in the interpretation of crustal deformations.

It is also to be remarked that even in the southern part of the epicentre where the slipperry pumice layer was lacking, the landslides were also conspicuous at steep mountain sides, and at many places they turned into mud avalanches and destroyed houses and buried several persons to death at several places. Indeed, most of lives lost and missing in the present earthquake were the result of these landslides. (cf. Figs. 7, 8.)

---

[8] H. KAWASUMI, *Rep. of Fukui Earthq.* (1950). 24.

Another fact to be mentioned on the landslides is that, almost none have occured on the northern side of the Daiya River, making marked contrast to the case of the 1683 earthquakes.

Damage and Casualties.

As has been stated already, the acceleration of the present earthquake was exceedingly large in the central part of the present disaster area, which, instead, was comparatively narrow owing to the smallness of the magnitude and the hypocentral depth. However, it is a wonderful fact that wooden dwelling houses in the meizoseismic area were but slightly ruined and levelled to the ground, although the joints of pillars and beams etc. were badly broken. But it is no wonder that the stone and brick buildings and stone plates which were nailed to the outside of wooden store house were almost completely shaken down in most part of the disaster area. The apparently slight damage of wooden dwelling houses were probably due to the smallness of duration and period of the principal part of the earthquake motion.

The statistics, prepared by the state police, of the damage and casualties are tabulated in Table 2.

The distribution of the number of totally collapsed houses, as shown in Fig. 3. is in accordance with the positions of epicentres instrumentally determined.

The principal damage done to the government railway line was between the stations Fubasami and Imaichi while that done to the Tōbu company line was between Shimokoziro and Kami-Imaichi. The main damage was subsidence, fissuring and slumpage of railroad embankments. The approaches of bridges also suffered subsidence and some abutments of them were sheared off and displaced. Some cars between the above intervals were derailed.

A word on the damage at Nikko may also be added for the sake of comparison with those of historical earthquakes. According to the authorities of the Tōshōgu and Futarasan shrines and the Rinnōji temple, the stone walls (520 sq. m.), stone fences (550 m.) and 2 stone stairs were badly shaken or shattered and 40 stone or bronze lanterns (tōrōs) were overturned, while the buildings in the shrines and the temple were scarcely damaged, although masonry buildings in the Town was badly shaken. It is also to be remarked that at the copper refinary plant at Kiyotaki, about 5 km. SW of Nikko, a brick chimney was broken down and a concrete chimney cracked badly.

Thus the damage due to the present earthquake at Nikko is lighter than

Table 2. Statistics of the damage and casualties caused by the Imaichi Earthquake of Dec. 26, 1949.

Locality	Casualties				Dwelling houses			Not-dwelling houses			Rice paddies		Dry field		Forest		Road damaged	Bridges destroyed	Houses afflicted	Men afflicted
	Dead	Missing	Wounded Heavily	Wounded Lightly	Totally collapsed	Half destroyed	Slightly damaged	Totally collapsed	Half destroyed	Slightly damaged	Buried	Fissured	Buried	Fissured & slid	Buried	Slid down				
1. Imaichi Town	5		1	158	228	2820	496	303	713	146	5.15 h.a.		6.3 h.a.		30 h.a.		22	3	3606	14436
2. Ōsawa Village		1			1	9	134	58	163	212							3		377	1156
3. Ochiai V.	1				49	49		137	52	47			0.1		20		3		236	944
4. Nikkō Town		1			6	22	66	2	13	4						20 h.a.	10		93	358
5. Itaga Village						2	200	9	49	250	0.4	1 h.a.	0.6			50	10	3	260	1184
6. Sinoi V.						1	13	7	65										65	324
7. Toyooka V.						62	750	82	1200	2200							3	4	812	2450
8. Okurugawa V.					4	6		1	25	100		0.2	0.1				12	1	84	382
9. Higasiōasi V.					2	8		10	16								1		36	148
10. Nisiōasi V.	1					13											7	1	14	56
11. Kaso V.								5	8								3	1	13	48
12. Funyū V.	1		1	3			1	3	2	20									30	123
13. Ōmiya V.						2													2	13
14. Kikuzawa V.								1	1										2	11
Total	8	2	2	161	290	2994	1660	618	2307	2979	5.55 h.a.	1.2 h.a.	7.1 h.a.		50 h.a.	50 h.a.	74	13	5630	21633

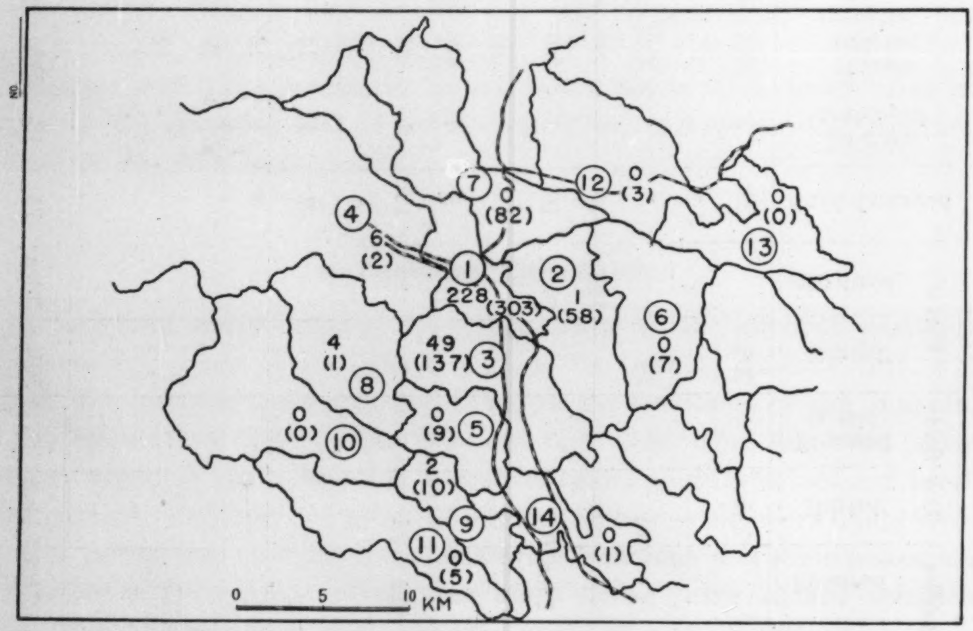

Fig. 3. Distribution of totally collapsed dwelling houses. The numbers in the brackets are those of not-dwelling houses. The number within the circle denote the locality in the Table 2.

in the case of 1683 earthquakes. This difference is due to the larger magnitude and to the proximity of the epicentres of the 1683 earthquakes, which might have occurred in the northern vicinity of Nikko. The 1755 earthquake was almost equal in intensity at Nikko, while the other shocks were inferior as compared with the present earthquake. At any rate the present earthquake is the strongest earthquake in the Nikko area in 194 years.

Summary and Remarks.

The Imaichi earthquake of Dec. 26, 1949 was the severest earthquake felt in the Nikko area in last 194 years. It originated in the southern vicinity, within several km. of the Imaichi Town. The hypocentral depth might have been under 20 km. The principal shock was preceeded 7 min. by a severe shock. The energy of the principal shock was estimated to be 10^{21} ergs, while that of the first shock was about 1/3 of the latter one.

Numerous aftershocks followed, but they decreased regularly. One aftershock at 17 h. 54 m. on the 27 th was so severe as to do slight damage again to the railway line.

Maximum intensity within the epicentral tract was so great as to exceed the acceleration due to gravity. Landslides were conspicuous in consequence, and the foundation of about 6 m. in thickness of the Imaichi town, which in-

Fig. 4. Damage of houses at Imaichi Town.

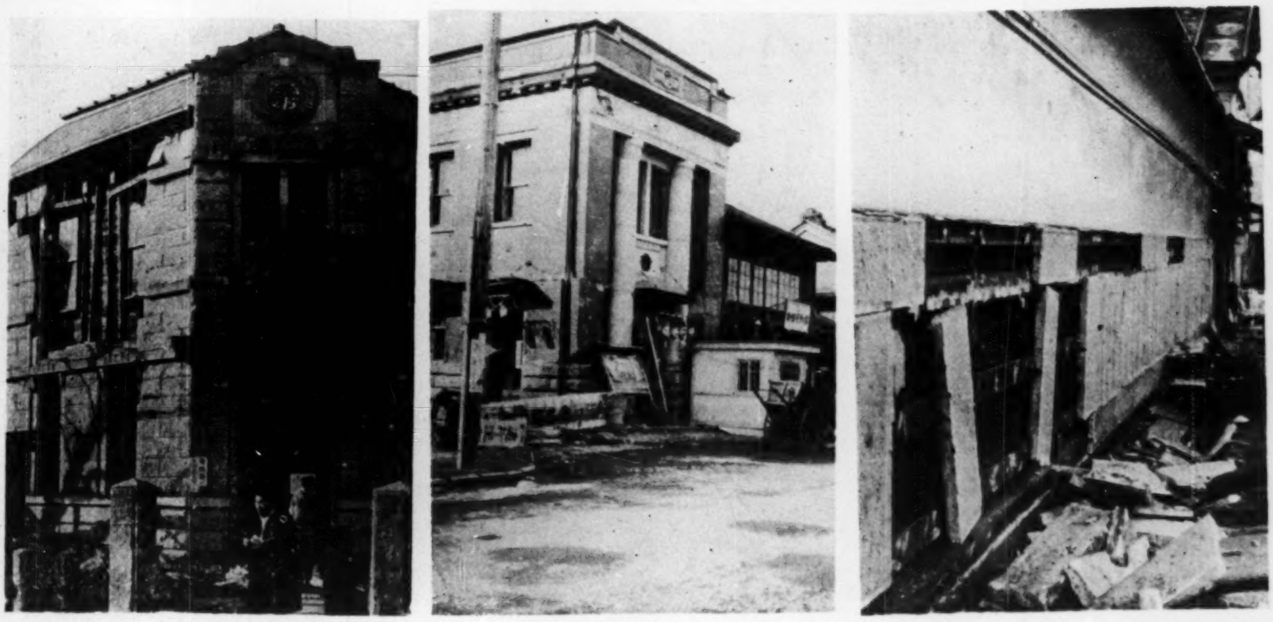

a. Town office. b. Police station. c. Wall of storehouse.

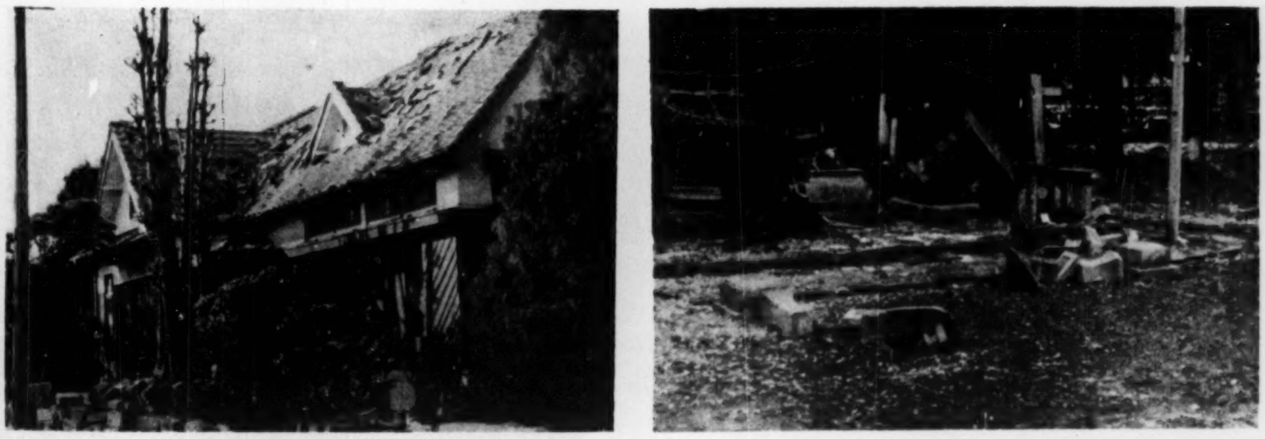

d. Wooden dwelling house. e. Subversion of smaller constructions at the Takinowo Shrine.

（震研彙報　第二十八號　圖版　河角）

Fig. 5. Effect of Earthquake at Nikko. Wooden buildings suffered almost no damage.

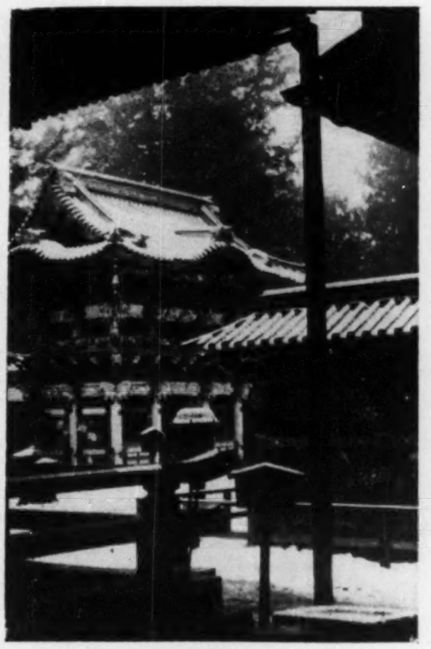

a. The Yōmeimon (gate).

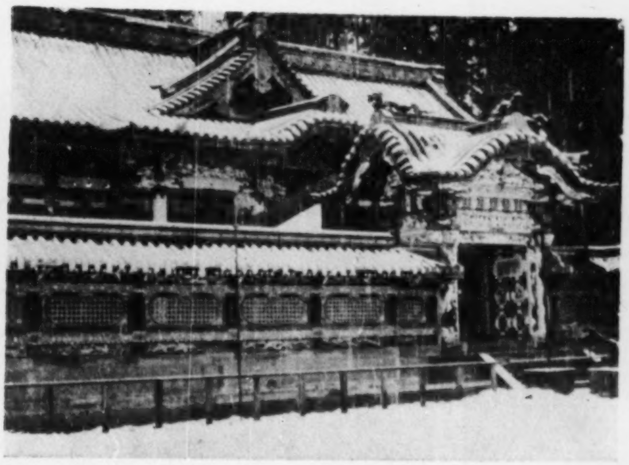

b. The Shrine and Kara-mon.

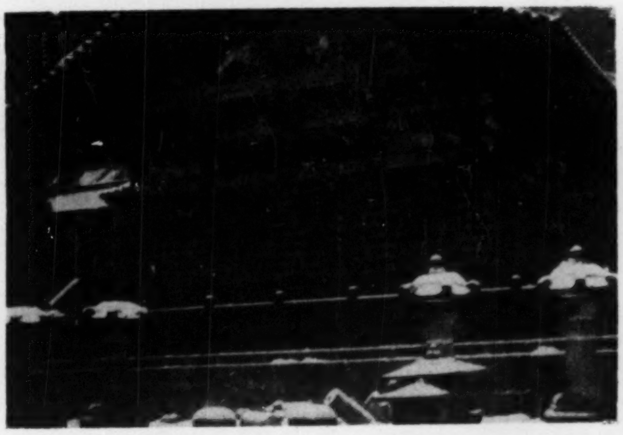

c. A few stone-lanterns in the foreground were overturned

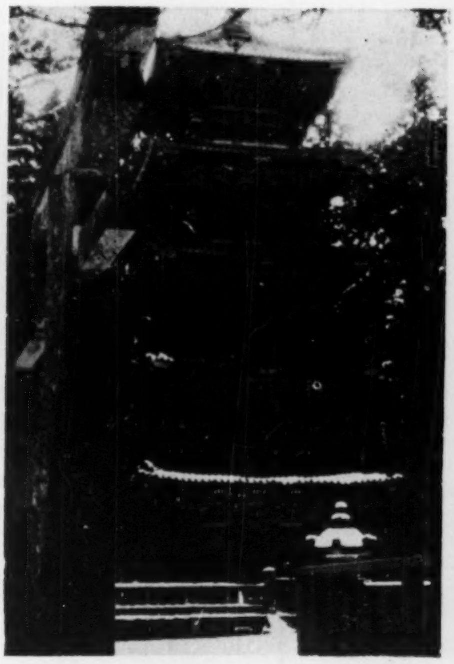

d. The pagoda suffered no damage. The upper part of *torii* (above the crack) was twisted a few cm.

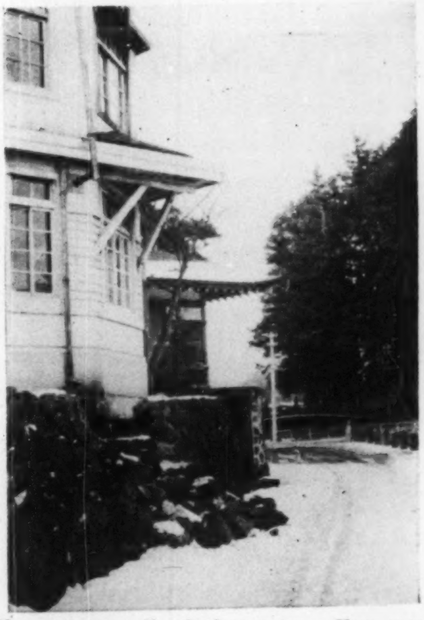

e. The stone wall of the town office was destroyed very slightly.

（震研彙報 第二十八號 圖版 河角）

Fig. 6.

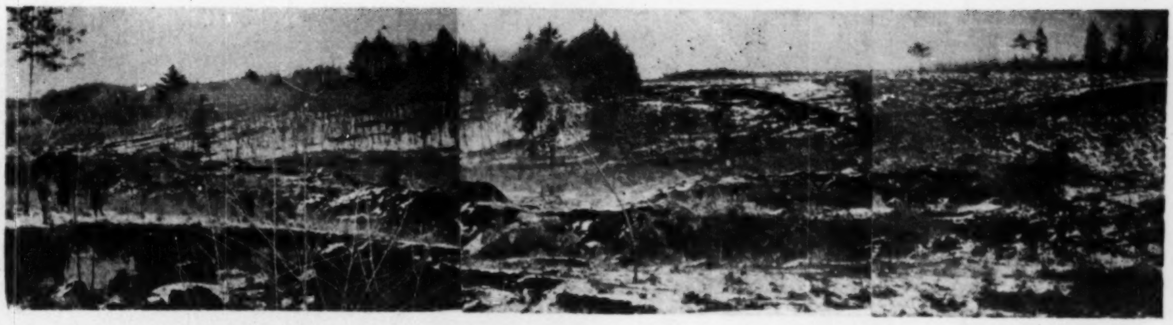

a. Low angle landslide at Tsuchizawa, Imaichi Town. Land before the brack fissure in the central part slid bodily with forrest almost undisturbed. The ridge in the foreground is the result of upthrust at the margin of the slid land.

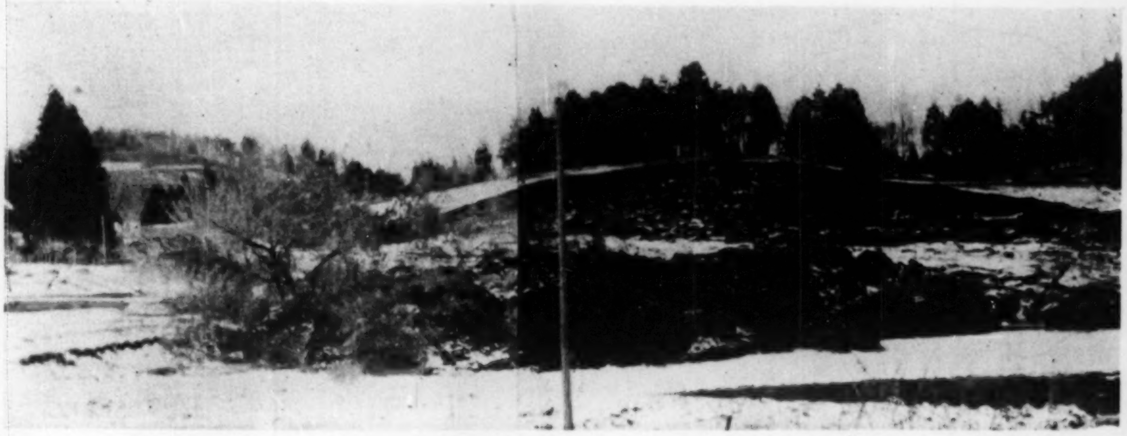

b. Low angle land slide at Numauchi, Nikko Town (above), c. with temporary pond at the right margin. (left).

（震研彙報 第二十八號 圖版 河角）

Fig. 7. a.

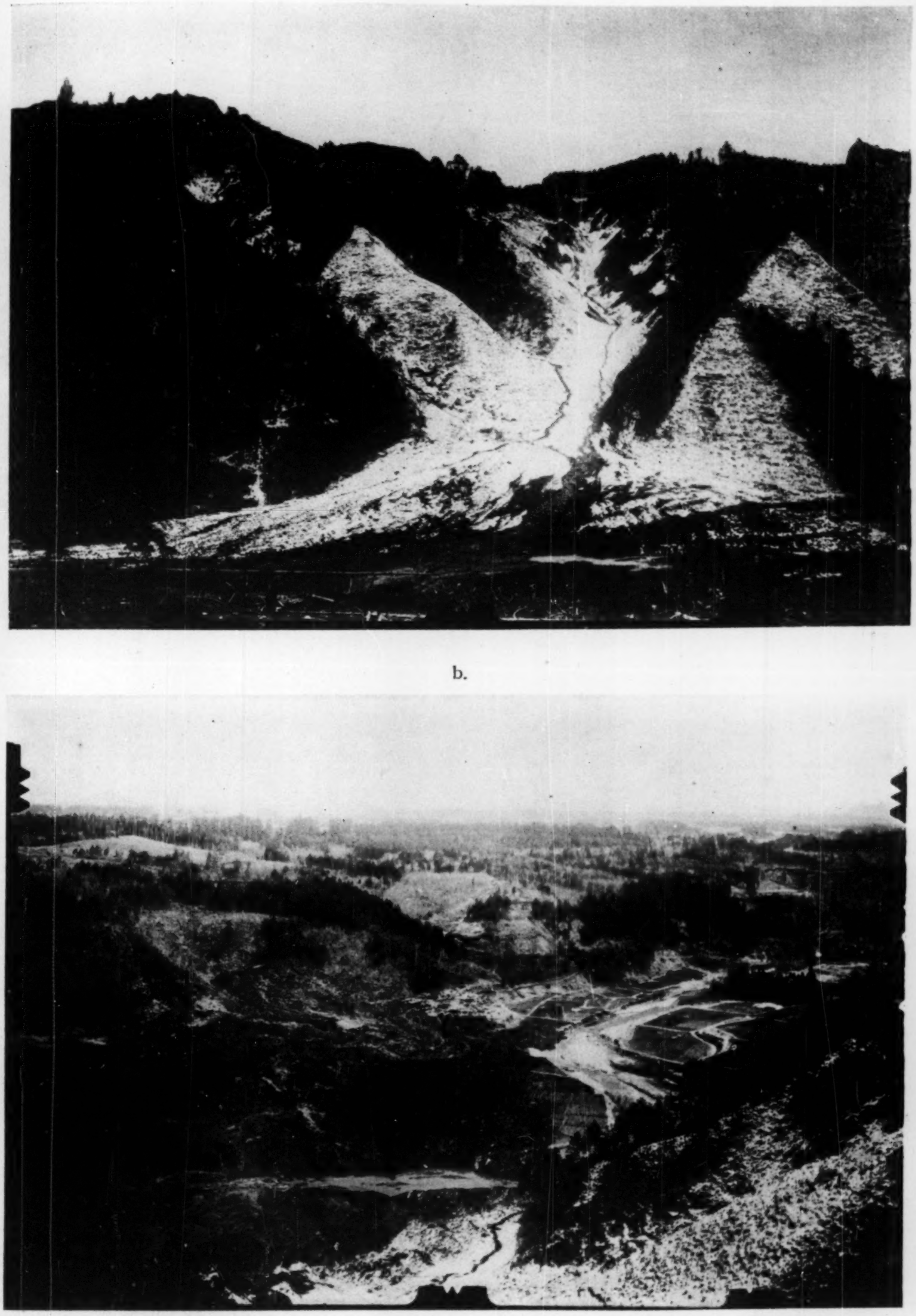

b.

High angle landslide (a) and the debris flowed down from it and buried 2 houses and 4 men and 1 horse (b). Murose-Namekawa, Imaichi Town.

（震研彙報 第二十八號 圖版 河角）

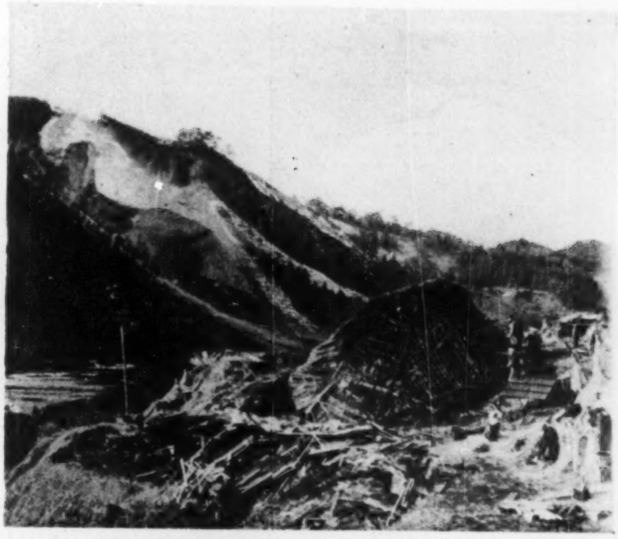

Fig. 7. c. The house pushed down and half buried by the mud flow. A horse was buried to death under the house. Stream line of the mud-avalanche is seen on the slope of the valley side in the back-ground.

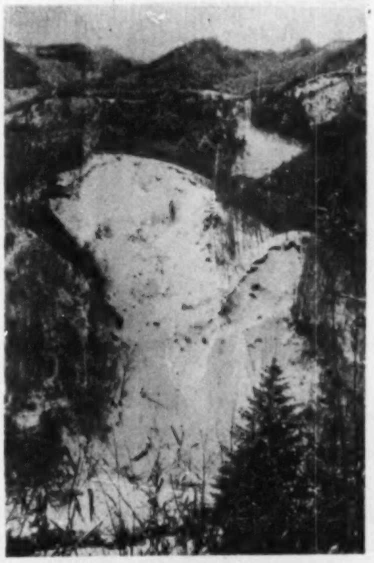

Fig. 8. a. High-angle landslide at Matsunokiuchi, Nikko Town.

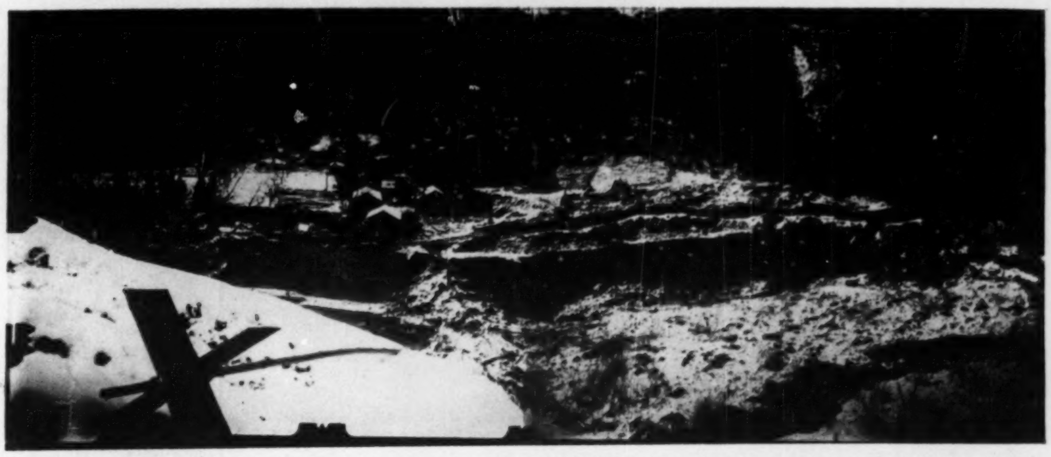

b. The mud flow flowed down the slope across the river in the foreground and leaped over the road and destroyed and buried a house standing at the higher level. The present road runs on the debris.

（震研彙報 第二十八號 圖版 河角）

Fig. 9.

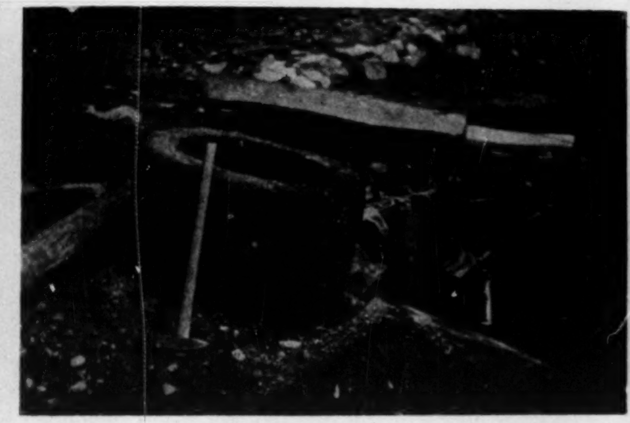

a. An "ishiusu", a stone implements for making rice cake, which was tossed some 20 cm several times like bounding rubber ball by the earthquake motion. At Nagahata, Ochiai Village.

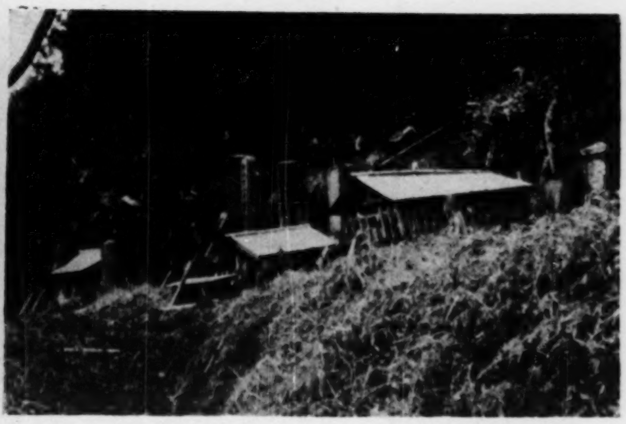

b. The tomb stone in the vicinity was disturbed but slightly.

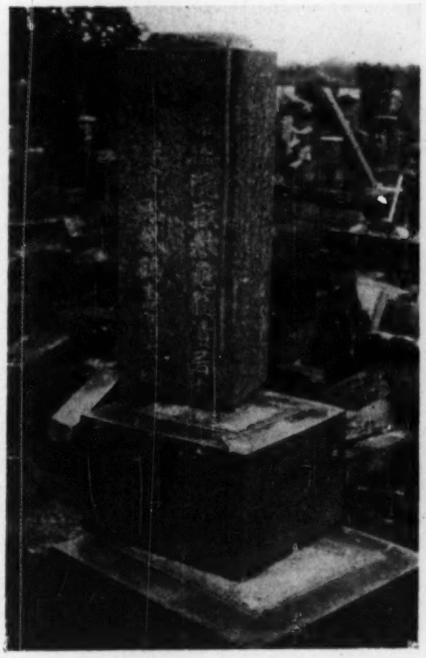

c. The tomb at the Imaichi Town was much disturbed and only very few tomb stones remains standing.

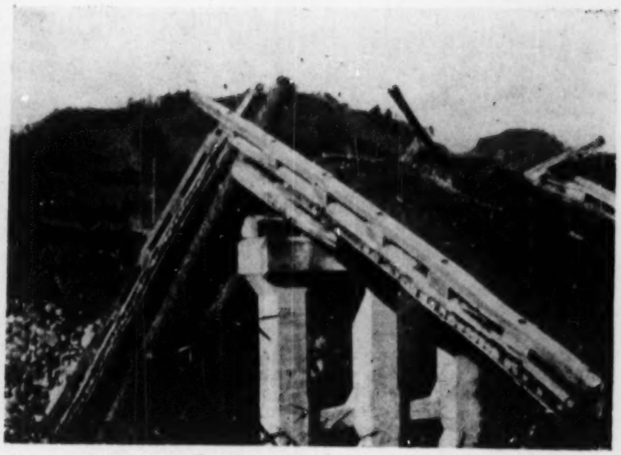

d. A broken bridge at Myōjin, Ochiai Village.

Fig. 10.

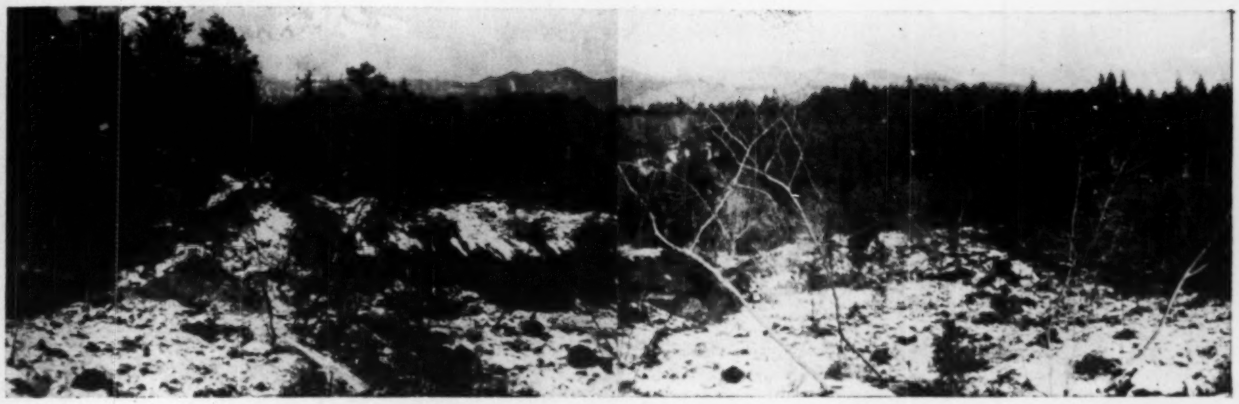

a. Devastation of a forrest at Yamakubo, Nikko Town.

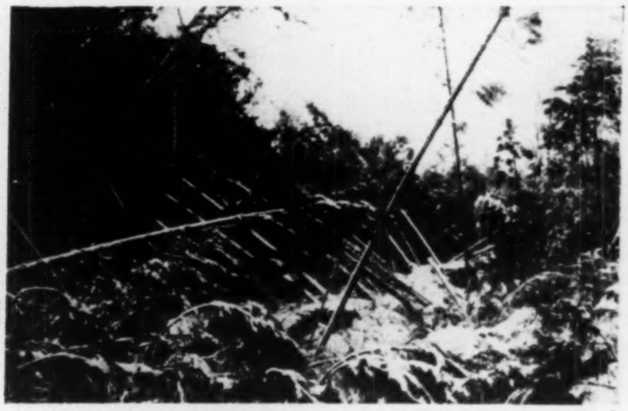

b. The trees pushed together compactly at the terminus of the mud flow.

clines only 1 degree eastward from the horizon, slid bodily eastward by about 6 cm. But the subversion of wooden houses in the meizoseismic area was rather slight owing perhaps to the shortness of duration and period of earthquake motion.

The mechanism of occurrence of the shock, as seen from the distribution of the first impulsions, was of conical type. And in harmony with this mechanism, we could not find any topographic changes which suggest the appearance of earthquake fault, while the provisional result of the levelling rerun after the earthquake, by the Geographical Survey Institute along the route from Utsunomiya to Nikko, revealed an upheaval more than 30 cm. in the vicinity of Imaichi with no indication of faulting.

Distribution of the first impulsions of the conical type was ascribed by M. Ishimoto to the mechanism of magma intrusion, and F. Omori attributed the earthquakes in this area to the volcanic earthquakes, but there is nevertheless no positive testimony to affirm the volcanic origin of the present earthquake. Although the writer has no intention to stress the volcanic hypothesis, since no Nikko earthquakes on record were acompanied by similar phenomena as follows, the apparent simultaneous activities of near volcanoes with the present earthquake must be mentioned. The Azuma, belonging to the Nasu volcanic zone, at 120 km. NE of Nikko manifested a slight activity on Feb. 10 and 13, and the Mihara at Oosima Island in the Sagami Bay which is 220 km. south of Nikko began its strong activity on July 16 and continued till Sep. 23 the Stronmolian phase forming a new central cone and emitting abundant lava, and recently the Asama at 100 km. SW by W made an unusually big explosions on Sept. 23, and Oct. 4, 1950.

---

25. 今市地震概説

地震研究所　河角廣

昭和24年12月26日朝8h 16m 及 8h 25m に栃木縣上都賀郡今市町附近を中心とする小區域破壞的地震が起り，死者8，行方不明2，全潰住家299戸半潰住家618戸の被害を生じた.

此の地震の震央附近の震度は極めて强かつたようであるが，振動週期極めて小なりし僞か石藏家屋の外は全潰（現建築費50％以上の損害）とは云へ倒潰と云ふやうなものは少かつた．従つて火事の發生を見なかつたのは幸であつた．然し山崩，地辷りは極めて著しく，山地田畑の荒廢著しく，人命の損失の大部分もこれによるものであつた．余震の頻發した事，及び初動の圓錐型分布，及び所謂地震斷層と思はれる如きものの見へなかつた事も本地震の特徴と云ふべく，今市町全體に互る地震後井戸壁の變形から約6mの厚さの地層が東方に約6cm移動した事が判明したが，之は測地學上重要問題を指唆するものである．尙水準測量の結果は今市町近傍數粁の間だけ約30～40cmの隆起があつた由である．震後の火山活動との關係も興味ある問題であらう.

[illegible]

[illegible]

[illegible]

[illegible]

[illegible]

[illegible]

[illegible]

26. *Seismometrical Study of the Imaichi Earthquake on Dec. 26, 1949.*

By Yoshiaki KOSHIKAWA.

Earthquake Research Institute.

(Read July 18, 1950.—Received Sept. 20, 1950).

1. Introduction.

On the morning of Dec. 26, 1949, Imaichi, Nikkô and the adjacent villages of Tochigi Pref. were severely shaken at 8 h 17 m and at 8 h 25 m (Japanese Civil Standard Time). The writer executed the seismometrical study of this earthquake. Original seimograms as observed at twelve meteorological stations and at the Earthquake Research Institute, Tokyo University, were analysed by the writer himself. Furthermore, seismological reports from 62 meteorological stations throughout Japan were placed at his disposal. Based on these data, the location of epicentres and the construction of travel-time curves were carried out.

2. Effect of the superficial layer.

At first a tentative epicentre was located as 139° 39.′5 E long. and 36° 41.′9 N lat. by means of arrival times. Travel-time curve of the first earthquake thus constructed showed the assumed epicentre to be fairly satisfactory. Next, the focal depth was tentatively determined by means of the duration of preliminary tremor τ, by the formula;

$$\sqrt{\Delta^2+h^2}=k\tau$$

where Δ, h and k denote the epicentral distance, the focal depth and Omori constant respectively. But the values of thus determined from τ_s at various stations were very divergent. This might have been due not only to oservation errors, but also to the fact that the effect of the superficial low-velocity layer is larger than the effect of the focal depth in case of such shallow earthquake, to say nothing of the mistake of identification of τ, with $\overline{P}-S^*$; $P^*-\overline{S}$; or P^*-S^* instead of $\overline{P}-\overline{S}$. This can be seen from the following considerations. In Fig. (1), d and H indicate the thickness of the superficial (sedimentary) layer and the granitic layer respectively. U and V correspond to the propaga-

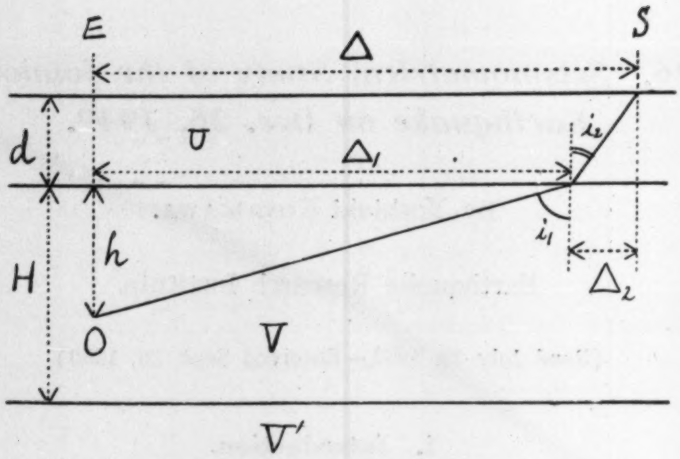

Fig. 1. Model of the earth-crust.
O: Hypocentre; E: Epicentre; S: Station.

tion velocities of seismic waves in the respective layers, while h denotes the part of focal depth in the granitic layer. Epicentral distance Δ is divided into the two parts Δ_1 and Δ_2 as shown in Fig. (1). Then the travel-time of $\overline{P}$– (or $\overline{S}$–) wave is written as follows;

$$\overline{T}=\frac{\sqrt{\Delta_1^2+h^2}}{V}+\frac{d}{U}\cdot\frac{1}{\sqrt{1-r^2\sin^2 i_1}}$$

$$=\frac{\sqrt{\Delta_1^2+h^2}}{V}+\frac{d}{U}\cdot\frac{\sqrt{\Delta_1^2+h^2}}{\sqrt{\Delta_1^2+h^2-r^2\Delta_1^2}},$$

where $r=U/V=\dfrac{\sin i_2}{\sin i_1}$.

$$\therefore\ \overline{T}\fallingdotseq\frac{\sqrt{\Delta_1^2+h^2}}{V}\left\{1+\frac{d}{r}\cdot\frac{1}{\Delta_1}\left(1+\frac{r^2}{2}-\frac{h^2}{2\Delta_1^2}\right)\right\}.$$

Now expanding this formula in terms of h/Δ_1 and neglecting its terms of higher order, we obtain

$$\overline{T}\fallingdotseq\frac{1}{V}\left\{\Delta_1+\frac{d}{r}+\frac{rd}{2}+\frac{1}{2}\,\frac{h^2}{\Delta_1}\right\}.$$

Since, $\Delta_1=\Delta-\Delta_2$ and $\Delta_2\fallingdotseq rd\left(1+\dfrac{r^2}{2}-\dfrac{h^2}{2\Delta_1^2}\right)$,

we have $$\overline{T}\fallingdotseq\frac{1}{V}\left\{\Delta+\frac{2-r^2}{2r}\,d+\frac{1}{2}\,\frac{h^2}{\Delta_1}\right\}\qquad\text{(1)}$$

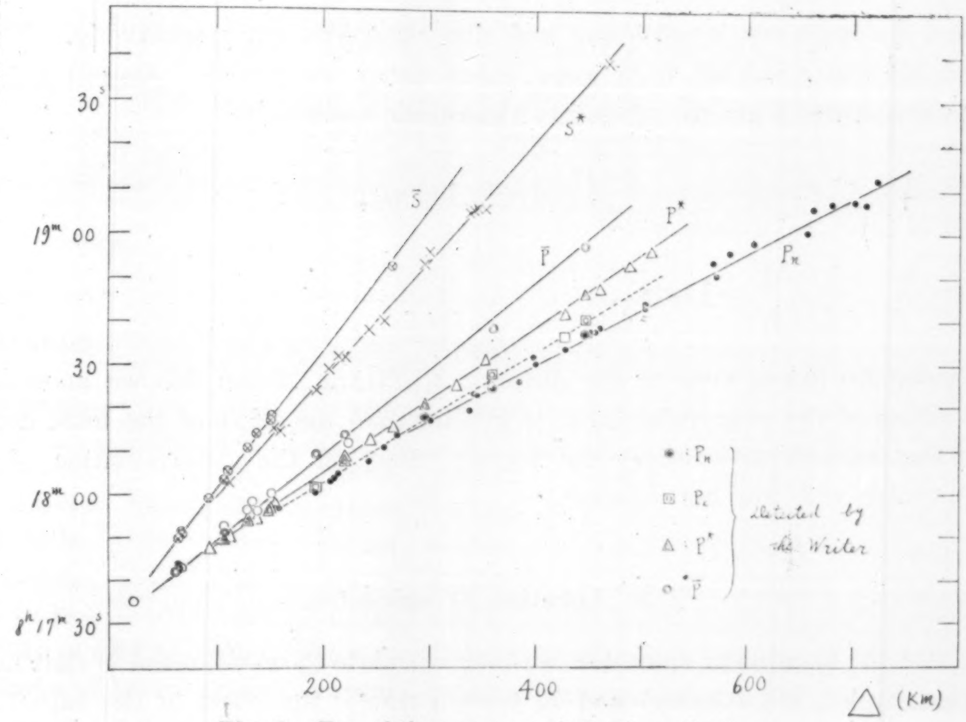

Fig. 2. Travel-time curves of the first shock.

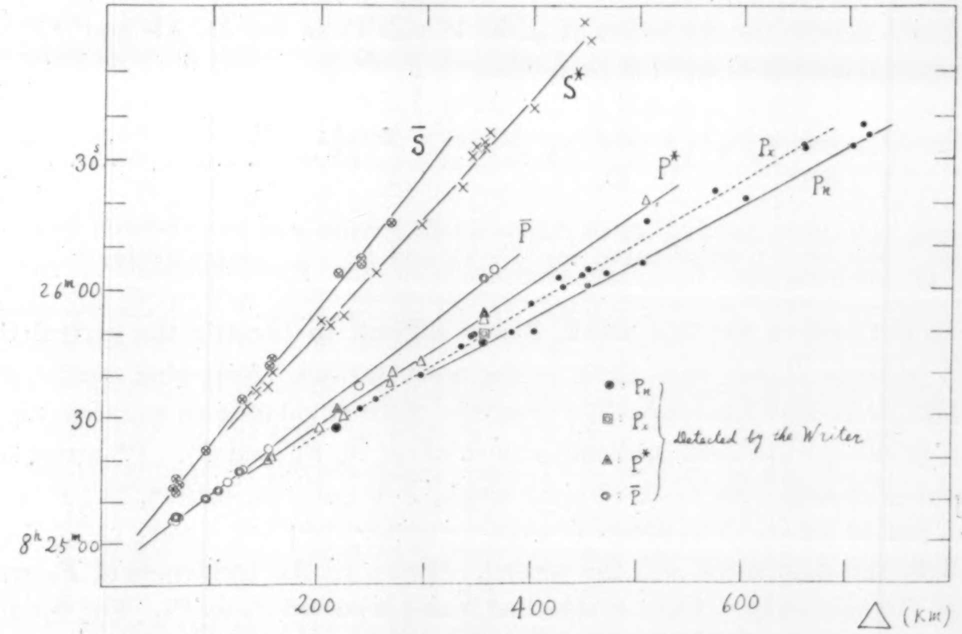

Fig. 3. Travel-time curves of the second shock.

According to Prof. T. Matuzawa,[1] U_P=1.94 km/s, U_S=1.14 km/s, V_P=5.0 km/s, V_S=3.15 km/s and d=3.83 km in the Kwantô Plain. Here, suffixes

---

1) T. MATUZAWA and T. FUKUTOMI, *Bull. Earthq.Res. Inst.*, 10 (1932), 511.

P and S denote the longitudinal and distortional waves respectively. Then, $r_P=0.384$ and $r_S=0.368$, their mean value being about 0.37. Assuming here $r=0.37$ and $d=4$ km for simplicity's sake, we have

$$\frac{2-r^2}{2r}\,d=10.1\,(km)\,,$$

whereas $\frac{1}{2}\,\frac{h^2}{\Delta_1}=1\,(km)$,

provided $h=10$ km, even at the distance $\Delta_1=50$ km. From this we know that the effect of the superficial layer is greater than the effect of the focal depth, and the necessity to consider the former effect in the determination of the hypocentre will now be apparent.

3. Location of epicentre.

For the location of epicentre ,we may calculate those values of φ (latitude), λ (longitude), V (velocity) and T_0 (origin time); the effect of the superficial layer $\frac{2-r^2}{2r}\,d$ is included in T_0 as a constant term.

If we denote the deviation of φ, λ, V and T_0 as $\delta\varphi$, $\delta\lambda$, δV and δT, observation equation is written as follows;

$$\frac{1}{V}\,\frac{\partial\Delta}{\partial\varphi}\,\delta\varphi+\frac{1}{V}\,\frac{\partial\Delta}{\partial\lambda}\,\delta\lambda-\delta T-\frac{t}{V}\,\delta V=m\,, \quad\text{..................}(2)$$

where t and m are substituted for $T-T_0$ and $t-\frac{\Delta}{V}$ respectively.

In the case of the first shock, it was difficult to identify the arrival time of $\overline{P}$, whereas $\overline{S}$ was very clear to the near stations. Assuming $\varphi=36°\ 41.'9$, $\lambda=139°\ 39.'5$, $V_S=3.15$ km/s, $T_0=17$ m28.7s, the method of least squares was applied to obtain the most probable values of φ, λ, V_S and T_0. P^*-wave, also, appeared clearly. As to the second shock, $\overline{P}$-wave was distinct, but P^* and $\overline{S}$ were not so clear. The bands of time variation of P_n-wave were rather broad in both the first shock and the second. Owing to the feebleness of P_n-wave, many stations seem to have overlooked it and reported P_x as P_n. For example, the seismograms of Morioka as examined by the writer, show P_x-phase distinctly, especially in the vertical movements, 2.0 sec. later than the very feeble movement of P_n.

The epicentre of the first shock was located independently from P^* as well as from $\overline{S}$ and obtained the fairly concordant results as shown in Table

Table 1. Data used to locate the epicentre.

Tentative epicentre $\begin{cases} 36^\circ\ 41.'9 \text{ N lat.} \\ 139^\circ\ 39.'5 \text{ E long.} \end{cases}$

Station	Δ	$\frac{\partial\Delta}{\partial\phi}$	$\frac{\partial\Delta}{\partial\lambda}$	1st shock		2nd shock
				P^*	$\overline{S}$	$\overline{P}$
	km			m s		
Maebashi	62.4	0.5290	0.6804	17 41.9	——	——
						m s
Kumagaya	65.7	0.9315	0.3026	——	——	25 06.4
					m s	
Tsukuba	66.6	0.8010	−0.4771	42.4	17 49.7	05.2
Shirakawa	68.0	−0.6860	−0.5835	——	50.9	05.3
Kakioka	69.8	0.7388	−0.5409	42.9	51.3	06.1
Chichibu	94.7	0.8377	0.4379	47.2	59.1	10.9
Oiwake	106.9	0.3742	0.7444	——	——	12.8
Tokyo (E.R.I.)	110.1	0.9963	−0.0714	49.2	18 03.7	——
Tokyo (C.M.O.)	113.0	0.9970	−0.0643	50.5	05.4	15.0
Onahama	113.6	−0.2363	−0.7790	49.9	——	——
Nagano	130.1	0.0195	0.8016	53.5	10.6	17.6
Takada	133.0	−0.3426	0.7526	——	——	17.8
Fukushima	137.1	−0.8551	−0.4155	53.9	13.8	——
Chôshi	152.5	0.6991	−0.5734	56.6	16.9	22.9
Kofu	153.7	0.7666	0.0514	——	18.2	——

(2). The epicentre of the second shock which were located from the arrival time of $\overline{P}$ coincided with the macroseismic data. It was situated in the western outskirts of Imaichi where the largest acceleration in this earthquake was experienced.

To evaluate the focal depth, the differences of intercept time between the direct waves ($\overline{P}$ or $\overline{S}$) and the refracted waves (P^* or S^*) were used.

The travel-time of the refracted wave T^* is written in the form,

$$T^* = \frac{\Delta}{V'} + \frac{(2H-h)\cos i}{V} + \frac{d}{r}\,\frac{\sqrt{1-r^2R^2}}{V}\,, \qquad \ldots\ldots\ldots\ldots\ldots\ldots\ldots(3)$$

where V' means the velocity in the intermediate (basaltic) layer, and $R=\sin i=V/V'$. Taking the difference of the values of the equations (1) and (3), at $\Delta=0$, we have

$$T^* - \overline{T} = \frac{(2H-h)\cos i}{V} + \left(\sqrt{1-r^2R^2} - \frac{2-r^2}{2}\right)\frac{d}{rV}\,.$$

Now that $\sqrt{1-r^2R^2} - \dfrac{2-r^2}{2} = 0.02$, and therefore may be neglected, when $r=0.37$ and $R=0\ 85$.

$$\therefore\quad T^* - \overline{T} \doteqdot \frac{(2H-h)\cos i}{V}.$$

Table 2. Results obtained by the method of least squares.

	The first shock		The second shock
	By the arrival times of		
	$\overline{S}$	P^*	$\overline{P}$
$\delta\varphi$	$-0'.837\ \pm0'.120$	$+0'.171\pm1'.095$	$+1'.743\ \pm0'.436$
$\delta\lambda$	$+0'.351\ \pm0'.226$	$+1'.503\pm1'.357$	$-0'.715\ \pm0'.557$
δV (km/s)	$-0.334\ \pm0.320$	-0.103 ± 0.240	-0.0531 ± 0.0743
δT (sec.)	-0.0318 ± 0.0146	$+0.276\pm1.901$	$+0.578\ \pm0.858$
$\varphi\ \left(\begin{smallmatrix}N\\ \text{lat.}\end{smallmatrix}\right)$	36° 41′.06±0′.12	36° 42′.1±1′.1	36° 43′.6±0′.4
$\lambda\ \left(\begin{smallmatrix}E\\ \text{long.}\end{smallmatrix}\right)$	139° 39′.85±0′.23	139° 41′.0±1′.4	139° 38′.8±0′.6
V (km/s)	3.118±0.015	6.00±0.24	5 05±0.074
T	17m 29.05s±0.33s	17m 31.32s±1.90s	24m 51.92s±0.86s

Intercept time (T_o) of

$\overline{P}$	P^*	S^*	P^*	S^*	$\overline{S}$
17m s s 29.31±0 92	s s 31.33±0.29	s s 32.25±0.64	24m s s 54.33±0 71	s s 55.58±0.62	s s 51.48±0.59

Velocity of S^*: 3.689±0.016 (km/s)

For the longitudinal wave of the first shock,

$$(T^*-\overline{T})_P = 17\text{ m }31.32\text{ s} - 17\text{ m }29.31\text{ s} = 2.01\text{s},$$

$$\therefore\quad 2H-h = 18.8\text{ (km)}.$$

For the distortional wave of the first shock,

$$(T^*-\overline{T})_S = 17\text{ m }32.25\text{ s} - 17\text{ m }29.05\text{ s} = 3.20\text{ s},$$

$$\therefore\quad 2H-h = 18.7\text{ (km)}.$$

The mean value of $2H-h=18.8$ (km).

Similarly, for the second shock,

$$(T^*-\overline{T})_P = 24\text{ m }54.33\text{ s} - 24\text{ m }51.92\text{ s} = 2.41\text{ s},$$

$$\therefore\quad 2H-h' = 22.6\text{ (km)},$$

$$(T^*-\overline{T})_S = 24\text{ m }55.58\text{ s} - 24\text{ m }51.48\text{ s} = 4.10\text{ s},$$

Table 3. Data used to determine the intercept time.

Station	1st shock				2nd shock			
	Δ	$\overline{P}$	P^*	S^*	Δ	P^*	S^*	$\overline{S}$
	km	m s	m s	m s	km	m s	m s	m s
Shirakawa	68.9	——			66.4			25 13.4
Maebashi	63.0	17 41.9			64.3			
Tsukubasan	64.7	42.4			69.3			
Kakioka	68.0	42.9			72.4			14.4
Kumagaya	65.0	43.5			68.9			
Chichibu	94.1		17 47.2		97.3			22.7
Tokyo (E.R.I.)	108.4	51.0	49.2		113.3			
Onahama	113.2		49.9		113.1			
Tokyo (C.M.O.)	111.4		50.5		117.2			
Nagano	129.0		53.5		127.6			
Fukushima	138.1		53.9		134.7		25 32.4	
Yokohama	139.4	56.-			144.2			
Niigata	149.2		55.8		144.3		36.1	
Chôshi	151.0		56.6		155.3			42.2
Kôfu	152.0	18 00.2			154.8	25 20.4	37.3	
Matsumoto	159.8			18 14.5	158.4	21.1		
Funatsu	154.7		57.8		158.1	20.7		
Takada	134.2	17 58.5			131.2			
Aikawa	193.8	18 09.5		24.-	189.3			
Sendai	206.8			29.2	203.4	27.4	52.8	
Ōshima	214.8			32.2	219.4			
Toyama	221.1	13.7	18 07.7		219.3	31.7		
Shizuoka	221.5		08.-	32.0	224.9	30.-		
Takayama	224.3	12.0			224.2			
Ishinomaki	243.7			38.1	240.6			
Sakata	245.0		12.5		240.3			26 07.2
Wajima	257.6			40.4	254.8		26 04.0	
Omaezaki	266.3		15.2		269.7	40.6		
Nagoya	296.0		20.7	53.2	297.5		15.0	
Mizusawa	301.1			56.-	297.3	43.-		
Irako	325.8		25.-		328.1			
Akita	339.3			19 04.9	334.7			
Tsuruga	343.0			05.4	344.1		30.7	
Hikone	345.7			05.8	346.6		32.6	

(to be cotinued)

Table 3. (continued)

Station	1st shock				2nd shock			
	Δ	$\overline{P}$	P^*	S^*	Δ	P^*	S^*	$\overline{S}$
	km	m s	m s	m s	km	m s	m s	m s
Kameyama	353.6			19 05.8	355.2	25 52.8	26 33.7	
Morioka	360.1	18 38.5			356.1	54.4	32.5	
Tsu	357.7				359.5			
Owase	428.5		18 41.5		430.7			
Osaka	448.-	57.5	46.2		449.-			
Kôbe	462.0		47.5		472.0			
Wakayama	490.4		52.7		491.8			
Tottori	509.5		56.0		509.2			
Shionomisaki	505.1				507.5	26 20.6		
Kanazawa	269.7				268.1	25 38.0		

$\therefore \quad 2H-h'=23.8$ (km).

The mean value of $2H-h'=23.2$ (km).

Then $h>h'$, and $h-h'=23.2-18.8=4.4$ (km). The values of H, h and h' which satisfy $2H-h=18.8$ and $2H-h'=23.2$ are listed in Table (4). The accurate values of h and h' could not be determined, but h may be about 15 km and h' may perhaps be 10 km.

Discussions concerning P_n and P_x will be held at some future date.

Table 4.

h'	h	H
km	km	km
0	4.4	11.6
2	6.4	12.6
4	8.4	13.6
6	10.4	14.6
8	12.4	15.6
10	14.4	16.6
12	16.4	17.6
14.4	18.8	18.8

Summary.

Considering the effect of the superficial layer, the location of epicentres was executed by means of the method of least squares, using the arrival times of $\overline{S}$ and P^* of the first shock and of $\overline{P}$ of the second. The epicentre of the first shock was obtained at a situation about 4.5 km southwards Imaichi. The second epicentre was located at a position in the western outskirts of Imaichi, about 5 km NNW from the first epicentre.

The focal depth of the former may be 15 km or so, and the latter's depth may be a few kilometers shallower than the former.

In conculsion, the writer wishes to express his sincere thanks to Professor

H. Kawasumi who gave him kind advices and Dr. W. Inouye, the head of the Seismometrical Section of C. M. O. and the other members of the section who offered him every facility for analysing the seismograms.

26. 今市地震の計測

地震研究所　越川善明

淺い地震を稍々遠い所で觀測した結果に基いて震源の深さを求めようとする場合，表面の低速度層の影響が大きいということを考察した．次に發震時を用いて最小自乘法によつて震央の決定を行つた．第一の地震については P^* 波と $\overline{S}$ 波との發震時を用いて別々に震央を定めたが，よく一致する結果が得られた．その震央位置は落合村長畑附近となつた．第二震はこれより北北西約5kmで，今市町の西端の邊りになる．深さは正確には定め得ないが第一震は15km位，第二震はそれより4～5km淺いということを，走時曲線の震央における時間差から求めた．所謂花崗岩層の厚さは17 km前後と考えられる．

花崗岩層及び玄武岩層における縱波，横波の傳播速度は次の樣に求められた．(單位は km/s).

$\overline{P}$: 5.05;　$\overline{S}$: 3.12;　P^*: 6.00;　S^*: 3.69.

27. *Geology of Imaichi District with Special Reference to the Earthquakes of Dec. 26th., 1949. (1)*

By Ryōhei MORIMOTO,

Earthquake Research Institute.

(Read Jan. 17, Apr. 18, 1950.—Received Sept. 20, 1950.)

I. Introduction.

Dec. 26th., 1949, the area around Town Imaichi, 7 km to the east of Nikkō, Kamitsuga-gun, Pref. Tochigi, and about 110 km to the north of Tokyo, was attacked by severe earthquakes that took place successively at 8:18, and 8:26 a. m. (Fig. 1). The wrier reached the town at the scene of the earthquake when the most severe aftershock of 5:54 p. m., Dec. 27th., rocked this area. Not only the focus of this most conspicuous aftershock, but also the focusses of the quakes that occurred in quick succession after the heaviest, are situated exclusively in depth within 10 km from the surface, the aftershocks with focusses estimated at about 5 km or less in their depth being the most common.[1] In spite of the small magnitude of the present earthquakes, the change of surface took place remarkably in the meizoseismic area, especially where the thick aeolian pumice deposits such as "Kanuma-zuchi" and "Imaichi-zuchi" are distributed. The epicentres of the two principal quakes are situated near Imaichi, the town built on the alluvial fan of the River Daiya which, in this area, runs eastwards through the valley between Ashio mountain land and Nikkō volcanic region.[2] And the focusses of the many aftershocks which

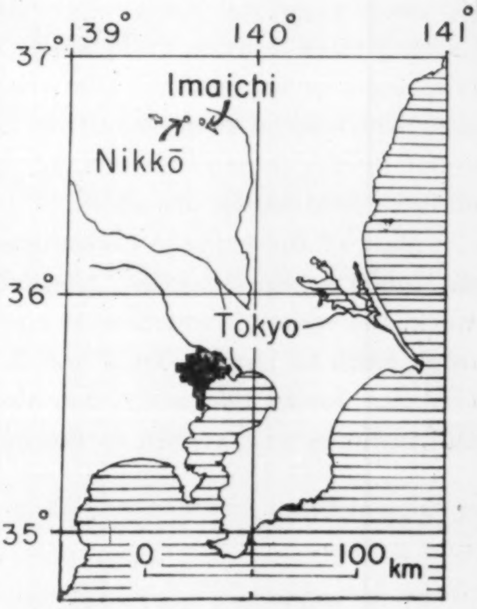

Fig. 1. Index map showing the locality of Imaichi district.

---

1) T. HAGIWARA, etc., *Bull. Earthq. Res. Inst.*, 28 (1950), 393 400.

2) Y. KOSHIKAWA, *Bull. Earthq. Fes. Inst.*, 28 (1950), 369-377.

took place successively for about three months are distributed in an area of about 100 km^2 including the town of Imaichi as its northernmost margin, the valley of Ogurugawa as its westernmost, the village of Itaga as its southernmost, and the lower reach of the River Namegawa as its easternmost.3) The geology of this area is mainly composed of hard compact Palaeozoic formations intruded by biotite granite or granite-porphyry, and the earthquake vibration through these strata sounds like an explosion of dynamite in mines. These sounds could be heard during the writer's field work whenever the aftershocks were felt, and the inhabitants said that such mountain rumblings conld be heard ever since the beginning of last August or about 5 months before the present earthquakes.4)

The area has long been neglected without any further geological investigation being made except that carried out by Nasa long years ago.5) While on the other hand, the Nikkō and Shiobara volcanic regions belonging to the socalled Nasu volcanic zone, northeast of this area, have been investigated repeatedly or in detail.6) The writer investigated the general geology of this area with special reference of the change of surface that had been brought about by the present earthquake, and in this paper, brief notes on the results of these field works are given.

Most of the expense necessitated for the investigation was defrayed from the funds for the Scientific Research of the Educational Ministry. In his field work, the writer is indebted to the Tochigi Prefectural Government, and he owes much to Drs. F. Tada and G. Imamura for their kind instruction and criticism during this study, and also to Y. Fukuda's of Itaga who gave him full facilities with regard to the field station during his stay there.

---

3) T. HAGIWARA and etc, *op. cit.*,

4) Oral communication from S. Fukuda, a mail deliverer of Miyanoshita, Ogurugawa. Another inhabitant of Yamanaka, the outskirts of Ogurugawa-village, said that he also had heard such sounds for 10 days or more before the quakes. And a villager of Oohara, Itaga also testified to 20 days or more. But it must be noted here that they without exception thought that these sounds were the explosion of dynamite in the working mines distributed in the southern vicinity.

5) T. NASA, *Explanatory Text of the Geological Map of Japan*, Scale 1:200,000. "Nikkō" (1899).

6) S. TSUBOI and K. SUGI, "Geological guide to the Nikkō district", *Guide Book of the excursions, Pan-Pacific Science Congress, Japan*, (1926).

S. IWAO, *Bull. Geol. Survey of Japan*, **3** (1913), 4–14 (in Japanese).

M. YAMAZAKI, *Jour. Geol. Soc. Japan*, **56** (1950), 38 (in Japanese).

H. NIINO, *Jour. Geol. Soc. Japan*, **40** (1930), 517–532 (in Japanese). etc.......

II. Geology of Imaich District.

Topography and general outline of geology.

The area consists of two topographic units: one is the alluvial fan of the River Daiya, and the other is an isolated topographic unit surrounded by the comparatively higher Palaeozoic mountain ridge passing through Mts. Keimei (961 m), Sasamekura (799 m), and Sekison (594 m), (Fig. 2). The former is diverging and is gently sloping eastwards, and combined with the fan of the River Kinu and her tributaries, it adjoins the great Kwanto plain. The latter is divided from the Ashio mountain land by the above-mentioned circularly arranged mountain ridge and is bounded by the River Namegawa from the flood plain developing in the east of the area. In short, the topography of the area is closely related with the geology of this district, and its present relief may be ascribed mainly not to the results of the denudation of the ground but to the results of differential erosion. Silicified Palaeozoic conglomerate or shale gives sharp slope to the higher mountain ridge while the rocks exposed at the valley or at the lower lands in this area are exclusively granite, especially monzonitic biotite-granite containing remarkable porphyritic potash felspar. Non-porphyritic biotite-granite, as well as the Palaeozoic rocks, however, resisting the exogenous agencies, forms the mountain such as Nakayama in the central portion of this area. Quartz-porphyry or granite-porphyry which forms the ridge running from NNW to SSE along the right side of the River Namegawa is also often capped by the quite silicified Palaeozoic rock. Some destructive land slides of large scale occurred along this ridge.

On the pediment developing at the foot of these mountains, uniform aeolian deposits of pumice are distributed. It covers extensively the northeastern part of this area, especially the Diluvial gravel of the River Daiya and sometimes amounts to several metres in thickness. As will be mentioned in the succeeding chapter (Chapter III), these pumice beds play an important rôle in bringing about the remarkable land slips of various scale that did the most conspicuous damage to civil engineering, forestry, and agriculture.

Tertiary formation developing in the north and northeast of the area is almost lacking in this area except at Itagabata where scanty outcrops of the formation composed mainly of pyroclasts are found. But the accurate geological relation to the associating rocks could not be ascertained during this investigation. Description about each rock and their geological relations will be given briefly as follows:

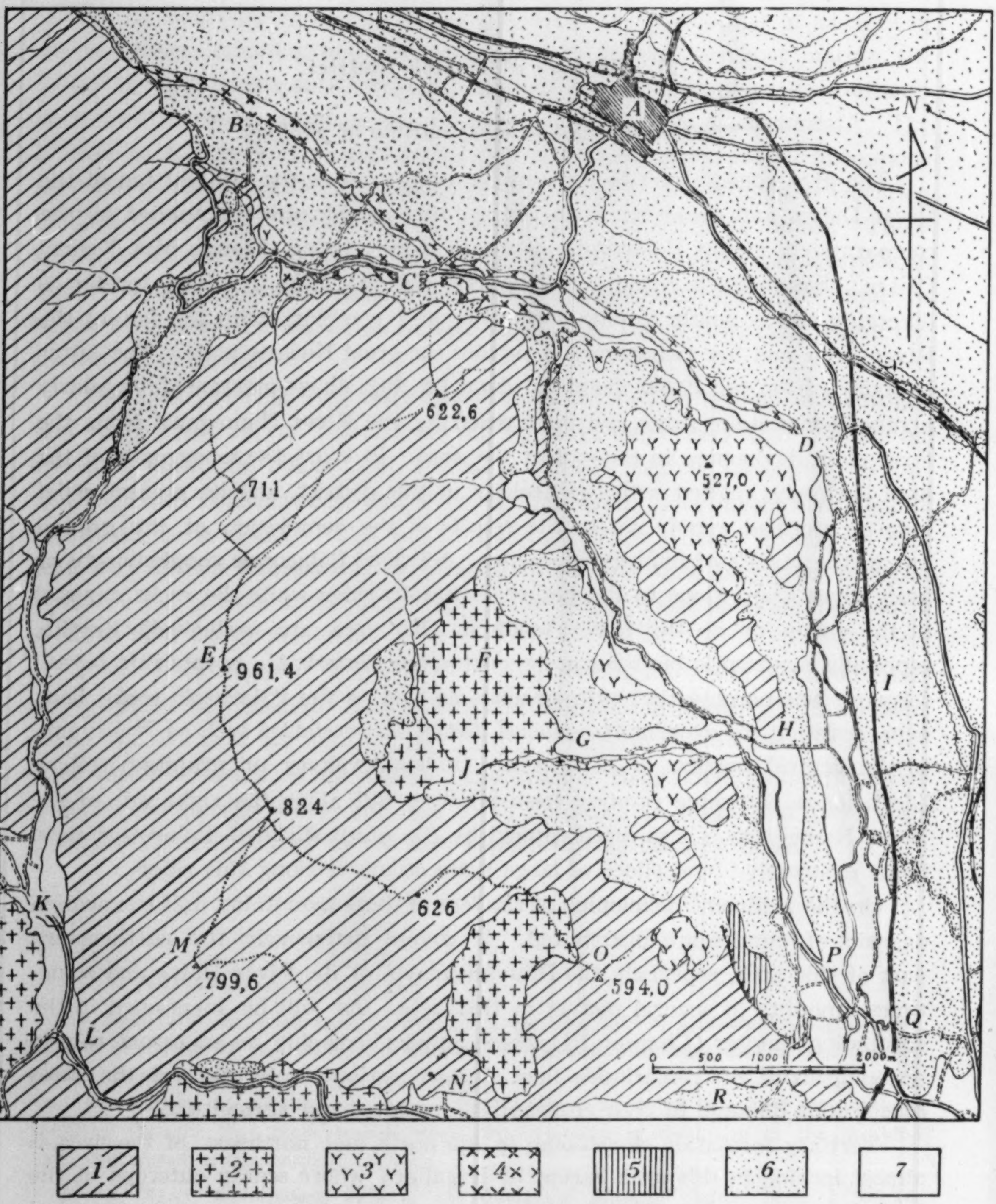
A
B
C
D
E
F
G
H
I
J
K
L
M
N
O
P
Q
R
N
622,6
711
527,0
961,4
824
626
799,6
594,0
0 500 1000 2000m
1
2
3
4
5
6
7

Fig. 2. Geologic map of Imaichi district.

A...Town of Imaichi, B...Numauchi, C...Matsunokiuchi, D...Murose-namegawa, E...Mt. Keimei, F...Mt. Nakayama, G...Nagahata-nakai, H...Ushiroyama, I...Myōjin station (Tōbu line), J...Keimei mine, K...Ogurugawa, L...Yamaguchi, M...Mt. Sasamekura, N...Oohara, O...Mt. Sekison, P...Itagabata, Q...Shimokojiro station of Tōbu line, R...Itaga, 1...Chichibu system, 2...Granite, 3...Granite-porphyry or quartz-porphyry, 4...Andesite flow, 5...Liparitic rock associated with pyroclastics, 6...Diluvium, 7...Alluvium.

(1) Chichibu System.

The Chichibu System, the oldest formation in this district, occupies a large area of the southwestern portion of the present macroseimic region. It continues to the Palaeozoic strata forming Ashio mountain land which shows an uniform valley system. The formation consists mainly of sandstone (composed of angular fragments of quartz, plagioclase, orthoclase, and shaly patches) and slate, and is more or less metamorphosed into compact hornfels owing to the intrusion of granitic rocks. Contact portion of the cherty hornfels and the porphyritic biotite-granite was found at the river bed, in the western outskirts of Oohara, where remarkable quartz veins were observed in both rocks (Fig. 3). The structure of the formation is not clear owing to its conspicuous silicification and shattering. But judging from the general trend of the distribution of each rock facies, it takes generally the NE–SW direction, dipping in most cases northwestwards.

Highty silicified rocks are often found as remnants of the roof pendants in or around the outcrops of the granitic rocks mentioned in the following sections. Reddish brown biotite frakes are commonly contained in the slate or in the cementing portion of the sandstone, while no other contact minerals are found.

(2) Granitic rocks.

Coarse-grained biotite-granite shows sometimes porphyritic appearance owing to the remarkable perthite crystals amounting up to 1 cm or more. The monzonitic facies of the granite is apt to be decomposed. Thus the granite occupies the valley or the rounded hill, while the highly silicified Palaeozoic strata form a sharp slope or ridge. Contact-effect on the Palaeozoic strata of this granite is not so remarkable as to bring about complete recrystallization of the surrounding rock. The only metamorphic mineral to be found is biotite. The strata were hardened along the contact zone by conspicuous silicification. According to these metamorphic feature shown by the Palaeozoic strata in this area, it may be considered that the boundary between the sedimentary rocks and the igneous body is not deep, being less than several hundred metres from the surface even where the Palaeozoic formation is distributed extensively. The granite exposed at the southwestern side of Mt. Sekison (Fig. 2), seems to change its facies gradually into granite-porphyry or quartz-porphyry. Near the contact with the hornfels showing quartz spots, it becomes aplitic, and contains dark greenish biotite. On the contrary, in the granite-porphyry exposed at the northeastern side of the same mountain, coarse grained granite-like facies are observable. These granitic rocks such as granite, granite-porphyry, and quartz-porphyry seem to be mutually transitional though such outcrops that would clearly show the mutual transition among each rock facies could not be found. At the river bed, south of the tribe of Nagahatanakai, however, the quartz-porphyry comes into sharp contact with granite, and the blocks of the granite are included in the former (Fig. 5). And this quartz-porphyry gradually changes into granite-porphyry in its rock facies. The latter biotite-granite continues to the country rock of Keimei mine where the tiltmeter and extensometer were equipped after the earthquakes and also to the biotite-granite forming Mt. Nakayama. No conspicuous porphyritic crystals of perthite are recognizable in the granite, being compared with the granite exposed near Kusakyū, Nishi-ōashi. Topography indicated by the granite was discussed in the foregoing chapter. At the mine, fractures in the country rock, impregnation veinlets of quartz or aplite, in which minute frakes of molybdenite are often observable, are conspicuous. Besides the molybdenite, other minerals have been reported from this mine by K. Sakurai.[7] Such a pneumatolytic deposit of molybdenite or wolframite is not rare in the southern vicinity of this district.

As shown in an annexed geologic map (Fig. 2), quartz-porphyry forms a ridge represented by a triangulation point 527 m. On the northern and southern sides of the spot, destructive collapse of the rock took place at the time of the earthquake of 8:26 a. m. At the foot of the ridge, along the river side or at the bed of the River Namegawa, the quartz-porphyry is exposed. Above the quartz-porphyry, the highly silicified rocks which seem to have been derived from the slate or shale belonging to the Chichibu system, forms rocky cliffs. Rock fall occurred at several points along these cliffs. Granite-porphyry with regular columnar jointing is observable along the road, 1 km to the south of Numauchi, near the elementary school of Yamakubo. And this porphyry is overlained by the agglomeratic andesite flow at the joint of the road with the River Namegawa. Quartz-porphyry, liparitic rock and its pyroclastsics are recognizable at the bed of the River Namegawa near Shimokojiro and Itagabata. White tuffaceous rock including glassy breccias of liparite covered by Diluvial loam and other pumice beds is found at the western slope of Mt. Sekison, near the tribe of Itagabata. These rocks with such rock facies may be of the Tertiary age, though there are no palaeontological data. In this narrow area less than 1 km^2 near Itagabata, the rocks of various facies such as quartz-porphyry, liparite, white tuff breccia, etc., are associated and intermingled with each other. And the boundary between the Palaeozoic hornfels of Mt. Sekison and this acid igneous complex may be supposed as a fault, judging from the geographical

---

7) K. SAKURAI, *Our minerals* 9 (1940), 374-375. (in Japanese)

distribution of these rocks in this narrow area. From the above-mentioned observations, it may be allowed to say that these igneous rocks may be consangunious and that no remarkable chronological gap is to be supposed among them, though the mode of intrusion, eruption, and of deposition is quite complicated and must be cleared up by further study.

(3) Diluvium.

The essential member of the Diluvium distributed extensively in this district are, arranged from the older to the younger, the gravel of the flood plain of the ancient river of Daiya, the so-called loam, the reddish brown pumice bed called "Imaichi-zuchi", and the yellow pumice bed, called "Kanuma-zuchi." (Fig. 5). The gravel may be correlated to of that of the River Watarase and further to that of Musashino. And the loam continues to that of "Narita bed" distributed widely at the northern Kwantō Plain. Blocky partially auto-brecciated lava flow is continuously observable along the River Namegawa. The two pyroxene andesite varies in its appearance; porphyritic or non-porphyritic, dark grey or purplish, compact or slaggish, rich or poor in mafic phenocrysts, etc. The lava covers directly the Palaeozoic sandstone, granite-porphyry or quarth-porphyry at the southern margin of the Diluvial flood plain of the ancient River Daiya, but it is underlain as a whole by the Diluvial gravel of the same river. The lava is overlain by the successive beds of loam, Imaichi-zuchi, and Kanuma-zuchi, and the flow terminates at the cliff of Murose-namegawa. The present river Namegawa cuts down this lava, making it form the cliff of the valley along the river. It may be said, therefore, that the present shape of the valley indicates the topography due to erosion, not of the structural valley, even though the ancient river Daiya might had run through the valley formed by Tertiary or pre-Tertiary faulting. In the present stage of our knowledge, it may be said and may be denied at the same time that the great tectonic line passes through this valley. Waving and inclination of the beds of Kanuma and Imaichi soil, aeolian pumice deposits, show the olden relief of the surface in most cases, and never suggests crustal deformation. The slipping of these bed in the Pleistocene age are commonly observable along the scarp of the river terrace (Fig. 6). Of the changes of surface brought about remarkably on these Diluvial beds, the writer will make mention in the comming chapter (Chapter III).

(To be continued.)

27. 栃木縣今市町附近の地質 (その一)

地震研究所　森本良平

昭和24年12月26日の今市地震に際して調べた同地方の地質の概要を述べた. 地變の重要な原因の一つとなつた同地方に特有な洪積期浮石質堆積物の性質と地變の記述は第2報にゆづる.

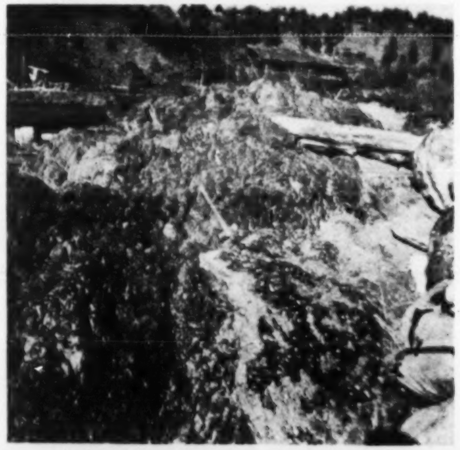

Fig. 3. Contact portion between porphyritic biotite-granite and Palaeozoic cherty hornfels. Oohara, Itaga village.

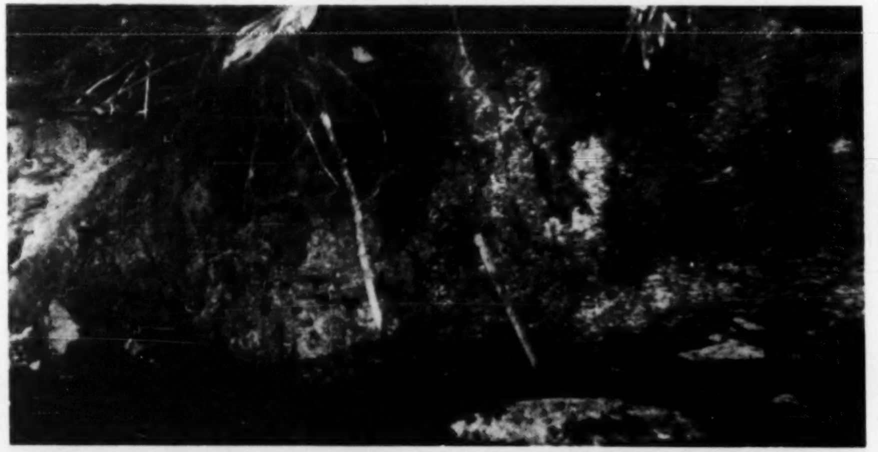

Fig. 4. Intrusion contact of quartz-porphyry into biotite-granite, Nagahata-nakai, Ochiai village.

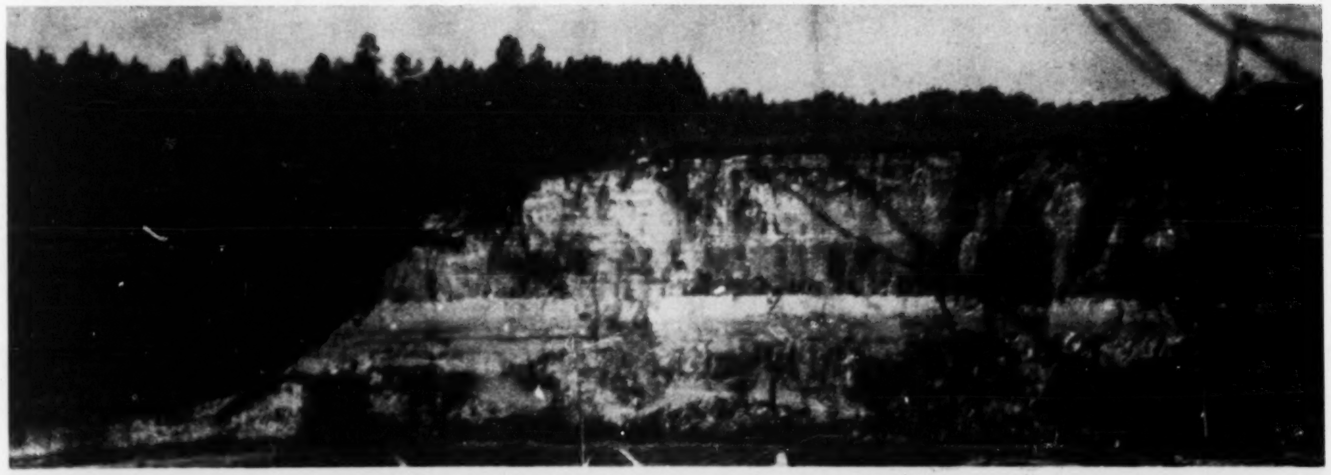

Fig. 5. Cliff showing the representative succession of the Diluvial beds. Collapsed cliff at Tashirouchi, east of Myojin, Ochiai village.

（震研彙報　第二十八號　圖版　森本）

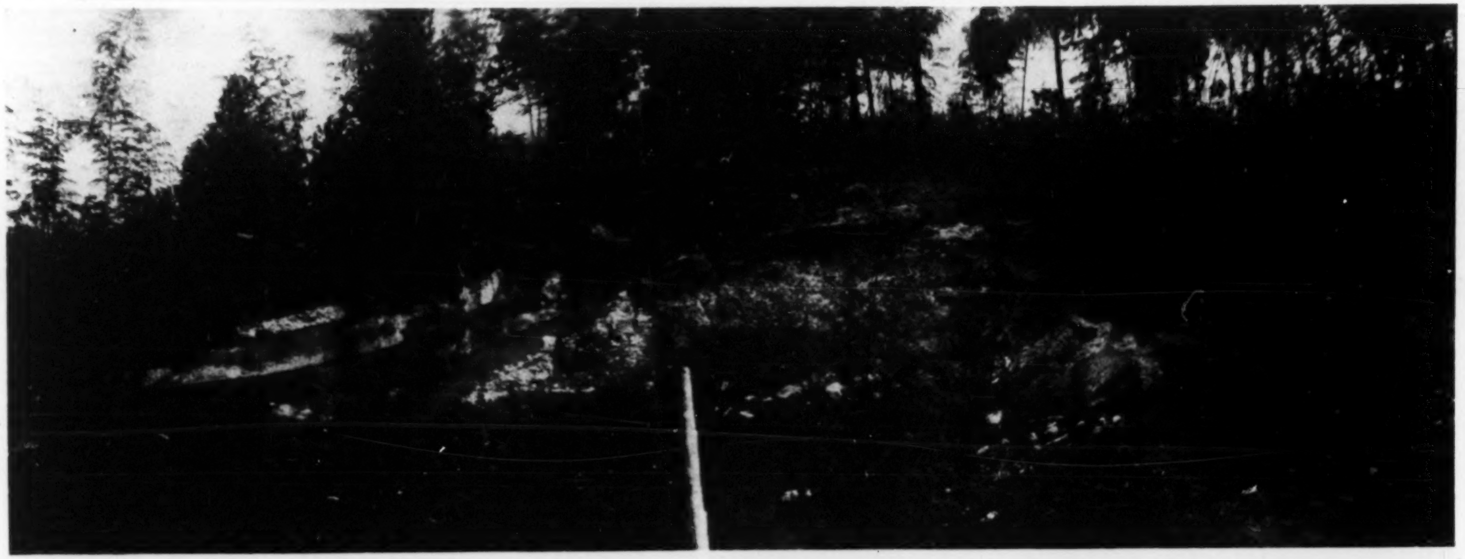

Fig. 6. Succession of the horizontal beds (right, facing the cliff) is clearly cut by the another succession of same order with a curved boundary line. Collapsed cliff at the east side of the River Namegawa, Murose-namegawa, Town of Imaichi (Cf. p. 385).

28. *Observation of Aftershocks Carried out in Imaichi District, Tochigi Prefecture.*

By the Earthquake Research Institute.

(Read Feb. 21 and Mar. 20, 1950.—Received Sept. 22, 1950.)

On the morning of December 26, 1949, a strong earthquake took place in the vicinity of Imaichi, Tochigi Prefecture, and considerable damage was caused in that area. The following day, the members of the Earthquake Research Institute hurried to the district with many instruments to set up a temporary seismological net-work there. Five points were chosen as the stations, that is, Funyū, Imaichi, Kanuma, Nikkō and Nishi-ōashi. Each station began its operation on Dec. 28, except Nishi-ōashi, where the observation was commenced on Dec. 31. The location of the stations and the instruments installed there are shown in Fig. 1 and Table I.

Table I. List of instruments installed at the stations and the period of observation.

Station	Constants of seismographs			The period of observation	
	Component	Natural period	Magnification	from	to
Funyū	E-W	0.1 sec.	187	Dec. 28, 1949	Jan. 10, 1950.
	N-S	0.1	187		
	U-D	0.1	206		
Imaichi	E-W	1	230	Dec. 28	Dec. 30
	E-W	6	30	Dec. 28	
	N-S	0.1	120		Jan. 10
Kanuma	E-W	6	30	Dec. 28	
	N-S	6	30		
	N-S	0.1	120		Jan. 8
Nikkō	E-W	6	30	Dec. 28	
	N-S	0.1	120		Jan. 28
Nishi-ōashi	E-W	1	230	Dec. 31	
	N-S	1	230		
	U-D	0.1	220		Jan. 6

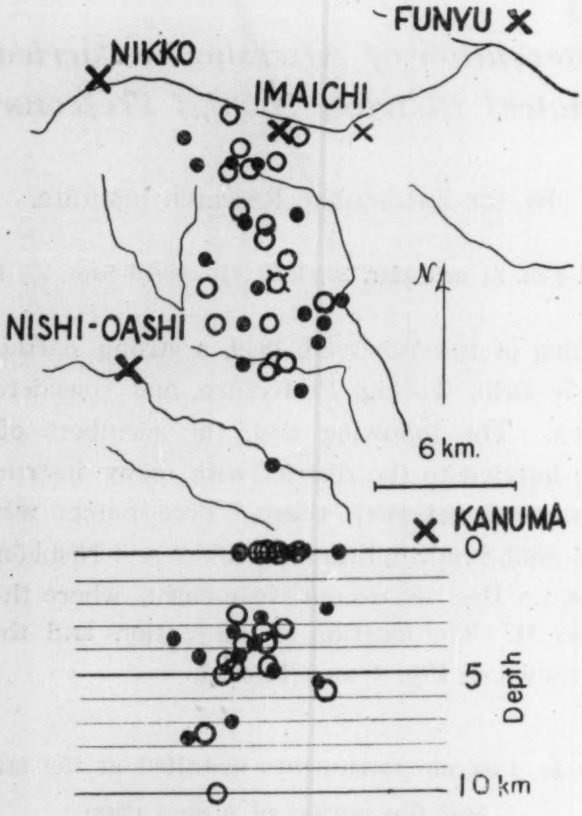

Fig. 1. Distribution of hypocenters.
○: Foci determined by P–S times obtained at four stations.
●: Foci determined by P–S times obtained at three stations.
×: Stations.

The earthquake was accompanied by so many aftershocks that some people in Imaichi could count more than 18 fairly strong earthquakes during the half an hour just following the main shock. Although our party missed the most active period following just after the main shock, with the seismographs brought there we could record many numbers of aftershocks in the earlier period of our observation. The aftershocks were recorded most frequently at the stations Imaichi and Nishi-ōashi, but not so often at station Kanuma, the most distant station from the damaged region. At station Nikkō we succeeded in catching a good number of shocks, and at station Funyū, in spite of its distant position, numbers of aftershocks were recorded with acceleration seismographs, which were twice as sensitive as those of the other stations. For instance, the daily number of aftershocks, recorded at stations Imaichi and Nikkō are given in Fig. 2, in which we numbered aftershocks whose maximum amplitudes exceed 2 mm on the record of the acceleration seismograph.

The aftershocks were distinguished by short P–S times (the name we gave

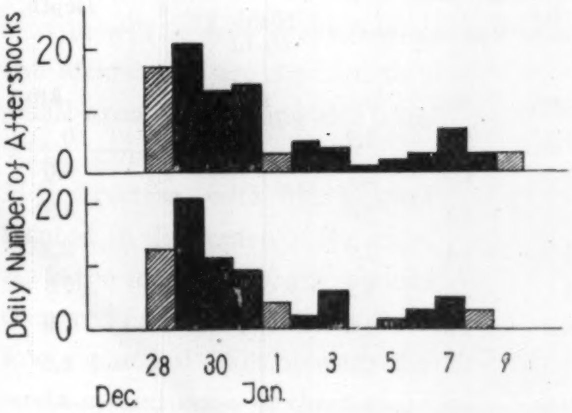

Fig. 2 Daily number of aftershocks.
Upper: Imaichi. Lower: Nikkō.

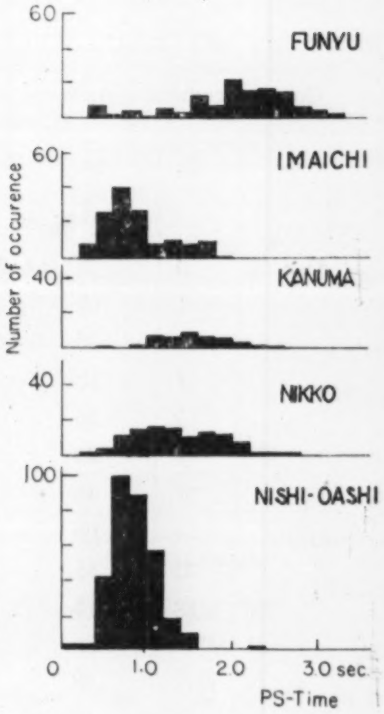

Fig. 3. Frequency distribution of P-S times.

to the duration time of preliminary tremor for the sake of convenience) and rapid vibration as may be seen in Fig. 5, and sometimes they were accompanied by earthsound. Frequency distribution of P-S times observed at our stations are shown in Fig. 3, in which we found that P-S times are quite short in general and even at station Kanuma, no P-S times exceeding 4 seconds were observed.

It was not always easy to find correspondence between seismograms obtained at different stations, because in such a case when very small aftershocks occurred frequently in the neighbourhood of a station, they could not be recorded at distant stations notwithstanding the remarkable amplitude recorded at the nearer station.

To determine the position of the hypocenters of the aftershocks, the ordinary method in which P-S time is used was employed. In this case, the first requisite is to evaluate k in the formula $D=kt$, in which D is the hypocentral distance, t the $P-S$ times, and k the constant. If we obtain $P-S$ times at four stations, we can calculate the value of k1). The data used for this purpose are shown in Table II. We adopted as the mean value of them 7.1±0.4, where the value of k was considered as free from focal depth

---

1) For instance, see T. HAGIWARA, *Bull. Earthq. Res. Inst.*, 18 (1940), 255.

Table II. List of the aftershocks, whose hypocenters have been determined.

Commencement time*)			*P—S* time					*k*	Depth
d.	h.	m.	Funyū	Imaichi	Kanuma	Nikkō	Nishi-ōashi		
			sec.	sec.	sec.	sec.	sec.		km
Dec. 29	0	36	2.2	1.0		1.9			0
	1	09	2.2	1.3	1.7	2.1		7.1	6.0
	1	36	3.1		1.2	2.6			4.9
	3	12		1.2	1.4	2.0			2.3
	5	39		1.2	2.8	1.3			7.8
	7	24		0.9	1.8	1.6			2.8
	22	45		1.5	1.5	2.2			5.5
	23	08		0.6	2.5	1.2			3.8
	23	41		1.1	2.2	1.4			4.4
30	18	17	2.0	0.8	2.4	1.2		7.5	5.2
31	0	38	2.5		1.8	1.8			4.6
	2	49	1.8	0.4		1.5			0
	18	49	2.2		2.0	1.7	1.1	6.1	0
	18	52	2.3		1.9	1.8	1.1	6.9	4.9
	20	46	2.5		1.1		1.0		0
Jan. 1	12	37	1.8	0.7	2.6	1.0		7.7	4.8
2	0	23	2.6	1.4			0.7		0
	1	37	2.9	1.8	2.2	2.1		7.3	10.0
	6	07	1.8	0.5	1.9	1.2	1.2	7.8	3.3
	18	53	1.8	0.6		1.1	1.4	7.6	4.0
	19	17	2.0	0.5		1.1	1.6	6.6	2.7
	19	51		1.0		2.0	1.3		0
	23	30	2.9	1.6	1.5		0.9	6.2	0
	23	59	2.0		2.0	1.4	1.1	7.1	0
3	11	44		1.5	1.5	2.2	1.1	6.6	3.3
	15	36	1.6	0.5	2.2	1.2	1.3	7.8	4.4
	15	38		0.8		0.8	1.5		3.9
	15	46	1.9	0.8		1.2	1.2	8.0	5.0
	23	36	2.5	1.2	1.7	1.9		6.8	3.9
6	6	06		0.7	2.2	1.3			3.3
	8	31	1.5	0.2	2.5	1.2	1.6	7.2	0
7	17	59	2.2	1.1		1.4			7.2
	19	25	2.8	1.4	1.4	2.1		6.5	0
8	3	34	2.6	1.4	2.2	1.7		7.3	7.9

Mean value of $k = 7.1 \pm 0.4$

*) For commencement times the date at Funyū were adopted, in most cases.

(Fig. 4). After *k* was evaluated, the hypocenters can be determined by $P-S$ times obtained at only three stations. Fig. 1 shows the epicentral distribution determined by the above method.

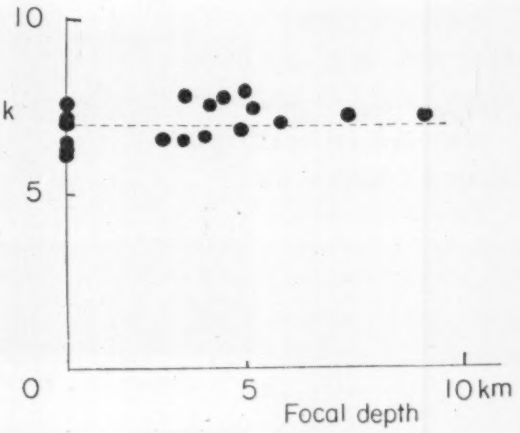

Fig 4. Valued of constant "*k*."

As will be seen in the figure, the aftershocks are confined to a small area, 15 km long and 6 km wide, somewhat elongated in the N-S direction, with Mt. Keimei located in the centre of the area. As to the focal depth, aftershocks occurred most frequently in shallower place, 0–5 km beneath the surface, and none of them could be found in depth exceeding 10 km. In Fig. 1, the hypocenters are projected on a vertical plane, and we find in the figure that the aftershocks with large focal depth are generated, in some measure, in the western side of the region.

Shifting of seismic active area with the lapse of time, which was often discussed in the studies on the characters of seismic activity, could not be seen in the present case. The push-pull distribution of the initial motion will be described in a separate paper.[2]

Concluding Remarks.

The outlines of the observation of aftershocks carried out in the Imaichi district were reported in this peper. More details related to the characters of aftershocks observed at each station, will be reported in separate papers, by the persons in charge of that station.

The present observation owes much to many persons who cooperated with the members in carrying out the work, and the authors wish to express their hearty thanks to all of them.

In conclusion, the members of the party are listed as follows:
(Station Funyū) S. Miyamura, T. Akima and T. Chigira,
(Station Imaichi) T. Hagiwara, T. Rikitake and K. Kasahara,
(Station Kanuma) F. Kishinouye, and R. Ikegami,
(Station Nikkō) K. Kanai, T. Tanaka and T. Suzuki,
(Station Nishi-ōashi) S. Omote and T. Fukuda.

---

2) T. HAGIWARA and K. KASAHARA, *Bull. Earthq. Res. Inst.*, 28 (1950), 393.

28. 今市地震餘震觀測報告

地震研究所

今市地震発生直後より約2週間に亘り，同地方において餘震の出張觀測が行われた．觀測點には船生，今市，鹿沼，日光及び西大芦が選ばれ，研究室單位に各々一點の業務を擔當したが，こゝに報告するのはその一般的な結果である．

震源の決定された餘震は期間中に34を数えたが，今回の餘震は極めて地表近く且局限された區域内に多く起つている模樣で，その中心は落合村の鶏鳴山附近と推定される．

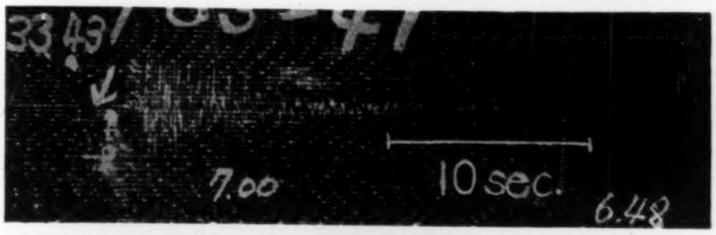

Earthquake of 3h34m,
Jan. 8, 1950.
(1.2× the actual)

Funyū, Acceleration seismograph, *N*—*S* Component.

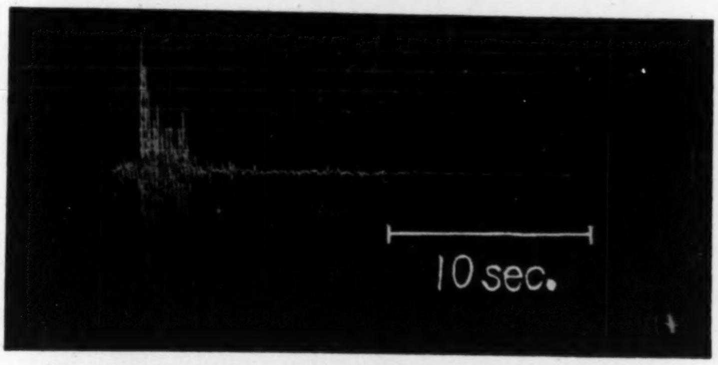

ibid.
(2.4× the actual)

Imaichi, Acceleration seismograph, *N*—*S* Component.

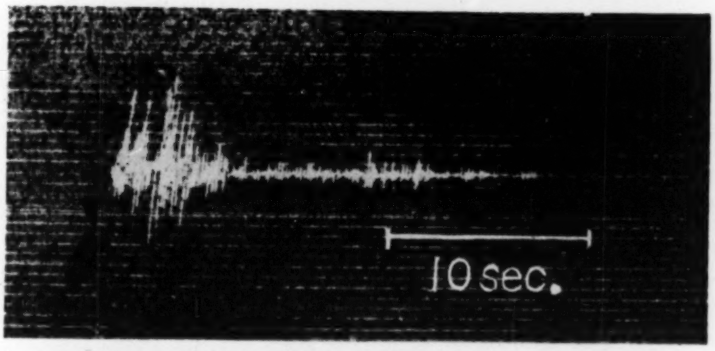

ibid.
(2.4× the actual)

Kanuma, Acceleration seismograph, *N*—*S* Component.

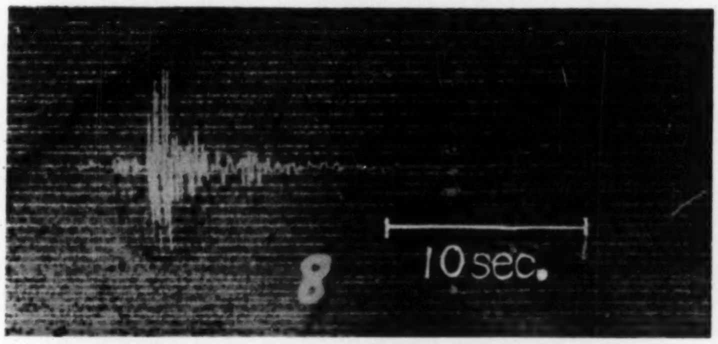

ibid.
(2.4× the actual)

Nikkō, Acceleration seismograph, *N*—*S* Component.

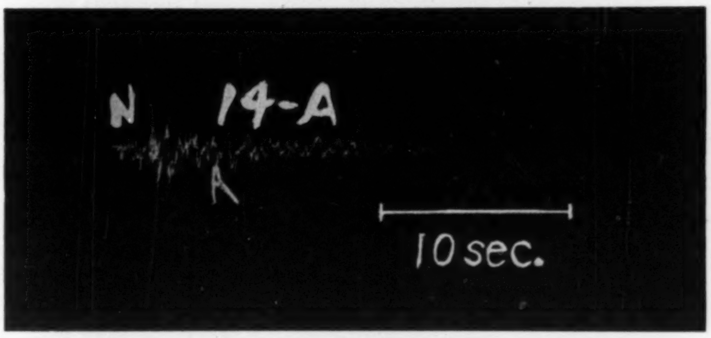

Earthquake of 8h31m.
Jan. 6, 1950.
(2.4× the actual)

Nishi-ōashi, Displacement seismograph, *N*—*S* Component.

29. *On Aftershocks Accompanied the Imaichi Earthquake, December 26, 1949.*

By Takahiro HAGIWARA and Keiichi KASAHARA,

Earthquake Research Institute.

(Read Jun. 20, 1950 – Received Sept. 22, 1950.)

Following the occurrence of the Imaichi Earthquake, December 26, 1949, the members of the institute hurried to the Imaichi district and set up a network of seismological stations temporarily to study the aftershocks. The observation was continued for about half a month and closed on January 8, as has been reported in the previous paper. After these stations were closed, the present authors attempted to continue the observation in a reduced scale for some long interval of time, because, in an observatory temporarily set up in the Keimei mines, Ochiai village, the observation of extension and inclination of the earth's crust had just commenced at that time,[1] and besides, the activity of aftershocks was not so diminished yet. New seismological stations were set up at three points, Imaichi, Nikkō and Ochiai and the observations commenced on Jan. 10, 1950. Among them, for the station of Nikkō the older

Table I. List of seismographs installed at the stations and the period of observation.

Station	Constants of seismographs			The period of observation	
	Component	Naturl period	Magnification	from	to
		sec.			
Imaichi *)	E-W **)	6	30	Jan. 10,	
	N-S	0.1	120	1950	——
Nikkō	E-W	6	30	Jan. 10,	Mar. 20,
	N-S	0.1	120	1950	1950
Ochiai	E-W	1	230	ibid.	
	N-S	0.1	120		
	N-S	1	230		
	U-D	0.1	220		

*) The station is about 2 km apart from the old station of Imaichi.
**) This has been exchanged for an acceleration seismograph, afterwards.

---

[1] T. HAGIWARA and T. RIKITAKE, *Bull. Earthq. Res. Inst.*, 28 (1950), 435.

station was appropriated but the other two were newly constructed. Two months after the stations of Nikkō and Ochiai were closed on Mar. 20, while, the station of Imaichi, alone, was kept intact and is still operating. The position and the instruments of each station are respectively shown in Fig. 1 and Table I.

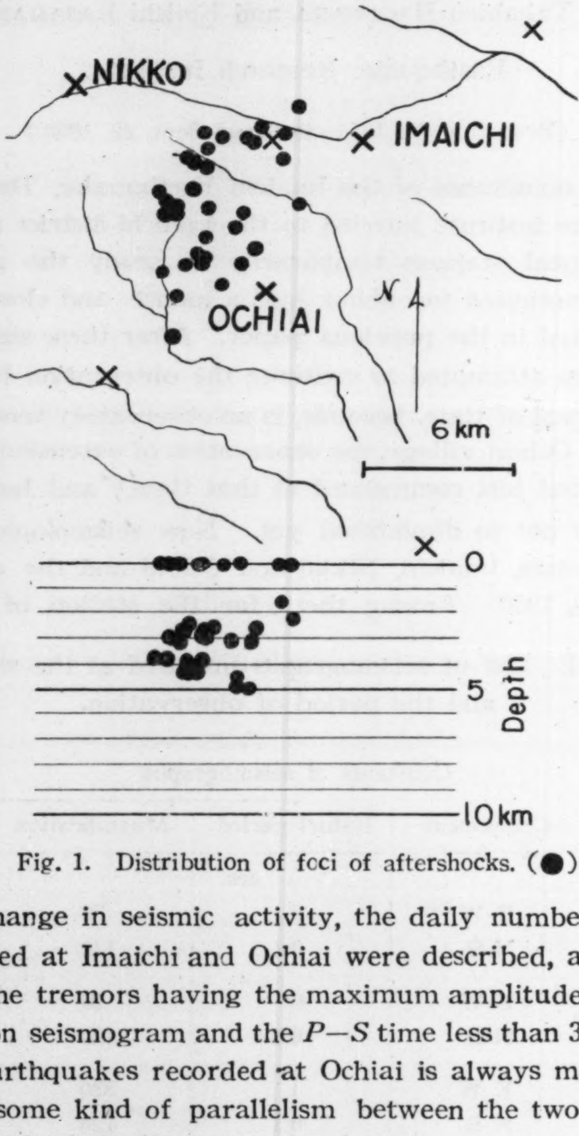

Fig. 1. Distribution of foci of aftershocks. (●)

To see the change in seismic activity, the daily number of occurrence of aftershocks counted at Imaichi and Ochiai were described, as shown in Fig. 2, with respect to the tremors having the maximum amplitude larger than 2 mm on the acceleration seismogram and the $P-S$ time less than 3 seconds. Though the number of earthquakes recorded at Ochiai is always much greater than that of Imaichi, some kind of parallelism between the two curves is clearly seen in the figure, both declining day by day.

Some examples of records of each station are shown in Fig. 7. The frequency distribution of $P-S$ times of the aftershocks observed in the above mentioned interval are shown in Fig. 3. In general, $P-S$ times are small in each station, and even in Nikkō which is considered to be far away from the seismic active center, we find no $P-S$ times exceeding 2 seconds.

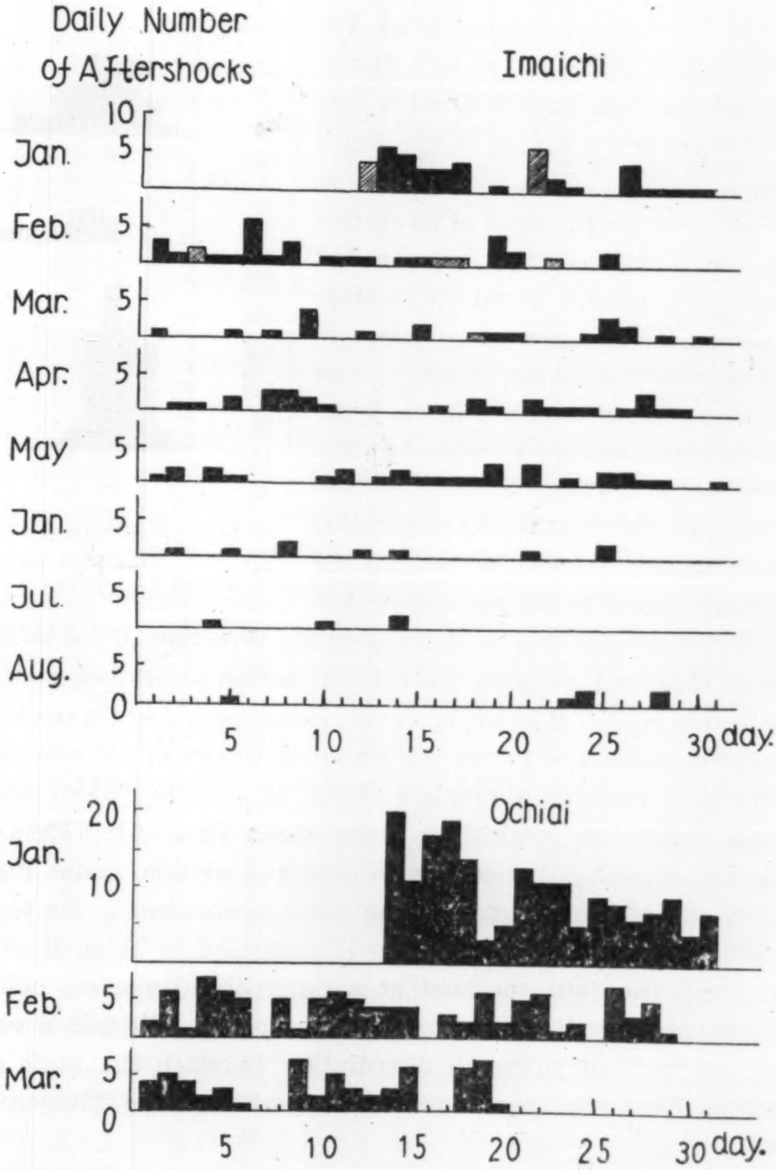

Fig. 2.

When the $P-S$ times of an aftershock are determined at three stations, we can determine its hypocenter. In this case, we need to know the value of k the constant of the so-called Ōmori's formula $D=kt$, where D is the hypocentral distance, t the $P-S$ times, k a constant. To serve this purpose, we can use the result of the preceding seismic net-work, in which k was determined to be 7,1. During the observation period, 33 aftershocks were available for the procedure and their hypocenters thus determined are shown in Table

II and Fig. 1 together with their commencement-times and *P—S* times. Comparing the epicentral distribution of this period with that of the preceding period, it is quite noticeable that there is no epicenter in the region to the south of the station of Ochiai. This fact, however, may be attributed to the presence of no station to the south. As a matter of fact, we can find a similar tendency in the epicentral distribution of the first period if we neglect the data obtained at the southern stations, Kanuma and Nishi-ōashi. The general tendency in the hypocentral distributions, therefore, may be considered to be approximately the same in both periods, except that the aftershocks originating in deeper position, say 10 km or so beneath the surface, were not found in the present period.

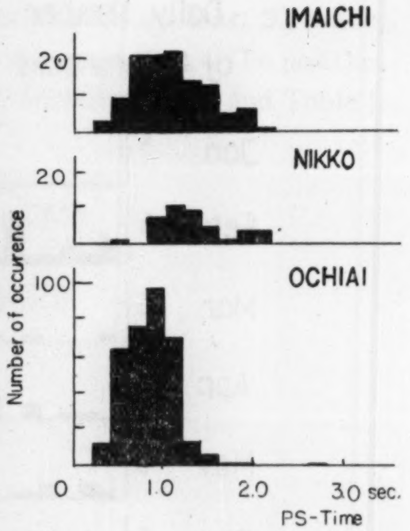

Fig. 3. Frequency distribution of *P-S* times.

It was not always possible to determine the direction of initial motion of the aftershocks observed, because the seismic motion sometimes commenced in a quite complicated mode. We can, however, recognize a certain tendency in the direction of initial motion at every station. For instance, the seismic motion seems to commence towards the origin (pull) at station Nikkō and Ochiai, but backwards (push) at Imaichi, in most cases (Fig. 4). Thus we may presume a mode of push-pull distribution of initial motion, under the assumption that every aftershock occur with the same mechanism.[2] As to the main shock, the mode of push-pull distribution is presumed to be such as is shown in Fig. 5, in which the data obtained at various observatories, belonging to the Central Meteorological Observatory, were plotted. We find a remarkable difference in the mode of push-pull distribution between the main shock and the aftershocks. However, more detailed discussion on the phenomenon will be postponed.

We consider, in the next step, frequencies of the time interval of occurrence of aftershocks. From the view-point of the theory of random walk, some investigators have tried to study the time interval of occurrence with regard to ordinary or volcanic earthquakes,[3] but not with regard to aftershocks

---

[2] T. HAGIWARA, S. MURAUCHI and J. YAMADA, Special Report of the Earthq. Res. Inst., No. 5 (1947), 164.

[3] F. KISHINOUYE and H. KAWASUMI, *Bull. Earthq. Res. Inst.*, 4 (1928), 75.
S. YAMAGUTI, *Bull. Earthq. Res. Inst.*, 11 (1933), 46; *ibid.*, 14 (1936), 399.
S. WATANABE, "*Riken-iho,*" 15 (1936), 1083.

Table II. List of the aftershocks, whose hypocenters have been determined.

Commencement time			*P—S* time			Depth
d.	h	m.	Nikkō	Imaichi	Ochiai	
Jan.			sec.	sec.	sec.	km
10	6	00	1.4	0.5	0.9	0
	6	07	1.4	0.6	1.1	1.7
12	21	39	1.1	0.7	1.0	0
14	12	18	1.3	1.7	0.8	0
17	10	27	1.1	1.3	1.3	4.0
	16	49	1.2	1.1	0.8	0
21	17	34	1.6	1.5	1.0	4.5
	19	04	1.6	1.5	0.9	4.0
	23	05	0.9	1.0	1.2	0
22	15	04	1.6	1.6	1.0	4.3
23	0	01	1.5	1.1	0.7	3.1
	21	48	0.9	1.2	0.8	0
26	7	19	1.1	1.3	0.9	0
	21	50	1.3	0.9	1.2	3.2
28	19	32	1.2	1.5	1.2	3.8
Feb.						
2	17	12	1.4	1.3	0.9	2.9
5	15	21	1.8	1.3	0.9	4.9
6	5	12	1.1	1.1	1.1	2.7
7	0	15	1.6	1.6	0.8	0
	18	12	1.3	0.8	1.2	2.7
10	2	07	1.6	1.2	1.0	4.7
	5	35	1.1	1.2	1.0	2.5
11	5	23	1.9	1.9	1.0	3.0
16	22	55	1.6	1.5	1.0	4.5
19	2	38	1.2	0.3	1.1	0
25	19	24	1.7	0.7	0.7	2.2
Mar.						
9	3	14	1.1	1.0	1.2	2.6
	22	25	1.6	1.4	0.4	0
11	0	16	1.1	1.1	1.2	3.1
12	12	54	1.8	1.4	0.9	5.0
15	3	23	1.0	1.2	1.2	2.7
18	21	46	1.1	1.5	1.3	3.9
19	13	13	1.2	1.4	1.1	3.2

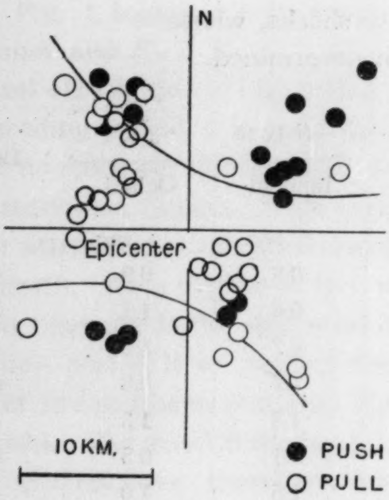

Fig. 4.

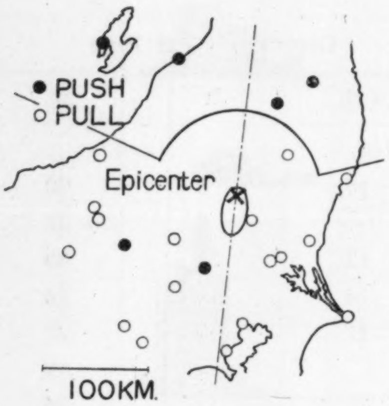

Fig. 5.

occurring in a limited region. The authors took as material the time intervals between two adjoining aftershocks observed at station Ochiai with an acceleration seismograph during the period from Jan. 14 to 23. In those days, about three weeks after the occurrence of the main shock, seismic activity was diminished to a certain extent and the activity could be approximately considered as stationary.

Aftershocks were observed 193 times, during the total observation time which amounts to 12044 minutes (about 8 days), and consequently the mean interval of occurrence Θ4) was determined to be 62.4 minutes. According to the theory of statistics, the probability of the time interval of two adjoining aftershocks lying between the interval $t_n \sim t_{n+1}$ is given as follows:

$$\int_{t_n}^{t_{n+1}} \psi(t)\,dt = e^{-ct_n} - e^{-ct_{n+1}}, \quad \text{where } c = \frac{1}{\Theta},$$

provided every aftershock occurs completely at random.

Now, taking the time interval $t_n \sim t_{n+1}$ as 10 minutes and calculating the probability, we obtain Table III and Fig. 6, where the observed frequencies are also shown. It is noticeable in the figure that the observed line is similar to the calculated one for large values of t, but when t is less than 10 minutes the former is far higher than the latter. The reuslt seems to suggest that the present group of aftershocks occurs rather successively than entirely at random, though the quantity of the material is not large enough to ascertain the conclusion.

---

4) R. FÜRTH, Schwankungserscheinungen, S. 35.

Table III. Relation between time intervals and number of occurrence.

Time interval	Number of occurrene	
	Obs.	Calc.
min.		
0—9	47	29
10—19	24	24
20—29	17	21
30—39	11	18
40—49	12	15
50—59	11	13
60—69	10	12
70—79	10	11
80—89	6	10
90—99	5	10
100—	39	30

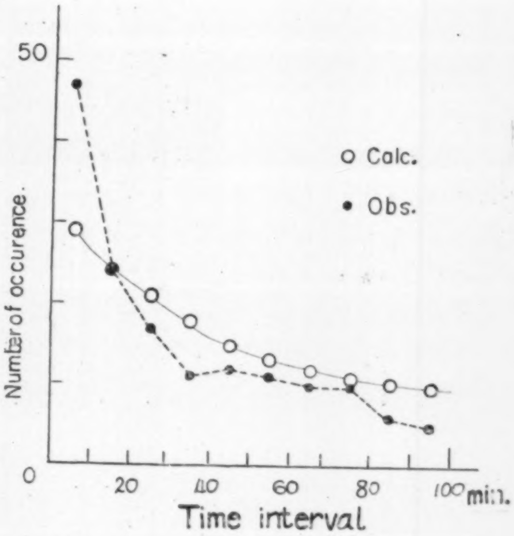

Fig. 6.

The tendency is, however, confirmed only for the present aftershocks, observed by a portable acceleration seismograph. It will be interest to examine whether the similar tendency is found or not in case of another great earthquake.

Summary and acknowledgement.

In the present paper the authors reported the result of the observation of aftershocks which accompanied the Imaichi Earthquake, during the period following the first observation carried out by the party of our Institute. It was found out that the distribution of hypocenters did not differ materially from that in the preceding period, and the general characteristics of aftershcoks during the two preriods were almost the same.

The character of the occurence of aftershocks was also examined from the view-point of the theory of random walk, and some successivity in their occurrence was concluded. According to the data obtained at the station of Imaichi, where the observation is still going on, seismic activity degenerated considerably since June, but a number of aftershocks were sometimes counted as before.

In conclusion, the authors' thanks are extended to J. Yamada and M. Watanabe for their as istance in operating the Ochiai station, and also to Mr. Y. Mori and Mr. T. Honda for their cooperation with the authors in constructing and maintaining the stations at Imaichi and Nikkō.

29. 今市地震の餘震

地震研究所 萩原尊禮
笠原慶一

前記共同觀測の後をうけて，筆者等は今市，日光，落合の三觀測所を３月下旬まで維持したが，その結果によると，餘震は依然，共同觀測期間中と同一の地域内に發生している模樣である．觀測所のうち，今市のそれは引續き現在まで觀測を行つており，餘震活動が次第に減衰してゆく狀況を見ることができる．

なお，報告中，落合で得られた資料につき，統計現象論的な立場から簡單な考察を行つて見たが，その結果では，餘震の發生の仕方に若干續發的な傾向が認められた．

Fig. 7. The earthquake of 2h38m, Feb. 19, 1950.

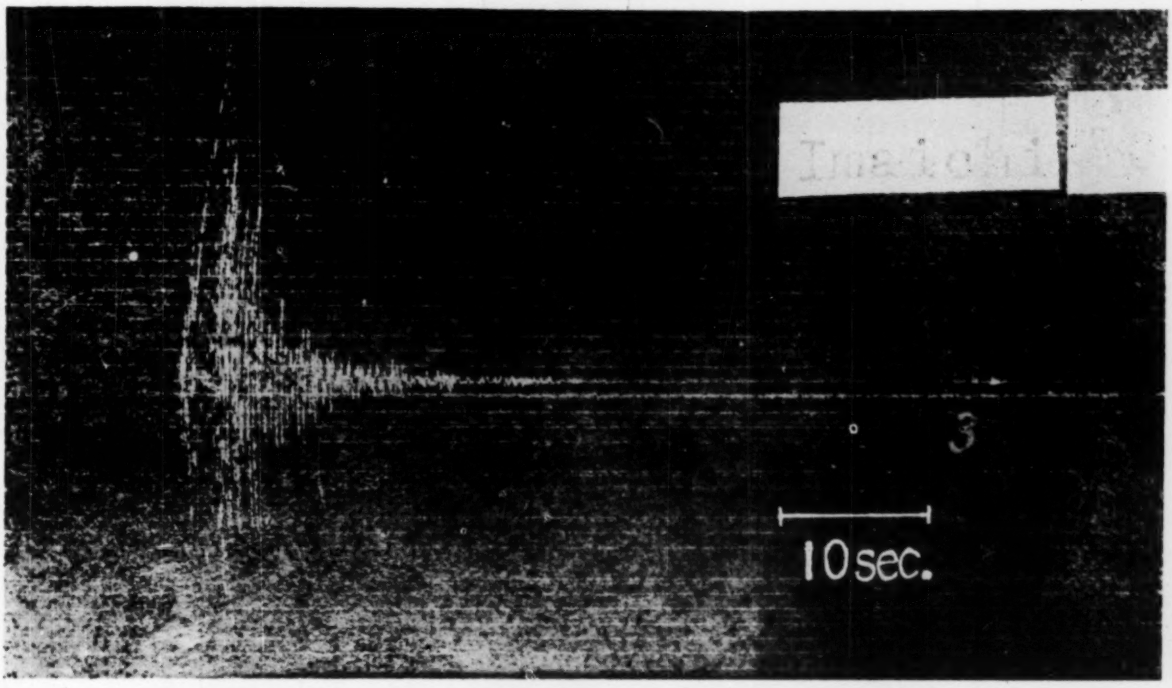

Imaichi, Acceleration seismograph (*N*—*S*). (1.7× the actual)

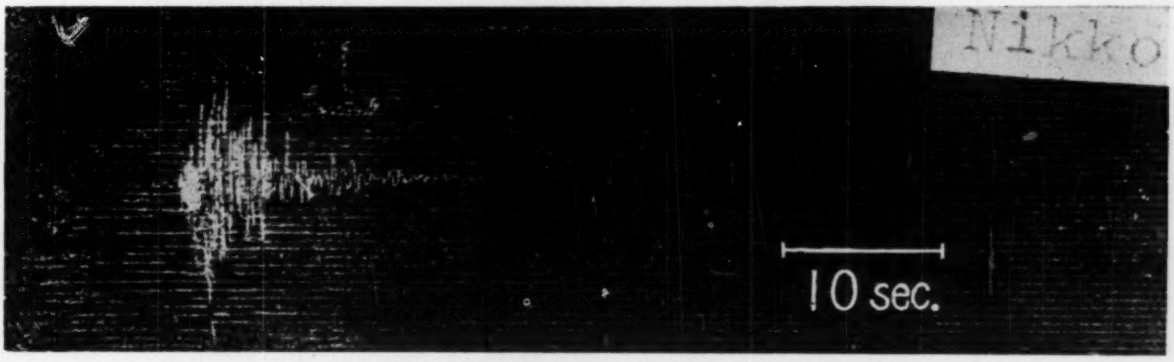

Nikkō, Acceleration seismograph (*N*—*S*). (1.7× the actual)

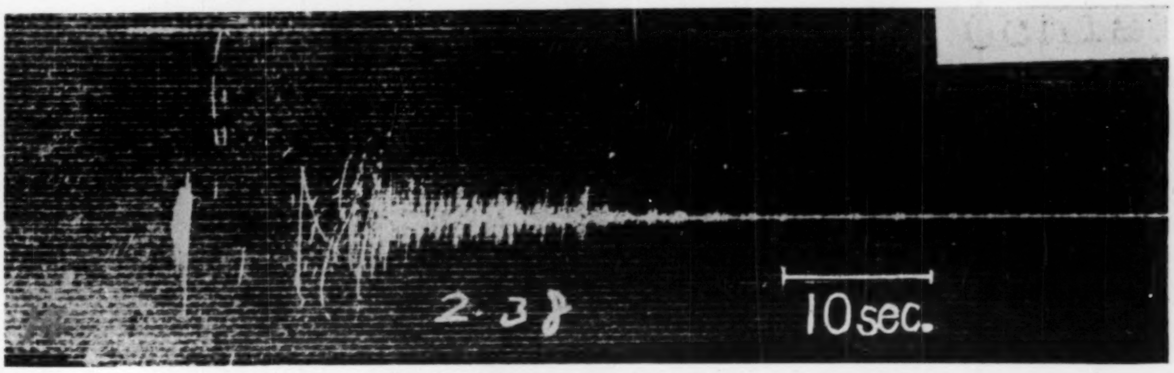

Ochiai, Acceleration seismograph (*N*—*S*). (1.7× the actual)

（震研彙報 第二十八號 圖版 萩原・笠原）

30. Aftershocks of Imaichi Earthquake Observed at Nishi-oashi Station.

By Syun'itiro OMOTE,

Earthquake Research Institute.

(Read Sep. 17, 1950—Received Sep. 20, 1950).

1. Introduction.

The Imaichi earthquake that shook the northern part of the Kwanto District on Dec. 26, 1949, was followed by a fairly large number of aftershocks. For the purpose of observing these aftershocks a temporary network of seismic stations was established soon after the main shock. These stations were Imaichi, Nikko, Funyu, Kanuma and Nishi-oashi, and at the last named station the author installed two seismometers of horizontal components and one of vertical component and carried out the registration of aftershocks in terms of three components of seismographs. In the former studies on aftershocks, such as those of Tango,[1] Tottori,[2] Fukui[3] and even of this Imaichi earthquake,[4] the location of foci was made entirely by the so-called "difference time method"[5] of three or four stations. The distribution of the foci of Imaichi aftershocks is discussed in another article[4] in this same bulletin. The number of shocks whose foci were located and reported on in that article in the period from Dec. 29 to Jan. 8 was 21 or so. In the case of the present observation, however, highly sensitive horizontal motion seismometers were installed at Nishi-oashi Station, and by the aid of a vertical motion seismometer, we were able to locate the foci of some one hundred aftershocks from the data obtained at the single station, Nishi-oashi, the result of which study will form the subject of the present article.

2. The Observations at Nishi-oashi Station.

The observation of afterocks at Nishi-oashi Station began on Dec. 31 and continued until Jan. 6 of the next year. The instrumental constants of the seismographs used then are listed in Table I.

---

[1] N. NASU, *Jour. Fac. Sci. Tokyo. Univ.*, 3 (1929), 29.
[2] S. OMOTE, *Bull. Earthq. Res. Inst.*, 22 (1944), 33.
[3] S. OMOTE, *Rep. Fukui Earthq.*, (1950, Tokyo), 37.
[4] EARTHQ. RES. INST., *Bull. Earthq. Res. Inst.*, 28 (1950), 387.
[5] BULLEN, "Introduction to the Theory of Seismology." 1924, (London).

Table I.

Type	Component	Period sec.	Weight kg.	Geomtrical magnification	Damping ratio
Displacement seismograph	Horizontal	1.0	50	235	8 : 1
Acceleration seismograph	Vertical	0.1	25	165	8 : 1

As soon as observations were started at Nishi-oashi we noticed that shocks of short *P—S* times were recorded frequently here and that these near shocks had energy large enough to give distinct beginnings to the records of the first motions. Some examples of these seismograms will be reproduced in the Plate. Daily numbers of shocks recorded at the Nishi-oashi Station and the frequency distribution of *P—S* times of these aftershocks will be seen in Figs. 1 and 2.

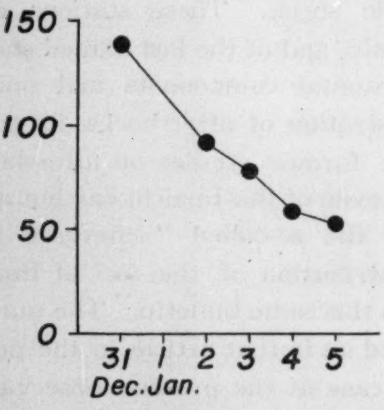

Fig. 1. Daily numbers of recorded shocks at Nishi-oashi.

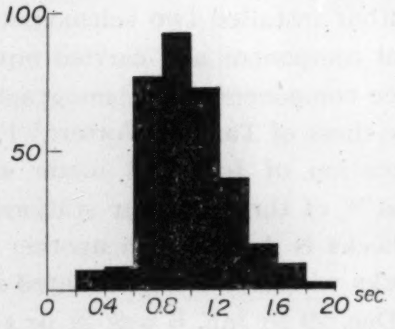

Fig. 2. Frequency diagram of *P—S* times.

The amplitudes of the first maximums of the respective shocks were read from the seismograms and are tabulated in Table II. The direction of the epicenter from the station was obtained by compounding the amplitudes of the first waves of *P* on the *E—W* and *N—S* component seismograms as vectors. The focal distance was computed from the *P—S* intervals observed at the station, the Omori constant k being given the value $k=7.1$ according to the result computed in the study of Imaichi aftershocks by the difference time method. In order to examine the accuracy of the epicenters determined by this single station method, we compared them with the epicenters of the same aftershocks determined by the difference time method. In Fig. 3 the foci of seven shocks obtained by these two different methods are compared. Open circles in Fig. 3 represent the foci located by the difference time method, and black dots those located by the single station method. Figures attached to

Table II.

Earthq. No.	Commencement time.			Trace amplitude of initial motion. (× 1/20 mm)			*P—S* time	Period of initial motion.		α	β	θ
	d	h	m	E-W	N-S	U-D	sec.	T_V sec.	T_H sec.			
1	31	12	16	− 1.0	+ 3.5	− 9.0	0.8	0.12	0.36	0.08	0.59	1°40′
2		12	33	+ 6.5	+ 13.0	− 6.0	1.2	0.04	0.12	0.55	0.84	40°55′
3		13	02	− 3.5	− 1.0	− 1.0	0.9	0.08	0.24	0.22	0.72	19°20′
4		15	31	− 5.0	− 8.5	+ 4.0	1.4	0.05	0.15	0.43	0.83	34°46′
5		15	49	+ 9.0	+ 9.0	− 11.5	1.7	0.08	0.24	0.22	0.72	10°06′
6		16	04	+ 10.0	+ 6.0	− 10.5	0.9	0.08	0.24	0.22	0.72	10°29′
7		17	52	+ 9.0	+ 1.0	− 11.0	1.0	0.08	0.24	0.22	0.72	8°07′
8		18	57	+ 18.0	+ 15.0	− 2.5	1.1	0.11	0.33	0.12	0.62	51°11′
9		22	25	− 3.0	− 2.0	− 1.0	1.1	0.04	0.12	0.55	0.84	53°21′
10		23	08	+ 2.0	− 4.0	− 2.0	0.9	0.06	0.18	0.37	0.78	33°30′
11		23	43	+ 8.0	+ 7.0	− 18.5	0.8	0.08	0.24	0.22	0.72	5°29′
12	1	0	11	+ 2.0	− 1.5	− 1.5	0.7	0.08	0.24	0.22	0.72	15°28′
13		0	13	+ 17.0	− 19.5	− 13.0		0.06	0.18	0.37	0.78	30°16′
14		0	34	− 6.5	− 6.5	+ 5.0	1.2	0.06	0.18	0.37	0.78	28°21′
15		0	37	+ 19.0	+ 3.5	− 7.0	1.4	0.08	0.24	0.22	0.72	24°42′
16		0	51	+ 2.0	+ 3.5	− 2.0	1.2	0.06	0.18	0.37	0.78	30°21′
17		0	54	− 4.5	− 7.5	+ 7.5	1.3	0.04	0.12	0.55	0.84	22°35′
18		1	07	+ 3.5	− 1.5	+ 5.0	1.3	0.08	0.24	0.22	0.72	7°14′
19		1	11	− 3.0	− 2.0	+ 2.5	1.2	0.04	0.12	0.55	0.84	27°03′
20		1	11	+ 2.0	− 6.0	+ 7.5	1.3	0.04	0.12	0.55	0.84	16°22′
21		16	35	− 2.5	− 3.0	+ 4.5	1.2	0.06	0.18	0.37	0.78	14°08′
22		16	50	− 2.0	− 1.5	+ 3.0	1.0	0.02	0.08	0.67	0.88	18°54′
23		17	08	+ 2.5	+ 2.0	− 2.0	0.8	0.06	0.18	0.37	0.78	25°06′
24		17	54	− 2.5	− 2.5	+ 5.5	0.7	0.04	0.12	0.55	0.84	12°42′
25		18	15	+ 2.0	+ 1.5	− 3.5	0.9	0.08	0.24	0.22	0.72	6°49′
26		19	08	+ 20.0	+ 13.0	− 7.0	0.9	0.10	0.30	0.13	0.65	2°24′
27		20	18	− 4.0	+ 3.0	− 3.0	0.9	0.04	0.12	0.55	0.84	30°35′
28		22	00	− 2.0	− 2.0	+ 2.0	1.2	0.04	0.12	0.55	0.84	26°22′
29		22	17	− 3.5	− 1.5	+ 6.0	1.1	0.08	0.24	0.22	0.72	6°02′
30	2	0	19	− 6.0	− 2.0	− 94.0		0.12	0.36	0.08	0.59	2°48′
31		1	37	+ 332.0	+ 440.0	− 112.0	1.6	0.10	0.13	0.05		19°10′
32		2	07	+ 2.0	+ 1.0	− 3.5	0.9	0.04	0.12	0.55	0.84	12°29′
33		2	14	− 3.0	− 3.0	+ 2.0	1.5	0.08	0.24	0.22	0.72	19°49′
34		3	38	− 1.5	− 1.0	+ 2.0	1.2	0.01	0.03	0.83	0.95	23°03′
35		3	50	− 2.0	− 2.0	+ 2.0	1.2	0.06	0.18	0.37	0.78	22°19′

(to be continued)

(continued)

Earthq. No.	Commencement time. d	h	m	Trace amplitude of initial motion. (× 1/20 mm) E-W	N-S	U-D	P—S time sec.	Period of initial motion. T_V sec.	T_H sec.	α	β	θ
36		3	57	− 2.0	− 2.5	− 0.5	1.2	0.04	0.12	0.55	0.84	10°38′
37		10	50	+ 7.0	0	− 3.0	1.0	0.09	0.27	0.17	0.68	17°21′
38		11	10	+ 1.5	− 2.0	− 2.0	0.4	0.04	0.12	0.55	0.84	24°12′
39		12	14	− 1.0	− 1.5	+ 4.0	0.6	0.04	0.12	0.55	0.84	9°04′
40		13	43	− 2.0	+ 1.5	− 1.0	0.8	0.08	0.24	0.22	0.72	11°59′
41		15	11	+ 16.0	+ 6.0	− 11.5	1.0	0.04	0.12	0.55	0.84	27°47′
42		15	50	− 6.0	− 6.0	+ 9.0	1.1	0.08	0.24	0.22	0.72	8°52′
43		16	30	+ 2.5	+ 1.0	− 2.0	0.8	0.06	0.18	0.37	0.78	21°31′
44		18	43	− 5.5	− 7.5	+ 3.0	1.4	0.07	0.23	0.30	0.73	27°55′
45		18	52	+ 1.0	+ 2.5	− 1.0	1.7	0.06	0.18	0.37	0.78	38°30′
46		19	23	+ 24.0	+ 8.5	− 10.5	1.3	0.08	0.24	0.22	0.72	33°30′
47		20	02	+ 2.0	− 1.0	+ 1.0	1.2	0.06	0.18	0.37	0.78	18°10′
48		20	32	+ 23.5	0	− 10.0	1.3	0.08	0.24	0.22	0.72	21°26′
49		20	54	+ 2.0	+ 3.5	+ 1.0	1.4	0.04	0.12	0.55	0.84	57°31′
50		21	18	− 7.0	− 6.5	+ 5.0	1.2	0.10	0.30	0.13	0.65	11°42′
51		23	53	− 12.0	− 42.0	+ 21.0		0.08	0.24	0.22	0.72	19°15′
52	3	6	15	− 1.5	− 4.0	+ 3.5	1.3	0.04	0.12	0.55	0.84	23°34′
53		7	27	− 4.0	− 3.0	+ 6.5	0.8	0.06	0.18	0.37	0.78	12°43′
54		8	27	+ 15.0	+ 10.0	− 7.5	0.6	0.08	0.24	0.22	0.72	21°50′
55		9	33	− 1.5	− 2.0	+ 3.0	1.0	0.04	0.12	0.55	0.84	16°24′
56		12	22	+ 4.0	+ 1.5	− 5.0	0.9	0.06	0.18	0.37	0.78	14°09′
57		15	47	−101.5	− 10.3	+ 55.0	1.4	0.10	0.30	0.13	0.65	20°40′
58		15	49	− 3.5	− 3.0	+ 2.0	1.7	0.07	0.21	0.29	0.76	26°06′
59		15	52	− 6.0	− 9.0	+ 3.0	1.5	0.06	0.18	0.37	0.78	47°17′
60		17	14	+ 19.5	− 30.0	− 10.0	1.0	0.10	0.30	0.13	0.65	20°14′
61		21	44	+ 2.0	+ 2.0	− 3.0	0.8	0.04	0.12	0.55	0.84	18°16′
62		22	22	+ 2.5	+ 1.5	− 4.0	0.9	0.04	0.12	0.55	0.84	14°25′
63		22	34	− 1.5	− 31.0	− 12.0	0.8	0.06	0.18	0.37	0.78	21°05′
64		22	35	+ 3.0	+ 1.5	− 3.0	0.9	0.05	0.15	0.46	0.83	18°45′
65		22	35	− 2.0	− 5.0	− 2.0	0.8	0.04	0.12	0.55	0.84	42°02′
66	4	8	56	− 2.5	− 7.0	+ 2.0	1.4	0.10	0.30	0.13	0.65	24°29′
67		9	06	+ 3.5	+ 1.5	+ 11.0	0.9	0.04	0.12	0.55	0.84	9°50′
68		9	20	+ 3.0	+ 3.0	− 4.5	0.9	0.06	0.18	0.37	0.78	15°26′
69		13	16	+ 4.5	+ 3.5	− 6.0	0.9	0.08	0.24	0.22	0.72	8°24′
70		13	46	− 4.0	− 6.0	+ 1.5	1.5	0.10	0.30	0.13	0.65	28°00′

(to be continued)

(Continued)

Earthq. No.	Commencement time. d h m	Trace amplitude of initial motion. (× 1/20 mm) E-W	N-S	U-D	P—S time sec.	Period of initial motion. Tv sec.	Th sec.	α	β	θ
71	4 16 18	− 5.0	+ 9.0	+ 6.0	1.1	0.08	0.24	0.22	0.72	15°43′
72	18 02	− 1.0	− 5.5	+ 3.0	1.1	0.10	0.30	0.13	0.65	11°21′
73	20 03	+ 7.0	+ 3.5	− 6.5	1.0	0.08	0.24	0.22	0.72	11°13′
74	22 11	+ 9.0	+ 10.0	− 8.5	0.7	0.08	0.24	0.22	0.72	14°57′
75	22 33	+ 6.0	− 14.0	− 6.5	1.1	0.04	0.12	0.55	0.84	39°51′
76	22 54	− 5.0	− 5.0	+ 7.0	1.3	0.04	0.12	0.55	0.84	21°13′
77	23 22	+ 6.0	+ 1.5	− 6.5	1.2	0.06	0.18	0.37	0.78	15°32′
78	23 28	− 3.7	− 4.5	+ 5.0	0.9	0.07	0.23	0.30	0.73	11°21′
79	5 2 46	+ 9.5	+ 2.0	− 9.0	0.7	0.06	0.18	0.37	0.78	17°42′
80	2 54	+ 3.0	+ 4.0	− 4.5	1.1	0.06	0.18	0.37	0.78	17°57′
81	3 46	− 1.0	− 4.0	+ 1.5	1.6	0.08	0.24	0.22	0.72	23°57′
82	12 11	+ 6.0	− 24.5	− 9.0	1.2	0.16	0.49	0.05	0.47	9°11′
83	12 59	− 1.5	− 4.5	+ 3.5	1.0	0.04	0.12	0.55	0.84	20°23′
84	13 35	+ 18.5	− 44.0	− 9.0	0.8	0.14	0.42	0.07	0.53	20°49′
85	13 54	+ 30.0	− 40.5	− 12.5	1.1	0.12	0.36	0.08	0.59	16°27′
86	16 41	+ 7.5	+ 3.5	− 4.5	0.9	0.08	0.24	0.22	0.72	17°09′
87	21 14	− 1.5	− 3.5	+ 2.0	0.8	0.04	0.12	0.55	0.84	34°03′
88	22 17	+ 2.0	− 8.0	− 3.0	1.4	0.06	0.18	0.37	0.78	38°50′
89	23 52	+ 2.0	− 7.5	− 2.0	0.9	0.04	0.12	0.55	0.84	55°37′
90	23 54	− 2.5	− 3.0	+ 4.0	0.3	0.06	0.18	0.37	0.78	16°05′
91	6 7 15	+ 3.0	+ 2.5	− 5.5	0.3	0.08	0.24	0.22	0.72	7°26′
92	7 55	− 2.0	− 1.0	+ 1.5	0.6	0.04	0.12	0.55	0.84	27°58′
93	7 56	+ 2.0	+ 1.5	+ 1.0	0.4	0.06	0.18	0.37	0.78	36°19′
94	8 06	+ 4.5	+ 3.5	− 3.0	1.0	0.06	0.18	0.37	0.78	29°06′
95	8 33	− 1.5	− 4.5	+ 1.0	1.9	0.12	0.41	0.22	0.55	59°10′

the circles refer to the earthquake numbers in Table II. It will be seen that, with respect to some aftershocks, considerable differences have resulted in the focal distances of the same shocks. This is because in Fig. 3 the focus located from single station data was assumed to exist on the surface of the earth. For our present purpose, then, only the azimuths of foci should be compared. The difference in azimuth is tabulated in Table III, and the mean deviation in azimuth was calculated as 12°.3±4°.5.

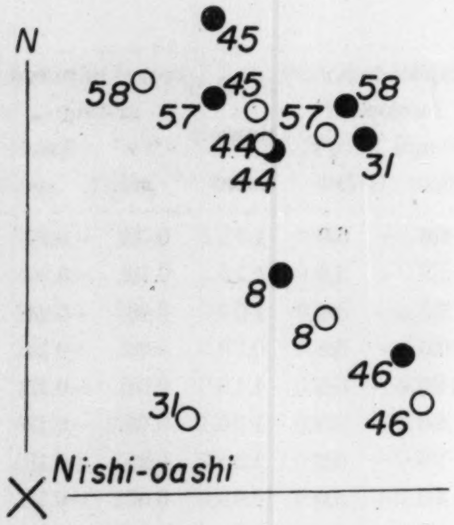

Fig. 3. Comparison of epicenters.
○ ; epicenter by difference time method.
● ; epicenter by single station method.

Table III. Azimuth of epicenter determined by
A ; the difference time method,
B ; the single station method.

Earthq. No.	46	8	31	57	45	44	58
A (from N to E)	78.5	60.2	66.0	40.3	32.0	35.0	16.5
B („)	71.0	50.2	45.0	26.5	21.5	36.2	40.0
Difference	7.5	10.0	21.0	14.3	10.5	-1.2	—

3. The Epicenters Located by the Data at a Single Station.

Through the investigations explained in the preceding paragraphs we were convinced that fairly reliable locations of epicenters were to be obtained from the data at a single station. Referring to Table II we were able to locate the foci of the shocks, assuming that focal depths of these shocks were all zero kilometer. Geographic distribution of these foci is shown in Fig. 4. For the sake of comparison the map of epicenters of aftershocks during the same period, prepared by the difference time method, is reproduced in Fig. 5. These two maps closely resemble each other. As seen in Fig. 4, the result obtained by the single station method also shows that large numbers of aftershocks have occurred in the region to the northeast of Nishi-oashi Station.

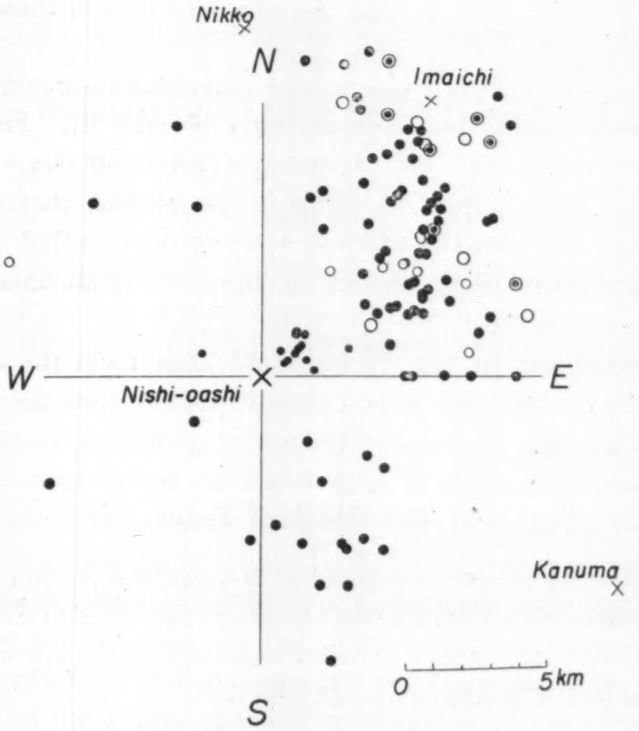

Fig. 4. Distribution of epicenters of shocks from Dec. 31 to Jan. 6 determined by the single station method.

Now when the area is divided into four quadrants by *E—W* and *N—S* lines intersecting at Nishi-oashi Station, some points of difference will be noticed between these two maps:

1) Not a small number of foci are seen located in the quadrant IV or the southeast quadrant by the single station method, while only a few shocks were located in this quadrant by the difference time method. The frequency curves of the *P—S* durations at Kanuma Station show that a considerable number of earthquakes of short *P—S* duration times (less than 2 seconds) are observed there, and it will be reasonable to consider that although small shocks had certainly occurred in this quadrant, the foci of such shocks were so distant

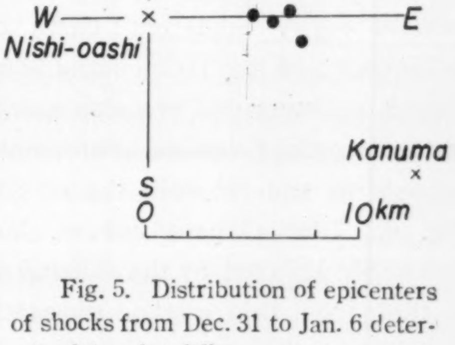

Fig. 5. Distribution of epicenters of shocks from Dec. 31 to Jan. 6 determined by the differnce time method. (After T. Hagiwara)

from Nikko or Imaichi Stations that the seismometers in these stations failed to catch them.

2) According to the result due to the difference time method, not a single epicenter has been located in the quadrants II and III. Nevertheless, our single station method reveals the existence of seven shocks with their foci in these quadrants. With respect to these seven shocks careful examinations have been carried out with the original seismograms, so that it may safely be said that the location of these shocks in the two quadrants is to be relied upon.

3) In the quadrant III, the most distant area from the active region, at least three shocks—admittedly a very small number—are seen to have occurred during this period.

4. The Depth of Focus.

As Nishi-oashi Station was equipped with a vertical motion seismometer besides two components of horizontal motion seismometers, we tried to compute the true angle of incidence of P waves in order to acquire some knowledge concerning the depth of the foci of aftershocks. As will be seen in Table I the free oscillation period of the vertical motion seismometer was adjusted at 0.1 second, so that the amplitude in their seismograms represents the acceleration of the motion of the earth, while that of the horizontal motion seismometers was adjusted at 1.0 second, so that in their seismograms will be recorded the displacement of the earth movement whose period is about 0.3 sec. Such being the case, the use of direct trace amplitude of seismograms does not readily make possible the quantitative determination of the incident angle. Since true earth amplitude is to be obtained by twice integrating[6] the recorded seismograms, we also subjected some of the records of vertical seismometers to these procedures and obtained the results given in Fig. 6. Displacement curves, however, are inevitably affected by the shifting of zero lines, so that, from this method of calculation, the

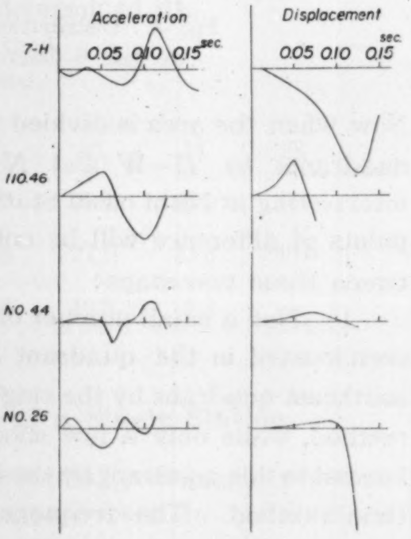

Fig. 6.
Acceleration: Original acceleration seismogram.
Displacement: Displacement curve computed from the acceleration seismogram.

---

[6] T. HAGIWARA, *Bull. Earthq. Res. Inst.*, 13 (1935), 138.

accurate value of the amplitude of the first motion is not to be measured. In order to eliminate this inaccuracy we made use of the results of calculation carried out by Dr. C. Tsuboi.⁽⁷⁾ He computed the motion of a pendulum when it was exposed to the external vibration of the forms:

$$\begin{cases} t<0 & f(t)=0 \\ t\geqq 0 & f(t)=a\sin\omega t \end{cases} \quad \cdots\cdots\cdots\cdots\cdots\cdots\cdots\cdots(1)$$

or

$$\begin{cases} t<0 & f(t)=0 \\ t\geqq 0 & f(t)=2\sin t-\sin 2t\,. \end{cases} \quad \cdots\cdots\cdots\cdots\cdots\cdots(2)$$

He also drew a graph that shows how much the recorded first maximum amplitude is reduced according to the fluctuation of the ratios of apparent period of the recorded initial motion to that of the seismographs. The apparent initial periods of the vertical motion were read from the seismograms and tabulated in column T_V in Table II, while the apparent initial periods of the horizontal motion were computed by T. Suzuki's method⁽⁸⁾ and shown in column T_H in the same Table. In our present study of Nishi-oashi records the initial motion of aftershocks had a sudden commencement as will be seen in the seismograms in the Plate, and so the equation (1) was made use of for computation. The coefficients for the correction of the initial apparent amplitudes on vertical and horizontal seismometers are seen in Table II, columns α and β. The apparent incident angle $\bar{i}$ will be calculated by

$$\tan\bar{i}=\frac{A_H}{A_V}=\frac{a_H}{a_V}\,\frac{\alpha}{\beta}\,\frac{V_H}{V_V}$$

where A_H and A_V are the true initial amplitudes of horizontal and vertical earth displacements, a_H and a_V the initial amplitudes of the observed motions, and V_H and V_V the magnification coefficients of the instruments. The true angle of incidence computed from these is shown in the last column in Table II. In computing the true incident angle, the value of V/v, the ratio of the velocities of longitudinal and transversal waves, was assumed to be 1.7 after T. Matuzawa⁽⁹⁾.

In Fig. 7 are shown the frequency diagrams of the incident angle due to every ten degrees. According to the data obtained by T. Suzuki⁽¹⁰⁾ at Tokyo and Mitaka some time ago, almost all the angles of incidence of seismic waves were found to be less than ten degrees, or in other words almost all seismic

---

7) C. TSUBOI, *Bull. Earthq. Res. Inst.*, 12 (1934), 426.
8) T. SUZUKI, *Bull. Earthq. Res. Inst.*, 12 (1934), 16.
9) T. MATUZAWA, *Bull. Earthq. Res. Inst.*, 6 (1920), 177.
10) T. SUZUKI, *Bull. Earthq. Res. Inst.*, 10 (1932), 518.

waves had nearly vertical directions. Contrary to this, in the case of Nishi-oashi observation, the majority of seismic waves had an incident angle from 10 to 30 degrees, only a small number of waves having angles less than ten degrees. Apparently this is because the geological conditions near the earth's surface in Nishi-oashi region are totally different from those in the Tokyo district, none of the soft layer of quaternary loam existing to disturb the wave paths to a remarkable extent.

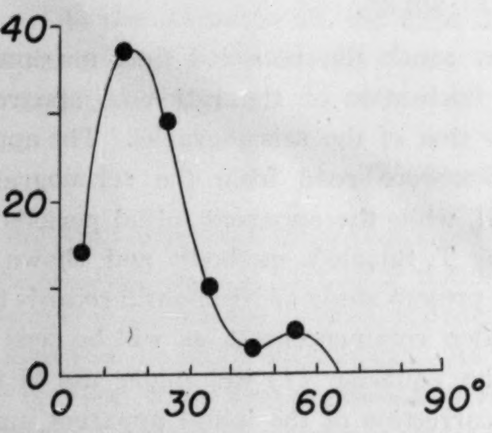

Fig. 7. Frequency diagram of incident angles.

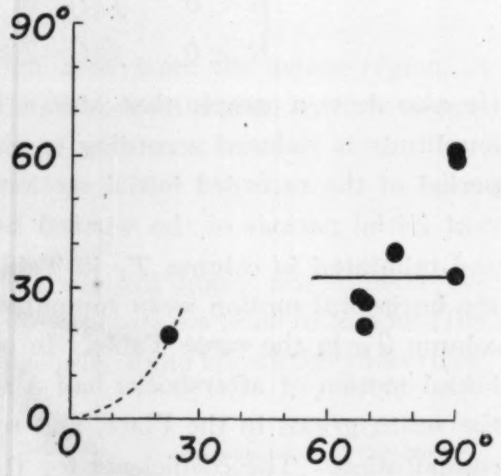

Fig. 8. Incident angles computed by the single station method (ordinate) as related to those computed by difference time method (abscissa).

The result of the study of aftershocks by the difference time method enables us to measure the angle formed by the wave path—namely the line from the focus to the station—and vertical line that passes through the station. This angle is contrasted in Fig. 8 with the incident angle computed by our single station method. As seen in the figure, the incident angle of the shock No. 5 is almost equal to the angle obtained by the difference time method, but when the incident angles calculated by the difference time method were 60~80 degrees, the angles computed by Nishi-oashi Station were about thirty degrees. The incident angles of four shocks that had very shallow origins will be contrasted with each other in Table IV. As seen in the table, though the incident angles observed at Nishi-oashi Station were fairly large with respect to the shocks whose epicentral distances were less than ten kilometers, shocks with longer epicentral distances had rather small incident angles.

In explanation of these facts we are led to suppose a discontinuity within the earth at the depth of a few kilometers. Supposing a *P* wave that started at some point near the discontinuous surface traveled along the boundary of

Table IV. Comparison of the incident angles computed by different methods.

θ : Incident angle computed by single station method.
i : Incident angle computed by difference time method.
Δ : Epicentral distance.

Earthq. No.	θ	i	Δ	Earthq. No.	θ	i	Δ
			km				km
8	51.2°	90.0°	8.1	46	33.5°	90.0°	9.4
31	19.2°	23.0°	4.2	57	20.7°	68.5°	10.8
44	27.9°	67.7°	9.8	58	26.1°	68.5°	9.8
45	38.5°	75.5°	10.3	95	59.2°	90.0°	12.0

the discontinuity and was refracted back to the observation station, such a wave will have the angle of incidence of 35 degrees, provided the second layer had a velocity of 7 km/s or so. Now as it is known that the focal depth of the majority of aftershocks is about five kilometers, if the above assumption is made, it will be understood that the peaks of the frequency curves of angles of incidence are seen at about 10~30 degrees. In the next place, assuming the depth of the discontinuity was less than 2.5 kilometers, the refracted waves will arrive at the station earlier than the direct waves, provided the origin of the shock was placed at the surface of the earth and the distance from the origin to the station was greater than 12 km. If such is the case it is possible that distant shocks will have smaller incident angles of the first wave than near ones.

It will be difficult to obtain positive geological evidences to support this view of subsurface structure, but it may not be altogether impossible to assume a discontinuous surface within the granitic layer.

As to the shocks with very small angles of incidence, we calculated their focal depths. If we use without any modification the values of the angles of incidence given in the last column, the epicentral distances will become too small. We therefore assumed that these small angles contained an error of 5 degrees. On this assumption the epicentral distances of these shocks were calculated and plotted in Fig. 4 by small dots. Small open circles show the location of foci when the shocks represented by the corresponding small dots are supposed to have the depth of zero meter.

5. The Distribution of First Impulsions.

As the foci of aftershocks have been determined in the preceding paragraphs, we will consider next the problem of the distribution of first impulsions. In this case too, as we did in the case of Fukui aftershocks,[11] we assume that a shock occurred at point 0 in Fig 9 and observation of it was made at positions designated by circles in the same figure. In reality we have one observation station and 95 foci distributed all around it, but now we assume that a shock occurred at the point 0 and was observed at 95 stations distributed all around it, the observation of first impulsions of *P* wave being carried out at the respective stations. Fig. 9 was drawn upon these assumptions, and the directions of the arrows indicate whether the first impulsions were directed toward or away from the epicenter, and the length of an arrow represents the ratio of the first horizontal amplitude of *P* wave to the amplitude of the largest motion, and a circle represents the sense of the first impulsion of the vertical component of the shock, open circles in it showing the downward motion and black ones the upward motion. From Fig. 9 it appears difficult to draw lines that bound the regions of the initial upward and downward motions. We notice, however, that all points in the northwest quadrant represent the initial downward motions, and in the southeast the majority of the points represent the upward, while in the southwest quadrant downward and upward signs are mixed together. Some similarities may be seen if we compare this map with the map showing the distribution of the first impulsions of the main shock.[12] In preparing Fig. 9, it is assumed that all the aftershocks took place with the same mechanism and at the same focal depth. These assumptions, however, involve exceptionnal conditions and are in reality almost impossible.

---

[11] S. OMOTE, *Bull. Earthq. Res. Inst.*, **28** (1950), 312.

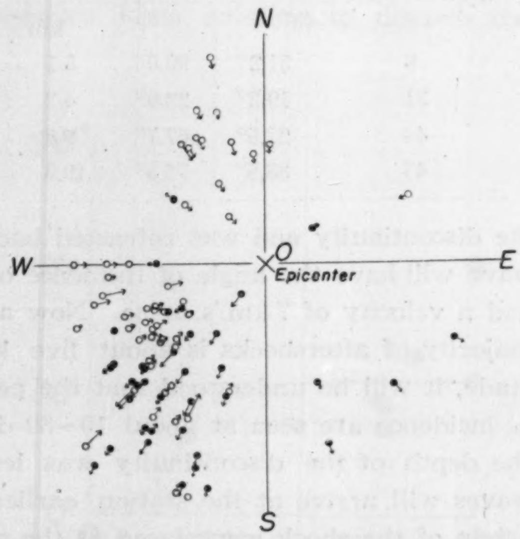

Fig. 9. Distribution of the direction of the initial motions.
Open circle; first condensational wave, black circle; first rarefactional wave.

6. Résumé.

In concluding these reports, the results obtained will be summarized as follows:—

---

[12] *loc. cit.,* 4).

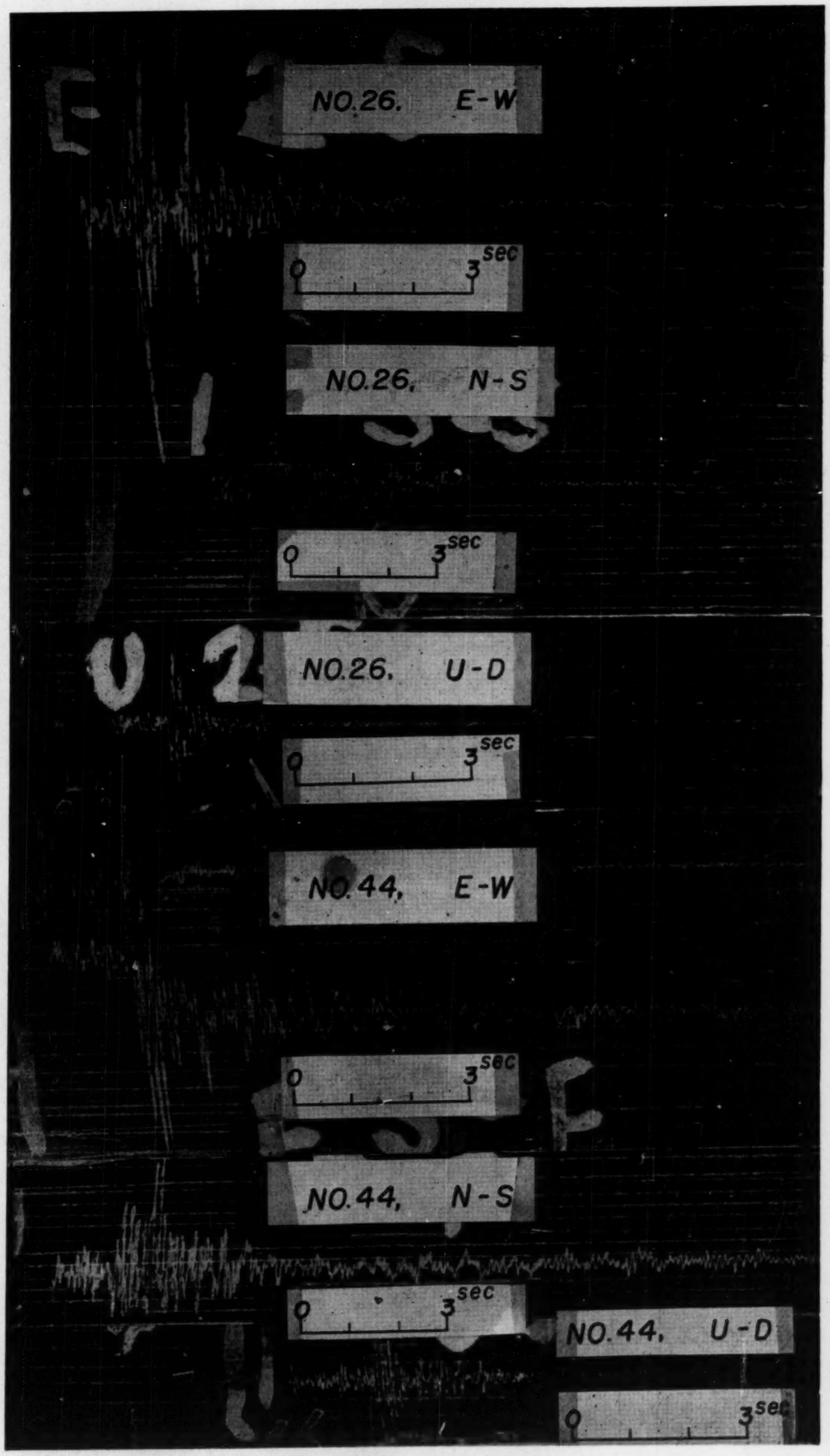

Fig. 10. a. Seismograms obtained at Nishi-oashi Station.

（震研彙報，第二十八號　圖版　表）

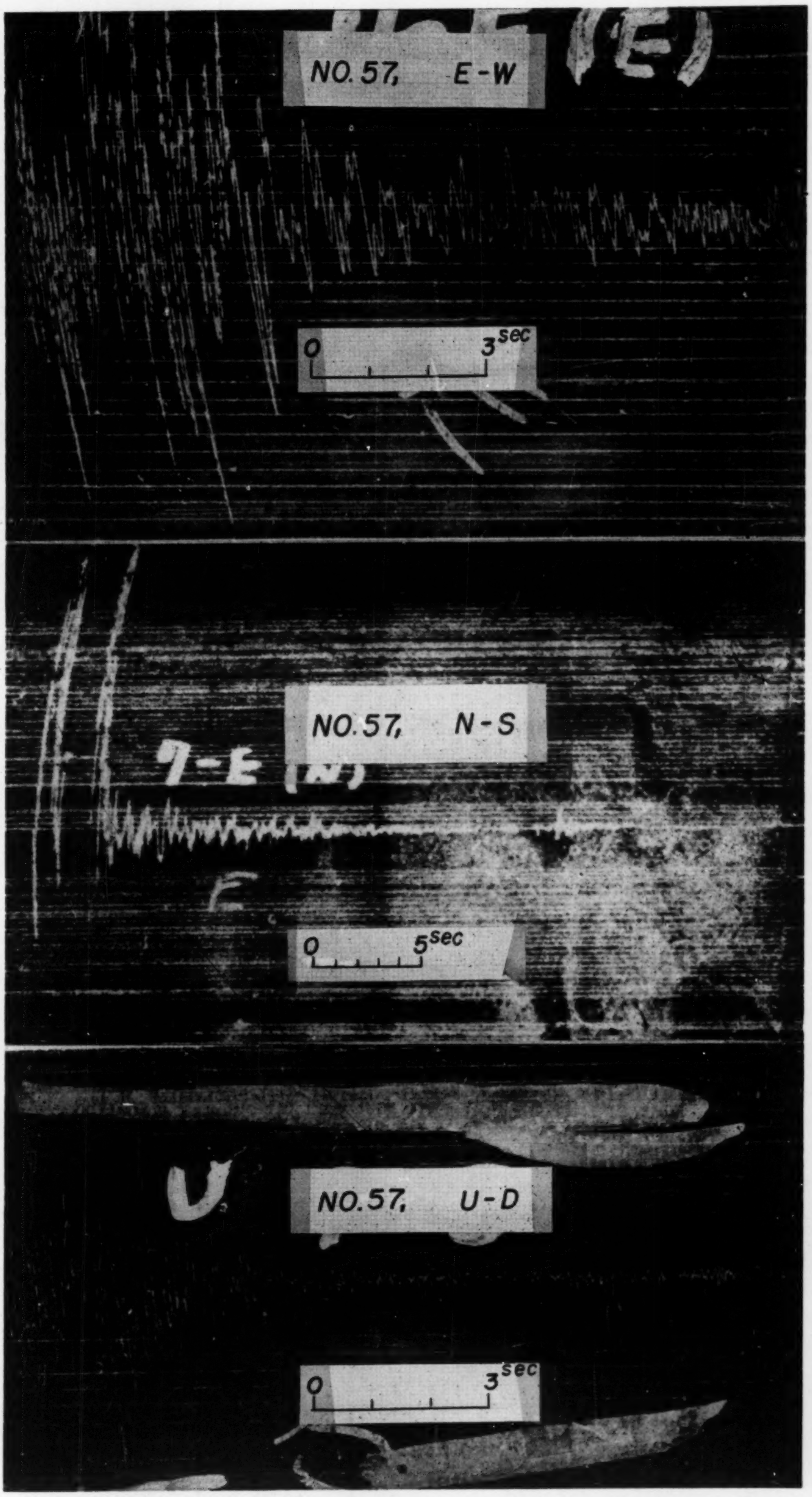

Fig. 10. b. Seismograms obtained at Nishi-oashi Station.

(1) Some 95 foci of Imaichi aftershocks were located by the data obtained at the single station, Nishi-oashi, which had three components of seismographs at its desposal.

(2) Epicenters of these aftershocks were mainly concentrated in the area bounded by a triangle, whose apices were Nishi-oashi, Imaichi and Nikko, and this fact was in good accord with the result obtained by the difference time method.

(3) Occurrence of shocks, though small in number, in the northwest and southwest quadrants was confirmed.

(4) The incident angle of the first P wave was calculated. In this, as the vertical motion seismometer had the free oscillation period of 0.1 sec., Tsuboi's method was made use of for the purpose of determining the true initial amplitude of the vertical component.

(5) The majority of shocks had incident angles of about 10°∼30° and the assumption of the existence of a discontinuity surface with a slightly bigger velocity within the earth was found to provide favourable explanation to it. The depth of this discontinuity will not be greater than 2.5 km.

(6) With respect to these shocks with small incident angles the depth of foci and the epicentral distance were calculated.

(7) Some observations were made regarding the distribution of the first impulsions of aftershocks.

In conclusion the author wishes to express his hearty thanks to Professor T. Hagiwara for his valuable advices. A part of the expense of this study was defrayed from the Scientific Research Fund of the Department of Education.

---

30. 西大芦村で観測された今市地震の余震

地震研究所 表 俊 一 郎

今市地震の余震観測は今市，日光，船生，鹿沼及西大芦で行はれそれらの結果より求められた余震の震央分布については別に報告されてゐる．筆者は西大芦に於て水平動の微動計2台，上下動の加速度計1台を用ひ三成分観測を行つた．微動計はしばしば針が外れ観測は困難であつたが初動は極めて明瞭な記録が得られたので之等の記録より一點觀測による震央を求めた結果，4點觀測による震央の位置と azimuth にして10°位の差違を生ずるが，その結果は充分信頼するに足るものであることが解つた．求められた震央は大部分西大芦の北東，日光今市西大芦を結ぶ三角形の中で發生しその他西大芦鹿沼間にも可なりの地震が發生したことが知られた．入射角を計算するにあたつては坪井教授の求められた初動の型を用ひてもとめた結果10°～30°の入射角をもつものが最も多いことが知られた．又極めて淺い地震についても震央距離の大きいものの方が入射角が反つて小となることが知られ之等より地下数粁の所に一つの層を考へられば之等の現象を説明するのに極めて好都合であることをのべた．

31. *On Micro-earthquakes Observed After the Imaichi Earthquake, Dec. 26, 1949.**

By Toshi ASADA and Ziro SUZUKI,

Geophysical Institute, Tokyo University.

(Read March 20, 1950—Received Sept. 20, 1950.)

1. C. F. Richter and J. M. Nordquist[1] observed small aftershocks, the principal shock of which occurred near Riverside, California, on Feb. 18, 1948. The Benioff seismometer at Riverside recorded 98 aftershocks during Feb. 18 and 19. The magnitude of the smallest aftershock was determined to be 0.4 in Richter's scale, and the energy released in the shock was 10^{12} ergs in the order of magnitude.

The present authors made the observation of very small aftershocks of the Fukui Earthquake[2] during the period from July 14 to Aug. 8, 1948 by means of the electromagnetic seismometers, of which the magnification was about 40,000 for the vibration of 20 c/s, and found that the micro-earthquakes, having the amplitudes of about a few hundredths of a micron, were occurring every three or four minutes on the average.

They also carried out the observation of micro-earthquakes in June, 1949, at Washishiki, Tokushima Pref., and at Kagami, Kochi Pref., in Shikoku District.[3] At Washishiki 16 micro-earthquakes were recorded during 16.6 hours, and at Kagami 9 were recorded during 43.2 hours. It is remarkable that many micro-earthquakes were registered at Washishiki and Kagami, although 30 months had elapsed after the Nankai Earthquake, Dec. 21, 1946.

The results of the observations above mentioned show that many micro-earthquakes can be registered if the sensitivity of seismometers is sufficiently high, especially in the area where aftershocks of an earthquake occur frequently, and moreover, Ishimoto-Iida's formula holds good between their frequency of occurrence and their amplitudes.

The present authors made the observation of micro-earthquakes after the Imaichi Earthquake, Dec. 26, 1949, for a further research on micro-earthquakes.

2. The seismometers used were of horizontal component type having the

---

* Communicated by T. MATUZAWA.

[1] C. F. RICHTER & J. M. NORDQUIST, *Bull. Seism. Soc Amer.*, 32 (1948) No. 4.

[2] T. ASADA & Z. SUZUKI, *Geophy. Notes*, 2 (1949) No. 16.

[3] Z. SUZUKI & T. ASADA, *Geophy. Notes*, 2 (1949) No. 17.

natural period of 1.2 seconds. Their transducers were of moving coil type. The type-D vibrators for YEW oscillograph were connected. The shunt resistances of 20 ohms were used and the seismometer-pendulums were over-damped. The frequency response curve of this seismometer is seen in Fig. 1. These seismometers are more sensitive than those used in the case of Fukui Earthquake. The frequency response curve of a Benioff vertical seismometer with a micro-moll-galvanometer is also given in Fig. 1 for reference' sake. The difference between the two curves is essential for obtaining legible records of such micro-earthquakes.

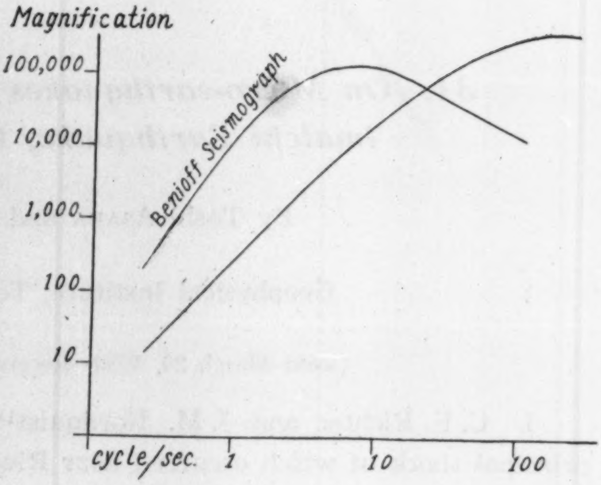

Fig. 1.

Three seismograms were recorded side by side on a photographic paper which was carried by a tape-recorder at the approximate speed of 9 cm/min or 30 cm/min. The temporary tripartite station was set at Tamozawa, Nikko, Tochigi Pref., the one side of the triangle being 150 meters long. The observation was made during the period from Dec. 29, 1949 to Jan. 10, 1950, and seismometers were operated exclusively at night, when the ground was not much disturbed by artificial noises. The total duration of the observation was 17.7 hours and 623 micro-earthquakes were registered, that is, they occurred every 1.7 minutes on the average.

3. The secular change in the frequency of occurrence of micro-earthquakes is given in Fig. 2. Those of the earthquakes registered by Ishimoto-accelerometers at Nikko and Imaichi are also seen in Fig. 3, A and B respectively. The tendency of the secular decrease in number of earthquakes recorded in a day is seen in all cases. The frequency distribution of $P—S$

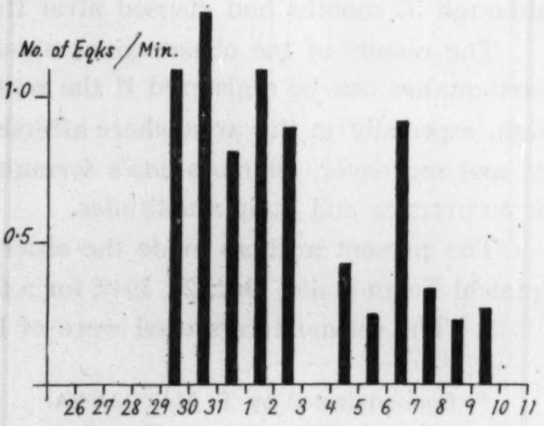

Fig. 2.

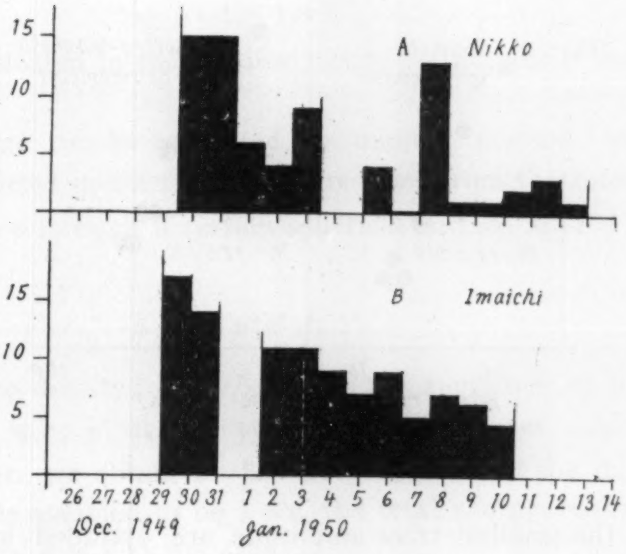

Fig. 3.

duration times of micro-earthquakes and of shocks recorded by the Ishimoto-accelerometer are shown in Fig. 4. The distributions in both cases are considerably different from each other. But it is premature to conclude from this fact that the geographical distribution of the foci of micro-earthquakes and those of comparatively large shocks are different. If the predominant periods of earthquake-motions are dependent on their epicentral distances, the earthquakes having larger epicentral distances might be missed more frequently in the observation by the electromagnetic seismometers than in the case by the Ishimoto-accelerometer, because the sensitivity of the electromagnetic seismograph becomes lower as the period becomes longer, then it is possible that the frequency distributions of $P-S$ intervals of earthquakes recorded by the electromagnetic seismometers and those of shocks recorded by the Ishimoto-accelerometer are apparently different.

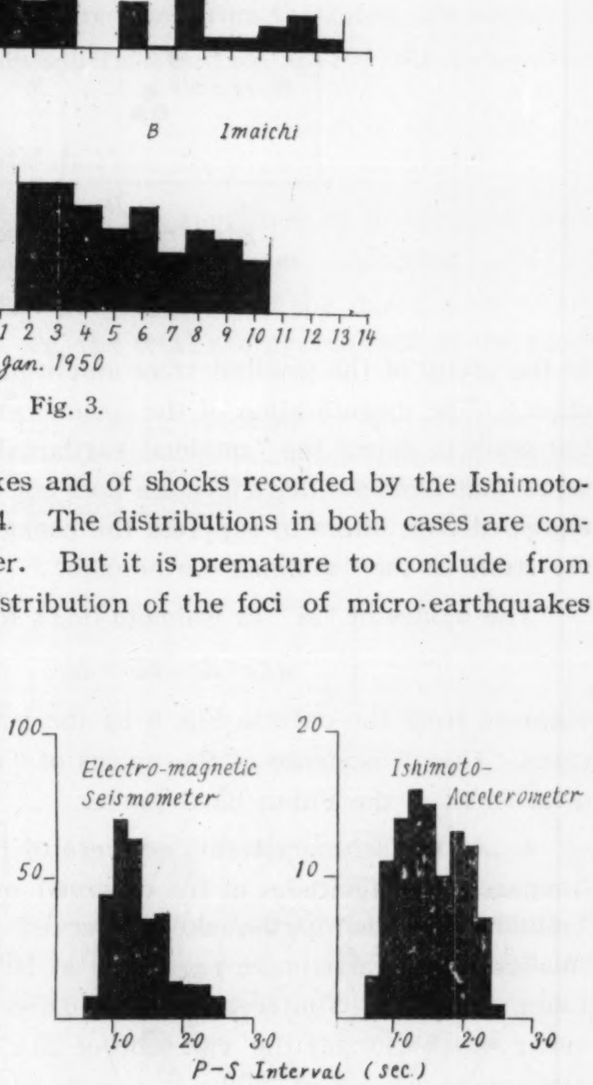

Fig. 4.

The frequency distribution curves of trace-amplitudes of micro-earthquakes and shocks registered by Ishimoto-accelerometer are given in Fig. 5. Both curves coincide well with Ishimoto-Iida's formula. (Earthquakes which belong

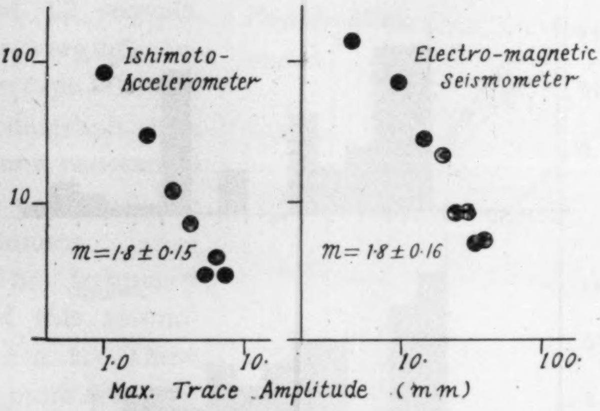

Fig. 5.

to the group of the smallest trace-amplitude are excluded in Fig. 5 in both cases.) The magnification of the seismometer used in the present case was too small to detect the "minimal earthquake", of which the amplitude is so small that Ishimoto-Iida's formula does not hold. More sensitive seismometers equipped with filters to suppress the background noises will be necessary for the study of the "minimal earthquake".

The values of "m" in Ishimoto-Iida's formula,

$$n(a)\,da=ka^{-m}da$$

obtained from the data in Fig. 5 by the least square method are 1.8 in both cases. This coincidence of the values of "m" was the case in the study of aftershocks of the Fukui Earthquake.

4. As the seismometers used were of horizontal component type, we can compare the magnitudes of the observed micro-earthquakes with that of the "minimal recorded earthquake" observed by Richter and Nordquist. The smallest micro-earthquake registered at Nikko has a trace-amplitude of about 1 mm, and its $P-S$ intervals is about 0.8 sec. The magnification of the seismometer was 6×10^4 for the vibration of 20 c/s, which was predominant in the earthquake-motions at Nikko as seen in Fig. 10. As Omori's constant connecting the $P-S$ interval and the hypocentral distance was determined to be 7 in the vicinity of Nikko by the members of the Earthquake Research Institute, Tokyo University, the hypocentral distance of the smallest micro-earthquake was about 6 km. Now it may be assumed that the amplitude decays in proportion to the square of the hypocentral distance. Then the amplitude of the smallest micro-earthquake would be 0.17μ, if it were recorded by the Wood-Anderson seismometer (magnification: 2800) at a station of which the hypocentral distance is 100 km, this value corresponding to magnitude -0.77

in Richter's scale. By the relation between energy and magnitude,[4]

$$\log E = 12 + 1.8\,M\,,$$

the energy released in the smallest micro-earthquake is estimated at 4×10^{10} ergs.

The energy can be estimated by another method. Assuming that the energy is emitted uniformly in all directions from the focus, the energy flux $\overline{F}$ which passes through a certain spherical surface around the hypocenter is expressed as

$$\overline{F} = \frac{1}{2}\cdot 4\cdot\pi\cdot\rho\, p^2\, r^2\, A_r\, V_s$$

where ρ is the density; $p=2\pi/T$; A_r is the amplitude on a spherical surface whose radius is r; V_s is the velocity of the waves. Adopting $\rho=2.7$, and $V_s=3.0$ km/sec., we obtain $\overline{F}=8.1\times10^{10}$ ergs/sec. If the duration of vibration at the focus is assumed to be 1 sec, the total energy released in the smallest micro-earthquake is 8.1×10^{10} ergs.

In both cases stated above the energy released in the smallest micro-earthquake is 10^{10} ergs in the order of magnitude, the value being one hundredth of the energy of the "minimal recorded earthquake".

5. The direction of the approach of initial waves and their apparent velocity could be calculated, as the tripartite station method was made use of. The frequency diagram of the directions is shown in Fig. 6. The distribution of the approach of wave fronts has a maximum of frequency between S 60° E and N 30° E. On the other hand, most of the foci of comparatively large aftershocks determined by the net of temporary seismological stations were located in the direction between S 30° E and S 60° E from Nikko. This result leads to three inferences: the first is that the geographical distributions of foci are actually

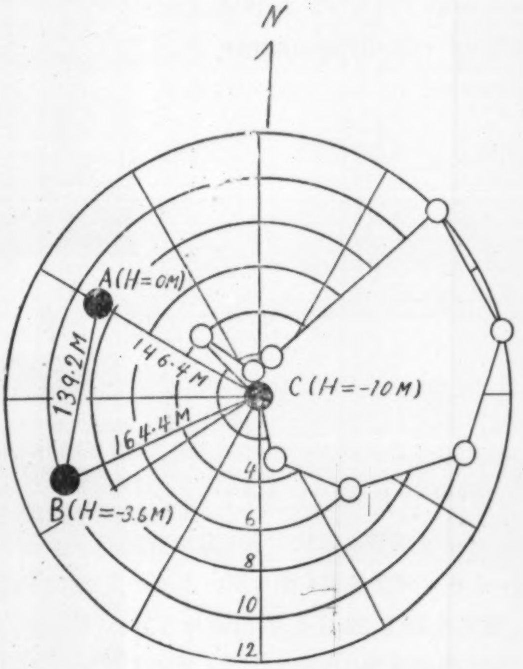

Fig. 6. H: relative heights of the stations.

---

[4] B. GUTENBERG & C. F. RICHTER, "*Seismicity of the Earth*" (1949).

different in both cases; the second is that the difference is an apparent one mainly caused by the difference in the ground structure near each station of the tripartite net; and the third is that the above result is caused partly by the first reason and partly by the second one. It will be necessary for the study of this problem to know the underground structure near the stations by seismic prospecting or other methods.

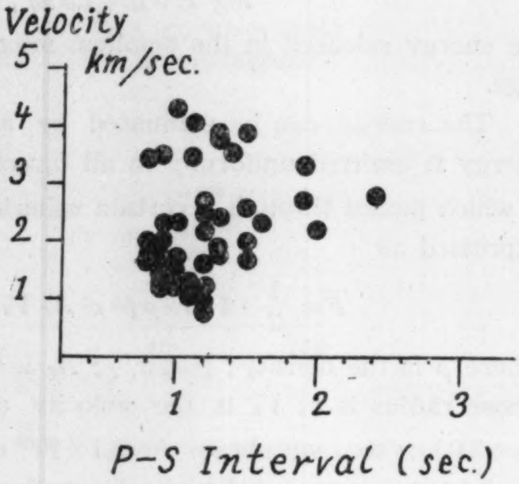

Fig. 7.

The relation between the $P-S$ interval and the apparent velocity obtained by the tripartite station mothod is given in Fig. 7. The velocity of the P-wave in the upper layer is estimated at 1 or 2 km/sec.

In conclusion the writers wish to express their thanks to Prof. T. Matuzawa and Prof. H. Kawasumi for their kind advices, to Prof. C. Tsuboi for his kind encouragements, and Mr. Y. Tomoda for his helpful assistance during the period of the observation.

---

31. 今市地震の際の微少地震に就て

地球物理學教室 淺田 敏
鈴木次郎

1949年12月26日に發生した今市地震後に著者等は日光町田母澤に於て微少地震の觀測を行つた．用いた器械は電磁式水平動地震計で20サイクルの振動に對して約60,000倍の倍率を持つて居る．これは福井地震の際に用いたものより高感度である．

觀測は12月29日より1950年1月10日まで，夜間のみ行われ，その結果は次の如くである．

1) 微少地震は平均して1.7分に1回の割合で記錄された．

2) 最も小さい地震のエネルギーは10^{10}エルグのオーダでRichter等によつて報告された最も小さい地震の1/100の大きさである．

3) 石本飯田の式はやはり，此等の微少地震にもあてはまつて居る．

4) 地震波の初動の波面の進行方向は，三點觀測法によればE及NEが多い．

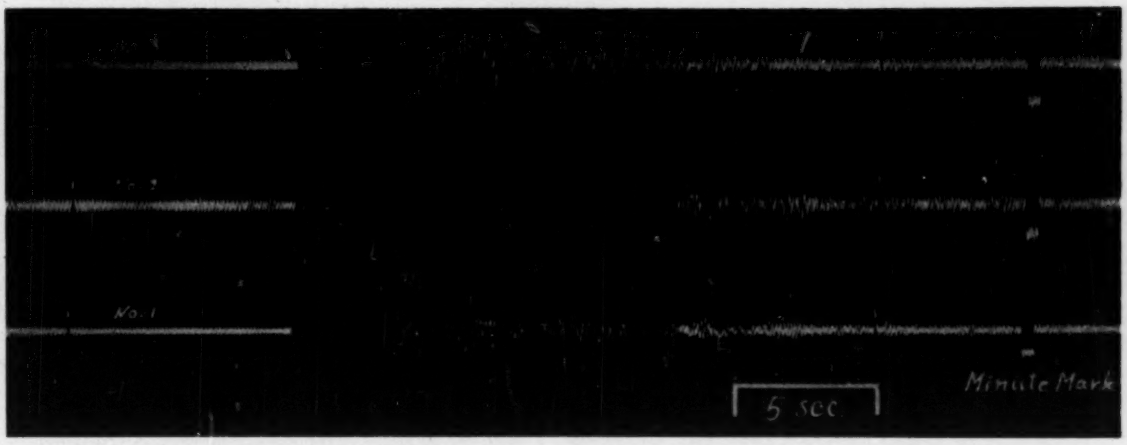
No. 1
Minute Mark
5 sec

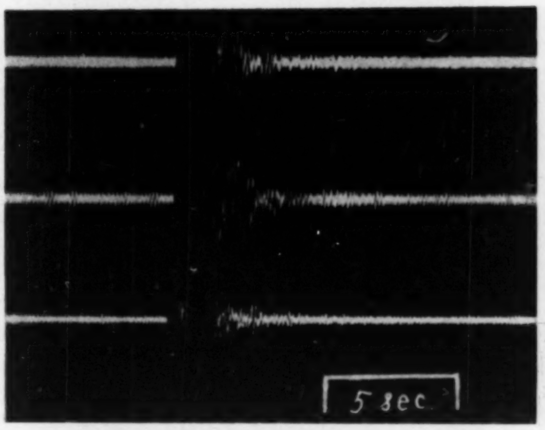
5 sec

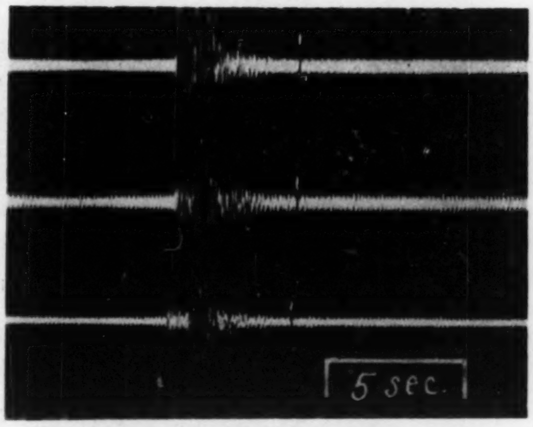
5 sec.

32. 今市地震余震の栃木縣船生（フニュウ）村における觀測について

地震研究所 宮村攝三
秋間哲夫

（昭和25年2月18日發表—昭和25年9月30日受理）

1. はしがき　餘震の計測的研究は那須信治[1]による丹後地震等にともなつた餘震の觀測[1]をはじめ，最近では萩原尊禮，水上武，表俊一郎，等によつて，機會あるごとにおこなわれて，徐々に計器，方法等もすゝんできた．しかし，大體において，餘震發生の時間的消長をしらべ，*P—S* 時間によつて震源をさだめ，その空間的分布，乃至時間的推移を論じ，大森常數をくらべ，あるいは *P—S* 時間の頻度をみる，といつたような程度のことがおこなわれていただけである．たゞ，最近になつて，萩原尊禮[3]が，各餘震の發震機構を同一と假定したときの初動分布をもとめ，表俊一郎[4]は福井地震餘震において，はじめて，とにかく發震時をえて走時を論ずるなど，ようやくあたらしい面があらわれるにいたつた．なおこのほか，餘震の比較觀測によつて，水上武，佐久間修三[5]が種々の地盤の震動性質の差違をしらべたことも，別の面でのあたらしい成果であつた．とにかく，餘震の計測的研究は，餘震そのものの研究としてはもちろん，それによつて地震動，地震波についての研究，地殼構造，發震機巧にいたる種々の問題の有力なてがかりを提供し，とくに震央にごくちかいところの地震動を觀測できるために，普通の觀測ではめつたにえられないような材料を豐富にあたえる機會になるのである．しかしながら，從來の程度の觀測では，數百の餘震を苦心して觀測しても，けつして充分の利用にたえるもののすくなかつたことも，また經驗者すべての知るところであり，したがつて，えられた結果もかぎられたものとならざるをえなかつたのは當然であつた．筆者らはこ

---

1) 那須信治，震研彙報 6 (1928), 7 (1929), 13 (1935), NASU, N. *Journ. Fcc. Sci. Tokyo. Univ. Sec.* II. Vol. III (1929) [丹後地震]，那須信治 震研彙報別冊3號 (1936) [臺灣地震].

2) 萩原尊禮・表俊一郎 震研彙報 15 (1937) [新島地震].
萩原尊禮 同上 18 (1940) [男鹿地震].
表俊一郎 同上 22 (1944) [鳥取地震].
表俊一郎 同上 24 (1946) [東海道地震，三河地震].
水上　武 同上 24 (1946) [東海道地震，三河地震].
OMOTE, S. *Report of the Special Committee for the Study of the Fukui Earthq.* (1950). [福井地震]

3) 萩原尊禮・他震研研究速報 5 (1947). [南海道地震].

4) 表俊一郎 地震學會第5回講演會 (1950, VI)，震研談話會 (1950. VII).

5) 水上武・震研彙報 22 (1944).
水上武・佐久間修三 同上 26 (1948).
佐久間修三 同上 26 (1948).

れらの點をいくらかでも改良して，豐富に餘震觀測を利用できるようにするために，とりあえずつぎの數點を考慮して觀測計畫を準備していた．すなわち，

(1) 震動を完全に記錄するために，よく檢定された水平動2上下動1の3成分の地震計を使用する．(これは，のちにのべるように，P, S のはじまりを決定するためだけにでも必要であり，1成分では P—S 時間さえたゞしい値がえられない危險がおゝいと考えなければならない.)

(2) 時刻精度を向上するために，精密な記錄裝置を採用する．

(3) 時刻精度向上と精密な震動分析とにたえるようにするために，記錄紙のはやさをます．(震源のちかい餘震の震動には短週期のものがおゝいので，從來，記錄線がはつきりたどれるような記象のえられないことが，特に加速度計ではおゝかつた．位相の決定にもこれは大きな誤差の原因となつていた.)

(4) 時刻精度を向上するために，刻時信號を，ある程度頻繁に，またできれば各觀測點に同一の時計であたえる．

等であり，これらによつて，餘震の計測約研究は相當現狀から前進しうるとかんがえた．

さて，このような計畫の具體的な準備をはじめてようやく1-2年のときに，今回の今市地震がおこつた．上下動地震計は組立てまえ，刻時法は實驗中というところであつたが，無理をして，餘震觀測網の1點だけをうけもち，今市北東約 10 km の船生村において觀測をおこなつた．準備不充分のためと，觀測位置が餘震々央からはなれすぎていたゝめに，大した結果がえられなかつたが，あたらしいこゝろみもあり，簡單に概略を報告しておくことにした．なお一般の餘震報告[6]にも船生村觀測の結果はふくまれているので，重復する點はすべてはぶいた．

2. 觀測器械および方法 うえにのべた計畫にもとづいて實施した，今回の觀測の器械および方法についてのべる．

(1) 地震計 まづ，上下動地震計の便利につかえるものというと，どうしても短週期のものになる．3成分は同一の常數のものをもちいたい．なお現狀としてすゝがきをとるのが種々の理由で適當である．これらの點をかんがえ，石本式加速度計[9]の携帶用のものを3成分つくつた．これは100倍の小型携帶用[9]ににた形で，おもりをその約2倍(15 kg)にし，倍率も2倍にしたものである．自巳週期は水平動，上下動ともに $T_0=0.08$ 秒，基本倍率は $V\fallingdotseq 200$，になつている．

位相の點で，加速度計がもつともよいこと[7]，震央近くで行う餘震觀測では加速度が大きいから，加速度計によれば比較的おゝくの地震をつかまえうること，などもこの採用の決定にあたり考慮したことである．さらに，われわれのつくつたねぢりふりこフィルター[8]をもちいれば，眞の加速度記象からは，任意の常數の地震計がかいたであろう記象をうることもできるはづである．(もちろん，加速度として記錄されてさえいればであるが)．そこで一應こうきめたわけである．

---

6) 地震研究所 今市地震余震觀測報告 震研彙報 28 (1950), 387〜392.

7) 中村左衞門太郎 學研天文地物邦文輯報 第1卷第2號 (1941).

8) 秋間哲夫 震研彙報 26 (1948), 坪井忠二・宮村攝三・秋間哲夫 震研談話會昭和21年7月.

9) 萩原尊禮 振動測定 (寶文館).

この地震計の減衰は，知られているように，空氣制振であるが，その使用時の値 h をしるには，たゝいてみるテストでは不充分である．今回，すでに諸所でおこなわれている，おもりに直接種々の周期の偏心廻轉の變位によるバネの力をあたえて，強制振動をさせる裝置[9]を，現場にもつてゆき，使用中の h を強制振動の倍率曲線をつくつてもとめた．東西，および南北に使用した地震計の現場における振動試驗の結果は第1圖にしめすとおりであり，ほゞ $h=0.35$ で使用されていたわけである．これはたゝき試驗で減衰比の目測をあやまつていたため制振がすこしよわすぎたのである．

(2)　記錄裝置　3成分を同一の圓筒に記錄することは，各成分の刻時のどれかゞぬけたとき，各成分の精確な時間位置の對應をつけるのに必要である．3成分用大型圓筒（圓周 600 mm 長さ 720 mm）をつかつた精密記錄裝置およびその驅動裝置等は坪井忠二および著者の一人等によつて，すでに製作されてあつた.[10] これに若干の變更をくわえ使用した．すなわち，廻轉は從來どおり坪井式二本吊振子制禦直流モーター（俗稱ブルブル）とし，よこにずらす方は，精度はいらないので，ブルブルの負荷をかるくするため，普通の直流モーターをもちいた．電源は交流 100V を 6V 電池充電用のセレン整流器で整流した直流 6V を常用し，停電時の用意に，これとともに乾電池を並列につなぎ，蓄電池の浮遊充電使用と同様な方式をこゝろみた．これは平時にも一種の電壓調整として役立ち，廻轉の一様性に好影響をあたえたようである．停電のとき放電した乾電池は，交流がくるとまた徐々に充電されて，ほゞ蓄電池のようなはたらきをした．半日以上の停電では乾電池が放電してモーターがとまつたが，ふたゝび充電後の停電では同様にはたらき，觀測期間中有効であつた．廻轉の精度は記錄の秒刻時によつてしらべると，もつともわるいときでも 1/10 秒以下であつた．

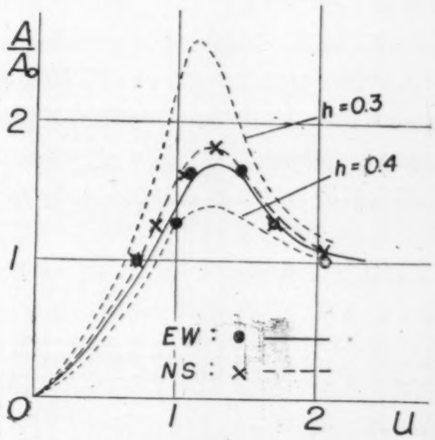

第1圖　使用加速度計の現場での振動試驗による倍率曲線．

Fig. 1. Dynamische Vergrößerung der horizontalen Seismographen durch eine Prüfung an die Meßstelle.

(3)　記錄紙速度　時間の精度を 0.1 秒として，從來の記錄紙速度の 1 mm/sec. では，長さの 0.1 mm までよまなくてはならない．これは紙の伸縮，よみとりの誤差，位相決定の誤差等から無理である．一方圓筒の廻轉が，圓周 600 mm のものでは 10 分 1 回轉までにおとさなくてはならない．この終段の齒車に 240 枚のものをもちいても，1 秒が $240/600=10/25$ 齒，0.1 秒は 1/25 齒にしかあたらない．これでは齒車の齒のところの不規則な偶然誤差がひゞくわけで，鋼ベルト等によつて改良するか，または 0.1 秒あたりの齒數をます，つまり廻轉をはやめる必要がある．しかしよこずりの線の間隔は

---

10)　坪井忠二・宮村攝三・實川顯　地震 13 (1941), 267. 14 (1942), 209.

加速度計でも，そうこまかくはできないし，一日一回以上の記象紙のとりかえは無理である．そこで，その範圍で最大の記錄紙速度をえるようにしたいと考えた．今回は，種々の都合で約2.5 mm/sec，つまり4分1回轉ほどになつた．これで，時間の精度と，震動記錄の短週期振動に對する分解能が相當にました．はやい振動で眞白くなつて $P-S$ がよめるだけのような記象からは解放された．

すゝがきにおいて記錄紙速度をはやくすると，固體摩擦變化をきたす點が問題となるが,11) われわれの場合のように短週期の地震計ではその影響は考える必要はない．

(4) 刻時　今回は1點だけであつたので，クロノメーターによる秒刻時をいれた．坪井研究室の好意により，重力測定用の時計とサイラトロン・リレー等を借用した．分の刻時では萬一回轉が不調の場合精度がおちると思つたのと，分刻時のできる時計がもちだせなかつたために，すこし頻繁すぎたが秒刻時計を採用した．サイラトロンの電源は交流であつたので，停電時には刻時できなかつた．刻時を記入する方法は成案がなかつたが，臨時的に，電磁スピーカーのコーンのかわりに金屬棒をつけ，それで，地震計の擴大装置のむぎわらのねもとのコの字をたゝいた．これで記象寫眞（第3圖～第8圖）でみられるようにわづかに振動する秒刻時がえられた．刻時の振動する時間は長くて0.2秒位で，時刻はそのたちあがりであつて，0.1秒よりよい精度がえられる．位相が刻時とかさなつた場合は0.2秒の誤差はさけられない．しかし，これはおくりののろい場合の從來の種々の刻時法よりは，はるかによいわけである．なおクロノメーターは1日1回ラヂオの時報を耳できいて，指針をよんで，すゝみをよみ，それによつて時刻の補正をおこなつた．

(5) 其他　すでに發表してあつた，すゝつけ装置，記錄白紙まきつけ臺，等10)を携帶用として利用した．

3. 觀測場所　栃木縣鹽谷（シオヤ）郡船生（フニユウ）村の驛前旅館の土間を利用した．同村は大體36°45′ *N*, 139°47′ *E*, 今市（イマイチ）町の北東約10 km の高原山（タカハラヤマ）の南麓にあり，南2 km には鬼怒（キヌ）川がながれている．驛附近は地質圖で沖積層になつているが，水田をうめて，土盛したところで，特に地盤はよくない．もちろん，山がちかいので，沖積層のあつさは，それほどあついとはおもわれないが，觀測してみて意外に軟弱地盤なのでおどろいた．これについては，のちに地盤の性質としてのべる．（第2圖參照）

4. 觀測結果　はじめにことわつたように，準備不充分で强行した觀測であつて，從來どうりの $P-S$ 時間などの觀測は別報6) のように一應できたが，あたらしいこゝろみによる成果は，期待したほどにあがらなかつた．つぎにおもな點について，のべる．

4.1 あたらしくこゝろみた上述の装備と方法とで，記錄された大部分の地震について0.1秒，すくなくとも0.2秒までの精度で初動の發震時をもとめることができた．そのうち，3點乃至4點の $P-S$ 時間によつて震源をきめることができた27ケの地震についての資料を第I表にのせた．發震時は1點のみではあまり役にたゝないが，こうしたことができたということは將來えの足場として一應しるしておく必要があろう．

初動はできるかぎり上下動によつてよんだ．第3圖～第8圖にしめした記錄寫眞にもみられるように，上下動ではすべて P は明瞭であるが，水平動では（P）としたよ

---

11) 岸上冬彦　地震 15 (1943), 44.

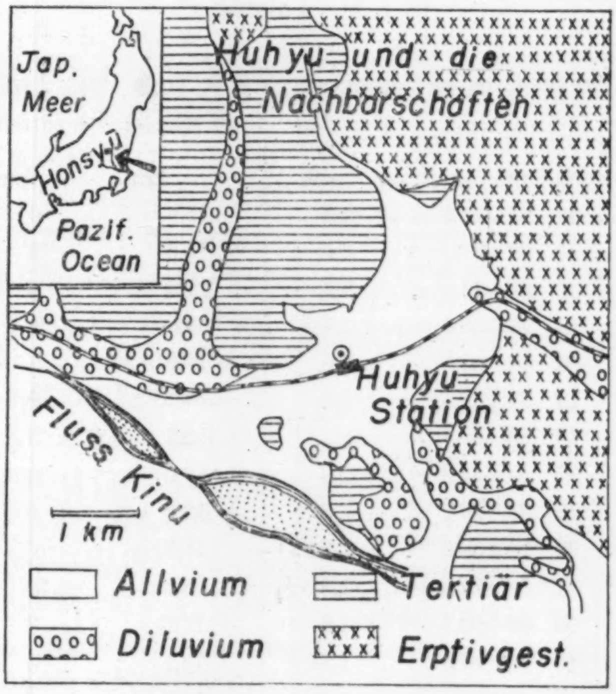
Jap. Meer
Honsyu
Pazif. Ocean
Huhyu und die Nachbarschaften
Huhyu Station
Fluss Kinu
1 km
Allvium
Tertiär
Diluvium
Erptivgest.

第2圖　船生村附近の地質圖
Fig. 2. Geologische Karte in der Umgebung von Hunyu.

うに，對應する時刻にまつたくうごきのみえない場合もある (Fig. 6, 7). 震源が決定されてないのではつきりはいえないが，大體進行方向にちかい *EW* でやゝ *P* がみえ，直角方向にちかい *NS* ではほとんど *P* はみえないのが普通である. (Fig. 3, 4, 5)

一方 *S* は Fig. 4 の *NS* 成分，Fig. 7 の *EW* 成分のように非常に一義的にきまるが，それらに直角の Fig. 4 の *EW*, Fig. 7 の *NS* では對應する位置に *S* をきめることが，非常に困難ではないが，まよいやすい場合もあり，Fig. 3,5, 6 のように一應兩成分ともに對應してきめうる場合，まれには Fig. 8 のようないづれにおいても非常にむつかしい場合などさまざまである. とにかく *S* はどうしても水平2成分の一方だけではきめられないことは，たしかである. 上下動の *S* に對應する位置は Fig. 3, 5 のように，やはりある位相をしめすものと，Fig. 4, 7 のように不明瞭のもの，逆に Fig. 6のようにあきらかに，ふれが急になくなる，つまり Negativer Einsatz (圖で $\overline{S}$ でしめす) とでもいうべき場合などがある.

さらに *P* と *S* とのあいだ，また *S* 以後においても，おゝくの位相がみられる. これを X_1, X_2…，およびY_1, Y_2…でしめしたが，これはまつたく各地震ごとに別々に記號としてしめしたので，Fig. 3 の X_1 と Fig. 4 の X_1 にはなんの對應もあるわけでない. Fig. 5, 6 はわれわれがきれいな，刻時いりの3成分記象をえたうちの，震源の決定されたたゞ2つの地震であり，震源位置はほゞひとしいが，記象もまたある程度にている. ことに X_1, X_2, X_3 などは，ほゞ對應しているように思える. しかし他の記象では大分かわつてくる. とにかく X_2 X_3, のようなはつきりした段を，すべての餘震

第 I 表 Tabelle I

番号 Nr.	月日 Datum	初動發震時 P-Einsatzzeit	初期微動 P-S Zeit	震央距離 Epiz. Distanz	震源の深さ Herdtiefe	震央方位 Epiz. Azimuth
		h m s	sek.	km	km	
7	XII 29	00 35 29,1	2,2	15,6	0	S 43° W
9		01 09 2-,-	2,2	14,5	6	40
10		01 35 4-,–	3,1	21,4	5	34
38	30	18 18 50,0	1,9	13,8	5	70
41	31	00 44 03,0	2,6	17,0	5	48
65		18 51 07,3	2,2	14,2	0	53
66		18 53 47,8	2,3	15,2	5	49
69		20 47 47,3	2,3	18,0	0	37
91	I 1	12 38 50,7	1.8	13,0	5	77
95	2	00 24 53,2	2,6	18,5	0	45
98		01 39 26,5	2,9	18,1	10	41
106		06 09 36,6	1,8	13,7	3	60
115		18 55 07,-	1,8	13,1	4	70
117		19 19 40,8	2,0	13,0	3	76
118		19 53 14,2	1,2	13,0	0	39
121		23 32 22,2	2,9	14,0	0	43
122	I 3	00 01 32,2	2,0	14,2	0	56
132		15 38 43,2	1,6	11,8	4	67
134		15 46 00,-	1,9	14,4	5	63
143		23 38 50,5	2,5	18,6	4	44
163	I 4	08 33 43,8	1,5	10,8	0	67
170	I 7	18 02 10,9	1.8	14,0	7	70
171		18 28 54,2	2,8	17,7	0	40
173		03 37 01,-	2,6	17,4	8	55
183	I 10	06 00 18,5	1,7	11,0	0	65
184		06 07 40,8	1,5	11,5	2	70
209	I 14	12 17 45,6	3,3	18,5	0	63

についてさがしてみると，このようななんらかの段が水平動においてはつきりみられるものは，はつきりした段のみられないものよりずつとすくない（小さい地震はみな段なしに分類されたから）．この段のある型と段のはつきりしない型とを *P—S* 時間にわけた頻度分布をつくつてみても，はつきりした區別はない．震央距離とともに，方位をとり，さらに發震機構まで考えなくてはならないのであろう．*P—X* 時間，*X—S* 時間等と *P—S* 時間の關係もきれいなものではない．つまり X_1, X_2… それぞれちがつたものであるから，それらをわけて考えられるようにもつと充分の材料をえなくては論ずることができないものと思われる．最後に上下動の初動であるが，これは第 9 圖にしめす

ように，するどい P_2 のまえに，かすかな微動 P_1 をともなうもの（A 型），まつたくするどい P が突然にはじまつているもの（B 型），次第に大きくなる振動ではじまつているもの（C 型）が區別された．これは震源のきまつたものについてみると，大體深くて遠いものに A 型があり，深くて近いものが B 型，淺いものが C 型がおゝいようであるから，震源のすぐ下の高速層をへた屈折波ともおもわれるが，量的にたしかめられてないので，今後の問題である．發震機巧によるものかもしれない．從來のろいおくりではこの A 型のはじめの微動はおそらくわからなかつたものとおもわれる．

4.2 記錄された地震は約200でそれらの加速度3成分の最大振幅を合成し（多少の位相差は無視した），地震の大體の大きさの目やすとして，發生の時間的推移をみると第10圖のようになる．これを時間の單位をかえてまとめると第11圖，第12圖のようになる．いくらか群發性がみられるようであるが，統計的吟味をしてみないとはつきりしたことはいえない．

4.3 記象寫眞（第3圖～第8圖）にもみられるように，晝間相當微動があり，特に EW-成分においていちゞるしい．これは，しらべてみると，附近の製材工場の動力によることがわかつた．鐵道は近いが，たまにとおる列車も大した微動はあたえなかつた．EW-成分のみ大きいことは，水平成分の2

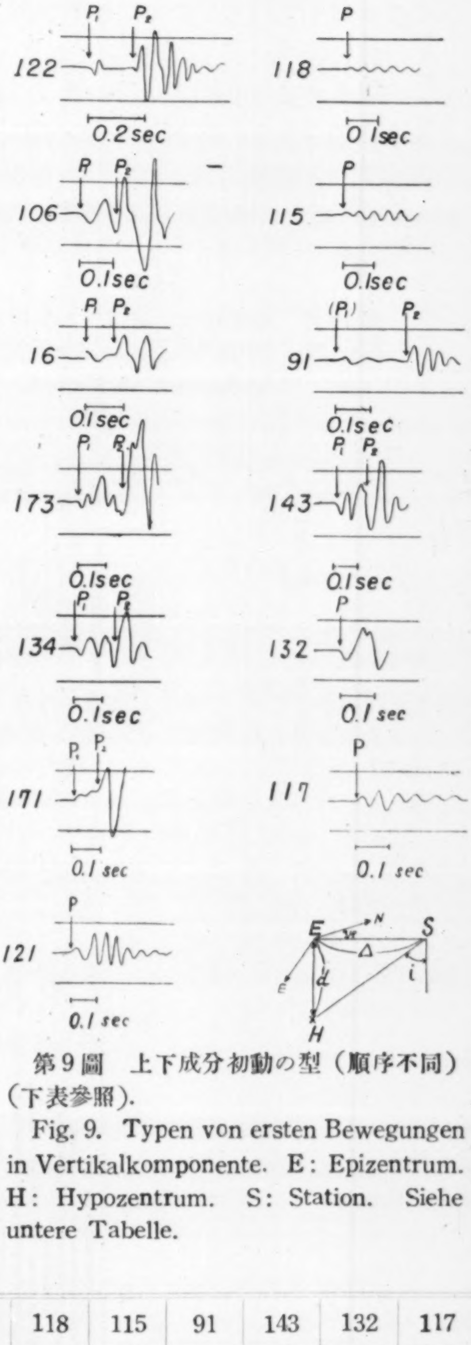

第9圖　上下成分初動の型（順序不同）（下表參照）.

Fig. 9. Typen von ersten Bewegungen in Vertikalkomponente. E: Epizentrum. H: Hypozentrum. S: Station. Siehe untere Tabelle.

Nr.	122	106	16	173	134	171	121	118	115	91	143	132	117
Δ(km)	15.4	15.0	18.6	17.0	12.6	17.0	28.0	7.4	12.4	12.8	16.8	11.6	14.6
d(km)	10	9	10	8	6	5	0	3	5	5	6	4	0
i	56°	60°	61°	64°	65°	73°	90°	68°	68°	69°	70°	72°	90°
φ	60°	61°	35°	53°	70°	40°	40°	40°	70°	74°	40°	62°	62°
Typus	A	A	A	A	A	A	C	C	C	A(B)?	A	B	C

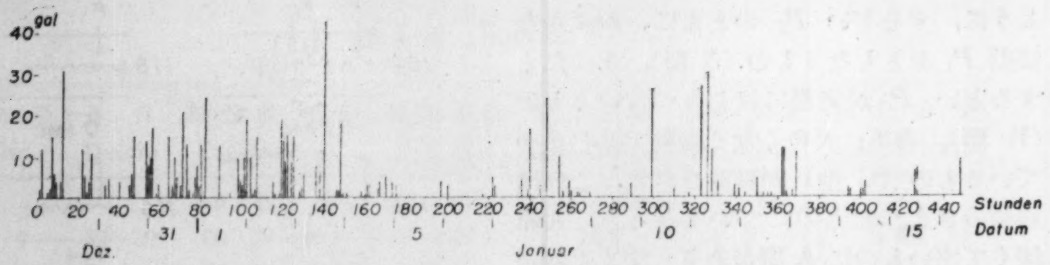

第10圖　船生村にて觀測せる余震とその最大加速度.

Fig. 10.　Zeitliche Folge der Nachbeben und ihrer maximalen Beschleunigungen beobachtet an Hunyu.

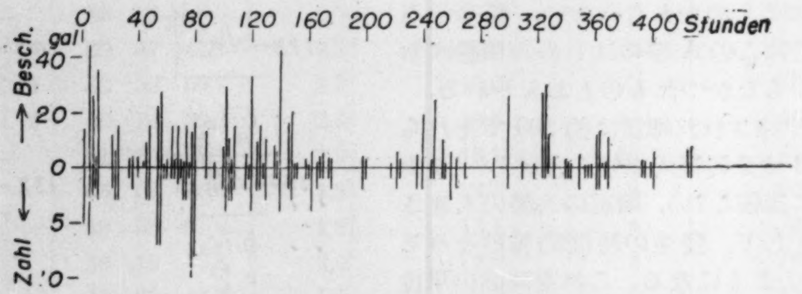

第11圖　船生村にて觀測せる余震の數および最大加速度の和

Fig. 11.　Zahlen der Nachbeben und die Summe der maximalen Beschleunigungen.

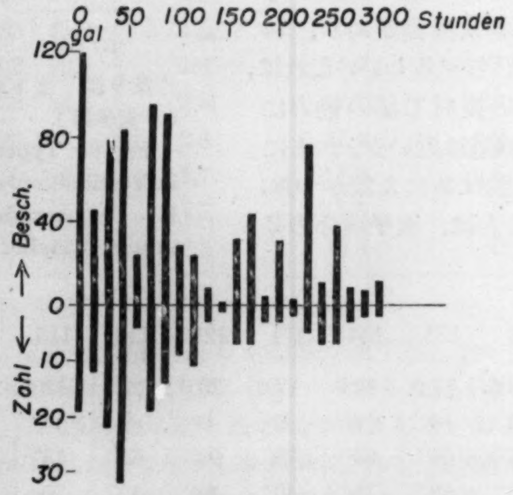

第12圖　船生村にて觀測せる余震の數と最大加速度の和

Fig. 12.　Zahlen der Nachbeben und die Summe der maximalen Beschleunigungen.

台の地震計を交換してみても同様であつたので，地震計のせいではないことはたしかめられた．これらの工場は第13圖にしめす①から⑨までの9ヶ所で，矢印が動力モーターにかけたベルトの方向（モーターの軸に直角）であつて，大部分が東西をむいていることは，*EW*–成分の微動の大きいことに相應している．（第14圖 A, B）村役場および製材業者の厚意により，1つ1つのモーターを別々にうごかして，他をすべてとめてみた．この實験では⑥のモーターだけが特に大きい *EW*–成分微動をあたえた（第14圖 C, D）．他のものは1ヶでは，みわけられるほどの微動をあたえない．この微動は特に大き場合は第14圖のように，うなりの形をしめす．個々の週期（どこでもほとんど一定，5ヶ所はかつてすべて0.13秒），うなりの週期（2.5～2.7秒）とモーターの廻轉（週期0.06秒のモーターをベルトで0.36秒の廻轉におとしている）とは直接の關係がみられない．つまりこれは土地に個有のもののようである．また南北にベルトのかゝつている①，⑤の2ヶだけを動かした場合も，やはり *NS*–成分よりも *EW*–成分の方が大きい微動をしめした．これで，あきらかにこの土地は異方性をもつていることがたしかめられた．

このような微動は地震の記錄のさまたげになるから，觀測點決定にあたり，充分注意してさけるべきであつたので，觀測上の失敗であるが，土地の振動性の異方性についての一例をえたことはおもしろいと思う．

4.4 表土の性質が地震動に影響すること，特に震害にそれが關係することはうたがいない．この場所はうえにのべたように，微動において異方性をしめすが，强制的振動についてはどうか．これらの問題を考え，表土の性質をしるため，簡單な實驗をおこなつた．

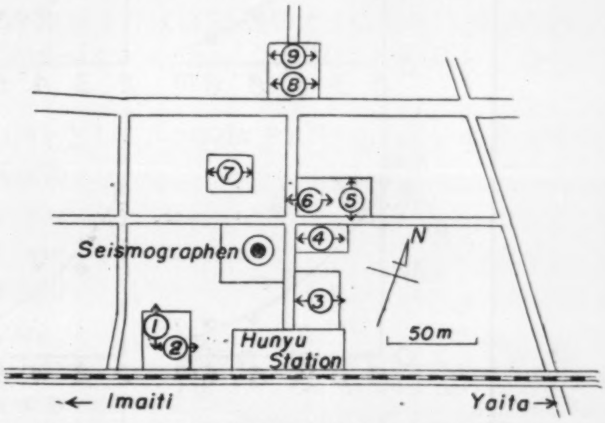

第13圖　船生村觀測點（●）および附近の製材工場モーターの位置（①～⑨，矢印はベルトの方向）

註．モーターの馬力．①20H.P.　②30H.P.　③5H.P.　④4H.P.　⑤15H.P.　⑥10H.P.　⑦2H.P.　⑧5H.P.　⑨3H.P.

モーターの回轉數．①，②，⑤，⑥；950～1150 R.P.M；③，⑧，⑨：1430～1730 R.P.M.；④，⑦：？

Fig. 13. Beobachtungsort am Huhuyu (●) und die Position der Sägemühlen (①～⑥. Pfeilen sind die Richtung der Belt).

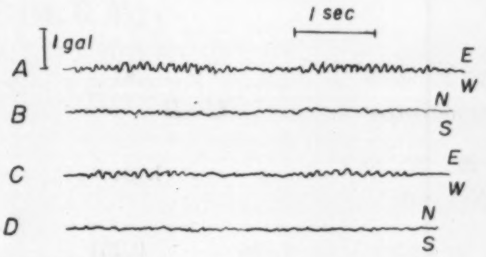

第14圖　モーターによる微動の一例．

A, B：すべてのモーターがうごいている．

C, D：⑥のモーターだけがうごいている．

Fig. 14. Eine Beispiel der Bodenschwingung durch Motor.

A, B: Alle Motoren.

C, D: Nur ⑥ allein.

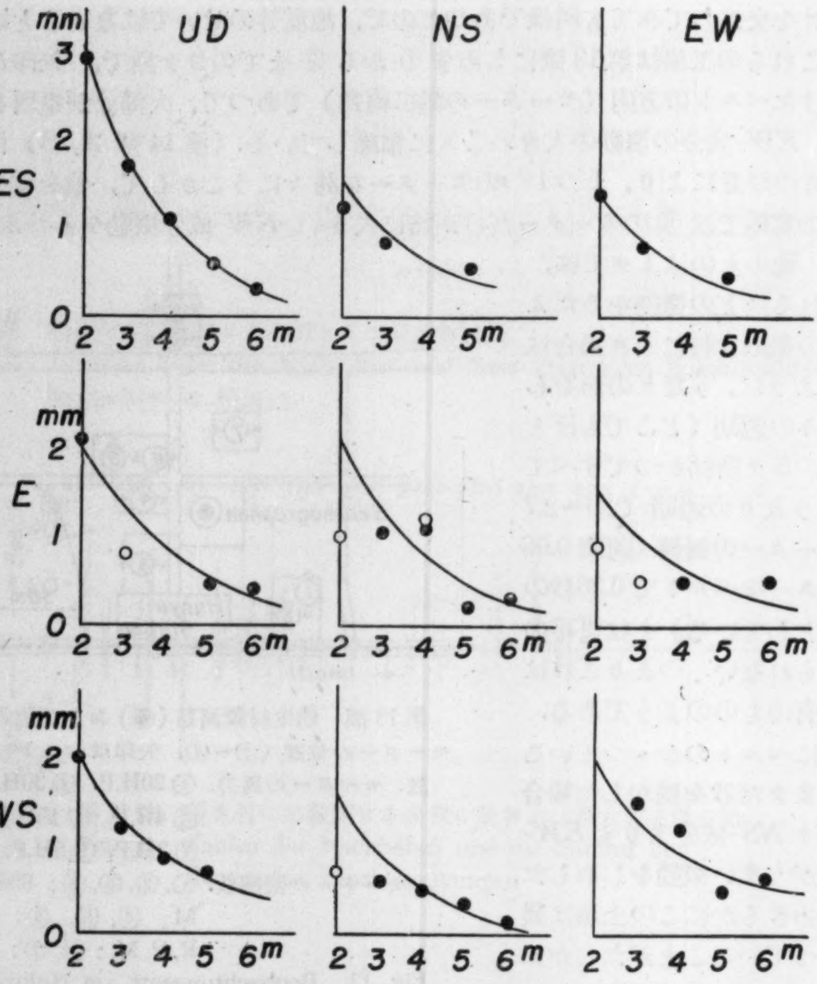

第16圖　砲丸落下による振動の距離による減衰（曲線は目のこでひいたものである）.

Fig. 16. Amplitudenverkleinerung der Bodenschwingung vom Kugelfall mit der Herddistanz.

第II表　Tabelle II

地震計成分 Komponenten	上下動 $U-D$		南北動 $N-S$		東西動 $E-W$	
震源方位 Azimuth	n	$k(m^{-1})$	n	$k(m^{-1})$	n	$k(m^{-1})$
南東 (*ES*)	0,726 ±,006	0,251 ±,004	1,32	0,11	1,18	0,10
東 (*E*)	0,81	0,17	1,09 ± 42	0,17 ±,30	—	—
南西 (*WS*)	0,67 ±,31	0,12 ±,24	0,29 ±,18	0,09 ±,06	0,69 ±,47	0,10 ±,33

$y=Ax^{-n}e^{-kx}$; y: Amplitude, x: Herddistanz.

12ポンド (約5.44 kg) の砲丸を 1 m の高さからおとす．地震計から，場所のゆるす範圍で南東，東，南西，の三方向に 2 m～6 m はなれて，震源をとつた場合地震計のふれをみる．上下動記錄の一例をしめすと第15圖のようである．Hubert12) の實驗によつても，このような場合でる波の週期は 1/20 秒程度以下であるから，この地震計はこゝでは變位計とみられる．記錄紙のおくりがこの週期に對してはのろいので第15圖のようにほとんど最大振幅がよみとれるだけである．それも針さきがかすれて，よみにくいこともある．最大振幅の距離によるへりを圖示すれば第16圖のようになる．圖の左側の *ES*, *E*, *WS* は砲丸をおとした點の地震計からみた方位，上の *UD*, *NS*, *EW* は地震計の成分である．

記象紙上の振幅を $y^{(mm)}$，距離を $x^{(m)}$ として，$y=Ax^{-n}e^{-kx}$ とおき，n, k をきめてみると，第II表のようになる．一番信用のおける *UD*-成分の各方位では大體 $n\fallingdotseq -0.7\sim0.8$ であり，表面傳播の場合の $n=-1$，立體傳播の場合の $n=-0.5$ の丁度中間となつていて，大體表面波にちかいが，下の方にもいくらかエネルギーがゆくという表面波と實體波の中間の形の傳播をすることがわかる．水平成分はふれが小さく，ばらつきも大きい．*ES*, *E* の二方位では精度がおちるが n が 1 にちかく，*WS* 方位ではすこし小さい．しかしとにかく微動のようないちぢるしい異方性はみられない．k はほゞ $0.1\sim0.2\,m^{-1}$ であつて，かなり大きい．もつとも，火藥爆發の波によつて福井平野でもとめられた値は，$n=1$ と假定して $k=0.06$ から $k=0.93$ におよんでいる.13) しかし Mintrop などは第4期層で週期 0.02 秒の波について $k=0.0023\,m^{-1}$ としている．なお長週期の地震波では $k\fallingdotseq10^{-6}$ 以下であることは周知のとおりである．

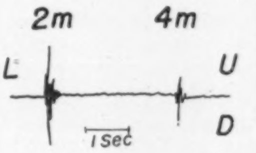

第15圖　砲丸落下による上下動の例．
Fig. 15.　Ein Beispiel der Vertikalbewegung von Kugelfall

5. むすび　おわりに本觀測はすべて本所千喜良利雄君の獻身的な熱意によつておこなわれたものであることを記し，こゝに心からの感謝のことばをのべる．

またクロノメーター其他の使用をゆるされた坪井忠二教授，終始御援助をえた坪井研究室實川顯氏，田島廣一氏にも感謝しなければならない．

さらに觀測地滯在中種々の便宜をあたえられた船生村のかたがたに特に御禮を申しのべたい．(本研究の費用の一部は文部省科學研究費によるものである.)

---

12)　HUBERT, F.,　Zeitschr. f. Geophys. (1924/25).
13)　吉川宗治　防災研究所報告 2 (1949).

32. *Über die Beobachtung der Nachbeben des Imaichi-bebens am Dorfe Hunyu, Provinz Totigi.*

Von Setumi MIYAMURA und Tetuo AKIMA.

Institut für Erdbebenforschung.

Nach dem letzten starken Lokalbeben vom 27. Dezember 1949 bei der Stadt Imaichi (139°42′ E, 36°42′ N) wurde wie gewöhnlich eine Expedition unseres Institutes für die Nachbebenbeobachtungen nach dem epizentralen Gebiet gesandt, und eine Zweigstation derseben am Dorfe Hunyu (139° 47′ E, 36°45′ N) (s. Fig. 2) wurde den Verfassern aufgetragen. Die dabei verwendeten neuen Verbesserungen in Ausrüstung und Methode für Nachbebenbeobachtung im Felde waren wie folgt:

1) Gebrauch von Dreikomponentenseismographen mit gleichen Konstanten, $T_0=0.08$, $V=200$, für jede Komponente.

2) Konstantenbestimmung an der Messtelle durch dynamische Prüfung. (s. Fig. 1)

3) Verwendung von einem Präzisions-registrierapparat, die eine grosse Trommel ($d=$ 195.5 mm, $l=740$ mm) für drei-komponenten Registrierung hat und durch einen von Bifilarpendel regulierten Gleichstrommotor betrieben wird.

4) Vergrösserung von Papiergeschwindigkeit der Registrierung. (d. h. ca. 2.5 mm/sec)

5) Sekundenzeitmarkierung durch einen mit Radiosignal verglichenen Chronometer.

u. s. w.

Folglich wurden die exakten Einsatzzeiten von *P* bis auf 1/10 Sekunde beinah zum ersten Mal in Feldbeobachtung der Nachbeben bestimmt. In Tabelle I ist ein Teil der Daten von 27 Beben zusammengestellt, deren Herdlagen durch *P—S*-Zeiten an 3 oder 4 Stationen bestimmt werden konnten. Einige Reproduktionen der Seismogrammen sind in Fig. 3~8 gezeigt.

Zwar man die näheren seismometrischen Studien nicht aus der Beobachtung von dieser einzigen Station (da andere Zweigstationen keine Zeitmarkierung und genügend schnelle Papiergeschwindigkeit hatten) durchführen kann, können wir doch für jetzt nur sagen, dass

1) *P*, *S*, und andere Einsätze aus einer einzigen Komponente nicht sicher bestimmt werden können,

2) bei gewissen Beben viele Phasen zwischen *P* und *S* bald in eine bald in andere Komponente klar festgestellt werden können, während bei anderen Beben keine solchen Einsätzen klar gefunnden werden,

3) in gewissen Beben kurz vor dem scharfen *P* in Vertikalkomponente eine leichte Bewegung getroffen wird. (s. Fig. 9) Leider finden diese Tatsachen 1)~3) für jetzt noch keine genügende Erklärung.

（震研彙報 第二十八號 圖版 宮村・秋間）

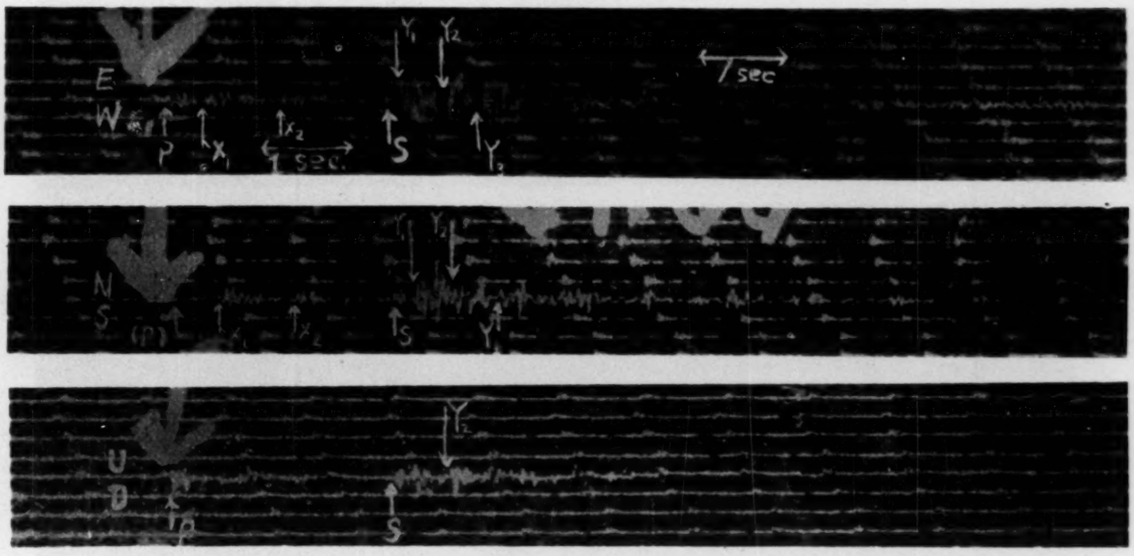

Fig. 3. Nachbeben Nr. 181 (Hunyu); 1950. I. 9; $00^m 19^h 24.^s 1$ $t_{p-s}=2.8$ sec.

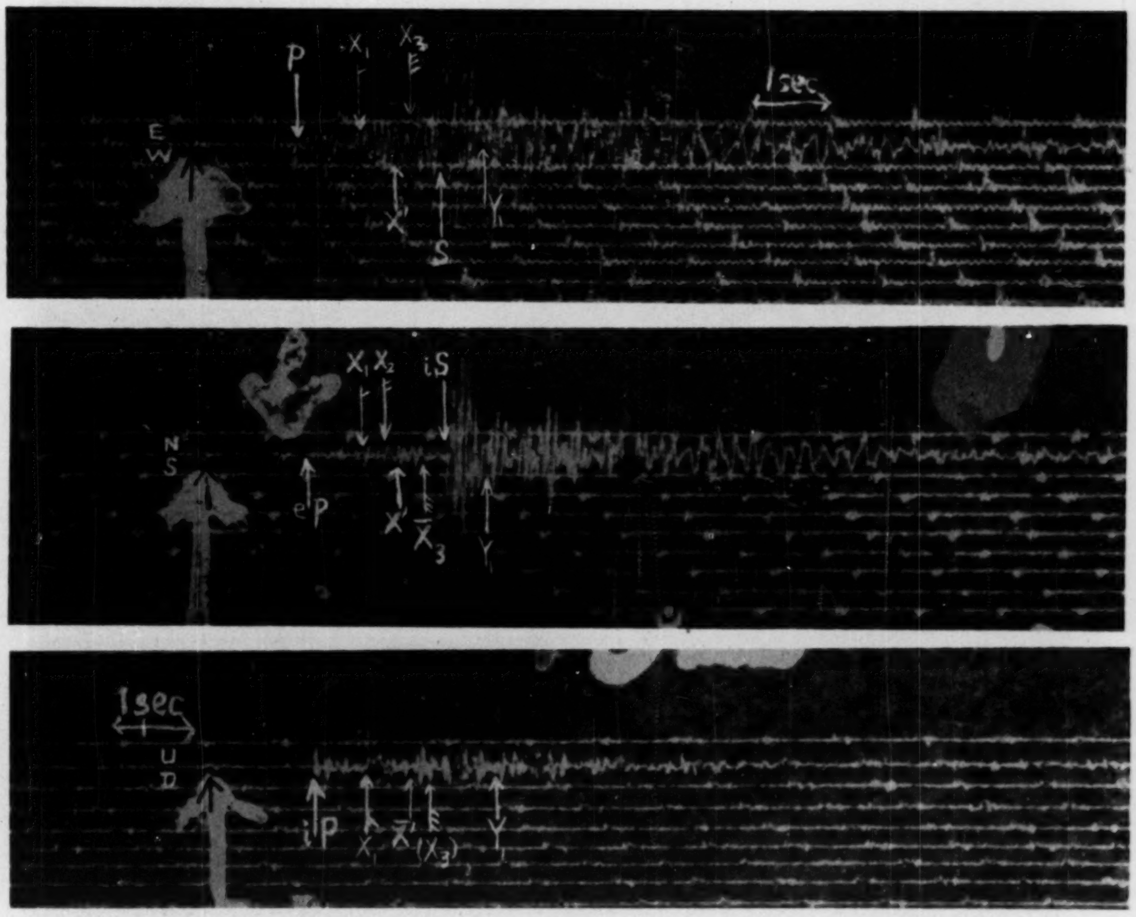

Fig. 4. Nachbeben Nr. 182 (Hunyu); 1950. I. 9; $20^h 32^m 30.^s 3$ $t_{p-s}=1.6$ sec.

N. B. (X): vermuteter Einsatz; $\overline{X}$: fehlender Einsatz (oder negativer Einsatz).

（電研彙報 第二十八號 圖版 宮村・和田）

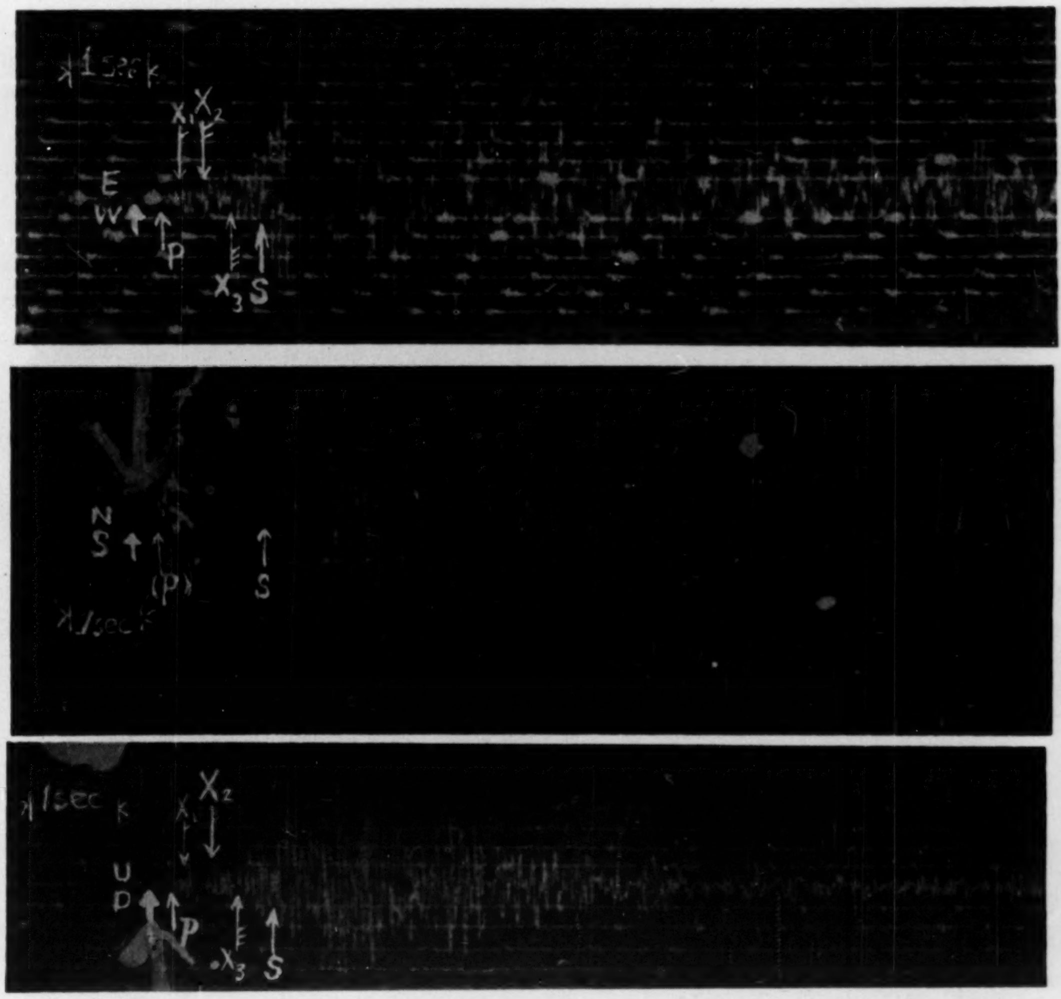

Fig. 5. Nachbeben Nr. 183 (Hunyu); 1950. I. 10; $0(^{h}00^{m}18.^{s}$. $t_{p-s}=1.7$sec
$\Delta=11.0$ km, $h=0$ km, $\varphi=S\,65°\,W$

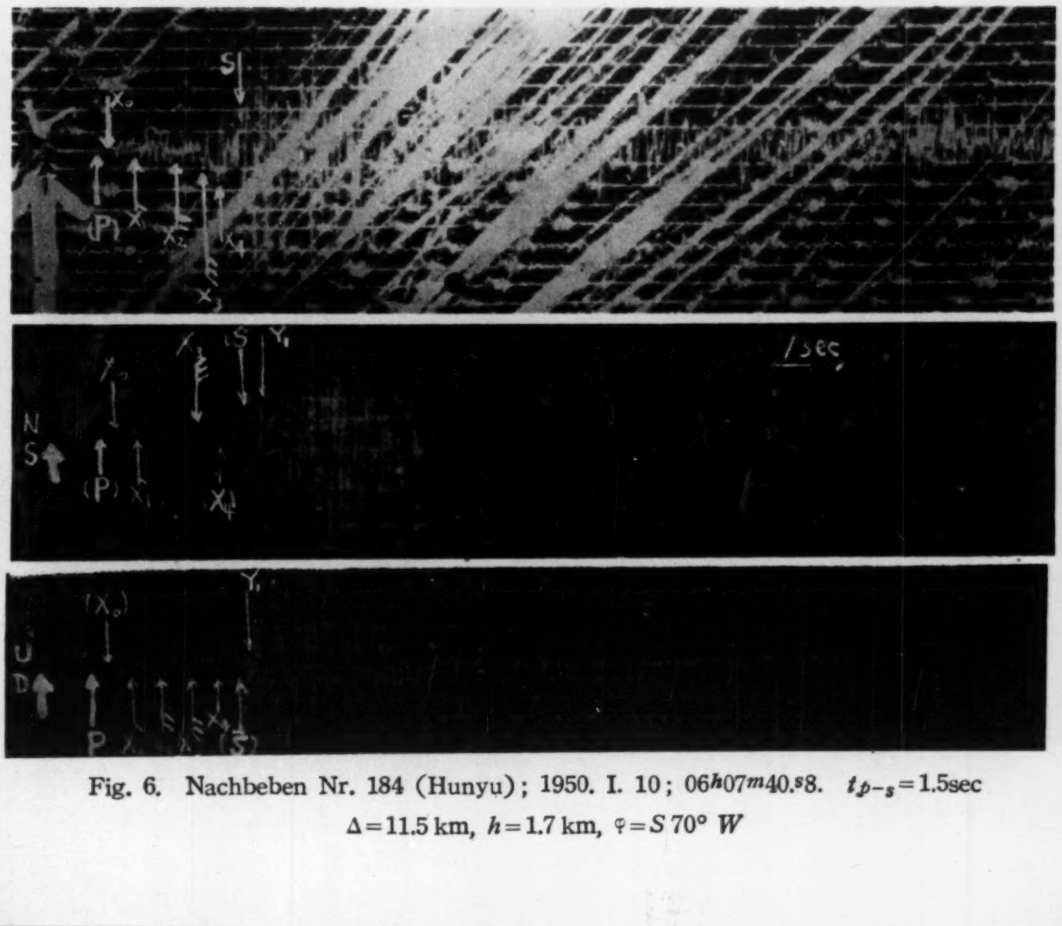

Fig. 6. Nachbeben Nr. 184 (Hunyu); 1950. I. 10; $06^{h}07^{m}40.^{s}8$. $t_{p-s}=1.5$sec
$\Delta=11.5$ km, $h=1.7$ km, $\varphi=S\,70°\,W$

（震研彙報 第二十八號 圖版 宮村・秋間）

（震研彙報 第二十八號 圖版 宮村・秋間）

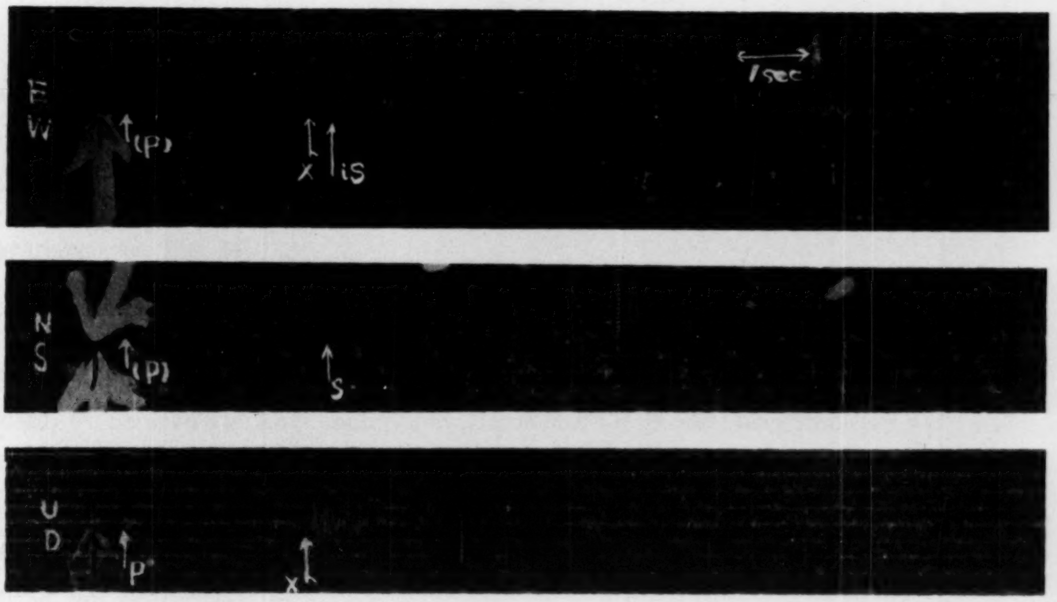

Fig. 7. Nachbeben Nr. 206 (Hunyu); 1950. I. 14; $05^h09^m34.^s5$ $t_{p-s}=2.7$ sec

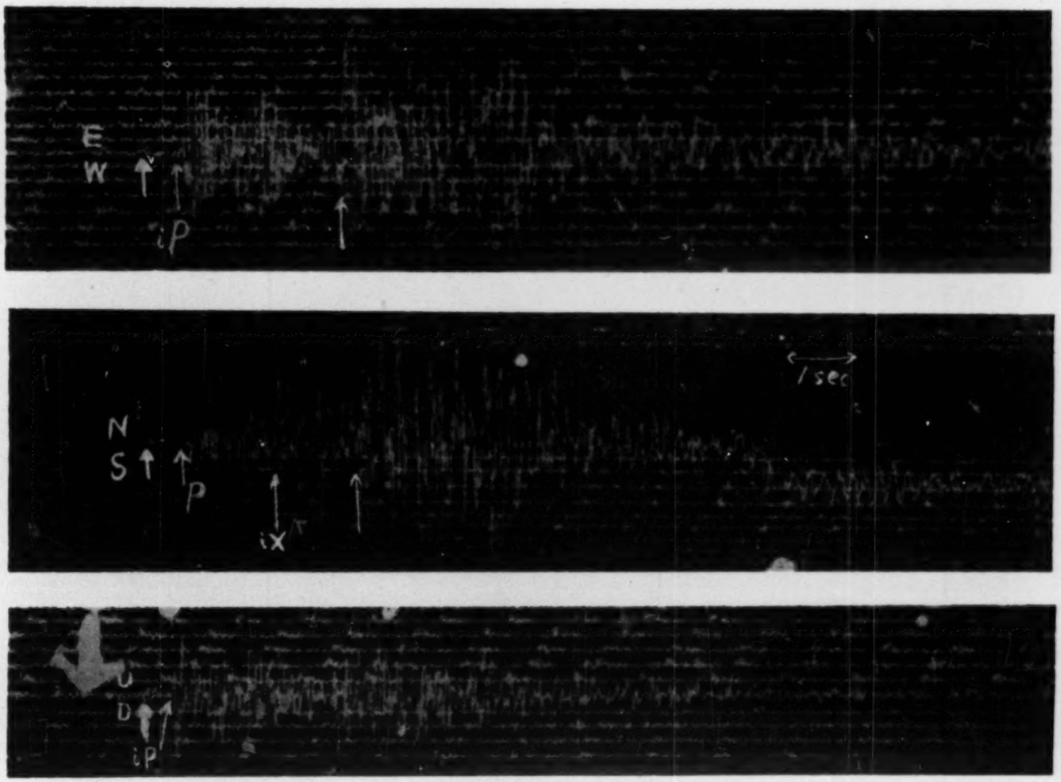

Fig. 8. Nachbeben Nr. 215 (Hunyu); 1950. I. 16; $12^h19^m0.9^s4$ $t_{p-s}=?$

Übrigens zeigten hier die Seismogrammen merkwürdige Bodenunruhe bei Tage besonders in O—W-Komponente. Zwar die Ursache dieser Bodenschwingung die umliegende Sägemühle (1-9 in Fig. 13) ist, gibt es keine direkte Relation zwischen der Periode der Bodenschwingungen und der der Motoren. Die Überwiegung in O—W-Komponente wurde auch von in N-S betriebenen Mühlen klar erzeugt, und daher müssen wir es zu einer Bodenanisotropie zuschreiben. (s. Fig. 14)

Freier Fall einer 12 Pfund Kugel von 1 m Höhe wurde auf den Boden in der Nähe 2～6 m von Seismographen versucht. (s. Fig. 15) Amplitudenverkleinerung mit der Herddistanz ist in Fig. 16 gezeigt und dort kann man keine obengenannte Anisotropie des Bodens finden. Wenn man die Amplitude y mit Herddistanz x in der Gleichung $y=Ax^{-n}e^{-kx}$ darstellen kann, kann man die Konstanten n und k aus diesem Experiment rechnen. (s. Tabelle II) Z. B. bei Vertikalbewegung sind n zwischen 1 und 1/2, und dies zeigt, dass die Wellenausbreitung wenigstens in diesem Fall sozusagen zwischen die der Oberflächenwellen und die der Raumwellen ist.

---

33. *Observation of the Deformation of the Earth's Surface in the Vicinity of the Epicentres of the Imaichi Earthquake.*

By Takahiro HAGIWARA and Tsuneji RIKITAKE,

Earthquake Research Institute.

(Read June 20, 1950—Received Sept. 20, 1950.)

1. Introduction.

After the Imaichi Earthquake of Dec. 26, 1949, an observation of the deformation of the ground was carried out with a water-tube tiltmeter and a silica-tube extensometer. The instruments were installed in disused mine at Ochiai Village about several kilometers distant from Imaichi-machi in the S-direction. According to the seismometric observation1), the epicentres of the main shocks were determined to be 139°39.′9 E, 36°41.′1 N for the first shock and 139°38′.8 E, 36°43′.6 N for the second one, both situated near the observation point. Almost all the aftershocks also occurred in the neighbourhood of the point. Hence, it may be said that the observation was executed at approximately the centre of the seismic activity related to the Imaichi Earthquake. Hitherto we have had some chances for similar observations on occasions of great earthquakes,2),3) but such observations were seldom carried out at seismic centres as in the present case. Thus it is natural to expect that a comparatively larger deformation would be observed, in case it exists, when compared with the former observations cited above.

2. The circumstances of the observation and the instruments.

The writers set a 24 m water-tube tiltmeter and a 12 m silica-tube extensometer in the so-called Keimei Mine, Ochiai village. Keimei Mine is a molybdenum mine drilled in metamorphosed granite rock at the foot of Mt. Keimei, the ore being out of use these several years. As shown in the map of Fig. 1, the mine is situated at the western part of the Ochiai Village where, as

---

1) Y. KOSHIKAWA, Read at the July Meeting of the Earthquake Research Institute, 1950.

2) T. HAGIWARA and J. YAMADA, *Special Bull. Earth. Res. Inst.*, No. 5 (1947), 179.

3) *Rep. Spec. Com. Fukui Earthq.* (1950), 124.

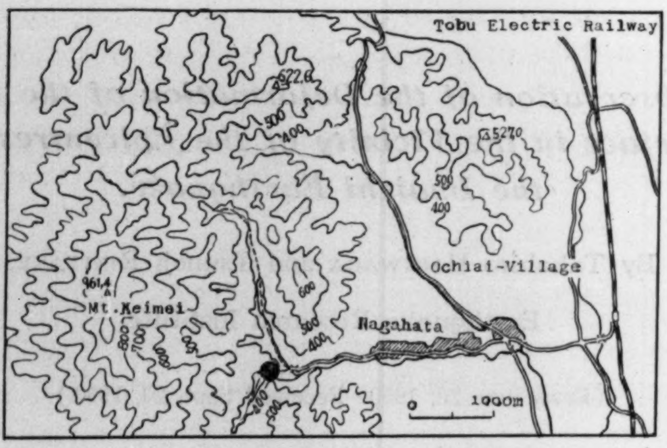
Tobu Electric Railway
622.6
500
400
527.0
500
400
Ochiai-Village
614
Mt. Keimei
800
700
600
500
400
Nagahata
0
1000m

Fig. 1. The map about the observing point, which is indicated with black circle.

already stated in the Introduction, may be regarded as the centres of the aftershocks as well as the main shocks. The main adit of the mine is drilled from the base of a river in the NW-direction about 1 km in length, while many branch adits are bored as shown in Fig. 2. The instruments were installed at a depth of about 50 m from the entrance. Their arrangement is also shown in Fig. 2. Photo. 1 shows the view of the entrance of the adit. The temperature in the mine was always kept at about 13°C within an error of ±0.°5.

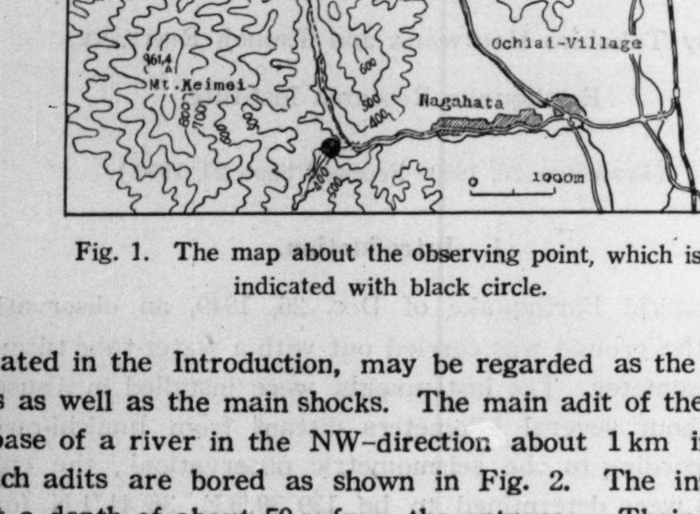
W
W
E
N
E
W
N
10m
S

Fig. 2. The plan of the adit.

About 10 days after the occurrence of the main shocks, the concrete blocks for the instruments were constructed. Observation was carried out from Jan.

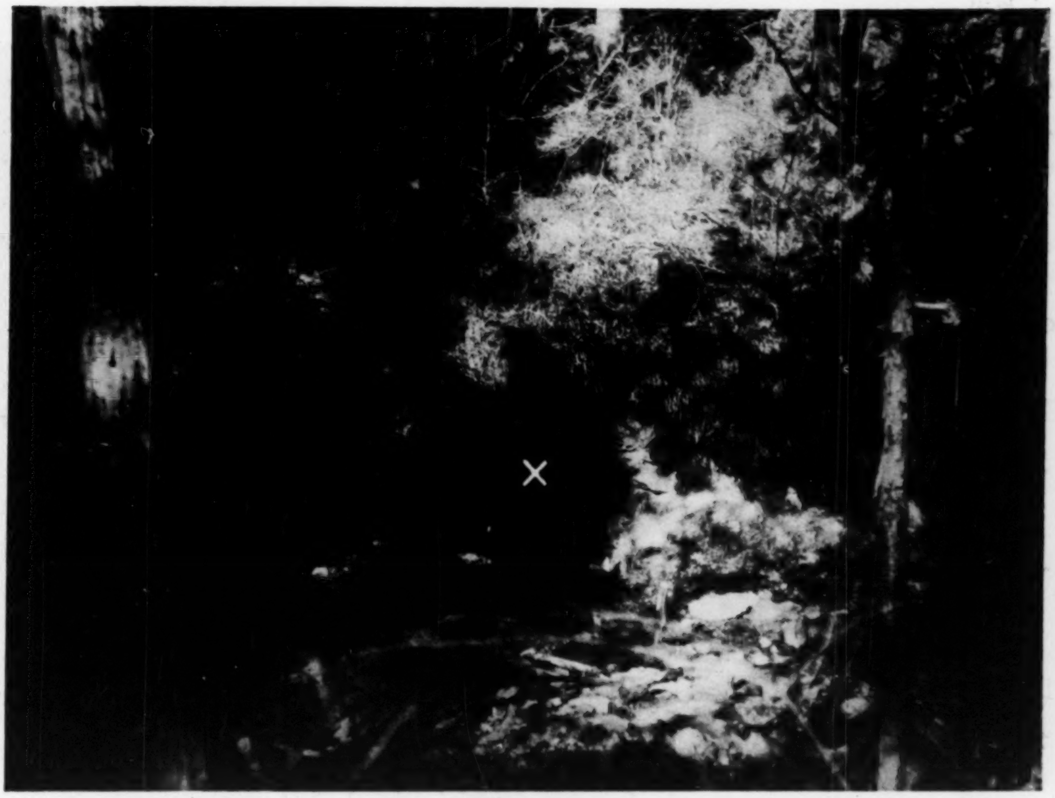

Photo. 1. The view of the entrance.

15. The instruments used here were almost the same with those used at Aburatsubo,[4] Matsuyama,[5] and Bandojima[3] at the time of Fukui Earthquake. The water-tube tiltmeter, however, was improved so as to measure the absolute difference of the heights of two bench marks which are fixed to the concrete blocks. A water-container is tightly mounted on a gun-metal stand with three legs, one of them made of stainless steel while the other two are gun-metal screws. After setting the stainless one on the bench mark which is also made of stainless steel, the inclination of the stand is adjusted with the screws so as to keep the container's height relatively constant to the bench mark. Two spirit levels attatched to the stand are used for adjustment. Then the water-level in the container is read off with a sharp point of stainless steel, its lower part being a micrometer. When the heights

---

4) T. Hagiwara, T. Rikitake, K. Kasahara and J. Yamada, *Spec. Bull. Earthq. Res. Inst.*, No. 6 (1949). *Bull. Earthq. Res. Inst.*, 27 (1949), 35 and 39. T. Hagiwara, T. Rikitake, and J. Yamada, *Bull. Earthq. Res. Inst.*, 26 (1948), 24.

5) T. Hagiwara, T. Rikitake and J. Yamada, Read at the June Meeting of the Earthquake Research Institute, (1949).

of the two bench marks are thus obtained with a pair of the container just mentioned, it is possible to find the difference between the heights of the two bench marks as follows. In the first place, we obtain the two readings h_1 and h_2 respectively for the containers No. 1 and No. 2, which are respectively set on the bench marks A and B. As the zeros of the micrometers are arbitrarily taken, the heights of the water-level above the bench marks A and B become respectively h_1+c_1 and h_2+c_2 where c_1 and c_2 are constants respectively proper to the containers No. 1 and No. 2. Hence the difference between the heights of the two bench marks is obtained as

$$\Delta h=(h_1-h_2)+(c_1-c_2)\,. \qquad \ldots\ldots\ldots\ldots\ldots\ldots\ldots\ldots(1)$$

On exchanging the containers, we have similar readings h_1' and h_2' respectively for No. 1 and No. 2, from which we obtain

$$\Delta h=(h_2'-h_1')-(c_1-c_2)\,. \qquad \ldots\ldots\ldots\ldots\ldots\ldots\ldots\ldots(2)$$

Adding (2) to (1), Δh becomes

$$\Delta h=\frac{1}{2}\{(h_1-h_2)-(h_1'-h_2')\}\,,$$

while, subtracting (2) from (1), the instrumental error c_1-c_2, which is peculiar to a combination of two containers, is determined to be

$$c_1-c_2=\frac{1}{2}\{(h_1-h_2)+(h_1'-h_2')\}\,.$$

Thus the change in the difference between the heights of two bench marks can be measured at any time even when we once take off the instrument from bench marks.

The height-differences of the pairs of bench marks (EW) and (NS) were measured at the beginning of the observation. Then the containers were set on N and S, the change being continuously observed. It is difficult, however, to carry out an exact measurement repeatedly, because it is dark in the adit where there is no electric supply and, moreover, the space is very narrow, full of humidity, and there is danger of weathered rocks falling from the ceiling. For these reasons, no measurement has been repeated.

As to the extensometer, since the instrument is just the same with that used at several places cited above, the description of the instrument will be omitted here.

3. The results of the observation.

The water-tube tiltmeter was read twice a day during the period from Jan. 15 to Mar. 22 and once a week after that period. The change in the inclination thus observed is plotted as shown in Fig. 3 together with the result

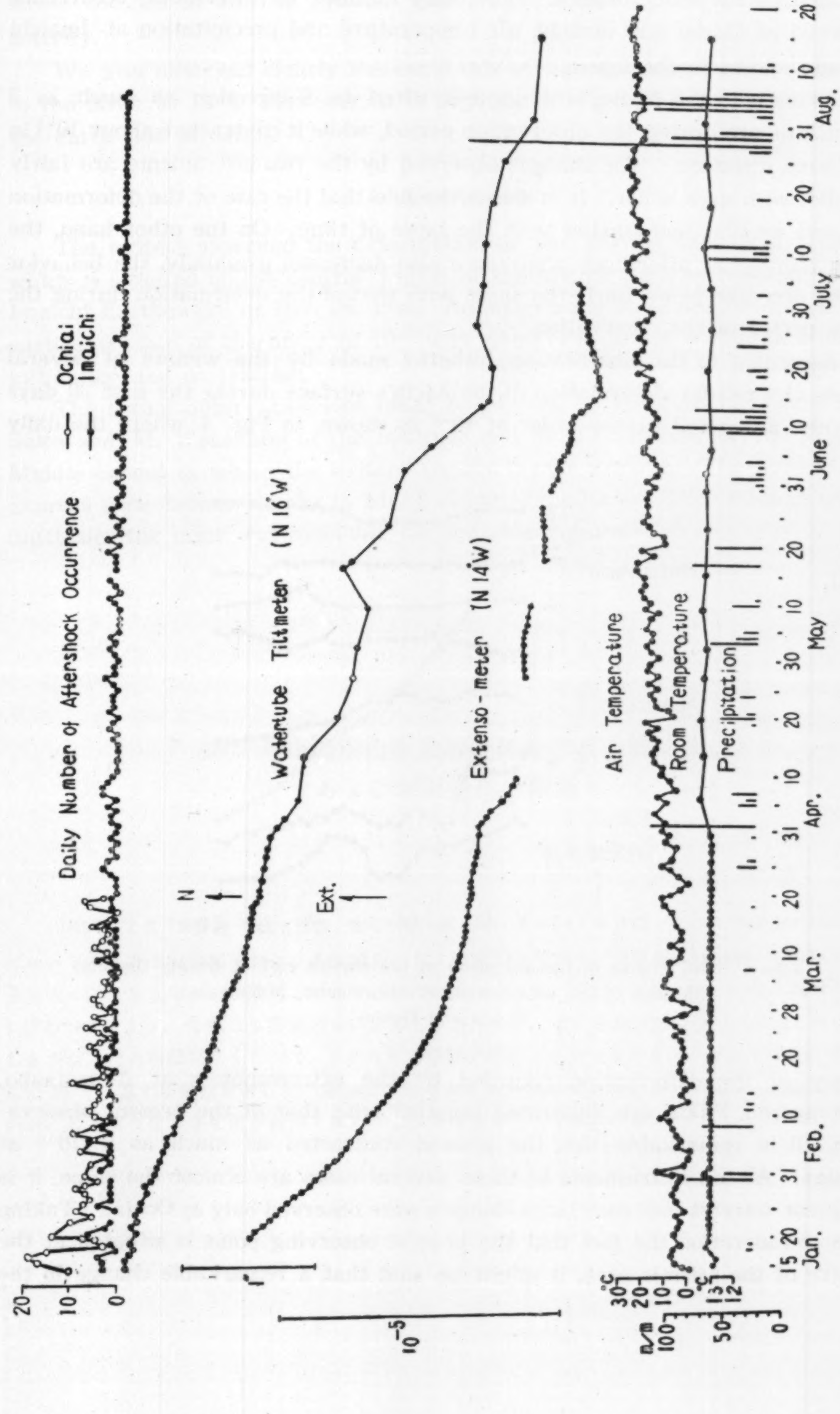

Fig. 3. The results of the observation.

obtained by the extensometer. The daily number of aftershock occurrence observed at Ochiai and Imaichi, air temperature and precipitation at Imaichi are also shown in the figure.

As seen in the figure, the ground tilted to S-direction as much as 3 seconds of arc during the observation period, while it contracted about 10^{-5} in the same direction. The changes observed by the two instruments are fairly parallel with each other. It is also noticeable that the rate of the deformation becomes smaller and smaller with the lapse of time. On the other hand, the daily number of aftershock occurrence also decreases gradually, the behavior of the decrease being fairly the same with that of the deformation during the early period of the observation.

According to the observation hitherto made by the writers at several places, the secular deformation of the earth's surface during the first 30 days scarcely amounted to the order of 10^{-6} as shown in Fig. 4 where the daily means of the deformation recorded by the extensometers at Aburatsubo, Matsuyama, Fukui are illustrated together with that of the present observation. It is remarkable that the ground contracted as much as 5×10^{-6} at Ochiai. As the instruments in these several cases are almost the same, it is of great interest that such large changes were observed only at Ochiai. Taking into consideration the fact that the present observing point is situated at the centre of the seismic area, it might be said that a remarkable change in the

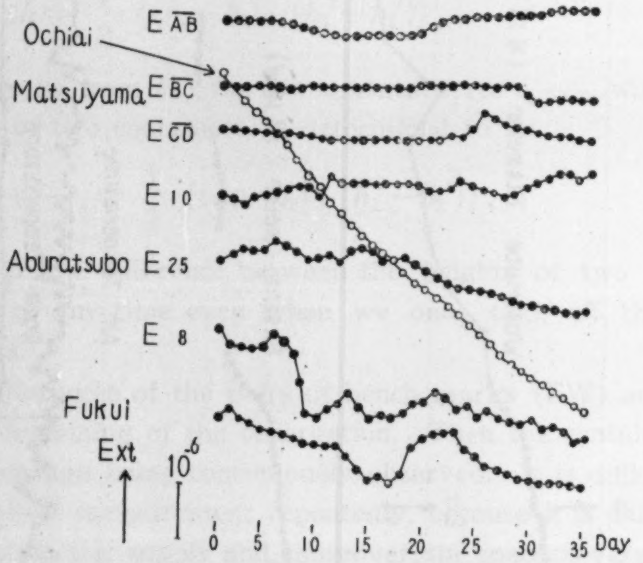

Fig. 4. The change in the extension of the earth's surface during the first 35 days of the observation at Aburatsubo, Matsuyama, Fukui and Ochiai

strain component of the ground was found at the centre of the seismic activity.

We also observed clearly the earth tide by the extensometer, it amounting to the order of 10^{-8}. However, it is beyond the scope of this paper to study the earth tide in detail.

4. Conclusion.

The writers observed the deformation of the earth's surface in a mine which is situated at the central region of the seismic activity related to the Imaichi Earthquake of Dec. 26, 1949. An abnormally large deformation of the earth's surface of the order of 10^{-5} was observed during 7 months both in inclination and contraction.

The actual observation was made by Messrs. K. Kasahara, J. Yamada, S. Saito and M. Watanabe of the Institute and Mr. T. Honda of the Imaichi Middle School to whom the writers' cordial thanks are due. The writers also express their hearty thanks to Mr. I. Ando of the Keimei Mine through whose courtesies the mine was available for the observation.

---

33. 今市地震の震央附近における土地伸縮および傾斜變化の観測

地震研究所 萩原尊禮
地震研究所 力武常次

1949年12月26日の今市地震後，1950年1月15日より約7ケ月間，その震央附近の鷄鳴鉱山において水晶管土地伸縮計および水管傾斜計による觀測を行つた．測定器類は油壺，松山および福井地震の際坂東島において使用されたものとほゞ同一である．從來大地震の際この種の觀測をしばしば行つてきたが，今回は本震震源のほとんど直上であり，また余震活動の中心に位置していた．したがつて過去の觀測にくらべて，より大きな變動が期待されたのであるが，果して傾斜，伸縮ともに10^{-5}に達する變動を示した．觀測はそれぞれ1成分のみであつたので，詳しい議論は出來ないが，このような大きな歪が觀測されたことは興味あることゝ思われる．

strain component of the ground is small at the centre of the seismic activity.

We also observed directly the earth tide by the extensometer, it amounting to the order of [illegible]. However, it is beyond the scope of this paper to study the earth tide [illegible] which will be reported [illegible] another paper.

4. Conclusion.

The writers observed the deformation of the earth's surface in a mine which is situated at the central region of the seismic activity related to the Imaichi Earthquakes of Dec. 26, 1949. An appreciable large deformation of the earth's surface of the order of [illegible] was observed during 7 months both in inclination and contraction.

The actual observation was made by Messrs. K. Kasahara, [illegible] and M. Watanabe of the Institute and Mr. [illegible] of the Imaichi Middle School to whom the writers' cordial thanks are due. The writers also express their hearty thanks to Mr. J. Ando of the Ashio Mine through whose courtesies the mine was available for the observation.

今市地震の震央地域における土地変形

（足尾銅山における観測）

地震研究所 萩 原 尊 禮
　　　　　 [illegible]

1949 年 12 月 26 日の今市地震 [illegible]

34. *Results of Precise Levellings Executed in the Epicentral Region of the Imaichi Earthquake.*

By Ryutaro TAKAHASI, Kintaro HIRANO and Isamu AITA,

The Earthquake Research Institute.

(Read March 20, 1950.—Received Sept. 20, 1950.)

During the first two weeks after the outburst of the Imaichi Earthquake, the decrease in number of aftershocks seemed to be abnormally slow, threatening with the possibility of occurrence of another earthquake. It suggested also that the post-seismic crustal movement was going on slowly, and we thought that this was a good chance to study the relation between the aftershocks and the post-seismic crustal movements. Although after a time the decrease in number of aftershocks proved to be not so abnormal, the levelling surveys were repeated as they were planned at first.

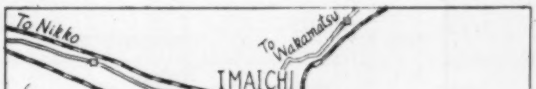
To Nikko
To Wakamatsu
IMAICHI
Nikko Highway
To Utsunomiya
R. Namekawa
Umaguchi
Toiri
OCHIAI-MURA
Takachiya
Zone of Subsidence
Keimei Mine
Nakai
Tajiri
Ushiroyama
Myojin
0
1
2
3
4 KM
□ G.S.B. BM.
○ E.R.I. BM.

Fig. 1.

In the vicinity of Imaichi, there are two levelling routes; one along the Nikko Highway, from Utsunomiya to Nikko via Imaichi, and the other along the Aizu Highway, from Imaichi to Wakamatsu. These levelling routes, which belong to the Geographical Survey Bureau, were not however utilized, since they are somewhat distant from the epicentre of the present earthquake as determined provisionally from the distribution of damage to houses and land-slides, and accordingly the crustal movement there was supposed to be small. Instead of these levelling routes, a new route was schemed, which starts from the BM at Imaichi towards the south, crosses the valley of Namekawa, runs through Ochiaimura, the most severely shaken village, and then turns to the east to reach the Myojin Station. A reconnaissance however proved that it is difficult for the precise levelling survey to cross the valley of Namekawa, owing to numerous land-slides and steep topographies. In these circumstances the present levelling was executed only in Ochiaimura along the route shown in Fig. 1 by thick lines.

Bench Marks.

Since it was necessary to execute the first levelling survey as fast as we can, iron rivets, cemented to natural rock or, in some cases, to huge boulders deeply imbedded into the ground, were used as bench marks. Their localities are given in Table I and in Fig. 1. No. N bench mark is a temporary one.

Table I Localities of Bench Marks

Bench Marks No.	Name of Locality	Note
No. 1	Ushiroyama	20 m east of Myojin Police Station.
No. 2	Nakai	Under the Jukuya stone tower.
No. 3	Takachiya	Under the fire-tower.
No. 4	Umaguchi	
No. N	Tajiri	On the handrail of a concrete bridge at the branch pt. to Takachiya.

Instruments and the method of survey.

The instruments used in the present survey were as follows:

Level: Zeiss 1st order levelling instrument
No. 5934.

Staffs: Invar tape staffs Nos. 841 and 842.

The method of survey was just the same as used by the Geographical Survey Bureau of Japan, except that two steel spikes, each 2.5 cm. in diameter and 30 cm. long, were used in place of the usual ground-plates for the staff, since the ground plates were found to sink into the frozen or muddy ground.

Results.

Results of the surveys, which were repeated three times, are given in Table II. In Table III are given the heights of each bench mark as found by the three surveys, as well as the variations in height in the intervals between each survey.

Table II

Section	Distance	First Survey		Second Survey		Third Survey	
		Jan. 10-15, 1950		Feb. 24-27, 1950		Apr. 11-13, 1950	
		Height Diff.	Closing Error	Height Diff.	Closing Error	Height Diff.	Closing Error
	km	m	mm	m	mm	m	mm
1-N	0.590	0.18784	0.27	0.19066	0.15	0.18819	1.52
N-2	1.840	44.84931	0.15	44.83741	1.05	44.83592	2.83
N-3	1.380	22.46240	0.07	22.44937	2.93	22.45127	3.13
3-4	2.080	56.18477	0.09	56.18963	1.35	56.18517	4.63

Table III

Survey / BM	I	II	III	II-I	III-II	III-I
	m	m	m	mm	mm	mm
1	0.00000	0.00000	0.00000	0	0	0
2	45.03715	45.02807	45.02411	− 9.08	−3.96	−13.04
3	22.65024	22.64003	22.63946	−10.21	−0.57	−10.78
4	78.83501	78.82966	78.82463	− 5.35	−5.03	−10.38
N	0.18784	0.19066	0.18819	2.82	−2.47	0.35

Conclusion.

Variations in heights of each bench marks are graphically shown in Fig. 2. The feature of the crustal movement is very complicated, but it seems that the bench marks No. 1 and No. N belong to a land-block different from that on which the remaining bench marks lie, and each of these two blocks made a south-eastery tilt in the interval II–I, and then a north-westery tilt in the interval III–II, making a zone of discontinuity at the boundary.

It seems that a zone of subsidence that appeared with the earthquake to the north of No. 1 bench mark in the direction NE, corresponds to this boundary of land-blocks. The surveyed area as a whole is inclining towards NW, but the absolute amounts of tilt have been gradually decreasing.

In connection with the present results, it will be interesting to mention that the Geographical Survey Bureau has found a remarkably upheaved zone to the west of Imaichi. Areal extension of this upheaved zone is not known but seeing that this is caused by the main earthquake, it can be said that the post-seismic crustal deformations surveyed by us are perhaps in the direction of recovery from the initial crustal deformations caused by the main earthquake.

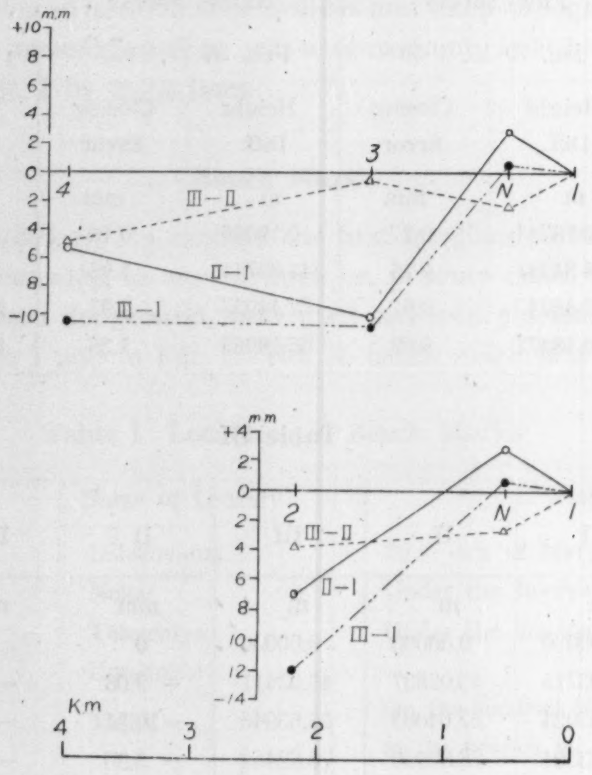

Fig. 2.

34. 今市地震の震央地域における精密水準測量結果（概要）

地震研究所
高橋龍太郎
平能金太郎
相田　勇

今市地震の震央地域と思わはる落合村において3回の精密水準測量を施行して本文第II表及第III表に示す如き結果を得た.

初め日光街道に沿つてある地理調査所の水準線路に今市町において取附ける豫定であつたが行川の兩岸が地形急峻で山崩が多く通過困難のため落合村内のみとした.

水準點は第I表及び第1圖に示す如く施置した. 急速を要するため岩盤に植附けた鐵ボルトを用ひた,

測量方法は凡て地理調査所の方式と規格とによつた．第2表の結果によれば水準點 No. 1, No. N と水準點 No. 2, No. 3, No. 4 とは別箇の地塊上にあるものの如くで，兩方の地塊は第1回，第2回の測量期間夫々南東に傾いて，兩地塊の境目に食違を生ずる様な運動をした．此の境目は宛も地震當時 No. N 水準點の直北に當つて，東北-西南の方向に沈下を生じた地帶に相当するものと思はれる．第2回，第3回の測量期の間には兩地塊は前と反対の方向に動き，全期間を通じて見ると，西乃至西北に傾いてゐる．傾斜の量は漸次に減少してゐる．

地理調査所の測量によれば今市町西方に著しい隆起地域があることと，此が本震によつて生じたものであることを考へ合せると，落合村の地塊の運動方向は本震に伴ふ地殼運動が恢復する方向に向つてゐるものと思はれる．

35. *Land Slip in the Imaichi District Revealed from the Breaks in the Well-Tubes.**

By Takao HONDA,

Imaichi Middle School.

(Read July 18, 1950.—Received Sept. 22, 1950.)

Introduction.

After the earthquake of Dec. 26, 1949, a large number of wells became dry or muddy in the Imaichi district, and the inhabitants found breaks in the well-tubes at some depth beneath the ground. The writer examined the water-wells distributed in and around the town of Imaichi and found out the horizontal slip of the strata of soil concealed under the ground. Then, with the cooperation of his 20 pupils of the Imaichi Middle School, he carried out more detailed investigations into this phenomenon from the end of May to the beginning of July, 1950.

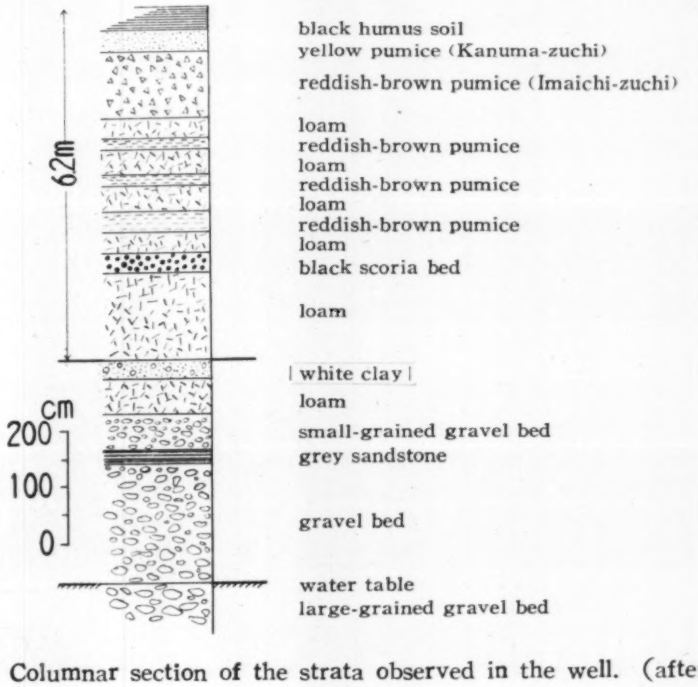
6.2m
cm
200
100
0
black humus soil
yellow pumice (Kanuma-zuchi)
reddish-brown pumice (Imaichi-zuchi)
loam
reddish-brown pumice
loam
reddish-brown pumice
loam
reddish-brown pumice
loam
black scoria bed
loam
white clay
loam
small-grained gravel bed
grey sandstone
gravel bed
water table
large-grained gravel bed

Fig 1. Columnar section of the strata observed in the well. (after J. Osaka)

---

* Communicated by T. HAGIWARA.

We carefully investigated whether the wall of the well was relatively displaced or not. The number of the wells investigated by us reached 168. When displacement was recognized, we measured the depth where the displacement occurred, and also the direction and amount of the displacement. As far as we know, the slip plane surely coincided with the white clayey bed

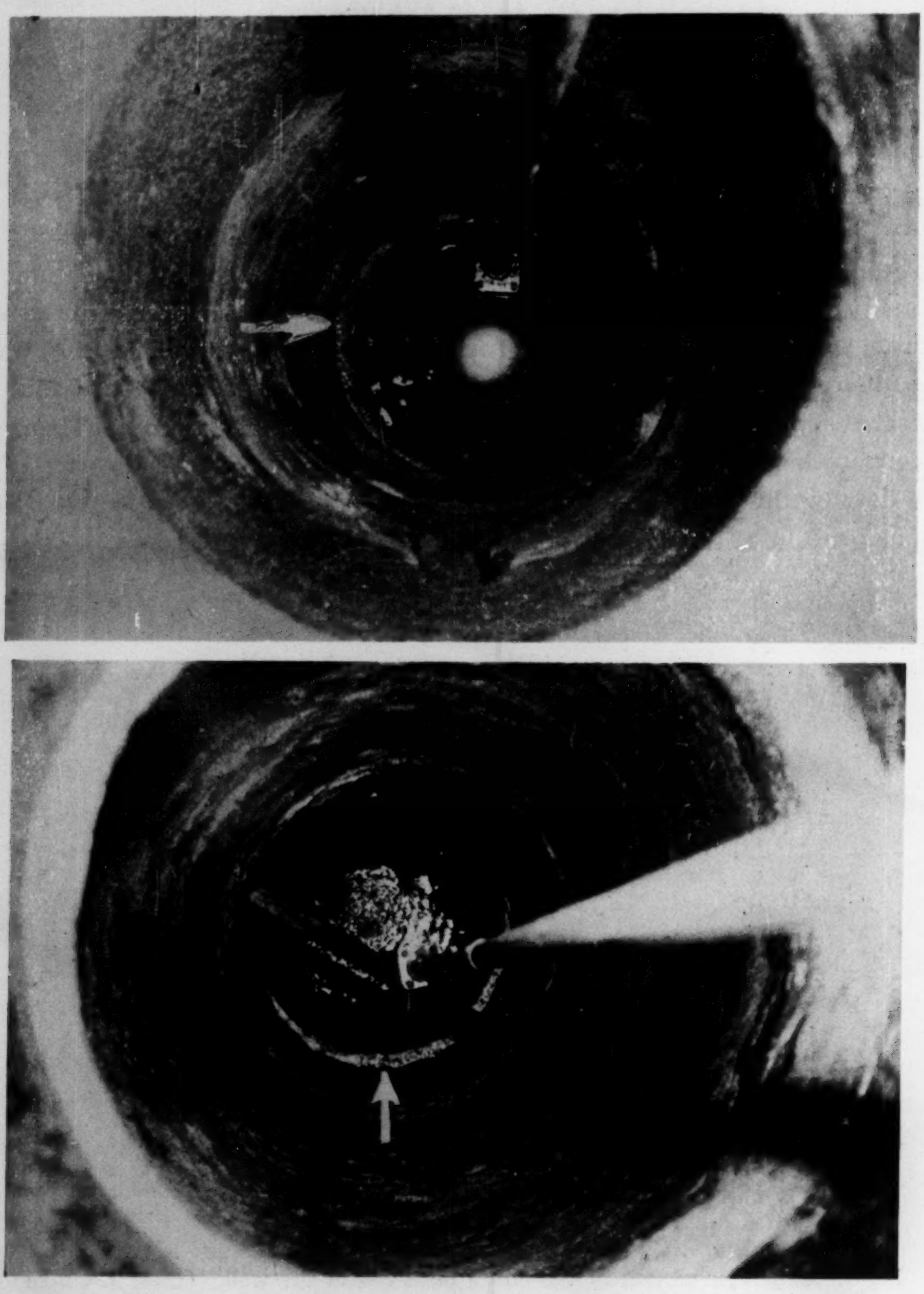

Fig. 2. White clayey bed is seen in a crescent-shape, showing the displacement of the side-wall of the well.

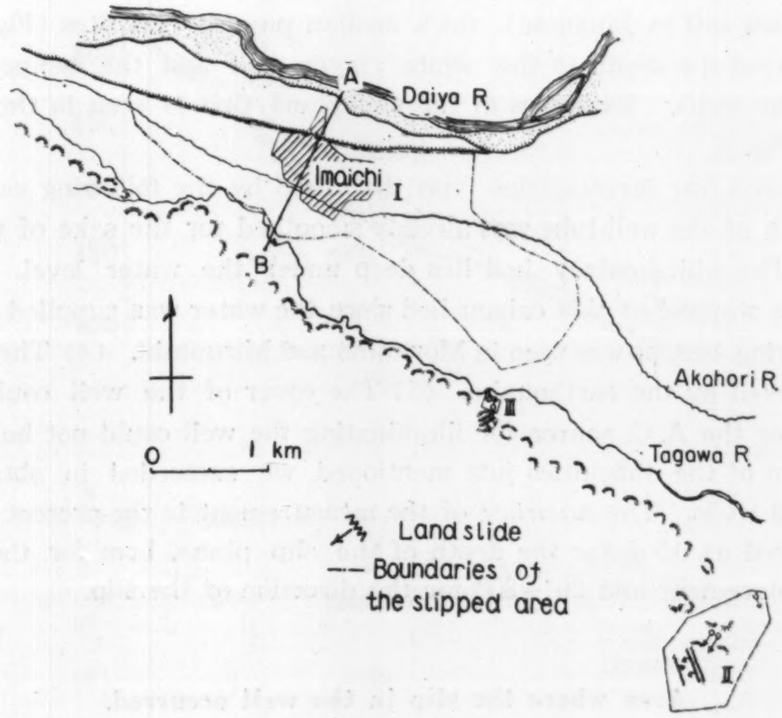
A
Daiya R
Imaichi
I
B
Akahori R
II
0
1 km
Tagawa R
Landslide
Boundaries of
the slipped area
III

Fig. 3. Distribution of the slipped area.

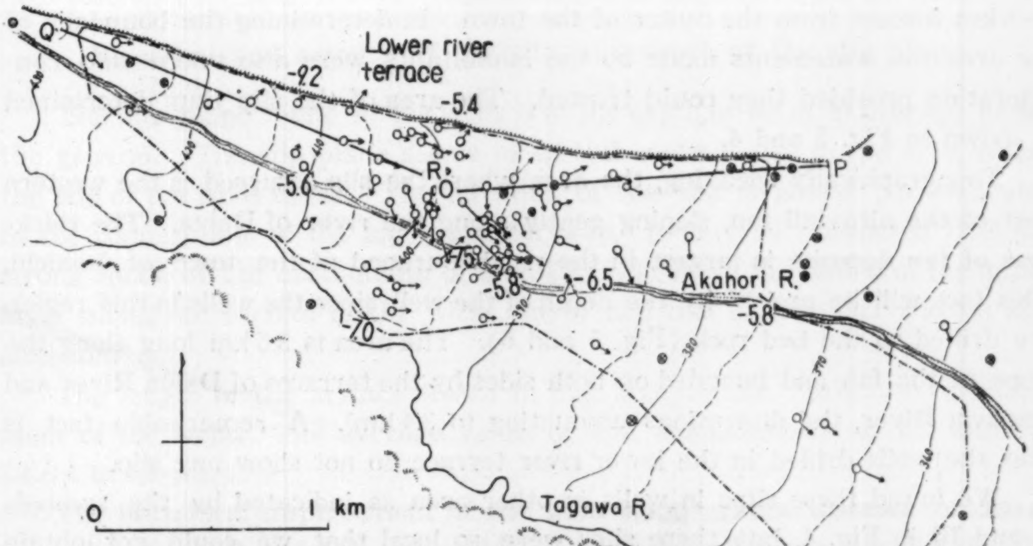
Q
Lower river
terrace
-22
-5.4
P
R
O
5.6
-7.5
-6.5
-5.6
Akahori R
-5.8
-7.0
0
1 km
Tagawa R
Slip amounting
to 10cm

Fig. 4. ⊸ Direction and amount of the slip. ⊗ Wells whose break could not be observed. Numbers (f.e. −5.8) Relative height (m); the surface of the alluvial fan being assumed as 0.

in the loam deposite overlaid by the so-called Imaichi-zuchi or Kanuma-zuchi (Zuchi means soil in Japanese), thick aeolian pumice deposites (Fig. 1). We also measured the depth to this white clayey bed and the temperature of water in the wells. Examples of the slip plane that is seen in the well are shown in Fig. 2.

Sometimes our investigation was disturbed by the following causes. (1) The surface of the well-tube was already smoothed for the sake of well-cleaning. (2) The white calyey bed lies deep under the water level. (3) The drlling was stopped at this calyey bed since the water was supplied from this water bearing bed, as was seen in Moritomo and Mizunashi. (4) The well-tube was destroyed by the earthquake. (5) The cover of the well could not be removed, or the A. C. source for illuminating the well could not be available.

In spite of the difficulties just mentioned, we succeeded in obtaining the data of 168 wells. The accuracy of the measurement in the present case may be considered as 0.5 m for the depth of the slip plane, 1 cm for the amount of the displacement and 20°~30° for the direction of the slip.

Area where the slip in the well occurred.

To determine the area where the slip in the well appeared, investigations were carried out in the town of Imaichi and in the surrounding villages, within 6~8 km distant from the center of the town. In determining the boundary of the area the statements made by the inhabitants were also taken into consideration provided they could trusted. The area of the slip thus determined is shown in Fig. 3 and 4.

Topographically speaking, the area where the slip occurred is the western part of the alluviall fan, sloping gently along the river of Daiya. The thickness of fan deposite is largest in the neighbourhood of the town of Imaichi. This fact will be proved by the depth of the well, since the wells in this region are drilled to the bed rock (Fig. 5 and 6). The area is 3.6 km long along the slope of the fan and bounded on both sides by the terraces of Daiya River and Tagawa River, the dimensions amounting to 3.4 km². A remarkable fact is that the wells drilled in the lower river terrace do not show any slip.

We found these slips in wells in other area as indicated by the symbols II and III in Fig. 4, but these slips were so local that we could not obtain sufficient data to discuss their character in detail. They seem to have been induced by the landslide which occurred in the neighbourhood of them, because the wells which slipped could not be found in places rather distant from there.

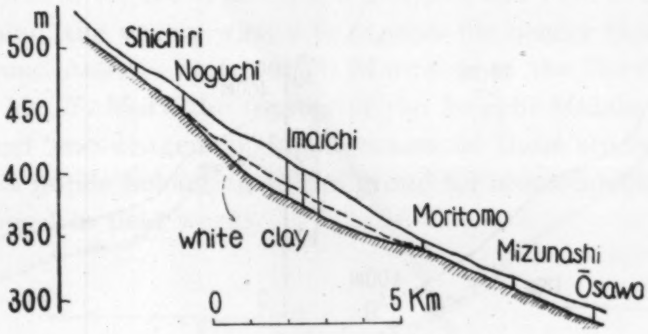
m
500
450
400
350
300
Shichiri
Noguchi
Imaichi
white clay
Moritomo
Mizunashi
Ōsawa
0
5 Km

Fig. 5.

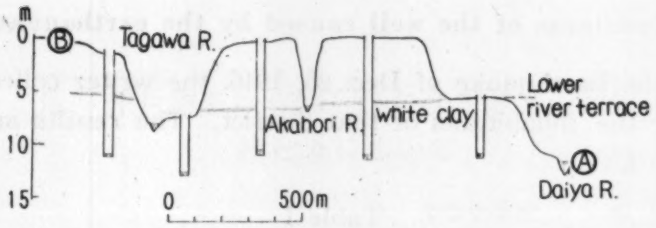
m
0
5
10
15
Ⓑ
Tagawa R.
Akahori R.
white clay
Lower river terrace
Ⓐ
Daiya R.
0
500m

Fig. 6.

Direction and amount of the slip, and depth of the slip plane.

The slip plane found in the wells is at the depth of 6.3 m in average under the ground. The slip plane seems to spread continuously in the area where the slip of the wells exists. The direction of the slip is almost perpendicular to the contour line of the topographical map. It may be considered that the strong shock of the earthquake of Dec. 26, 1949 caused the sliding of the upper layer along the surface of the white clayey bed that had smaller friction and adhesion.

The length of the arrows drawn in Fig. 3 shows the horizontal displacement of the wells. The average value of the displacements of 65 wells is 7.4 cm in length.

The horizontal displacement of the wells lying within distance of 100 m from the line QR and OP was projected to a vertical plane parallel to the line (Fig. 7 and 8). As will be seen in the Figure, the displacements are largest in the middle portion of the area (O, R) and smallest at the margins both north and south (Q, P). The mean inclination of the ground between Q and P is about 1° in angle.

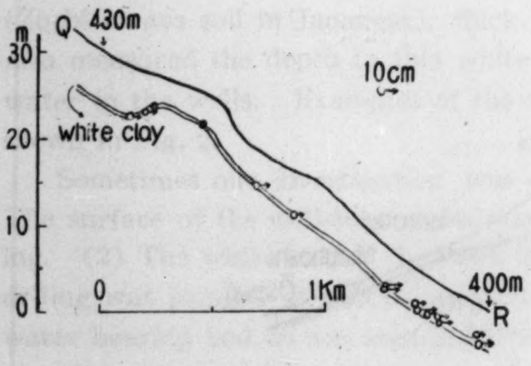

Fig. 7.

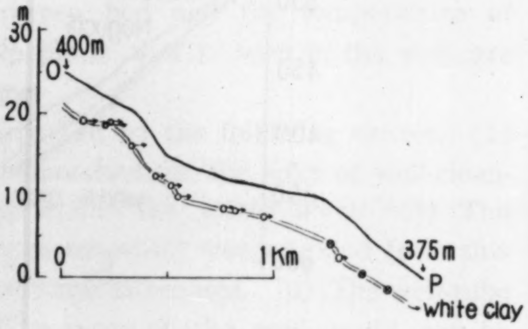

Fig. 8.

Muddiness of the well caused by the earthquake.

Following the Earthquake of Dec. 26, 1946, the writer collected the statements made by the inhabitants of that district. The results are classified as shown in Table I.

Table I

Well Colour of muddiness	Slipped	Not slipped	Undetermined
white	34	9	15
Red or yellow	27	21	7
Mixture of white & red, or white & yellow	1	—	1
Dark or others	—	3	—
Not muddy	8	17	1
Indistinct	6	8	10
Total	76	58	34

As will been in the Table, a large number of the wells which slipped became muddy in white colour. This fact means that the white clayey bed played an important rôle in the slip of the land.

Résumé.

Investigating the slip caused in the wells, it was found that the land around the town of Imaichi, which sloped in angle of 1°, slided downwards. The land block which slided was estimated to be 3.4 km² in area and 6~7 m in thickness. The amount of the distance slided is largest in the central part of

the area, smallest at the north and south margins, and 7 cm in length averagely.

In conclusion, the writer wishes to express his hearty thanks to Professor T. Hagiwara and Assist. Professor R. Morimoto of the Earthquake Research Institute and Mr. Y. Mori, the master of the Imaichi Middle School for their kind advice and encouragement in the course of these studies. Thanks are also due to his pupils belonging to the group for meteorological study for the helps they offered in field works.

---

35. 井戸調査から知られた今市地方の地層の横辷りについて

今市中學校　本田孝雄

今市地震後，同地方にある井戸の壁に，地層の横辷りを示す著しい食違いが認められたが，この現象に興味を抱いた筆者は，今市町を中心とする數 km の範圍に亘り井戸の調査を行つた．横辷りの有る場合は，井戸の壁上に附屬寫眞のような三日月型に白粘土層が認められるから，この型に着目して，横辷りの方向，距離を測定する事が出來た．調査に當つてはこの他，横辷りの起つている層迄の深さ，水位，水溫等も併せて測定し，同時に地震前後の井戸狀態の變化に關する質問を行つた．

調査の對象となつた井戸は總計 168 に上り，いろいろの理由で現象の確認できないものもあつたが，結果を綜合すると上記現象の認められる井戸は別圖の如く三地域内に分布している．この内 II, III の地域は現象がきわめて局部的なので，考察から除外するが，I の地域においては，殆んど例外なしに，井戸の上層部の地層が土地の傾斜方向に移動している模樣である．この地方の構造は，地理的及び地質的に二，三の研究者により調べられており，その結果を參照すると，上記現象は，今市町を含む面積 3.4 km^2, 厚さ 6〜7 m の土塊（附圖參照）が地震動の爲に白粘土層を境として，土地の傾斜方向に 7 cm 程度移動した結果と推定されるに至つた．

更に，この地塊の中央部において移動量は最も大きく，南北の兩端部に於て小さい事は，興味深く思われる．尙，横辷りのあつた井戸の場合，地震後白濁したものが最も多い模樣であり，これからも，白粘土層が横辷りに密接な關係を有していた事が想像される．

36. *Instrumental Recording of a Landslide caused by the Imaichi Earthquake of Dec. 26, 1949.*

By Fuyuhiko KISHINOUYE,

Earthquake Research Institute.

(Read Sept. 19, 1950 – Received Sept. 20, 1950.)

In the macroseismic area of the Imaichi earthquake, landslides occurred at many places. The abundance of the landslides may be due to the weakness of the tuff which lay under the great part the surface in this area. Some people of the district were anxious to know how the landslides would move afterwards in fear of the disaster caused by landslides. Then the writer made an apparatus and recorded continuously the movement of a landslide at Kisoyama in Nagahata, Ochiai Village, about 10 km SE of Nikkō.

The recording-method adopted was simple. A steel wire was stretched from a pole erected vertically at the sliding portion of the land, and the other end of the wire was connected to another pole set up on motionless ground through a helical spring. The recording drum was put on the ground near the spring and an end of a lever was connected with a joint to the recording pen clamped to the wire. When the lower pole moved the wire was pulled, and the pen connected to the wire with lever drew the movement of the landslide.

The measured landslide was oblong in shape, about 50 m in length and 40 m in width, and the wire was adjusted to record the maximum movement at the middle of the sliding portion. The length of the wire was 24.4 m, S 50° W in azimuth and the dip of the wire was about 15°.

The record obtained is shown in Fig. 1. The daily change on the record will be brought about by the elongation or contraction of the wire due to the daily variation in the air temperature. Although the recording was interrupted by various accidents, it may be allowed to consider that the sliding was continued till about April 10, 1950, and there after the record shows apparent approach of the two points. But it may be due to the leaning of the pole towards the upper one. Such inclination of the pole would be natural in the case of landslide, for the bottom plane of the sliding mass is considered as nearly cylindrical. So the writer concluded that the sliding almost stopped after April 10. The crustal deformation measured by levelling carried out by

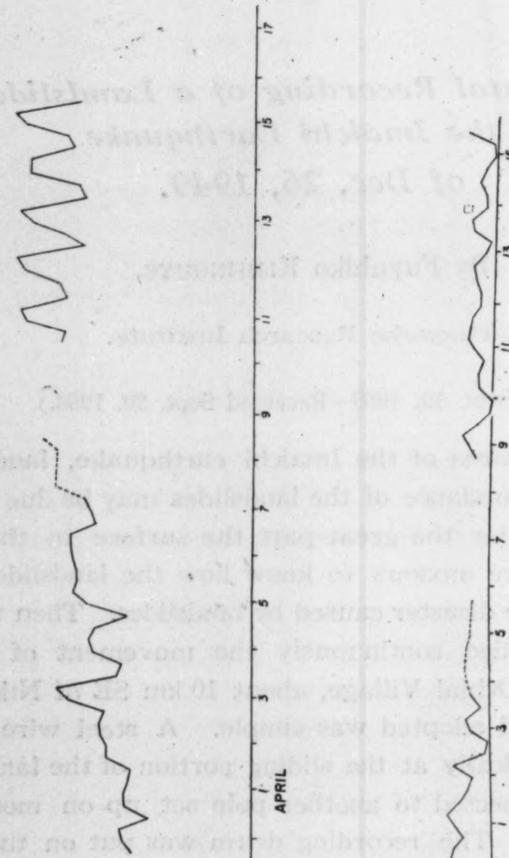

Fig. 1. Movement of a landslide after the Imaichi earthquake. (Relative movement of two places 24.4 m distant in S 50° W, dip 15°).

Fig. 2. Upper scarp of the landslide.

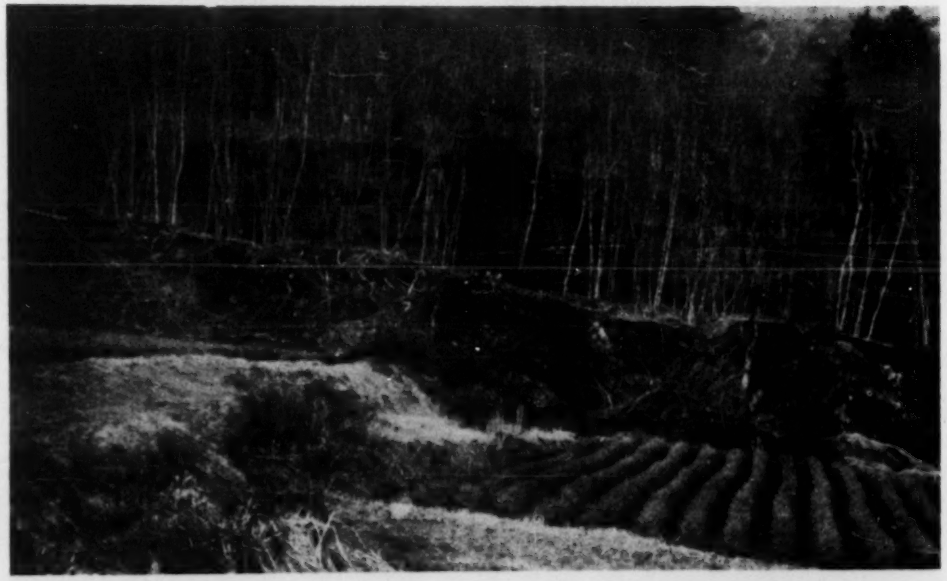

Fig. 3. Lower part of the lendslide.

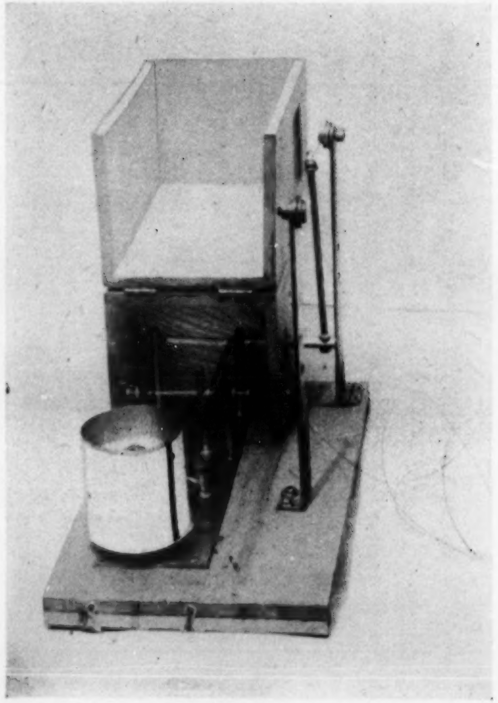

Fig. 4. An apparatus for recording the displacement of the landslide.

the other members of our institute[1] also reported the rate of the deformation became very small towards the above mentioned time.

In May 1950 at the recording place it rained much and the air was humid. The clock-work in the apparatus became rusty by water condensed from the humid air, and it stopped frequently, so the writer gave up the recording on May 15.

The writer expresses his best thanks to Mr. Moichirō Fukuda for his kindness in helping the witer with the observation, and he also thanks Miss Mieko Kotaka and Mr. Jōkichi Moroga for their assistance in this study.

36. 今市地震によつて起された地辷りの器械觀測

地震研究所　岸上冬彦

栃木縣上都賀郡落合村大字長畑の森東にある木曾山に今市地震によつて起された長さ50m巾40mの余り大きくない地辷りを，一端にらせんばねをつけた鋼線を二地點間にはりその線の動きと變えて記録した．その結果は第1圖の通りで，觀測したのは1950年3月17日から5月15日までで，途中故障が多かつたが4月10日頃までは辷りが進んでいたが，それ以後は止んだ．後の方で逆に動いているように見えるのは，地辷りの斷面は半圓形であると考えると當然のことゝ見做される．この測定の目的は地辷が其の後も大きくて災害を起す恐れがあるかないかを知るのであつた．終りにこの觀測には前記の土地の福田茂一郎氏の協力によるので，こゝに感謝する．

---

1) R. Takahasi, *Bull. Earthq. Res. Inst.*, 27 (1950), 443~447.

37. *On the Damage to Buildings by the Imaichi Earthquake of Dec. 26, 1949.*

By Kiyoshi KANAI and Teiji TANAKA,

Earthquake Research Institute.

(Read Jan. 17, 1950.—Recevied Aug. 20, 1950.)

1. Introduction.

Two destructive earthquakes occurred successively near Imaichi-town (Tochigi prefecture) at 8 h 18 m and 8 h 26 m on Dec. 26, 1949, and caused damage as shown in Fig. 1 and Table. I.

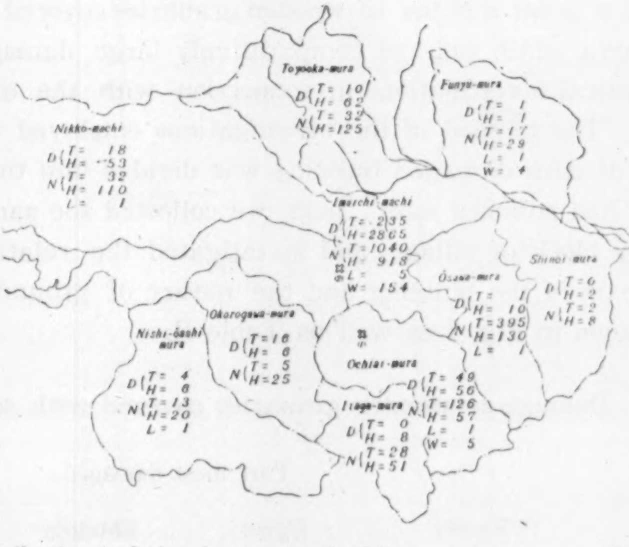
Toyooka-mura
D(T= 10, H= 62
N(T= 32, H=125
Funyu-mura
D(T= 1, H= 1
N(T=17, H=29
L= 1
W= 4
Nikko-machi
D(T= 18, H= 53
N(T= 32, H= 110
L= 1
Imaichi-machi
D(T= 235, H=2865
N(T=1040, H= 918
L= 5
W= 154
Shinoi-mura
D(T=6, H=2
N(T=2, H=8
Ōsawa-mura
D(T= 1, H= 10
N(T=395, H=130
L= 1
Okorogawa-mura
D(T=16, H= 6
N(T= 5, H=25
Nishi-ōashi-mura
D(T= 4, H= 6
N(T=13, H=20
L= 1
Ochiai-mura
D(T= 49, H= 56
N(T=126, H= 57
L= 1
W= 5
Itaga-mura
D(T= 0, H= 8
N(T=28, H=51

Fig. 1. Distributions of the damage to buildings and humans. Symbles *D* and *N*, represent dwelling houses and not-dwelling houses. Symbles *T*, *H*, *L* and *W* represent number of houses totally destroyed, half destroyed, lives lost and persons wounded. Mark × indicates the epicenter.

Table I. Damage of the Imaichi Earthquake

No. of Dwelling-houses		No. of Build. not for dwelling		No. of Lives loss	No. of Persons wounded
Totally destroyed	Half destroyed	Totally destroyed	Half destroyed		
334	3069	1690	1484	10	163

The buildings not for dwelling in the seismic region are mostly soft-stone granaries or wooden buildings covered with soft-stone.

Generally speaking, relatively flexible buildings as wooden dwellings received slight damage, but, the damage done to rather rigid structures like soft-stone granaries or wooden buildings covered with soft-stone was somewhat large.

Similar phenomena concerning the damage done to buildings were to be seen in the Tokyo Earthquake of Apr. 26, 1922.1)

The phenomena just mentioned are likely to be explained by the facts that the scale of the earthquake was small, and the afflicted area being very near to the origin, the period as well as the duration of shocks were short.

2. Results of the investigations regarding the wooden buildings covered with soft stone.

As there are a great number of wooden granaries covered with soft-stone in the afflicted area which suffered comparatively large damage, we carried out mainly statistical investigations in connection with the damage done to those buildings. The method of the investigations employed was as follows: first, the height of each damaged building was divided into three to examine which part of it had suffered most: next, we collected the same kind of destruction at every block of village, and investigated the relation between the most damaged part of the building and the nature of ground. The results arranged are shown in Fig. 2 as well as Table II.

Table II. Damage to wooden granaries covered with soft stone.

Ground condition	Part most damaged			
	Evenly	Upper	Middle	Lower
Up (Hard) lands	2%	87%	4%	7%
Plain (Soft) lands	11%	27%	20%	42%

From these results, it will be seen that, on plain lands, the rate of the buildings which suffered most damage at the upper part is high, while on uplands most buildings were damaged at their lowest part.

If we consider the problem of forced oscillation of structure according to the general idea, the part subjected to the maximum stress must be placed higher as the period of the earthquake shocks becomes shorter. Then, the

---

1) *Rep. Earthq. Inv. Comm.*, No. 99 (1925), 44.

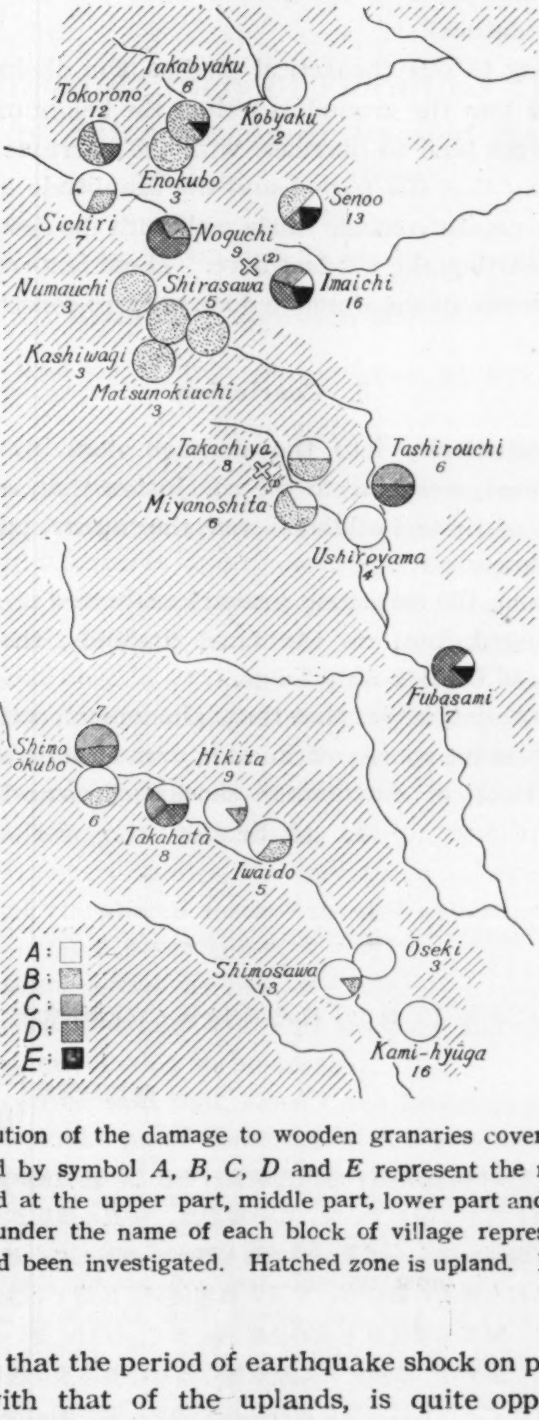
Takabyaku
6
Tokorono
12
Kobyaku
2
Enokubo
3
Senoo
13
Sichiri
7
Noguchi
9
(2)
Imaichi
16
Numauchi
3
Shirasawa
5
Kashiwagi
3
Matsunokiuchi
3
Takachiya
8
Tashirouchi
6
Miyanoshita
6
Ushiroyama
4
Fubasami
7
7
Shimo
okubo
Hikita
9
6
Takahata
8
Iwaido
5
Ōseki
3
Shimosawa
13
Kami-hyūga
16
A: □
B: ▨
C: ▨
D: ▨
E: ■

Fig. 2. Distribution of the damage to wooden granaries covered with soft stone. The spaces indicated by symbol *A*, *B*, *C*, *D* and *E* represent the rate of the buildings undamaged, damaged at the upper part, middle part, lower part and evenly, respectively. The figure written under the name of each block of village represents the number of buildings which had been investigated. Hatched zone is upland. Mark × indicates the epicenter.

general conception that the period of earthquake shock on plain lands is rather large compared with that of the uplands, is quite opposed to the above-mentioned phenomena.

However, it will be cleared up considerably by the results of our theoretical study based upon the idea that at the time of earthquake the vibration energy of buildings dissipates to the ground again as the elastic wave that starts from the foundation.[1]

Namely, according to our theoretical studies, the dissipation of vibration energy of structures into the ground as well as the height of the part subjected to the maximum stress tend to increase with the decrease in the rigidity of the ground, supposing that the period and the amplitude are constant.

This theoretical results coincide fairly well with the destructive phenomena of buildings in the earthquake studied here. These features had been already pointed out in the study of the damage done to ferro-concrete buildings in the Kwantô earthquake.[2]

3. Conclusion.

Investigating statistically into the damage done to wooden granaries covered with soft stone, we came to the conclusion that, on soft ground, the most damaged part of these buildings was the upper part, while on hard ground, it was the lower part.

On the other hand, the soft-stone granaries situated on the soft level lands were scarecely damaged, but, on the hard up-lands, the damage done to similar buildings were considerably large.

It is more natural to consider that these phenomena occurred by the nature of dissipation of vibration energy of buildings into the ground rather than by the difference of periods of earthquake shocks. In conclusion, we wish to express our hearty thanks to Mr. M. Suzuki who worked together in this investigation.

---

37. 昭和24年12月26日今市地震の建物被害について

地震研究所 金井　清
　　　　　 田中貞二

今回の地震被害は，比較的に柔構造の木造住家等に小さく，比較的に剛構造の石造及び貼石木構造の藏等に大きい傾向を明かに示していた．この現象は，地震の規模が小さく，激震地域が震源に近いために，地震動の周期が短く，震動繼續時間も短かかつたために起つたと考えてよかろう．

被害数の多かつた貼石木構造の藏について最大被害個所と地盤との関係をしらべたところ，軟い地盤上では上部で最大の被害を受けたものが比較的に多く，反対に硬い地盤上では下部のものが多いことがわかつた．この事実は，地盤による地震動の周期の差違では説明が困難で，地震時に建物の震動勢力が地下に逸散する性質に関する数理的研究結果と定性的によく合う．

---

1) K. SEZAWA and K. KANAI, *Bull. Earthq. Res. Inst.*, 14 (1936), 164.
2) K. KANAI, *Bull. Earthq. Res. Inst.*, 27 (1949), 97.

38. *Experimental Study of Vibrations of Structures Caused by After-shocks of Imaichi Earthquake of Dec. 26, 1949.*

By Kiyoshi KANAI and Tomisaburo SUZUKI,

Earthquake Research Institute.

(Read Jan. 17, 1950.—Received Sept. 20, 1950.)

1. Introduction.

If we could observe precisely the motions of structures or the motions of ground at the afflicted area of great earthquakes so as to make clear the collapsing process of structures due to earthquake, the problem of earthquake-proof buildings would make much more progress. These observations, however, being considerably difficult to carry out in practice, this problem has been hitherto attacked only in various indirect ways. Namely, the statistical and analytical studies of earthquake damage to buildings were started from the statical point of view,[1] but they have been developed gradually into dynamical treatments such as the studies of the relation between the earthquake damage of buildings and the nature of ground.[2] On the other hand, in the field of experimental studies, the measuring of vibration of buildings by means of artificial vibrational forces[3] as well as by actual earthquakes of small scale[4] has been tried many times.

These investigations showd us that the vibration problem of buildings caused by destructive earthquake are very complex and there many subjects concerning this problem remains to be treated.

Nevertheless it can be said that, since these investigation threw light on the problem of earthquake-proof construction to a considerable extent, its remarkable developement will be realized in the near future. With a view to obtaining some insight into the problem just mentioned, we investigated the effect of periods, displacement amplitudes and acceleration amplitudes of earthquake motions as well as the proper period and stiffness of buildings, on the strains of buildings in the after-shocks of the Imaichi earthquake.

---

[1] R. SANO, *Rep. Earthq. Inv. Comm.*, No. 83 (1916), A, 1; B, 1.

[2] M. ISHIMOTO, *Bull. Earthq. Res. Inst.*, 10 (1932), 171,
K. SEZAWA and K. KANAI, *Bull. Earthq. Res. Inst.*, 14 (1936), 164,
K. KANAI, *Bull. Earthq. Res. Inst.*, 17 (1939), 37; 27 (1949), 97.

[3] T. SAITA, *Rep. Earthq.-proof Const. Comm., Japan Soc. Prom. Scie. Res.*, No. 1, 60,
Rep. Special Comm. Fukui Earthq., (1950), 186-187,
K. KANAI, *Bull. Earthq. Res. Inst.*, 27 (1949), 91.

[4] T. SAITA and M. SUZUKI, *Bull. Earthq. Res. Inst.*, 14 (1936),
C. TSUBOI and S. MIYAMURA, *Bull. Earthq. Res. Inst.*, 20 (1942), 291,
Rep. Special Comm. Fukui Earthq., (1950), 187-190.

We carried out the observations of the after-shocks, using the acceleration seismograph together with the displacement seismograph and at the same time the strains of four kinds of buildings caused by the same shocks were measured during the period from Dec. 27, 1949 to Jan. 8, 1950 at Nikko-town in the slightly afflicted area. In the next period from Mar. 22 to Mar. 25, 1950, vibration experiments by means of a vibrator were made on the same buildings.

2. The method of observation.

The constants of the acceleration seismograph and the displacement seismograph used in the observation were as follows:

acceleration seismograph; period=0.1 sec, 1 mm=2.2 gal,

displacement seismograph; period=4 sec, magnification=12.

The four kinds of buildings with which we experimented were a wooden shed, a wooden building covered with mortar (an electric distributing station), a wooden dwelling house of Japanese temple type and a wooden granary covered with soft stone. The sketch of these buildings are shown in Figs. 1-4.

The strains of buildings were measured in a way so that the deflections of a part of column at some height above the base relative to the base may be recorded on a revolving smoked paper magnified mechanically about 50 times. Marks × in Figs. 1-4 show the location of the apparatus.

The vibrator which consists of one rotating wheel with eccentric weight driven manually was set on the place of mark ⊙ in Figs. 1-4. The wheel was driven faster than the proper period of a test building and then set free

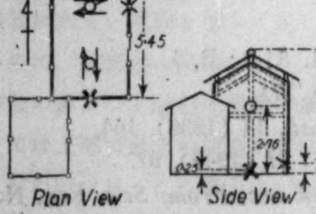

Fig. 1. Sketch of the wooden granary covered with soft-stone. Marks ○ and × indicate the locations of the vibrator and the apparatus.

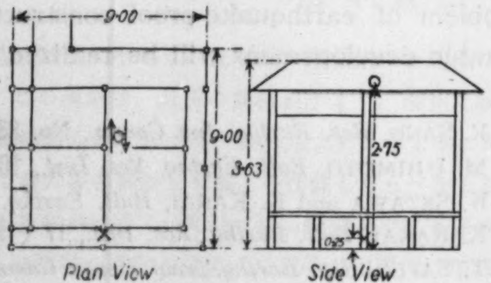

Fig. 2. Sketch of the wooden dwelling house of Japanese temple type. Marks ○ and × indicate the locations of the vibrator and the apparatus.

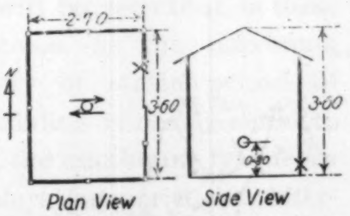

Fig. 3. Sketch of the wooden building covered with mortar. Marks ○ and × indicate the locations of the vibrator and the apparatus.

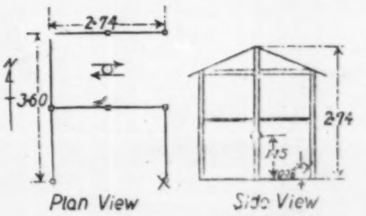

Fig. 4. Sketch of the wooden shed. Marks ○ and × indicate the locations of the vibrator and the apparatus.

in a state of free rotation. It keeps on running for quite a long time diminishing its speed gradually. Eccentric weight of 1 kg is set at the radius of 18 cm.

3. Results of observations and interpretation of them.

Displacement seismogram, acceleration seismogram and record of strain of building due to after-shocks are shown in Figs. 5, 6.

(i) *Cases of EW direction of the wooden granary covered with soft stone and the dwelling house of Japanese temple type.*

Using the observed records, we obtained the relation of vibration periods to their frequency, and that of vibration amplitudes to their periods, regarding the accelerations as well as the displacements of the after-shocks and strains of buildings due to the same shocks.

On the other hand, we also got the relation between the vibration period and amplitude of each building in the case of artificial vibration experiments. The results of them are shown in Figs. 7, 8.

Two figures tell us that the vibration amplitudes of after-shocks are large at frequent vibration period. In the case of the granary, it seems that both the frequency of vibration period and the amplitude of vibration strain due to after-shocks have two peaks at nearly the same vibration period, one of which corresponds to the vibration period where the period frequency and the amplitude of acceleration of after-shocks are large,and the other corresponds to the vibration period where the amplitude of strain of building due to artificial vibrational force is large.

In other words, the strains of the granary caused by after-shocks grow larger in two cases, that is when the acceleration amplitudes of shocks are large and when the proper period of the building coincides with the period of shocks, and the strains due to the former case are several times larger than those due to the latter.

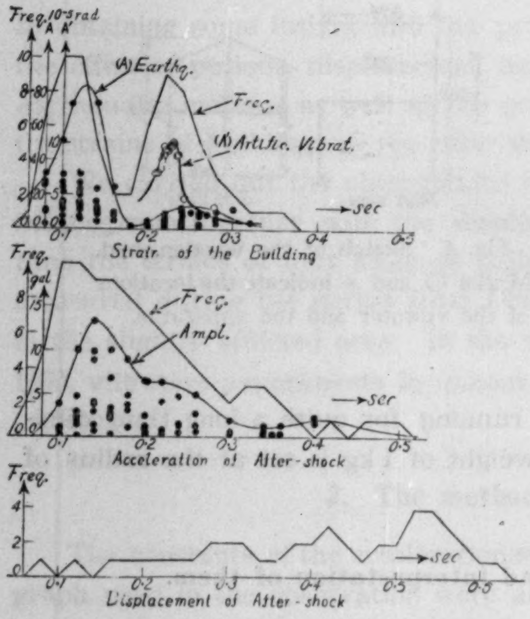

Fig. 7. Case of *EW* direction of the wooden granary covered with soft-stone.

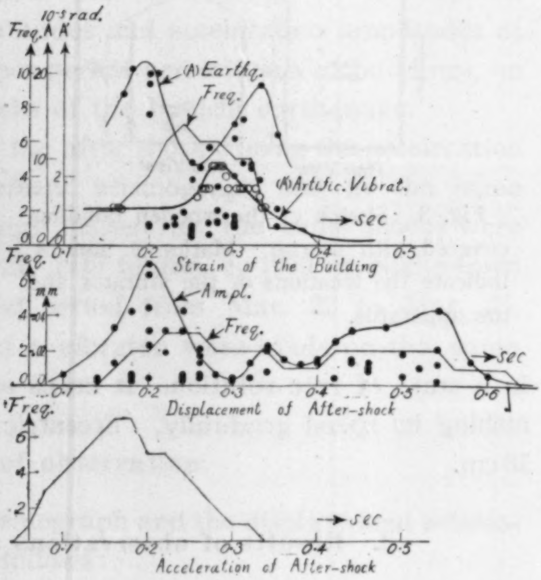

Fig. 8. Case of the dwelling house of Japanese temple type.

In the case of the temple-type house, as shown in Fig. 8 there are two peaks in the strain amplitudes due to after-shocks, but the period frequency has only one peak which is relatively flat. One of the two peaks of the strain amplitudes of the temple-type house corresponds to the vibration period of the large displacement amplitudes of after-shocks, and the other corresponds to the large strain amplitudes in artificial vibration experiments. The peak of the frequency of strain period approximately corresponds to that of the frequent displacement of after-shocks.

Thus we reached the following view, as already stated, that the vibration of wooden granary covered with soft stone was influenced by the accelerations of after-shocks, but the vibration of wooden dwelling-house of Japanese temple type was rather sensible to the displacements of after-shocks, and both buildings have the tendency to induce their free vibrations whether great or small.

(ii) *Cases of NS direction of the wooden granary covered with soft stone, the wooden building covered with mortar and the wooden shed.*

In these cases, using the observed records, we obtained the relation between vibration period and their frequency, regarding the accelerations as well as the displacements of the after-shocks and strains of each building due to the same shocks. On the other hand, we obtained the relation between vibration period and amplitude of each building in the case of artificial vibration experiments. The results of them are shown in Figs. 9–11.

It will be seen that, in these three cases, as the maximum frequency of strain period of each building is nearly equal to both of the maximum frequency of acceleration period of aftershocks and proper period of each building, it is naturally not clear which of them has more influence on the strain of building.

4. Conclusion.

The vibration problems of buildings caused by earthquake were to some extent made clear by investigating the displacement, the acceleration of aftershocks and strains of various kinds of buildings caused by those shocks in the Imaichi earthquake of Dec. 26, 1949.

The results of these investigations showed that relatively rigid buildings suffered by accelerations of successive earthquake motions, but relatively flexible buildings were rather affected by their displacements.[1]

And, free vibrations of buildings seems to be excited considerably in the case of relatively flexible buildings, but in the case of relatively rigid buildings the degree is rather low. At any rate, as free vibrations of buildings will be excited more or less by earthquake motions, it is

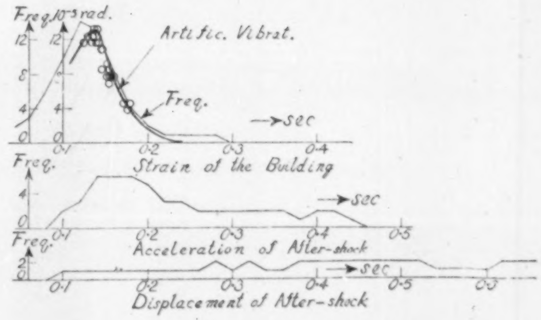

Fig. 9. Case of *NS* direction of the wooden granary covered with soft-stone.

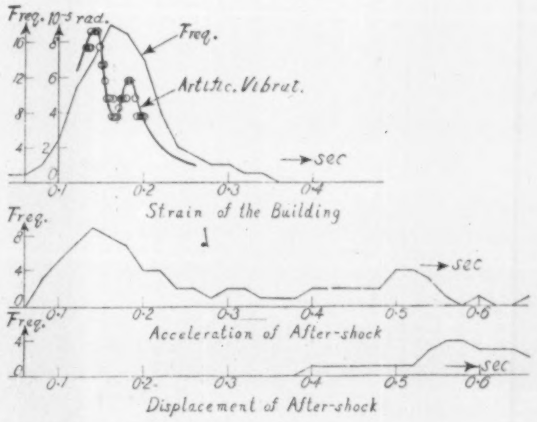

Fig. 10. Case of the wooden building covered with mortar.

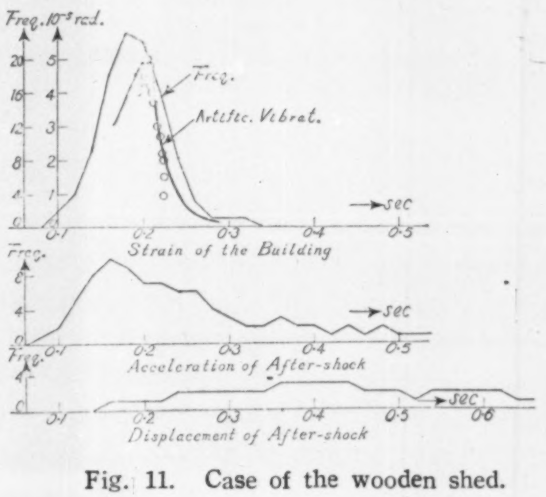

Fig. 11. Case of the wooden shed.

---

1) K. KANAI, *Bull. Earthq. Res. Inst.*, 25 (1947), 64, Fig. 4.

injurious for buildings to have proper periods near to the frequent periods of earthquake motion.

The phenomena of damage done to buildings in the past great earthquakes are likely to be explained to a degree through the results just mentioned.

In conclusion, we wish to express our hearty thanks to Mssrs. M. Suzuki, T. Tanaka and K. Osada, with whose aid the present investigations were successfully made.

---

38. 今市地震の余震による建物振動の観測結果

地震研究所 金井清
鈴木富三郎

今市地震の余震の加速度及び変位とその余震による種々の建物の歪とを觀測し，後にこれらの建物について人工的振動試験を行つた結果，次の事柄がわかつた．

即ち，貼石木構造の藏のような比較的に剛構造物の地震動による歪は地震動の加速度振幅に支配され安く，建物自體の自己振動を多少誘發される．これに反して，神殿作の住居のような比較的に柔構造物の地震動による歪は，むしろ地震動の變位振幅の影響を受け，建物自體の自已振動が相當に誘發される．

尙建物の歪は，何れの場合にも，地震動の大振幅の部分の繼續時間に非常に支配される．

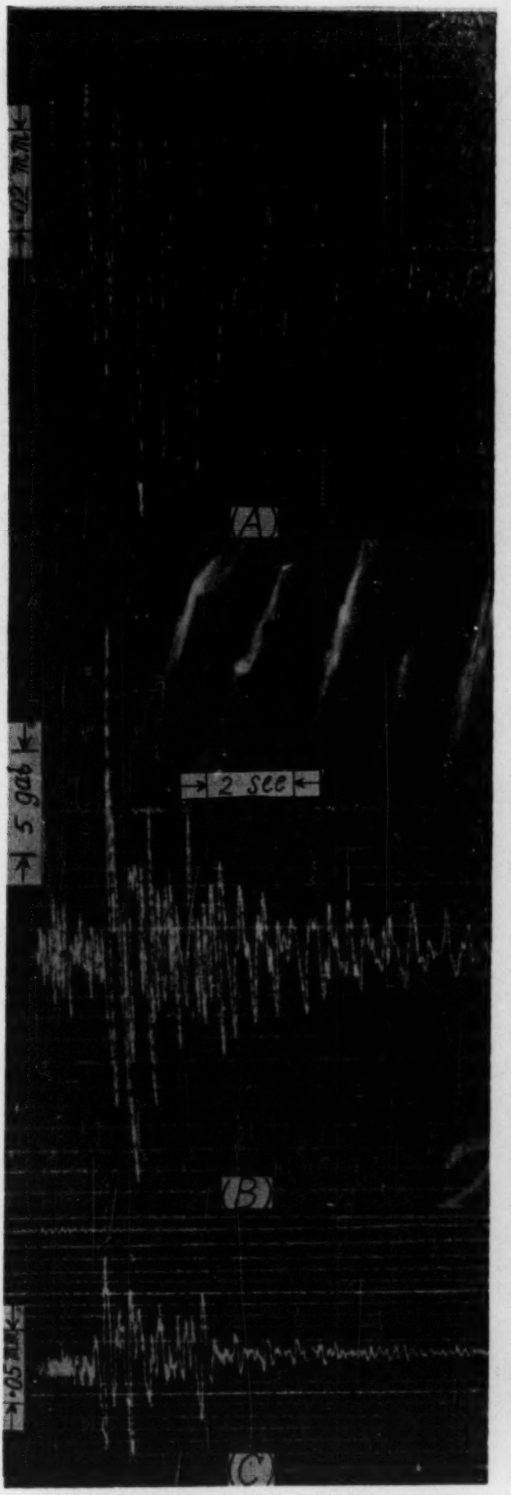

Fig. 5. (A); Displacement seismogram, (B); Acceleration seismogram, (C); Record of strain of the wooden building covered with mortar.

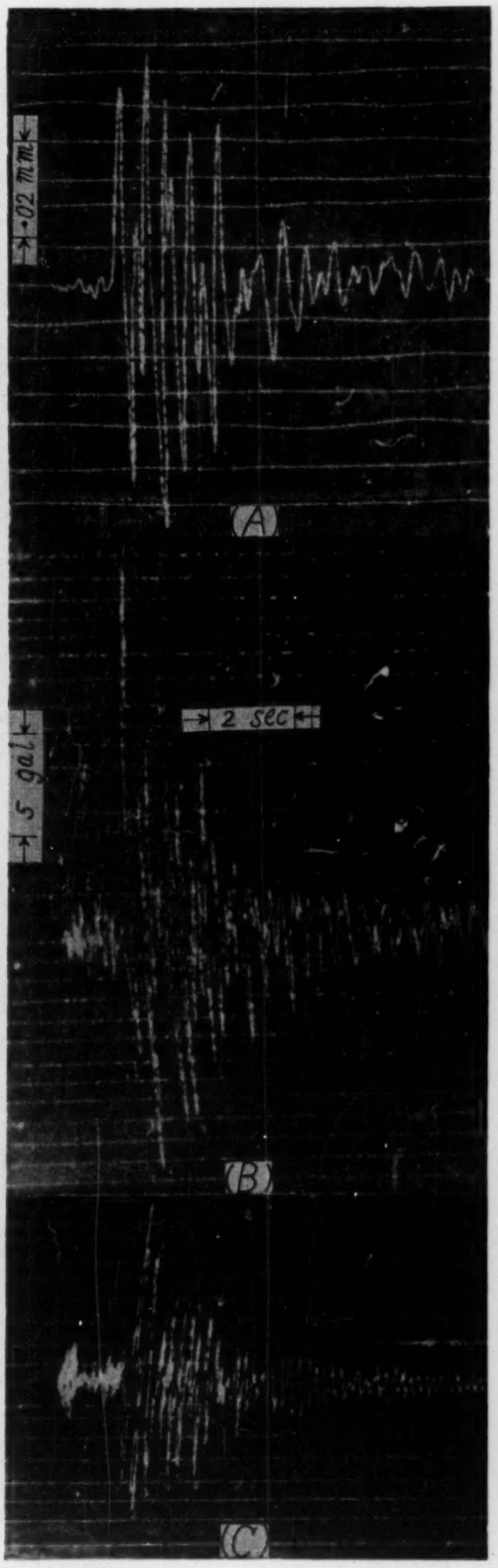

Fig. 6. (A); Displacement seismogram, (B); Acceleration seismogram, (C); Record of strain of the wooden shed.

39. *Seismometrical Data of the Imaichi Earthquake, Dec. 26, 1949.*

By the Earthquake Research Institute.

Table I.

Station	Coordinate	
	Longitude (E)	Latitude (N)
Tôkyô (Hongô)	139° 45′.0	35° 42′.7
Tsukuba	140° 06′.6	36° 12′.65
Mitaka	139° 32′.5	35° 40′.3
Amatsu	140° 09′.2	35° 07′.3

Table II. Time=Central standard time of Japan. (Mean solar time of the meridian 135° E.)

Notation:

Prel. tr. = Preliminary tremor.

N.S. = North south component.

E.W. = East west component.

2A = Range of motion.

T = Period of earthquake motion.

T_0 = Free vibration period of instrument.

V = Magnification.

h = Damping constant (ε/n).

No.	Station	Time of occurrence	Duration of prel. tr.	Maximum motion *N.S.* 2*A* (*T*)	Maximum motion *E.W.* 2*A* (*T*)	Direction of initial motion	Maximum acceleration *N.S.*(*T*)	Maximum acceleration *E.W.*(T)	Maximum acceleration *U.D.*(*T*)
		h m s	s s	mm	mm	mm	gal	gal	gal
1	Tôkyô	eP 8 17 49.2	12.85 ± 0.13	11.4 (5.8s)	11.5 (5.3s)	0.08 down	13.0 (0.2s)	8.0 (0.2s)	6.4 (0.15s)
		iP 17 50.4	14.27 ± 0.14						
(First main shock)	Tsukuba		8.0			*N* 36° *W*			
	Mitaka		13.5						
	Amatsu		19.1						
				mm	mm		gal	gal	gal
2	Tôkyô	8 25 13.0	13.1 ± 0.2	16.3 (5.6s)	14.3 (5.8s)		12.1 (0.3s)	12.9 (0.2s)	7.7 (0.25s)
(Second main shock)			14.6						
	Tsukuba		7.7			*N* 38° *W*			
	Mitaka		14.0						
	Amatsu		19.9						

Fig. 1. Tôkyô observation of the earthquake of $8^h 17^m$ on Dec. 26, 1949.

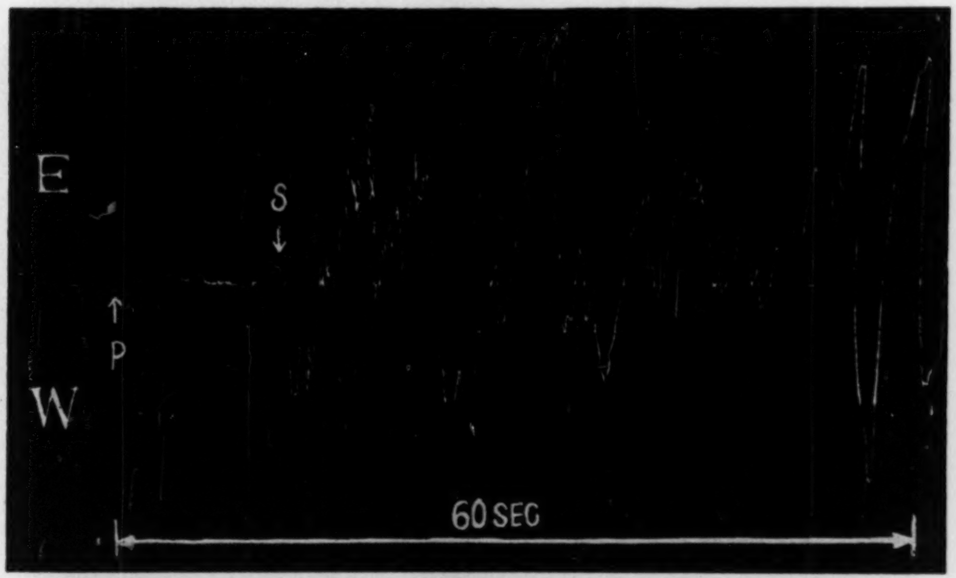

Original × 1.50

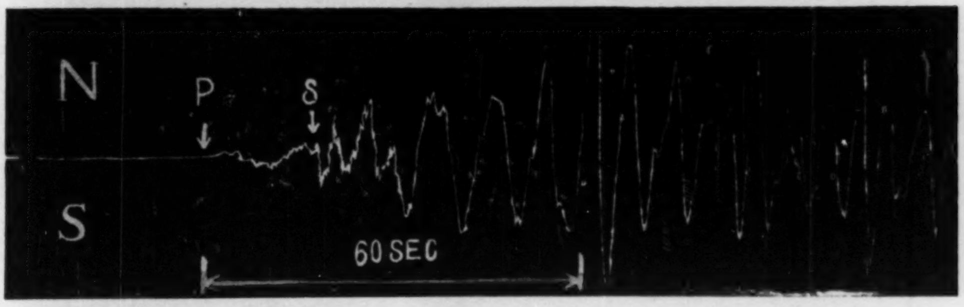

Original × 1.85

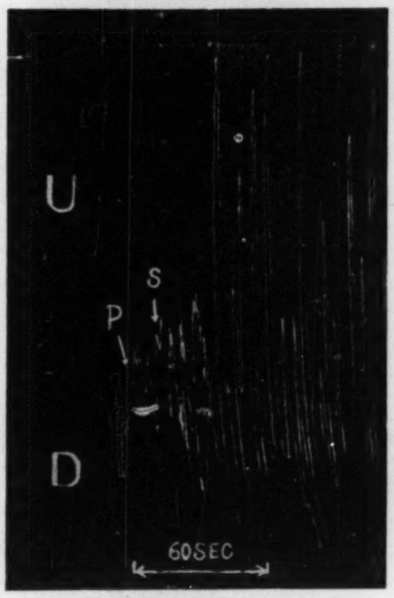

Original × 0.87

Instrumental constants:

Component	V	T_0	h
E.W.	5	45.0^s	1
N.S.	1.5	120.0	1
Vert.	20	8.5	0.016

Fig. 2. Tkôyô observation of the earthquake of $8^h 25^m$ on Dec. 26, 1949.

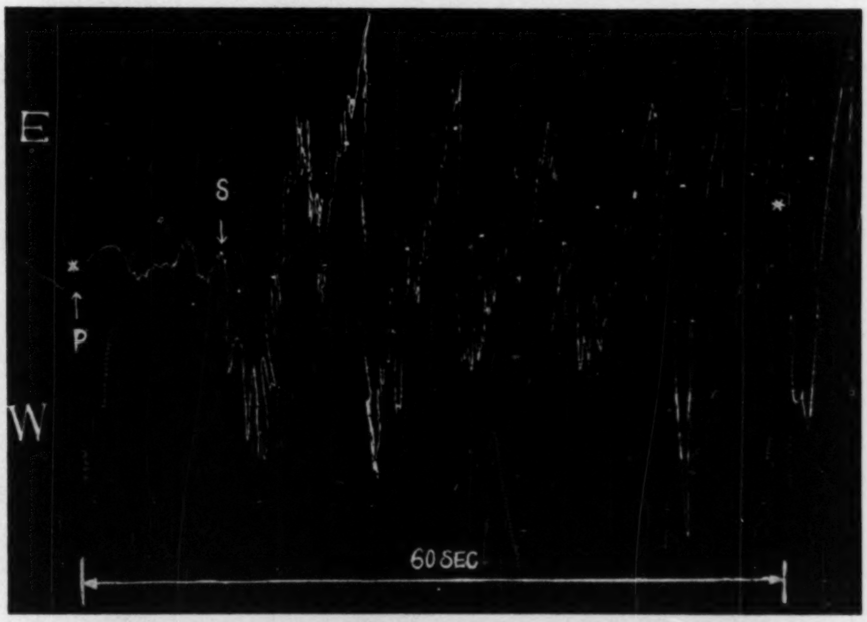

Original × 1.32

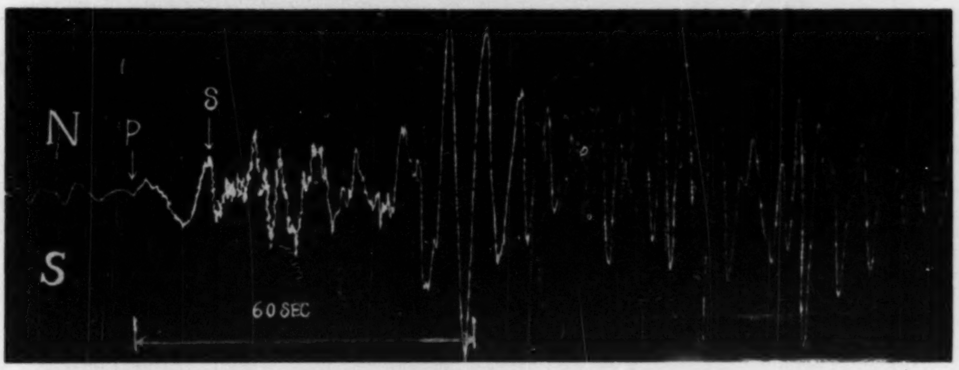

Original × 1.64

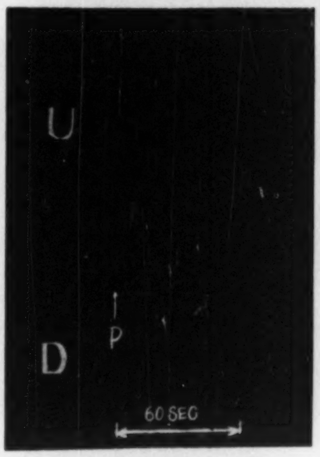

Original × 0.70

Instrumental constants :

Component	V	T_0	h
E.W.	5	45.0^s	1
N.S.	1.5	120.0	1
Vert.	20	8.5	0.016

（震研彙報　第二十八號　圖版　地震研究所）

Fig. 3. Tsukuba observation of the earthquake of $8^h 17^m$ on Dec. 26, 1949.

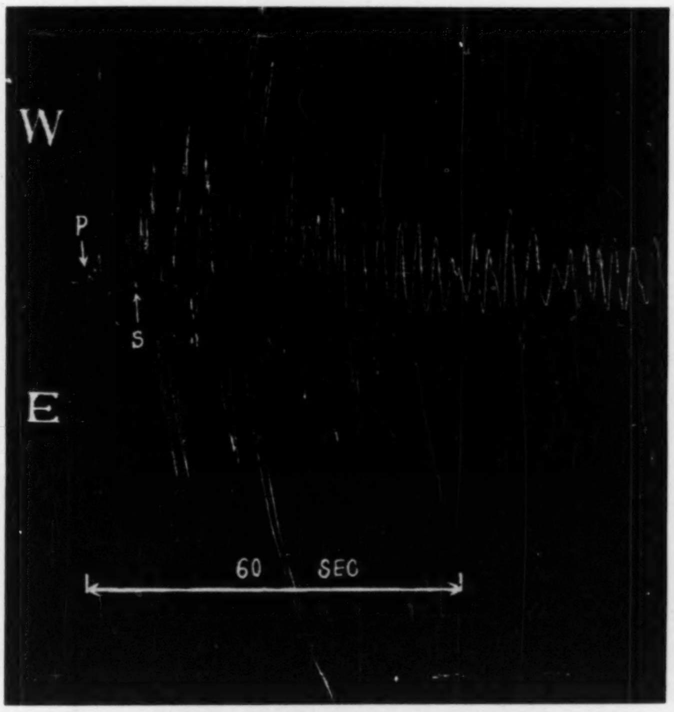

Original × 0.73

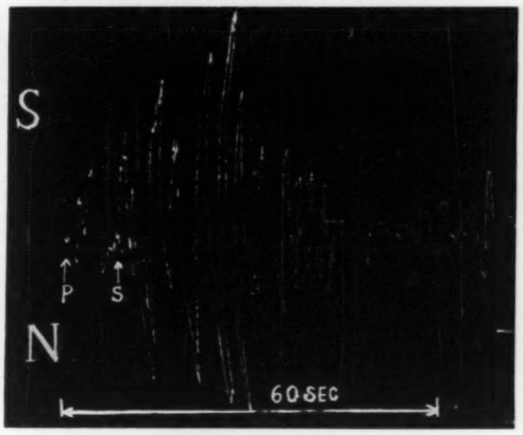

Original × 0.73

Instrumental constants:

Component	V	T_0	h
E.W.	38.8	4.3^s	0.63
N.S.	32.0	3.5	0.50

Fig. 4. Tsukuba observation of the earthquake of $8^{h}25^{m}$ on Dec. 26, 1949.

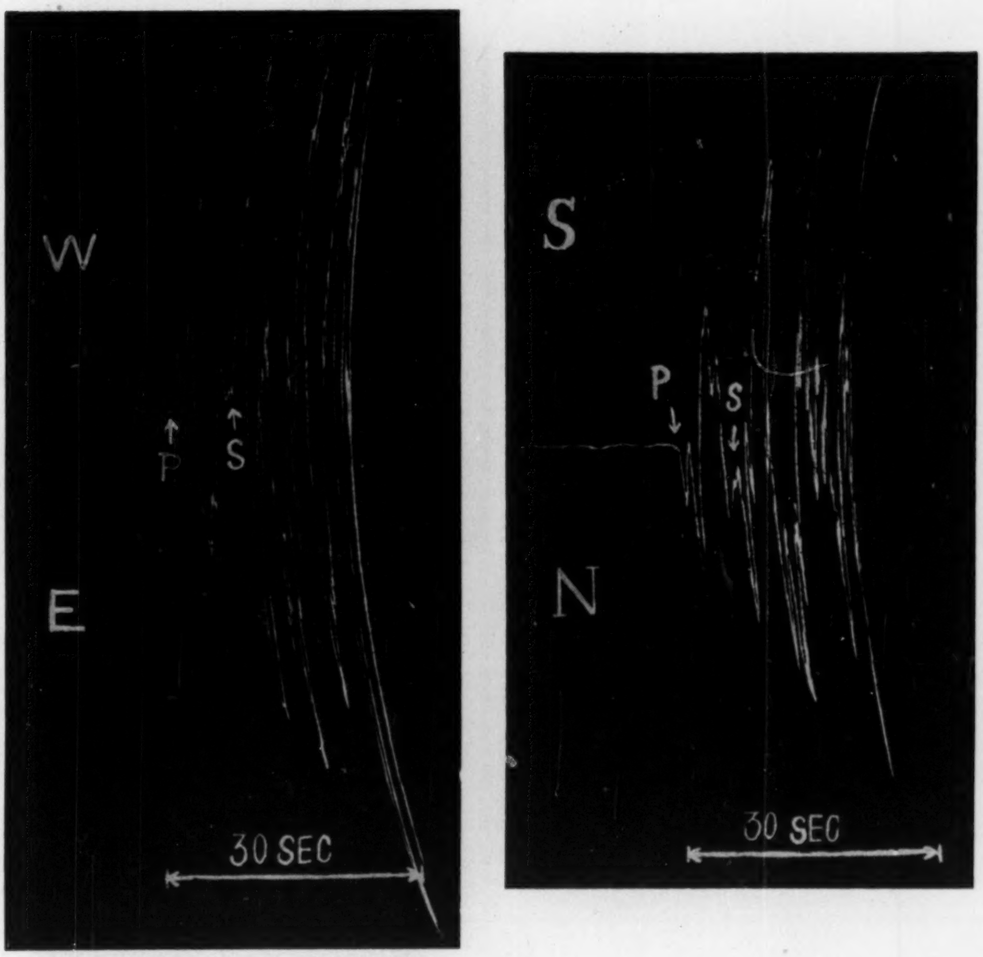

Original size

Instrumental constants:

Component	V	T_0	h
E.W.	38.8	4.3^{s}	0.63
N.S.	32.0	3.5	0.50

Fig. 5. Mitaka observation of the earthquake of $8^h 17^m$ on Dec. 26, 1949, (upper plates), and that of $8^h 25^m$, (lower plates).

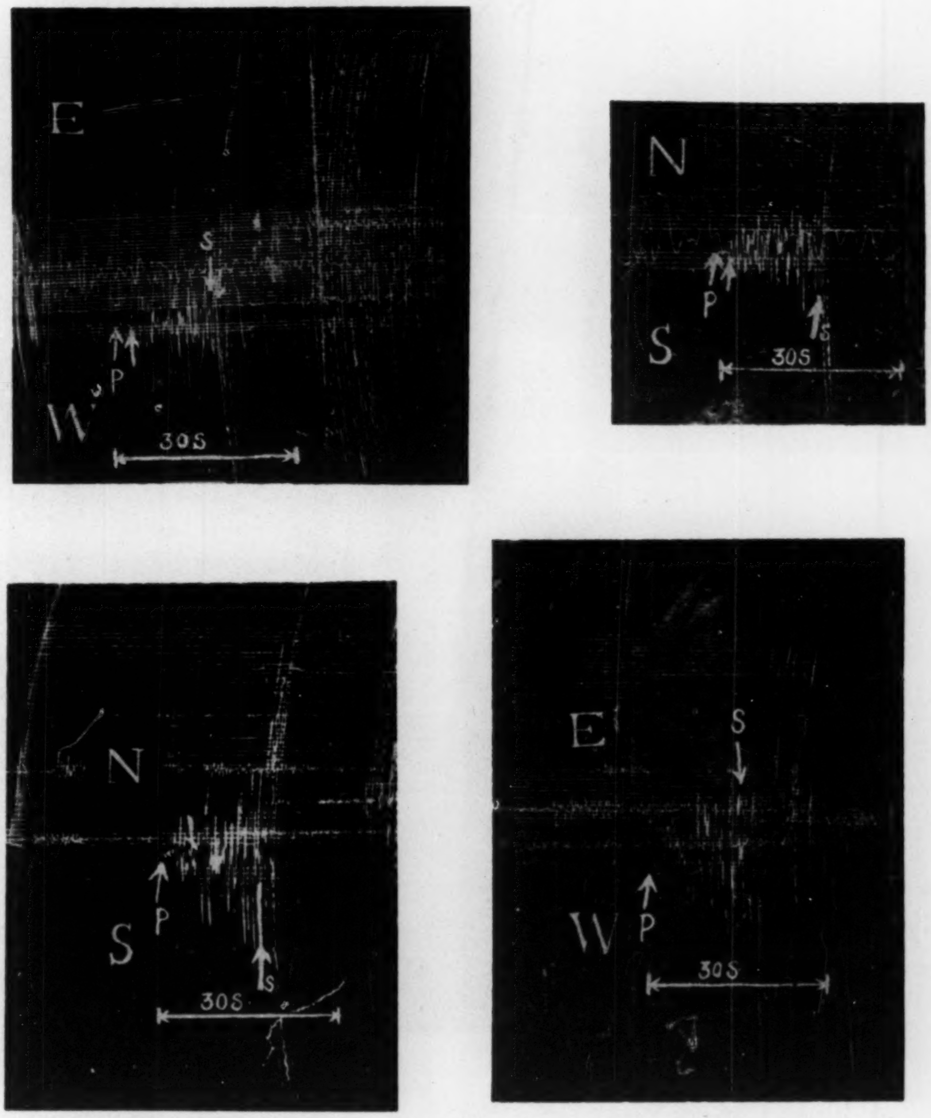

Original × 0.80

Instrumental constants:

Component	V	T_0	h
E.W.	80	1.4^s	0.09
N.S.	80	1.5	0.42

（震研彙報 第二十八號 圖版 地震研究所）

7

K. Sezawa

東京帝國大學地震研究所長 妹澤克惟教授小傳

妹澤克惟教授は明治28年8月21日，檢事妹澤政雄氏の次男として山口市で誕生された．昭和19年4月初めに病床に臥され，同月23日早朝病氣がにわかに革り，急逝されるところとなつた．

故妹澤教授は大正10年東京帝國大學工學部船舶工學科を卒業，間もなく講師，翌年助教授になられ，大正12年航空研究所員，大正14年地震研究所の創設と共に所員に補せられ，續いて昭和3年教授に任ぜられ，昭和17年地震研究所長に補せられた．

其間，大正13年工學博士，昭和14年理學博士の學位を授けられ，昭和18年帝國學士院會員を仰付けられた．その他，學術研究會議會員並びに同會議震災豫防研究委員會委員長，日本學術振興會學術部委員並びに同會非線型特別委員會委員長，測地學委員會委員等多くの要職について居られた．

昭和7年から9年にかけて，地球力學研究の爲に英國，獨國並びに米國に在留され，在留中に測地學及び地球物理學本邦委員を委囑された．

故妹澤教授が發表された研究論文は實に240編に及んだ．その中，地球物理學關係のものは“地震波の發生並びに傳播の理論的研究”を始めとして前人未踏の域を開發され，その論文數は135編に達し，地震研究所彙報に掲載されて居る．航空機の振動關係のものは“柱や薄板の挫屈”に關する不滅の研究を始めとして49編の論文が航空研究所彙報，同所報告等に發表された．又，船舶の振動關係では“周邊固定の矩形板の振動，彈性安定の研究”という先鞭的研究を始めとして17編が造船協會會報等に載せられて居る．尙，帝國學士院紀事に掲載された論文が14編あり，その他外國では Engineering, Nature, Physical Magazine, Zeitschrift für angewandte Mathematik und Mechanik, Journal of the Royal Aeronautical Society 等に少からず掲載されて居る．

地震波の生成傳播其他に關する理論的研究に對しては昭和6年帝國學士院より恩賜賞が授けられた．

故妹澤教授は彈性振動の理論的研究家として，研究內容から言つても又發表論文數から言つても，超人的とも言うべき業蹟を殘された譯であるが，特に，故教授の博識と慧眼は單に純理論的研究に止ることなく，その大部分は直ちに實用に供し得るところまで進められた．

晩年になつて，地震研究所長並びに各種の研究委員會の委員長として，卓越した御手腕と御熱意とによつて上げられた，斯界えの御寄與も亦極めて大なるものがあつた．

OBITUARY

Professor KATSUTADA SEZAWA, D. S., D. E.

Brief History of the Late Professor Katsutada Sezawa, the Director of the Earthquake Research Institute, Tokyo Imperial University.

Professor K. Sezawa, the second son of Masao who had been a public prosecutor, was born in Yamaguchi on Aug. 21, 1895. At the beginning of April, 1944, he was taken ill, and his sudden passing was reported early in the morning of 23rd of that month.

Professor Sezawa graduated from the Department of Naval Architecture of Tokyo Imperial University in 1921. Soon after that he became a lecturer at the university and in the next year was appointed assistant professor. Then he was proposed as a member of the Aeronautical Research Institute in 1923, and a member of the Earthquake Research Institute in 1925, the year when the institute was founded. In 1928 he was appointed professor of the same university and in 1942 the Director of the Earthquake Research Institute.

Through these years his academic life had been a brilliant one. In 1925 he received his degree of Doctor of Engineering and in 1939 his degree of Doctor of Science. He was elected to the Imperial Academy in 1943. He also occupied other important positions such as a member of the National Research Council of Japan, the chairman of the Investigation Committee for Earthquake-damage Prevention, a member of the Science Section of Japan Society for the Promotion of Scientific Research, a member of the Special Committee for the Study of Non-linear Problem of the same society, a member of Imperial Japanese Geodetic Commission, etc.

From 1932 to 34, he stayed in England, Germany and USA, to study geodynamics, taking an active part as a member of Japanese Geodetic and Geophysical Committee.

In the course of his research, he wrote papers exceeding two-hundred and forty in number. He acted as pioneer in the field of geophysics, publishing "The Theoretical Study on the Generation and Propagation of Seismic Waves" and other papers which amounted to one-hundred and thirty-five in Bulletin of the Earthquake Research Institute. The forty-nine writings on the vibration of aeroplanes, including the well-known "The Buckling of a Bar or a Thin Plate", was made public from time to time in Journal of the Aeronautical

Research Institute and Report of the Aeronautical Research Institute. Concerning the vibration of ships, he wrote seventeen papers of which particularly "The Vibration and its Stability of a Rectangular Plate Clamped at four Edges" was epoch-making. The Proceedings of Imperial Academy contains forteen papers written by this noted scholar. Not a few writings of the professor appeared even in foreign periodicals such as Engineering, Nature, Physical Magazine, Zeitschrift für Angewandte Mathematik und Mechanik, Journal of the Royal Aeronautical Society, and in the publications of a number of other learned societies.

In 1931, he was awarded the Imperial Prize by the Imperial Academy for his remarkable paper "The Theoretical Study on the Generation and Propagation of Seismic Waves and on the Other problems".

Professor Sezawa as a theoretical researcher of elastic vibration, may be said to have left a superhuman mark, both in quality and quantity of his study. Moreover his exhaustive knowledge and penetrating mind never left his studies in purely theoretical stage but always advanced them with a view to their practical application.

It is noteworthy too that he, in his last days, rendered great services through his outstanding ability and zeal as the Director of the Earthquake Research Institute and chairman of various committees.

——所　報——

◎ 談話會記事

第269回談話會（昭和25年7月18日）

1. 江戸川川口附近の干潟堆積物	村井勇
2. 井戸調査から知られた今市地方の横辷りについて	本田孝雄 （萩原所員紹介）
3. 今市地震の計測（その一）	越川善明
4. 地震のエネルギーと頻度に就いて	淺田敏 鈴木次郎 友田好文 （松澤所員紹介）
5. 小型磁氣感應儀の製作	力武常次
6. 建物の振動に伴う土地の震動の測定結果（第二報）	金井清 長田甲斐男
7. M_2 波について（續報）	金井清

第270回談話會（昭和25年9月19日）

1. 今市地震後の地辷り器械觀測	岸上冬彦
2. 今市地震の有感地震回數	岸上冬彦
3. 西大芦村で觀測された今市地震の餘震	表俊一郎
4. 筑波山觀測に基く今市地震の震央	萩原尊禮 笠原慶一
5. 地質時代の區別	長岡半太郎
6. 伊豆大島地磁氣伏角測量（第1報）	力武常次 笠原慶一 菱山よね子
7. 三原山噴火調査報告（1）　初期の活動經過	津屋弘逵 森本良平
8. 震害と地盤との關係（江東區砂町で行つた實驗）（序報）	表俊一郎 山崎良雄
9. 振動法による構築物の安全性の判定と對策の例（其一）	那須信治

第271回談話會（昭和25年10月17日）

1. 火薬の爆發によつて起される地動について	池上良平
2. 東京本郷における地電流	岸上冬彦 小高美江子
3. 地下における地震動の觀測結果 第1報	金井清 田中貞二 吉澤靜代
4. 地質時代轉換の説明（Archaen, Algonkian, Cambrian）	長岡半太郎
5. 三原山噴火に關する二，三の觀測結果	村内必典 高木勳 本多俊一 （水上所員紹介）

6. 三原山泉津熔岩流の粘性について	村井勇 奈須紀幸 杉村新 鮫島輝彦
7. 三原火山の最近の活動に就いて 中期及び後期	高橋龍太郎 下鶴大輔

第272回談話會（昭和25年11月21日）

1. 應力がかゝつた狀態に於ける岩石彈性率の動力學的研究 其の一 ヤング率の測定	下鶴大輔
2. 伊豆大島地磁氣伏角測量（第二報） 三原山噴火に伴う伏角變化について	力武常次 齋藤貞夫
3. 三原山火口附近に於ける放送電波の廻折	力武常次 齋藤貞夫
4. 富士山山麓に於ける地表傾斜變化の研究（昭和25年の水準測量）	萩原尊禮 表俊一郎 笠原慶一
5. 磯波に關する二三の觀測	高橋龍太郎 下鶴大輔 平能金太郎
6. 津浪の水槽實驗（第1報）	高橋龍太郎 平能金太郎 下鶴大輔
7. 地質時代は太陽系に數多の小惑星を生じたと渡因を均しくするを論ず	長岡半太郎
8. 石淵爆破地震動觀測	爆破地震動研究グループ
9. 名古屋市の地盤と震害との關係	表俊一郎 宮村攝三
10. 古來の地震活動より見たる日本各地の地震危險度及び耐震設計基準震度の決定	河角廣
追加 今市地震水準測量の結果について	井上英二 （河角所員紹介）

第273回談話會（昭和25年12月19日）

1. その後の本學內深井の水位	佐藤泰夫
2. 表面波の研究 ラブ波の極小群速度その他	佐藤泰夫
3. 石淵爆破地震動觀測（第2報）	爆破地震動研究グループ
4. 東京下町の地盤振動周期について	岸上冬彦 諸我丈吉
5. 吾妻山の小活動	水上武 同研究室員
6. 阿蘇山噴火の前兆地震	水上武 武石武
7. 三原山噴火に伴つた地震	水上武 同研究室員

BULLETIN
OF THE
EARTHQUAKE RESEARCH INSTITUTE

TOKYO UNIVERSITY

VOL. XXVIII

1950

東 京 大 學

地 震 研 究 所 彙 報

第 28 號

昭 和 25 年

Contents.

Vol. XXVIII.

Parts 1—2. January—June, 1950.

Papers and Reports

Page

1. Y. SATÔ, Transformations of Wave-functions Related to the Transformations of Coordinates Systems. I. (in English) 1
2. Y. SATÔ, Rayleigh Waves Propagated along the Plane Surface of Horizontally Isotropic and Vertically Aeolotropic Elastic Body. (in English) 23
3 K. KANAI, The Effect of Solid Viscosity of Surface Layer on the Earthquake Movements. (in English) 31
4 T. TAKAHASHI and Y. SATÔ, On the Theory of Elastic Waves in Granular Substance. II. (in English) 37
5. T. RIKITAKE, Electromagnetic Induction within the Earth and Its Relation to the Electrical State of the Earth's Interior. Part I (1) (in English) 45
6. R. MORIMOTO, Petrogenic Meaning of the Occurrence of Spinel in Xenoliths. (in Englisn) 101
7. F. KISHINOUYE and M. KOTAKA, A Statistical Investigation of Conspicuous Earthquakes in Japan during the Period 1933–1943. (in English) 109
8. R. IKEGAMI and F. KISHINOUYE, A Study on the Propagation of Microseismic Waves. Part II. (in English) 115
9. R. IKEGAMI and F. KISHINOUYE, The Acceleration of Earthquake Motion Deduced from Overturning of the Gravestones in Case of the Imaichi Earthquake on Dec. 26. 1949. (in English) 121
10. D. SHIMOZURU, Change of the Ground-water Level due to the Imaichi Earthquake. (in English) 129
11. S. OMOTE, Precise Leveling at the Eastern Foot of Volcano Usu. (in Englisn) 133
12. T. MINAKAMI, Recent Activities of Volcano Usu (V). Topographical Deformations During the 1943–1945 Eruption. (in English) 143
13. T. MINAKAMI, S. SAKUMA and A. OKADA, Recent Activities of Volcano Usu (VI). Precise Levelling Around Mt. Usu in 1949. (in English) 153
14. K. KANAI, A Method of Determining the Stiffness of Each Storey of a n-storied Building. (in English) 161

15. R. TAKAHASI, A Short Note on Kanai's Formula. (in English) 165
16. K. KANAI and S. YOSHIZAWA, Distribution of Suffered Frequency of Earthquake Damage to House in Japan. (in Japanese) 167

Parts 3—4. July—December, 1950.

17. Y. SATÔ, Transformation of Wave-functions related to the Transformation of Coordinates Systems. II. (in English) 175
18. T. RIKITAKE, Electromagnetic Induction within the Earth and Its Relation to the Electrical State of the Earth's Interior. Part I (2). (in English) 219
19. T. RIKITAKE, Electromagnetic Induction within the Earth and Its Relation to the Electrical State of the Earth's Interior. Part II. (in English) 263
20. S. OMOTE, On the Coda Waves of Earthquake Motions. (Part 5) (in English) 285
21. S. OMOTE, On the Aftershocks of the Fukui Earthquake. (Part 2) (in English) 311
22. S. MIYAMURA, Vermessung der Deformation der Erdoberflächen bei der Eruption eines neuen Flankenvulkans von Usu-dake. Hokkaido, 1944. (im Japanischen) 321
23. T. AKIMA, Experiments on the Overturnings of Circular Columns by the aid of a Shaking-Table. (in English) 333
24. N. NASU, Vibration Tests of Defective Buildings. (in English) 349
25. H. KAWASUMI, The Imaichi Earthquake of December 26th, 1949. General Description. (in English) 355
26. Y. KOSHIKAWA, Seismometrical Study of the Imaichi Earthquake on Dec. 26, 1949. (in English) 369
27. R. MORIMOTO, Geology of Imaichi District with Special Reference to the Earthquake of Dec. 26, 1949. (in English) 379
28. Observation of Aftershocks Carried out in the Imaichi District, Tochigi Prefecture. (in English) 387
29. T. HAGIWARA and K. KASAHARA, On Aftershocks Accompanied the Imaichi Earthquake, December 26, 1949. (in Englisn) 393
30. S. OMOTE, Aftershocks of Imaichi Earthquake Observed at Nishi-oashi Station. (in English) 401
31. T. ASADA and Z. SUZUKI, On Micro-earthquakes Observed After the Imaichi Earthquake, Dec. 26, 1949. (in English) 415
32. S. MIYAMURA and T. AKIMA, Über die Beobachtung der Nachbeben des Imaichi-bebens am Dorfe Hunyu, Provinz Totigi. (im Japanischen) 421

33. T. Hagiwara and T. Rikitake, Observation of the Deformation of the Earth's Surface in the Vicinity of Epicentres of the Imaichi Earthquake. (English) 435
34. R. Takahasi, K. Hirano and I. Aita, Results of Precise Levellings Executed in the Epicentral Region of the Imaichi Earthquake. (in English) 443
35. T. Honda, Land Slip in the Imaichi District Revealed from the Breaks in the Well-Tubes. (in English) 449
36. F. Kishinouya, Instrumental Recording fo a Landslide caused by the Imaichi Earthquake of Dec. 26, 1950. (in English) 457
37. K. Kanai and T. Tanaka, On the Damage to Buildings by the Imaichi Earthquake of Dec. 26, 1949. (in Engilsh) 461
38. K. Kanai and T. Suzuki, Experimental Study of Vibrations of Structures Caused by After-shocks of Imaichi Earthquake of Dec. 26. 1949. (in English) 465
39. Seismometrical Data of the Imaichi Earthquake, Dec. 26, 1949. (in English) 471

目　次

第 28 號

第1~2冊　昭和25年1~6月

論文及報告　　頁

1. 坐標變換にともなふ波動方程式の解の變換 I（英文）……… 佐藤泰夫 1
2. 水平等方彈性体表面を傳はるレーリー波（英文）………… 佐藤泰夫 23
3. 地表層の固体粘性が地震動の振幅に及ぼす影響（英文）…… 金井　清 31
4. 粒狀物體を傳はる彈性波の理論 II（英文）…………… 高橋健人 佐藤泰夫 37
5. 地球内の電磁感應およびその地球内部の電氣的性質との關係 第1報（1）（英文）………… 力武常次 45
6. 捕獲岩に見出される尖晶石の產狀とその成因（英文）……… 森本良平 101
7. 日本における1933年から1943年までの間に起つた著しい地震の統計的研究（英文）………… 岸上冬彦 小高美江子 109
8. 土地の脈動の傳播性の研究（第2報）（英文）………… 池上良平 岸上冬彦 115
9. 昭和24年12月26日今市地震に於ける墓石顚倒より推定した地震動の加速度（英文）………… 池上良平 岸上冬彦 121
10. 今市地震に依る地下水位の變化（英文）………… 下鶴大輔 129
11. 有珠山の活動と精密水準測量（英文）………… 表　俊一郎 133
12. 最近の有珠山の活動（其の5）噴火中（1944-1945）に現はれた地形變動（英文）………… 水上　武 143
13. 最近の有珠山の活動（其の6）有珠山周邊の精密水準測量（英文）………… 水上　武 佐久間修三 岡田　惇 153
14. n 層建實在建物の各階の水平剛度を調べる一つの方法（英文）………… 金井　清 161
15. 金井式小引（英文）………… 高橋龍太郎 165
16. 日本における建物に震害を受けた度數の分布（邦文）……… 金井　清 吉澤靜代 167

第3~4冊　昭和25年7~8月

17. 坐標變換にともなふ波動方程式の解の變換 II（英文）…… 佐藤泰夫 175
18. 地球内の電磁感應およびその地球内部の電氣的性質との關係 第1報（2）（英文）………… 力武常次 219
19. 地球内の電磁感應およびその地球内部の電氣的性質との關係 第2報（英文）………… 力武常次 263

20. 地震動の尾部について（其の5）（英文）…………………… 表 俊一郎 285
21. 福井地震の余震について（英文）…………………… 表 俊一郎 311
22. 北海道有珠岳新側火山發生にともなつた地表變形の測定（邦文）…………………… 宮村攝三 321
23. 振動臺による圓柱の轉倒に關する實驗について（英文）…… 秋間哲夫 333
24. 非健全家屋の振動試驗（英文）…………………… 那須信治 349
25. 今市地震概說（英文）…………………… 河角廣 355
26. 今市地震の計測（英文）…………………… 越川善明 369
27. 栃木縣今市町附近の地質（その一）（英文）…………………… 森本良平 379
28. 今市地震餘震觀測報告（英文）…………………… 地震研究所 387
29. 今市地震の餘震（英文）…………………… 萩原尊禮 笠原慶一 393
30. 西大芦村で觀測された今市地震の餘震（英文）…………………… 表 俊一郎 401
31. 今市地震の際の微少地震に就て（英文）…………………… 浅田敏 鈴木次郎 415
32. 今市地震余震の栃木縣船生村における觀測について（邦文） 宮村攝三 秋間哲夫 421
33. 今市地震の震央附近における土地伸縮および傾斜變化の觀測（英文）…………………… 萩原尊禮 力武常次 435
34. 今市地震の震央地域における精密水準測量結果（概要）（英文）…………………… 高橋龍太郎 平能金太郎 相田勇 443
35. 井戸調査から知られた今市地方の地層の横辷りについて（英文）…………………… 本田孝雄 449
36. 今市地震によつて起された地辷りの器械觀測（英文）…… 岸上冬彦 457
37. 昭和24年12月26日今市地震の建物被害について（英文） 金井清 田中貞二 461
38. 今市地震の余震による建物振動の觀測結果（英文）…… 金井清 鈴木富三郎 465
39. 昭和24年12月26日今市地震の觀測資料（英文）…… 地震研究所 471

Index to Vol. XXVIII.

Page

AITA, I., TAKAHASI, R. and HIRANO, K., (34) Results of Precise Levellings Executed in the Epicentral Region of the Imaichi Earthquake. (in English) 443

AKIMA, T., (23) Experiments on the Overturnings of Circular Columns by the aid of a Shaking-Table. (in English) 333

AKIMA, T. and MIYAMURA, S., (32) Über die Beobachtung der Nachbeben des Imaichi-bebens am Dorfe Hunyu, Provinz Totigi. (in Japanischen) 421

ASADA, T. and SUZUKI, Z., (31) On Micro-earthquakes Observed After the Imaichi Earthquake, Dec. 26, 1949. (in English) 415

HAGIWARA, T. and KASAHARA, K., (29) On Aftershocks Accompanied the Imaichi Earthquake, December 26, 1949. (in English) 393

HAGIWARA, T. and RIKITAKE, T., (33) Observation of the Deformation of the Earth's Surface in the Vicinity of the Epicentres of the Imaichi Earthquake. (in English) 435

HIRANO, K., TAKAHASI, R. and AITA, I., (34) Results of Precise Levellings Executed in the Epicentral Region of the Imaichi Earthquake. (in English) 443

HONDA, T., (35) Land Slip in the Imaichi District Revealed from the Breaks in the Well-Tubes. (in English) 449

IKEGAMI, R. and KISHINOUYE, F., (8) A Study on the Propagation of Microseismic Waves. Part II. (in English) 115

IKEGAMI, R. and KISHINOUYE, F., (9) The Acceleration of Earthquake Motion Deduced from Overturning of the Gravestones in Case of the Imaichi Earthquake on Dec. 26, 1949. (in English) 121

KANAI, K., (3) The Effect of Solid Viscosity of Surface Layer on the Earthquake Movements. (in English) 31

KANAI, K., (14) A Method of Determining the Stiffness of Each Storey of a n-storied Building. (in English) 161

KANAI, K. and TANAKA, T., (37) On the Damage to Buildings by the Imaichi Earthquake of Dec. 26, 1949. (in English) 461

KANAI, K. and YOSHIZAWA, S., (16) Distribution of Suffered Frequency of Earthquake Damage to House in Japan. (in Japanese) 167

KANAI, K. and SUZUKI, T., (38) Experimental study of Vibrations of Structures Caused by After-shocks of Imaichi Earthquake of Dec. 26, 1949. (in English) 465

KASAHARA, K. and HAGIWARA, T., (29) On Aftershocks Accompanied the Imaichi Earthquake, December 26, 1949. (in English) 393

KAWASUMI, H., (25) The Imaichi Earthquake of December 26th, 1949. General Description. (in English) 355

Kishinouye, F., (36) Instrumental Recording of a Landslide caused by the Imaichi Earthquake of Dec. 26, 1949. (in English) 457

Kishinouye, F. and Kotaka, M., (7) A Statistical Investigation of Conspicuous Earthquakes in Japan during the Period 1933–1943. (in English) 109

Kishinouye, F. and Ikegami, R., (8) A Study on the Propagation of Microseismic Waves. Part II. (in English) 115

Kishinouye, F. and Ikegami, R., (9) The Acceleration of Earthquake Motion Deduced from Overturning of the Gravestones in Case of the Imaichi Earthquake on Dec. 26, 1949. (in English) 121

Koshikawa, Y., (26) Seismometrical Study of the Imaichi Earthquake on Dec. 26, 1949. (in English) 369

Kotaka, M. and Kishinouye, F., (7) A Statistical Investigation of Conspicuous Earthquakes in Japan during the Period 1933–1943 (in English) 109

Minakami, T., (12) Recent Activities of Volcano Usu (V). Topographical Deformations During the 1943–1945 Eruption. (in English) 143

Minakami, T., Sakuma, S. and Okada, A., (13) Recent Activities of Volcano Usu (VI). Precise Levelling Around Mt. Usu in 1949. (in English) ... 153

Miyamura, S., (22) Vermessung der Deformation der Erdoberflächen bei der Eruption eines neuen Flankenvulkans von Usu-dake, Hokkaido, 1944. (im Japanischen) 321

Miyamura, S. and Akima, T., (32) Über der Beobachtung der Nachbeben des Imaichi-bebens am Dorfe Hunyu, Provinz Totigi. (im Japanischen) 421

Morimoto, R., (6) Petrogenic Meaning of the Occurrence of Spinel in Xenoliths. (in English) 101

Morimoto, R., (27) Geology of Imaichi District with Special Reference to the Earthquake of Dec. 26, 1949. (in English) 379

Nasu, N., (24) Vibration Tests of Defective Buildings. (in English) 349

Okada, A., Minakami, T. and Sakuma, S., (13) Recent Activities of Volcano Usu (VI). Precise Levelling Around Mt. Usu in 1949. (in English) 153

Omote, S., (11) Precise Levelling at the Eastern Foot of Volcano Use. (in English) 133

Omota, S., (20) On the Coda Waves of Earthquake Motions. (Part 5) (in English) 285

Omote, S., (21) On the Aftershocks of the Fukui Earthquake. (Part 2) (in English) 311

Omote, S., (30) Aftershocks of the Imaichi Earthquake Observed at Nishioashi Station. (in English) 401

Rikitake, T., (5) Electromagnetic Induction within the Earth and Its Relation to the Electrical State of the Earth's Interior. Part I (1). (in English) 45

Rikitake, T., (18) Electromagnetic Induction within the Earth and Its Relation to the Electrical State of the Earth's Interior. Part I (2). (in English) 219

Rikitake, T., (19) Electromagnetic Induction within the Earth and Its Relation to the Electrical State of the Earth's Interior. Part II. (in English) 263

Rikitake, T. and Hagiwara, T., (33) Observation of the Deformation of the Earth's Surface in the Vicinity of the Epicentres of the Imaicni Earthquake. (in English) 435

Sakuma, S., Minakami, T. and Okada, A., (13) Recent Activities of Volcano Usu (VI). Precise Levelling Around Mt. Usu in 1949. (in English) 153

Satô, Y., (1) Transformations of Wave-functions Related to the Transformations of Coordinates Systems. I. (in English) 1

Satô, Y., (2) Rayleigh Waves Propagated along the Plane Surface of Horizontally Isotropic and Vertically Aeolotropic Elastic Body. (in English) 23

Satô, Y., (17) Transformation of Wave-functions related to the Transformation of Coordinates Systems. II. (in English) 175

Satô, Y. and Takahashi, T., (4) On the Theory of Elastic Waves in Granular Substance. II. (in English) 37

Shimozuru, D., (10) Change of the Ground-water Level due to the Imaichi Earthquake. (in English) 129

Suzuki, T. and Kanai, K., (38) Experimental Study of Vibrations of Structures Caused by After-shocks of Imaichi Earthquake of Dec. 26. 1949. (in English) 465

Suzuki, Z. and Asada, T., (31) On Micro-earthquakes Observed After the Imaichi Earthquake, Dec. 26, 1949. (in English) 415

Takahashi, T. and Satô, Y., (4) On the Theory of Elastic Waves in Granular Substance. II. (in English) 37

Takahasi, R., (15) A Short Note on Kanai's Formula. (in English) 165

Takahasi, R., Hirano, K. and Aita, I., (34) Results of Precise Levellings Executed in the Epicentral Region of the Imaichi Earthquake. (in English) 443

Tanaka, T. and Kanai, K., (37) On the Damage to Buildings by the Imaichi Earthquake of Dec. 26, 1949. (in English) 461

Yoshizawa, S. and Kanai, K., (16) Distribution of Suffered Frequency of Earthquake Damage to House in Japan. (in Japanese) 167

(28) Observation of Aftershocks Carried out in the Imaichi District, Tochigi Prefecture. (in English) 387

(39) Seismometrical Data of the Imaichi Earthquake, Dec. 26, 1949. (in English) 471

Rikitake, T. (18) Electromagnetic Induction within the Earth and its Relation to the Electrical State of the Earth's Interior. Part I. (In English) 219

Rikitake, T. (19) Electromagnetic Induction within the Earth and its Relation to the Electrical State of the Earth's Interior. Part II. (In English) 263

Rikitake, T. and Hagiwara, T. (15) Observation of the Deformation of the Earth's Surface in the Vicinity of the Epicentre of the Imaichi Earthquakes. (In English) 139

Sassa, K., Minakami, T. and Okada, A. (11) Recent Activities of Volcano Usu (VI). Precise Levelling Around Mt. Usu in 1950. (In English) 157

Sato, Y. (1) Transformations of Wave-functions Related to the Transformation of Coordinate Systems. I. (In English) 1

Sato, Y. (2) Rayleigh Waves Propagated along the Plane Surface of Horizontally Isotropic and Vertically Aeolotropic Elastic Body. (In English) 23

Sato, Y. (12) Transformation of Wave-functions related to the Transformation of Coordinate Systems. II. (In English) 175

Sato, Y. and Takahasi, T. (9-44) On the Theory of Elastic Waves in Granular Substance. II. (In English) 91

Shimozuru, D. (16) Oscillations of the Groundwater Level due to the Imaichi Earthquakes. (In English) 133

Suzuki, M. and Kanai, K. (28) Experimental Study of the Vibrations of Structures Caused by After-shocks of Imaichi Earthquake of Dec. 26, 1949. (In English) 441

Suzuki, Z. and Suzuki, T. (25) On Micro-earthquakes Observed After the Imaichi Earthquake, Dec. 26, 1949. (In English) 403

Takahasi, T. and Sato, Y. (4) On the Theory of Elastic Waves in Granular Substance. II. (In English) 371

Takahasi, R. (13) A Short Note on [illegible] Formula. (In English) 195

Takagi, K., Hirono, K. and Aita, I. (29) Results of Precise Levellings Executed in the Epicentral Region of the Imaichi Earthquakes. (In English) 443

Tamura, T. and Kanai, K. (27) On the Damage to Buildings by the Imaichi Earthquake of Dec. 26, 1949 (In English) 461

Tominaga, S. and Kanai, K. (10) Distribution of Spectral frequency of Earthquake Damage to Houses in Japan. (In English) 107

(26) Observation of Aftershocks Carried out in the Imaichi District Tochigi Prefecture. (In English) 437

(27) Seismometrical Data of the Imaichi Earthquake, Dec. 26, 1949. (In English) 471

第28號　索　引

頁

相田　勇・高橋龍太郎・平能金太郎　(34) 今市地震の震央地域における精密水準測量結果 (概要) (英文)………………………… 443

秋間哲夫　(23) 振動臺による圓柱の轉倒に關する實驗について (英文)………… 333

秋間哲夫・宮村攝三　(32) 今市地震餘震の栃木縣船生村における觀測について (邦文) ……………………………… 421

淺田　敏・鈴木次郎　(31) 今市地震の際の微少地震に就て (英文)………………… 415

萩原尊禮・笠原慶一　(29) 今市地震の餘震 (英文)……………………………… 393

萩原尊禮・力武常次　(33) 今市地震の震央附近における土地伸縮および傾斜變化の觀測 (英文) ……………………………… 435

平能金太郎・高橋龍太郎・相田　勇　(34) 今市地震の震央地域における精密水準測量結果 (概要) (英文)……………………………… 443

本田孝雄　(35) 井戸調査から知られた今市地方の地層の横辷りについて (英文)……………………………… 449

池上良平・岸上冬彥　(8) 土地の脈動の傳播性の研究 (第2報) (英文)………… 115

池上良平・岸上冬彥　(9) 昭和24年12月26日今市地震に於ける墓石顚倒より推定した地震動の加速度 (英文) ……………………………… 121

金井　清　(3) 地表層の固體粘性が地震動の振幅に及ぼす影響 (英文) …………… 31

金井　清　(14) *n* 層建實在建物の各階の水平剛度を調べる一つの方法 (英文)…… 161

金井　清・田中貞二　(37) 昭和24年12月26日今市地震の建物被害について (英文) ……………………………… 461

金井　清・吉澤靜代　(16) 日本における建物に震害を受けた變數の分布 (邦文)……………………………… 167

金井　清・鈴木富三郎　(38) 今市地震の餘震による建物振動の觀測結果 (英文)……………………………… 465

笠原慶一・萩原尊禮　(29) 今市地震の餘震 (英文) ……………………………… 393

河角　廣　(25) 今市地震概說 (英文)……………………………… 355

岸上冬彥　(36) 今市地震によつて起された地辷りの器械觀測 (英文)……………… 457

岸上冬彥・小高美江子　(7) 日本における1933年から1943年までの間に起つた著しい地震の統計的研究 (英文) ……………………………… 109

岸上冬彥・池上良平　(8) 土地の脈動の傳播性の研究 (第1報) (英文)………… 115

岸上冬彥・池上良平　(9) 昭和24年12月25日今市地震に於ける墓石顚倒より推定した地震動の加速度 (英文) ……………………………… 121

越川善明　(26) 今市地震の計測 (英文)……………………………… 369

小高美江子・岸上冬彥　(7) 日本における1933年から1943年までの間に起つた著しい地震の統計的研究 (英文) ……………………………… 109

水上　武　(12) 最近の有珠山の活動 (其の5) 噴火中 (1944-1945) に現はれた地形變動 (英文) ……………………………… 143

ア

水上 武・佐久間修三・岡田 惇 (13) 最近の有珠山の活動 (其の6) 有珠山周邊の精密水準測量 (英文) …………………… 153
宮村攝三 (22) 北海道有珠岳新側火山發生にともなつた地表變形の測定 (邦文)… 321
宮村攝三・秋間哲夫 (32) 今市地震餘震の栃木縣船生村における觀測について (邦文) …………………… 421
森本良平 (6) 捕獲岩に見出される尖晶石の産狀とその成因 (英文) …………… 101
森本良平 (27) 栃木縣今市町附近の地質 (その一) (英文) …………… 379
那須信治 (24) 非健全家屋の振動試驗 (英文) …………… 349
岡田 惇・水上 武・佐久間修三 (13) 最近の有珠山の活動 (其の6) 有珠山周邊の精密水準測量 (英文) …………………… 153
表俊一郎 (11) 有珠山の活動と精密水準測量 (英文) …………… 133
表俊一郎 (20) 地震動の尾部について (其の5) (英文) …………… 285
表俊一郎 (21) 福井地震の餘震について (英文) …………… 311
表俊一郎 (30) 西大芦村で觀測された今市地震の餘震 (英文) …………… 401
力武常次 (5) 地球内の電磁感應およびその地球内部の電氣的性質との關係第1報 (英文) …………………… 45
力武常次 (18) 地球内の電磁感應およびその地球内部の電氣的性質との關係第1報 (2) (英文) …………………… 219
力武常次 (19) 地球内の電磁感應およびその地球内部の電氣的性質との關係第2報 (英文) …………………… 263
力武常次・萩原尊禮 (33) 今市地震の震央附近における土地伸縮および傾斜變化の觀測 (英文) …………………… 435
佐久間修三・水上 武・岡田 惇 (13) 最近の有珠山の活動 (其の6) 有珠山周邊の精密水準測量 (英文) …………………… 153
佐藤泰夫 (1) 坐標變換にともなふ波動方程式の解の變換 I (英文) …………… 1
佐藤泰夫 (2) 水平等方彈性體表面を傳はるレーリー波 (英文) …………… 23
佐藤泰夫 (17)坐標變換にともなふ波動方程式の解の變換 II (英文) …………… 175
佐藤泰夫・高橋健人 (4) 粒狀物體を傳はる彈性波の理論 II (英文) …………… 37
下鶴大輔 (10) 今市地震に依る地下水位の變化 (英文) …………… 129
鈴木富三郎・金井 清 (38) 今市地震の餘震による建物振動の觀測結果 (英文) …………………… 465
鈴木次郎・淺田 敏 (31) 今市地震の際の微少地震に就て (英文) …………… 415
高橋健人・佐藤泰夫 (4) 粒狀物體を傳はる彈性波の理論 II (英文) …………… 37
高橋龍太郎 (15) 金井式小引 (英文) …………… 165
高橋龍太郎・平能金太郎・相田 勇 (34) 今市地震の震央地域における精密水準測量結果 (概要) (英文) …………………… 443
田中貞二・金井 清 (37) 昭和24年12月26日今市地震の建物被害について (英文) …………………… 461
吉澤靜代・金井 清 (16) 日本における建物に震害を受けた度數の分布 (邦文) …………………… 167
地震研究所 (28) 今市地震餘震觀測報告 (英文) …………… 387
地震研究所 (39) 昭和24年12月26日今市地震の觀測資料 (英文) …………… 471

昭和26年3月20日印刷
昭和26年3月25日發行

東京都文京區本富士町一番地
東京大學構内
編纂兼發行者　東京大學地震研究所

東京都港區芝浦一丁目一番地
印刷者　富田元

東京都港區芝浦一丁目一番地
印刷所　株式會社ヘラルド社

東京都千代田區神田一ツ橋通
賣捌所　岩波書店

東京都中央區日本橋二丁目六番地
丸善株式會社

Sold by
Iwanami Shoten,
Hitotsubashi dôri, Chiyoda, Tôkyô,
and
Maruzen Co., Ltd.,
Nihonbashi dôri, Chûô-ku, Tôkyô.
Price of this copy: 1000 Yen. (Postage exclusive.)

BULLETIN OF

THE EARTHQUAKE RESEARCH INSTITUTE

TOKYO UNIVERSITY

Vol. XXVIII, Parts 3-4. July~Dec., 1950.

Contents.

Papers and Reports.

Page

17. Y. SATÔ, Transformation of Wave-functions related to the Transformation of Coordinates Systems. II. (in English) ... 175
18. T. RIKITAKE, Electromagnetic Induction within the Earth and Its Relation to the Electrical State of the Earth's Interior. Part I (2). (in English) ... 219
19. T. RIKITAKE, Electromagnetic Induction within the Earth and Its Relation to the Electrical State of the Earth's Interior. Part II. (in English) ... 263
20. S. OMOTE, On the Coda Waves of Earthquake Motions. (Part 5) (in English) 285
21. S. OMOTE, On the Aftershocks of the Fukui Earthquake. (Part 2) (in English) 311
22. S. MIYAMURA, Vermessung der Deformation der Erdoberflächen bei der Eruption eines neuen Flankenvulkans von Usu-dake, Hokkaido, 1944. (im Japanischen)... 321
23. T. AKIMA, Experiments on the Overturnings of Circular Columns by the aid of a Shaking-Table. (in English) ... 333
24. N. NASU, Vibration Tests of Defective Buildings. (in English) ... 349
25. H. KAWASUMI, The Imaichi Earthquake of December 26th, 1949. General Description. (in English) ... 355
26. Y. KOSHIKAWA, Seismometrical Study of the Imaichi Earthquake on Dec. 26, 1949. (in English) ... 369
27. R. MORIMOTO, Geology of Imaichi District with Special Reference to the Earthquake of Dec. 26, 1949. (in English) ... 379
28. Observation of Aftershocks Carried out in the Imaichi District, Tochigi Prefecture. (in English) ... 387
29. T. HAGIWARA and K. KASAHARA, On Aftershocks Accompanied the Imaichi Earthquake, December 26, 1949. (in English) ... 393
30. S. OMOTE, Aftershocks of Imaichi Earthquake Observed at Nishi-oashi Station. (in English) ... 401
31. T. ASADA and Z. SUZUKI, On Micro-earthquakes Observed After the Imaichi Earthquake, Dec. 26, 1949. (in English) ... 415
32. S. MIYAMURA and T. AKIMA, Über die Beobachtung der Nachbeben des Imaichi-bebens am Dorfe Hunyu, Provinz Totigi. (im Japanischen) ... 421
33. T. HAGIWARA and T. RIKITAKE, Observation of the Deformation of the Earth's Surface in the Vicinity of the Epicentres of the Imaichi Earthquake. (in English) 435
34. R. TAKAHASI, K. HIRANO and I. AITA, Results of Precise Levellings Executed in the Epicentral Region of the Imaichi Earthquake. (in English) ... 443
35. T. HONDA, Land Slip in the Imaichi District Revealed from the Breaks in the Well-Tubes. (in English) ... 449
36. F. KISHINOUYE, Instrumental Recording of a Landslide caused by the Imaichi Earthquake of Dec. 26, 1949. (in English) ... 457
37. K. KANAI and T. TANAKA, On the Damage to Buildings by the Imaichi Earthquake of Dec. 26, 1949. (in English) ... 461
38. K. KANAI and T. SUZUKI, Experimental Study of Vibrations of Structures Caused by After-shocks of Imaichi Earthquake of Dec. 26. 1949. (in English) ... 465
39. Seismometrical Data of the Imaichi Earthquake, Dec. 26, 1949. (in English) ... 471

Institute Notes.

Index.

(For the papers written in Japanese or in occidental languages, the abstracts are given in occidental languages or in Japanese respectively.)